THE UNIVERSITY *of* EDINBURGH

Uranium Associations and Migration Behaviour at the Needle's Eye Natural Analogue Site in SW Scotland

Xiaolu Xu

PhD

The University of Edinburgh

2013

Declaration

I certify that the work described in this thesis in my own, except where otherwise stated, and has not been previously submitted for any other degree at this, or any other university.

Xiaolu Xu

Abstract

This thesis investigated uranium (U) migration behaviour at the Needle's Eye natural analogue site, located close to Southwick Water, South West Scotland. The results of this study are important for the prediction of U behaviour in the far-field environments of nuclear waste repositories over long time-scales.

The Needle's Eye natural analogue site was selected because the processes involved in U mobilisation, the direction of water flow and the extent of retention of uranium in peaty soils had already been identified. To this end, previous results demonstrated that groundwater passing through the mineralisation oxidized U and transported it to the peaty area, where 80-90% of the released U has been retained. Sequential extraction of the peaty soils indicated that more than 90% of the solid phase U was bound to the organic fraction. However, in-depth characterisation of U associations within the soil porewaters and the peaty soils at this site was lacking. Therefore, the processes controlling the migration of uranium within this organic-rich system were the main focus of this study. There were five sampling trips carried out from 2007-2011, in which cave drip waters, bog waters and surface soil and soil core samples were selectively collected for analysis by a range of methods described below.

The cave drip waters emerging from the mineralisation were oxidizing and slightly alkaline (7.6-7.8), U was mainly in truly dissolved (<3 kDa) forms ($Ca_2UO_2(CO_3)_3^0$, $CaUO_2(CO_3)_3^{2-}$ and $UO_2(CO_3)_2^{2-}$). It is known that the formation of the ternary Ca-U^{VI}-CO_3 complexes inhibits the reduction of U and so it is likely that it is U^{VI} that is present within the peaty soils and their associated porewaters.

Sampling trip 1 quantified the U concentrations in cave waters and soil core porewaters. By 30 m from the cave, U concentrations in the soil porewaters had decreased by a factor of ~10. Ultrafiltration fractionated the colloidal fraction (3 kDa-0.2 μm) into large (100 kDa-0.2 μm), medium (30-100 kDa) and small (3-30 kDa) colloidal fractions. It was found that U was mainly associated with the large colloid (100 kDa-0.2 μm) but, with increasing distance from the mineralisation, the U distribution became bimodal with both large and small fractions being equally important. Iron (Fe) was exclusively associated with the large colloid fraction in the peaty soil porewaters. Gel electrophoresis and gel filtration, applied to study the interactions of U (and other elements) with humic substances (HS), showed

that the associations were quite uniform with increasing depth of the cores and increasing distance from the U mineralisation. Uranium (and other elements including Fe) was associated with the largest humic molecules.

Sampling trip 2 involved collection of three more soil cores and ultrafiltration again fractionated the total dissolved porewater into large, medium and small colloids. This time, the truly dissolved (<3 kDa) fraction was also analysed. Again, U was mainly associated with the large colloidal (100 kda-0.2 μm) fraction. With increasing distance and increasing depth, U was still predominantly associated with the large colloidal fraction, but the importance of the truly dissolved (<3 kDa) phase could not be neglected. At the same time, Fe was also mainly associated with the large colloidal fraction. The remainder of the experimental work on samples from trip 2 focused on determining the importance of U associations with both Fe and humic components of the solid phase. Sequential extraction of the whole soil mainly targeted different iron phases and found that U was mainly released in the sodium acetate and sodium dithionite solutions, which indicated U was associated with (i) Fe carbonates; and (ii) crystalline Fe oxides (e.g. goethite, hematite, and akaganetite). However, very little Fe was extracted in the "carbonate-bound" fraction and separate experiments showed that U was not associated with Fe carbonates but instead had been released from the surfaces of HS and humic-bound Fe surfaces. XRD spectroscopy showed that mineral compositions were in reasonable agreement with the sequential extraction results and SEM-EDX analysis indicated that U in the soil was generally not present in crystalline form, as only two particles with high U content were found after 4-hour searching. Exhaustive extraction of HS showed that >90% U was associated with organic substances, in agreement with previous work and novel experiments involving gel electrophoresis in conjunction with sequential extraction was used to study the relationships between U, Fe and the HS. It was demonstrated that ~20-25% U was weakly held by the HS or at humic-bound Fe surfaces, ~45% was incorporated into crystalline Fe oxides which were intimately associated with HS and the remainder was in the form of strong U-CO_3-humic complexes.

In sampling trip 3, U migration behaviour in the soil porewaters was the focus. A 30-m transect line, comprising seven0-5 cm soil samples, starting at the cave and passing through the peaty area towards the Southwick Water, was established. Soil porewaters from these surface soils were fractionated into colloidal (3 kDa-0.2 μm) fraction and truly dissolved (<3 kDa) phase. There was a major change in U speciation, from $Ca_2UO_2(CO_3)_3^0$,

$CaUO_2(CO_3)_3^{2-}$ and $UO_2(CO_3)_2^{2-}$ in the truly dissolved fractions of waters close to the cave to a predominant association with the highly coloured colloidal fractions as soon as the boggy area was reached. With distance through the boggy area, it was clear that the colloidal U was being incorporated into the solid phase since porewater concentrations had decreased ~100-fold by 30 m from the cave. Ultrafiltration in conjunction with acetate extraction was then used to extract U from the porewater colloids isolated from a soil core (20 m from cave). In the organic-rich portion of the core (0-30 cm), ~60-70% U was colloidally associated and ~85-95% of this U was extracted from the colloidal fraction. This indicated that the interactions between U and the porewater colloids were weak.

In sampling trip 4, U associations in the porewater colloids were still the main focus. Gel filtration of porewater colloids confirmed that U, Fe and humic colloids were intimately associated. It was concluded that although U in the cave drip water was mainly in truly dissolved forms, weak U----humic/Fe colloids were formed immediately when U entered the peaty area.

In sampling trip 5, results for soil core porewaters showed that Fe in the whole core was mainly in the form of Fe^{II}. Thus strongly reducing conditions prevailed through the core which was situated within the peaty area.

Combining the results from the five sampling trips, three zones within the peaty area were distinguished. Zone I was characterised by extremely high concentrations of dissolved HS and this was where the change in U speciation from dissolved to colloidal forms took place. Zone II contained most of the soil cores collected during this study and was characterised by strongly reducing conditions and moderate concentrations of HS. Colloidal U was removed to the solid phase as waters flow through this area. Zone III marks the transition to the saltmarsh. Focusing on Zone II, a conceptual model of U behaviour was developed: upon entering the peaty area, U is weakly held by very large humic-Fe colloids. These colloids are removed to the solid phase and over time the associations of U are transformed; some becomes incorporated into stable humic-bound crystalline oxides as a result of redox cycling of Fe, some becomes strongly complexed to HS and the remainder is weakly held by the HS and/or humic-bound Fe surfaces. The crystalline Fe oxides were transformed to Fe sulfides below 30 cm depth but the associated U was not transferred to these sulfides. Instead the weak associations became more important.

In the wider context, since only U^{VI} forms soluble complexes with acetate, U^{VI} does not appear to be reduced even under the strongly reducing conditions encountered within waterlogged organic-rich soils. Initial interactions between U^{VI} and porewater colloids appear to be weak but stronger interactions such as incorporation into Fe phases and complexation by HS occur once the colloids and associated U are removed to the solid phase. Waterlogged organic-rich soils appear to be a long-term sink for U but changing climatic conditions leading to the drying out of such soils may ultimately release U in association with smaller, more mobile organic-rich colloids.

Acknowledgements

First and foremost, I would like to thank my supervisor Dr. Margaret Graham. I am grateful for her guidance, encouragement and enthusiasm during my master and PhD studies. I am so lucky that I have been under an environment that is not only for teaching me to be qualified scientist, but to be better human being, I could not wish for a better supervisor. I would also like to thank Professor John Farmer for his kind assistance as my co-supervisor.

I have met many people who have a heart of gold in Edinburgh (though I did not know then, for when you are young you take the kindness people show you as your right). I would like to thank my colleagues Joanna Cloy, Helfrid Rossiter, David Blair and Peerapat Kosolsaksakul for assisting with field work, providing comments and useful information on my work and making my time in lab enjoyable. A special thanks to Dr Lorna Eades for the analysis of so many samples by ICP-MS and her patience for my questions. A big thank you to Dr Ian Oliver for providing a mock viva for me, which is really helpful. Another big thank you to Dr. Bryne Ngwenya for his help and encouragement during my PhD.

I would like to thank all of my friends in Edinburgh with whom I have shared so many excellent times. In particular, I would like to thank Mengmeng, Wei, Bibi and Tiantian.

Finally, I would like to thank my mum and dad, for their unconditional love and support.

Table of Contents

List of Figures

1 Introduction

2 Method

3 Results and discussion for sampling trip 1 on 11/12/2007: initial survey of the Needle's Eye site and method development

4 Results and initial interpretation for sampling trips 2-5

5 Synthesis and Discussion

List of Tables

1 Introduction

2 Method

3 Results and discussion for sampling trip 1 on 11/12/2007: initial survey of the Needle's Eye site and method development

4 Results and initial interpretation for sampling trips 2-5

5 Synthesis and Discussion

9 Appendix

1 Introduction

1.1 Investigations of uranium (U) behaviour at the Needle's Eye natural analogue site, SW Scotland – overview

1.1.1 Importance of investigations of the environmental behavior of U

As a result of nuclear energy production activities around the world over the past ~60 years, nuclear wastes containing U and other radionuclides, many of which have long half-lives and present a significant radiological risk to human health, have been released into the environment, e.g. via leaching from unprotected mine tailings at Rockhole, Northern Territory, Australia (Mudd, 2000), from authorized and accidental marine discharges relating to the nuclear fuel reprocessing at the British Nuclear Fuels (BNF) plant at Sellafield in Northwest England (Gray et al., 1995), and from improper waste storage at the Hanford site in the state of Washington (U.S.) (Wang et al., 2004). In addition, the ores which are used for extraction of U and subsequent production of nuclear fuels, e.g. uraninite (UO_2), coffinite ($U(SiO_4)_{1-x}(OH)_{4x}$), and autinite ($Ca(UO_2)_2(PO_4)_2.10\text{-}12H_2O$), can also be significant natural sources of U to groundwaters, especially in mineral-rich areas and some granitic terrains. Globally, groundwaters are increasingly being used as drinking water sources and there is concern that, in many countries, U contamination may pose a risk to human health (Nriagu et al., 2012).

There have been quite a number of recent studies of U in groundwater. For example, the typical concentration of U in groundwater is <1 μg L^{-1} but, from the analysis of 101 groundwater samples collected in England and Wales in 2005 and 2006, ~20% of samples contain U more than 2 μg L^{-1} (Smedley et al., 2006).

In Labrador, Canada (Figure 1.1), there has been recent concern that well water used for drinking water may potentially contain U at concentrations of >20 μg L^{-1}. Although no exceedences of this value have been recorded to date, the Canadian government have provided guidance recommending consumption of bottled water should the situation arise (http://www.env.gov.nl.ca/env/waterres/cycle/groundwater/well/uranium.html; accessed 01/04/2013).

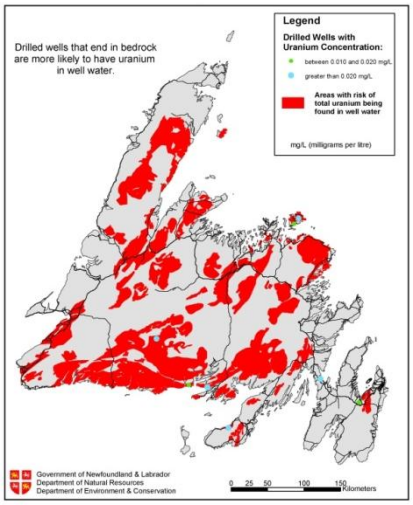

Figure 1.1: Areas of potential U contamination in well water in Newfoundland and Labrador, Canada (red areas show areas where total U concentrations >0.02 mg L^{-1}, i.e. >20 µg L^{-1}may be found) (http://www.env.gov.nl.ca/env/waterres/cycle/groundwater/well/uranium.html**; accessed 01/04/2013)**

Finally, in Mongolia, a country whose water resources are very fragile due to a combination of harsh winters, hot summers, low rainfall and human activity, Nriagu et al. (2012) found that the mean U concentration was ~4.5 µg L^{-1}, 10% of the 258 groundwater samples from Ulaanbaatar exceeded 10 µg L^{-1} and 5% exceeded 15 µg L^{-1} (Figure 1.2), the provisional WHO drinking water limit until 2012. This raises concerns about the potential impacts of U exposure on human health where groundwater is being used as a source of drinking water.

Very recently, however, a new provisional value of 30 µg L^{-1} (WHO, 2012) has been introduced in the light of recent epidemiological studies on populations exposed to high U concentrations (e.g. Kurttio et al., 2006). It should be stressed that this is still a provisional guideline value because of the difficulties in identifying an exposure level at which effects might be expected. A further point of caution is that this limit may provide protection for adult health but some studies have suggested that the kidney function in infants may be affected by much lower Uconcentrations. As a consequence the German limit for U in water used for preparing infant milk products is only 2 µg L^{-1} (ESFA, 2009). Clearly, even the mean value for U concentration in Ulaanbaatar groundwaters is greater than this lower limit.

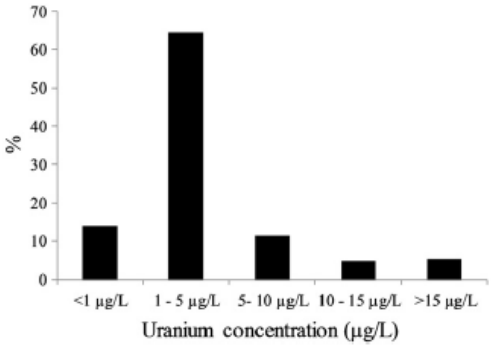

Figure 1.2: Uranium distribution in groundwater in Ulaanbaatar, Mongolia (Nriagu et al., 2012)

The release of U from solid phases into water bodies can be enhanced by the presence of both organic and inorganic colloids but the controlling processes are not fully understood. An investigation of U migration behaviour in both terrestrial and aquatic systems is therefore needed in order to (i) quantify the risks to human health; (ii) provide in-depth understanding of retention/release processes of relevance to both radioactive waste disposal and more generally to groundwater contamination; (iii) inform about appropriate remediation strategies to remove U from drinking water sources.

1.1.2 The use of natural analogue sites to study U migration behaviour

Transport or migration within the geosphere is largely controlled by groundwater flow (advection) which is driven by pressure gradients and/or diffusion which is driven by concentration gradients (Smellie, 2009). Advection representsthe mean transport flow whilst diffusive flow operates on the smaller scale and is affected by heterogeneities in the solid substrate.

Transport can be modified by retention and retardation effects. The most important of these arise from (i) direct interactions between solute and the solid phases (i.e. sorption) and (ii) matrix diffusion, when radionuclides diffuse into stagnant porewaters where they are transported more slowly than in the advective flow system. The presence of suspended particulate matter and/or colloids can further modify retention/retardation and is often considered to enhance the migration potential of U and other radionuclides (Smellie, 2009). The conditions prevailing within the natural system are also of prime importance. For example, the mobilization of U is often correlated with the flow of oxic water through the

mineral-rich rock and subsequent fixation involves processes such as complexation, reduction, adsorption and ion exchange (Smedley et al., 2006). Recent studies also indicate that microorganisms may also have a high radionuclide sorption capacity, possibly selective and irreversible, thus favouring radionuclide transport to the biosphere (Ohnuki et al., 2010).

Natural mineralisations, also called natural analogue sites, are areas in which U ores have been present for geologic time periods and so they provide the opportunity to study U migration over long time-scales. The results from such studies can enable the prediction of U migration behaviour from deep nuclear waste repositories, as well as from mineral areas and some granitic terrains through the near-field (within the repository) and far-field (after the repository has been breached) environment in the dimensions of both space and time (Miller et al., 2011).

There are many well-known examples of natural analogue sites, including Poços de Caldas (Brazil), Cigar Lake (Canada), Oklo/Okélobondo and Bangombé (Gabon, Central Africa), El Berrocal (Spain), Palmottu (Finland), Needle's Eye (SW Scotland) (Table 1.1).

Table 1.1: Examples and descriptions of U mineralisations and natural analogue sites around the world (modified from Bruno et al., 2002)

Site	Geological Description	Example References
Po ços de Caldas	Mesozoic volcanic ring structure hosting a U-Th mineralisation	Chapman et al., 1993
Cigar Lake	1.3 billion year old U deposit located in a water-saturated sandstone where the ore is surrounded by a clay-rich halo	Cramer and Smellie, 1994
Oklo	Fossil nuclear reactor system located in a Precambrian sedimentary basin	Louvat et al., 1998
El Berrocal	Granitic Hercinian massif intercepted by quartz vein; associated primary Umineralisations	Enresa, 1996
Palmottu	U deposit located within Precambrian metamorphosed supracrustal and sedimentary rocks	Blomqvist et al., 2000
Needle's Eye	U deposit located within the Criffel pluton; late Caledonian granodioriteintrusion of Silurian metasedimentary rocks	Miller and Taylor, 1966 Halliday et al., 1980

These natural analogue sites have been widely used over recent decades to study within-repository processes (e.g. MacKenzie et al., 1992; Vilks et al., 1993; Smellie and Karlsson, 1999), develop and test geochemical transport models (e.g. Bruno et al., 1997; Bruno et al., 2002), and to investigate the long-term behaviour of U as it is released into near-surface soil environments (e.g. Hooker et al., 1986; Basham et al., 1989; Hooker, 1990; MacKenzie et al., 1990; Jamet et al., 1993).

This study involves the investigation of U migration from the Needle's Eye natural U mineralization through organic-rich soils. Detailed description of the natural analogue site at Needle's Eye, SW Scotland, is included in Chapter 2, whilst the sections that follow within this chapter will focusonthecharacteristics of soils, especially relating to mineral phases and organic matter (section 1.2), the properties of U including its aqueous geochemistry (section 1.3), the major processes which retain/retard U as it migrates through soil (section 1.4) and methods which have been used to study U interactions in

soils (section 1.5). Finally, section 1.6 sets out the aims of this study.

1.2 Soils and their properties

Since the focus of this study is on U migration through near-surface soils, the sections which follow describe the main inorganic and organic components of soils and the processes which affect soil composition.

1.2.1 Soil formation

The first step in soil formation occurs when mineral material from rocks and organic matter from plants and animals are combined together. Rocks are the main mineral inputs to the soil and physical and chemical weathering are the main factors to transform rock to soil (Brady and Weil, 2007). Physical weathering includes the processes of thermal weathering, abrasion by water, ice and wind, and disintegration by plants and animals. Temperature differences cause thermal stress between the outer and inner parts of the rock, and different expansion rates between different minerals in the rock. Water and plant roots can penetrate into the small cracks of rocks, and ice can exert an expanding force on the rock. These processes eventually lead to the disintegration of the rock. Further breakdown of rocks is theneffected by chemical weathering which includes the processes of hydration, hydrolysis, acid hydrolysis, dissolution and oxidation-reduction. Water must be in contact with the rock before chemical weathering takes place but these processes are enhanced by the presence of dissolved carbon dioxide and oxygen, or biological agents such as the acids produced by microbial and plant-root metabolism (Ashman and Puri, 2008).

Plant and animal residues are the main source materials from which soil organic matter is formed. Weathered rock eventually becomes soil when organic matter is incorporated into rock-derived minerals to form a distinct structural unit. The initial accumulation of soil organic matter on mineral surfaces relies on certain bacteria, fungi and plant species that can live in water- and nutrient-limited environments, especially those which can obtain nitrogen from the atmosphere. When these special organisms die, their tissues are combined within the minerals to form the first organic matter of the soil. When the amount of the organic matter increases to the extent that other plants may obtain nutrition from the soil, it can form an on-going sink for soil organic matter(Ashman and Puri, 2008) (see section 1.2.2.4).

During the whole process of soil formation, there are five factors that affect the outcome, including the parent materials, climate, biota, topography and time. The chemical and mineralogical composition of the parent material is important since it is the primary source of mineral nutrients upon which plant sustenance will depend. Climate determines the nature and intensity of the physical and chemical weathering. The effect of biota on soil formation is composed of the role of natural vegetation and the role of animals. For example, the nature of the vegetation will determine the composition of the organic material entering the soil. Living vegetation can also accelerate mineral weathering by taking up these elements from the soil; enhanced mineral dissolution will result. Animals such as earthworms and ants mix the soil, transporting material from one horizon to another. Topography is a term to describe differences in elevation, slope, and landscape position. The importance of topography on soil formation lies in the shape and slope of the landscape, which have an effect on run-off, erosion and drainage. Finally, soil formation is a slow process; the younger a soil is, the more closely its composition will resemble the parent material (Brady and Weil, 2007).

During soil formation, mineral and organic materials move down to the lower layers of soils by dissolving or suspending in the water and moving along with water. In this way, the soil can form a number of distinct layers as some layers are enriched with new compounds while others are depleted with removal of mobile compounds (Ashman and Puri, 2008). The term “soil profile” refers to the top layers of soil and all underlying layers down to the unaltered parent material from which the soil has formed (Figure 1.3).

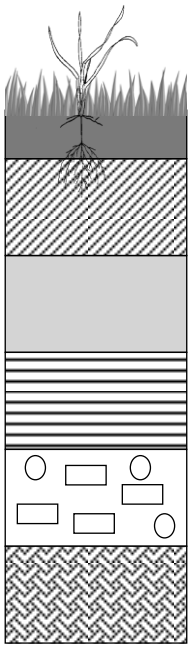

Figure 1.3: Hypothetical soil profile showing the major horizons1 that may be present in a well-drained soil in the temperate humid region (Ashman and Puri, 2008)

[1]not all soils have all of these horizons; the parent material need not be the bedrock

The soil layers are commonly labelled as O, A, E, B, C and R with increasing depth (Figure 1.3). The O horizon is an organic-rich layer occurring at the surface of some soils. When present, it is often dark-brown in colour, and originates from dead plant and animal residues. This may include fresh inputs, partially degraded material where residues are still recognizable, through to highly decomposed humus material with no recognizable plant or animal remains. The A horizon is the first mineral horizon of the soil and is often dark brown in colour due to the presence of the soil humus. The texture in this zone is usually quite coarse, especially wheresome of the fine particulate material has been translocated into lower horizons. The E horizon is the main zone of eluviation (loss) and it tends to be pale in colour due to the loss of soluble organic matter and mineral components. Resistant and insoluble minerals including quartz, Al oxides, and aluminosilicates, most of which are pale in colour, remain in this zone while soluble ions, e.g. Ca^{2+}, Fe^{2+}, Fe^{3+}, K^{+}, Mg^{2+}, Mn^{2+}, Na^{+}, NO_3^{-}, NO_2^{-}, and neutral species, e.g. $H_4SiO_4^{0}$, are leached from the upper layers and often accumulate in the B horizon, the zone of accumulation. It has the greatest

accumulation of Fe and Al oxide amongst all the horizons. In some cases, e.g. forest soils, an orange-brown coloured iron (Fe) pan may be formed here. The C horizon is below the zones of most biological activities, so, in contrast with the B horizon, it does not undergo significant chemical weathering and still contains some features of the original parent material (Ashman and Puri, 2008; Brady and Weil, 1999). The R horizon is the parent material from which the soil has formed. This need not be the same as the underlying bedrock since glaciation may have transported rock material from elsewhere and this may have become weathered to form the soil.

1.2.2 Soil composition

Soils consist of four major components: air, water, mineral and organic matter, which are mixed in a complex pattern. Under optimal conditions for plant growth, the proportions of these four components in a surface (loam) soil are 20-30% air, 20-30% water, 45% mineral and 5% organic matter by volume, respectively, but significant deviations from ideal conditions are observed (Brady and Weil, 2007).

1.2.2.1 Soil Water

The amount of water held in the soil is dependent on the number and size of soil pores, the amount of organic matter present as well as the climate-related availability of water entering the soil. Soil pores may be filled with either air or with water, the latter sometimes being referred to as the soil solution or soil porewater. The soil porewater contains soluble inorganic and organic substances, which are mainly released from the soil solids (although some may come from rain water). These include truly dissolved cations and anions, e.g. Ca^{2+}, Mg^{2+}, Na^{+}, K^{+}, and PO_4^{3-}, NO_3^{-}, SO_4^{2-}, respectively, but also dissolved organic compounds and organic and inorganic colloids (1 nm-~0.2 μm). Many soil chemical and biological reactions, including those affecting contaminants such as U, are dependent on the pH of soil porewater (Brady and Weil, 2007).

1.2.2.2 Soil Atmosphere

The composition of soil gas varies from place to place, but usually the concentration of carbon dioxide is much higher, e.g. up to several hundred times more concentrated (Brady and Weil, 2007), than that commonly found in atmospheric air (~380 ppbV) due to the

metabolic activities of plant roots and microorganisms. Usually the air preferably occupies the large transmission pores (>50 μm), followed by medium-sizedstorage pores (0.5-50 μm) and finally the small residual pores (<0.5 μm) in the soil. As a consequence, soilswith mainly residual pores tend to be poorly aerated. In such soil, water is predominantly present in the pores and this will have high levels of dissolved CO_2 as a consequence of root/microbial activity, which may change the chemical reactions that could occur in the soil (Brady and Weil, 2007).

1.2.2.3 Soil minerals

Within the solid phase, there are two kinds of minerals in the soil, primary minerals and secondary minerals which range in size from clay-sized particles (<2 μm) to gravel and stones (>2 mm) (Table 1.2).

Table 1.2: The UK, US and International System for classification of soil mineral particles according to size (Ashman and Puri, 2008)

Fraction	UK System	US System	International System
Stones/gravel	>2.0 mm	>2.0 mm	>2.0 mm
Coarse sand	2.0 – 0.2 mm	2.0 – 0.2 mm	2.0 – 0.2 mm
Fine sand	0.2 – 0.06 mm	0.2 – 0.05 mm	0.2 – 0.02 mm
Silt	60 – 2 μm	50 – 2 μm	20 – 2 μm
Clay	<2 μm	<2 μm	<2 μm

Primary minerals are components that are derived directly from the rocks by physical weathering without being chemically altered. This means they are the same as the mineral material in the parent rock. Examples of primary minerals includerelatively resistant minerals such as quartz (SiO_2), micas (e.g. $K(Mg,Fe)_3AlSi_3O_{10}(F,OH)_2$), chlorites (e.g. $(Mg,Fe)_3(Si,Al)_4O_{10}$) and feldspars (e.g. $KAlSi_3O_8$) and more readily altered minerals such as pyroxenes (e.g. $CaMgSi_2O_6$) and monomer silicates (e.g. $(Mg,Fe)_2(SiO_4)$). Primary minerals are relatively large and are mainly found in the sand fraction with some being found in the silt fraction (Table 1.2). The combined effect of hydrolysis, hydration, and dissolution cause rocks to break down into their chemical constituents, such as silicon (Si), Fe, Al, magnesium (Mg), potassium (K) and calcium (Ca). Where these combine to form new solid phases, they are defined as secondary minerals. Common secondary minerals are aluminosilicate clay minerals such as kaolinite ($Si_2Al_2O_5(OH)_4$), oxides such as goethite

(Fe_2O_3), amorphous-to-poorly-crystalline material such as allophone ($Al_2O_3.(SiO_2)_{1.3\text{-}2}.2.5\text{-}3H_2O$), and sulfur- and carbonate-containing minerals (e.g. FeS_2 and $FeCO_3$, respectively). Secondary minerals are predominantly found in the clay size fraction, but are also found in the silt fraction (Cresser et al., 1993; Sparks, 2003; Brady and Weil, 2007; Ashman and Puri, 2008). Section 1.2.5 will describe the properties of these minerals in more detail.

1.2.2.4 Soil Organic Matter

In comparison with soil minerals, organic matter often comprises a small fraction of the solid phase soil; its influence on soil properties is, however, far greater than its small proportion, e.g. <5% w/w in mineral soils, suggests. In contrast to mineral soils, organic-rich soils and peats often have organic matter contents of >90% w/w. Soil organic matter includes living organisms, carbonaceous remains of organisms, and organic compounds produced by metabolic processes. Organic matter interacts with mineral particles to form mixed soil aggregates and to create a granular soil structure, which is, to a large extent, essential for a loose, easily managed, productive soil. It also increases the amount of water held within the soil and provides nutrients for plants and soil organisms.

Water retention is especially significant in the formation of organic-rich soils since it is swampy, water-logged conditions that favour the preservation of organic matter. Indeed, the amount of organic matter preserved in soils depends on several factors including hydrology and climate. In water-logged soil areas, the dead plant material sinks into the water, where the circulation of air in the soil is largely restricted. The dead plant residue decomposes much slower and peat starts to accumulate.

In the UK, a soil is classified as a peat when its surface organic-rich layer is at least 40 cm thick (Pitty, 1979). In those areas, residues from wetland plants such as pondweeds, cattails, sedges, reeds, mosses, shrubs, and certain trees accumulate over centuries (Brady and Weil, 2007). The UK has significant areas of peatlands and peaty soils (Figure 1.4) and there is considerable current interest in their carbon storage status in the light of changing climatic conditions. This in turn depends on the stability of the organic matter present at these locations.

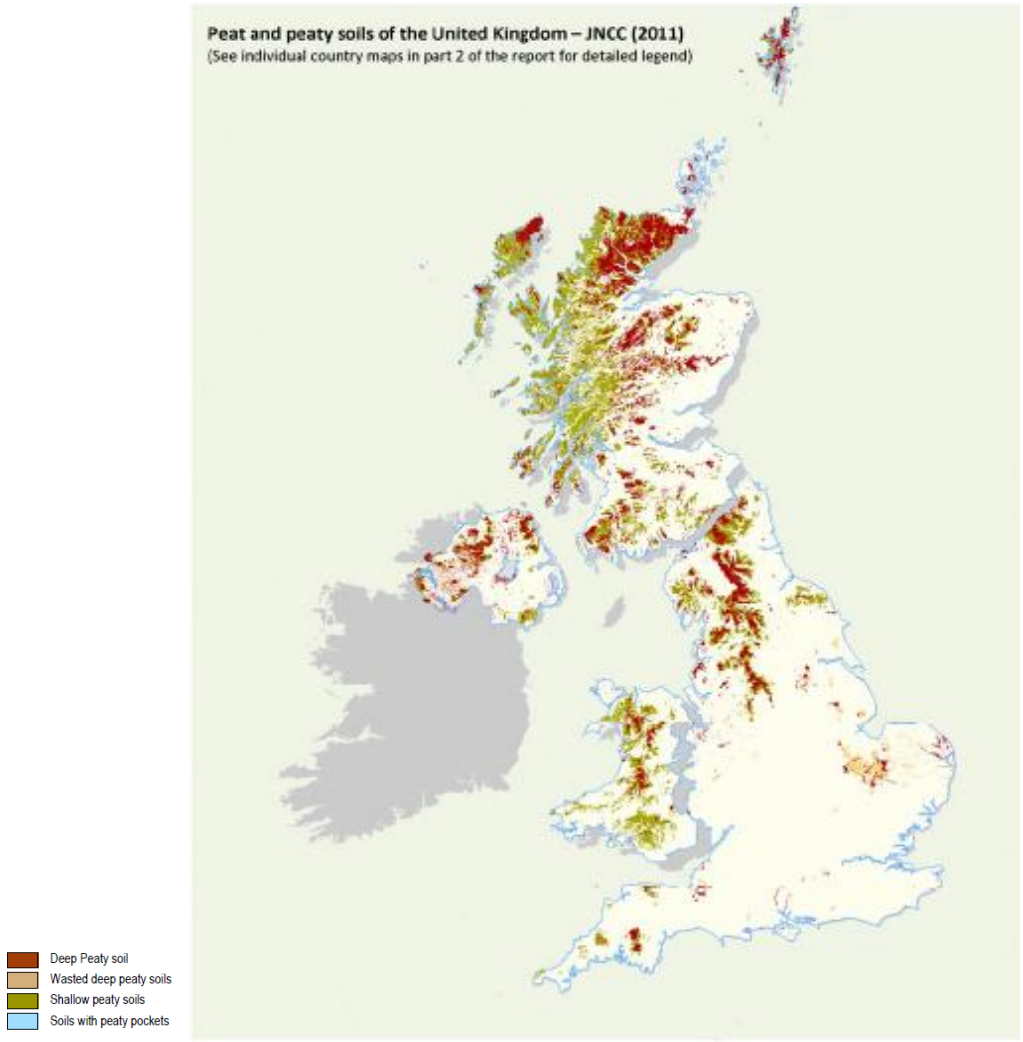

Figure 1.4: Distribution of peatland and peaty soils across the UK (JNCC, 2001)

Humus is the sub-micron sized fraction, stable component of soil organic matter which displays a large surface area with high net-negative surface charge. In addition to the stability of this component, the properties of humus in the soil are of great interest because it is this fraction which has the highest capacity to attract and hold water, nutrients and other elements. Soil organic matter and humic substances, a major component of soil humus, will be discussed in more details in section 1.2.6.

1.2.3 Soil texture

The proportion of particles with different sizes is important as it affects the soil behaviour. As shown in Table 1.2, soil mineral particles can be divided into five broad classes on the

basis of their sizes. Stones and gravel that are larger than 2.0 mm may have some impact upon soil properties, but they are not used to classify different types of soil. The proportion of sand, silt and clay is referred to as the soil's textural class and is used to determine the type of soil textural group. A soil textural triangle is often used to make the classification of the soil when the proportions of sand, silt and clay are known (Figure 1.5). Clay minerals and oxides are the predominant secondary minerals present in the clay size fraction. Their small particle size means that they have very large surface areas. This together with the composition of the particle surfaces means that, in comparison with other mineral particles, those in the clay size fraction has the greatest capacity to hold water and other substances (Brady and Weil, 2007).

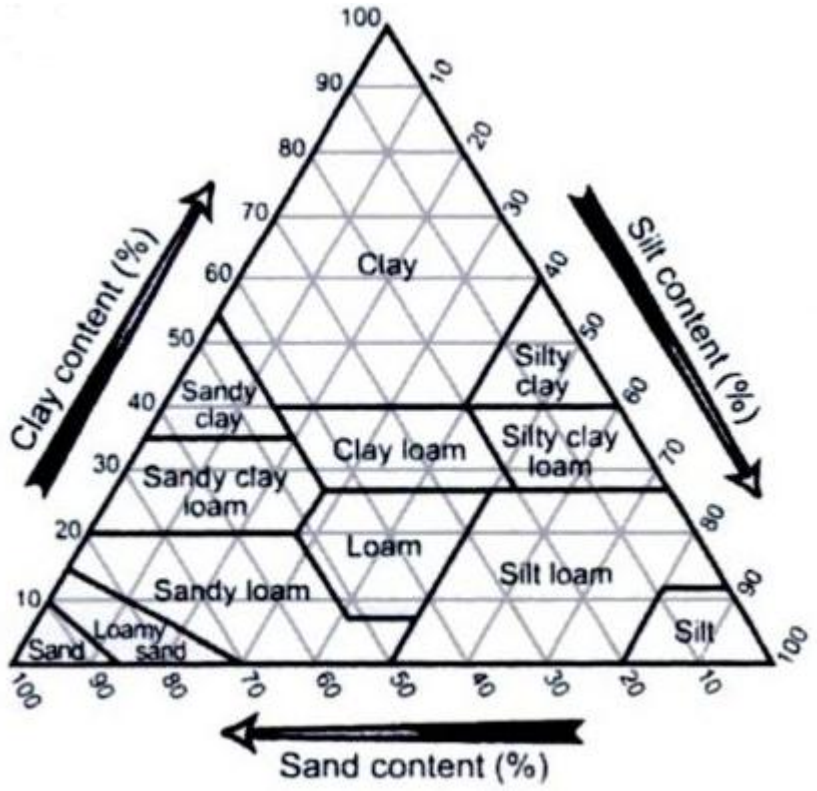

Figure 1.5: Soil textural class triangle (Schaetzl and Anderson, 2005)

In general, the texture of a soil at any particular location remains relatively constant and so it is regarded as a fundamental soil property. There are two main reasons why soil texture is important. Firstly, the combination of different sizes of soil particles results in different numbers and sizes of pores within the soil, which further affects the gas exchange with the atmosphere, soil mechanical strength and the amount of water held in the pores. Secondly, the soil texture affects the soil's capacity to store plant nutrients and to retain other

elements.

The textural class system applies primarily to mineral soils, i.e. organic matter content <5% w/w. In organic-rich and peaty soils, mineral content is significantly reduced. However, mineral particles in the clay size range may still be present at the percent (w/w) level and may still play significant roles relating to nutrient storage etc.

1.2.4 Soil aggregate structure

Aggregates can be broadly divided into two forms according to their sizes: microaggregates (<250 μm) and macroaggregates (>250 μm). The first step to form microaggregates involves flocculation of clay minerals to form small stacks, which are called 'domains'. This process requires ions with more than one charge such as Ca^{2+}, Mg^{2+} and Al^{3+}. When these ions are associated with the surface of clay, they help clay minerals to form domains. The domain can further bond with organic matter to form microaggregates. The association of organic matter with microaggregates leads to organic matter that is more resistant to microbial degradation. Microaggregates can coalesce to form macroaggregates, usually not as one massive block but frequently as a series of large aggregates (Brady and Weil, 2007). The factors that affect aggregate stability have been reviewed and these include soil texture, clay mineralogy, cation content, the presence of Al and Fe oxides, and soil organic matter (Amezketa, 1999; Bronick and Lal, 2005; Abiven et al., 2009). Mixed aggregates (organic matter and minerals), in particular, are important because they break up massive clay blocks and allow roots, water and nutrients to penetrate the soil. Although they may play a less significant role, these mixed aggregates will also be present in organic-rich soils and peats.

1.2.5 Surface properties of secondary minerals

Secondary minerals are especially important because they characteristically have small particle size and large surface areas. For example, the surface areas of Fe oxides vary and can be up to several hundred $m^2\ g^{-1}$, e.g. soil goethite has a surface area of 20-200 $m^2\ g^{-1}$ (Schwertmann, 1988). This contributes to their ability to interact with contaminants as well as other soil components. Sections 1.2.5.1-1.2.5.2 describe the composition and surface properties of both clay minerals and metal oxides.

1.2.5.1 Composition of clays and hydrous metal oxides

Clays can be divided into two main groups: 1:1 clay minerals, e.g. kaolinite, and 2:1 clay minerals, e.g. smectite, vermiculite, illite and chlorite (note – chlorites can be classified as either primary or secondary minerals). A 1:1 silicate clay contains one tetrahedral silica and one octahedral Al oxide sheet whilst 2:1 silicate clays contains one octahedral sheet sandwiched between two tetrahedral sheets.

Hydrous oxides of Fe, aluminium (Al) and manganese (Mn) do not contain tetrahedral sheets nor Si in their structure. They are composed of modified octahedral sheets with either Fe^{3+}, Al^{3+} or Mn^{4+} in the cation position. They usually possess a small, pH-dependent (see section 1.2.5.2) net charge from removal or addition of hydrogen ions at the surface hydroxyl groups. They can also form coatings on the surface of clay minerals (or primary minerals such as biotite), masking their charge sites and thus changing the properties of the clay minerals (Brady and Weil, 2007).

The major Fe oxides, oxyhydroxides and hydroxides are shown in Table 1.3. The octahedral structure is the basic unit for all Fe oxides and oxyhydroxides (Figure 1.6). This structural unit includes Fe surrounded either by six O, six OH or a mixture of O and OH ions. The structural differences among types of Fe oxides lies in the octahedral arrangements and the way they link (Kampf et al., 2000). For example, the layers that the O and OH ions form in goethite and hematite are approximately hexagonally closed-packed; these are defined as α phases. The layers in lepidocrocite and megahemite are approximately cubic closed-packed and defined as γ phases. The γ phases are described as metastable and can be converted to α phases at high temperature.

The structure of akaganeite is different from otherFe oxides as it contains square molecular channels bound by four double rows of octahedra, which are large enough to arrange anions in a body-centre array. This structure is defined as a β phase and is less dense than α and γ phases. Magnetite has a cubic structure with 1/3 of the interstices tetrahedrally coordinated and 2/3 octahedrally coordinated and filled by Fe (Schwertmann and Cornell, 2000). The basic structure of ferrihydrite is not yet fully elucidated according to a review by Michel et al. (2010) but it is considered to be a poorly crystalline, hydrated Fe oxyhydroxide.

Table 1.3: Major hydrous Fe oxides

Oxyhydroxides		**Oxides**		**Hydroxides**	
Formula	Mineral	Formula	Mineral	Formula	Mineral
α-FeOOH	Goethite	α-Fe_2O_3	Hematite	$Fe(OH)_{3\ (am)}$	Bernalite
β-FeOOH	Akaganeite	γ-Fe_2O_3	Maghemite	$Fe(OH)_{2(am)}$	
γ-FeOOH	Lepidocrocite	Fe_3O_4	Magnetite		
$Fe_5HO_8.4H_2O$	Ferrihydrite	FeO	Wüstite		

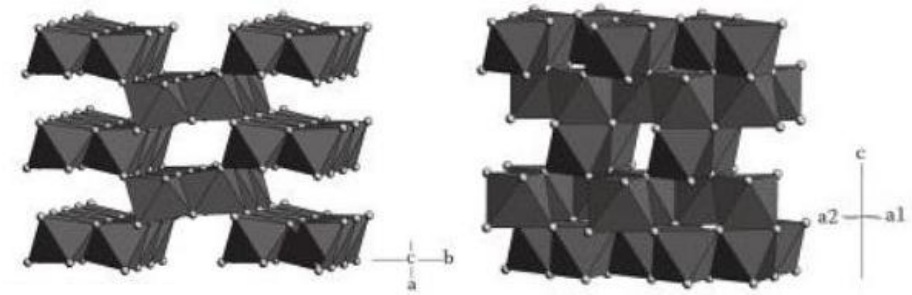

(a) Goethite (b) Hematite

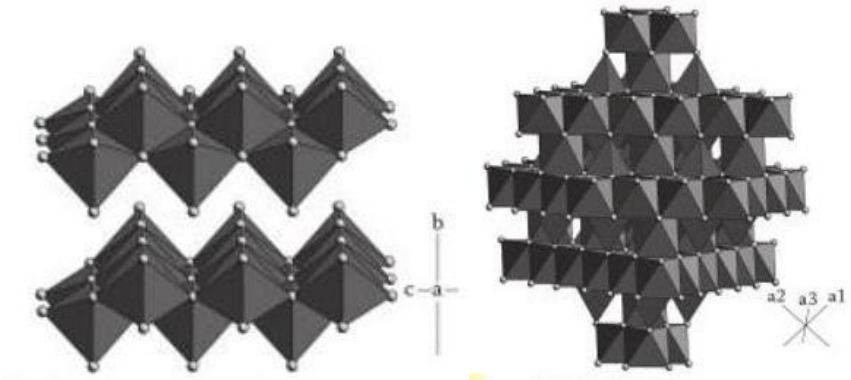

(c) Lepidocrocite (d) Magnetite; Maghemite

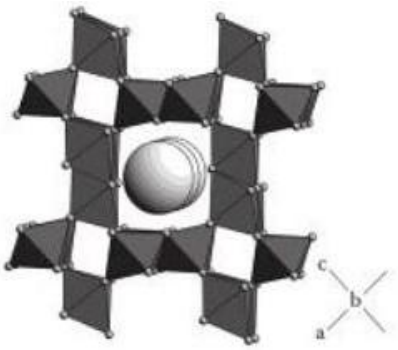

(e) Akaganeite

Figure 1.6(a)-(e): Structures for selected hydrous Fe oxide minerals in soils (Kampf et al., 2000)

Similarly to Fe, Al also exists as a number of hydroxides, oxides and oxyhydroxides. Gibbsite (γ-$Al(OH)_3$), a common soil crystalline hydroxide, is made up of Al octahedral sheets which are linked by hydrogen bonding via the hydroxyl groups (Brady and Weil, 2007). Less common forms include boehmite (γ-AlOOH) and corundum (α-Al_2O_3). Manganese also forms octahedral oxides and oxyhydroxides and the most common forms are birnessite (δ-MnO_2), pyrolusite (β-MnO_2) and manganite (MnOOH).

1.2.5.2 Surface charge on clays and hydrous Fe oxides

In general, there are two main sources of surface charges on soil minerals: (i) permanent (near-surface) charge which derives from isomorphous substitution by ions of similar size but different charge at the time of mineral formation; and (ii) pH-dependent charge arising from hydroxyls and other functional groups on the surfaces of colloidal particles that release or accept H^+ to provide negative or positive charge (Brady and Weil, 2007).

The magnitude of surface charge depends on the surface area, the extent of isomorphous substitution (permanent charge), the number of acidic surface functional groups (pH-dependent surface charge) and the environmental chemical conditions, such as pH (pH-dependent surface charge). For most minerals, a negative charge is predominant, but some minerals, e.g. Fe oxides, can bear a net positive charge even under near-neutral environmental conditions. For example, the pH of point of zero charge of hematite was reported to be between 7.2 and 9.5 (James and Parks, 1982; Penners et al., 1986; Lyklema et al., 1987; Chorover et al., 1997); it therefore bears a net positive charge at pH 7-8. Mineral surfaces with net negative charges can adsorb positively charged ions to the surface by electrostatic attraction, such as those of UO_2^{2+}, Ca^{2+}, Mg^{2+}, K^+, H^+.

For soils that contain predominantly 1:1 and 2:1 silicate clays, extensive isomorphous substitution by Fe^{2+}, Mg^{2+} or Mn^{2+} for Al^{3+} in the octahedral layers or Al^{3+}or Fe^{3+} for Si^{4+} in the tetrahedral layer of the mineral structure results in a permanent near-surface negative charge. As a consequence, cations in the soil solution will be attracted to the clay mineral surfaces. For Fe and Al oxides, the net charge of the colloid is mainly dependent on the pH values of the environment. Under acidic to slightly alkaline conditions, the net charge on these oxides is often positive and so anion attraction predominates (Brady and Weil, 2007).

Both surface charge and surface area are important in determining the interactions between

species in solution and mineral surfaces. Mineral particles with extensive isomorphous substitution and/or ionisable surface functional groups in combination with large surface areas will have the greatest potential to attract ions from solution. Where the net charge is negative, this is expressed as the cation exchange capacity (CEC) which is defined as the sum total of the exchangeable cations that are absorbed onto soil surfaces with units of $cmol_c kg^{-1}$.

CEC is an important soil property as it is used to assess the environmental behaviour of soil. Due to their surface charge properties described above, the 1:1 clay minerals make a very large contribution to the total CEC of the mineral fraction of soil. However, the contribution to total CEC by humus is much greater (~tenfold) in comparison with inorganic clays, and Fe, Al oxides (Brady and Weil, 2007). The importance of ion exchange processes in organic-rich soils may therefore be greater than in mineral soils.

1.2.6 Organic matter and humic substances

1.2.6.1 Organic matter - decomposition and humification

Soil organic matter is composed of a wide range of organic substances, which are mainly divided into three groups: (i) the living soil biota including microorganisms, animals and intact plants; (ii) the decomposing residues of plants as well as animals and microbes; (iii) soil humus (Cresser et al., 1993).

Plant biomass is the major material that undergoes decomposition and becomes the primary precursor of soil organic matter. The whole process involves the decomposition of the plant residues and formation of the more resistant forms of soil organic matter, especially humic material (Cresser et al., 1993). Figure 1.7 shows the average composition of terrestrial plants, but it should be noted that different plants may vary in composition. The major constituents, in general order of decreasing decomposition rate, are carbohydrates (sugars and starches, cellulose and hemicelluloses), proteins, lipids (fats and waxes), and lignin and other polyphenolic compounds (Brady and Weil, 2007).

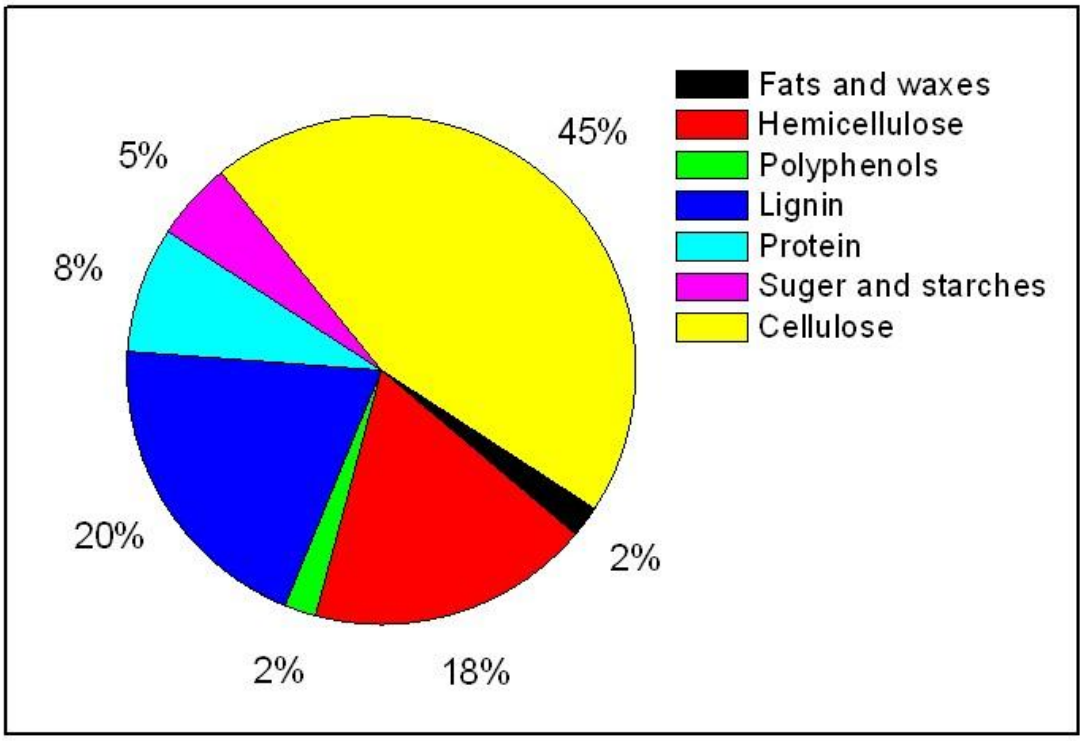

Figure 1.7: Typical composition of representative green-plant material

The initial stage of the decomposition process involves earthworms and other animals breaking down fresh plant material. Further transformation requires enzymes produced by microorganisms. When the soil environment is well-aerated, the organic matter is subject to microbially controlled oxidation, and the ultimate end product is carbon dioxide. However, many intermediate reactions occur during the overall process. For example, cellulose and starch are polysaccharides comprising long chains of sugar molecules, which can be broken down microbially to short chain molecules before degrading into individual simple sugar molecules, e.g. fructose, sucrose etc. The complete decomposition of proteins again generates carbon dioxide, but enzymatic hydrolysis produces amino acids (partial hydrolysis produces peptones) that can be further decomposed to give ammonium, nitrate and sulphate ions. A high proportion of amino acids are readily assimilated by living organisms. Lipids are less readily broken down and products include hydroxy-fatty acids which are relatively stable in the soil environment. Lignin, the least readily degraded plant-derived substrate, is composed of 3d-interlinked phenolic ring subunits, most of which are phenylpropene-like structures with various methoxyl ($-OCH_3$) groups attached. This structure is very strong and resistant, thus only a few microorganisms can break it down (Stevenson, 1982). After the degradation of lignin into its phenolic subunits and then the oxidation of these phenolic subunits to quinones, it is thought that soil microbes

metabolize the resulting simpler components and synthesize resistant humic molecules or their precursors by combining mainly amino acids, and to a lesser extent, nucleic acids and phospholipids with the aromatic quinones (Cresser et al., 1993). The structure of humic substances thus formed is unrelated to those of the main compound classes, i.e. proteins, carbohydrates, lipids and lignin. However, the synthetic processes by which humic substances are formed are still not well-understood. For example, studies have shown that amide N in peptides is the predominant chemical form of N in humic substances whilst free amino acids make a small contribution (Knicker et al., 1995; Schmidt et al., 1997). This means that the previously accepted "polymer model" which suppresses amide N functional groups during the formation of humic substance cannot be the main synthetic pathway occurring in natural systems (Sutton and Sposito, 2005). One of the main reasons why there has been considerable difficulty in elucidating these processes is that humic substances comprise mixtures of many thousands of dark-brown coloured natural organic molecules. Further research is required to determine molecular composition within these complex mixtures. This will lead to improved models of the formation process and also understanding of their role in binding natural and contaminant metals.

1.2.6.2 Methods used to isolate and fractionate humic substances

The first problem faced in characterising soil humic substances is that they must be isolated from the soil. An ideal extraction method should meet the following objectives: (i) the humic material is not altered during isolation; (ii) the extracted humic substances are free of inorganic contaminants, such as clay and polyvalent cations; (iii) extraction can represent the entire molecular-weight range of humic substances; (iv) the method is applicable to all soils. In reality, no extraction methods have achieved all of these objectives (Stevenson, 1982).

Extraction reagents

Quite a lot of reagents have been used for humic substances extraction, including strong bases, neutral salts, organic chelates, formic acid, and acetone-H_2O-HCl solvent mixtures. In addition to the concerns about co-extraction of inorganic materials, all of these methods may co-extract organic impurities such as carbohydrates, proteinaceous compounds (Stevenson, 1982). Only alkali and mild reagents are discussed here as these are considered to give the most representative humic extracts (Table 1.4) (Stevenson, 1982).

Table 1.4: Reagents used for extraction of humic substance in the soil (Stevenson, 1982)

Category of extractant	Extractant	Humic substance extraction rate (%)
Alkali extractant	NaOH	≤80
	Na_2CO_3	≤30
Mild extractant	$Na_4P_2O_7$, NaF	≤30
	Organic acid salts	≤30

NaOH and Na_2CO_3 solutions (0.1- 0.5 M) with a soil:extractant ratio of 1:2 to 1:5 (g mL^{-1}) are widely used for recovery of humic substances. The extraction efficiency of NaOH is up to 80% of humic substances while that of Na_2CO_3 is up to only 30%. The extraction process is considered to be the conversion of acidic components to ions and subsequent formation of soluble sodium salts in aqueous solution(Stevenson, 1982) (Equation 1.1).

$$\text{Humic-COOH} + \text{NaOH} \leftrightharpoons \text{Humic-COO}^- \text{Na}^+ + \text{H}_2\text{O} \qquad \text{Equation 1.1}$$

There are some disadvantages of alkali extraction for humic substances: (i) alkali solutions can co-extract silica from the soil mineral phase as well as protoplasmic and structural components from fresh organic tissues, resulting in contamination of the humic extract; (ii) alteration of humic functionality occurs, e.g. oxidation of some organic components under alkaline conditions when exposed to the air; (iii) formation of humic-like compounds via chemical reactions occurs, e.g. condensation between amino acids and the C=O group of aromatic aldehydes or quinones to form humic-type compounds through browning reactions (Tinsley and Salam, 1961).

Many of these problems can be overcome by optimising the extraction conditions, e.g. by (i) 0.2 μm-filtering the alkaline extract to remove fine mineral particulates and plant residues that have been mobilised; (ii) preventing oxidation by carrying out extractions under nitrogen; and (iii) minimising oxidation and condensation reactions by using short extraction times followed by immediate dialysis.

Milder extractants have been investigated as alternatives for extraction with strong alkali. Calcium (Ca^{2+}) and other polyvalent cations such as Fe^{3+} and Al^{3+} are essential in maintaining organic matter in a flocculated and insoluble condition. $Na_4P_2O_7$ and other organic acid salts can form insoluble precipitates or soluble complexes with these cation

sands, as a result, organic matter dissolves in Na^+, K^+, or NH_4^+-containing pyrophosphate solutions. This method is believed to modify the humic molecules to a lesser extent (Stevenson, 1982) but the recovery rate is significantly lower and so a representative extract may not be obtained. Thus a controlled alkaline extraction is favoured in this study.

Traditional fractionation based on humic solubility

As mentioned above, humic substances can be extracted from soils using alkali, e.g. 0.1 M NaOH. After the alkali extraction, the resistant organic material that remains in the soil is classified as humin, a precursor to coal. The alkali solution is then acidified to pH 1 to separate humic acid and fulvic acid. Figure 1.8 shows the classification of humic materials in relation to these chemical extraction methods (Brady and Weil, 2007).

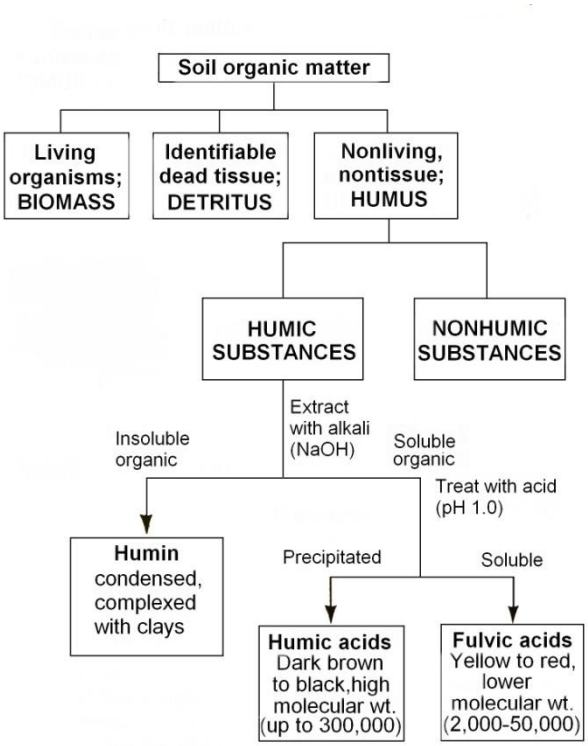

Figure 1.8: Schematic of classification of soil organic matter components separable by chemical and physical criteria (Brady and Weil, 2007).

As shown in Figure 1.8, humic materials may be distinguished according to their solubility in acid and alkaline solutions. Based on these chemical methods, an extrapolation has then been made to the environmental behaviour and occurrence of these materials. Fulvic acids are considered to comprise organic macromolecules that are soluble in water at all pH

values. Humic acids are thought to represent those macromolecules that are insoluble at acidic pH values (pH<2) but soluble at higher pH values. Humin is thus the faction of natural organic matter that is insoluble at all pH values (Brady and Weil, 2007). Although chemical and physical differences are the cause of the variations in solubility and the separation of humic substance into three groups is feasible, it does not indicate that three distinct types of organic molecule exists (Hayes et al., 1989).

The use of strong acids and bases in such methods has been criticized for several reasons. Those relating to the use of strong base have been covered in the sections above but those relating to the use of strong acids include: (i) associated metals are released during the acid precipitation step and so it is not possible to study the metal or mineral interactions with humic materials as they occurred in the natural environment (Graham, 1995); (ii) the functionality of the humic materials may be altered during this part of the extraction procedure (Worobey and Webster, 1981). For the purposes of this study, the former is especially important and so the best method for isolation of a representative humic extract was considered to be alkaline extraction over a short time period followed by immediate dialysis (as per Graham, 1995).

Purification of humic materials

Stevenson (1982) described several methods that have been used to attempt to remove the organic impurities (e.g., proteins and carbohydrates) from crude humic acids. For example, aqueous phenol was used to separate a protein-rich component from humic acid (Biederbeck and Paul, 1973; Simonart et al., 1967). Recent findings reveal that this is unsatisfactory as the procedure to purify the humic substances by removing the strongly associated biomolecules (Stevenson, 1982) may significantly alter the chemical properties of humic substance (Sutton and Sposito, 2005). Similar concerns have been raised over the use of hydrofluoric acid to remove strongly associated siliceous material (Piccolo, 1988). In this study, no such purification methods were used.

1.2.6.3 Structure of humic macromolecules

The size, chemical composition, structure, and functional groups of humic materials vary, depending on the origin and age of materials (Brady and Weil, 2007). It has proven very difficult to identify the actual structure of humic materials, but a proposed structure typical of humic acid is shown in Figure 1.9.

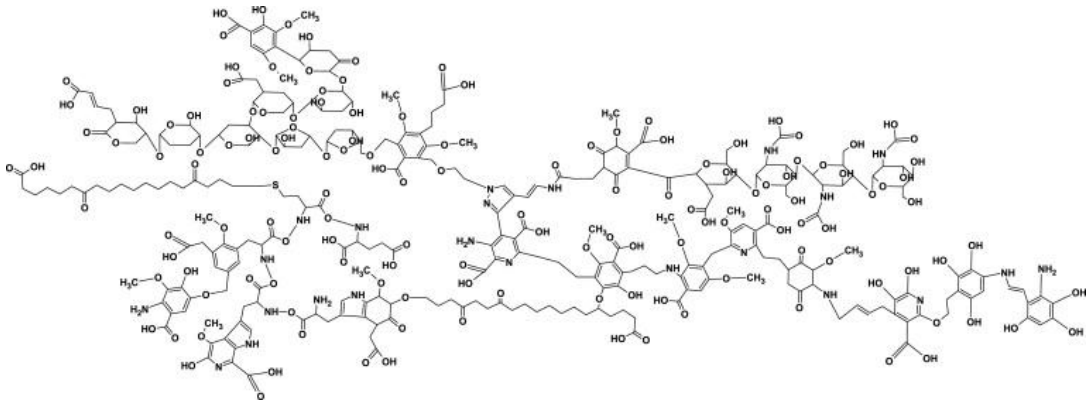

Figure 1.9: Proposed macromolecular structure of a soil humic acid (HA) (Stevenson, 1982)

It was thought that humic substances were composed of randomly coiled macromolecules which have elongated shapes in basic or low-ionic strength solution, but form coils in acidic or high-ionic strength solutions (Stevenson, 1982). A proposed new model encompasses all molecules found to be intimately associated with humic substances, even including biomolecules. Piccolo et al. (2001) found that after humic fractions with different hydrophobicities were added to carboxylic and mineral acids, the aggregate disruption was greatest when the more hydrophobic humic acids were combined with the simple organic acids. Also fulvic acid, which is of lower hydrophobicity and is not linked by hydrogen bonds and hydrophobic interactions, was found to be minimally changed under different solution conditions (Simpson, 2002). Ferreira et al. (2001) found that hydrophobic regions form under acidic conditions, but disperse under basic conditions. From these observations, humic substances are now being considered to be a supramolecular association, in which many relatively small and chemically diverse organic molecules form groups linked by hydrogen bonds and hydrophobic interactions. In such organic molecules the hydrophilic exterior area shields the hydrophobic interior, preventing contact with water molecules in aqueous solution (Sutton and Sposito, 2005).

The studies supporting this new theory of lower molecular weight have involved the use of advanced spectrometric methods such as diffusion-ordered nuclear magnetic resonance (NMR) spectroscopy and mass spectrometry (MS) with optimised spray conditions and soft ionisation techniques for sample introduction (Simpson et al., 2002; Leenheer et al., 2001). In conclusion, it is now important to recognise both that humic substances comprise a collection of much smaller molecules (average molecular weight, M_n~600 Da, e.g. Figure

1.10) but that they can form supramolecular associations via hydrogen bonding, van der Waals etc. since it is the latter that may influence their behaviour in the natural environment (Simpson et al., 2003).

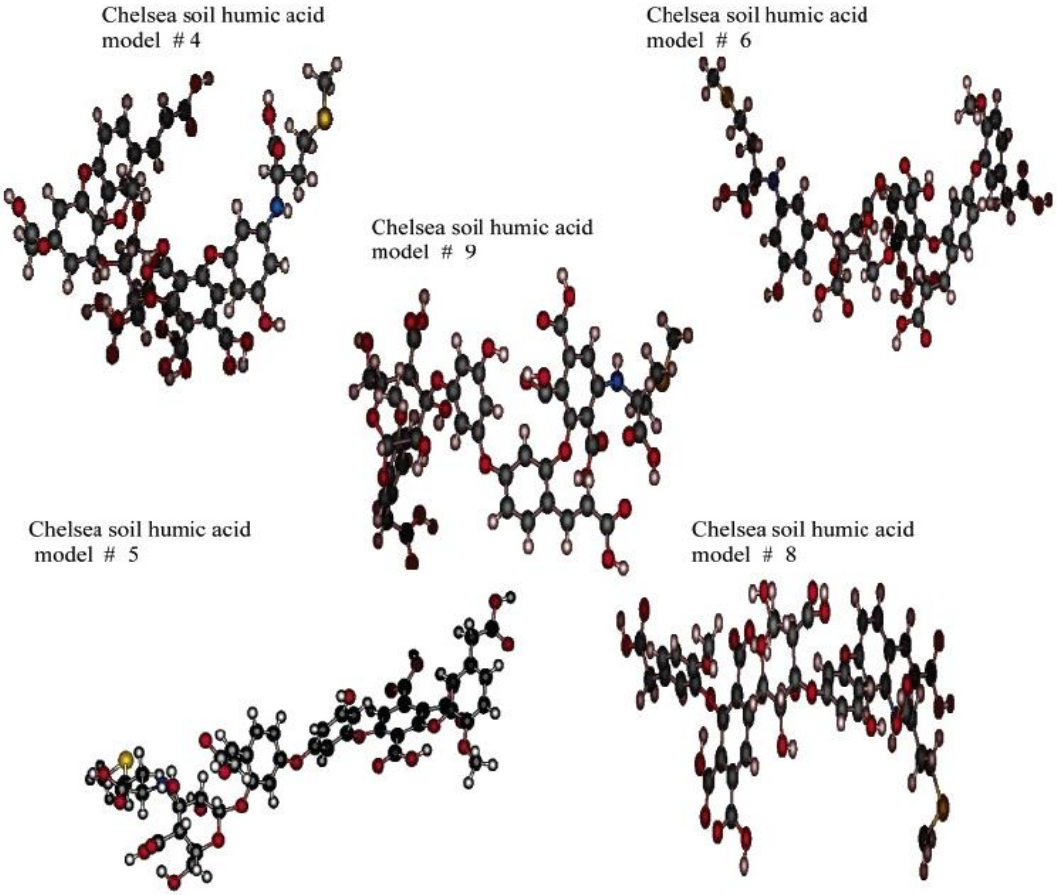

Figure 1.10: Suggested structures for low molecular weight humic acids (Simpson et al., 2003). C atoms are in black, O atoms are in red, N atoms are in blue, S atoms are in yellow, and the remaining atoms are H atoms

1.2.6.4 Surface properties of humic substances

As shown in both Figures 1.9 and 1.10, the proposed humic acid molecular structures contain a series of carbon chains and ring structures with numerous chemically active functional groups, among which 'OH' groups are considered to be most responsible for the high amount of molecular charge. The charge derives largely from ionization of COOH groups, although there is some contribution from phenolic OH as well as NH groups. Under most natural conditions in soils, humic molecules have a strong negative charge and mainly adsorbcations (Brady and Weil, 2007).

Soil humus has a high specific surface area as great as 800-900 m^2g^{-1} and, combined with the high negative surface charge, this gives a cation exchange capacity (CEC) that ranges from 150 to 300 $cmol_c kg^{-1}$. Thus it is an important sorbent of heavy metal cations (Sparks, 2003). It is considered that up to 80% of the CEC of the soil may be caused by organic matter, but for highly organic soils and humus layers of forest soils, practically all of the CEC is attributed to organic matter. Unlike some clay minerals, i.e. those with predominantly permanent surface charge, soil organic matter does not have a fixed CEC as it is dependent on the soil pH. The CEC increases markedly with increasing pH due to dissociation of the wide range of different carboxylic functional groups and then, beyond pH 8-9, the dissociation of phenolic groups (Stevenson, 1982).

1.2.7 General soil colloid properties

The term colloidal soil particle usually refers to clay-sized particles and the humus fraction because of their extremely small particle/molecular sizes. For the same mass, soil colloids expose a large external surface area, which is more than 1000 times the surface area of sand particles. They are implicated in adsorption, catalysis, precipitation, microbial colonization and other surface phenomena (Brady and Weil, 2007). Figure 1.11 illustrates the relationship between soil components of different sizes.

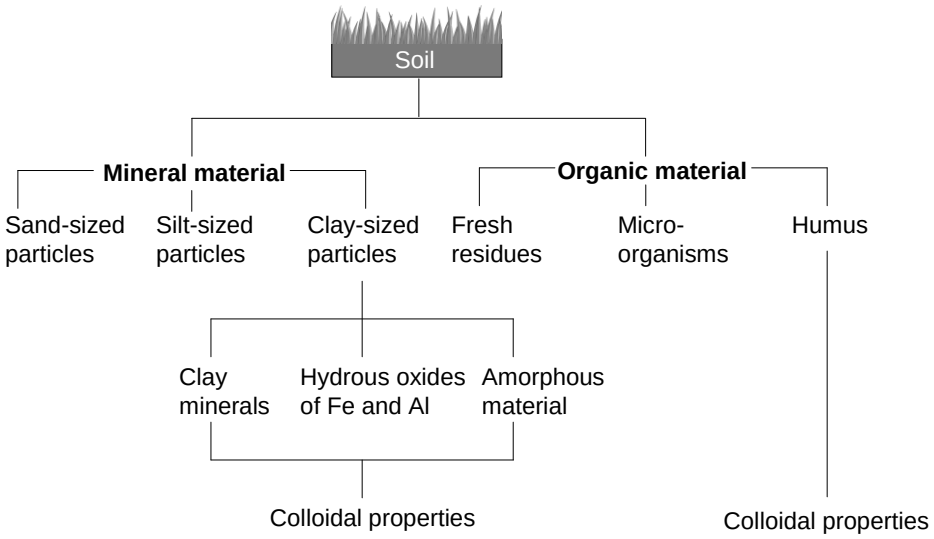

Figure 1.11: Illustration of the relationship between soil fractions of different sizes (Ashman and Puri, 2008)

Within the soil porewaters, filterable components of greater than 1 nm but smaller than 1 μm are considered to comprise the aqueous colloidal size fraction. A wide range of entities can be included within this definition, including Fe or Al hydroxides, Mn oxides, clays, carbonates, humic substances, polysaccharides, virus, bacteria, etc. (Ure and Davidson, 2008). These vary considerably in terms of their hydrophobic/hydrophilic character and also their size (Table 1.5 and Figure 1.12).

Table 1.5: Hydrophobic and hydrophilic status of aquatic colloids (adapted from Ranville and Schmiermund, 2002)

Hydrophobic colloids	**Hydrophilic colloids**
Phyllosilicates, clays	Humic substances
Fe, Mn, Al hydrous oxides	Polysaccharides
Framework silicates	Proteins
Phosphates, carbonates, sulphides	Silica gel
Bacteria	Alumina gel
Viruses	
Organic detritus	

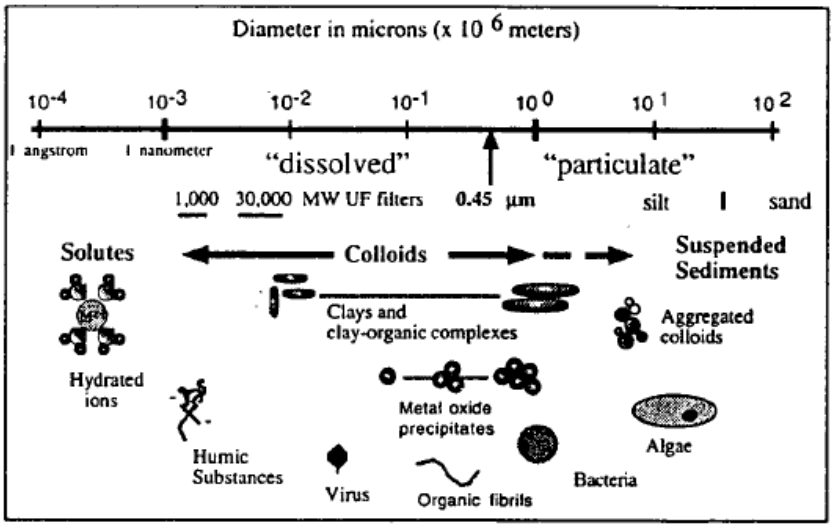

Figure 1.12: Illustration of the size ranges of colloids present in aquatic systems including soil porewaters (Ranville and Schmiermund, 2002)

Although 1 nm and 1 µmare commonly used to define the lower and upper size limits, respectively, for colloidal particles, field-based aqueous speciation studies often use upper limits of 0.2 and 0.45 µm to separate colloidal from particulate matter (Figure 1.12). The 0.2 µm cut-off membrane excludes bacteria as well as particulate matter (e.g. Pearce, 2007), and is used in many aqueous U speciation studies (Jackson et al., 2005; Graham et al., 2008, 2011; Oliver et al., 2008). Ultrafilters with cut-off values such as 10, 30, 100 kDa have been used to distinguish between different colloidal components while those with lower cut-off values such as 1 and 3 kDa have been used to separate truly dissolved from colloidal components (e.g. Graham et al., 2008, 2011; Vasyukova et al., 2010; Claveranne-Lamol ère, 2011). Ultrafiltration as a method to study U speciation in aqueous solutions will be described in section 1.5.2.

In addition to characterising the roles of colloidal and dissolved components in transporting metals in aquatic systems, some researchers also classify 1-20 µm size fractions as particulate matter that can be stabilized in aquatic systems during high energy events, such as storm flow conditions (Jacobsen et al., 1997; Ryan et al., 1998; Graham et al., 2006). This is especially important for contaminant metals such as lead which have very low solubility in aqueous solution and are highly particle-reactive (Shafer et al., 1997; Graham et al., 2006) but was shown to be insignificant for the transport of DU at the MoD firing range at Dundrennan, SW Scotland (Graham, pers. comm.).

The colloidal properties of clay minerals and hydrous Fe oxides were described in section 1.2.5.2 whilst those of humic substances were detailed in section 1.2.6.4. These mineral and organic colloids both have high affinity for U, as will be discussed in section 1.4.4.4.

1.2.8 Geochemical conditions in soils

Redox potential and soil porewater pH are two of the most important soil parameters that may influence metal and indeed U speciation within soil porewaters. Metal speciation within the porewater is of paramount importance in determining its interactions with the soil solid phases described in the preceding sections.

1.2.8.1 Soil redox potential

Redox potential, expressed as Eh with unit mV, is an electrical measurement that indicates the oxidation-reduction status of soils. The Eh value reflects the tendency of a soil solution to transfer electrons to or from a reference electrode (Vorenhout et al., 2004), which an indication of whether the soil conditions are aerobic or anaerobic. High (more positive) values are indicative of a tendency for electron loss, i.e. oxidation, whilst low (more negative) values signify a tendency for electron gain, i.e. reduction. The first main oxidant in natural soil systems is atmospheric oxygen and organic matter is often the main substance that is oxidised. This microbially controlled process decreases the concentration of dissolved oxygen in the soil solution (Equation 1.2) and, when this occurs at a rate much faster than oxygen can be re-supplied, conditions become more reducing (or anaerobic). Anaerobic conditions also influence the behaviour of trace metals such as U, Fe, Mn, which may be present in both reduced and oxidized forms in the soil and soil porewater. It should be noted that the Eh of a soil need not be constant over time since it may be affected by a fluctuating water table (Vepraskas and Faulkner, 2001); indeed, due to spatial heterogeneity and the presence of plant roots, it need not be uniform throughout the soil.

$$CH_2O + O_2 \leftrightharpoons CO_2 + H_2O \qquad \text{Equation 1.2}$$

Soil oxidation-reduction reactions often involve both electron and proton transfer and thus many redox reactions are also pH dependent (Table 1.6). The common electron acceptors available in soil are O_2, NO_3^-, MnO_2, $Fe(OH)_3$, SO_4^{2-}, CO_2. Table 1.6 lists the Eh values (mV) for the major reduction half-reactions occurring in soils (Cresser et al., 1993).

Organic matter is the main source of electrons, which are released when organic matter and bacteria are oxidized. In theory, O_2 will be the only electron acceptor used until it is depleted, NO_3^- will be the next electron acceptor followed by other acceptors in the order listed in Table 1.6. However, this order requires Eh to be at an equilibrium state, which is not the case for many environmental situations. Indeed, the Eh value may vary within the same horizon because soils are typically heterogeneous and organic materials are not distributed evenly (Vepraskas and Faulkner, 2001).

Table 1.6: Redox potential (Eh; mV) for major soil reduction half-reactions (adapted from Russell, 2008).

	Eh (mV) at 25 ℃	
Half-reaction	**pH 5**	**pH 7**
$O_2 + 4H^+ + 4e^- \leftrightharpoons 2H_2O$	930	820
$NO_3^- + 2H^+ + 2e^- \leftrightharpoons NO_2^- + H_2O$	530	420
$MnO_2 + 4H^+ + 2e^- \leftrightharpoons Mn^{2+} + 2H_2O$	640	410
$Fe(OH)_3 + 3H^+ + e^- \leftrightharpoons Fe^{2+} + 3H_2O$	170	-180
$SO_4^{2-} + 10\ H^+ + 8e^- \leftrightharpoons H_2S + 4\ H_2O$	-70	-220
$CO_2 + 8e^- + 8H^+ \leftrightharpoons CH_4 + 2H_2O$	-120	-240

1.2.8.2 Soil porewater pH

According to the IUPAC convention, pH is defined as a measure of the activity of hydrogen ions in a solution. The degree of soil acidity, expressed as soil pH, is determined by the balance between those processes that produce H^+ ions and those that consume H^+ ions. There are several sources of H^+ ions released to the soil: formation and subsequent dissociation of carbonic acid from hydration of dissolved CO_2, organic acid dissociation, nitrification, oxidation of sulfides to give sulfuric acid, atmospheric H_2SO_4 and HNO_3 deposition, plant uptake and exchange of cations for H^+ ions. Another important acid-generating process derives from the dissolution of Fe- and Al-containing minerals. For example, when H^+ ions attack such minerals, Fe^{3+} and/or Al^{3+} ions are released into the soil porewaters and these have strong tendency to hydrolyze. They abstract the OH^- ions from water molecules, leaving the H^+ to acidify the soil solution (see example equations 1.3-1.6).

$Fe^{3+} + H_2O$	$\leftrightharpoons Fe(OH)^{2+} + H^+$	K_1	Equation 1.3
$Fe(OH)^{2+} + H_2O$	$\leftrightharpoons Fe(OH)_2^+ + H^+$	K_2	Equation 1.4
$Fe(OH)_2^+ + H_2O$	$\leftrightharpoons Fe(OH)_3^0 + H^+$	K_3	Equation 1.5
$Fe(OH)_3^0 + H_2O$	$\leftrightharpoons Fe(OH)_4^- + H^+$	K_4	Equation 1.6

In near-neutral to slightly alkaline soils, the hydrolysis will progress to the formation of the third hydrolysis products, i.e. $Fe(OH)_3$, $Fe(OH)_2$, or $Al(OH)_3$, which often precipitate and are removed from solution (Figure 1.13).

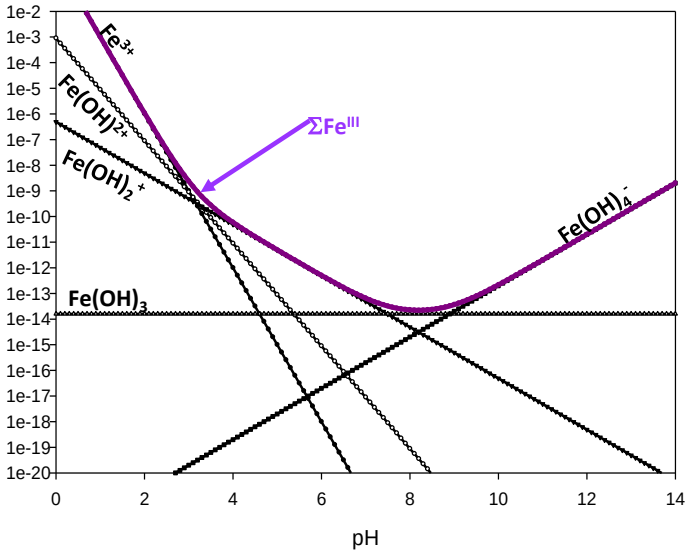

Figure 1.13: The pH dependent solubility of Fe^{III} in aqueous solution. Black lines show concentrations (molar) of individual species; the purple line shows the overall solubility (ΣFe^{III})

At the same time as H^+ is being released, several processes can consume the H^+, e.g. reactions with carbonate or bicarbonate ions (Equation 1.7), reduction of nitrate (Equation 1.8), acid hydrolysis of minerals such as primary aluminosilicates which release non-acidic cations (Ca^{2+}, Mg^{2+}, K^+, Na^+) (Equation 1.9), protonation of pH-dependent surface sites (Equation 1.10) (Brady and Weil, 2007).

$CaCO_{3(s)} + H_2CO_3$	$\leftrightharpoons Ca^{2+} + 2HCO_3^-$	Equation 1.7
$NO_3^- + 2e^- + 2H^+$	$\leftrightharpoons NO_2^- + H_2O$	Equation 1.8
$2KAlSi_3O_8 + 2H^+ + 9H_2O$	$\leftrightharpoons Al_2Si_2O_5(OH)_4 + 4H_4SiO_4 + 2K^+$	Equation 1.9
$Surface\text{-}O^- + H^+$	$\leftrightharpoons Surface\text{-}OH$	Equation 1.10

The overall pH of a soil is determined by the balance between the processes which consume hydrogen ions and those which release them. Natural soil pH values range from ~4 to ~8 but more extreme values can be found under certain circumstances. For example, pH values in the range 3-4 are not uncommon for near-surface horizons of coniferous forest soils, attributable to the large contribution of organic acids from the breakdown of pine needles. Values of <2 and >10, however, are usually indicative of anthropogenic influences with the former being typical of acid-mine drainage and the latter being associated with man-made concrete materials in contact with the soil.

The influence of both redox and pH conditions on U speciation will be discussed in section 1.3.4.

1.3 Properties of U

1.3.1 Uranium characteristics and natural occurrence

Uranium is a heavy, silver white, ductile, and slightly paramagnetic metal which, although harder than most metals, is slightly softer than steel. It has an elemental density of 19.05 g cm^{-3} and a melting point of 1135 °C (Greenwood and Earnshaw, 1997). In metallic form, it reacts readily with air to form a dark coating of U oxide on its surface (Bleise et al., 2003). More generally, it reacts with almost all non-metallic elements and their compounds; reactivity is enhanced with increasing temperature but, in finely divided form, it will even react with cold water.

As the heaviest naturally occurring element, U is found at an average concentration of 0.0004% in the Earth's crust (Priest, 2001). U is widely distributed within the geosphere; it is present in oceanic and fresh waters (including surface and groundwaters) and in a range of sedimentary and igneous rocks (Figure 1.14). It is most commonly found as a minor constituent of the continental crust and of rocks such as granites and shales but it is found in most concentrated form in ores such as the microcrystalline pitchblende (U_3O_8) and the macrocrystalline uraninite (UO_2). These, along with coffinite, are examples of primary minerals, i.e. unaltered by chemical weathering (see section 1.3). U is also found in weathered secondary mineral forms and examples of these include the phosphate, autunite ($Ca(UO_2)_2(PO_4)_2.10\text{-}12H_2O$), and the vanadate, carnotite ($K_2(UO_2)_2(VO_4)_2.1–3\ H_2O$). Pure

mineral deposits are rare and U ores are often found in association with sandstones, phosphates, lignites, and shales.

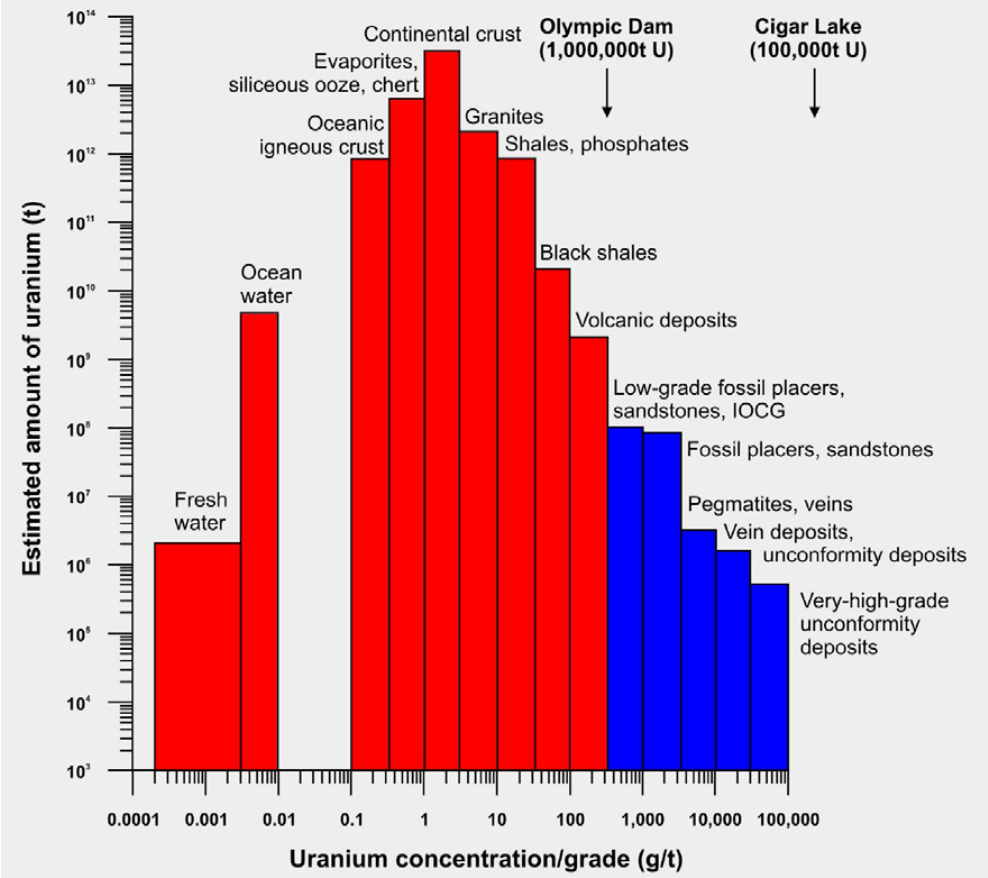

Figure 1.14: Estimates of the amount of U contained in ore deposits (blue bars) and in other geological settings (red bars) (adapted from Deffeyes and MacGregor, 1980). The low grade deposits at Olympic Dam (Australia) and high grade deposits at Cigar Lake (Canada) contain 1 million and 1 hundred thousand tonnes of U, respectively.

In the environment, U occurs mainly as three of its seventeen isotopes, ^{238}U (99.27%), ^{235}U (0.72%) and ^{234}U (0.0054%) with half-lives of 4.47×10^{9}, 7.04×10^{8}, 2.46×10^{5} years, respectively (Table 1.7). Both ^{238}U and ^{235}U are considered to be primordial (present since the formation of the Earth) and ^{234}U is part of the ^{238}U decay series (Figure 1.15).

Table 1.7 Properties of selected U isotopes

Isotope	Mass	Half-life	Mode of Decay	Natural Abundance	Specific Activity**
^{238}U	238.0507847(23)	$4.47x10^{9}$ y $8.94x10^{13}$ y	α to ^{234}Th SF	99.27%	12.5kBq g^{-1}
^{237}U	237.048723	6.75 d	β^- to ^{237}Np	-	
^{236}U	236.045561	$2.34x10^{7}$ y $2.44x10^{14}$ y	α to ^{232}Th SF	Trace*	
^{235}U	235.0439242(24)	$7.04x10^{8}$ y $1.01x10^{19}$ y	α to ^{231}Th SF	0.72%	80.0kBq g^{-1}
^{234}U	234.0409468(24)	$2.46x10^{5}$ y $1.44x10^{16}$ y	α to ^{230}Th SF	0.0054%	2.31 MBq g^{-1}
^{233}U	233.039628	$1.59x10^{5}$ y $2.27x10^{17}$ y	α to ^{229}Th SF	Trace*	
^{232}U	232.03715	68.9 y	α to ^{228}Th	Trace*	
^{231}U	231.03626	4.2 d	α to ^{227}Th	-	
^{230}U	230.03393	20.8 d	α to ^{226}Th	-	

*natural reactors, e.g. Oklo in Gabon, Central Africa

**www.iaea.org

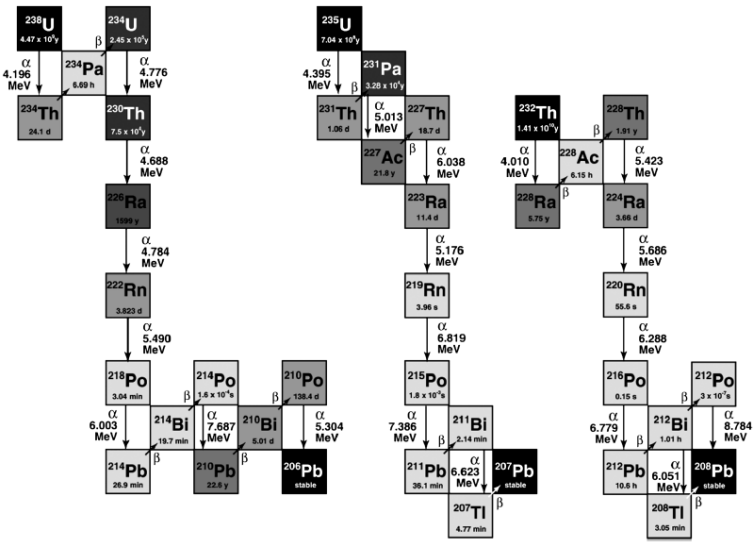

Figure 1.15: U and Th decay series (from Vanhaecke et al., 2009)

The radioactivity of isotopes depends on the half-life, and the corresponding specific

activity for ^{238}U, ^{235}U and ^{234}U is 12.5 $kBqg^{-1}$, 80.0 $kBqg^{-1}$, 231 $MBqg^{-1}$ (Table 1.7). As shown in Table 1.7, most of the U isotopes decay by emitting alpha particles but some also undergo spontaneous fission. In the natural environment, spontaneous fission occurs only rarely and alpha or beta particle emission occurs instead. For example, the probability of spontaneous fission per decay is 7.0×10^{-11} and 5.4×10^{-7} for ^{238}U and ^{235}U, respectively (Shultis and Faw, 2007). Further discussion about modes of decay and about nuclear fission will be covered in section 1.3.3 on radiotoxicity of U and in section 1.3.2 on anthropogenic sources of U, respectively.

Another important property of U is its ability to exist in several different oxidation states. It can occur in +4, +5, +6 oxidation states but it is the +4 and +6 states that are more commonly found in the natural environment. The former is commonly found in the solid phase whilst the latter is frequently found in aqueous phase environments and so the mobility of U is strongly dependent on its oxidation state. For example, uraninite, which contains U^{IV} and occurs in reducing environments, is considered to be immobile and non-bioavailable (Langmuir, 1978). In contrast, U^{VI} is present primarily as the uranyl ion, UO_2^{2+}, and in complexed species such as $UO_2(OH)^+$ and $UO_2(CO_3)_3^{4-}$, depending on pH and presence of dissolved CO_2. As these complexes are found to be unsusceptible to adsorption, they are mobile and potentially bioavailable in the environment. Clearly, oxidation-reduction processes may play a very important role with respect to U mobility in natural systems. This will be discussed further in section1.3.4.

1.3.2 Anthropogenic sources of U to the environment

There are several sources of anthropogenic radionuclides in the environment, such as operations associated with (i) nuclear weapon programmes including weapon production and testing; (ii) nuclear power production including U mining and milling, near-surface storage of low-level solid wastes, aqueous discharge of low-level liquid wastes following power production, on-site storage of intermediate level wastes, commercial fuel reprocessing, deep geological storage of high-level nuclear wastes and nuclear accidents (Hu et al., 2010); (iii) industrial processes including coal combustion (e.g. Beck and Miller, 1980) and phosphate ore-processing (e.g. McCartney et al., 1990); (iii) medical, academic research-related, and military use of isotopes including gold isotopes (e.g. ^{198}Au; $t_{½}$=2.7 d; Handfield et al., 2008) for cancer treatment, depleted U (DU) for armour-plating of military vehicles and for tank piercing munitions tips (e.g. Oliver et al., 2007).

Examples of environmental U contamination arising from each of these four main categories are detailed in sections 1.3.2.1-1.3.2.4 below.

1.3.2.1 Nuclear weapons production and testing

Uranium contamination of the Hanford site in Washington State, US, which was established in 1943 and used during both the Second World War and Cold War era, is a legacy of nuclear weapon production and nuclear fuel reprocessing. During the process, fissile materials (e.g. ^{235}U and ^{239}Pu) were separated from fission products in spent fuel rods to produce weapon-grade material. High-level nuclear waste products remaining after extraction of the fissile material from spent fuel rods were stored in 177 underground storage tanks, many of which have subsequently discharged large quantities of radionuclides such as $^{235, 238}$U, ^{60}Co, ^{90}Sr, ^{99}Tc, $^{152, 154}$Eu and ^{137}Cs, into the vadose zone and groundwater (Ahearne, 1997; Catalano et al., 2004). For example, U, together with other contaminants, was released to the vadose zone through leakage from the storage tanks and through discharges of lower concentration wastewaters into retention basins, cribs, and trenches (Wan et al., 2009). The single largest discharge occurred from the overfilling of Tank BX-102 in 1951 when an estimated 10 000 kg of U^{VI} entered the deep vadose zone. Figure 1.16 shows the U plume that has been identified in groundwater. Concentrations of U and the spread of the plume have increased over time.

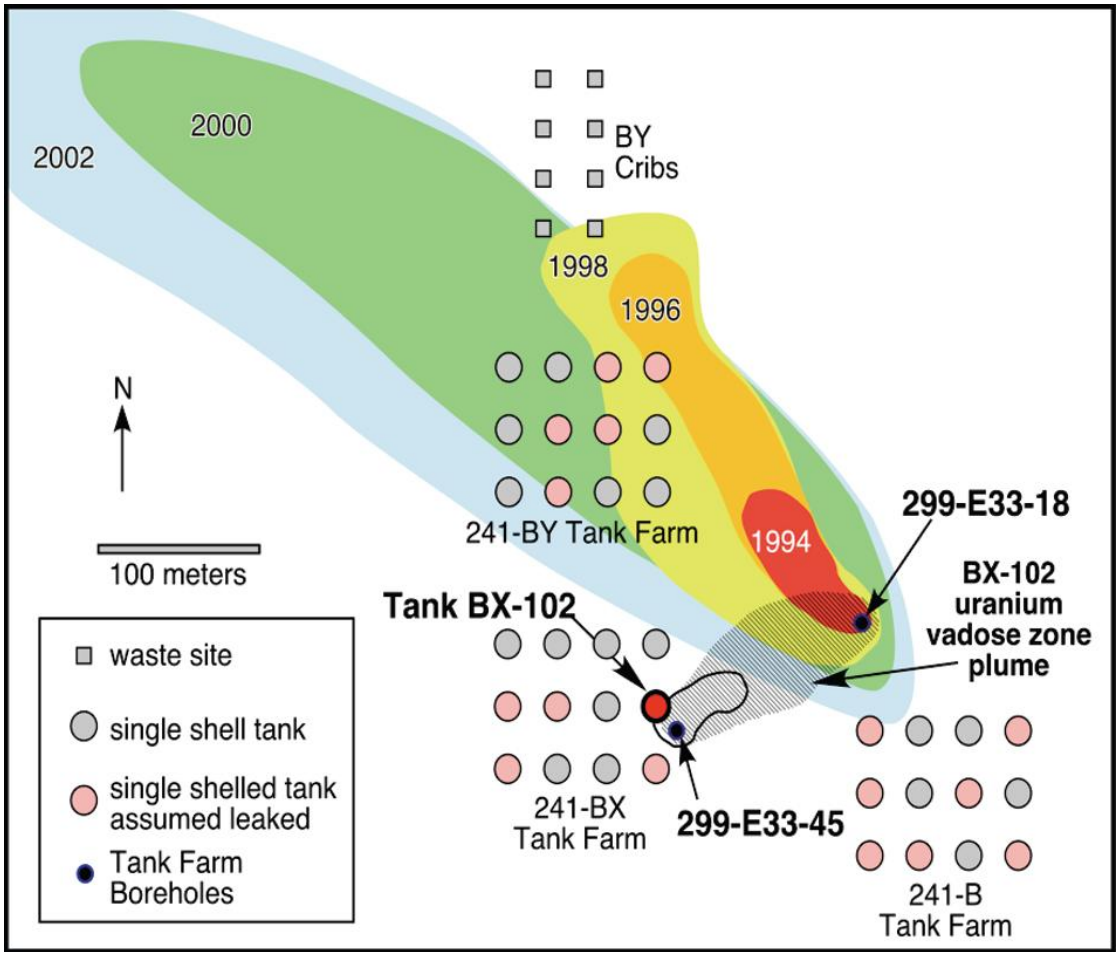

Figure 1.16: Accidental release of U into groundwater at the Hanford site, Washington State, US (Wan et al., 2009)

The Semipalatinsk test site is located in the northeast of the Republic of Kazakhstan, covering 19,000 km^2. The Soviet Union carried out about 460 nuclear weapon tests at this location during the period 1949-1989, including more than 300 underground tests. It was found that 13 underground tests generated radioactive gases which were released into the atmosphere (IAEA, 2008). In addition, there has been recent concern that groundwater may have become contaminated with isotopes of U, plutonium (Pu) and americium (Am). With respect to U, Leon Vintro et al. (2009) showed that total U concentrations in groundwater were in the range 6.0-17.3 μg L^{-1}. These were much higher than values obtained for nearby river water. Moreover, the $^{235}U/^{238}U$ ratio was slightly elevated above the value expected for natural U and so it was concluded that some of the groundwater U had come from the underground nuclear tests. Many of the groundwater samples were obtained from wells and although none exceed the US EPA limit of 30 μg L^{-1} for drinking water, some do exceed the WHO guideline value.

1.3.2.2 Nuclear power production

Uranium mining and milling are the first stages in the nuclear fuel cycle and involve ore extraction and subsequent physical and chemical extraction of U from the ore. The radionuclides associated with U mill tailings include U isotopes (^{238}U, ^{235}U, ^{234} U), ^{230}Th, ^{226}Ra and ^{222}Rn. It is estimated that the total volume of mill tailing worldwide is 938×10^6 m^3 produced from 4384 mines in countries such as Kazhakstan, Canada, Australia, Russia, United States, Namibia, and the Niger. The radioactivity associated with these tailings depends on the grade of the ore (Abdelouas, 2006). In addition, the environmental impact usually depends on the extent to which the tailings have been protected from infiltration by rainwater and surface/groundwater. More recent tailings dams have impermeable linings and are often capped with clays. However, Lottermoser and Ashley (2005) reported seepage of U and other radionuclides from the capped tailings dam at the rehabilitated Mary Kathleen U mine, Australia. Over time, the tailings have developed stratified porewaters with highly acidic (pH<4), metal-rich waters in the upper layers and near-neutral metal-poor waters at greater depth. Seepage is occurring through the dam walls and the emerging waters are slightly acidic (~pH 5.5) and transport ~5 kg U per year. Surface waters downstream of the dam contain U at concentrations higher than the Australian livestock drinking water limit of 200 µg L^{-1} (NWQMS, 2000). The environmental impact of tailings in Tajikistan has also been the subject of a recent study (Skipperud et al., 2012). Again, waters emanating from the tailings were enriched in U which was considered to be both mobile and bioavailable (defined as the portion of an element which may be taken up by a living organism).

The British Nuclear Fuels plant at Sellafield (formerly Windscale and Calder Works) is the largest nuclear complex in UK. The Windscale reactors, called piles, were constructed in the 1940s and were used for irradiation of U and the subsequent production of weapons-grade Pu (Gray et al., 1995). Nearby, four reactors comprising the Calder Hall nuclear power station were officially opened in October 1956 and these were used for electricity generation. A serious fire at the Windscale Piles occurred in October 1957 when insufficient core instrumentation failed to detect overproduction of heat generated from the reaction of hot metallic U and graphite with air. The fire caused the release of significant radioactivity to the environment, e.g. 180 TBq ^{137}Cs; 1800 TBq ^{131}I (Garland and Wakefield, 2007). In addition, however, it has been estimated that ~5 kg U was lost during the fire (Chamberlain, 1981) and investigations during the 1970s-80s showed that U-rich fuel

particles were present in the surrounding soils and coastal sediments (Hamilton, 1981). These pose a significant risk to human health if ingested (Charles and Harrison, 2007).

Small quantities of U, Pu, Am, caesium (Cs) and other radionuclides were also released as part of authorised discharges of low-level radioactive liquid wastes *via* a 2.5 km pipeline into the Irish Sea. On an annual basis, it is estimated that a maximum of 4 tonnes U were discharged. This is at least an order of magnitude lower than the amount of U being discharged from the nearby Marchon phosphate processing plant near Whitehaven whose annual discharges over the period 1954-1988 were ~30 tonnes U (McCartney et al., 1990) (see section 1.3.2.3). Summed over this period, the combined discharges from Sellafield and Marchon (≤1300 tonnes) are still negligible in comparison with the amount of U present naturally in seawater (Figure 1.14).

The Enhanced Actinide Removal Plant (EARP) considerably reduced discharges into the Irish Sea and, with the completion of the Thermal Oxide Reprocessing Plant (THORP) in 1994, BNF added the capability to carry out spent fuel reprocessing and associated waste management operations. However, in 2005, it was discovered that 83,000 L of acidic, U-containing radioactive waste had leaked from a cracked pipe into an underlying stainless steel-lined sump. Subsequently, 19 tonnes of U and 150 kg of Pu have been recovered. Although there was no contamination of the surrounding environment, there will be implications for final decommissioning of the site.

1.3.2.3 Industrial processes

Due to its natural occurrence, U can also be released into the environment from non-nuclear industrial sources, e.g. coal combustion and phosphate ore-processing (Figure 1.17).

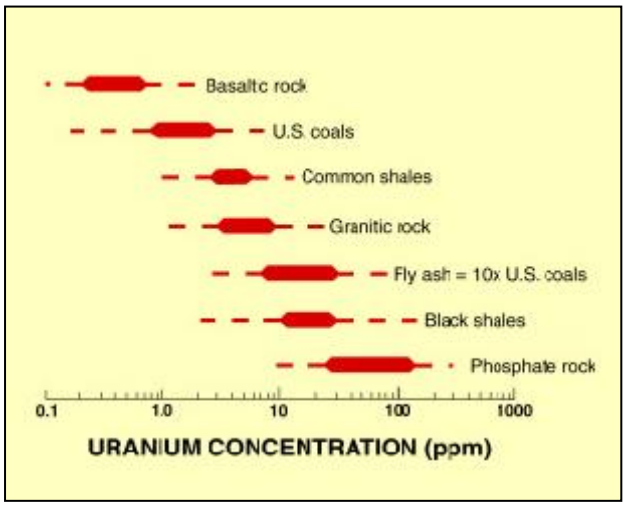

Figure 1.17: Concentration of U in US coals and fly ash in comparison with various rocks including phosphate rock (http://pubs.usgs.gov/fs/1997/fs163-97/FS-163-97.html)

Upon combustion, most uranium in coal is retained in the fly ash, especially in the finer sized particles. Fly ash may be placed in lagoons as a disposal option, where leaching of soluble components may result in mobilisation of U and other radionuclides. However, USGS researchers showed that U is not commonly present on the surface of the fly ash particles and will therefore have a low susceptibility to leaching (http://pubs.usgs.gov/fs/1997/fs163-97/FS-163-97.html). Fly ash is also used in building materials and there is concern that levels of radioactivity in housing may be increased as a consequence (Papastefanou, 2010). The main risk, however, is likely to be from ^{222}Rn gas rather than from U directly.

Phosphate rock is the raw material used in the manufacture of all phosphate products. This contains natural U at concentrations in the range of 10s-100s mg kg^{-1}. Additionally, it contains many of the U decay series radionuclides, some of which present significant risk to human health. The Albright and Wilson Marchon phosphate-ore processing plant mentioned above was situated at Whitehaven, northwest England. From the 1950s to the late 1980s, phosphoric acid was produced from the phosphate and the U-containing effluent was discharged under licence into the Irish Sea. Several studies (e.g. McDonald et al., 1991; McCartney et al., 1992; Keating et al., 1996) have shown that there are enhanced activities of U and its decay products in coastal areas in the vicinity of the plant.

1.3.2.4 Military uses

Depleted uranium (DU) is the by-product of the U enrichment process within the nuclear fuel cycle (Figure 1.18). The fissile isotope ^{235}U is preferentially concentrated for the production of nuclear fuel or nuclear weapons via gas centrifugation or gaseous diffusion. The enriched product contains ~3% w/w ^{235}U and the depleted by-product, DU, contains only ~0.2% w/w. As such DU is less radioactive than both natural and enriched U.

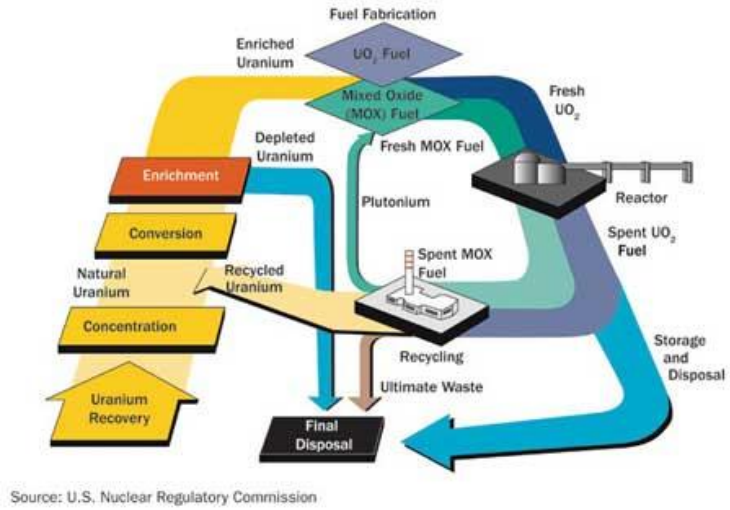

Figure 1.18: The nuclear fuel cycle showing the separation of enriched and depleted U (www.nrc.gov)

As for natural U, DU has a high density (19.05 g cm^{-3}) and, because of its low cost as well as its lower radioactivity, it has been used for armour-plating military vehicles (Oliver et al., 2007). Its ability to self-sharpen and its pyrophoric properties have also been exploited for military purposes (Oliver et al., 2007). DU-tipped munitions have been developed and tested at UK Ministry of Defence (MoD) sites. For example, the Dundrennan Firing Range, SW Scotland was used for firing accuracy trials for DU projectiles over the period 1982-mid 1990s. Of the 1800 test firings, there were 71 malfunctions which caused the shells to break up over the firing range. This resulted in soil contamination along the direction of fire and in the downwind direction (Oliver et al., 2007). DU was also detected in soil porewaters, earthworms and plants in the vicinity of the firing area and it was demonstrated that DU was more mobile than natural U (Oliver et al., 2007; Oliver et al., 2008a).

1.3.3 Radiotoxicity and chemical toxicity of U

As alluded to in the previous sections, U from both natural and anthropogenic sources can cause significant contamination of terrestrial and aquatic environments.

It is generally considered that the toxicity of natural U mainly comes from its chemical and, to a lesser extent, its radiological properties (Venugopal, 1978; Van Horn and Huang, 2006). Its radioactivity is considered to be low because of the long-life of the main isotope, ^{238}U (Craft et al., 2004). Bosshard et al. (1992) reported that no radiation effects have been found in either animals or humans after exposure to natural U.

The health risks associated with U depend on the route by which it enters the human body. Inhalation of small particles which may lodge in the lungs presents a different type of risk from that associated with ingestion of particulate or dissolved forms of U.

With respect to inhalation, the chemical properties of U, which lead to toxic effects, are similar to other heavy metals. Ochiai (1977, 1987) reported that the mechanisms of metal-ion toxicity include blocking biologically essential pathways, substituting the essential metal ion from biomolecules and functional cellular units, conformational modification, disruption of cellular and organellar membrane integrity and denaturation and inactivation of enzymes. For example, U can destroy enzyme function by replacing metals such as Cu^{2+} and Zn^{2+}, which play important roles in some enzymes. In a separate study, Wise et al. (2007) used human bronchial fibroblasts exposed to uranium trioxide and uranyl acetate to show that natural U was cytotoxic and clastogenic to human lung cells.

With respect to ingestion, it has been found that insoluble forms of U present the lowest risk since they are excreted via the digestive track. Soluble forms, however, do interact with biological ligands (Figure 1.19) and can cause toxicological effects, e.g. dissolved forms are considered to be nephrotoxins (causing kidney damage and failure) (Van Horn and Huang, 2006).

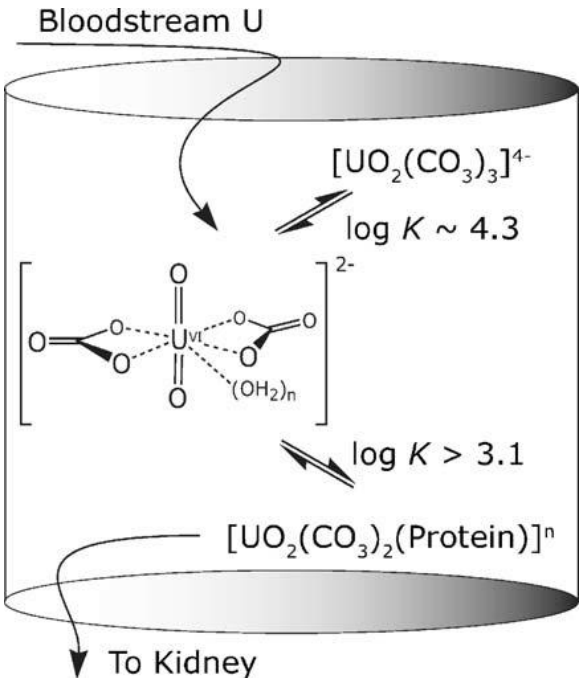

Figure 1.19: Current understanding of how soluble U is transported to the kidneys within the human body (Van Horn and Huang, 2006)

Some early studies of the effects of U on the human body indicated that the minimum dose required to have a nephrotoxic effect was 70-100 µg U kg^{-1} whilst a kidney concentration of more than 2 mg U kg^{-1} resulted in catalasuria and proteinuria (Luessenhop et al., 1958; Hursh and Spoor, 1973). In a more recent study of human exposure via consumption of U in drinking water, Kurttio et al. (2002) found it difficult to establish a lower limit for nephrotoxicity but concluded that a guideline value of 100 µg L^{-1} was too high while values of 2-30 µg L^{-1} would be more appropriate. The most recent WHO guideline value of 30 µg L^{-1} is at the top end of this range. However, a report from the UK Committee on Toxicity in 2006 calculated the Tolerable Daily Intake (TDI) for infants (~4.5 kg body weight; consuming 700 ml milk prepared with water containing 15 µg L^{-1} (the previous WHO guideline value) and found that the TDI exceeded the WHO limit of 0.6 µg kg^{-1} (body weight) per day by a factor of 4 (http://cot.food.gov.uk/pdfs/cotstatementuranium06.pdf). It is also possible that the absorption of U by young infants is greater than in adults and so the consequences of this exceedence are unclear. As a precautionary measure, it would appear that the German guideline value of 2 µg L^{-1} for water used to prepare infant milk products (ESFA, 2009) should be more widely recommended to protect infant health.

1.3.4 Influence of redox potential and pH on the aqueous phase speciation of U

The chemical behaviour of U in the natural aquatic system is mainly influenced by the pH, redox potential and the presence of various complexing agents (also see section 1.4.2). Under oxidising conditions, soluble U^{VI} species prevail in aqueous solutions. The uranyl ion (UO_2^{2+}) is stable only at low pH (<5); thereafter, hydrolysis complexes prevail in the absence of dissolved CO_2.

$UO_2^{2+} + H_2O \leftrightharpoons UO_2(OH)^+ + H^+$ Equation 1.11

$UO_2(OH)^+ + H_2O \leftrightharpoons UO_2(OH)_2^0 + H^+$ Equation 1.12

$UO_2(OH)_2^0 + H_2O \leftrightharpoons UO_2(OH)_3^- + H^+$ Equation 1.13

At extremely low concentrations, the mononuclear species, $UO_2(OH)^+$, $UO_2(OH)_2^0$, and $UO_2(OH)_3^-$, form progressively as pH increases (Equations 1.11-11.13) but even at total U^{VI} concentrations of 10^{-8} M (~2.4 μg L^{-1}, i.e. similar to slightly contaminated groundwaters; see section 1.1.1), polynuclear complexes such as $(UO_2)_2(OH)_2^{2+}$ and $(UO_2)_3(OH)_5^+$ form (Equations 1.14-1.15), albeit at significantly lower concentrations than the mononuclear complexes (Figure 1.20).

$2UO_2^{2+} + 2H_2O \leftrightharpoons (UO_2)_2(OH)_2^{2+} + 2H^+$ Equation 1.14

$3UO_2^{2+} + 5H_2O \leftrightharpoons (UO_2)_3(OH)_5^+ + 5H^+$ Equation 1.15

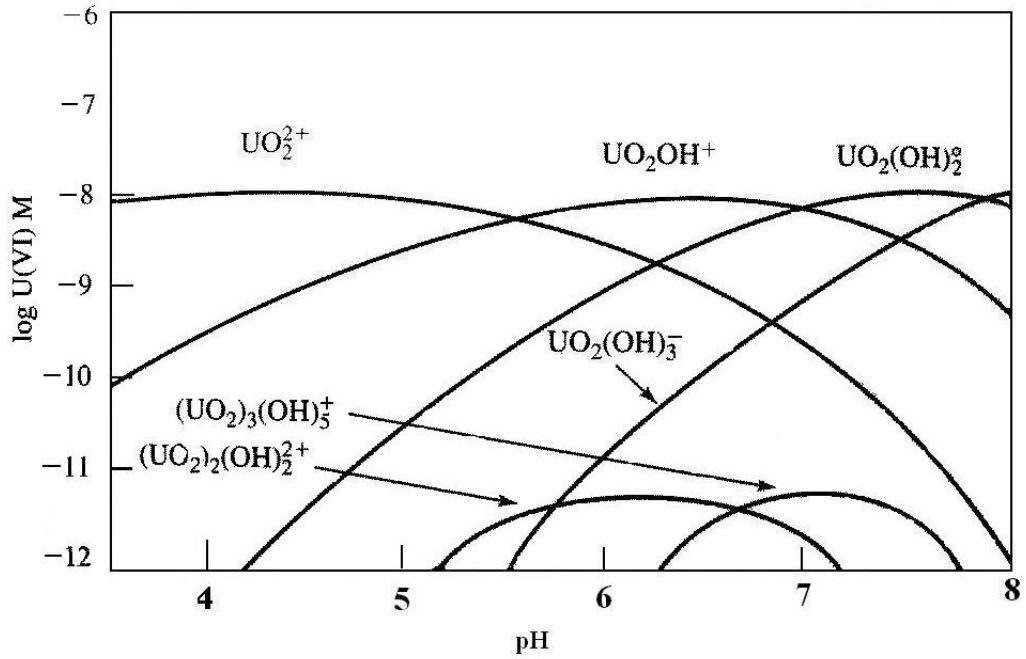

Figure 1.20: Distribution of U^{VI} species at 25 ℃ and I=0.1 M for ∑U=10^{-8} M, pCO_2= 0 bar (Waite et al., 1994).

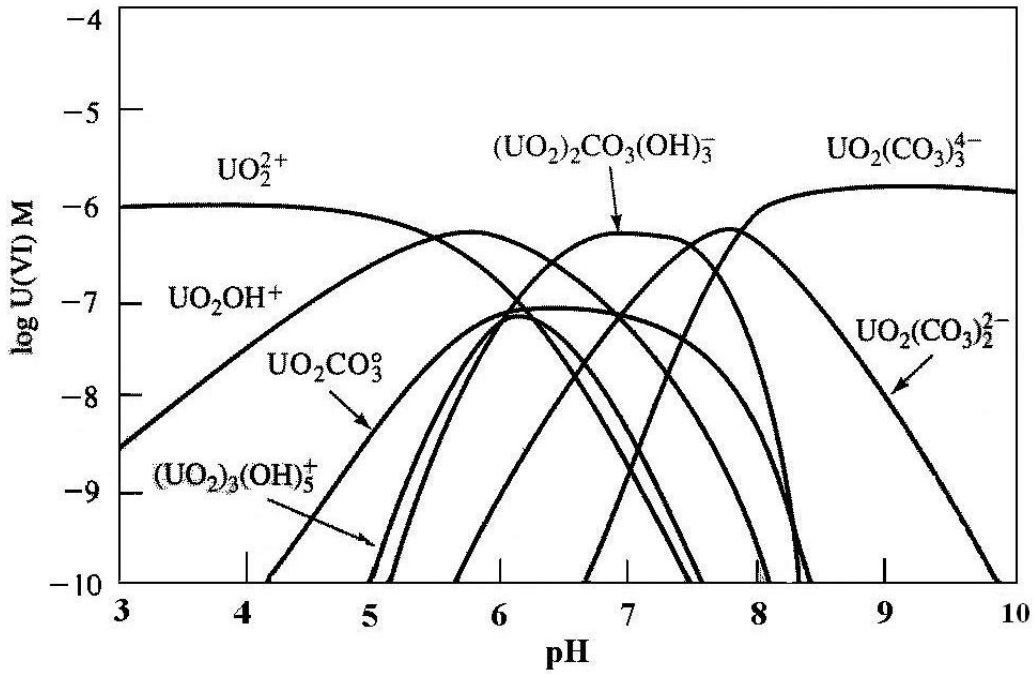

Figure 1.21: Distribution of U^{VI} species at 25 ℃ and I=0.1 M for ∑U=10^{-6} M, pCO_2= $10^{-3.5}$ bar (Waite et al., 1994).

In the presence of dissolved CO_2, however, uranyl-hydroxy-carbonato and carbonato

species largely replace the uranylhydroxy species above pH 6-7. For example, Figure 1.20 shows that, below pH 6, the uranyl ion (UO_2^{2+}) dominates, between pH 6-8, the main species are UO_2OH^+, $(UO_2)_2CO_3(OH)_3^-$, $(UO_2)_3(OH)_5^+$ and $UO_2(CO_3)_2^{2-}$ and above pH 8, $UO_2(CO_3)_3^{4-}$ dominates. The speciation calculations shown in this figure are based on a total U^{VI} concentration of 10^{-6} M (~238 μg L^{-1}, similar to some mining impacted groundwaters in Australia, e.g. Rossiter et al., 2010) and, in comparison to the 10^{-8} M solution shown in Figure 1.21, it is clear that, over the pH range 6-7.5, polynuclear species make a much greater contribution to the speciation of U.

More generally, however, due to widespread presence of dissolved carbon dioxide and acid-base reactions involving dissolved inorganic carbon species, uranyl-hydroxy-carbonato and carbonato complexes are the dominant U^{VI} species in many natural water systems at pH 7 and above (Langmuir et al., 1997). In relation to mobility, of particular importance are the negatively charged U complexes, e.g. $UO_2(CO_3)_2^{2-}$, $UO_2(CO_3)_3^{4-}$ which have very low affinity for the predominantly negatively charged mineral phases present in soil, and thus tend to remain in the solution phase (Renshaw, 2011). Carbonate complexation has also been found to increase the solubility of U minerals, facilitating U^{IV}re-oxidation as well as limiting the extent of U adsorption. Complexation and adsorption processes will be discussed in more detail in sections 1.4.2 and 1.4.3, respectively.

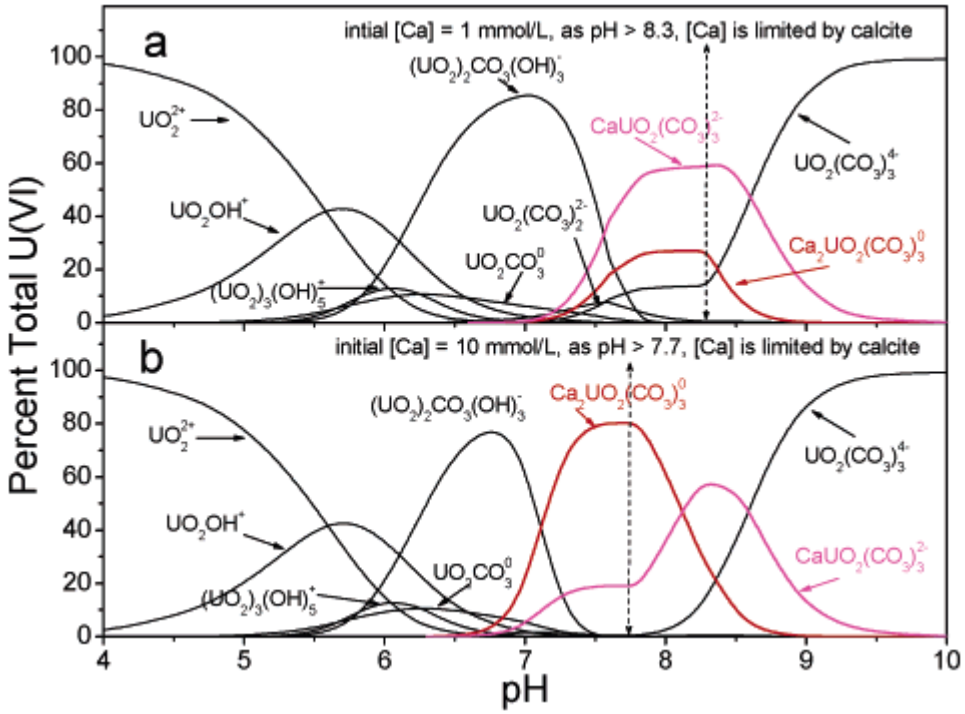

Figure 1.22: Distribution of U^{VI} species at 25 °C and I= 0.1 M for ∑U= 10^{-6} M, pCO_2= $10^{-3.5}$ bar (a) Ca^{2+}= 1 mmolL^{-1}, and (b) Ca^{2+}= 10 mmol L^{-1}. The formation constants for $CaUO_2(CO_3)_3^{2-}$ and $Ca_2UO_2(CO_3)_3^0$ are from Dong and Brooks (2006) and the others from Guillaumont and Mompean (2003).

Other inorganic species in solution such as Ca^{2+} ions can also have an impact on U speciation (Figure 1.22). The main effect on speciation occurs in the pH range 7-8.5 and the species formed depend on the Ca^{2+} concentration. For example, at lower concentrations, e.g. 1 mmol L^{-1} (= 40 mg L^{-1}), the negatively charged $CaUO_2(CO_3)_3^{2-}$ is the main species in solution at pH 7.5-8 whilst, at higher concentrations, e.g. 10 mmol L^{-1} (= 400 mg L^{-1}), the neutral species $Ca_2UO_2(CO_3)_3^0$ predominates at pH 7.5. At higher pH values, the concentrations of the calcium carbonato species is limited by the formation of calcite (K_{SP} = 3.36 x 10^{-9}) which removes Ca^{2+} from solution.

Organic species including humic acids often have a much wider influence on the aqueous speciation of U. For example, U^{VI} speciation modelling of groundwaters at the Aberdeen Proving Ground (APG) in Maryland, U.S. was carried out by Dong et al. (2006) using the complexation model developed by Choppin and Allard (1985) in conjunction with other measured chemical characteristics of the APG surface water (Figure 1.23). It is evident that, below pH 4.5, inorganic ligands dominate, UO_2A dominates between pH 4.5-7.5, while

uranyl carbonate complexes, $UO_2(CO_3)_2^{2-}$ and $UO_2(CO_3)_3^{4-}$, dominate under alkaline conditions (pH> 7.5). When compared with Figure 1.21, the carbonate complexes have been replaced by humic substances to a large extent between pH 6-8.

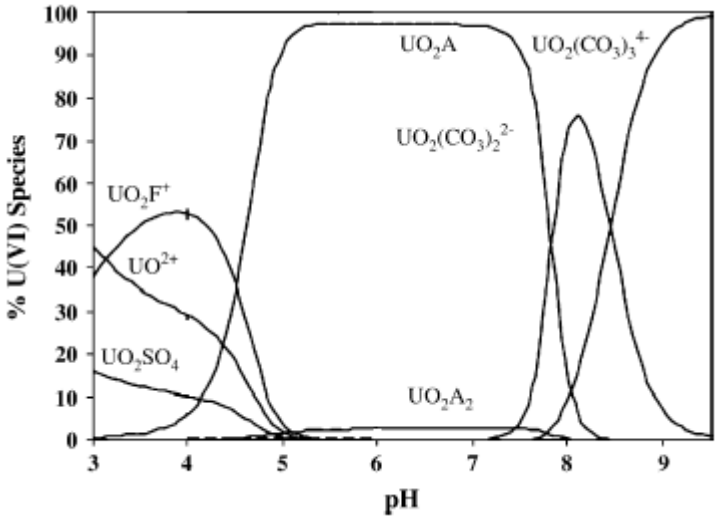

Figure 1.23: Distribution of U^{VI} species in surface water (I= 0.001) in the presence of humic substances (DOC= 13.9 mg/l) as a function of pH at pCO_2= $10^{-3.5}$ bar for ∑U= 0.013 M, calculated using a humic acid complexation model (Choppin and Allard, 1985). The symbol A in UO_2A and UO_2A_2 represents free carboxylic acid groups in molecules of humic substances.

As mentioned in section 1.3.1, U is mainly found in the oxidation states U^{IV} and U^{VI} in natural systems. Under reducing conditions, the U concentration in waters is usually very low as U^{IV} has quite low solubility. Ahonen et al. (1992) studied U speciation in groundwater samples from drill holes at the Palmottu Natural Analogue Site, Finland. The measured redox potentials were in the range -92 to 55 mV and the pH values ranged from ~6.9-9.1. They found that 93-97% U was in the form of U^{VI} when the redox potential was between -70 to 55 mV while 97% was present as U^{IV} at -92 mV.

As for U^{VI}, the speciation of U^{IV} in aqueous solution is also pH dependent.

$U^{4+} + H_2O \leftrightharpoons UOH^{3+} + H^+$ Equation 1.16

$UOH^{3+} + 3H_2O \leftrightharpoons U(OH)_4^0 + 4H^+$ Equation 1.17

The hydrolysis of U^{IV} occurs at much lower pH than for U^{VI} and the first hydrolysis

product forms below pH 1. Hydrolysis progresses rapidly as pH increases and there is no stability zone for either the second or third hydrolysis products. Complete hydrolysis to form $U(OH)_4^0$ occurs by pH 4 (cf stability zone for first hydrolysis product of U^{VI} occurs at pH 5-6).

An Eh-pH diagram for a system $U\text{-}O_2\text{-}CO_2\text{-}H_2O$ at 25°C with a groundwater U concentration of $\sum U(aq) = 10^{-8}$ M in the presence of 10^{-2} bar CO_2 is shown in Figure 1.24. Note that the value for pCO_2 is much greater than in Figure 1.20 and so theuranyl carbonate complexes dominate U^{VI} speciation above pH 5. U^{IV} is present only at low Eh values over the pH range 0-9.

The hatched line in Figure 1.24 shows the Eh-pH conditions under which U precipitates as uraninite when the total solution phase U concentration is increased to 10^{-5} M (~2.4 mg L^{-1}). Precipitation reactions will be discussed further in section 1.4.1.

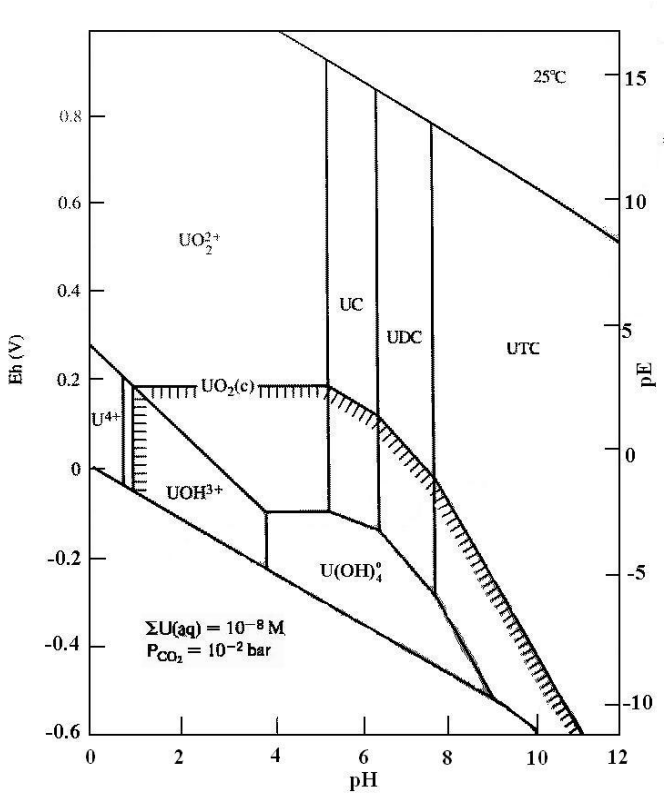

Figure 1.24: Eh-pH diagram for aqueous species and solids in the system $U\text{-}O_2\text{-}CO_2\text{-}H_2O$ at 25°C and 1 bar total pressure. Solid/aqueous boundaries (hatched) are drawn for $\sum U=10^{-5}$ M. UC, UDC and UTC are $UO_2(CO_3)^0$, $UO_2(CO_3)_2^{2-}$ and $UO_2(CO_3)_3^{4-}$, respectively (Langmuir et al., 1997).

1.4 Processes controlling the migration behaviour of U in soil and aquatic environments

The parameters described above (i.e. solution phase composition, redox potential, pH value, as well as the presence of solid mineral phases and organic material) control U speciation and migration behaviour (Renshaw et al., 2011). There are four key processes that may affect the mobility of U: precipitation, complexation, sorption and colloid formation. The influence of geochemical parameters on each of these processes will be discussed in turn in sections 1.4.1-1.4.4.

1.4.1 Precipitation

Under strongly reducing conditions, where U^{IV} is the main oxidation state, U readily precipitates as uraninite (UO_2) over the entire pH range typically encountered in natural soil and aquatic systems, i.e. pH 4-10 (Figure 1.24). Under slightly less strongly reducing conditions, precipitation can be induced by reduction of U^{VI} to U^{IV} to form uraninite (UO_2) (Figure 1.24). However, when U^{VI} is present at concentrations in excess of its solubility product (Table 1.8), U^{VI} minerals can precipitate from the solution. Where equilibrium conditions are reached, all of these processes will limit the amount of U in solution, thus limiting the mobility of U (Langmuir et al., 1997).

U^{VI} minerals are often the products of the oxidation and weathering of nearby U^{IV} ore minerals such as uraninite (UO_2) and coffinite ($USiO_4$) (see section 1.1) but they also form by precipitation from dissolved U^{VI}. For example, carnotite ($K_2(UO_2)_2(VO_4)_2$) and tyuyamunite ($Ca(UO_2)_2(VO_4)_2$) have been found in calcrete deposits in Western Australia (Mann and Deutscher, 1978) and in sandstone-hosted U deposits of the arid southern United States (Hostetler and Garrels, 1962). Autinite ($Ca(UO_2)_2(PO_4)_2 \cdot 10\text{-}12H_2O$), a low solubility phosphate, is slightly more soluble than the vanadates but has been found in precipitates near Mt. Spokane, Washington (Leo, 1960). Although relatively soluble and rare, U^{VI} is also found as the mineral schoepite ($UO_3\ 2H_2O$) in contaminated soils at a U.S. Department of Energy site (Morris et al., 1996).

Table 1.8: Solubility products for selected U^{VI} minerals

Mineral	Formula	Log K_{sp}	Reference
Schoepite	$UO_3(H_2O)_{2.25}$	-12.55	Mann, 1974
Metaschoepite	$UO_3(H_2O)_2$	4.68-6.23	Meinrath and Kimura, 1993; Sandino and Bruno, 1993
Leibigite	$Ca_2UO_2(CO_3)_3(H_2O)_{10}$	-36.9 ±2.1	Alwan and Williams, 1980
Swartzite	$CaMgUO_2(CO_3)_3(H_2O)_{12}$	-37.9 ±1.4	Alwan and Williams, 1980
Bayelite	$Mg_2UO_2(CO_3)_3(H_2O)_{18}$	-36.6 ±1.4	Alwan and Williams, 1980
Andersonite	$Na_2CaUO_2(CO_3)_3(H_2O)_6$	-37.5 ±4.2	Alwan and Williams, 1980
Autinite	$Ca(UO_2)_2(PO_4)_2.10\text{-}12H_2O$	-44.7	Shelobolina et al., 2009

Bioremediation has become a primary focus in reducing U^{VI} to U^{IV} since Lovley (1991) published the result that dissimilatory Fe^{III}-reducing microorganisms (*Geobactermetallireducens* GS15) could transport electrons to U^{VI}. In laboratory and *in situ* groundwater studies, it was observed that the presence of humic materials enhanced the bioreduction rate of U^{VI} under strict anaerobic conditions (Gu and Chen, 2003; Gu et al., 2005; Dong et al., 2006). Gu and Chen (2003) also reported that the reduction rate varied among the NOM fractions, humic and fulvic acids, with humic acid being more reactive in the microbial reduction of U^{VI} due to its high contents of polycondensed and conjugated aromatic organic moieties and greater solubility and conformational changes under circumneutral pH conditions. Aromatic functional groups including phenolic groups are considered to be responsible for electron transfer reactions (Chen et al., 2003).

In a study of bioreduction involving microorganisms and Fe^{III} under anaerobic conditions, it was concluded that humic substances accepted electrons from humic-reducing microorganisms and then donated electrons to Fe^{III} or Fe^{III}-containing minerals to release Fe^{II}. Thus humic substances were postulated to play a beneficial role as electron mediators or shuttles in bioreduction (Lovley et al., 1996). These shuttling processes can also explain the bioreduction of U in the presence of humic substances. Gu et al. (2005) reported that the reduced U was in the form of U^{IV}-humic complexes with no U^{IV} mineral precipitates

being formed by the reduction process.

1.4.2 Complexation

In the aquatic environment, cations can be present as free aquated ions, as part of an ion pair, or complexed by ligands, such as hydroxide, carbonate, sulfate, phosphate, chloride, fluoride, nitrate, and silicate, and natural organic matter. It is reported that the strength of inorganic ligand complexation decreases in the order of CO_3^{2-}, OH^->HPO_4^{2-}, F^-, SO_4^{2-}> NO_3^-, Cl^- (Renshaw et al., 2011). The inorganic ligands that complex U can be the same ones discussed under precipitation in section 1.4.1 since, in general, cations and ligands which form strong complexes form low solubility mineral phases. At first this might seem counter-intuitive since, for example, uranyl carbonate is very stable in solution and yet there are a number of very low-solubility U^{VI} carbonate phases. However, in natural systems, the formation of a sparingly soluble phase and its relationship with species in an aqueous solution is not as straightforward as a thermodynamic equilibrium reaction in a homogenous solution (Stumm and Morgan, 1995).

Natural organic matter, with its well-known complexation capabilities, also affects the retention and release of U in soil and into solution, respectively. Natural organic matter can be present in solution in both dissolved and colloidal forms, and is also present as a component of the solid phase soil (Choppin, 1992). Thus, whether it retains or releases U depends on whether U is complexed with NOM in the solution or solid phase. For example, the ready complexation of the uranyl ion with organic molecules such as humic acid (Haas and Northup, 1999) is thought to account for the strong retention of U in humic-rich environments such as peaty soils and peat bogs (MacKenzie et al., 1991; González et al., 2006; Regenspurg et al., 2010). However, the nature of the complexes formed between U and humic substances have yet to be fully elucidated.

Some studies have used humic acids (HAs) as a proxy for solid phase natural organic matter (Steelink, 2002; Schmidt et al., 2011). In general, carboxylate functional groups are considered to be the primary functional groups which complex actinide elements (Stevenson et al., 1982; Pompe et al., 2000). Other functional groups such as phenolic groups (Pompe et al., 2000; Kremleva et al., 2009), amino groups (Gunther et al., 2007) are also considered to provide complexation sites on HA for the uranyl ion. However, as discussed in section 1.3.4, aqueous phase U is present as hydroxylcarbonato, calcium

carbonato and carbonato species at the pH values prevailing in many soils. Although the uranyl ion may interact strongly with carboxylate groups it is not immediately clear that less strongly positive charged hydrolysis products (e.g. UO_2OH^+) nor neutral (e.g. $UO_2CO_3^0$, $CaUO_2(CO_3)_2^0$) or negatively charged (e.g. $(UO_2)_2(CO_3)(OH)_3^-$, $UO_2(CO_3)_2^{2-}$, $UO_2(CO_3)_3^{4-}$) U species should interact in the same way with highly negatively charged humic molecules.

Direct complexation of the uranyl ion by humic acid is described as a binary interaction and this occurs at low pH. Beyond pH 5, it is necessary to consider the effects of hydrolysis and carbonate complexation on U speciation. Complexes between hydroxy, calcium carbonato, hydroxycarbonato, and carbonato U species and humic acid are described as ternary interactions. A small number of recent studies have characterised some of these ternary complexes. For example, the ternary complex $UO_2(OH)HA$ formed by complexation of UO_2OH^+ with HA at pH 7 under exclusion of CO_2 was studied by Sachs et al. (2007) and the stability constant was determined as $\log \beta = 6.58 \pm 0.24$. In comparison, if the calculation was carried out for the interaction between HA and non-hydrolyzed UO_2^{2+}, the overall constant was 14.89 ± 0.54. Thus the ternary complex formed at pH 7 is less strong than the binary complex formed between U and humic acid at low pH. Very recently, Steudtner et al. (2011a) for the first time directly verified spectroscopically the formation of ternary U^{VI} humate complexes in solutions containing dissolved CO_2. The stability constant for $UO_2(CO_3)HA$ was found to be 24.47 ± 0.70, indicating that a strong complex had been formed (Steudtner et al. 2011a).

Besides pH and the available ligands in the environment, humic molecular size is another factor that must be considered when investigating the interactions between U and humic substances. Christl et al. (2000) investigated the chemical heterogeneity of humic substances in relation to molecular size and found clear differences between the humic size fractions, e.g. lower molecular weight fractions contained more chargeable functional groups (e.g. carboxylic group) and larger amounts of aromatic carbon than higher molecular weight fractions. Since many studies have shown that smaller, more hydrophilic humic fractions may be more environmentally mobile, it is important to determine whether U interacts to differing extents with different humic sizefractions. Graham et al. (2000) demonstrated that the association of U in soils was skewed towards the larger molecules in soils from the banks of the River Esk, NW England, consistent with their presence in the solid phase. In contrast, Graham et al. (2011) showed that association of DU with small

organic colloids inhibited their removal from soil porewaters at the Eskmeals Firing Range, NW England.

The pH dependence of interactions between U^{VI} and humic acids was investigated in an earlier study. Li et al. (1980) fractionated humic acid into five size fractions, namely <1.9 nm, 1.9-2.4 nm, 2.4-3.1 nm, 3.1-5.1 nm and >5.1 nm. Their results indicated that U^{VI} associated with humic acid in the largest size fraction (> 5.1 nm) at pH ≤3, but with that inone of the smaller size fractions (1.9 nm- 2.4 nm) at pH ≥5. In another study, Lenhart et al. (2000) found that U^{VI} became strongly bound to both humic and fulvic acids, but humic acid formed slightly stronger complexes and that complexation was more pH dependent. Finally, with respect to humic composition, Yang et al. (2012) recently used NMR to determine the alkyl content of different humic acids and reported that the mobility of humic acid-complexed U was positively correlated with the hydrophobicity of the humic acids.

Overall, it is clear that there is notaunique relationship between humic molecular size or hydrophilicity/hydrophobicity and ability to complex U^{VI}. This may be due to the location-specific structural characteristics of the humics themselves as well as to differences in prevailing environmental conditions.

1.4.3 Adsorption

Adsorption can be defined as the accumulation of substance or material at an interface between the solid phase and the bathing solution. Physical and chemical forces are responsible for the adsorption of metals from solution (Sparks, 2003).

There are a number of methods for modelling adsorption, from simple models which only use a single parameter (e.g. K_d) to represent this uptake to more detailed models such as a surface complexation model (SCM), in which interaction between dissolved species and surface functional groups are modelled using information obtained for complex formation with ligands in solution. Speciation programmes such as MINTEQA2 can be used to compute the equilibrium distribution of all species in the system, which includes dissolved, precipitated and adsorbed form. Although SCMs have been widely used, there are two problems that have not been solved. Firstly, reliable experimental sorption data are lacking for some species. Secondly, it is difficult to establish the identity of surface species. These two problems do not just apply to SCM, but also to many other models.

Even where the model fit to the data is good, it may simply be a consequence of the adjustment of a sufficient number of fitting parameters. Nowadays, Extended X-ray Absorption Fine Structure (EXAFS) and Fourier Transformed Infrared (FTIR) Spectroscopy (Bargar et al., 2005; Ulrich et al., 2006) are being used as independent means for identifying surface species (Waite et al., 1994), which can help to support modeling studies (Payne et al., 1998).

There are three main ways for U to adsorb onto solid phases: adsorption by a formation of an outer-sphere complex (e.g. electrostatic attraction only), ion exchange and formation of an inner-sphere complex (e.g. covalent bonding to mineral phase).

Adsorption of U onto solid surfaces has been extensively studied as it significantly affects migration behaviour. Sylwester et al. (2000) investigated the adsorption of the uranyl ion (UO_2^{2+}) to amorphous silica (SiO_2), γ-alumina (Al_2O_3), and montmorillonite surfaces between pH 3.1-6.5. The results suggested that adsorption of uranyl ion onto montmorillonite at low pH occurred via ion exchange, but at near neutral pH and in the presence of a competing ion, adsorption via inner-sphere complexes dominated. For silica and γ-alumina, the adsorption also occurred via inner-sphere complexes at near-neutral pH. At low pH, no possible complexes were confirmed for silica and γ-alumina.

U^{VI} also binds to Fe hydroxides (goethite and hydrated ferric oxide) through the formation of inner sphere complex (Waite et al., 1994; Reich et al., 1998; Walter et al., 2003). The adsorption of the uranyl ion onto the surfaces of as well as its incorporation into the structure of Fe oxides have both been extensively studied (Moyes et al., 2000; Dodge et al., 2002; Duff et al., 2002; Cheng et al., 2006; Ulrich et al., 2006; Sherman et al., 2008; Hiemstra et al., 2009; Nico et al., 2009). For example, Moyes et al. (2000) showed that U uptake by goethite and lepidocrocite via surface complexation ceased when the surface was saturated. Xray absorption spectroscopy (XAS) indicated that bidentate inner-sphere surface complexes were formed on the surface via coordination of two surface oxygens from an Fe octahedron in the equatorial plane of the complex. This is a bidentate-edge sharing surface complex which has also been proposed by other authors (Waite et al., 1994; Ulrich et al., 2006). More recently, however, a bidentate corner-sharing surface complex was suggested to be the dominant form of U^{VI} adsorbed on goethite in carbonate-free system (Sherman et al., 2008).

All the studies mentioned above used synthetic mineral phases and controlled laboratory conditions. It is worth remembering that interactions may be different in the natural environment where: (i) minerals are not pure, (ii) multiple different mineral phases may co-exist and (iii) mineral surfaces may be coated to some extent with organic matter.

The presence of dissolved carbon dioxide in aqueous solution can also affect the adsorption of U^{VI} on hydrous Fe oxide surfaces. For example, Wazne et al. (2003) found that when carbonate concentrations increased, FTIR spectroscopy showed a shift in the antisymmetric stretching vibration of the uranyl U−O bond toward lower wave numbers, indicating that uranyl carbonato complexes were adsorbed onto the surface. The experimental pH is an additional factor that affects the adsorption of U onto Fe oxides in the presence of carbonate. Ulrich et al. (2006) characterized U^{VI} sorption on ferrihydrite and found that the binary surface complex species $\equiv Fe(O)_2{=}UO_2$ was dominant at pH 5-6 in equilibrium with atmospheric CO_2 while ternary U^{VI}-carbonato surface complexes were of minor importance. However, at pH8, the ternary carbonato complex was dominant. The uranyl surface complex was found to greatly change in the presence of carbonate due to the specific adsorption of carbonate ions as well as the formation of ternary uranyl-carbonate surface complexes. In respect of the ternary carbonato complex, two types of binding mode were postulated (Figure 1.25). For type A, a uranyl edge-sharing surface complex is formed where a binary uranyl surface complex is directly bound through singly-coordinated surface groups present at particular edges of Fe-octahedra of ferrihydrite. This complex is similar to the species reported by Waite et al. (1994) for carbonate-free systems. For type B, a uranyl tris-carbonato surface complex ($\equiv(UO_2)(CO_3)_3^{4-}$) is singly-bound to an Fe atom in the solid phase through a carbonate group. Here, a carbonate ligand rather than the uranyl entity is singly coordinated to the Fe atom on the solid surface (Hiemstra et al., 2009). This complex is mostly found under conditions of high pH and at higher carbonate concentrations.

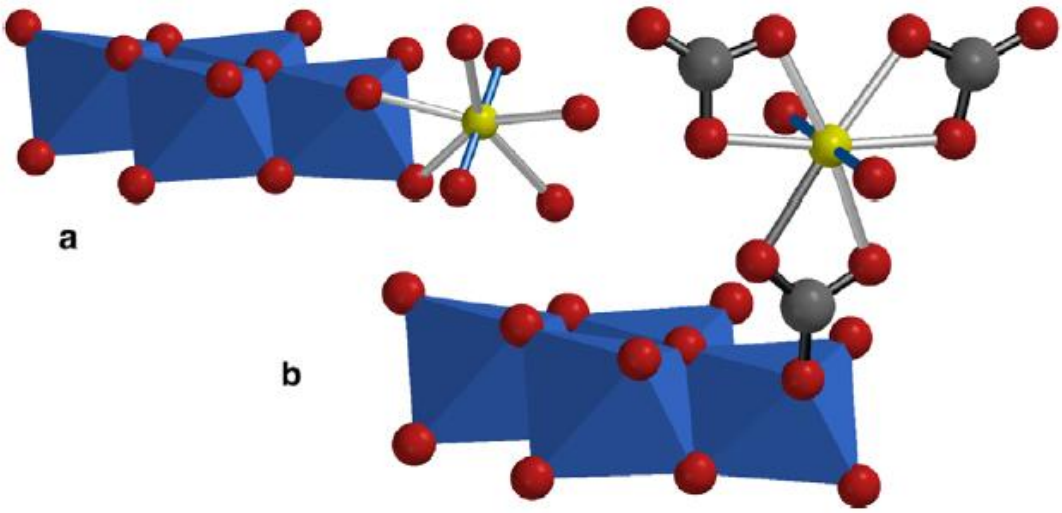

Figure 1.25: Representation of prominent uranyl surface complexes in open systems, i.e. (a) type A: uranyl bound by two singly-coordinated surface groups present at a free edge, the outer ligands of the uranyl surface complex may be OH, OH_2 or CO_3 (not shown) and (b) type B: A uranyl tris-carbonato complex that is singly-coordinated to an Fe atom on the solid surface via a carbonate group (Hiemstra et al., 2009).

Some recent studies have suggested another possible interaction between U and Fe oxides; instead of sorption onto the surface of the oxides, it is thought that U can become incorporated into the mineral structure. For example, Duff et al. (2002) observed that U^{VI} (0.72-0.8 Å) was incorporated into the Fe oxide mineral phase until a point of saturation was reached. As the radius of UO_2^{2+} (~1.8 Å) is much larger than that of Fe^{3+} (0.65 Å), UO_2^{2+} is not likely to replace the Fe^{3+} in the Fe^{III} oxide structure. However, although solid phase U^{VI} can form UO_2^{2+} species with two axial U-O bonds and four or more equatorial U-O bonds it is also possible to form uranate species e.g. γ-UO_3, without axial U-O bonds. The uranate species is much smaller and it was proposed that U^{VI} incorporated in the Fe oxides was in the form of uranate. Stewart et al. (2009) examined the sorption mechanism for U^{VI} reacted with ferrihydrite in the presence of Fe^{II}, dissolved Ca and carbonate. They found that the stability of U^{VI} incorporated into Fe(hydr)oxide mineral was dependent on the Fe^{II} concentrations during the Fe crystalline process under reducing and oxidizing conditions. In 3 mM Fe(II) reduced system, U can be incorporated into Fe^{III} (hydr)oxide (goethite), the product of ferrihydrite transformation. This U was resistant to release from the goethite even after exposure to oxidizing condition. By contrast, 10 mM Fe^{II} under reduced condition caused U^{VI} incorporation into $Fe^{II/III}$ (hydr)oxide (magnetite) and

subsequent formation of UO_2. When exposed in the oxic condition, Fe^{II} in the $Fe^{II/III}$ (hydr)oxide was oxidized, followed by subsequent release of U^{VI} into solution. UO_2 was also re-oxidized to U^{VI} and dissolved in the solution. The presence of dissolved Ca and carbonate promoted the formation of Ca-UO_2-CO_3 complex, which made U^{VI} more resistant to chemical reduction when it was incorporated into the Fe (hydr)oxide. These findings were implicated in co-association of U^{VI} and Fe minerals found in nature.

Finally, with respect to sorption reactions occurring in natural soil systems, it is important to recall that mineral particles are often part of mixed aggregates (section 1.2.4) and, as mentioned above, that many mineral surfaces are coated with natural organic matter. There have been a few studies providing information about ternary U-humic-mineral interactions in recent years (Krepelova et al., 2007; Sachs et al., 2007; Steudtner et al., 2011a; Steudtner et al, 2011b). For example, time-resolved laser-induced fluorescence spectroscopy (TRLFS) was applied to analyse a ternary system comprising U^{VI}-HA-kaolinite. Results indicated that U^{VI} was preferentially binding to kaolinite, with HA additionally attached as a uranyl-humate complex (Krepelova et al., 2007).

Other ternary interactions that may affect U migration behaviour include those involving U^{VI}-HA-Fe oxides. Payne et al. (1996) found that the U uptake on ferrihydrite was increased at pH<7 with addition of HA; little effect was observed above this pH value. Lenhart and Honeyman (1999) investigated U^{VI} sorption to hematite in the presence and absence of humic acid (HA) under a range of conditions (e.g. pH, ionic strength, hematite concentration, HA concentration). In the absence of HA, U^{VI} adsorption was influenced only slightly by ionic strength, consistent with the formation of inner sphere surface complexes, but to a larger extent by hematite concentration. The pH range over which sorption occurred was widened from 5-8 to ~4-9.5 by a one hundred-fold increase in hematite concentration, which was attributed to the increase in solid/solution ratio. In the presence of HA, the U^{VI} adsorption "window" shifted to slightly lower pH values, e.g. ~3.5-9 for the higher hematite concentration conditions. Interestingly, the enhanced adsorption at lower pH was most evident at low hematite concentrations. Lenhart and Honeyman (1999) tried to simulate the ternary system (hematite/HA/U^{VI}) through the combination of binary bimodels, e.g. CO_3^{2-}/hematite, U^{VI}/HA, U^{VI}/hematite and HA/hematite but they found that this gave an "under-estimation" of the experimental results – the predicted adsorption windows were consistently narrower. This was interpreted as further evidence for the formation of the ternary complexes among U^{VI}, HA

and hematite. They subsequently postulated that an inner sphere reaction (Equation 1.1.8) had occurred (L_2 represents carboxylic functional group):

$\equiv Fe\text{-}OH + HL_2 + UO_2^{2+} \leftrightharpoons \equiv FeOUO_2L_2 + 2H^+$ Equation 1.18

$\equiv Fe\text{-}OH + HL_2 + UO_2^{2+} \leftrightharpoons \equiv FeOH\text{---}UO_2L_2 + 2H^+$ Equation 1.19

However, the incorporation of this reaction into the model resulted in a poor fit for the experimental data. The outer sphere association shown in Equation 1.19 gave a much better match. It is not proposed that this ternary complex is truly "outer sphere" in nature but that there may be some "inner sphere" character, i.e. the charge from the uranyl species is distributed in some way between the surface and the electric double layer (Lenhart and Honeyman, 1999). The nature of such interactions is highly significant as this will determine how easily U might be removed from the mineral surface upon changing conditions in natural systems.

In conclusion, there are several factors that affect U^{VI} adsorption in natural environment system, including the pH of the contacting solution, aqueous carbonate concentration, aqueous calcium concentration, organic ligand e.g. HA, and Fe(II) concentration. Careful consideration of these factors will be essential in the investigation of U^{VI} adsorption behaviour at Needle's Eye Natural Analogue site.

1.4.4 Colloid Formation

Actinide colloids in natural waters are divided into two groups: intrinsic colloids and carrier colloids.

Intrinsic colloids are composed primarily of the actinide and are formed by condensation of actinide molecules or ions as the first step in hydrolytic or precipitation processes, e.g. leading to the formation of $UO_2.xH_2O_{(am)}$. Van der Lee et al. (1992) suggested the potential route to form this type of colloid is when U dissolves as U^{VI} species under oxidizing conditions, e.g. in a repository, and migrates with groundwater to a more reducing environment, where U^{VI} is reduced to form $UO_2.xH_2O_{(am)}$ colloids. Waterborne U^{IV} nanoparticles ($UO_2.xH_2O$) of comparatively high concentrations are relatively easy to produce at pH<3 (Opel et al., 2007; Ikeda-Ohno et al., 2009). However, when the pH israised to near-neutral region, this $UO_2.xH_2O$ colloid suspension will form aggregates and

sedimentation of particles follows (Dreissig et al., 2011). Dreissig et al. (2011) also observed concentrations of $\leq 10^{-3}$ M silicate-containing U^{IV} colloids in the near-neutral to slightly alkaline pH range; these remained stable in aqueous suspensionfor several years. In this study, the next-neighbour coordination of U^{IV} in U^{IV}-silica colloids was comparable with that of coffinite ($USiO_4$). In general, however, only a little knowledge has been attained about the nature of intrinsic U^{IV} colloids in reduced natural waters compared with the larger number of papers published on carrier colloids.

Carrier colloidsare formed through sorption or complexation of radionuclides onto colloids of other materials. There are several carrier colloids withwhich actinides are known to associate, including clay mineral colloids from the weathering of rock material, colloids of precipitated secondary minerals (e.g.aluminosilicate, siderite, Fe oxide) andhumic colloids(Warwick et al., 2002; Zanker et al., 2007). More specifically, these materials have been implicated in the formation of colloidal U species (Artinger et al., 2002; Pokrovsky and Schott, 2002; Jackson et al., 2005; Mibus et al., 2007; Vandenhove et al., 2007; Oliver et al., 2008a; Claveranne-Lamolère et al., 2009; Crançon et al., 2010; Pokrovsky et al., 2010; Graham et al., 2011; Yang et al., 2012).

Crancon et al. (2010) studied the transport of U through a sandy podzolic soil in columns, and observed that fast elution of U related to its interactions with humic colloids. Specifically, ~1-5% of the totalU input was transported through the column in association with the humic colloids at the mean porewater velocity. Claveranne-Lamolère et al. (2009) also found that only a small proportion (≤1%) of the U content of a soil leachate was transported by colloids. These colloids comprised humic-like substances in near-surface soils butinorganic entities (a mix of carbonatenano-particles or clay probably coated by organic particles) at depth. A more detailed examination of the humic-like substances suggested that it could be a mixture of clays, humic substances transporting Fe and Al, Fe oxyhydroxides and organic carbon. However, it was difficult to determine whether these different types of colloids found in the humic-like fraction were truly separate materials or whether they were associated with each other. A Gaussian peak profile did suggest a homogeneous colloid distribution. The carbonate colloids found at depth related to the nature of the soil, which was derived from a carbonated bed-rock.

Graham et al. (2011) characterized soil porewater samples from two DU-weapon testing sites, which were at Dundrennan, Scotland and at Eskmeals, Cumbria, NW England. The

soils from Dundrennan were Fe- and Al-rich clay-loam soils, whilst those from Eskmeals were Fe- and Al-poor sandy soils; both soil types had similar organic contents. Result showed that 80-100% porewaterU was in colloidal form and that the U was split between large (100 kDa-0.2 μm) Fe/Al/humic colloidsand small (30-100 kDa) organic colloids atDundrennan. In contrast, at Eskmeals, although 70-90% porewater U was colloidally associated, a higher proportion was present in the small (3-30kDa) organic colloid fraction, which had little associated Fe/Al, or in the truly dissolved (<3 kDa) fraction.

From the studies described above, it is clear that the conclusions regarding the nature of the colloids and indeed the importance of U colloidal transport vary quite considerably.

Association of U with colloids can either enhance or retard transport in natural systems. For example, U^{IV} is sparingly soluble but formation of intrinsic colloids and/or association with carrier colloids can significantly enhance transport. Although U^{VI} colloids are usually considered to be highly mobile, association with colloids which are only stable under certain conditionsmay significantly inhibit its mobility as a consequence of adsorption, colloid aggregation and/or aggregate sedimentation (Zanker et al., 2007). For example, the soil porewater study by Graham et al. (2011) proposed that association with large Fe/Al/organic colloids was a precursor to removal of U from porewater to the solid phase in clay-loam soils, whilst the association of U with small organic colloids in sandy soils promoted U migration. Indeed, Mibus et al. (2007) reported that the presence of humic acid accelerated U^{VI}, and possibly U^{IV}, migration through soil columns.

For carrier colloid-borne U, the nature of Uinteractions with these colloids must also be taken into account when evaluating migration behaviour. To this end, Rao et al. (1994) reported that there were two binding modes (strong and weak) between actinides and humic colloids: “strong” actinide binding within the coiled humic acid structure was linked with slow dissociation kinetics whilst“weak” actinide binding to peripheral sites had fast dissociation kinetics. Geckeis et al. (2002) compared the dissociation process for colloid-borne U^{IV} and U^{VI}. After 105 days, 43% of U remained associated with natural humic colloids in the desorption experiment, indicating the formation of irreversible binding of at least a part of colloid-borne polyvalent U. They suggested that U^{VI} and U^{IV} states co-existed in association with the humic colloid and that the U^{VI} occurred as ionic carbonato complex. They concluded that U^{VI} dissociation was relatively fast whilst U^{IV} dissociation was inhibited. Finally, the prevailing pH value is another fact that affects the

dissociation of U from humic colloid. Zeh et al. (1997) reported that the sorption of UO_2^{2+} on humic colloids increased at pH 1-4, but desorption occurred at pH>4.5.

As demonstrated above, U association with colloidscan, under certain conditions, facilitate transport from the site of origin and it is important to consider the consequences in terms of U bioavailability. Oliver et al. (2008a) investigated the mobility of DU along a down-sloping transect at the Dundrennan Firing Range in SW Scotland (Figure 1.26) and found that DU was detectable at a distance of ~200 m from the test-firing position with U dispersion attributable to aerial deposition, surface water flow and possibly within-soil transformations. Oliver et al. (2008a) also analysed the earthworms present in soils along the same transect and showed that, in comparison with the soil and even the soil porewaters, earthworms were more highly contaminated with DU (Figure 1.27). This showed that the transported DU was more mobile and bioavailable than natural U and it is likely that the association with soil organic matter is implicated in this process (Oliver et al., 2007; Oliver et al., 2008a; Graham et al., 2008).

Figure 1.26: Photograph of the MoD firing range at Dundrennan showing the downslope transect (solid line) leading from the DU munitions firing pad (arrow) towards a receiving stream (Dunrod Burn, shown by the dashed line)

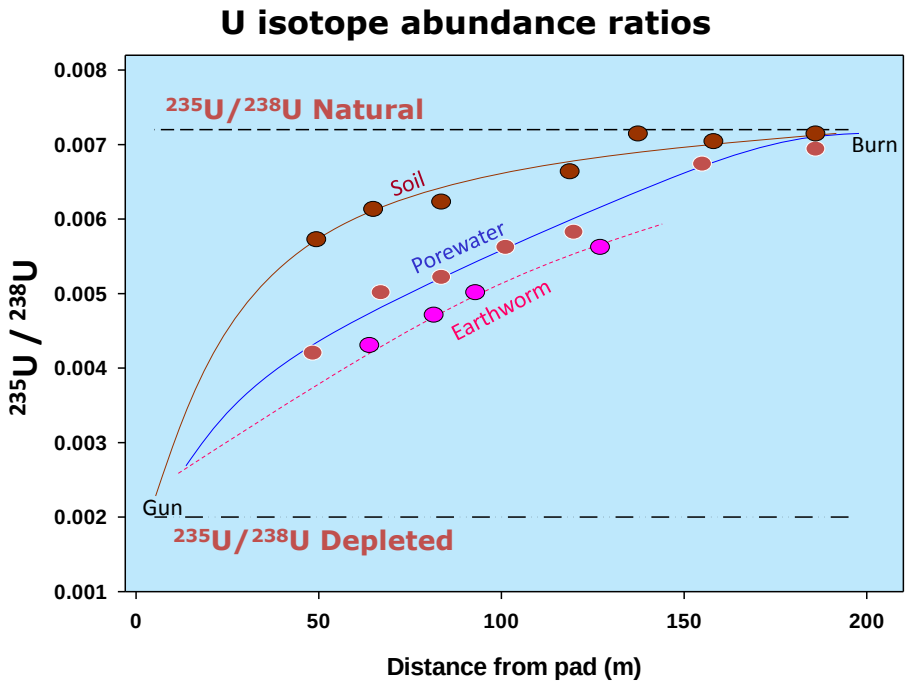

Figure 1.27: $^{235}U/^{238}U$ ratio for soil, soil porewater and earthworms collected along a downslope transect at the Dundrennan Firing Range, SW Scotland (adapted from Oliver et al., 2008a)

As demonstrated in sections 1.4.1 to 1.4.4, understanding U speciation in groundwater and adsorption, precipitation and incorporation, complexation processes involving soil minerals, especially Fe-bearing minerals, and soil organic matter are all key aspects for understanding the migration behavior U insoil systems.Therefore, when U migration behaviour is examined in the natural environment, methods which look at the combined effects of the whole system are preferable to controlled laboratory experiments involving single phases and studying single processes.

With respect to this study, >90% of the U released from the U mineralization at the Needle's Eye natural analogue site has been retained in organic-rich soil by interaction with humic substance in the soil (MacKenzie et al., 1991; Jamet et al, 1993). However, many questions remain to be answered:

(i) after release from the mineralisation, does U become associated with colloids?

(ii) if so, what type of the colloids and does the nature of associations change with migration distance?

(iii) what are the mechanisms of retention ofUby the organic-rich soil?

(iv) if U is directly bound to organic matter, which components of the organic matter are responsible for its retention in the solid phase?

(v) do mineral phases, especially Fe oxides, in the solid phase play a role in U retention?

(vi) what forms of U are not retained by the organic-rich soils?

In section 1.5, different characterization techniques will be evaluated with respect to their potential to determine the solid and aqueous phase U associations in the Needle's Eye soils.

1.5 Methods used to study solid and aqueous phase U associations

1.5.1 Sequential extraction to determine the solid phase associations of U in soils

As described in the preceding sections, trace metals, including U, can interact with different soil components via processes including adsorption, complexation and co-precipitation. It is important to determine the relative importance of these different modes of retention since this information can lead to estimations of potential mobility and availability in the environment. Solid phase physical characterisation techniques such as X-ray diffraction (XRD) spectroscopy and Scanning Electron Microscopy-Energy Dispersive X-ray spectroscopy (SEM-EDX) are widely used to characterise mineral phases but are of limited use in determining U speciation in soils since their detection limits are usually ~1-2% w/w, i.e. 10-20 g U kg^{-1} soil. Instead, chemical methods such as sequential extraction have been used to fractionate the solid phase forms of metal in the soil. This section gives a brief general account of sequential extraction procedures and then focuses on methods which have been developed to determine the role of Fe oxides in binding U in soils.

Sequential extraction consists of multi-step treatment of a soil sample with increasingly aggressive extracts to dissolve selectively targeted components. There have been a wide variety of procedures published in past decades (Tessier et al., 1979; Forstner, 1983; Thomas et al., 1994; Raiswell et al., 1994; Rauret et al., 1999; Poulton and Canfield, 2005). Although some procedures involve a different number of steps, most are variations of the method that Tessier (1979) proposed, which determines trace metal associations with five

fractions: exchangeable, carbonates, Fe and Mn oxides, organic matter and the residual phase. It is generally considered that all the schemes have disadvantages, such as non-exclusivity of extractants for the target fraction (Filgueiras et al., 2002; Bacon and Davidson, 2008) and re-adsorption of extracted metals onto the residual soil (Kazi et al., 2005). However, it can still be a useful method to provide information on trace metal mobility in the environment where careful validation of the methodology has been carried out and with careful interpretation of the results.

Table 1.9 gives details of a sequential extraction scheme that has been used to investigate the associations of U in the organic-rich soils present at the Needle's Eye natural analogue site.

Table 1.9: Sequential extraction scheme used by MacKenzie et al. (1991) to investigate U interactions in organic-rich soils, in which the first four steps were directlyfrom Cook et al. (1984)

Target Phase	**Reagent**
Exchangeable	0.05 M $CaCl_2$
Less readily exchangeable or carbonate bound	0.5 M CH_3COOH
Organically bound	0.1 M $Na_4P_2O_7$
Magnetite and easily reducible oxides, e.g. ferrihydrite and lepidocrocite	0.175 M $NH_4C_2O_4$/ 0.1 M $H_2C_2O_4$
Residual	concentrated HCl, HF, HNO_3

1.5.1.1 Exchangeable metals

Metals extracted in the exchangeable fraction are weakly-bound species retained on the soil surface by relatively weak electrostatic interactions which can be released by anion-exchange process. Cations such as Ca^{2+} and Mg^{2+} (in reagents such as 0.05 M $CaCl_2$ or 1 M $MgCl_2$) can displace the weakly-bound metals and do not attack the silicate, oxyhydroxide phases, organic matter or metal sulphide (Tessier, 1979; Pickering, 1986).

1.5.1.2 Carbonate bound metals

Hydrogen ions released from dilute acetic acid (CH_3COOH) have been found to be less specific than the chloride salts used for the exchangeable fraction since they partly attack

carbonate and silicate (Rapin and Forstner, 1983) in addition to removing exchangeable metals. When used as the second step in a sequential extraction scheme, however, 0.5 M CH_3COOH is used to target less readily exchangeable and carbonate bound metals. The latter may be important when Fe-Mn minerals and organic matter are present at low concentrations (Stone and Droppo, 1996).

In addition to its use by Cook et al. (1984) (Table 1.9), Farrah and Pickering (1993) also used CH_3COOH to extract metals associated with the carbonate fraction from dried lake sediment. However, an alternative reagent used in a number of other studies has been a buffered $CH_3COO^-Na^+/CH_3COOH$ solution but it can also release metals that are specifically sorbed on the surface of clays, organic matter and Fe/Mn oxyhydroxide (Pickering, 1986) and so care is required when interpreting the associations of U when this reagent has been used.

1.5.1.3 Organic bound metals

As mentioned in section 1.2.6.2, sodium pyrophosphate ($Na_4P_2O_7$) and sodium hydroxide (NaOH) can both extract the organically-bound fraction of a soil. With respect to sequential extraction schemes, 0.1 M $Na_4P_2O_7$ is a convenientreagent for organic matter extraction although amorphous Fe oxides are co-extracted at pH 10 during the process (Pickering, 1986). NaOH is usually only applied for the samples of very high amount of organic matter, but it also attacks aluminosilicates and clays (Stevenson, 1982). H_2O_2/CH_3COONH_4 has also been used for extracting organic-bound fraction, but it also removes sulphide at the same time (Calmano and Forstner, 1983). Thus the best reagent may depend on the composition of the soils being investigated.

1.5.1.4 Iron bound metals

A buffered ammonium oxalate/oxalic acid solution (0.175 M $NH_4C_2O_4$/0.1 M $H_2C_2O_4$) has been used in some studies to extract Fe oxides (magnetite and easily reducible oxides such as lepidocrocite and ferrihydrite) (Cook et al., 1984). However, several other studies have used hydroxylamine hydrochloride ($NH_2OH.HCl$) to target only the amorphous Fe oxides (ferrihydrite and lepidocrocite) (Ure et al., 1993; Poulton and Canfield, 2005; Oliver et al., 2008b). To avoid problems with re-adsorption of the released metals, it is often acidified with 25% v/v acetic acid (Gleyzes et al., 2002). A potential drawback is that it has been

suggested that 0.1 M acidified $NH_2OH.HCl$ mainly attacks amorphous Mn oxide rather than amorphous Fe oxide (Shuman, 1982).

As with all the steps discussed so far, the length of extraction time is also important. Tessier et al. (1979) investigated the extraction time and found that the total dissolution of the reducible Fe fraction in sediment occurred within 6 hours but Arunachalam et al. (1996) subsequently purported that this could not be achieved for the high levels of Fe in soil samples. More recently, Poulton and Canfield (2005) demonstrated that a 48-h extraction of 1 M hydroxylamine-HCl effectively dissolved amorphous Fe oxides (ferrihydrite and lepidocrocite) from pure mineral phase and sediment samples, removed a minor amount of akaganeite, and left the remaining Fe minerals almost intact. This was part of a multi-step extraction scheme (Table 1.10) developed and tested by these authors to distinguish between metal interactions with different Fe phases (rather than the single step usually incorporated in most other sequential extraction schemes).

Table 1.10: Sequential extraction scheme developed by Poulton and Canfield (2005) to investigate metal associations with Fe phases in soils

Target Phase	**Reagent**
Exchangeable	1 M $MgCl_2$, pH 7
Less readily exchangeable or carbonate bound	1 M CH_3COONa acidified with CH_3COOH to pH 4.5
Easily reducible (amorphous) oxides, e.g. ferrihydrite and lepidocrocite	1 M $NH_2OH.HCl$ in 25% v/v CH_3COOH
Reducible (crystalline) oxides, e.g. goethite, hematite, akaganetite	50 g/L $Na_2S_2O_4$ acidified with 0.35 M CH_3COOH /0.2 M $NaC_6O_7H_7$ to pH 4.8
Magnetite	0.2 M $NH_4C_2O_4$/ 0.17 M $H_2C_2O_4$, pH 3.2
Poorly reactive sheet silicate Fe	Boiling 12 M HCl
Residue, e.g. pyrite and unreactive silicate Fe	Concentrated HF, HBF_4 (Yafa and Farmer, 2006)

The first three steps are exchangeable, carbonate bound and associated with amorphous Fe oxides and the reagents used are 1 M $MgCl_2$, 1 M CH_3COONa acidified with CH_3COOH to pH 4.5, and 1M $NH_2OH.HCl$ in 25% v/v CH_3COOH, all of which have been discussed in the preceding paragraphs.

The next step uses sodium dithionite, a strong reducing reagent that can reduce both crystalline and amorphous Fe oxide phases. Acetic acid is added to buffer the pH and stabilize the oxidation potential while sodium citrate is applied to avoid FeS precipitation (Gleyzes et al., 2002). During method development, Poulton and Canfield (2005) used a single dithionite extraction to test its efficiency for dissolving Fe (oxyhydr)oxides. The results showed the quantitative dissolution of ferrihydrite, lepidocrocite, goethite, hematite, akaganetite, as well as 5-7% of magnetite (Table 1.11). Thus, sodium dithionite can be used after hydroxylamine hydrochloride to selectively remove only the crystalline oxides.

It has been shown that ammonium oxalate efficiently extracts amorphous Fe oxide in addition to the crystalline oxide magnetite (Canfield, 1988). Used after hydroxylamine hydrochloride, however, it can selectively remove magnetite ($Fe^{II}Fe^{III}_2O_4$). The oxalate reagent effectively complexes Fe with log K ranging between 4.35 and 18.49 for Fe^{3+} and between 3.20 and 5.15 for Fe^{2+} (Gleyzes et al., 2002). A major disadvantage is that it also forms strong complexes with Al (log K=15), so it can be hard to distinguish whether the trace metals present in this extract are associated with Al oxides or Fe oxides (Shuman, 1982). It has also been found to complex Fe from organic complexes (Chao and Zhou, 1983).

According to Table 1.11, when extraction sequences of hydroxylamine, dithionite, oxalate are considered for targeting Fe phases, the fact that dithionite can extract 4.1-5.1% magnetite would suggest that hydroxylamine extraction should be followed by oxalate extraction in order to gain a more targeted extraction of magnetite in the sediment. However, the presence of dissolved Fe(II) during oxalate extraction can catalyse dissolution of crystalline ferric oxyhydr(oxide), and the extent of dissolution depends on the amount of Fe(II) released (Suter et al., 1988). Thus, the optimal extraction sequence is in the order of hydroxylamine, dithionite, oxalate.

Table 1.11: A comparison of the concentrations of Fe (in wt.% removed by different reagents (for optimum extraction order) (Poulton et al., 2005).

Mineral	Total	Na acetate pH 4.5, 24 h	Hydr.–HCl 48 h	Dithionite 2 h	Oxalate 6h
$FeCO_3$ (syn.)	46.2	46.2	ND	ND	ND
Roxbury siderite	28.9	24.4	ND	ND	ND
Biwabik siderite	22.3	12.3	ND	ND	ND
Ankerite	13.9	13.6	ND	ND	ND
Ferrihydrite	54.7	0.95	54.2	54.7	54.2
Lepidocrocite	62.8	0.85	61.9	62.9	62.8
Akaganéite	63.1	0.08	2.44	63.2	2.37
Goethite	62.8	0.02	0.05	62.8	0.60
Hematite	69.8	<0.001	0.05	65.7	0.30
Magnetite (syn.)	72.3	0.01	0.34	5.1	72.3
Magnetite (nat.)	72.3	0.01	0.41	4.1	72.0
Nontronite	22.7	0.003	0.34	3.5	0.24

ND=not determined.

Finally, Raiswell et al. (1994) compared the solubility of a variety of Fe minerals in ditihionite and boiling 12 M HCl and reported that HCl extracts greater amounts ofFe from silicates. HF and HBF_4 are normally used in the mixture to dissolve silicates that are present in the samples but these acids can also dissolve any remaining mineral material and total dissolution is usually achieved (Krachler et al., 2002; Yafa and Farmer, 2006). Thus HF or HBF_4 can be used as a final step in order to attain a mass balance for U and other metals in soils.

1.5.2 Determination of U associations with soil porewater colloids

Most methods used to isolate colloids from aquatic systems involve a filtration step to remove suspended particulate matter (e.g. 0.45 µm or 0.2 µm membrane) and then one of a number of approaches including asymmetrical flow field-flow fractionation (A4F), nanofiltration (NF) or reverse osmosis, tangential flow (or cross-flow), ultrafiltration and centrifugal ultrafiltration.

A4F-fractionation has been used in a number of recent studies of U-colloid associations (Jackson et al., 2005; Ranville et al., 2007; Claveranne-Lamolère et al., 2009). Ranville et al. (2007) studied U associations with dissolved organic carbon in clay-rich aquitard porewaters using A4F coupled with ICP-MS and UV spectroscopy. Following UV

detection, direct input to an ICP-MS enables quantification of Ucomplexed with different humic colloid fractions. However, 10-50% of the DOC in the porewaters was lost during the fractionation and the detection limits for total Uwere calculated to be ~50 μg L^{-1}. Although it was concluded that U transport by humic colloids was unimportant at pH>7, the possibility remained that U could be transported by low molecular weight ligands that would be lost through the membrane. In addition, the colloids that are retained cannot be recovered for further experimentation.

In contrast to A4F, nanofiltration (NF) membranes have been shown to retain 81-99% U in direct groundwater treatment (Raff and Wilken, 1999). Rossiter et al. (2010) analysed the factors that are likely to affect U removal from brackish groundwater using a NF and reverse osmosis (RO) membrane. They concluded that the retention by the membrane was caused by adsorption at pH 4-7 and co-precipitation with Ca at pH 10-11. However, this technique can not readily be applied to samples that contain organic colloids since they often cause fouling of the membranes (Shäfer et al., 1998).

Tangential flow ultrafiltration and centrifugal ultrafiltration techniques have been used where additional colloid characterisation as well as quantification of U-colloidal interactions is a requirement of the study. Tangential flow methods are predominantly used where large volumes of water require to be analysed, e.g. low concentrations of U in seawater, lake water etc. Centrifugal ultrafiltration is more suited to small water volumes such as those typically encountered in studies of U associations in soil porewaters (e.g. Graham et al., 2008, 2011). Ultrafiltration and gel filtration methods used to isolate and fractionate colloids in aquatic systems were briefly mentioned in sections 1.2.7 and 1.4.4. The paragraphs which follow consider in more detail the advantages as well assome of the artefacts that need to be avoided during colloid isolation and fractionation by ultrafiltration.

There are several advantages relating to the use of ultrafiltration to isolate and fractionate soil porewater colloids. The procedure is very simple, and requires no additional separation media and auxiliary reagents, which are commonly used in, for example, (i) the isolation of colloidalhumic acids and fulvic acids, e.g. macroporous ion exchange resins DAX-8 and XAD-4 and mineral acids (e.g. Aiken et al., 1992); (ii) the fractionation of porewater colloids using AF4, e.g. carrier solutions such as 0.001 M NaCl + 0.003 NaN_3 (Ranville et al., 2007).

There is also evidence supporting the reproducibility of separations and for the minimal chemical compositional alteration of humiccolloids (Burba et al., 1998). However, a considerable number of concerns have also been raised. Guo et al. (2007) reported that up to 30-60 % low molecular weight dissolved U species (<1 kDa) were retained on a 1 kDa ultrafiltration membrane as an artefact retentate through preferential rejection by negatively charged membranes. The membrane comprised regenerated cellulose material which had been pre-cleaned with 0.05 M NaOH and 0.02 M HCl (Guo and Santschi, 1996). Large volumes (~20 L) of estuarine waters were ultrafiltered through the micon cartridges while small volumes (~500 mL) were filtered through a stirred cell membrane disk. Since the high colloidal U concentrations were attributed to erroneous retention, colloids play only a very minor role in transporting U in such systems. The results showed only a low colloidal association of U in the estuarine waters.

As for nanofiltration, humic acid fouling can be a concern during ultrafiltration. Susanto and Ulbricht (2006) modified a polyethersulfone (PES) ultrafiltration membrane by simultaneous photograft copolymerization of polymethacrylate onto PES membrane to reduce the humic acid fouling. Humic acids, especially those that have been commercially produced, e.g. Aldrich humic acid, are more prone to cause membrane fouling than, for example, humic colloids present in natural waters. Nevertheless, it is important to carefully evaluate the efficacy of such fractionation methods even for soil porewater colloids. For example, Graham et al. (2008) used ultrafiltration (PES membrane) to fractionate colloids into three fractions, 100 kDa-0.2 µm, 30-100 kDa, 3-30 kDa, and separate them from the truly dissolved fraction (<3 kDa). They investigated whether: (i) the resulting fractionation may have been method-dependent; (ii) artefacts had been generated during separation, e.g. fluorescent components may have come from the ultrafiltration membrane material itself; (ii) the membrane caused retention of dissolved metals because of charge effects (as in Susanto and Ulbricht, 2006; Guo et al., 2007). It was demonstrated that none of these problems had arisen. However, the 100 kDa ultrafilter did not efficiently separate higher molecular weight molecules from <100 kDa molecules as it was observed that some molecules in the 3-30 kDa size range had been retained. The results of this study emphasised the importance of using multiple fractionation methods to characterise the U interactions with humic colloids within the soil porewater.

1.5.3 Determination of U associations with fractionated humic substances

Most methods for determining U interactions with solid phase soil humic substances require pre-extraction of the organic matter. The methodology relating to extraction of bulk humic substances has been covered in section 1.2.6.2 and so sections 1.5.3.1-2 deal with techniques used to characterise U interactions with fractionated humic substances from both solid phase humic extracts and isolated porewater colloids.

Techniques such as X-ray photoelectron spectroscopy (XPS) (Memon et al., 2009) and U L_3-edge X-ray adsorption spectroscopy (XAS) (Regenspurg et al., 2010) have been used to study those interactions. There have been reports that XAS can probe the local atomic environment around U atoms at environmentally relevant concentrations (Kelly, 2010) but its detection limit is still ~0.1% w/w (Francis et al., 2004). XPS is another technique for defining the elemental composition of a solid's outer surface (van der Heide, 2011), but it requires elemental concentration to be at least ~1% w/w. Thus although some bulk soil samples at Needle's Eye might be suitable for XAS or XPS analysis, it was considered that these methods were unlikely to be useful for studying U associations with fractionated humic extracts from the soils. Instead, gel filtration and gel electrophoresis were used in conjunction with ICP-MS analysis.

1.5.3.1 Gel filtration chromatography

Gel filtration (or size exclusion) chromatography (GFC or SEC) is a simple and relatively effective method to fractionate humic molecules into different size ranges. Porous gel with carefully controlled ranges of pore sizes are typically suspended in an aqueous (e.g. 0.1 M NaOH or deionised water) solvent (Figure 2.28). When additional solvent is passed through the column, humic molecules which are too large to enter any pores are excluded from the gel and emerge from the column first (defining the exclusion limit). Molecules which can enter all of the gel pores can access the entire column volume and emerge at the permeation limit. Assuming no interactions between the humic molecules and the gel, those with sizes in between the exclusion and permeation limits are then fractionated according to size.

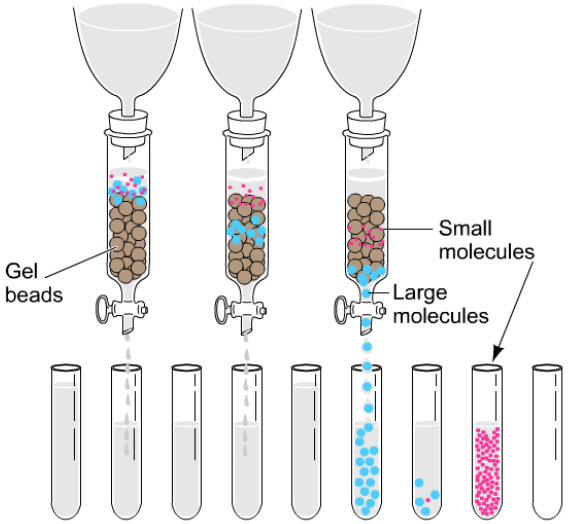

Figure 1.28: Separation of molecules according to size on a gel filtration column (www.wiley.com/college/fob)

However, careful interpretation of the separation achieved by such columns requires consideration of possible exclusion effects which are not related to molecular size. The dissociated functional groups on humic substances cause intra-molecular electrostatic repulsion, which leads to stretching of the molecule. These electrostatic forces are affected by ionic strength due to the presence of cationic species and ion-pairing agents. For example, at low ionic strength, the forces are especially important and so molecules which are smaller than the exclusion limit may co-elute with larger excluded molecules. At high ionic strength the intra-molecular forces are masked to a large extent and so the effective size of the molecules is decreased; thus larger ones may actually enter the gel pores and appear to be fractionated by the column. Therefore, the same molecule with certain molecular mass may elute at different times depending on the medium and experimental condition. Thus, the molecular masses of humic substances measured by SEC are operationally defined rather than true values (Janos, 2003). In addition, the SEC separation is further complicated by the nature of humic substances as will be discussed in the paragraph below.

There are further two problems relating to humic substance separations using SEC: (i) coulombic forces (ion-exchange or ion-exclusion interactions between the solute and stationary phase) and (ii) adsorption or reversed phase partitioning (Swift and Posner, 1971; Ralph and Catcheside, 1996). It is known that dextran gel such as Sephadex contains residual carboxyl groups, and their ionization generates negative charges on the polymer

chains. Humic substances also bear ionizable carboxyl and phenolic groups, therefore a charge exclusion effect occurs between the gel and the humic substances. This means that, under low ionic strength conditions, small molecules may co-elute with excluded molecules. Phenolic groups are known to adsorb reversibly to dextran gel via the formation of hydrogen bonds. This effect, which leads to the retardation of the adsorbed molecules is particularly marked when distilled water is used as eluent (Swift and Posner, 1971). Both of these problems are more important for dextran gels which have lower size cut-off values, i.e. have a greater degree of cross-linking. For example, Graham (1995) demonstrated that while no effect was observed for a G200 gel (MWCO = 200 kDa), strong retardation effects were demonstrated for a G25 gel (MWCO = 5 kDa).

Overall SEC using 0.1 M NaOH as the eluent can be used with care to compare the relative size of components of humic substances. Water can be used as an eluent where it is recognised that additional mechanisms may affect the separations that are achieved. For example, Graham et al. (2008) used gel filtration as a complementary size fractionation method for comparison with the separations achieved by electrophoresis and ultrafiltration in the investigation of DU interactions with porewaterhumic colloids (3 kDa-0.2 μm) with deionised water as eluent during the SEC process. Results showed that the two humic bands separated by SEC were consistent with the electrophoretic distribution pattern and with the proposed mechanism of separation achieved by ultrafiltration. Clearly deionised water can be used for SEC separation of porewater humic colloids, but for humic substances from solid phase samples, other eluents such as borate buffer or alkaline buffer are recommended to ensure that all components remain in solution and to eliminate coulombic interactions and adsorption or reversed phase partitioning effects (Swift and Posner, 1971).

UV-Vis spectroscopy is still the most commonly used detection method for humic substances separated by SEC because of its simplicity and sensitivity. UV absorbance in the region 220-280 nm is used as a measure of humic substance concentration (Zhou et al., 2000; Graham et al., 2008).

1.5.3.2 Gel electrophoresis

Electrophoresis is a technique based on the use of migration of electrically charged particles or ions under application of an electric field between an anode and cathode. There

are several electrophoretic methods which have been used to characterise humic substances and/or humic interaction with metals. These include isoelectric focusing (IEF), isotachophoresis, polyacrylamide gel electrophoresis (PAGE) and agarose gel electrophoresis.

Isoelectric focusing (IEF), carried out in a pH gradient, has been used to study the organic matter extracted from soil (De Nobili et al., 1990; Alianiello and Fiorelli, 1998; Alianiello, 2003). IEF separation is a technique for separating molecules by their different isoelectric point. A medium of amphoteric electrolytes is firstly electrophoresed through a gel to establish a pH gradient under an electric field. Then the molecule mixtures move through the gel until they reach their isoelectric point (pI) in the pH gradient. The pI of any molecule is defined as the specific pH at which it does not bear any electrical charge. Molecules become focused into well-defined, sharp zones at pH values corresponding to their specific isoelectric point (Garfin and Ahuja, 2005). This technique separates humic molecules mainly based on the pK_a of their acidic functional groups (Duxbury, 1989). IEF has been extensively used for characterizing humic substances (Cavani et al., 2008; Karim et al., 2013), and seldom used for characterization of metal-humic acid interaction. Jimenez et al. (2010) for the first time used IEF as separation technique with LA-ICP-MS (laser ablation-inductively coupled plasma mass spectrometry) as detection system to successfully study the distribution of metal-humic acid complexes in environmental samples. It provided two main humic regions: (A) with $3<pI<4.5$ and (B) with $pI>5$, with the biggest metal signals found in region A.

Isotachophoresis is carried out in a discontinuous buffer, including a leading electrolyte with a high mobility ion and terminating electrolyte with a low mobility ion. In theory, the mixed molecules migrate between the electrolytes and get separated into pure zones of individual substances according to different mobilities (Krivankova et al., 1996). Isotachopherograms of humic substances comprising up to 18 zones have been achieved by capillary isotachophoresis, which used a chloride solution as leading electrolyte and a caproate solution as terminating electrolyte (Kopacek et al., 1991). However, it is possible that those zones were not pure and the mixed zones couldn’t be attributed to any specific humic fraction. The capillary isotachophoresis technique to separate humic substances was improved with the application of discrete spacers (inorganic and organic acid, amino acid of suitable acid-base and migration properties exhibiting no light adsorption in the UV-region of the light spectrum) and photometric detection (Nagyova and Kaniansky,

2001).

Polyacrylamide gel electrophoresis (PAGE) has been used to fractionate the humic substances into four discrete bands according to different electrophoretic mobility (Trubetskoj et al., 1991). PAGE in the presence of urea was also used to check the purity of humic acid fractions obtained by SEC or ultrafiltration (Trubetskoj et al., 1997), and the results indicated that SEC gave a better separation of humic acid than ultrafiltration. More recently, the technique has been applied in conjunction with other techniques, e.g. SEC and laser ablation-inductively coupled plasma mass spectrometry, to characterise humic substances (Cavani et al., 2008) and metal-humic acids (Jimenez et al., 2010), respectively.

The use of agarose gel in horizontal bed gel electrophoresis is in many ways similar to that described for polyacrylamide gel electrophoresis. The difference between them is simply that the pore size of the agarose gel (up to 0.1 μm for a 1% w/v agarose gel) is relatively large compared to polyacrylamide gel. This enables a wider range of natural humic molecules to enter the gel and thus be fractionated. It can also be used directly to isolate and fractionate humic substances from soils. Graham et al. (2000) demonstrated that direct extraction and fractionation of more than 70% of the ^{238}U-humic complexes extracted by 0.1 M NaOH can be attained using agarose gel electrophoresis (0.05 M Tris-HCl loading buffer/1% agarose/20 mA/60 min). The fractionation only method has also been applied in an initial investigation of Cr interactions with humic substances from contaminated ultrafiltered groundwaters and showed that free Cr^{VI} migrated more rapidly than humic-Cr^{III} material in the gel (Farmer et al., 2002). More recently, Graham et al. (2008) used gel electrophoresis to evaluate the interactions between DU andhumic substances in soil porewaters. The separations achieved by electrophoresis were in good agreement with those achieved by ultrafiltration and by gel filtration chromatography, giving additional confidence in this approach. In this study, gel electrophoresis will be used not only to fractionate the humic substances, but the approach will be developed further to investigate the metal interactions with the different humic fractions.

1.6 Summary

With the pressure on freshwater resources, U contamination in groundwater is becoming an increasingly important environmental issue with respect to potential impacts on human health. In addition, concerns about the safety of long-term deep repositories and the

potential for U to be released into the far-field environment reinforce the need to fully understand its migration behaviour. It is well-known that U interacts strongly with organic matter and, since many rural areas in the UK have organic-rich surface soils, an improved understanding of the mechanisms of U retention by solid phase organic matter or, alternatively, of U stabilisation in the aqueous phase would be beneficial. The interactions of U with mineral phases, especially Fe oxides, have been heavily studied under laboratory conditions and it is also well-known that organic matter forms coatings on the surface of such oxide phases. The relative importance, however, of U binding to organic matter and to Fe oxides, under natural conditions is not yet well understood. In natural systems there are also many other parameters that must be taken into account, including pH, pCO_2, redox status, Ca^{2+} concentration etc.. These may: (i) influence the speciation of the aqueous phase U; (ii) affect interactions between U and the solid phase; (iii) change the nature of solid phase. Finally, there are many methods which can be used to study U behaviour but it is important to select and carefully evaluate appropriate methods for characterising its interactions in natural soil systems.

1.7 Aims and Objectives of this Study

For the organic-rich soils at the Needle's Eye Natural Analogue site, the overarching aims of this study were to:

(i) provide an improved understanding of U speciation in groundwaters and soil porewaters and of U associations in solid phases of the soils with increasing distance from a U mineralisation;

(ii) develop a mechanistic understanding of the processes by which U is transferred from the aqueous to the solid phase.

The specific objectives were to:

(i) characterise the interactions of U with soils from different depths and with increasing distance from the mineralisation using a range of extraction and characterisation techniques, e.g. 0.1 M NaOHhumic extraction/gel chromatography/ICP-MS, sequential extraction/ICP-MS, acid digestion/ICP-MS;

(ii) develop novel methods combining sequential extraction, humic extraction and gel electrophoresis/ICP-MS in order to differentiate between U interactions with mineral and organic components of the solid phase;

(iii) determine the distribution of U amongst colloidal and dissolved components of groundwaters and soil porewaters using ultrafiltration/ICP-MS;

(iv) apply the novel methods described in (ii) to evaluate U interactions with mineral and organic colloids;

(v) use data for an extended transect from the mineralisation through the organic-rich soils, establish mechanisms by which U is being removed to the solid phase and identify U binding components which remain in the aqueous phase.

2 Sampling Site Description and Experimental Methods

2.1 Introduction to the Needle's Eye natural analogue site, SW Scotland

The Needle's Eye Natural Analogue Site is located in the vicinity of the town of Dalbeattie on the north shore of the Solway Firth at Southwick, SW Scotland (Figure 2.1). Needle's Eye itself is a natural arch formed by coastal erosion of an ancient cliff, with uranium occurring in polymetallic-carbonate breccia veins in the cliff. This area is mainly underlain by strongly folded Silurian sediment rocks which were locally hornfelsed. The Criffell granodiorite, a late Caledonian body, is the main intrusive body in the area, which had intruded into the Silurian sediments, faulted against downthrown Carboniferous strata. This faulting marks the line of the cliff and Southwick Water, following a northwest (NW) to southeast (SE) direction. At this location groundwater, flowing from NW to SE originating from the cliff emerges at the cliff base before flowing towards the Southwick Water (Jamet et al., 1993; MacKenzie et al., 1991).

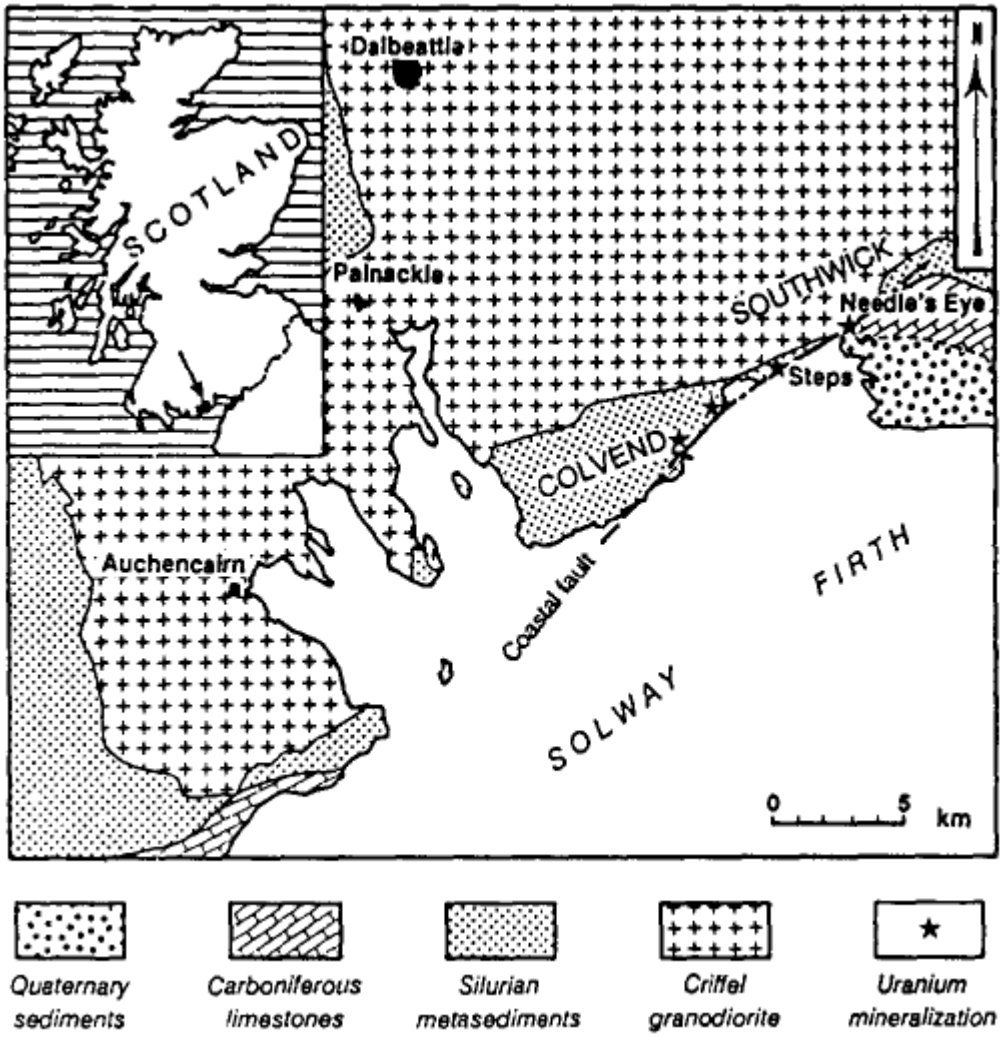

Figure 2.1: Map showing the locationand geology of Needle's Eye Natural Analogue Site, and the black arrow in the insert-map showing the location of Needle's Eye in Scotland (Jamet et al., 1993)

Uranium is present within the vein in the form of pitchblende (UO_2) in association with secondary phases such as uranophane (Ca-U-silicate). Since the groundwater is oxic, it oxidizes some of the U^{IV} to U^{VI}, leading to its dissolution in the groundwater and brings it down to the base of the cliff, where there is a quaternary sediment deposit composed mainly of quartz-rich silts with a variable minor to subordinate amount of clay and humic debris (Figure 2.2). However, previous research has shown that 80-90% of U has been retained in the organic-rich layer so that very little flows into the Southwick Water. The organic-rich anoxic soil is of about 1 m depth, and extends outward for a distance of 30 m from the base of the cliff (Hooker, 1990; Jamet et al., 1993; MacKenzie et al., 1991).

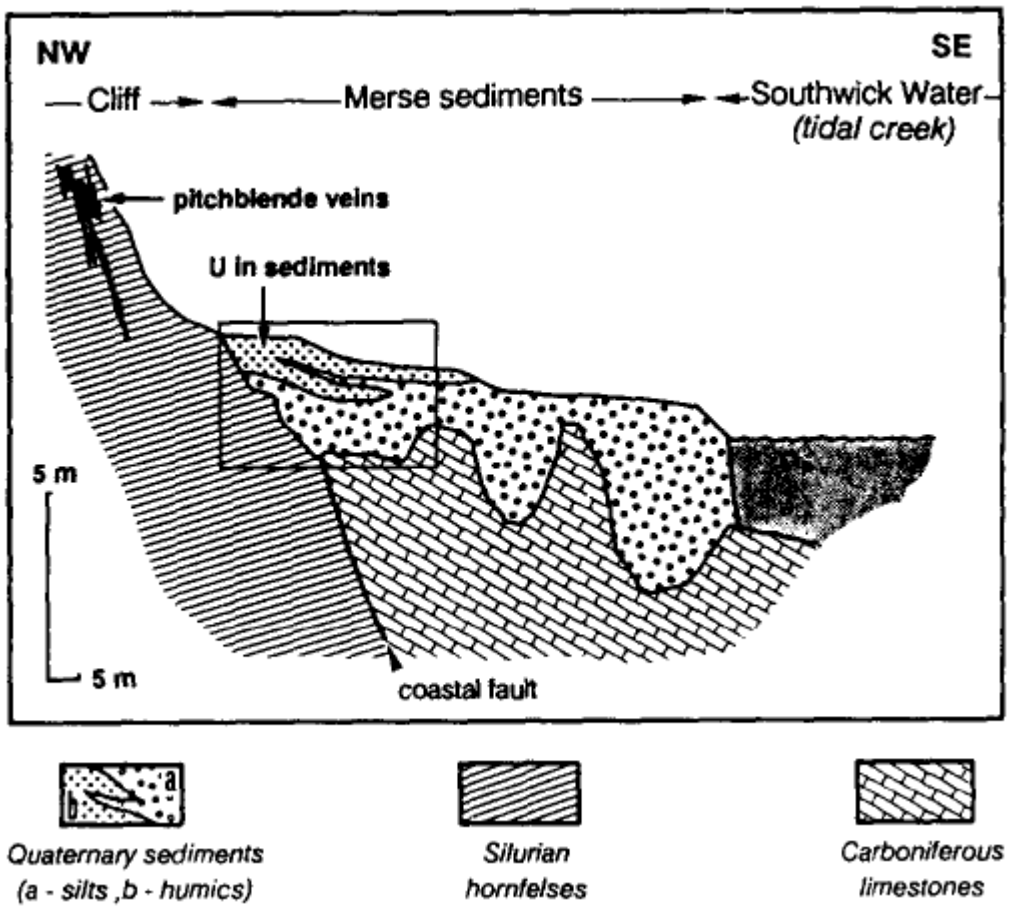

Figure 2.2: Uranium mineralisation at Needle's Eye (Jamet et al., 1993)

The soluble U^{VI} complexes originating from pitchblende mineralisation in the cliff are transported into the organic-rich soil via surface flow from the cliff and groundwater flow from the underlying rocks (Figure 2.3). Surface waters pass through the organic-rich soils before flowing into the Southwick Water (red arrow in Figure 2.3). The situation for the groundwater flow is more complicated. The high flow at the base of the sediment near the cliff had the highest hydraulic pressure, imposing a horizontal vector on the flow. The hydraulic pressure drives the groundwater flow toward Southwick Water (blue arrow in Figure 2.3) (Hooker, 1990; Jamet et al., 1993; MacKenzie et al., 1991).

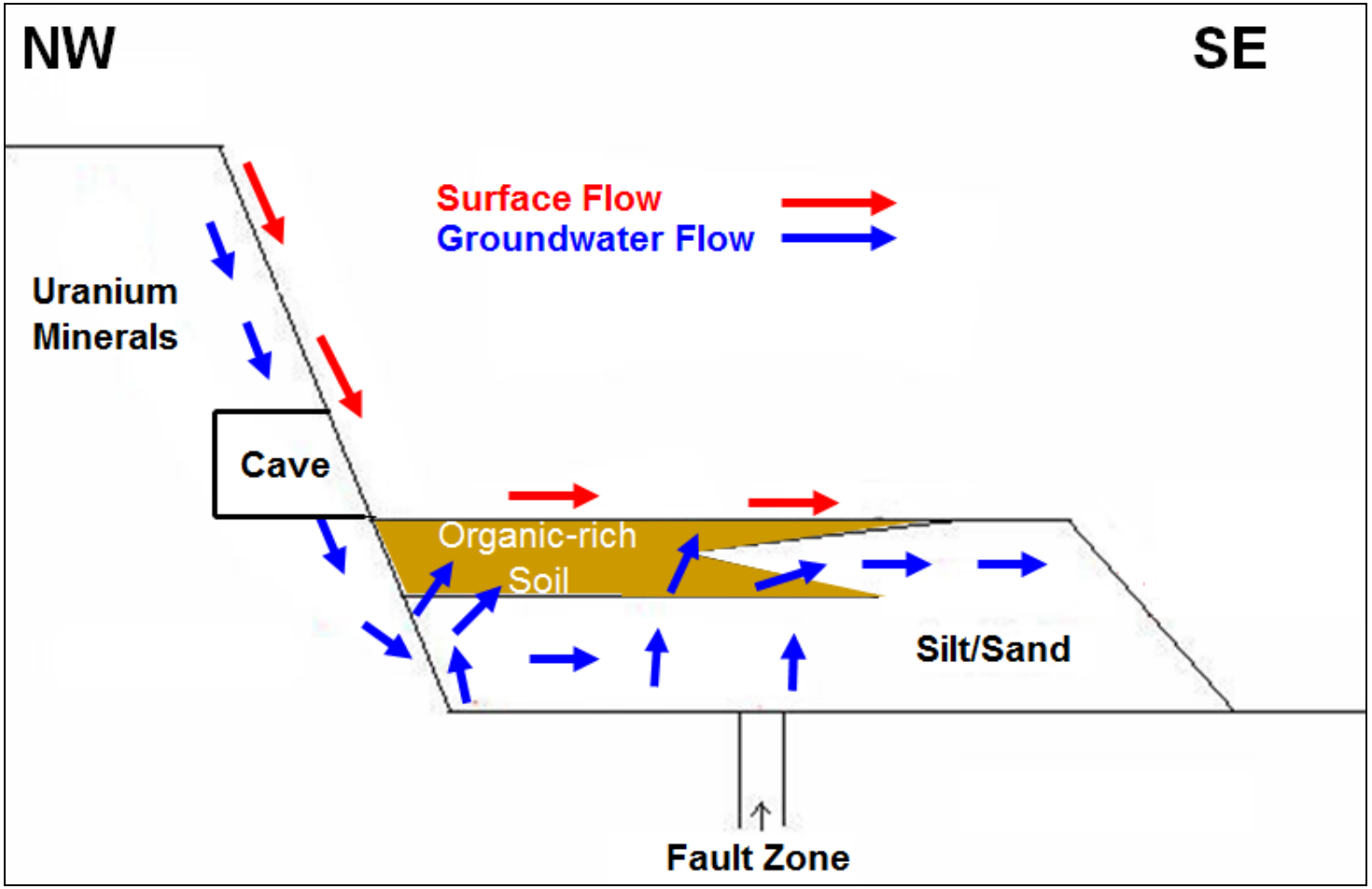

Figure 2.3: Overview of Needle's Eye sampling location (adapted from Jamet et al., 1993)

2.2 Sample collection

The sampling strategy focused on the area situated on a NW-SE line between the cave in the cliff and the organic-rich soils at the base of the cliff in the direction of the Southwick Water. Waters emerging in a cave at the base of the cliff were collected on several occasions during the sampling period. In addition, soil cores and transect surface soils, along with their associated porewaters and other groundwaters, were selectively collected from an area stretching some 30 m from the base of the cliff (see Tables 2.1) so that the U behaviour in solution and solid phase could be studied. Since (i) measurements relating to U and other elemental associations in porewaters need to be carried out rapidly in order to minimise sample alteration; (ii) there is a limit to the number of samples that can be processed in short periods of time; (iii) volumes of porewaters may be small, multiple sampling trips were required during this study. While some general parameters were determined on each trip, other procedures were developed to address specific questions that arose from the results of preceding trips.

2.2.1 Collection of water emerging from the mineralisation

Within the cave, water emerges from the rock and often drips slowly onto the ground. The U concentration in the drip waters has been shown to be influenced by the water flow rate (MacKenzie et al., 1991). All cave drip water samples were collected in cleaned (see nitric acid wash in Section 2.5.1) and labelled polyethylene bottles (Figure 2.4).

Figure 2.4: Cave drip water collection

Table 2.1: Sample ID and corresponding information (sampling date, description, distance from mineralisation, dimensions, core sectioning) for all samples

Sampling date	Sample ID	Description	Distance from cave (m)	Dimensions of the core cm depth x cm x cm	Thickness of each core slice (cm)
Trip1 11/12/2007	Cave drip water 1	Water from front cave	0	-	-
	Cave drip water 2	Water from back cave left hand side	0	-	-
	Cave drip water 3	Water from back cave right hand side	0	-	-
	Core 1	Soil core and porewaters	20	45 x 15 x 11	5
	Bog water 1	Water at the bottom of pit 1	20	-	-
	Core 2	Soil core and porewaters	30	42 x 15 x 11	5
	Bog water 2	Water at the bottom of pit 2	30	-	-
Trip2 02/10/2008	Cave drip water 4	Water from back cave left hand side	0	-	-
	Cave drip water 5	Water from back cave right hand side	0	-	-
	Core 3	Soil core and porewaters	20	44 x 15 x 11	3
	Bog water 3	Water at the bottom of pit 3	20	-	-
	Core 4	Soil core and porewaters	25	36 x 15 x 11	3
	Bog water 4	Water at the bottom of pit 4	25	-	-
	Core 5	Soil core and porewaters	35	20 x 15 x 11	5
	Bog water 5	Water at the bottom of pit 5	35	-	-
Trip3	Cave drip water 6	Water from back cave left hand side	0	-	-

26/10/2010	Cave drip water 7	Water from back cave right hand side	0	-	-
	Core 6	Soil core porewaters	20	48 x 15 x 11	2
	NE1	Surface soil porewaters	1	5 x 15 x 15	5
	NE2	Surface soil porewaters	11		
	NE3	Surface soil porewaters	14		
	NE4	Surface soil porewaters	17		
	NE5	Surface soil porewaters	24.5		
	NE6	Surface soil porewaters	27.5		
	NE7	Surface soil porewaters	30		
Trip4 21/06/2011	Cave drip water 8	Water from back cave left hand side	0	-	-
	Cave drip water 9	Water from back cave right hand side	0	-	-
	Core 7	Soil core porewaters	25	40 x 15 x 11	1
Trip5 11/10/2011	Core 8	Soil core porewaters	25	-	~2.5-3

[Table 2.1: Sample ID and corresponding information (sampling date, description, distance from mineralisation, dimensions, core sectioning) for all samples ….ctd.]

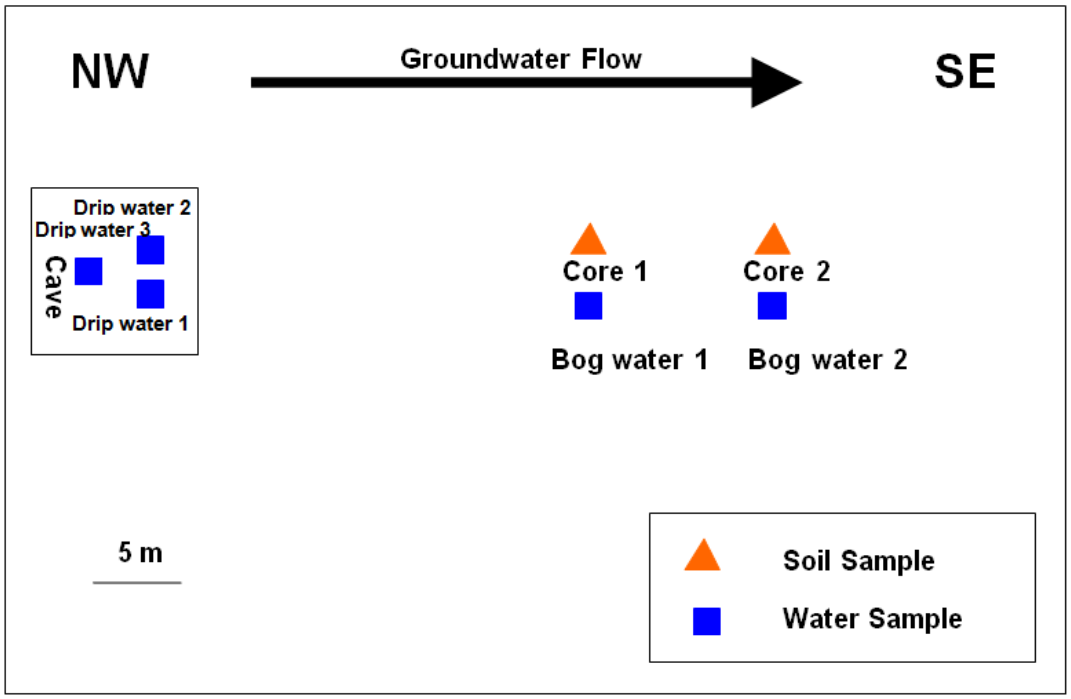

Figure 2.5: Map showing location of samples collected on 11/12/2007 (trip 1)

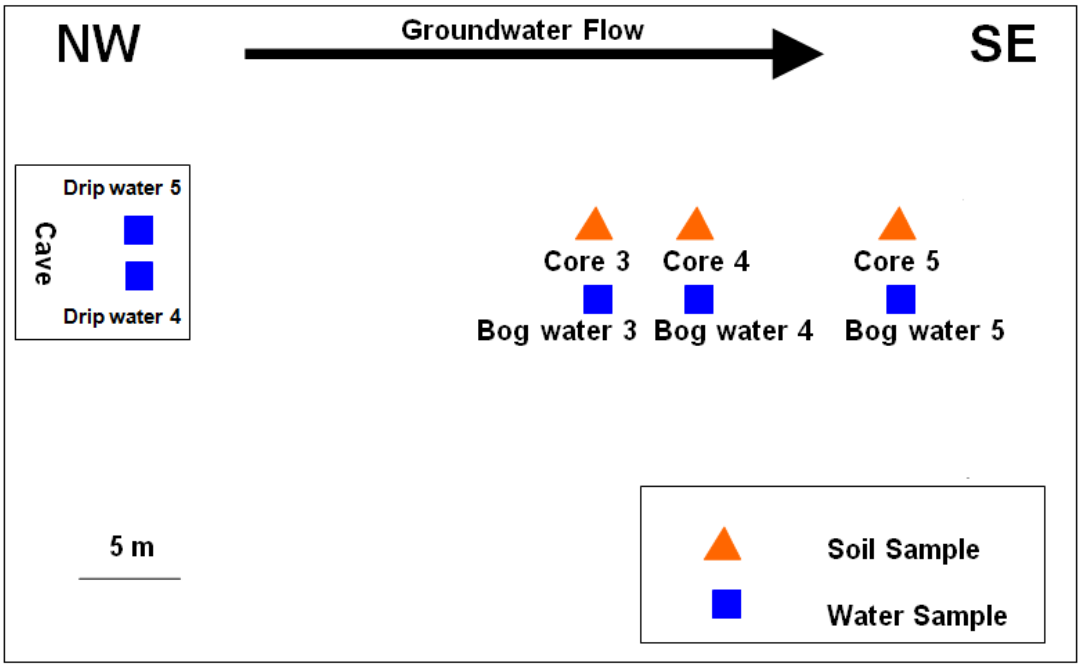

Figure 2.6: Map showing location of samples collected on 02/10/2008 (trip 2)

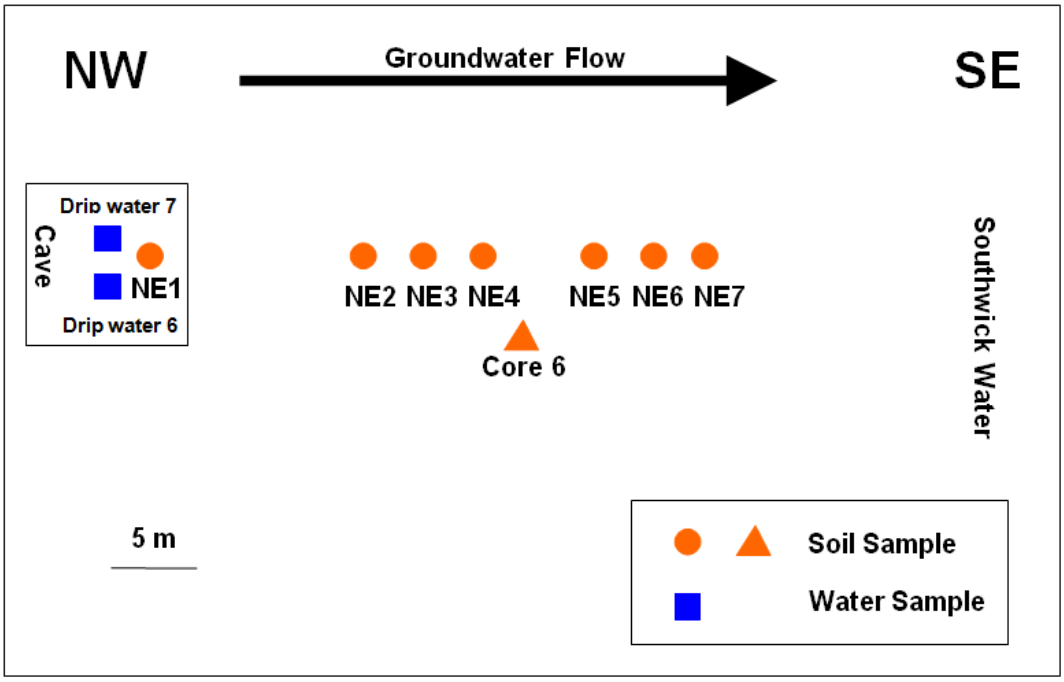

Figure 2.7: Map showing location of samples collected on 26/10/2010 (trip 3)

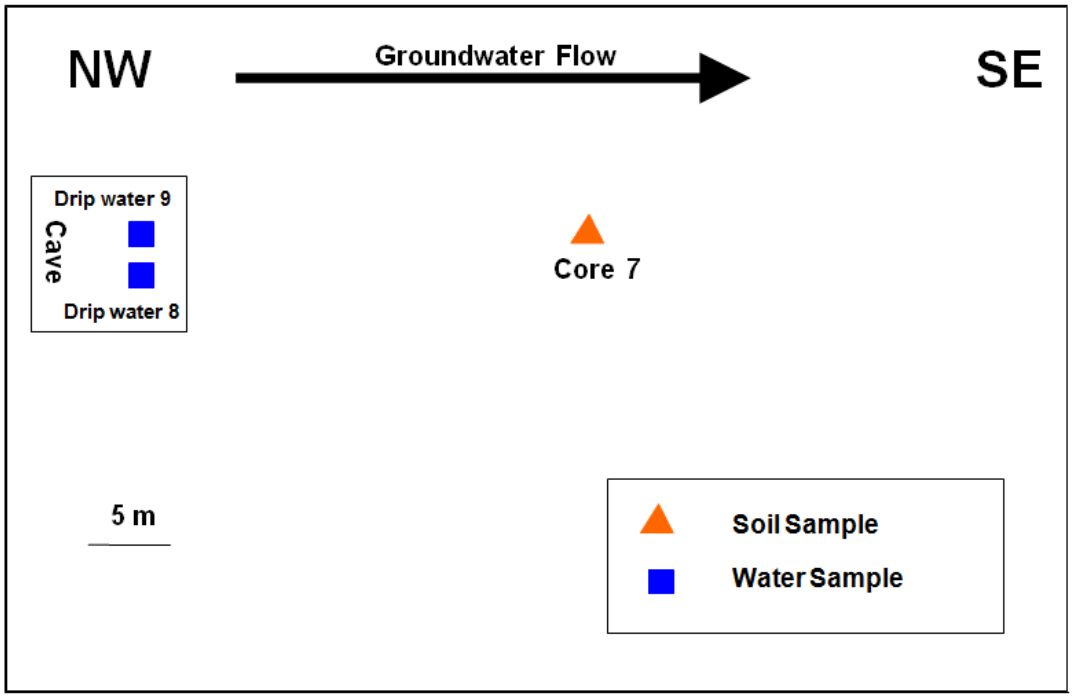

Figure 2.8: Map showing location of samples collected on 21/06/2011 (trip 4)

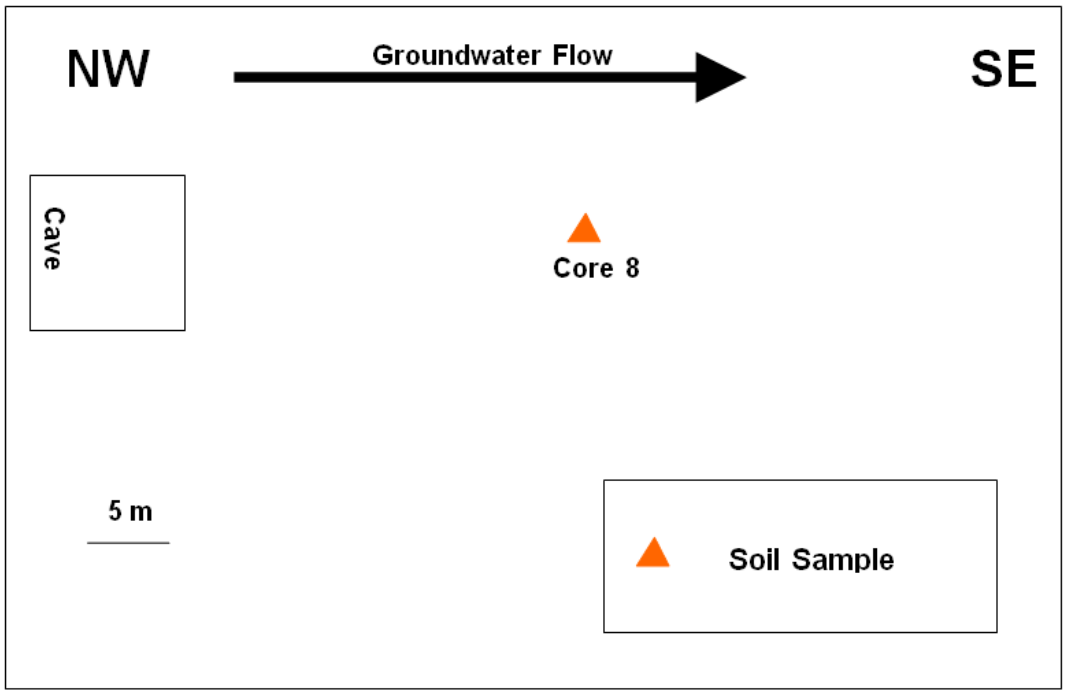

Figure 2.9: Map showing location of samples collected on 11/10/11 (trip 5)

2.2.2 Collection of soils from the organic-rich zone extending from the mineralisation towards Southwick Water

There were five sampling trips during 2007 to 2011. Table 2.1 shows the sample ID and descriptions for each trip (Table 2.1). Figures 2.5-2.9 shows the location of each sampling site during the five trips.

Cores 1 to 7 were collected using a 50 x 7 x 15 cm monolith tin. A spade was used to excavate a 50 x 30 x 30 cm pit and the monolith tin was placed vertically against one of the pit walls and hammered into the soil using a wooden mallet. A kitchen knife was used to remove soil around the outside of the tin and the spade was then used to assist the removal of the soil core (contained within the monolith tin). After recovery of the soil core, it was laid horizontally on the ground and the outer layer was carefully removed using the kitchen knife. The core was then sliced into 1-5 cm depth intervals and each depth section was placed in a separate, labelled plastic bag (Figure 2.5). Table 2.1 showed the accurate thickness of cutting intervals for each of the cores. Initially, air was excluded by hand squeezing and sealing of the sample bags but during the third and fourth sampling trips, helium was applied to flush each bag before it was sealed properly. All the samples were placed into a fridge at 4 ℃ when they reached laboratory prior to further use.

Surface soils NE1-7 from the soil transect in the third sampling trip were collected using a spade to excavate a 20 x 20 x 5 cm section. The soil removed from the pit was then placed in a separate, labelled plastic bag, flushed by helium and then sealed.

Bog waters from Cores 1-5 at the bottom of the pits were collected in polyethylene bottles after the removal of the soil core.

The sample collection procedurewas different from sampling trip 1 to 4. A pit was excavated but depth sections (~2.5 cm) were cut directly from one of the pit walls and the porewater from each section was squeezed by hand into a plastic bag which was immediately flushed with helium and then sealed.

Figure 2.10: Soil sample and bog water collection

2.3 Field measurement of soil redox potential (Eh)

When the Cores 3-4 were removed from the peat bog, a redox potential meter (HI98121, Hanna) was immediately inserted into one side of the pit wall to record the redox potential. This was done in less than 1 minute after the core was removed since exposure to air can cause an increase in the measured value.

2.4 Overview of the entire experimental programme

Figure 2.11 provides an overview of the experimental programme for this research project.

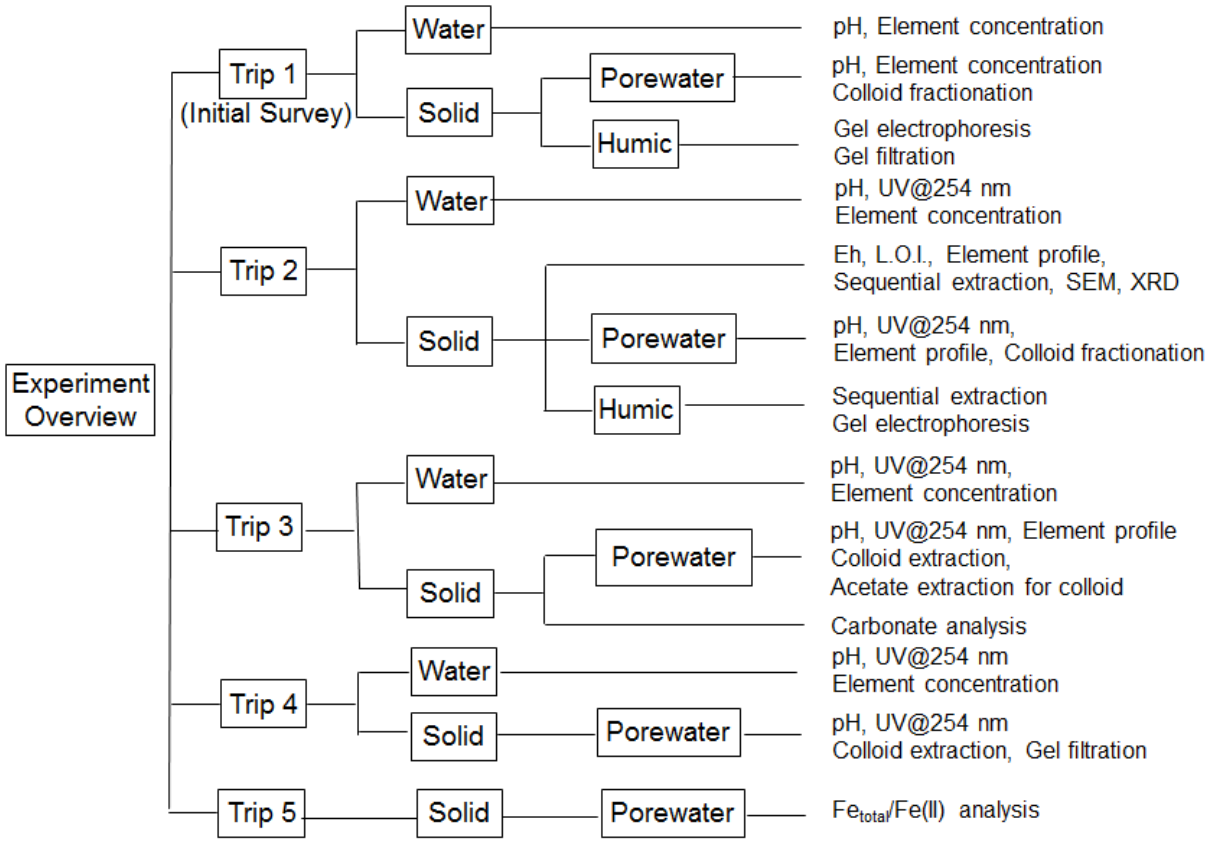

Figure 2.11: Overview of the experimental programme

2.5 Experimental methods

2.5.1 Quality control procedures for all experimental work

2.5.1.1 Cleaning of glassware and plasticware

All glassware was boiled in 5 M nitric acid solution (see Appendix section9.1.1) for 3 hours on a hot plate, rinsed thoroughly with deionized water, then re-boiled in a deionized water bath for another 3 hours. Once cooled, all glassware was rinsed with deionized water before being transferred to a drying cupboard. All plasticware was cleaned by soaking in 5 M nitric acid at room temperature for 24 hours, rinsed with deionized water, then placed in deionized water bath for another 24 hours, before being transferred to a drying cupboard.

2.5.1.2 Sample blank controls

There was a series of blank controls carried out before each method was applied to the samples.

0.2 µm hydrophilic membranes

~5 mL deionised water was filtered through 0.2 µm hydrophilic membranes (Sartorious), the filtrate was transferred into a sterilin container and accurately weighted. The concentration of elements released from the membranes was determined by ICP-OES (see section 2.5.16).

Ultrafiltration units

For sampling trips 1 and 2, 5 mL deionised water was transferred to the ultrafiltration units (100 kDa, 30 kDa, 3 kDa, Vivaspin) and centrifuged at 6000 g for ~15 min. until < 0.1 mL water was retained in the top compartment (Figure 2.13). After centrifugation, each filtrate (bottom compartment) was transferred to a sterilin container and accurately weighed. The concentration of elements released from the membrane was determined by ICP-OES (see section 2.5.16).

A separate blank test was carried out for sampling trip 3, where ~3 mL, 6.5 mL, 10 mL, 18 mL deionised water was transferred to the ultrafiltration tube (3 kDa, Vivaspin) and centrifuged at 6000 g for 15 minutes. The amount of deionised water used here was in

accordance with the amount of porewater from Core 3 for ultrafiltration because some of the soil samples were quite dry and only small volumes of porewater could be extracted for ultrafiltration. After centrifugation, each filtrate was transferred to a sterilin container and accurately weighed. 1.5 mL 1 M sodium acetate was then added to the same ultrafiltration unit and the same procedure was again carried out. The element concentrations in all filtrates were determined by ICP-MS (see section 2.5.17). The 1 M Na acetate solutions collected from the bottom compartment of the ultrafiltration unit were diluted by a factor of 10 prior to ICP-MS analysis.

Microwave-assisted digestion

As 9 mL HNO_3 and 0.2 mL HBF_4 or 1 mL HF were used for microwave-assisted digestion of soil samples, a separate vessel filled with only 9 mL HNO_3 and 0.2 mL HBF_4 or 1 mL HF was reserved to run the reagent blank digestion. After the microwave programme was complete (see section 2.5.8), the solution in the vessel was transferred to a Teflon beaker, evaporated on a hotplate to less than 1 mL and made up to 25 mL in plastic volumetric flask with 2% v/v Aristar HNO_3. The element concentrations in the reagent blank were determined by ICP-OES (see section 2.5.16).

Sequential extraction

A solution of each reagent used in steps (i)-(v) of the sequential extraction procedure described in 2.5.11 (see Table 2.4) was analysed by ICP-OES after appropriate dilution. For steps (vi)-(vii), a protocol similar to that described for microwave-assisted digestion was adopted.

Gel electrophoresis

~1.5 g agarose gel powder was typically prepared with 150 ml 0.045 M tris-borate buffer to form a 1% agarose gel for fractionating humic substances. Since U and other elemental interactions with the humic materials were to be investigated, it was important to recognise that the gel itself also contained some trace metals. Trial runs where no sample was applied to the gel well were undertaken and the whole gel cut into 1-cm strips (parallel to the direction of ion flow). This was done once where the current was not applied and again where the standard operating conditions were applied (20 mA; 30 minutes). Selected strips (several from each end of the gel and several from the middle sections) were digested separately with 5 mL 2% nitric acid and 1 mL H_2O_2 before being transferred tosterilin containers and weighed accurately. The element concentrations in the blank were

determined by ICP-OES (see section 2.5.16). The element concentrations in each 1-cm gel strip were calculated as the average value of those three gel strips from the middle of the gel.

ICP-OES/ICP-MS

For ICP-OES or ICP-MS, blankswere prepared in accordance with the matrix for the samples. In every run, 2% v/v nitric acid was run as part of the standard calibration procedure (see sections 2.5.16 and 2.5.17). The reagent blanks described in the sections above were analysed along with the appropriate set of samples, i.e. filtered and ultrafiltered porewaters; soil digests; sequential extracts; gel digests.

2.5.1.3 Detection limits for ICP-OES and ICP-MS

The intensity of ten aliquots of blank was obtained to establish the standard deviation of the mean for the blank after running a sample blank solution through the instrument ten times. Analytical detection limits for each procedure were determined as three times the standard deviation of the blank divided by the slope of the calibration curve (Vandecasteele and Block, 1997). Details of detection limits relating to each element and each procedure are given in the appendices along with each data set.

2.5.1.4 Sample replicates

Where possible procedures (soil digestions, sequential extractions, carbonate determination) were carried out in duplicate, multiple samples at a single location were collected (cave waters), or pseudo-replicates were used (sequential extraction-humic extraction-gel electrophoresis). In other instances, it was not possible to obtain duplicates (filtered and ultrafiltered porewaters, acetate extraction of colloids, gel chromatographic fractionation of colloids). Percentage elemental recovery was used as means of establishing quality control for porewater samples.

2.5.1.5 Reference materials and reference solutions

Certified reference materials were available only for total soil and the certified

ombrotrophic peat reference material NIMT/UOE/FM/001 and International Atomic Energy Agency soil IAEA-326 were used to determine the effectiveness of total digestions. The results for these will be presented in section 2.5.8. Certified reference solutions such as Multielement Standard Solution MVI (Merck) were run along with every set of ICP-OES and ICP-MS analyses as a check on calibrations and also on instrumental stability throughout sample runs (see sections 2.5.16 and 2.5.17).

2.5.2 Water sample pre-treatment

For sampling trips 1 to 4, all samples were processed immediately upon return to the laboratory. All the bog water and cave drip water samples were filtered through 0.2 µm hydrophilic membranes (Sartorious); a portion of the filtered samples was then immediately analysed by ICP-OES and/or ICP-MS (see sections 2.5.16-2.5.17) and the remainder was retained in sterilin containers at 4°C for further use.

2.5.3 Soil sample pre-treatment

Sample pretreatment includes porewater extraction, soil homogenization and humic extraction.

2.5.3.1 Porewater extraction

A portion of each depth section from each of soil Cores 1-7 was packed into centrifuge tubes (Fisherbrand) for centrifugation at 8000 g for 10 minutes. Porewater was subsequently collected from the top of the tube and passed through 0.2 µm hydrophilic membranes (Sartorious).

Each soil section from Core 6 was packed into centrifuge tubes within a glove bag (Aldrich AtmosBag) which was filled with N_2 (Figure 2.12). After the lid was tightened, the centrifuge tube was sealed with packing tape to maintain anaerobic condition and centrifuged at 8000 g until enough porewater had accumulated on the top of the soil. The tube was unwrapped by removing the tape and immediately returned to the glove bag. Porewater was then removed from the tube and passed through 0.2 µm hydrophilic membranes (Sartorious) inside the glove bag.

A glove bag (Aldrich AtmosBag) is an inflatable chamber with built-in gloves that creates isolated working environment (Figure 2.12). N_2 was purged into the glove bag and gently flowed out of bag front opening. All necessary equipment was placed in the bag, such as soil samples, centrifuge tube, ultrafiltrator, pipette and disposal nitrile gloves. The bag was then sealed and the N_2 was purged again to inflate the whole bag. The gas was turned off and the bag was opened to allow the gas to escape before it was sealed. This inflation/deflation cycle was repeated ~10 times to achieve N_2 environment in the bag. Finally, the bag was inflated to a very soft-pillow level, which allows the plastic gloves to move easily within the bag. The N_2 was then turned off and the bag opening was folded over twice to prevent the diffusion of air into the bag (Figure 2.12). Hands were inserted into the built-in gloves to carry out the experimentswithin the bag.

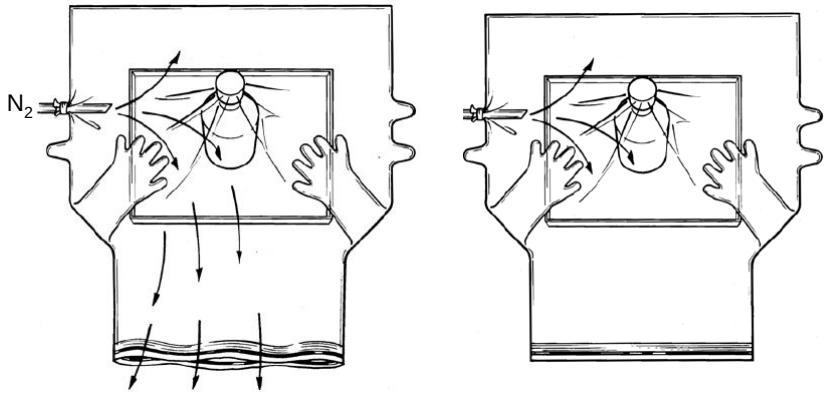

Figure 2.12: Schematic of glove bag

For sampling trip 5, a salad spinner was used as a centrifuge to extract the porewater from the soil. These samples were immediately placed in He-filled bags until a small portion could be removed and filtered through 0.2 μm hydrophilic membranes (Sartorious) at the sampling site. A portion of the samples were used for Fe^{II} analysis on the site and the rest was preserved in the sterilin containers (flushed with He) for total Fe analysis by ICP-MS in the laboratory.

2.5.3.2 Soil homogenization

After the powater was extracted, a portion of each of the soil samples from Cores 3-5 was air-dried at 30 ℃ until constant weight was achieved. After large pieces of vegetation and stones were removed, homogenisation was achieved by grinding with a mortar and pestle.

The dried, ground soil was placed in labelled plastic bags, sealed and stored in a cool, dark cupboard for further use.

2.5.3.3 Humic extraction

In order to extract humic substances, a portion of soil from each depth section from each soil was suspended in 0.1 M NaOH in an approximate liquid to solid ratio of 5 mL:1 g with manual stirring at regular intervals for 4 hours.

Sampling trip 1

Although it is known that more than 90% of U in the soil was associated with humic substances at Needle's Eye (MacKenzie et al., 1991), many questions remain about the U associations with these materials: (i) is it bound directly to humic substances or bound indirectly through minerals?; (ii) are there any differences of the U-humic binding in relation to humic size or with increasing depth or increasing distance from mineralization? Thus, humic substances were extracted from soil sections of different depths and different distances from mineralization so that later gel electrophoresis (GE) and gel filtration (GF) could be applied to investigate in sampling trip 1.

The alkaline solutionfrom each sample suspension from Cores 1 and 2 was then decanted and filtered through 20-25 μm filter papers (Qualitative Filter Paper, Grade No.4, Whatman). The dark brown filtered humic extract was then transferred into a dialysis membrane (Dialysis Membrane 12,000-14,000 MCWO, Spectra/Por) and placed in deionised water for dialysis. To remove the NaOH in the humic solution, the water outside of the membrane was changed every day until its pH value was lower than 7. A portion of the dialysed humic extract was used for gel electrophoresis (2.5.9). This had to be concentrated by partial freeze-drying prior to gel electrophoretic fractionation because the elemental concentrations in the gel fractions were too low for analysis by ICP-OES. The rest of the dialysed extract was freeze-dried to obtain humic substances for gel filtration (see Section 2.5.10).

Sampling trip2

Core 3 16.5 cm and 19.5 cm depth samples were labelled as Core 3 S6 and Core 3 S7 as they were the sixth and the seventh depth sections of the core.

The first experiment was designed to test whether there was definitely more than 90% of U associated with humic substances. The exhaustive humic extractions were carried out for Core 3 S6 and Core 3 S7 soil samples. The procedures described above were used, but it was repeated until the colour of the extract was pale brown. The alkaline extracts from the Core 3 samples were decanted. The residue of soil samples were digested by microwave-assisted digestion and the U amount in the residue was determined by ICP-OES.

In the second experiment, there were two groups of humic extracts which were labeled accordingly: Core 3 S6-1, S7-1 and Core 3 S6-2, S7-2. The difference between those two groups will be explained in Section 2.5.11 (Table 2.5). The procedures described above were again used but the alkaline extracts from the Core 3 samples were decanted and then filtered through a 0.2 μm hydrophilic membrane (Sartorious) to remove co-extracted mineral matter. The extracts were then transferred to a dialysis membrane (Dialysis Membrane 12,000-14,000 MCWO, Spectra/Por) for dialysis against deionized water. Once the pH of the deionized water decreased below 7, the dialysed extract was freeze-dried to obtain humic substances for sequential extraction in conjunction with gel electrophoresis (see Section 2.5.11.4).

2.5.4 Measurement of soil porewater pH

After the samples were transported to the lab, porewater from each portion of the soil was extracted and filtered through 0.2 μmhydrophilic membrane as mentioned in Section 2.5.2. The pH meter (Jenway Model 3505) was calibrated using pH 4 and pH 7 standard solutions. It was then placed in the 0.2 μm-filtered porewater and cave drip water and the pH value was recorded when the reading was stable.

2.5.5 Relative concentration of DOC measured by UV-Visible Spectroscopy

UV-vis measurement at 254 nm has been found to be effective for monitoring the concentration of dissolved organic matter (DOM) (Egeberg et al., 2002; Graham et al., 2008). The basic assumption is that the DOM concentration is linearly related to the UV absorbance (Dobbs et al., 1972). The part of an organic molecule responsible for producing colour is referred to as a chromophore. The chromophores that absorb light in the

ultraviolet (200 to 400 nm) region are usually aromatic groups with various degrees and types of substitution, including monosubstituted and polysubstituted phenols and various aromatic acids. Aromatic groups such as those described above are thought to be major structural components of humic substances. However, there can be variations in the type and amount of these components and so this method is only valid for humic compounds of similar origins (Stevenson, 1982). As all the humic materials were extracted from the same location, application of this method was appropriate.

The absorbance at 254 nm for aliquots of 0.2 μm-filtered water samples was recorded using a Perkin Elmer Lambda 900 UV/VIS/NIR spectrophotometer. The samples were diluted when absorbance at 254 nm was >1.5. Deionised water was used for background blank absorbance.

2.5.6 Loss on ignition

Loss on ignition (LOI) was used to determine the percentage of organic matter in each soil section from cores 3-5. ~0.25 g air-dried, homogenised soil was accurately weighed into beakers and placed in an oven (Gallenkamp) for 12 hours at 105°C for moisture content correction. After cooling in a dessicator and reweighing, the beakers were then covered with watch glasses and placed in an ashing furnace (Carbolite) at 450 ℃ for 8 hours. When the ashing was finished, the beakers were again transferredto a glass desiccator for cooling. Once the beakers were cooled to room temperature, the beakers containing the residue were reweighed. The difference in mass between the ashed sample and the 105°C-dried weight was used to calculate the organic matter content.

2.5.7 Isolation and fractionation of porewater colloids using centrifugal ultrafiltration

The principle of centrifugal ultrafiltration is that a hydrostatic pressure is created by centrifugation, which forces a liquid against a semi-permeable membrane. The membrane can separate marcromolecular species and solvents based on their sizes. Larger colloidal molecules are retained by the membranes while truly dissolved phase and smaller colloidal molecules pass through the membrane (Figure 2.13).

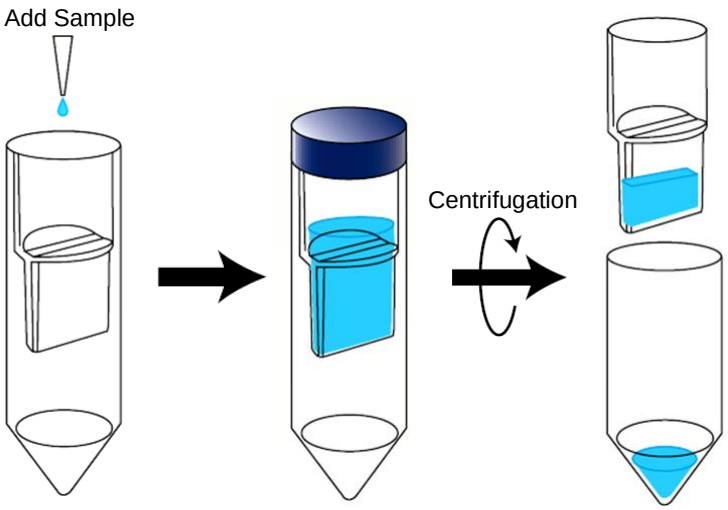

Figure 2.13: Schematic showing the centrifugal ultrafiltration procedure

Size fractionation by ultrafiltration was carried out using a defined set of centrifugal ultrafiltration units (Vivaspin 20, polyethersulfone membrane, Vivascience) with different molecular weight cut-offs (Table 2.2).

Table 2.2: The size ranges of different colloids and truly dissolved phase species (http://www.millipore.com/publications.nsf/a73664f9f981af8c852569b9005b4eee/ce8d86a76a8048f08525738e005ac086/$FILE/pf1172en00.pdf).

Fraction	Molecular weight cut-off (MWCO)	Diameter
Large colloid	100 kDa-0.2 µm	~3.6 nm-0.2 µm
Medium colloid	30-100 kDa	~2.3 nm-3.6 nm
Small colloid	3-30 kDa	~1 nm-2.3 nm
Truly dissolved phase	< 3kDa	< ~1nm

2.5.7.1 Sampling trips 1 and 2

For sampling trips 1 and 2, ultrafiltration was used to fractionate the porewater (<0.2 µm) from each depth section of Cores 1-5 into 100 kDa-0.2 µm, 30-100 kDa, 3-30 kDa and <3 kDa fractions. This was used to build up a distribution profile for U with regards to soil depth and distance from the mineralisation. An aliquot (20 mL) of porewater samples was transferred to a 100 kDa centrifugal ultrafiltration tube and centrifuged at 6000 g for one hour. After centrifugation, each filtrate at the bottom was transferred to a 30 kDa centrifugal ultrafiltration tube and centrifuged again. The process was then repeated with a

3 kDa centrifugal ultrafiltration tube. In this way, fractions 100 kDa- 0.2 µm, 30-100 kDa, 3-30 kDa were retained in the top half of the ultrafilter tubes. In order to efficiently remove the retentate, 100 µL buffer (0.05 M Tris-HCl, pH 8.5, see Appendix Section 9.3) and a little deionised water was added to the top half of the unit and a 1 mL plastic pipette was used to mobilise any colloidal materials sticking to the membrane. The washings were then transferred to a sterilin container and the accurate weight was recorded. The truly dissolved (<3 kDa) fraction was not preserved for analysis during preparation of samples from trip 1 but this fraction was retained from samples collected during trip 2. This was because the results for trip 1 samples showed that, for some elements, there was a difference between the summed concentrations of elements in the colloidal fraction and the total elemental concentrations in the porewater. As some of these elements may have been present in the dissolved (<3 kDa) forms, it was necessary to retain and analyse this fraction in orderto attain a complete mass balance.

2.5.7.2 Sampling trip 3

For sampling trip 3, porewater from seven surface soils (NE1 to NE7) were collected along a transect line from near the cave towards Southwick Water. Those porewaters were fractionated into colloidal (3 kDa-0.2 µm) fraction and truly dissolved (<3 kDa) fraction. This procedure provided information on U behaviour in surface flow. Both fractions were transferred into sterilin containers separately as mentioned in Section 2.5.7.1.

Aliquots of surface soil porewaters NE1-NE7 were subjected to colloid extraction via 3 kDa centrifugal ultrafiltration. The colloidal (3 kDa- 0.2 µm) fraction was again collected in the top compartment of the ultrafilter unit.

Porewaters were extracted from Core 6 samples with and without the exclusion of air; and the former was carried out in the glove bag using N_2following the same procedures described in 2.5.3.1. It should be noted that Core 6 samples were flushed using helium in the field and $N_2$was used in the lab. Both gases were used to establish anaerobic conditions for the samples. Helium was used in the field because the helium tank was much lighter than the N_2, making it easy to carry in the field. After extraction, an aliquot (3.5-19 mL) of each porewater sample was placed in the top section of a 3 kDa centrifugal ultrafiltation unit and centrifuged at 6000 g until less than 0.2 mL remained on the top. Fraction <3 kDa truly dissolved phase was collected in the bottom compartment. The colloid (3 kDa- 0.2 µm)

fraction remained in the top compartment and 1.5 mL 1 M acetate was then added to carry out acetate extraction. After acetate extraction, the unit was centrifuged at 8000 g to separate the acetate extractable components from the colloids which remained in the top compartment. Those two fractions were transferred to sterilin containers using acetate and deionised water separately before accurate weights were recorded. The elemental concentrationsin these solutions were measured by ICP-OES or ICP-MS (see section 1.5.16-1.5.17).

2.5.7.3 Sampling trip 4

Soil sections from 3.5 cm, 8.5 cm, 17.5 cm and 35.5 cm depths were labelled as Core 7 S4, S8, S17 and S35, respectively. ~10 mL 0.2 µm-filtered porewater from each of these sampleswere passed through a 3 kDa centrifugal ultrafiltration unit to obtain the colloid (3 kDa-0.2 µm) fraction. The colloidswere later separated by gel filtration chromatography to explore the U associations in relation to colloidal size (Section2.5.10).

2.5.8 Microwave-assisted digestion of soil samples

2.5.8.1 Principle of microwave accelerated reaction system

The microwave accelerated reaction system is a technique for digesting a wide range of materials which are considered difficult to solubilise. The advantage of the system lies in its ability to achieve significantly higher pressure and working temperature than the traditional hot plate digestion.

Closed pressurization means digesting samples in a sealed vessel. This provides the advantage that the whole reaction is isolated from the laboratory environment. Potential cross-contamination of samples is avoided and the volume of acid required to digest them is significantly reduced.

The microwave acts as a source of intense energy to rapidly heat the sample within the digestion mixture. Although the technique makes use of microwave energy, simply microwave heating alone cannot rupture molecular bonds directly because the proton energy is less than the strength of chemical bond (Nadkarni, 1984). Thus it is more correct

to use the expression “microwave-assisted digestion”rather than “microwave digestion”. Instead it is the action of the hot acids upon the soil that results in sample dissolution. When the soil/acid mixture is heated by microwave, the vapour generated from the liquid does not absorb microwave. Thus the temperature of the vapour phase is lower than the temperature of the liquid phase. Vapour condensation occurs on cold vessel walls. Thus, reflux conditions are established within the microwave vessel.

2.5.8.2 The microwave instrument

A CEM Mars 5 microwave accelerated reaction system was used in this study. The microwave system consists of a microwave power system, a fluoropolymer-coated microwave cavity, a cavity exhaust fan and tubing, a programmable computer, explosion proof reaction vessels and one specialized vessel for monitoring pressure and temperature, a carousel, a door safety interlock system.

Figure 2.14: Schematic of microwave running system (carousel, closed system vessels, blue pressure sensor tube)

The programmable computer provides parameter settings including the percentage of power applied, the total wattage, control temperature, pressure, ramp and hold time, and the number of reaction stages or circles. It also provides pre-programmed settings including

EPA methodused for this study.

The carousel holds 14 vessels and rotates the samples by 360 degrees through the microwave field, which ensures homogeneous distribution of microwave radiation for all vessels. The exhaust tubing, which allows removal of the fumes generated from the vessels, vents into a fume cupboard.

The 14 vessels can be held at temperatures up to 260 ℃, or pressure up to 500 psi. The liners are composed of polyfluoroalkoxy (PFA) polymer, which is transparent and has extreme resistance to chemical attack. Each vessel contains a plastic membrane pressure disc fitting between the exhaust port in the vessel lid and the cap with a small hole drilled in it. When the pressure in the vessel exceeds 500 psi, the membrane will burst and the exhaust gas will be removed via the exhaust port to prevent over pressurization in the vessel.

One of the 14 vessels acts as a control to monitor pressure and temperature. The control vessel is made from the same material as the other vessels but it contains a glass well that penetrates in the vessel so that a temperature sensor can be placed into the vessel. The lid of the vessel also contains a port connected to the pressure sensor.

2.5.8.3 Procedure

~0.25 g air-dried, homogenised soils were accurately weighed out and placed in 105 ℃ oven for moisture content correction before being ashed at 450 ℃ (8 hours). The ashed samples were then subjected to a microwave-assisted (CEM Mars 5) total digestion using 9 mL HNO_3 and 0.2 mL HBF_4. This method is based on the USEPA Method 3052 and, with the exception of the replacement of HF with HBF_4, was identical to that described in Yafa et al. (2004). After cooling, the digests were transferred to Teflon beakers, evaporated on a hotplate to less than 1 mL and made up to 25 mL in plastic volumetric flasks with 2% v/v Aristar HNO_3. All samples were prepared in duplicate or triplicate as appropriate and then analysed by ICP-OES. The certificated peat material, Ombrotrophic Peat NIMT/UOE/FM/001, was also used simultaneously to provide a measure of the accuracy of elemental (Fe, Mn, Pb, Cu, Zn, Al, As) concentrations determined by this method (Yafa et al., 2004). International Atomic Energy Authority certified material IAEA-326 was used toe determine the accuracy of U concentration measurements.

Table 2.3: Mean measured and certified values for elemental concentrations in certified reference material ombrotrophic peat (NIMT/UOE/FM001) and IAEA326.

Analysed Metal	**Measured Value Range (mg kg^{-1})**	**Mean Measured Value (mg kg^{-1})**	**Certified Value for NIMT/UOE/FM001 (mg kg^{-1})**
Fe	574-925	840 ± 60 (n = 7)	921 ± 84
Al	2794-4006	3563 ± 443 (n = 7)	3692 ± 347
Mn	5.54-8.65	7.19 ± 0.76 (n = 7)	7.52 ± 0.41
Pb	119-167	147 ± 14 (n = 6)	174 ± 8
Cu	3.59-4.70	4.13 ±0.56 (n = 7)	5.28 ± 1.04
As	n.d.-3.71	2.13 ± 1.27 (n = 7)	2.44 ± 0.55
Analysed Metal	**Measured Value Range (mg kg^{-1})**	**Mean Measured Value (mg kg^{-1})**	**Certified Value for IAEA-326 (mg kg^{-1})**
U	0.62-5.48	2.62 ± 1.75 (n=7)	3.2 ±1.5

For all elements except Pb, the measured values were in good agreement with the certified values and the level of precision attained was similar to that quoted for the certified values. This gives confidence in the data obtained in this study. The certified values for Pb were determined by ICP-MS and the measured values in this study were determined by ICP-OES. Interferences (e.g. relating to Fe in the sample digests) can impact on the quantification of Pb by ICP-OES and it is recommended that, in future, steps are taken to identify and eliminate the interference and/or the samples are analysed by ICP-MS.

2.5.9 Gel electrophoresis

2.5.9.1 Principle of gel electrophoresis

Electrophoresis is a technique used to separate macromolecules that differ in size, charge or conformation. Electrophoresis is applied to pull or push the molecules through a gel. By placing the molecules in wells in the gel and applying an electric current, the molecules will move through the gel at different rates.

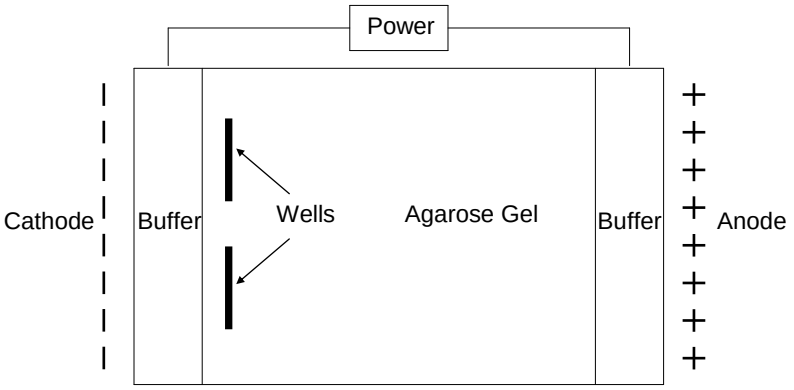

Figure 2.15: Schematic of the gel electrophoretic extraction experiment

Ionisable molecules in aqueous solution carry a defined electrical charge at all pH values except their isoelectric point. Therefore, they migrate in an electric field. The migration velocity of the molecules is determined by the magnitude of the net charge, size and shape of the molecule, electric field strength and viscosity of electrophoresis medium. Electrophoretic separation can be performed in a solution containing a non-conductive matrix, e.g. agarose gel which is a net-like matrix with pore of different diameters. These pores can perform a sieving effect, which means it can separate the molecules on the basis of their sizes and shapes. The size of the pores and the migrating molecules has already determined the viscosity of electrophoresis medium, thus humic molecules are separated based on both charge and size. Molecules with greater net negative charges and smaller size migrate towards the anode more quickly (Figure 2.15) (Manz et al., 2004).

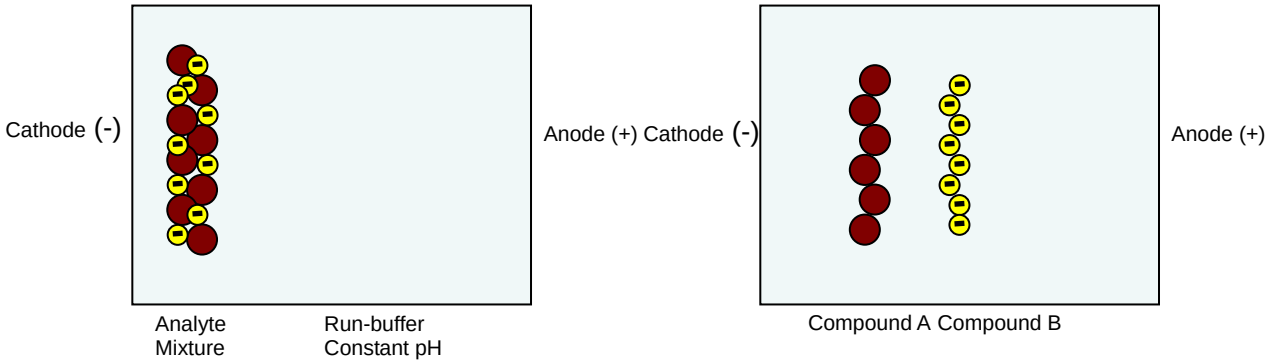

Figure 2.16: The separation principle of electrophoresis

2.5.9.2 Method

A 1% w/v agarose gel was prepared by adding 1.5 g agarose powder to 150 mL 0.045 M Tris-borate (See Appendix Section 9.2) in a beaker. The beaker was placed in a microwave (300 w, ~3 minutes) to heat the mixture until the agarose dissolved in the buffer. The melted agarose gel was then poured into the gel tray (secured with rubber seals) which has a comb at one side, and then left to set for 30 minutes at room temperature. When the gel has solidified, the seals and comb were pulled out, leaving empty wells for the humic samples. The gel, together with the gel tray, was placed into an electrophoresis tank. As humic molecules have a strong negative charge, the sample wells were located closest to the electrode that had the negative charge. 0.045 M Tris-borate buffer was added into the chambers at each side of the gel tray until level with the top of the gel.

Aliquots of 350 µL samples were loaded into the gel wells using an adjustable 0-100 µL pipette. The lid was placed tightly onto the electrophoresis unit to connect the power supply. Electrophoretic separation was carried out at a fixed current (20 mA) for 30 minutes. The gel was then cut into 8 1-cm strips (sampling trip 1 samples) or 7 1-cm strips (sampling trip 2 samples) and labelled from F1 to F8 or F1 to F7 according to increasing mobility from cathode to anode. The location of the brown sample band can be determined visually. The gel was then placed under an ultraviolet lamp, by which the location of fluorescence bands can be viewed (Figure 2.17).

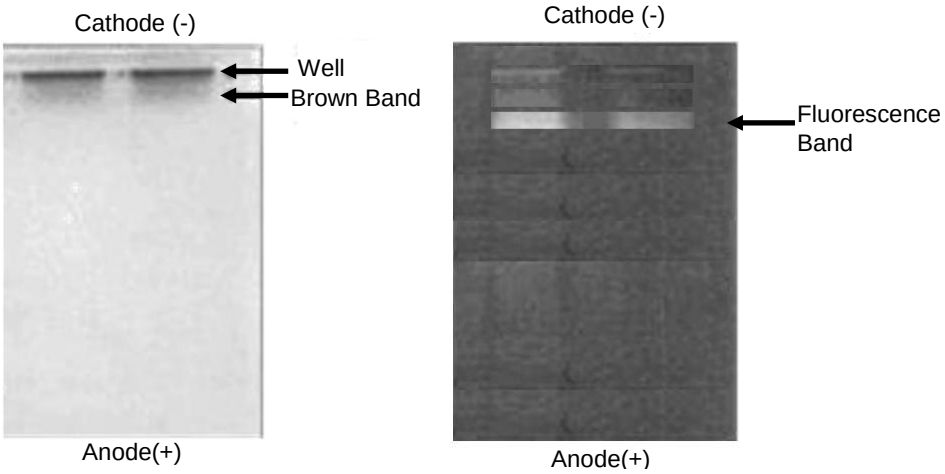

Figure 2.17: Humic substances separation by gel electrophoresis, brown band can be observed under natural light while fluorescence band can be observed under UV light (Vinogradoff et al., 1998)

Each strip was digested on a hotplate with 5 mL 2% (v/v) HNO_3 (Aristar, VWR). 1 mL 30% w/v H_2O_2 (Fisher scientific) was then added to totally destroy the organic material and release all the elements bound to the humic substances. After volume reduction, each solution was accurately diluted to around 5 mL with 2 % nitric acid. Element concentrations were determined by ICP-OES (see Section 2.5.16).

Validation of the gel electrophoretic fractionation procedure

As gel electrophoresis was to be used to investigate the interaction between U and humic substances, initial experiments (i) investigated the effect of gel cutting efficiency and (ii) quantified the contribution of metal contaminants from the gel.

After the gel was cut into several strips of 1-cm width by a blade, each strip was accurately weighed. This was to test how evenly it was cut and whether the slight cutting difference would affect the result. Each strip was then digested as described above and transferred to a sterilin tube before analysed by ICP-OES. This step was to determine the elemental (U, Fe, Mn, Pb, Cu, Zn) concentrations in the gel blank.

Figure 2.18 (a) shows the mass of selected 1-cm weight gel strip (F1, F2, F3, F7, F8, F12, F13, F14) and (b) and (c) show the corresponding element concentrations without application of current. In theory, the elemental content of each gel strip should be similar if the gel cutting has

been carried out well. However, it should be noted that the gel strip close to the edge of the gel casting tray may have come into contact with the rubber used to seal the tray during gel casting and setting. Thus the gel strips (F1, F2, F3 and F12, F13, F14) closest to the seals were selected, in addition to two strips located in the middle of the gel. In the first experiment, the gel was prepared according to the method described in Section 2.5.9.2, but no current was applied. The mean mass (and standard deviation) of the gel strip was 4.39±0.22 g (n=8). It should be noted that strip F1 has a slightly higher mass simply due to the removal of the gel well which usually leaves a little extra gel. The mean elemental contents for U, Fe and Zn were 1.0±0.077, 0.45±0.23, 7.7±3.7 μg per gel strip while no Mn, Cu and Pb were detected in the gel. As shown in Figure 2.18, in comparison with all of the other elements, much higher Zn concentrations were obtained. This was particularly evident for F14 which had ~2 times the amount of Zn contained in any of the other fractions.The same effect is not observed for F1 because there is gel material behind the gel well which is not used (the sample will migrate in the opposite direction).

Overall, it can be seen from Figure 2.18 that the gel contains trace amounts of U relatively evenly distributed in the gel, but trace amounts of Fe and larger amounts of Zn unevenly distributed in the gel. Cutting is likely to be the main reason for the Fe pattern as F1 and F14 both had a higher amount of Fe than the rest of the strips. However, this will be unlikely to have a major impact where Fe concentrations in humic extracts are significantly greater than for the gel blank. Cutting is also unlikely to be the main reason for the Zn pattern and it is speculated that the rubber used to seal the gel tray released a large amount of Zn as the hot liquid gel cooled and solidified.

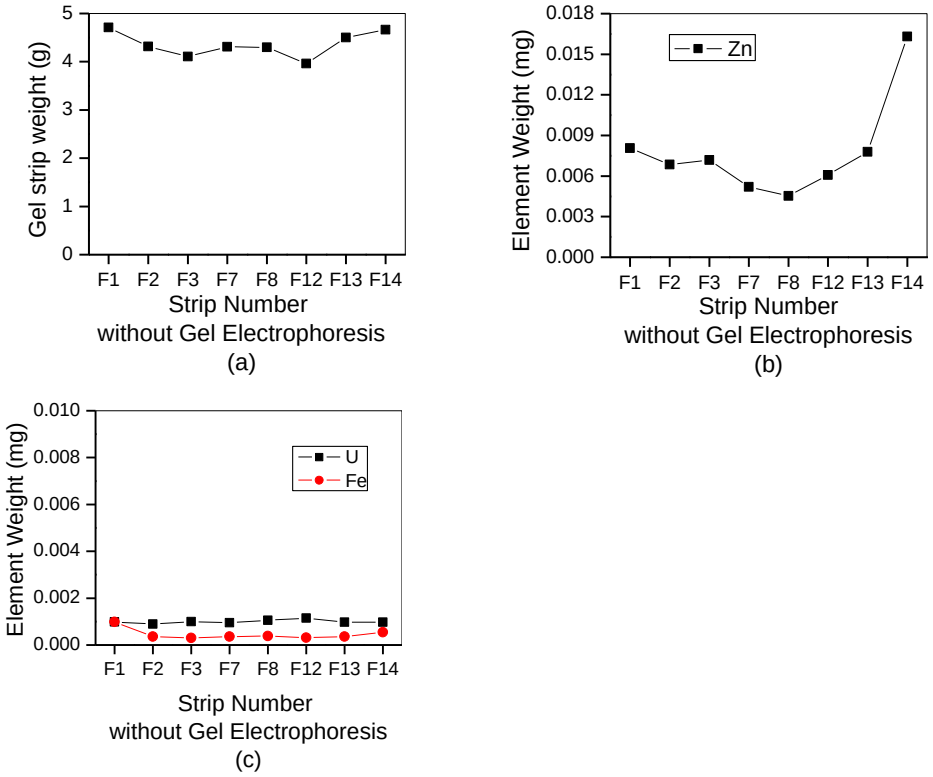

Figure 2.18: (a) Gel strip mass and (b)-(c) corresponding elemental content of gel strips without application of current

The same procedure was carried out again but this time 20 mA was applied for 30 minutes. Afterwards, the element distribution patterns remained almost the same as those shown in Figure 2.19, where no current had been applied. Importantly, the small amounts of U (Mn, Pb, Cu not detected) remained evenly distributed across the gel. F3 and F12 had slightly higher amount of Fe than the rest of the strips although cutting was not the reason as F1 and F14 had higher weights than the rest of the strips. The Zn contamination in the gel remained in F14, indicating that the form of Zn present was immobile under the applied conditions with humic and other colloidal entities from the environmental samples in this study. In all subsequent electrophoretic experiments, Zn was omitted from the elemental analyses.

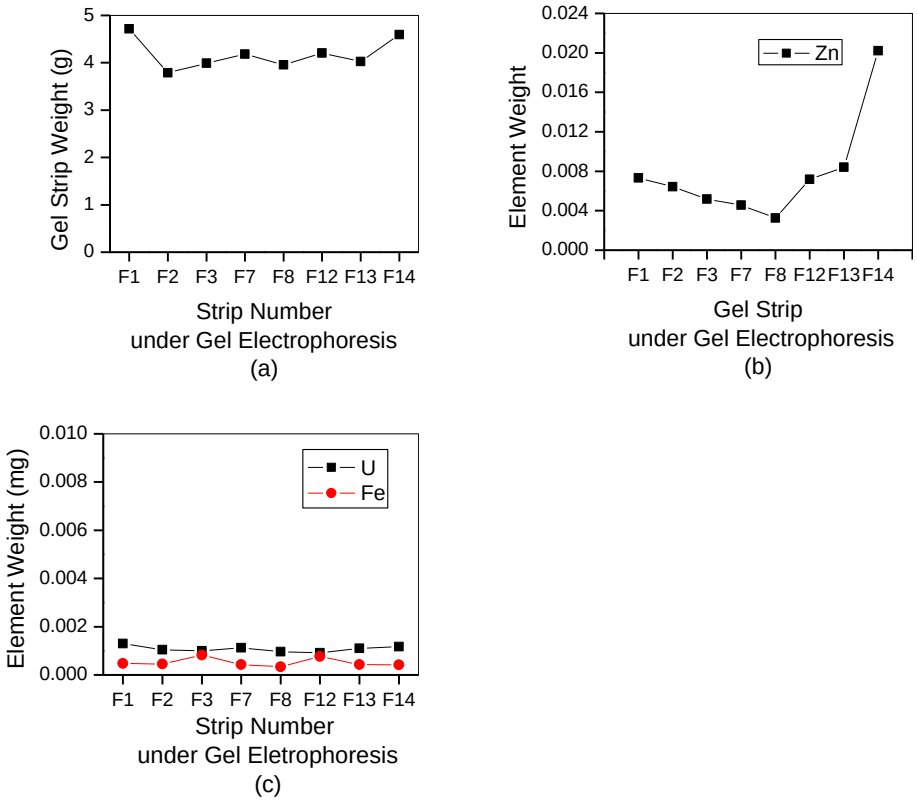

Figure 2.19: (a) Gel strip mass and (b)-(c) corresponding elemental content of gel strips following application of current (20 mA for 30 minutes)

Sampling trip 1

The concentrations of elements associated with the humic extract (Section 2.5.3.3) from Core 1 were determined by ICP-OES prior to gel electrophoresis.Since the elementalconcentrations in the humic extracts were too low in comparison with those in the gel blank, the extracts need to be pre-concentrated by partial freeze-drying before being run by gel electrophoresis. ~400 µL of the concentrated humic extract was loaded into the gel well using an adjustable 100 µL pipette.

Sampling trip 2

0.0090 g freeze-dried humic substances from Core 3 S6 and Core 3 S7 (Section 2.5.3.3b) from each sample was dissolved in 350 µL dionised water and loaded into the gel well using an adjustable 100 µL pipette. Details of the samples will be given in section 2.5.11.4.

2.5.10 Gel filtration

2.5.10.1 Principle of gel filtration chromatography

Gel filtration is a technique used to separate the molecules in solution according to differences in their sizes by passing through a column packed with gel particles in bead form (Figure 2.20). The gels are formed from polymers by cross-linking to form a three-dimensional heterogeneous network, in which the gel beads are the stationary phase and the solvent used for swelling is mobile phase. Sephadex gel, which is a polymer formed by cross-linking dextran, was used in this study. The pores in the gel matrix should be comparable in size to the molecules to be separated. Relatively small molecules can diffuse into the gel beads while relatively large molecules will be prevented from diffusing into the gel bead to the same degree, which causes the large molecules to appear in the earlier fractions of the elute followed by the smaller molecules in the order of their sizes (Pharmacia LKB, 1991).

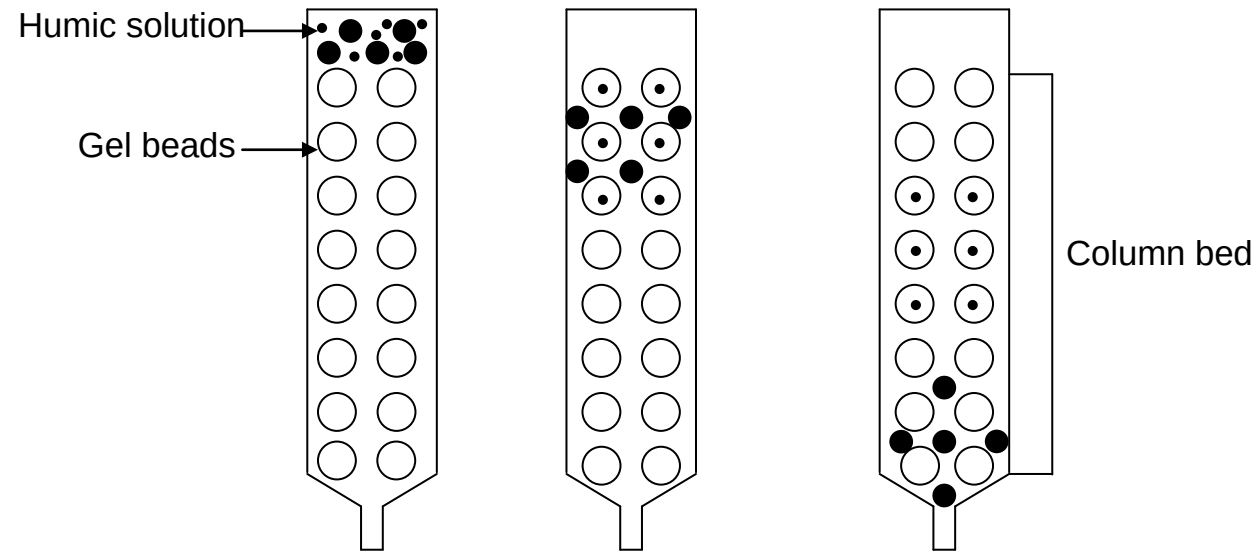

Figure 2.20: Schematic of size separation by gel filtration

2.5.10.2 Method used for gel filtration chromatography

Sampling trip 1

About 6 g gel powder (Sephadex G-75) was added into 100 mL 0.1M NaOH to swell for 24 hours ready for use. After 10 mL 0.1 M NaOH was added into the column (2.5 diameter × 30 cm), the gel was slowly poured into the column using a glass rod. The column then stood for an hour so that the gel bed settled evenly in the column. Excess NaOH solution was run off and the position of the gel bed was marked by pen to ensure the height (23.5 cm) of the gel bed remains the same every time.

The void volume (34 mL) of the gel bed was determined by running Blue Dextran 2000 at a concentration of 2 mg mL^{-1}. Needle's Eye humic substances (50 mg) were dissolved in 5 mL 0.1 M NaOH, which was then placed on top of the gel bed to form a thin band. Fractionation was achieved by passing through 0.1 M NaOH at a flow rate of ~ 2 mL min^{-1}. Fractions (5 mL) containing humic substances were collected after the first brown colour emerged (usually at or just beyond the exclusion limit). The elemental concentrations in each fraction were determined by ICP-OES (see Section 2.5.16).

Sampling trip 4

Porewater colloids (3 kDa-0.2 μm) from Core 7 S4, S8, S17, S35 (Section 2.5.7.3) were fractionated by gel filtration. Here deionized water was used as the mobile phase to avoid a mismatch in ionic strength between the porewater sample and the eluent. G200 Sephadex powder was thus suspended in deionised water to obtain gel slurry. Mini-columns of 3 mL gel slurry were prepared with a small piece of cotton wool at the bottom of a plastic pipette. Each sample (100 μL) was loaded in a thin, even layer onto the gel surface, and water was used as eluent. 8 fractions (~1 mL) for each sample were collected in sterilin containers, and labeled as F0 to F7. F0 represents the fraction before the brown colour emerged from the column. Each fraction was analysed by UV-Visible Spectroscopy at 254 nm (Section 2.5.5) and by ICP-MS (Section 2.5.17).

2.5.11 Sequential extraction

2.5.11.1 Sequential extraction and sulfide analysis for soil

~2.5-3 g wet soil for selected samples from core 3, core 4 and core 5 was accurately weighed into centrifuge tubes and subjected to a sequential iron extraction. Each step of the sequential extraction involved different extraction conditions (Table 2.4) (also see Appendix Section 9.4), (i) 25 mL 0.1 M magnesium chloride at pH 7 for 2 hours, (ii) 25 mL 1 M sodium acetate buffered to pH 4.5 with acetic acid for 24 hours, (iii) 25 mL 1 M hydroxylamine-HCl in 25% v/v acetic acid for 48 hours, (iv) 25 mL 50 g L^{-1} sodium dithionite buffered to pH 4.8 with 0.35 M acetic acid and 0.2 M sodium citrate for 2 hours, (v) 25 mL 0.2 M ammonium oxalate buffered to pH 3.2 with 0.17 M oxalic acid for 6 hours, (vi) 5 ml 12 M HCl boiling for 1 minute, (vii) 9 mL c.HNO_3 (Aristar) and 0.2 mL c.HBF_4 (Aristar), after the residual soil in step (vi) was ashed for 8 hours at 450 ℃. This is a modified method based on the iron sequential extraction of Poulton and Canfield (2005). Poulton and Canfield (2005) used chromus chloride distillation to extract reduced inorganic sulphur phases, e.g. pyrite, elemental surfur and acid volatile monosulfides after step (i) to (v), but this was fulfilled separately in my work (see Section 2.5.11.2). In addition, they used a near boiling 6 M HCl for 24 hours instead of HNO_3 and HBF_4 to extract Fe in residual.

Steps (i)-(v) were carried out in centrifuge tubes which were continually agitated using bench-top shakers. Between each successive extraction, separation was achieved by centrifugation at 8000 g for 15 minutes. Step (vi) was carried out in beakers. After the extraction, the sample was transferred back to the centrifuge tube, and centrifuged at 8000 g for 15 minutes. The supernatant was collected into a beaker, and heated until nearly dry before each solution was accurately diluted to around 5 mL with 2 % v/v HNO_3 (Aristar). Step (vii) involved the HNO_3/HBF_4 microwave assisted acid digestion method mentioned in Section 2.5.8.3. All sequential extracts were analysed in duplicate. The elemental concentrations in each extract were determined by ICP-OES or ICP-MS as appropriate with the standards prepared in the same matrix as each extractant (see Section 2.5.16 and 2.5.17). There were no certified reference materials for this method and so % recovery was used as a QC measure. In addition, further experiments were carried out to validate several of the steps (sections 2.5.11.2-2.5.11.3).

Table 2.4: Details of sequential extraction scheme with extractive reagent, target fraction and the condition

Extractive reagent	Target Fraction	Condition
(i) $MgCl_2$ (pH 7)	F1: Exchangeable Fe	2 h, room temperature
(ii) CH_3COONa (pH 4.5)	F2: $FeCO_3$, including siderite and ankerite	24 h, room temperature
(iii) NH_2OH-HCl	F3: Ferrihydrite, lepidocrocite	48 h, room temperature
(iv) $Na_2S_2O_4$ (pH 4.8)	F4: Goethite, akaganeite, hematite	2 h, room temperature
(v) $(NH4)_2(COO)_2$ (pH 3.2)	F5: Magnetite	6 h, in the dark, room temperature
(vi) 12 M HCl	F6: Sheet silicate Fe	1 min, boiling
(vii) HNO_3 and HBF_4	F7: Residual	Microwave digestion

2.5.11.2 Additional experiment to test the efficacy of step F2 in the sequential extraction

According to the sequential extraction results (see Section 4.1.8), the greatest proportion of U was extracted in F2 which was thought to represent that associated with the iron carbonate fraction (Table 2.4). However, very little Fe was extracted in F2 for Cores 3 and 4 (see Result Section 4.1.8, Figure 4.9). Therefore, an additional experiment was added to verify whether the extracted U was associated with carbonate or whether some other release mechanism was taking place.

~3 g (the same amount as that used in sequential extraction) subsamples of wet soil from Core 3 S4 (10.5 cm depth) were suspended in 25 mL DI water (the same volume of extract used in sequential extraction) in a centrifuge tube. The same mass of soil and the same solution volume of pH-adjusted DI water were used so that the concentrations of U and Fe released in the pH-adjusted water can be compared directly. The aim of the experiment was to change the pH from 7 (the same as that used for F1) to 4.5 (as used in F2). However, the test started from pH 6.09 which was the value obtained when the soil was suspended in DI water. The pH was adjusted by 0.2 unit increment via addition of 0.1 M HCl and continually agitated using bench-top shakers for 24 hours. It should be noted that it was a separate soil sample for each pH value. Separation was then achieved by centrifugation at 8000 g for 15 minutes. The supernatants were transferred to sterilin containers and analysed by ICP-OES. The samples were

run in duplicate.

2.5.11.3 Total reduced inorganic sulphur and acid volatile sulfide extraction

The whole procedure was modified based on the method reported by Fossing and Jorgensen (1989). The only difference is that they used ZnAc to trap the H_2S while 0.1 M NaOH was used to trap it in this study.

Selected subsamples of wet soils (7-11 g) from Cores 3 and 4 were accurately weighted and placed in a reaction flask which had been purged with N_2 for 30 minutes. 1 M $CrCl_2$ in 0.5 M HCl was produced by filling a glass bottle with 1 M HCl-rinsed mossy zinc (Fisher Scientific), then filling the bottle with the Cr^{3+} solution (1M $CrCl_3.6H_2O$ in 0.5 M HCl). The solution was again purged with N_2 for 30 minutes, whereby Cr^{3+} was reduced to Cr^{2+} by mossy zinc. 15 mL 1 M $CrCl_2$ in 0.5 M HCl and 10 mL 12 M HCl were then injected into the sample flask using a syringe. The reaction in the extraction suspension proceeded for 1 hour with continuous bubbling of N_2. Total reduced inorganic sulphur (TRIS), which includes both acid volatile sulfide (AVS: H_2S+FeS) and the remaining chromium reducible sulfur (CRS: S^0, FeS_2), was stripped as H_2S and trapped in 20 mL 0.1 M NaOH solution. The solutions were stored at 4 ℃ until analysis by ICP-OES (section 2.5.16).

Further portions of wet soil from the same selected subsamples (~ 4 – 15 g) of core 3 and core 4 were extracted with 50 mL degassed 1 M HCl. The suspension was magnetically stirred for 1 hour under N_2. AVS was released from the slurry as H_2S and trapped in 20 mL 0.1 M NaOH solution. The solutions were stored at 4 ℃ until analysed by ICP-MS (section 2.5.17).

2.5.11.4 Sequential extraction for humic substances in conjunction with gel electrophoresis

The results of the sequential extraction for soil showed that uranium was mainly released in steps (ii) acetate and (iv) dithionite (see section 4.1.8; Figure 4.9). In this section, acetate and dithionite extractions were used to study the associations between humic substances, U, and other metals (especially Fe).

As mentioned in section 2.5.9, there were two extraction orders of humic substances performed on the same soil samples, which are labelled as Core 3 S6-1, Core S7-1 series and Core 3 S6-2, Core 3 S7-2 series.

For the Core 3 S6-1 and Core 3 S7-1 series, humic substances were extracted from the soil AFTER (i) acetate extraction; (ii) dithionite extraction; (iii) acetate and then dithionite extraction of metals from the soil. Gel electrophoretic fractionation of HS followed.

For the Core 3 S6-2 and Core 3 S7-2 series, humic substances were extracted from the soil BEFORE (i) acetate extraction; (ii) dithionite extraction; (iii) acetate and then dithionite extraction of metals from the HS. Gel elctrophoretic fractionation of HS followed.

In the first series, ~5 g soil from Core 3 S6 and Core 3 S7 was accurately weighted into centrifugal tubes and subjected to three different extractions, which include (i) 42 mL 1 M sodium acetate buffered to pH 4.5 with acetic acid for 24 hours, (ii) 42 mL 50 g L^{-1} sodium dithionite buffered to pH 4.8 with 0.35 M acetic acid and 0.2 M sodium citrate for 2 hours, (iii) a sequential application of (i) and (ii). The experiment was carried out in the centrifuge tubes which were continually agitated using bench-top shakers. Separation was achieved by centrifugation at 8000 g for 15 minutes. After the supernatant was decanted, 42 mL deionised water was added in the centrifuge tube to wash the soil samples for 15 minutes before separation by centrifugation at 8000 g for 15 minutes. The supernatant was decanted again, and 25 mL 0.1 M NaOH was added to extract humic substances for 4 hours. After separation by centrifugation, the humic extract was filtered through 0.2 μm hydrophilic membrane (Sartorious) and transferred into a dialysis membrane (Dialysis Membrane 12,000-14,000 MCWO, Spectra/Por) for dialysis against deionized water. Once the pH had dropped below 7, the humic extract was freeze-dried and stored in a sterilin tube. As described in section 2.5.9, 0.0090 g dried humic substance was dissolved in 350 μm deionised water and loaded into the gel well for further gel electrophoresis. There were six humic samples generated during this procedure which were labelled as Core 3 S 6-1 after acetate, core 3 S6-1 after dithionite, Core3 S 6-1 after both, and Core 3 S 7-1 after acetate, Core 3 S 7-1 after ditnionite, Core 3 S 7-1 after both.

In the second series, ~5 g soil from core 3 S6 and Core 3 S7 was suspended in 25 mL 0.1 M NaOH for 4 hours to extract humic substances. The extract was then prepared as described above. There were two humic samples obtained and labeled as Core 3 S6 NaOH and Core 3 S7

NaOH. The humic substances were subjected to three different extractions including acetate extraction, dithionite extraction, or both in the approximate liquid to solid ratio of 1 mL: 0.01 g carried out in the centrifuge tubes. As the humic substances can be dissolved in the solution, centrifugation was not able to separate the humic substances from the extract. The whole solution was therefore transferred into the membrane for dialysis to remove the acetate or dithionite reagent from the humic solution before being freeze-dried to obtain humic substances. Again, 0.0090 g dried humic substance was dissolved in 350 µm deionised water and loaded into the gel well for gel electrophoretic fractionation (see section 2.5.9). There were six humic samples generated during this procedure, which were labelled as Core 3 S 6-2 after acetate, Core 3 S6-2 after dithionite, Core3 S 6-2 after both, and Core 3 S 7-2 after acetate, Core 3 S 7-2 after dithionite, Core 3 S 7-2 after sequential extractions of acetate and dithionite solution..

Overall, the aim was to compare the amount of elements (U, Fe, Mn, Al) associated with total humic substances with that associated with the same materials after acetate extraction, after dithionite extraction and after both acetate and dithionite extraction. In total, there were 14 humic samples fractionated by gel electrophoresis which are summarised in Table 2.5.

Table 2.5: Explanation of labelling of humic substances

Humic substances (no reagent extraction)	**Humis substances of Core 3 S6-1, Core 3 S7-1 series (after reagent extraction)**	**Humic substances of Core 3 S7-1, Core 3 S7-2 series (after reagent extraction)**
Core 3 S6 NaOH	Core 3 S6-1 after acetate Core 3 S6-1 after dithionite Core 3 S6-1 after both	Core 3 S6-2 after acetate Core 3 S6-2 after dithionite Core 3 S6-2 after both
Core 3 S7 NaOH	Core 3 S7-1 after acetate Core 3 S7-1 after dithionite Core 3 S7-1 after both	Core 3 S7-2 after acetate Core 3 S7-2 after dithionite Core 3 S7-2 after both

2.5.11.5 Acetate extraction for elements associated with porewater colloid (3 kDa-0.2 µm)

The porewater samples from Core 3 collected during sampling trip 3 were split into two parts. One was handled in the glove bag with continuous purging with N_2 while the other was handled in air. The aim was determine whether the air affects the element distribution between the colloidal and dissolved fractions.

Porewater samples (see Section 2.5.3.1) isolated from each sub-fraction of Core 6 were fractionated by centrifugal ultrafiltration to obtain colloid (3 kDa-0.2 µm) in the porewater. An aliquot (3-20 mL) of porewater was transferred to a 3 kDa centrifuged ultrafiltration tube (Vivaspin 20 membrane, Vivascience) and centrifugationat 6000 g until less than 0.1 mL of porewater retained on the top. The filtrate was transferred to a sterilin container, and the accurate weight was recorded and designated as the '<3 kDa fraction'. 1.5 mL 1 M CH_3COONa/CH_3COOH at pH 4.5 was then added to the top of ultrafiltration unit and, continually agitated using bench-top shakers for 24 hours. Further ultrafiltration was then carried out at 8000 g until less than 0.1 mL acetate solution remained in the top compartment. A little deionised water was added and a 1 mL plastic pipette was used to wash any materials sticking to the membrane and to remove the retentate. The washings were then transferred to a tube and the accurate weight was recorded and labelled as '3 kDa- 0.2 µm remaining after acetate extraction'. Filtrate labelled as '3 kDa- 0.2 µm extracted by acetate' was transferred to a tube and accurate weight was recorded.

In total, there were three fractions generated in this experiment, including fractions <3 kDa, 3 kDa- 0.2 µm remaining after acetate extraction and 3 kDa- 0.2 µm extracted by acetate.

2.5.12 Scanning electron microscopy- energy dispersive X-ray spectroscopy (SEM-EDX)

SEM-EDX is used to characterize the morphology of the particles on a nanometer (nm) to micrometer (µm) scale. Analysis was carried out on a Philips XL30CP Scanning Electron Microscope equipped with a backscattered electron detector (BSE) and a secondary electron detector (SE). An X-ray detector PGT (Princeton Gamma Tech) was used for obtaining the X-ray spectra from U-contained particles (beam voltage: 15 kV, beam current: 1.00 nA). Dried grounded soil from Core 3 S7 was attached to SEM disks and immediately

coated with gold. The sample was then placed in a dessicator until analysed by SEM-EDX. The topography of the sample was obtained using SEM, the bright spot on the photograph was then selected to analyse the chemical composition using EDX. If the spot contained U, BSE or SE was selected to obtain a clear image of U grain.

2.5.13 X-ray diffraction (XRD)

X-ray diffraction (XRD) is a technique for qualitative identification of crystalline minerals by powder diffraction. Dried, and ground soil samples from Core 3 13.5 cm, 25.5 cm, 37.5 cm, Core 4 4.5 cm, 19.5 cm, 31.5 cm and Core 5 7.5 cm were ashed in a furnace at 450 ℃ for 4 hours. The reason to shorten the ashing time from 8 hours (Section 2.5.13) to 4 hours was to minimise the decomposition or alteration of some minerals. The ashed samples were analysed by XRD (Philips PW 1800). The XRD system was used in conjunction with the PC-APD software to collect and analyse the diffraction data. Quantitative XRD analysis was performed using Siroquant V2.5 phase analysis software.

2.5.14 Carbonate analysis

A portion of dried, homogenised sub-sample from Core 6 was accurately weighed and placed in an oven at 105 ℃ oven for moisture content correction before being placed in the ashing furnace at 450 ℃ for 8 hours (this was necessary to ensure that all organic matter had been completely destroyed as organic matter decomposition would also generate carbon dioxide). When the ashing was finished, the beakers were removed and allowed to cool in a glass desiccator. Once cooled to room temperature, the beakers which contained the residue were reweighed. ~0.1–2 g residue was accurately weighted and placed in a reaction flask and degassed with N_2 for 30 minutes. 20 mL 2 M HCl was injected in the flask. The reaction on the suspension proceeded for 20 minutes with continuous bubbling of N_2. The carbonate in the residue was stripped as CO_2 and trapped in 20 mL 0.1 M NaOH solution. Determination of the amount of carbonate dissolved in 0.1 M NaOH was achieved by titration with 0.01 M HCl using phenolphthalein and methyl orange as indicator (British Standard Institution, 1996). The carbonate concentration in a 0.1 M reagent blank was pre-analysed to correct the carbonate concentration trapped in NaOH. All samples were run in duplicate where soil mass permitted.

2.5.15 Fe^{II}/Fe total analysis

The Fe^{II} determination was based on the method provided by Viollier et al. (2000). To 1 mL porewater was added 100 µL ferrozine (Aldrich) prepared in 10 M ammonium acetate (Aldrich) solution to form a magenta complex species, for which the maximum ultraviolet absorbance was recorded at 562 nm (see Appendix Section 9.4.6). A series of Fe^{II} standards were prepared to obtain the Fe^{II} calibration curve (Figure 2.21) (see Appendix Section 9.16 Table 9.38).

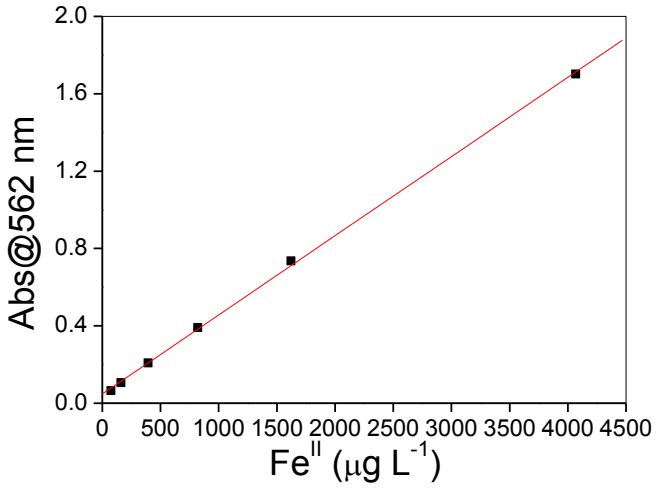

Figure 2.21: Calibration curve with Fe^{II} standards

The equation of the calibration curve in Figure 2.20 is:

$$Abs=0.0475+4.092\times10^{-4}C_{Fe(II)}$$

Equation 2.1

The Fe^{II} determination in each sub-section of Core 8 was carried out in-situ. After all the porewater samples were processed within 20 minutes, another 1 mL of the first analysed porewater sample was added with ferrozine again to check whether exposure to oxygen in the field had caused rapid oxidation of the Fe^{II} to Fe^{III}. The test showed that the Fe^{II} remained stable in the porewater over the time period of sample processing.

Three hours later, when the samples were transported back to the lab, Fe^{II} concentrations were immediately determined using a UV/VIS/NIR spectrophotometer (Perkin Elmer

Lambda 900). The Fe^{II}analysis method from Viollier et al. (2000) reported that changes in the absorbance of the Fe^{II}-ferrozine complex remained under 1% for periods of up to 3 hours. Total Fe concentration in the porewater was analysed by ICP-MS (section 1.5.17).

2.5.16 Inductively coupled plasma-optical emission spectrometry (ICP-OES)

2.5.16.1 Principle of ICP-OES

ICP-OES is a technique used to determine the concentrations of a wide range of elements over a wide concentration range (0.0002-1000 mg L^{-1}) in aqueous or organic solutions. The main advantages of ICP-OES over atomic absorption (AAS) techniques are its simultaneous multi-element analysis capabilities, longer linear dynamic ranges, and fewer condensed phased interferences (Boss and Fredeen, 2004).

In ICP-OES, the sample is nebulized and transported to the plasma where it is desolvated, vaporized, atomized, and excited and/or ionized by the plasma. The excited atoms and ions emit their characteristic radiation which is collected by a device that sorts the radiation by wavelength. The radiation is detected and turned into electronic signals that are converted into concentration information for the analyst (Figure 2.22) (Boss and Fredeen, 2004).

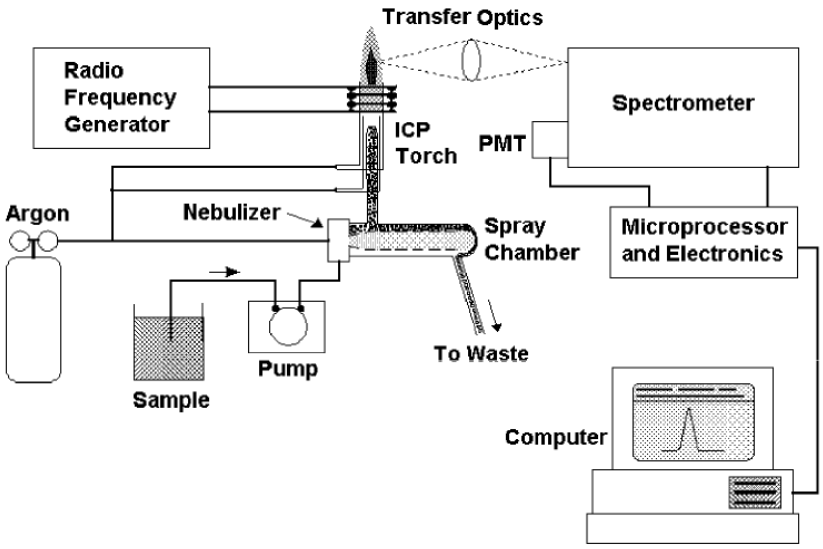

Figure 2.22: Major components and layout of an ICP-OES instrument (Boss and Fredeen, 2004)

The ICP torches contain three concentric tubes for argon flow and aerosol injection. The plasma flow (usually 7 – 15 L min^{-1}) spirals tangentially around as it proceeds upward to keep the quartz walls of the torch cool. The auxiliary flow (about 0.75 L min^{-1}) keeps the plasma discharge away from the intermediate and injector tubes and makes sample aerosol introduction into the plasma easier. The nebulizer flow, which carries the sample aerosol, is injected into the plasma through the central tube or injector (Figure 2.23) (Boss and Fredeen, 2004).

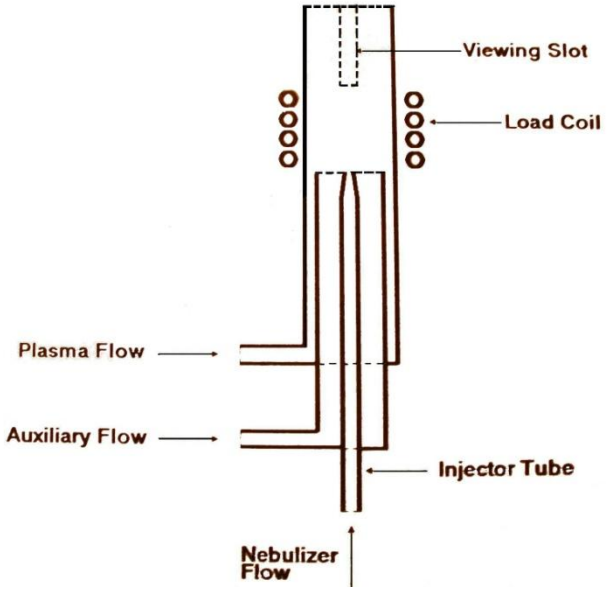

Figure 2.23: Schematic of a torch used for ICP-OES (Boss, 2004)

Inductively coupled plasma (ICP) is generated during the coupling of free electrons from argon to the energy radio frequency (RF) magnetic field. The magnetic field is formed when RF power (typically 700 – 1500 watts) is applied to the load coil, which surrounds the top end of the torch. With argon gas being swirled through the torch, a spark is applied to the gas causing some electrons to be stripped from their argon atoms. These electrons are caught up and accelerated by magnetic field. These high-energy electrons in turn collide with other argon atoms and continue in a chain reaction, forming an ICP discharge (Figure 2.24) (Boss and Fredeen, 2004).

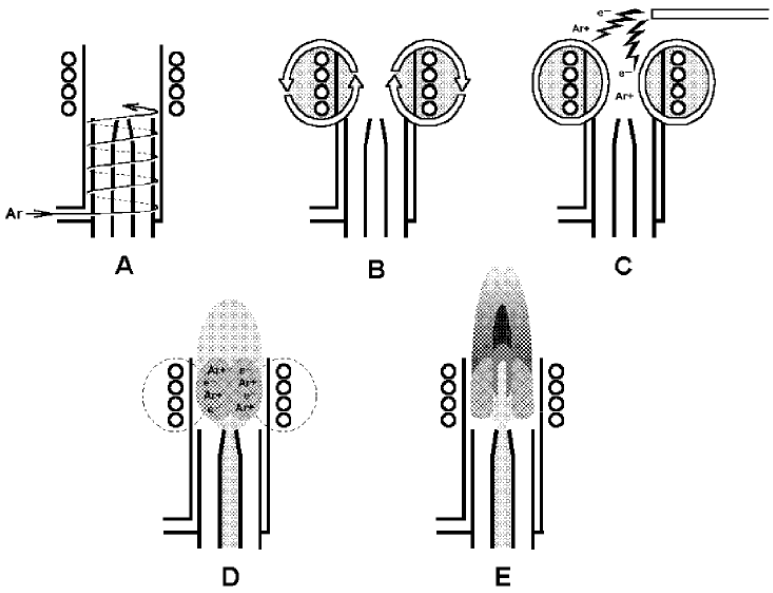

Figure 2.24: Cross section of an ICP torch and load coil depicting an ignition sequence. A – Argon gas is swirled through the torch. B – RF power is applied to the load coil. C – A spark produces some free electrons in the argon. D – The free electrons are accelerated by the RF fields causing further ionization and forming a plasma. E – The sample aerosol-carrying nebulizer flow punches a hole in the plasma (Boss and Fredeen, 2004)

In optical emission spectrometry (OES), the sample is subjected to temperatures high enough to cause not only dissociation into atoms but to cause significant amount of collisional excitation (and ionization) of the sample atoms to take place. The atoms or ions can decay from their excited states to lower states though thermal or radiative (emission) energy transitions. Every element has its own characteristics set of energy levels and thus its own unique set of emission wavelengths. In OES, the intensity of the light emitted at specific wavelengths is measured and used to determine the concentrations of the elements of interest (Figure 2.25) (Boss, 2004).

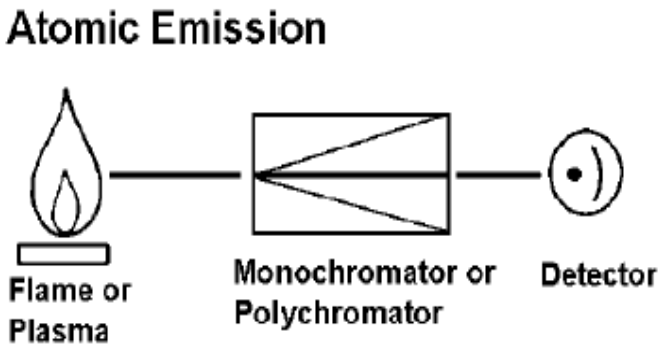

Figure 2.25: Schematic of Atomic Emission spectrometry systems (Boss and Fredeen, 2004)

2.5.16.2 Method used for ICP-OES analysis

Total elemental concentrations in solution were determined using a Perkin Elmer 5300 DV ICP-OES (Perkin Elmer, Seer Green, UK). Elemental calibration standards for U, Fe, Mn, Pb, Cu, Zn, Al, As were prepared from 1000 mg L^{-1} stock solutions (in 1 M HNO_3) to span a concentration range of 0.02-10 mg L^{-1}. The emission intensity was measured at 409.014 nm for U, 238.204 nm and 239.562 nm for Fe, 257.610 nm and 260.568 nm for Mn, 220.353 nm for Pb, 324.752 nm and 327.393 nm for Cu, 188.979 nm for As, 213.857 nm for Zn, 308.215 nm for Al. Table 2.6 shows the values of the key instrumental parameters used in all analyses.

Table 2.6: ICP-OES conditions adopted for all analyses

Instrument		**Parameters**
Argon flow	Coolant	15 L min^{-1}
	Auxillary	0.2 L min^{-1}
	Nebulizer	0.8 L min^{-1}
Pump flow rate		1.5 L min^{-1}
RF power		1400 W

For quality control purposes, a standard reference solution M6 (CertiPUR - ICP multielement standard solution VI) was analysed along with each batch of samples. This solution includes all elements being determined in this study. Good agreement was typically obtained between the measured (e.g. U= 0.093 mgL^{-1}) and certified (U= 0.1 mgL^{-1}) values.

2.5.17 Inductively coupled plasma-Mass spectrometry (ICP-MS)

2.5.17.1 Principle of ICP-MS

ICP-MS is a technique that is suitable for the ultra-trace analysis of a wide range of elements (0.0005-100 μg L^{-1}). The difference between ICP-MS and ICP-OES is that mass spectrometry separates the ions generated from ICP based on their mass-to-charge ratio, while ICP-OES separates the light according to its wavelength.

The ICP-MS instrument has the following components: sample introduction system, inductively coupled plasma (ICP) source, sometimes a collision cell, interface vacuum, ion lenses, analyzer, detector, vacuum system, RF generator (Figure 2.26). In ICP-MS, the sample is nebulized and transported to the plasma where it is desolvated, vaporized, atomized and excited and/or ionized by the plasma. After the analyte ion beams are formed and then passed through a collision cell (He gas), they are extracted through a series of cones, focused by ion lenses before entering into a quadrupole mass spectrometer. The samples are then separated on the basis of their mass-to-charge ratio by the quadrupole. The ion signals are measured by the electron multiplier detector (Becker, 2008).

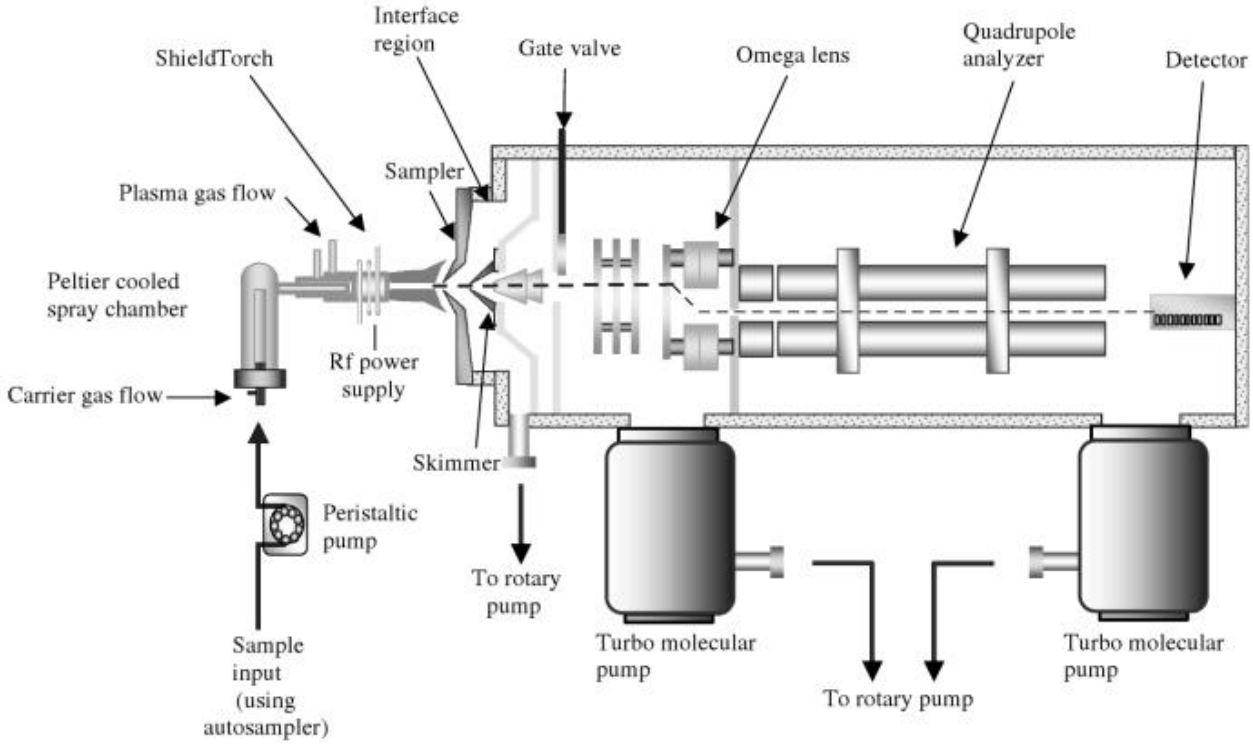

Figure 2.26: Major components and layout of an ICP-MS instrument (Becker, 2008)

The quadrupole is composed of four long metal rods whichhave RF and DC voltages applied to them (Figure 2.27). The rods behave as a mass filter by changing the voltages. A mixture of ions with different mass-to-size ratios pass through the center space of the rods and only ions of a specific mass-to-charge ratio are allowed to exit at the end and enter the detector. All other masses collide and were rejected by the rods, such as electrons and neutrons (Becker, 2008).

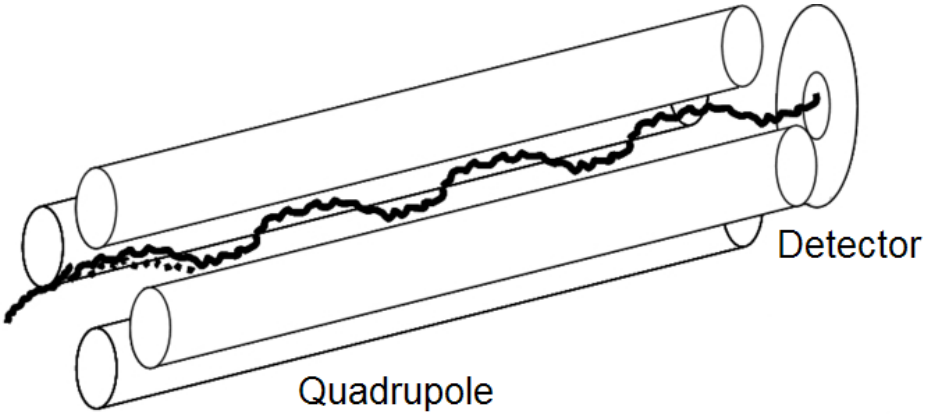

Figure 2.27: Quadrupole mass spectrometry (adapted from Taylor, 2001)

The electron multiplier detector has many dynodes. When the ion hits the first dynode, a shower of electrons is generated. The electrons are multiplied by successively hitting the next dynodes and converted into a measurable electrical current (Becker, 2008).

2.5.17.2 Method of ICP-MS

Total element concentrations in solution were determined using an Agilent 7500ce ICP-MS. Elemental calibration standards for U, Fe, Mn, Pb, Cu, Zn, Al, Pb, As, Ca were prepared from 1000 mg L^{-1} stock solutions (Perkin Elmer, Seer Green, UK) in an appropriate solution to span a concentration range of 0.1-1000 µg L^{-1}. For multiple-element analysis, the ICP-MS was carried out in spectrum acquisition mode, where relevant mode was selected for each element (Table 2.7). If there was uncertainty about which gas mode was better, an element would be analysed under both modes, and the best one would be selected according to the standard reference material.

Table 2.7: Acquisition modes selected for the elements analysed

Acquisition modes	Relevant for elements
He mode	^{56}Fe, ^{57}Fe, ^{55}Mn, ^{63}Cu, ^{65}Cu, ^{66}Zn,^{68}Zn, ^{27}Al, ^{75}As
No-gas mode	^{238}U, ^{55}Mn, ^{206}Pb, ^{207}Pb, ^{208}Pb, ^{63}Cu, ^{65}Cu, ^{27}Al,^{64}Zn, ^{66}Zn, ^{68}Zn

For quality control purpose, the standard reference material SRM 1643e was analysed after the standards for calibration were run whilst the standard reference solution M6 was run after all the samples were analysed. One standard was chosen to run after every six samples, followed by a rinse using blank solution. Table 2.8 shows the values of the key instrumental parameters used in all analyses.

Table 2.8: ICP-MS conditions adopted for all analyses

Instrument	Parameters
RF power	1540 W
Reflected power	1
Argon gas carrier flow	0.82 L min^{-1}
Argon gas make-up flow	0.21 L min^{-1}
Nebuliser up-take rate	0.2 ml min^{-1} (0.06 rps)
Analyser pressure (vacuum)	3×10^{-6} Pa
IF/BK pressure (vacuum)	8.5×10^{-1} Pa
Rinse speed (rinse port)	0.3 rps
Between sample rinse time, rinse vial	40 sec
Rinse speed (rinse vial)	0.1 rps
Between sample rinse time, rinse port	10 sec

3 Results and discussion for sampling trip 1 on 11/12/2007: initial survey of the Needle's Eye site and method development

3.1 Aims

The key aims were to: (i) determine the elemental (U, Fe, Mn, Pb and Cu) concentrations in the cave water emerging from the mineralization and toquantify the changes in groundwater elemental concentrations with increasing distance from the cave; (ii) to characterize the groundwater colloids in terms of their composition and metal binding behaviour; (iii) to characterize humic substances extracted from the organic-rich soils in terms of their size and metal binding behaviour via gel electrophoretic and gel filtration fractionation; and (iv) to optimize protocols for investigating U interactions in both water and solid phase samples.

3.2 Lateral variations in elemental concentrations in Needle's Eye water samples

The concentrations of U, Fe. Mn, Pb and Cu in each of the water samples are shown in Table 3.1.

3.2.1 Uranium concentrations

Uranium concentrations in the cave drip water emerging from the mineralization ranged from 60-110 μg L^{-1}. At 20 m from the cave, U concentrations in the soil core porewaters were in the range of 5-60 μg L^{-1} and that in the bog water collected as the sampling pit filled up was within this range, at ~22 μg L^{-1}. At 30 m from the cave, the range for soil core porewaters and the value for bogwater were 2-8 μg L^{-1} and ~11 μg L^{-1}, respectively. Thus,

by 30 m from the base of the cliff, the U concentrations had decreased by a factor of ~10. This clear trend of decreasing U concentration with increasing distance from the mineralization agrees with previous work which showed that the organic soil at Needle's Eye retained more than 90% of the uranium released from the mineralisation (MacKenzie et al., 1991).

3.2.2 Other elemental concentrations

For the same samples, the highest concentrations of Fe, Mn, Pb were found in Core 2 porewaters, the site furthest from the mineralization. For Cu, there was no consistent relationship with distance from the mineralization.

Redox potential and pH conditions were not recorded during the initial survey. In terms of the geochemistry of the water samples, higher concentrations of Mn and Fe were found in core porewaters compared with the cave drip waters. In particular, the highest concentrations of both Mn and Fe were found for the core furthest from the mineralization. Since reducing conditions promote dissolution of Mn and Fe minerals, it is likely that the conditions at 30 m from the cave are probably more strongly reducing than at Core 1.

Table 3.1: Elemental concentration data for water samples collected during the initial survey (11/12/2007)

Site	Distance from cave (m)	Sample description	Aqueous phase concentrations				
			U (μg L^{-1})	Fe (mg L^{-1})	Mn (mg L^{-1})	Pb (mg L^{-1})	Cu (mg L^{-1})
Cave	0	Drip water 1	107	0.020	0.004	0.019	0.014
		Drip water 2	70.4	0.021	0.003	0.021	0.026
		Drip water 3	67.5	0.012	0.003	0.018	0.040
Core 1	20	Porewater	5.6-58.6	0.099-0.457	0.004-0.018	0.021-0.031	0.023-0.079
		Bog water 1	21.6	0.110	0.004	0.017	0.023
Core 2	30	Porewater	1.9-7.6	0.284-1.498	0.005-0.031	0.026-0.031	0.018-0.030
		Bog water 2	11.1	0.173	0.003	0.025	0.011

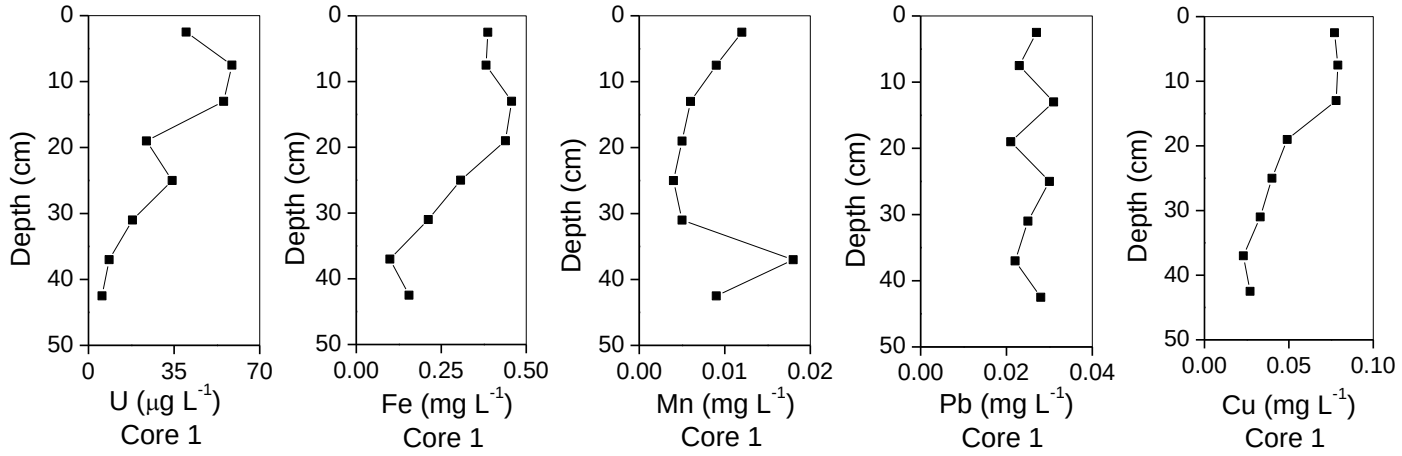

Figure 3.1: Vertical concentration profiles for U, Fe, Mn, Pb and Cu in soil porewaters from Core 1 (20 m from cave)

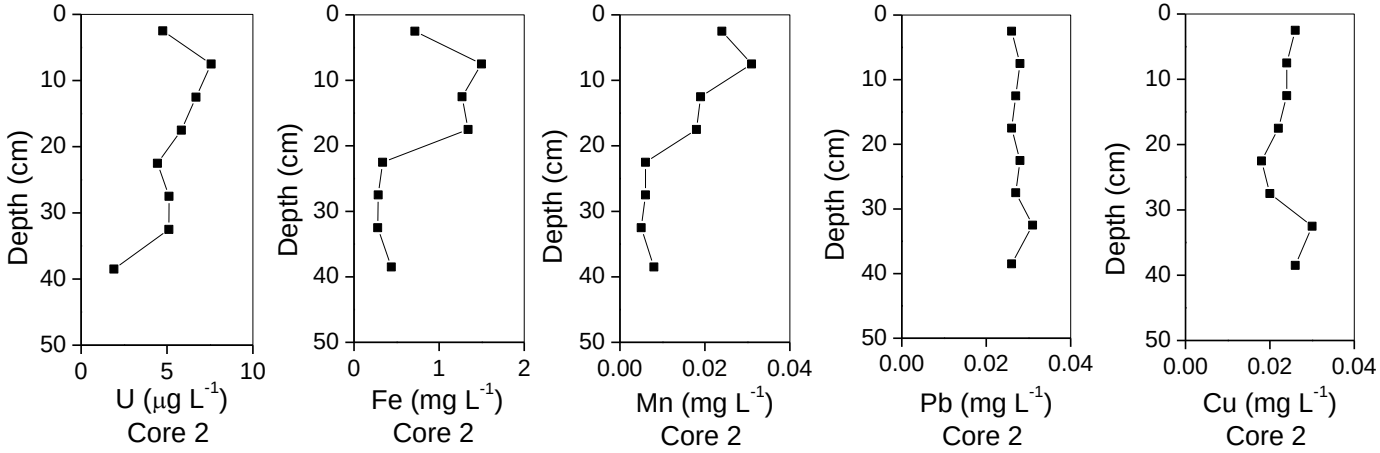

Figure 3.2: Vertical concentration profiles for U, Fe, Mn, Pb and Cu in soil porewaters from Core 2 (30 m from cave)

3.3 Vertical profiles for U and other elements in the porewaters of soil samples from Cores 1 and 2

3.3.1 Core 1 (20 m from the cave)

After reaching a maximum concentration of ~60 μg L^{-1} at 5-15 cm depth, U concentrations in soil Core 1 porewaters showed a ten-fold decrease to ~6 μg L^{-1} at the bottom of the core (~45 cm depth). Fe and Cu also had concentration maxima in the uppermost 20 cm sections, and then showed a similar trend of decreasing concentration towards the bottom of the core. Mn concentrations decreased from the surface down to 25 cm depth but the maximum value of ~0.02 mg L^{-1} occurred at 35-40 cm depth. Porewater Pb concentrations did not vary significantly with depth and were close to detectable limits by ICP-OES (Figure 3.1) (see Appendix section 9.8, Table 9.4).

3.3.2 Core 2 (30 m from the cave)

After reaching a maximum concentration of ~8 μg L^{-1} at 5-10 cm, U concentrations showed a gradual decrease to ~5 μg L^{-1} at 27-35 cm, and then amore rapid decrease to ~2 μg L^{-1} towards the bottom of the core (Figure 3.2). Fe had a broad maximum concentration of ~1.5 mg L^{-1} at 5-20 cm, below which it decreased towards the bottom of the core. The maximum Mn concentration of 0.03 mg L^{-1} occurred at 7.5 cm; as for Fe, there was a decrease in concentration towards the bottom of the core. There was no significant change in Pb concentration with increasing depth and again concentrations were close to detectable limits; in contrast, Cu concentrations gradually decreased from surface to a depth of 22.5 cm, after which it increased to 0.03 mg L^{-1} at 32.5 cm (see Appendix section 9.8, Table 9.4).

The information obtained from these graphs can be very useful when it comes to assessing

the redox status of a system. Equations 3.1-3.4 show reduction half-reactions along with standard reduction potentials (Eh) fortwo important oxidizing agents (Mn and Fe) present in mineral phases as well as for U^{VI} in soils.

Mn Oxide (Bricker, 1964)

$1/2Mn^{IV}O_{2(s)} + 2H^+ + e^- = 1/2Mn^{2+}_{(aq)} + H_2O$ $E_h = 1.29$ V Equation 3.1

Goethite (Robie et al., 1978)

$Fe^{III}OOH_{(s)} + 3H^+ + e^- = Fe^{2+}_{(aq)} + 2H_2O$ $E_h = 0.67$ V Equation 3.2

Hematite (Robie et al., 1978)

$1/2Fe^{III}O_{3(s)} + 3H^+ + e^- = 1/2Fe^{2+}_{(aq)} + 3/2H_2O$ $E_h = 0.66$ V Equation 3.3

Uranyl ion (Essington, 2003)

$1/2U^{VI}O_2^{2+} + 2H^+ + e^- = 1/2U^{4+} + H_2O$ $E_h = 0.308$ V Equation 3.4

In a soil profile, the conditions often change from oxidizing at the surface to reducing conditions at depth. Water saturating the pore spaces between soil particles decreases the movement of oxygen into and through the soil, but biological activity such as the breakdown of organic matter continues to consume oxygen in the soil (see Section 1.2.8.1). After the soil oxygen becomes depleted, anaerobic microorganisms use other compounds as electron acceptors in redox reactions, following the progression NO_3^-, Mn^{IV}, Fe^{III} and then SO_4^{2-} reduction. In the deeper anaerobic soil, reduced forms such as Mn^{II}, Fe^{II}, NH_4^+ and sulfide are dominant (Mitsch and Gosselink, 2007). Thus the soil depth profile can show a decrease in oxidation-reduction potential (Eh) with increasing depth. In theory, the species on the left hand side of the redox couple with highest potential will undergo reduction first, e.g. solid phase Mn^{IV} will be reduced to soluble Mn^{II} before solid phase Fe^{III} is reduced to soluble Fe^{II} (Stumm and Morgan, 1996). This means that the porewater Mn

peak should be nearer the surface than the Fe peak and a U^{VI} should be reduced to U^{IV} at greater depth than the Fe peak. However, in core 1, U concentration maximum lies slightly above that for Fe while in core 2, U, Fe and Mn peaks occur at the same depth, indicating other factors may be controlling uranium speciation in the surface soil porewaters. Possible explanationsarethat (i) Mn/Fe (hydr)oxides have adsorbed U^{VI} species on their surfaces and so reductive dissolution of these mineral phasescould release U into solution at the same depth as the reduced forms of Mn/Fe, (ii) U^{VI} may be reduced and complexed by humic substances and so the presence of U in the solution phase is controlled by processes related to solubilisation of the humic materials, and (iii) the humic substances themselves may form coatings on the Mn/Fe (hydr)oxide surfaces; here, reductive dissolution of the mineral phase may release humic-complexed U into solution.

3.4 Element associations with colloids in soil porewaters from Cores 1 and 2

Figures 3.3 and 3.4 show the distribution of U, Fe, Mn, Cu, Pb amongst colloidal fraction (100 kDa-0.2 μm, 30-100 kDa and 3-30 kDa) of porewaters obtained from Cores 1 and 2. The <3 kDa fraction was not analysed and so the sum of elemental concentrations from the analysed colloidal fractions was significantly less than the values for total (<0.2 μm) porewaters in some cases.

As described in Section 3.2, at 20 m from the cave, there was a marked decrease in soil core porewater U concentration with increasing depth whilst at 30 m from the cave, there was a more gradual decrease in U concentration with increasing depth. Centrifugal ultrafiltration of the porewaters from selected depths (top, middle, bottom) was used to investigate the U associations with colloids within these porewaters.

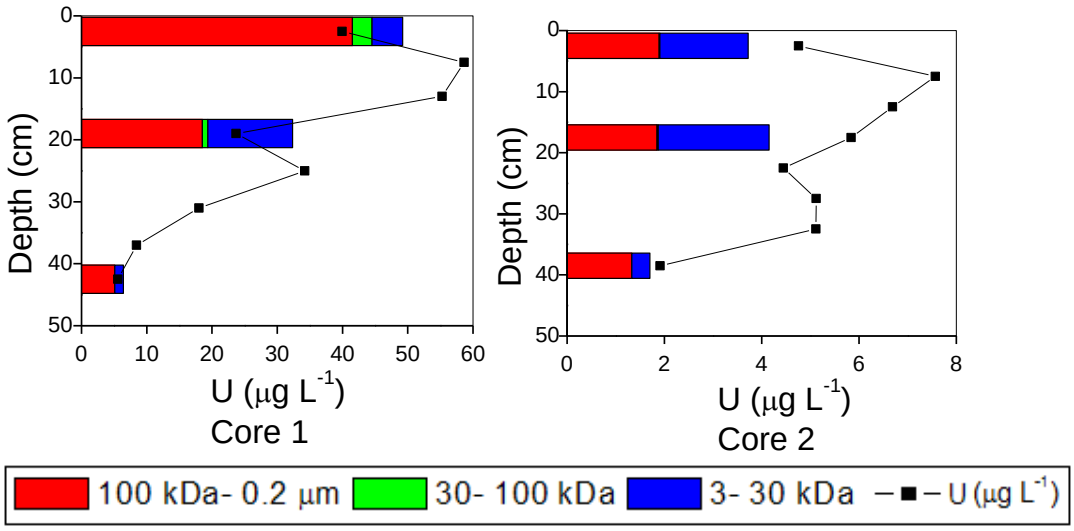

Figure 3.3: Total vertical concentration for U in soil porewater (line) and corresponding colloidal association (bars) from selected depths for Core 1 and Core 2

At 20 m from the cave, the sum of the U concentrations in the colloidal fractions was slightly greater than the measured total U (<0.2 µm) concentrations. Nevertheless, the trend in total colloidal U with increasing soil depth matched that for total U.For the surface sample, >85%waspresent in the large colloid (100 kDa-0.2 µm) fraction, but, at the mid-depth, >40% was found in the small colloid (3-30 kDa) fraction. At 30 m from the cave, however, there was a clear bimodal split of U between large and small colloids at depths for both the surface and mid-depth samples (Figure 3.3) (see Appendix section 9.9, Table 9.10). It was clear, however, that for future work, (i) the fractionation procedure must be carried out more precisely; and (ii) the dissolved fraction must be analysed to ensure that a mass balance had been achieved.

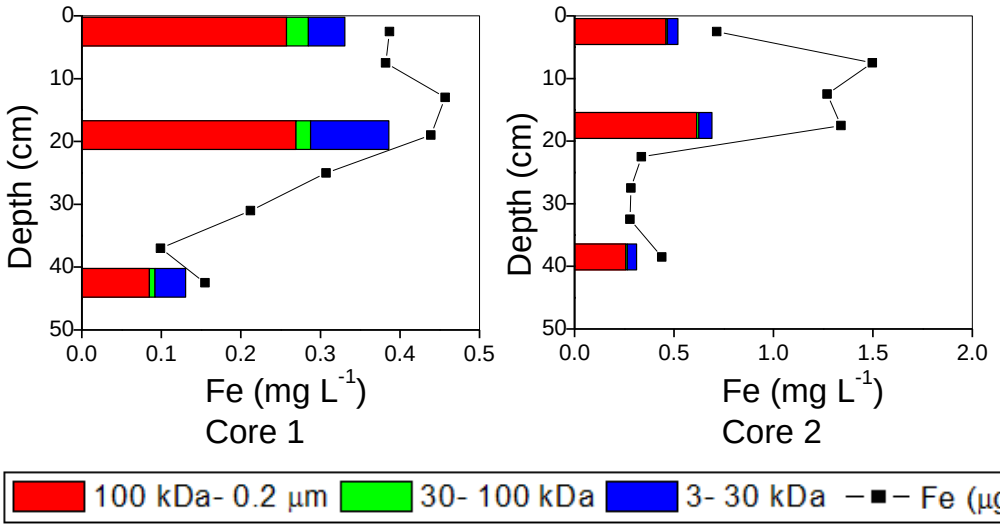
Depth (cm)
Fe (mg L-1)
Core 1
Core 2

100 kDa- 0.2 µm
30- 100 kDa
3- 30 kDa
Fe (µg L-1)

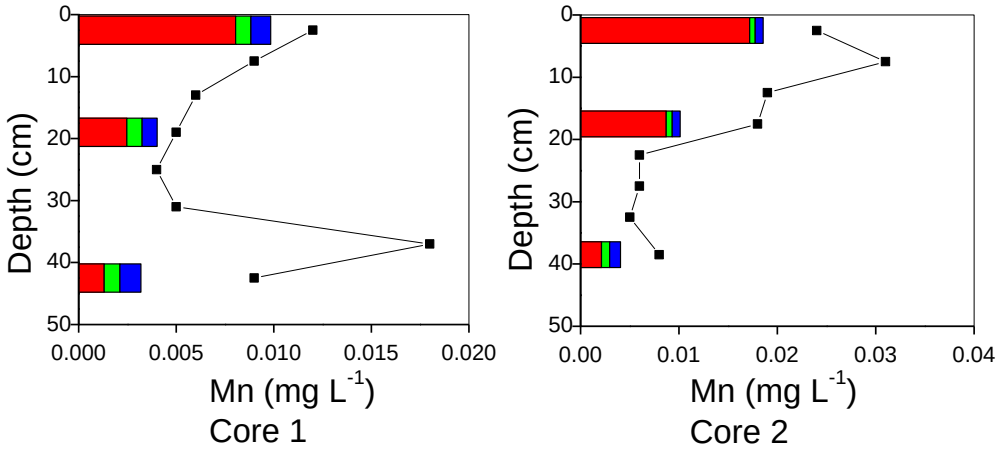
Depth (cm)
Mn (mg L-1)
Core 1
Core 2

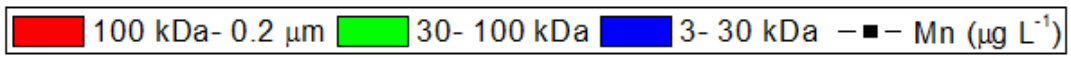
100 kDa- 0.2 µm
30- 100 kDa
3- 30 kDa
Mn (µg L-1)

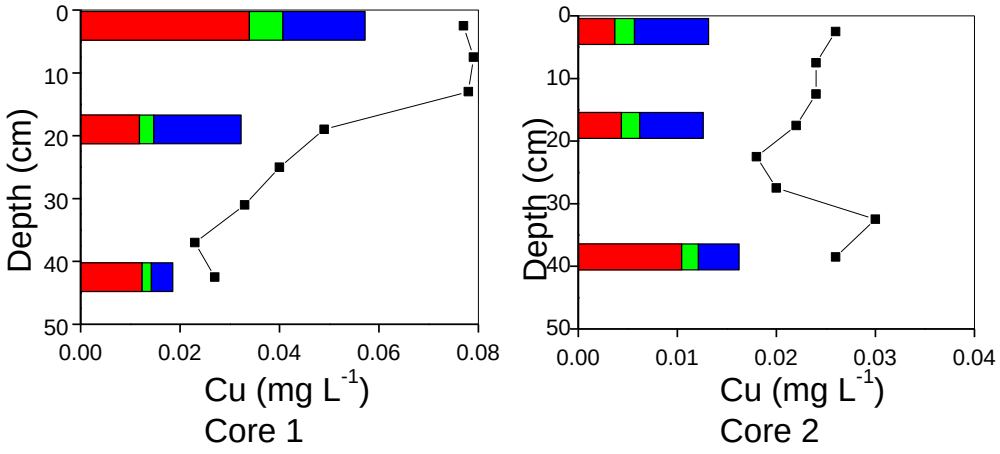
Depth (cm)
Cu (mg L-1)
Core 1
Core 2

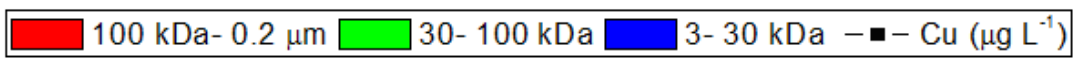
100 kDa- 0.2 µm
30- 100 kDa
3- 30 kDa
Cu (µg L-1)

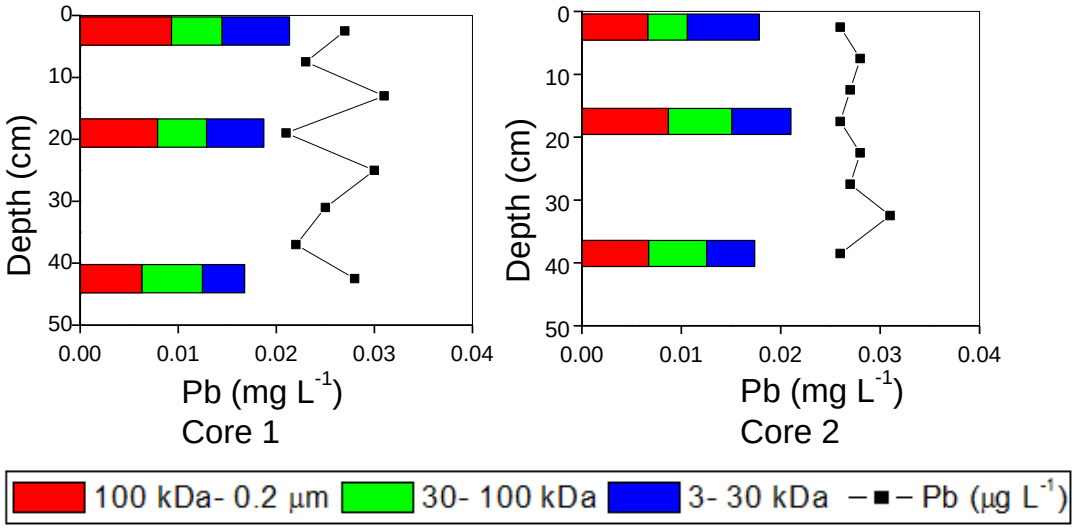

Figure 3.4: Total vertical concentration for Fe, Mn, Pb and Cu in soil porewater (line) and corresponding colloidal association (bars) from selected depths for Core 1 and Core 2

At 20 m from the cave, Fe and Mn were predominantly present in the large colloid (100 kD-0.2 µm) fraction. In contrast with Fe and Mn, a lower proportion of Cu and Pb was associated with the large colloids. Cu showed a split between large and small (3-30 kDa) colloid fractions, especially in the top 0-20 cm sections, whilst Pb was more evenly distributed across the three colloidal size fractions. A similardistribution pattern for each of these elements (Fe, Mn, Cu and Pb) was observed at 30 m from the cave (Figure 3.4) (see Appendix section 9.9, Table 9.11).

A series of both field and laboratory studies have reported that organic colloid or organic-mineral colloids are implicated in the transport of uranium in the environment (Artinger et al., 2002; Sachs et al., 2006; Oliver et al., 2008a; Crancon et al., 2010; Pokrovsky et al., 2005, 2010; Claveranne-Lamolere, 2011; Graham et al., 2008, 2011). However, as discussed in Section 1.4.4, the extent to which uranium associates with colloids seems to vary and may be dependent on the site studied. Ranville et al. (2007) reported that only ≤ 2% of the U, likely in the form of U(VI), was complexed with humic colloid at pH>7 and in the presence of substantial dissolved carbonate. Bednar et al. (2007)

studied interaction of uranium with humic acid and aqueous plant extract, and demonstrated that nearly 100% of U was bound to organic ligands, which generally decreased uranium sorption to soils. Uranium was also found to associate with inorganic mineral or ligands such as Fe colloids and carbonate (Langmuir, 1978; Krawczyk-Barsch et al., 2004). In addition, it has been suggested that association with large Fe/Al/organic colloids was a precursor to the removal of U from the porewater to solid phase. For example, Oliver et al. (2008a) reported the depleted uranium at the Dundrennan Firing Range was mainly split into the large (100 kDa-0.2 μm) and small (3-30 kDa) colloid fraction. The Fe/Al/organic colloids in this large size fraction were believed to be responsible for limiting the transport of uranium in the field (Graham et al., 2011).

From the results of these initial experiments, in comparison with the Core 1 samples, there was a greater proportion of Core 2 soil porewater U in the small colloid fraction, indicating that small colloids may be more effective in the lateral transport of U. Since at 30 m, Fe and Mn are still found in the large colloidal fractions, it cannot be ruled out that the U in this size fraction is associated with these elements rather than humic colloids, and further investigation is needed to characterize these colloids.

For further work, changes to the ultrafiltration procedure were implemented. Firstly, recognizing that porewater comprises both colloidal (3 kDa-0.2 μm) and truly dissolved (<3 kDa) components and that not analysing the <3 kDa fractions was an oversight. Comparison of the colloidal concentrations with the total porewater values showed that the truly dissolved fraction (<3 kDa) potentially contained a considerable proportion for some elements. Thus, all subsequent work involved analysis of the truly dissolved fraction. Secondly, only DI water was used to remove the retentate from the ultrafilter membranes, but it was observed there was some brown colour left on the membrane, indicating that DI water only was not able to efficiently recover the retentates from the membrane. In the next phase of work, a small amount of 0.045 M Tris-borate buffer was used to aid recovery of

the humic colloids that are retained by the ultrafilters (see Appendix Table 9.12).

3.5 Characterization of humic substances extracted from solid phase soil samples

After rapid alkaline extraction followed by dialysis and then concentration, 5 ml aliquots of each soil humic substance extract were digested and analysed by ICP-OES for total elemental content (see Section 2.5.3.3 sampling trip 1), which isshown in Table 3.2. The data in Table 3.2 cannot be used to quantify elemental associations with humic substances in mg kg^{-1} dry weight soil at different depths because the alkaline extraction was performed using wet fresh soil samples for which the water content was not determined. The purpose of these experiments was, however, to compare the associations of U and other elements with electrophoretically and gel chromatographically separated humic components at different soil depths. In order to compare the efficacy of these two separation methods, the concentrations shown in Table 3.2 were then used to calculate elemental ratios, e.g. Fe/U.

Table 3.2: Element concentrations (U, Fe, Mn, Cu and Pb) in each soil humic extract

Core 1 Depth (cm)	U	Fe	Mn	Cu	Pb	Core 2 Depth (cm)	U	Fe	Mn	Cu	Pb
	mg L^{-1}						mg L^{-1}				
2.5	0.67	3.69	0.13	0.80	0.19	2.5	0.53	14.19	0.17	0.51	0.14
7.5	0.35	5.27	0.11	0.66	0.15	7.5	0.77	25.59	0.22	0.75	0.14
13	1.28	3.45	0.10	0.94	0.20	12.5	0.41	15.13	0.16	0.44	0.18
19	1.16	6.22	0.05	1.60	0.19	17.5	0.58	11.25	0.09	0.51	0.12
25	0.60	3.41	0.01	0.62	0.14	22.5	0.42	2.39	0.04	0.29	0.16
31	0.84	7.57	n.d.	0.88	0.25	27.5	0.25	8.04	0.08	0.31	0.19
37	0.47	7.34	0.03	0.41	0.17	32.5	0.66	9.58	0.05	0.41	0.37
42.5	0.63	7.79	0.01	0.59	0.23	38.5	0.37	13.58	0.13	0.37	0.13

Further investigation of metal associations with the soil humic substances was then achieved by using gel electrophoresis and gel filtration techniques.

3.5.1 Gel electrophoretic fractionation of soil humic substances extracted from Cores 1 and 2

Where the elementalconcentrations in Table 3.2 were too low in comparison with those found in digested electrophoretic gel blanks, the extracts were concentrated by partial freeze-drying before being fractionated by gel electrophoresis. The elemental concentrations in the gel blank were shown in section 2.5.9.2 (validation of the gel electrophoretic fractionation procedure). Taking account of the elemental concentrations in blank gel stripsand the fact that only 350 µL solutions is placed in the each gel well, it was calculated that all the soil humic substances required to be concentrated prior to gel electrophoresis to ensure that the U concentrations in the fractionated samples were much higher than those in gel blanks.

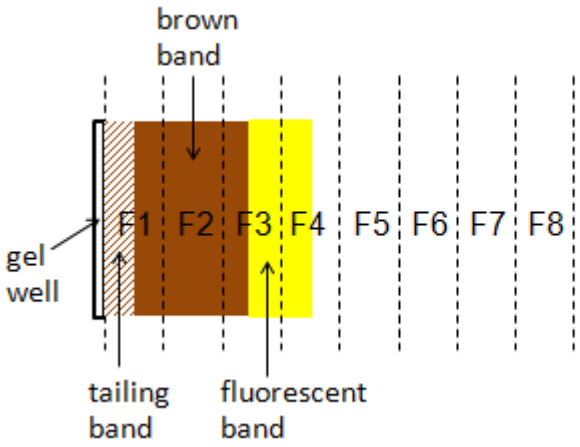

Figure 3.5: Schematic of the gel electrophoretic pattern for Core 1 and Core 2 samples obtained after 30 minutes showing the position of the tailing, brown and fluorescent bands

For each of the humic substances from Core 1 (20 m from cave) and Core 2 (30 m from cave), visual observation of the gel after running for 30 minutes showed that a dark brown band had emerged from the gel well. Viewed under UV light, a fluorescent band was also observed (Figure 3.5). Decreasing size and/or charge results in increased electrophoretic mobility (increased movement from left to right of the gel). The gel was then cut into eight 1-cm width strips and the positions of the band were noted. For all samples, the tailing bands were located in F1, dark brown bands were in F1-F3, while the florescent bands were in F3 and F4, with the fluorescent being slightly ahead of the brown band.

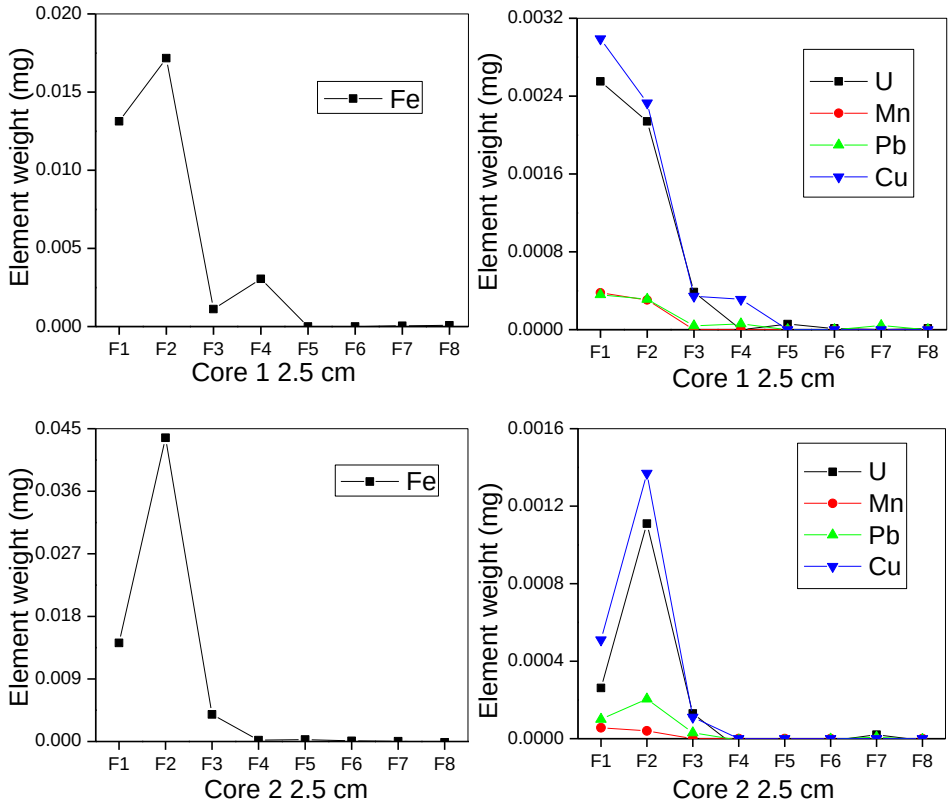

Figure 3.6 Mass of elements (U, Fe, Mn, Pb and Cu) in gel electrophoretic fractions from Core 1 2.5 cm and Core 2 2.5 cm (F1-F8 represents 1-cm sections of the gel strip that have been digested and analysed for element concentration by ICP-OES).

The electrophoretic patterns (in mg element per digested gel strip) for elements associated

with humic extracts from Core 1 2.5 cm and Core 2 2.5 cm depth sections are shown in Figure 3.6 (see Appendix section 9.12.2, Table 9.22). The patterns for Fe are shown in separate graphs because the maximum amounts were ~10-100 times greater in comparison with the other elements.

The first important observation was that each of the elements was almost entirely present in the fractions which contained the humic substances (F1-F4). Thus, no dissociation from the humics had occurred during the fractionation procedure. Secondly, for each sample, all elements had a very similar distribution pattern and the majority of each element was found in association with the least mobile humic fractions (F1-F2). This was particularly evident for the Core 1 2.5 cm sample where the largest amounts of U (also Cu, Mn and Pb) were found in F1. For the Core 2 2.5 cm sample, the highest amounts of each element were obtained for F2. It was also evident that there was a slightly greater spread for some elements for the Core 1 2.5 cm sample in that there were detectable amounts of Fe and Cu in F4. The smaller organic molecules within this fraction have fluorescent properties.

For the humic substances from the other depths, the element distributions are very similar to those shown in Figure 3.6. Since it is difficult to examine the gel eletrophoretic patterns for each element in each depth, e.g. whether there is trend in association with larger or smaller humic substance with increasing depth, all the elements were presented in another way, which grouped the individual element with each depth (Figure 3.7).

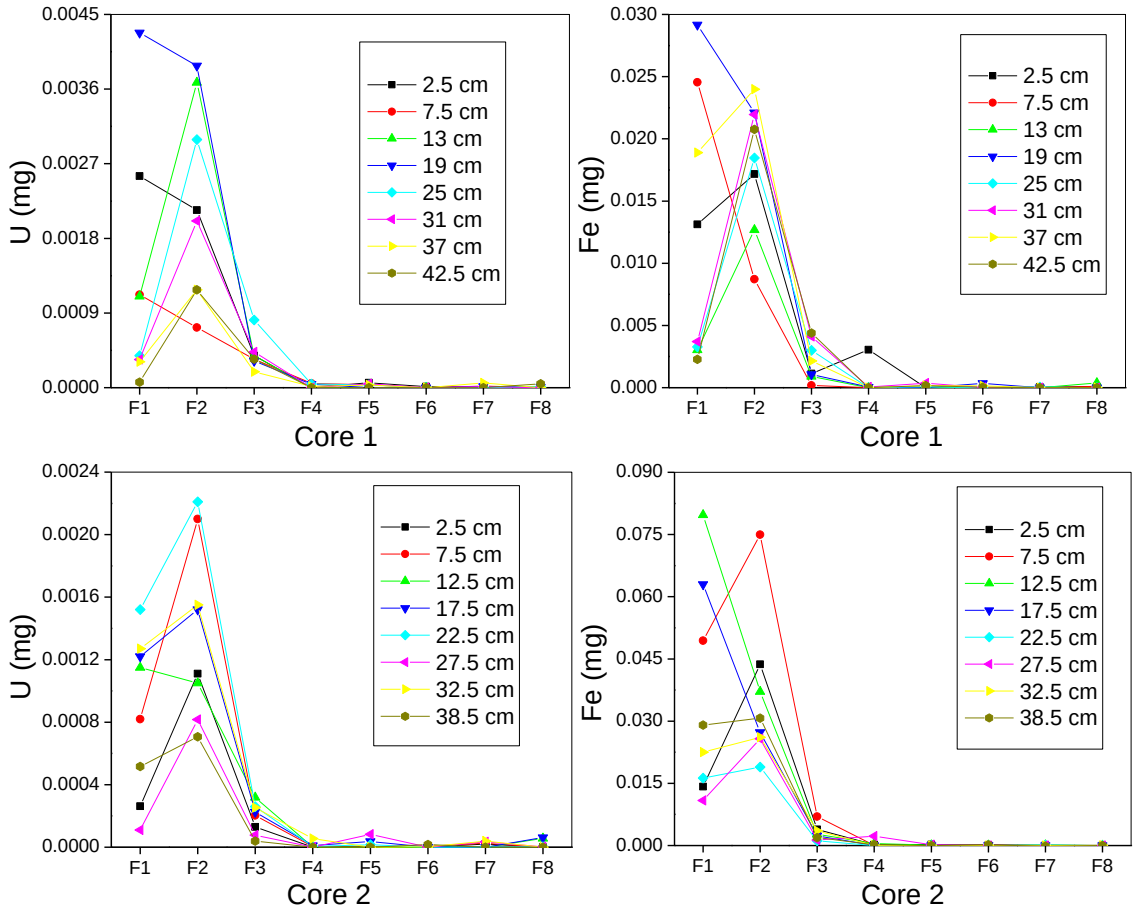

Figure 3.7(a) Mass of elements (U and Fe) in gel electrophoretic fractions of humic substances extracted from different depths in Core 1 and Core 2

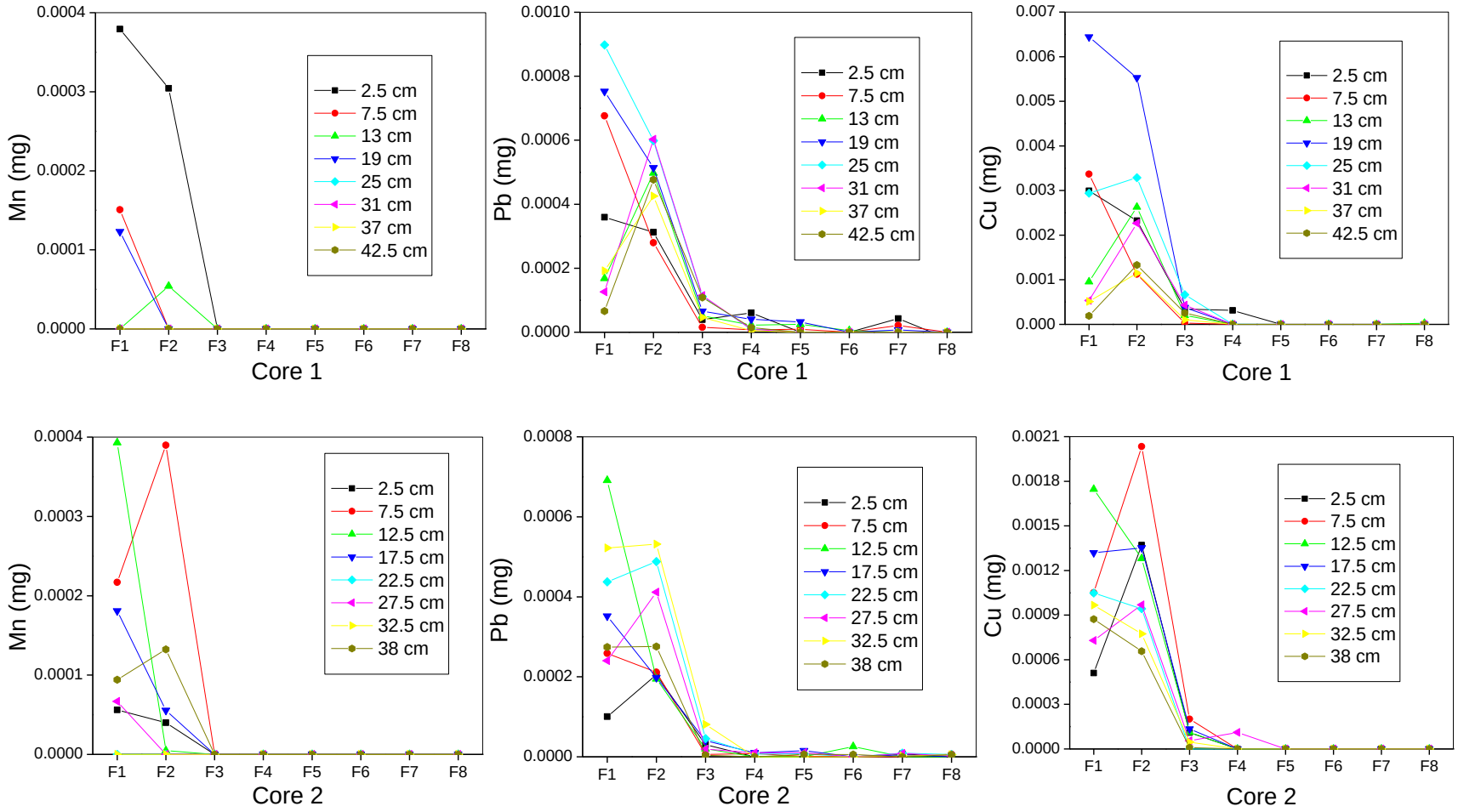

Figure 3.7(b) Mass of elements (Mn, Pb and Cu) in gel electrophoretic fractions of humic substances extracted from different depths in Core 1 and Core 2

From Figures 3.7(a) and (b), it can be clearly seen that, in almost all cases, gel strips F1-F3 contained>90% of each element, coincident with the position of the brown and tailing bands. In agreement with the results presented in Figure 3.6, the elements (U, Fe, Mn, Pb and Cu) did not migrate further than the fluorescent material. In addition, the maximum element concentration was present in either F1 or F2.

More specifically, comparing the U associations with humic substances from all depths at Core 1 (20 m from the cave), most of the U is contained in F1 and F2, indicating that solid phase U is associated with the less electrophoretically mobile, large humic fractions (Figure 3.7(a)). This agrees with the results for organic-rich forest soils reported by Graham et al. (2000). The position of the maximum concentration (mass of U per gel strip) varied between these two fractions and with a gradual change from F1→F2 (Figure 3.7(a)) and there is a suggestion of association with slightly more electrophoretically mobile humic material with increasing depth. The patterns for each of the other elements (Figure 3.7(b)), including those for Fe (Figure 3.7(a)), were generally very similar to those described for U.

For Core 2, 30 m from the cave, the gel electrophoretic patterns for the elements were very similar to those obtained for Core 1 in that U was mostly found in F1 and F2 (Figure 3.7(a). Here there was no consistent change in the position of the U maximum (mass per gel strip) with increasing soil depth, although the maximum moved from F2 to F1/2 in the middle sections of the core (12.5 cm and 17.5 cm depth). At these depths, there was some separation of Fe, Mn and Pb peaks from those of U and Cu in that clear Fe, Mn and Pb maxima were found in F1 at some depths whilst the U and Cu peaks in F1/2 were skewed more toward F2 (Figure 3.7(b)) (see Appendix section 9.12.2, Tables 9.23-9.27).

Overall, however, there were no major variations in U-humic association either with vertical soil depth or with lateral distance from the U mineralization. This could be due to

the uniformity in composition of the humic material present in the Needle's Eye soils.

3.5.2 Gel filtration chromatography

3.5.2.1 Optimization of the gel filtration procedure

The initial gel filtration protocol was based on previously published procedures (Graham, 1995; Perez-Sanz et al., 2006). The samples were fractionated using Sephadex G75 (2.5 diameter × 30 cm length column) and 0.1 M NaOH as the eluent. The void volume (34 ml) of the gel bed was determined by running Blue Dextran 2000 at a concentration of 2 mg mL^{-1}. At the same time, the quality of the packing can be checked by watching the progression of Dextran 2000 through the gel bed; it should elute as a single band and the gel bed height should not decrease. To prevent compaction of the gel bed during separations, samples were passed through the column at a low flow rate of approximate 2 mL min^{-1} (see section 2.5.10.2 sampling trip 1). The permeation limit was determined using a potassium dichromate solution.

A trial sample (humic extract from Core 2 7.5 cm) was applied to evaluate the performance of the column, e.g. elution within the exclusion and permeation limits. The first fraction (5 mL) was collected as the first hint of brown colour emerged from the column, close to the exclusion limit. The colours of each fraction (5 mL) ranged from dark brown (F1-F8) to amber yellow (F9-F15) then to pale yellow (after F15). Figure 3.8 shows the elution profile for each element. The maximum concentrations of U occurred in F2-F3 whilst the maximum for the other elements was clearly in F2. For most elements, the vast majority eluted within the fractions F1-4 (U: 100%; Fe: 86%; Mn: 100%; Pb: 100%; Zn: 66%). The exception to this was Cu, which was spread across F1-11 (Figure 3.8) (see Appendix section 9.15, Table 9.35). Again, as for the gel electrophoresis experiments, the elution profiles for the elements U, Fe, Mn, Pb and Cu, did not extend beyond the profile for the

humic materials. However, there was still measurable Zn eluting in the last fractions and it is possible that some of this may no longer be associated with the humic substances. This would not be inconsistent with the greater general lability of Zn in comparison with the other elements.

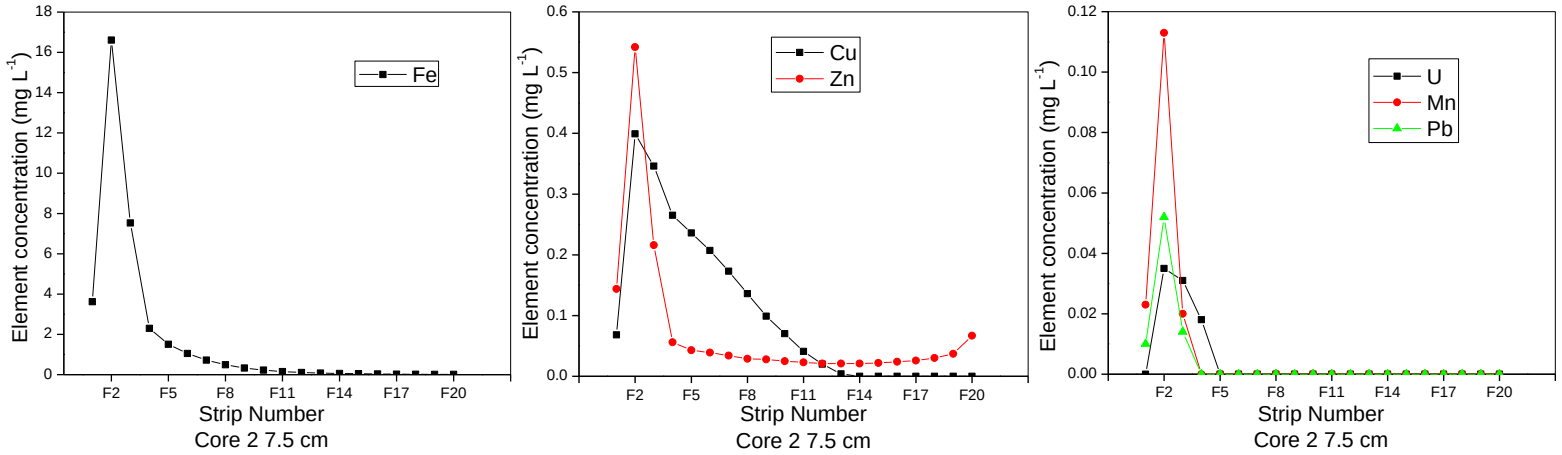

Figure 3.8: Distribution of elements in gel filtration fractionation of Needle's Eye humic substance from Core 2 7.5 cm

3.5.2.2 Gel filtration fractionation of soil humic substances from Core 1

Figure 3.9 illustrates the results of gel filtration fractionation of humic substances isolated from soils at three different depths in Core 1 (20 m from cave). Core 1 rather than Core 2 was selected because the gel electrophoresis results suggested that there was a slight change in uranium associations with Core 1 humic substances trend with increasing soil depth (Figure 3.7(a)). Core 1 31 cm, 37 cm and 42.5 cm were selected with the original objective of determining the extent to which the gel can differentiate between humic substances extracted from soils at consecutive depths. AgainF1 (5 mL) was collected at the exclusion limit, as the first hint of brown colour emerged from the column. Thus F2 is the first strongly brown coloured fraction and, for all elements and for each soil depth, the maximum concentration was obtained in F2 or F3. These correspond to large humic molecules which are eluted at/close to the exclusion limit of the gel (~75,000 Da). For many of the elements (Fe, Mn, Pb and Cu), concentrations decreased rapidly after F5 but for U and particularly Cu, there was a more gradual decrease to F12-F14. Only for Zn was there any increase in concentration for the later eluting fractions (F20-F25), which may indicate that some Zn had dissociated from the humic substances.

Table 3.3 shows the proportion of total eluted elements (U, Fe, Mn, Pb, Cu, Zn) in F1-F4 and F5-F9 for Core 1 31 cm, 37 cm and 42.5. The U peak occurred in F2/3 at all three depths and the proportions of the total eluted U present F1-F4 were 78%, 57% and 74% for the 31 cm, 37 cm and 42.5 cm samples, respectively. Correspondingly, the proportions of total eluted U in F5-F9 were 22%, 26% and 25% for Core 1 31 cm, 37 cm and 42.5 cm, respectively. The maximum Fe concentrations also occurred in F2/3 and 80%, 77% and 81% eluted in F1-F4 for the 31 cm, 37 cm and 42.5 cm samples, respectively. Fe eluted in F5-F9 constituted 18%, 19% and 16% of the total eluted Fe in the same samples. It is interesting to note that Mn, Pb, Cu and Zn also exhibit a very specific association with the

largest humic molecules only (F2/3) (see Appendix Table 9.36).

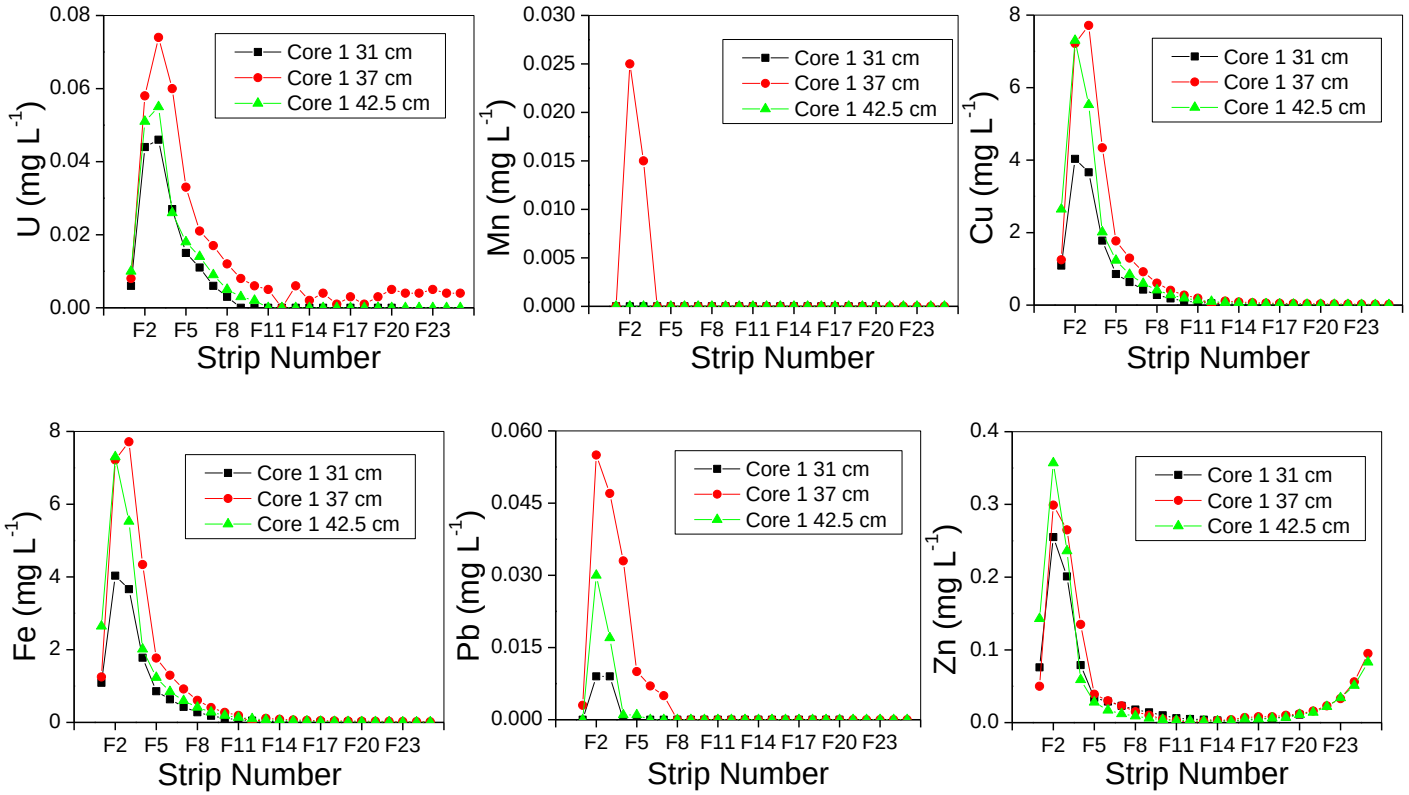

Figure 3.9: Distribution of elements (U, Fe, Mn, Pb, Cu, Zn) in gel filtration fractions of humic substances extracted from Core 1

Table 3.3: The proportion of total eluted elements (U, Fe, Mn, Pb, Cu, Zn) in F1-F4 and F5-F9 for Core 1 31 cm, 37 cm, 42.5 cm

		U	Fe	Mn	Pb	Cu	Zn
Core 1 31 cm	F1-F4	78%	80%	n.d.	100%	58%	77%
	F5-F9	22%	18%	n.d.	n.d.	35%	23%
Core 1 37 cm	F1-F4	57%	77%	100%	86%	54%	65%
	F5-F9	26%	19%	n.d.	14%	36%	10%
Core 1 42.5 cm	F1-F4	74%	81%	n.d.	98%	54%	71%
	F5-F9	25%	16%	n.d.	2%	36%	6%

n.d. for Mn = 0.0002 mg L^{-1}

n.d. for Pb = 0.002 mg L^{-1}

As can be seen from Figures 3.7 and 3.9, gel electrophoresis and gel filtration both showed that all the elements were predominantly associated with large humic molecules at all depths within the peaty soils. However, a major difference between the results obtained for the two fractionation approaches should be noted. The Fe/"other element" ratio is much higher in gel filtration compared with those obtained by gel electrophoresis. For gel electrophoresis technique, the gel together with the humic samples were completely digested and analysed, so the recovery rate of the humic samples in each strip is almost 100%. Comparison of the humic extract data and gel electrophoresis data in Table 3.4 demonstrates that the Fe/"other elements" ratios were very similar. For gel filtration, this is not the case because the humic substances are spread over a larger number of fractions and thus considerable dilution takes place. Thus the concentrations of elements in later fractions were often close to or below detection limits, affecting the reliability of calculations of the total amounts especially of the elements which are present at much lower concentrations (cf. Fe was often present at concentrations ~10-100 times greater than the other elements).

Table 3.4: Ratio of Fe/other element obtained from humic extract, gel electrophoresis data and gel filtration data

	Fe/U	Fe/Mn	Fe/Pb	Fe/Cu	Fe/Zn
Humic extract Core 1 31cm	9.0	/	30.2	8.6	6.6
Humic extract Core 1 37 cm	15.6	272	43.2	17.9	10.5
Humic extract Core 1 42.5 cm	12.4	556	33.9	13.2	8.9
Gel electrophoresis Core 1 31 cm	10.8	/	35.4	9.3	/
Gel electrophoresis Core 1 37 cm	26.0	/	67.4	25.5	/
Gel electrophoresis Core 1 42.5 cm	17.6	/	41.4	15.5	/
Gel filtration Core 1 31 cm	84.0	/	737	3.6	16.8
Gel filtration Core 1 37 cm	76.4	665	166	10.1	23.1
Gel filtration Core 1 42.5 cm	112	/	441.3	7.5	19.3

3.6 Initial findings

(i) U concentrations in cave water emerging from the mineralization weretwo orders of magnitude greater than the typical concentration of <1 μg L^{-1} in UK groundwaters (Smedley et al., 2006). At 20 m from the cave, the 0-20 cm soil porewater U concentrations were typically greater than 30 μg L^{-1}, the current guideline value for drinking water. There was a clear trend of decreasing U concentrations with increasing distance from the cave.

(ii) The colloid data for water samples suggested that the lateral migration of U may be more strongly influenced by association with smaller colloids since such associations in the soil porewaters were more important at 30 mcompared with 20 m from the cave.

(iii) It is worth noting that, at 20 m from the cave, U, Fe and Mn were all found in the large colloidal fraction in water samples. Therefore, it cannot be ruled out that the U in this size fraction is associated with Fe and Mn colloids rather than humic colloids in water. However, at 30 m from the cave, U was split between large and small colloid fractions while Fe and Mn were still predominantly in the large colloid fraction. The low concentrations of Mn and Fe in the small colloid fraction, in conjunction with the greater presence of U in this fraction with increasing distance from the cave,suggests that small organic colloids may be especially important for migration of U.

(v) The gel electrophoresis results demonstrated that, in the solid phase soil, U was predominantly associated with larger, brown-coloured and less electrophoretically mobile soil humic molecules. Processes such as complexation, reduction followed by complexation and/or adsorption to humic-coated Fe/Mn mineral phases must therefore be responsible for the attenuation of mineralization-derived U in the Needle's Eye soils.

(vi) The lack of any significant change in electrophoretic mobility of the soil humic substance with distance from the mineralization and with increasing soil depth suggest that the humic material present in these soils is fairly uniform in composition and mainly comprises very large molecules.

(vii) Comparing the results of porewater fractionation (by ultrafiltration) with those for the fractionation of solid phase humic substances (by gel electrophoresis and by filtration) reveals some interesting similarities. The main similarity is that U and Fe are associated

with very large humic molecules in both the porewater (Figure 3.5) and in the solid phase soil (Figures 3.7, 3.8 and 3.9). Thus, the relative importance of U associations with organic matter or Fe-containing minerals bound to organic matter could not be distinguished.

3.7 Implications for subsequent sampling trips based on initial findings

For subsequent sampling trips, an improved protocol for ultrafiltration of porewaters would need to be applied to ensure that good recoveries of colloids and associated elements were attained. In addition, in-depth investigation of the solid phase associations (mineral and organic) of U would be required. Thus the objectives of subsequent sampling trips were as follows:

(i) Lateral and vertical trends in elemental concentrations again to be determined followed by ultrafiltration to fractionate porewater into large (100 kDa-0.2 μm), medium (30-100 kDa) small (3-30 kDa) colloids and truly dissolved fraction (<3kDa).

(ii) Redox potential and pH in the porewater needed to be measured as they are helpful in evaluating processes controlling U behaviour in the environment.

(iii) XRD and SEM to examine the composition of the solid phase and sequential extraction to quantify U associations with Fe minerals within the solid phase.

(iv) Sequential extraction applied to humic substances extracted from the soil in conjunction with gel electrophoresis and ICP-OES in order to differentiate between U associated directly with humic substances from that associated with Fe minerals bound to humic substances.

4 Results and initial interpretation for sampling trips 2-5

This chapter consists of four main parts, each of which presents the resultsfromone sampling trip. Overall, the chapter contains the results for redox conditions (Eh), whole soil characterization (soil porewater pH, organic matter content, SEM, XRD), elemental distribution in both solid and aqueous phase, sequential extraction for soil, humic substances and porewater colloids, as well as colloid fractionation and characterization for porewater samples from the Needle's Eye natural analogue site, SW Scotland. Multiple sampling trips were required because of limitations in sample sizes, e.g. small volumes of porewaters, and in the number of samples that could physically be processed within acceptable time periods upon return to the laboratory. For trips 2-4, background information, e.g. pH, dissolved organic matter content, as well as porewater elemental concentration profiles and elemental concentrations in cave drip waters were determined so that between-trip and seasonal variations could be evaluated. Section 4.1 contains elemental concentrations in porewaters and solid phase samples from three cores. Colloidal fractionation by ultrafiltration was then carried out on the soil porewaters and the distribution of elements amongst colloidal and dissolved fractions has been presented.This was followed by sequential extraction, SEM and XRD characterization of the mineral components of the solid phase. Finally, sequential extraction in conjunction with gel electrophoresis was developed to investigate the interactions of U with both humic substances and Fe phases. In section 4.2, colloid isolation in conjunction with acetate extraction was undertaken to provide comparison with the solid phase sequential extraction results. To provide supporting evidence for the XRD data, the results for carbonate determination in the solid phase soil are also presented in this section. In section 4.3, gel chromatography was used to further charaterize U interactions with colloids of different sizes. Section 4.4 finally examines the Fe^{II}/Fe^{III} distributions in porewater from a vertical soil profile.

4.1 Results from sampling trip 2 on 02/10/2008

4.1.1 Redox potential for Cores 3, 4 and 5 and for the water emerging from the uranium mineralization

As shown in Table 4.1, the Core 3 and Core 4 soils had very low Eh values of 48 and 13

mV, respectively, indicating that the conditions in the boggy soils were strongly reducing. In contrast, the water emerging from the mineralisation had a much higher value of 294 mV, indicating it was oxidizing. At Core 5, a redox measurement was not successfully obtained due to the lower moisture content of the soil.

Table 4.1: Redox potential measurements at the sampling sites

Site	**Redox potential (mV)**
Cave drip water emerging from mineralisation	294
Core 3	48
Core 4	13
Core 5	n.d.

n.d. = not determined

4.1.2 pH values for porewater samples from Cores 3, 4 and 5

The pH was recorded for the porewaters obtained from each depth section of Cores 3, 4 and 5. The range of values obtained from the three cores was ~6.0-7.2, indicating that the porewaters were slightly acidic to circumneutral. Core 3 showed a small decrease from a surface value of 6.3 to 6.1 at ~5 cm depth; below this there was agradual increase to pH7.1 at ~28 cm. The values stabilized at ~6.9 towards the bottom of the core. Core 4 had a near surface maximum pH value of 7.1. Thereafter the values fluctuated between 6.3 and 6.9. The pH values for Core 5 decreased from 6.8 at the surface to 6.8 at ~12 cm depth, and then increased to ~6.4 at the bottom of the core. Thus all three cores had distinctive pH depth profiles (Figure 4.1) (see Appendix section 9.5, Table 9.1).

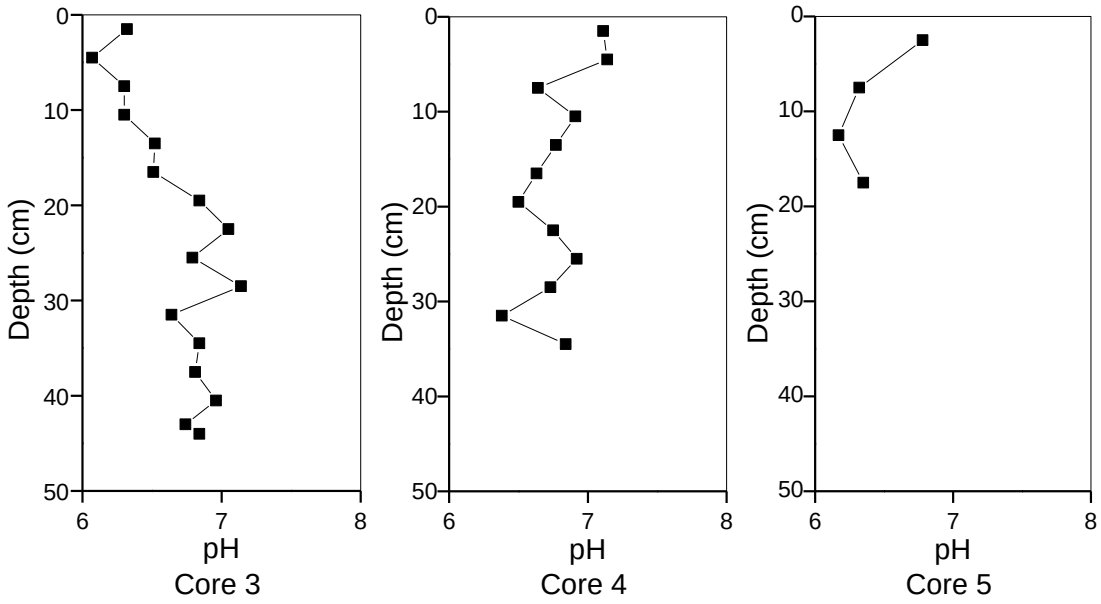

Figure 4.1: Soil porewater pH values for Cores 3, 4 and 5

4.1.3 UV absorbance at 254 nm in porewaters from Cores 3, 4, and 5

The UV absorbance at 254 nm has been used as a measure of the relative amount of dissolved organic matter (DOM) in water samples (Egeberg et al., 2002; Graham et al., 2008). Where absorbance values were greater than 2.0, measurements were made on diluted samples and then the final value calculated using the dilution factor. It should also be noted that the term DOM refers to both colloidal and truly dissolved OM since the water samples were simply filtered through 0.2 μm hydrophilic membranes.

The absorbance values for porewaters obtained from each depth section of Core 3, 4 and 5 are shown in Figure 4.2. For Core 3 porewater absorbance values showed a gradual decrease from ~2.5 at the surface to only 0.5 at 32 cm. Thereafter, there was a small increase to a value of 1.2 at the bottom of the core. Core 4 porewaters had a near-surface DOM maximum. Below 10 cm, lower values of ~0.6-0.7 were obtained to a depth of 13.5-25.5 cm and there was a slight increase to a value of 1.0 towards the bottom of the core. Although the absorbance values were slightly higher, the shape of the profile for Core 5 was similar to that observed over the top 0-20 cm sections of Core 4 (see Appendix section 9.6, Table 9.2).

It can be seen from Figures 4.1 and 4.2 that there was an inverse relationship between UV absorbance and pH values at Core 3 whilst UV absorbance at Cores 4 and 5 did not appear to be directly or indirectly related to the pH values.

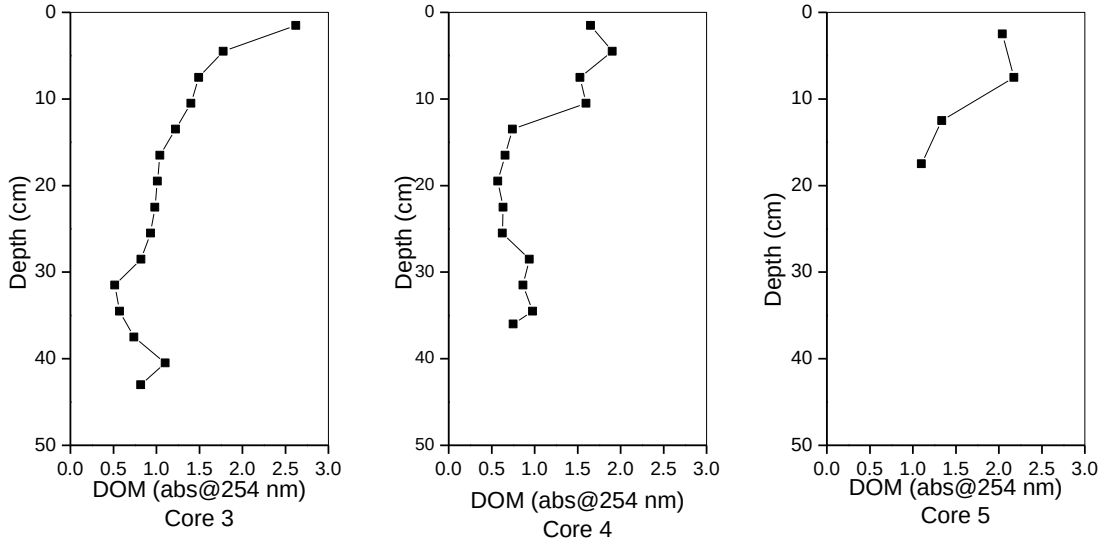

Figure 4.2: Soil porewater UV absorbance values for Cores 3, 4 and 5

4.1.4 Organic matter content in the soil samples from Cores 3, 4 and 5: loss on ignition (LOI)

The organic matter (OM) content of the soil samples was determined by loss on ignition (LOI) by ashing at 450 ℃ for 8 hours. The results were expressed relative to 105 ℃-dried weights of the samples (Equation 4.1) and are displayed in Figure 4.3. The OM content of the soils decreased from ~90% and 85% d.wt.at the surface to ~40% and 35%d.wt. at the bottom of Core 3 and Core 4, respectively.In each case, the decrease over the top 0-25 cm sections was gradual but then there was a more marked drop starting at ~25 cm towards the bottom the core.Core 5 showed a gradual decrease from 50% at the surface to 37% at ~17.5 cm. Although less organic-rich, the trend for Core 5 was similar to that observed for Cores 3 and 4 (see Appendix section 9.7, Table 9.3).

LOI (wt%) = 100 ×(105 ℃ d.wt.-450 ℃ ashed wt.)/ 105 ℃ d.wt. Equation 4.1

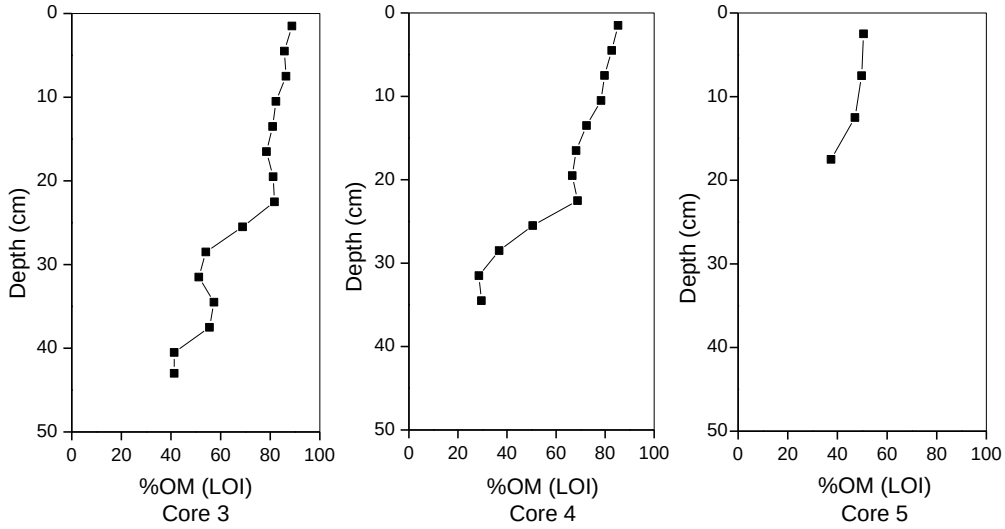

Figure 4.3: Loss on ignition (LOI) profiles for Cores 3, 4 and 5

It can be seen from Figures 4.2 and 4.3 that the DOM profile did not mirror that of solid phase precisely although there was a general decrease with increasing soil depth. Although the solid phase organic content in Core 5 was in the range of 40-50%, i.e. much lower than that for Cores 3 and 4, the pattern of DOM at Core 5 was similar to that observed in the top 0-20 cm sections of Cores 3 and 4.

4.1.5 Lateral variations in elemental concentrations in Needle's Eye water samples

The concentrations of a range of elements (U, Fe, Mn, Pb, Cu, Zn, Al and As) in soil porewaters, bog waters and cave drip waters emerging from the U mineralisation collected duringsampling trip 2 are shown in Table 4.2. The U concentrations in the cave drip waters were in the range of ~210-240 μg L^{-1}. At 20 m from the cave, U concentrations in the porewaters from soil Core 3 were in the range of ~7-90 μg L^{-1} and that in the groundwater collected as the sampling pit filled up with water was below this range at ~3 μg L^{-1}. At 25 m from the cave, the range for Core 4 porewaters and the value for groundwater were 3-10 μg $L^{-1}$and ~1 μg L^{-1}, respectively. This represented a 20-fold decrease in U concentration in comparison with those in the cave drip waters. The U concentrations in Core 5 porewaters were similar to those for Core 4.

For the same samples, the highest concentrations of Fe, Mn and Pb were found for Core 5, the site furthest from the mineralisation. For the other elements analysed, higher concentrations of Cu, Al and As were found in soil core porewaters in comparison with the waters emerging from the mineralisation, but there was no consistent relationship with distance.

Table 4.2 also confirms the visual observation that the soil porewaters were highly coloured and therefore organic-rich while the cave drip waters were crystal clear.The UV absorbances at 254 nm were in the range ~0.5-2.6 for the former but only 0.03-0.07 for the latter. There was no consistent trend in DOM content with increasing distance from the cave.

Table 4.2: Geochemical and elemental concentration data for water samples collected during sampling trip 2 (02/10/2008)

Site	Distance from cave (m)	Sample description	UV absorbance at 254 nm	Aqueous phase concentrations						
				U ($\mu g\ L^{-1}$)	Fe ($\mu g\ L^{-1}$)	Mn ($\mu g\ L^{-1}$)	Pb ($\mu g\ L^{-1}$)	Cu ($\mu g\ L^{-1}$)	Al ($\mu g\ L^{-1}$)	As ($\mu g\ L^{-1}$)
Cave	0	Drip water 4	0.03	235	13.7	0.4	0.06	4.8	3.8	12.0
		Drip water5	0.07	213	7.3	1.5	0.07	7.0	2.5	11.0
Core 3	20	Porewater	0.52 – 2.62	7-85	41-384	3-38	0.9-6.6	5.6-68	18-223	37-239
		Bog water 3	0.65	2.9	57.9	0.4	0.1	4.4	5.5	3.2
Core 4	25	Porewater	0.57 – 1.90	3-10	130-150	8.8-142	1.9-7.1	3.9-11.2	13-102	25-388
		Bog water 4	0.75	1.2	67.9	0.1	2.1	1.9	27.6	25.7
Core 5	35	Porewater	1.1-2.2	11-14	3490-12800	29-229	25.5-37.5	13.8-19.8	194-255	76-273
		Bog water 5	1.5	1.5	3960	2.3	4.4	1.1	42.5	99.1

4.1.6 Vertical concentration profiles for U and other elements in the solid phase and porewaters of soil samples from Cores 3, 4 and 5

The bars in Figure 4.4-4.6 show the elemental distributions with depth in the solid phase soil from Cores 3, 4 and 5 (see Appendix section 9.8, Table 9.5). The highest solid phase U concentrations of ~2400 mg kg^{-1}, ~190 mg kg^{-1} and ~110 mg kg^{-1}occurred at 19.5 cm, 13.5 cm and 7.5 cm for Cores 3, 4 and 5, respectively. Below these depths, the U concentrations gradually decreased towards the bottom of the cores.

The solid phase Fe profiles for Cores 3, 4 and 5 usually had a peak occurring within the 10-20 cm depth range but for Core 3, the main peak occurred at 30-40 cm. Maximum Fe concentrations in the solid phase varied from ~0.75% w/w for Core 3 to ~2.5% w/w for Core 5.

The maximum solid phase Mn concentrations of ~370 $mgkg^{-1}$, ~600 mg kg^{-1} and ~400 $mgkg^{-1}$ occurred in the top sections of Cores 3, 4 and 5, respectively. In each case, the solid phase Mn concentrations decreased rapidly over the top 0-20 cm. For Core 3, there was a smaller sub-surface maximum at 20 cm but for Cores 4 and 5, the decrease in Mn concentration continued to the bottom of the cores.

Aluminium concentrations in the solid phase were obtained as a proxy for the mineral (alumino-silicate) content of the organic-rich soils. The solid phase Al concentration profiles for Core 3 and Core 4 indicated a major change towards the bottom of cores. For Core 3, the change at ~25 cm was very marked; above this concentrations are typically <0.6% w/w while below this depth, values are typically closer to 2% w/w. The trend towards higher concentrations with increasing depth for Core 4 was more gradual. Nevertheless, particularly high values of up to 2% w/w were observed for the bottom 4 sections. For both cores, the depth at which this change occurs coincided with the marked decrease in %OM (Figures 4.3-4.4). Thus a major change from organic-rich to mineral-rich soil was evident in each of these cores at about the same depth. Core 5 was not sufficiently lengthy to observe this transformation.

The maximum solid phase Pb concentrations of 115 mg kg^{-1}, 140 mg kg^{-1} and 101 mg kg^{-1} occurred at 25-30 cm, 25 cm and 12.5 cm for Cores 3, 4 and 5, respectively. For Cores 3

and 4, the Pb concentrations gradually increased and reached maxima at 20-25 cm, and gradually decreased towards the bottom afterwards. Core 5 was not sufficiently lengthy to observe this trend. Maximum concentrations of ~560-570 mg kg^{-1}, ~140 mg kg^{-1} and 75 mg kg^{-1} occurred in the solid phase Cu profiles at ~20-25 cm for Core 3, ~15-25 cm for Core 4 and at 12.5 cm for Core 5. Finally, the solid phase As profile for Core 3 had a maximum at 30-40 cm while those for Cores 4 and 5 occurred at 20-30 cm and 5-10 cm, respectively. The highest As concentrations were ~190 mg kg^{-1}, ~260 mg kg^{-1}, and ~230 mg kg^{-1} occurred at 37.5 cm, 10.5 cm and 7.5 cm in Cores 3, 4 and 5, respectively.

Observations and initial interpretation

For Cores 3 and 4, the U solid phase profile showed broad similarity with Cu solid phase profile. At Core 3, they both hadmaximum values at ~20 cm depth: below this the concentration of both elements decreased to the bottom of the core. At Core 4, again they had broad maxima over the depth range 15-25 cm. It is well-known that both elements show strong associations with natural organic matter but there is no correlation with OM content. The sharp decrease in Core 3 and the gradual decrease in Core 4 concentrations towards the bottom of these cores did, however, occur at the point where the composition of the solid phase changes from predominantly organic- to more mineral-rich. Again for Cores 3 and 4, the solid phase profiles for Fe and As showed similarity. In Core 3, the concentrations of both elements gradually increased towards the bottom of the core with maximum occurred at 37.5 cm. In Core 4, they increased to maximum at depth of 10.5 cm and then decreased towards the bottom of the core. The behaviour of As is often closely related to that of Fe in many natural systems. Although the Al and, to some extent, Pb profiles were similar to the Fe profile for Core 3, those for Core 4 were distinctly different from its Fe profile. The main difference was that the Fe maximum was in the upper part of the core whilst, in agreement with Core 3 Pb and Al profiles, the Pb and Al maxima are towards the bottom of the core. Differences in redox status of Cores 3 and 4 may account for the position of the Fe maxima and will be explored in later sections.

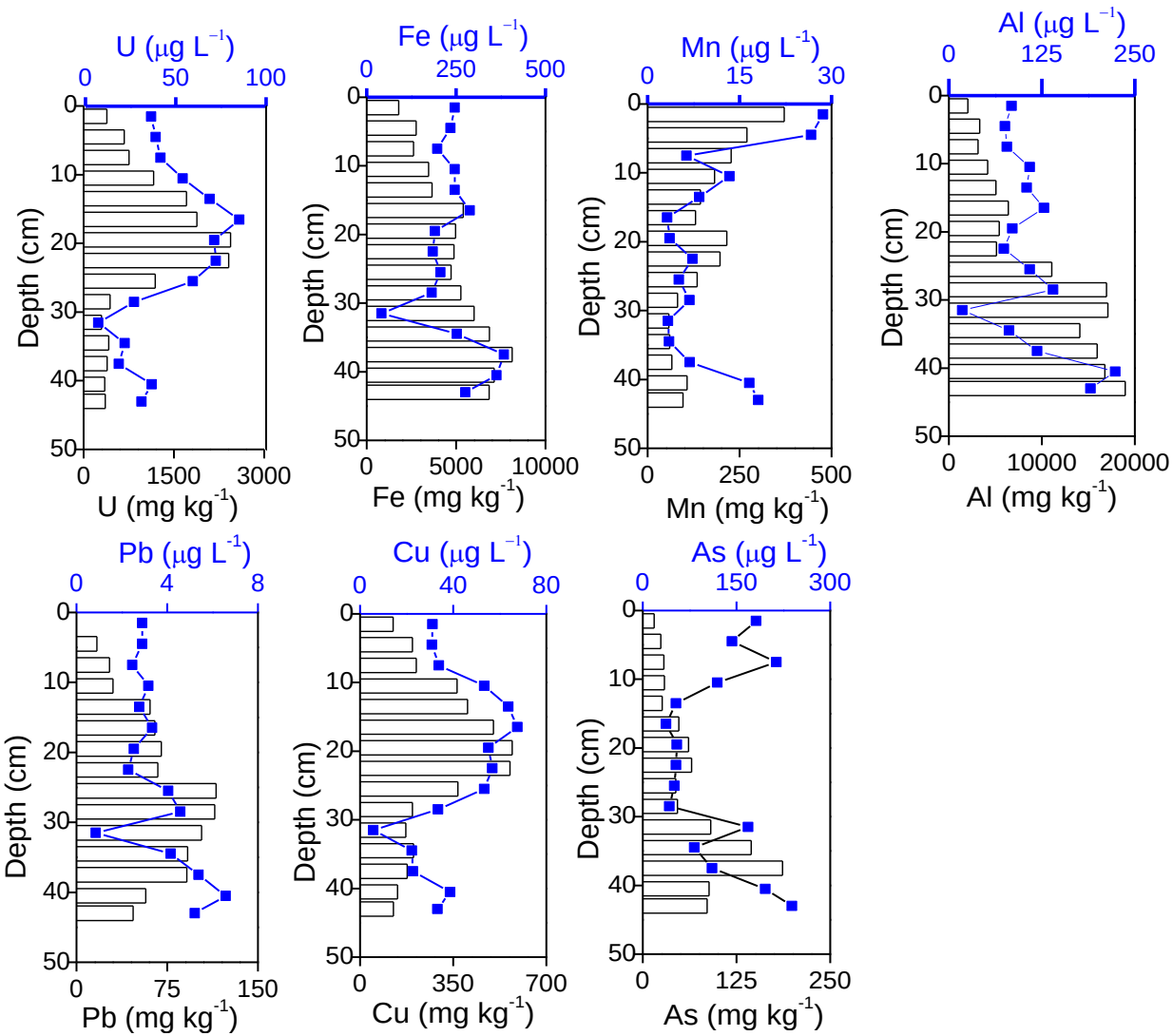

Figure 4.4: Vertical concentration profiles for U, Fe, Mn, Al, Cu, Pb and As in soil porewaters and solid phase from Core 3 (the blue lines show the elemental distributions in the soil porewaters, and the bars show the elemental distributions in the soil

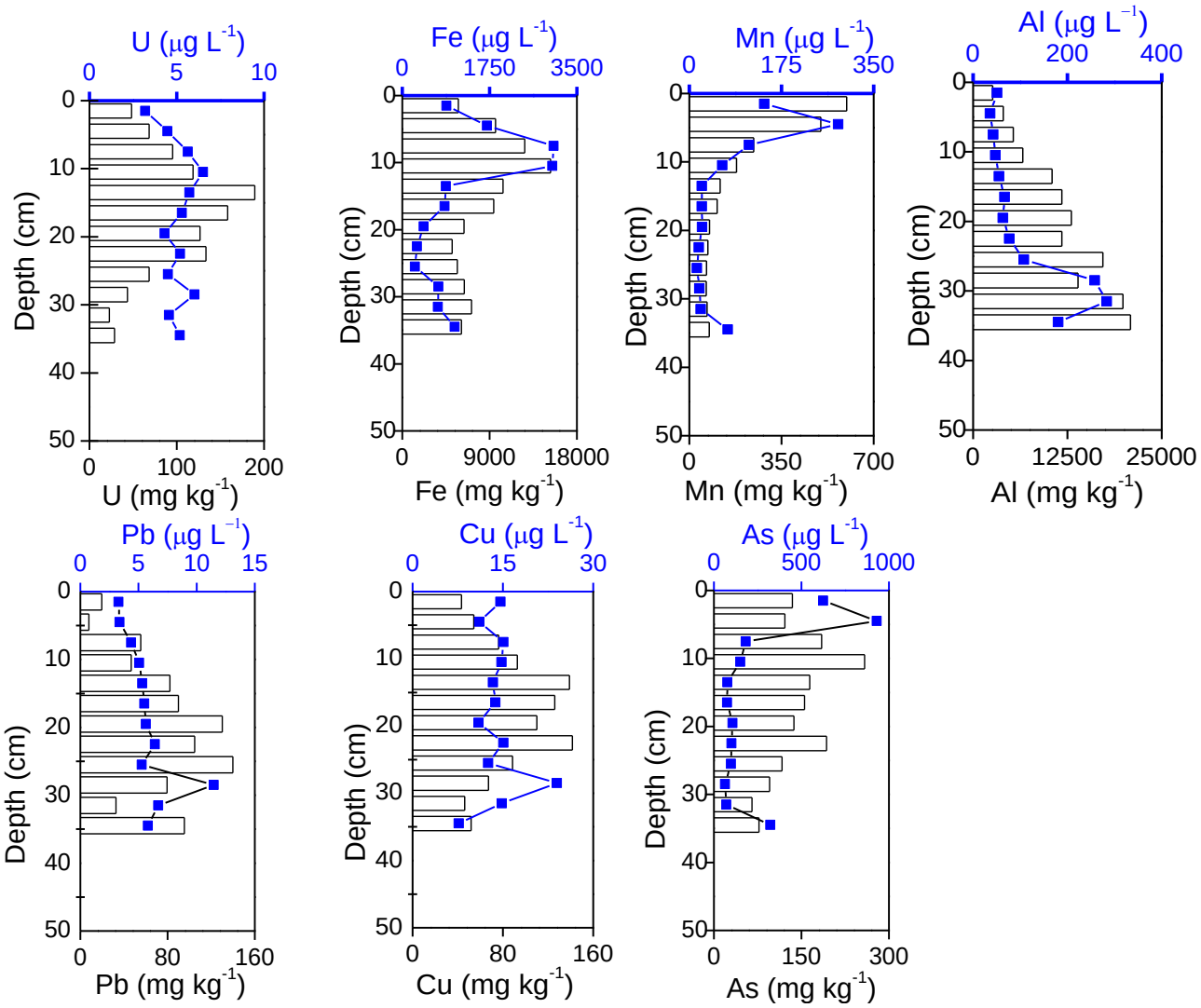

Figure 4.5: Vertical concentration profiles for U, Fe, Mn, Al, Cu, Pb and As in soil porewaters and solid phase from Core 4(the blue lines show the elemental distributions in the soil porewaters, and the bars show the elemental distributions in the soil)

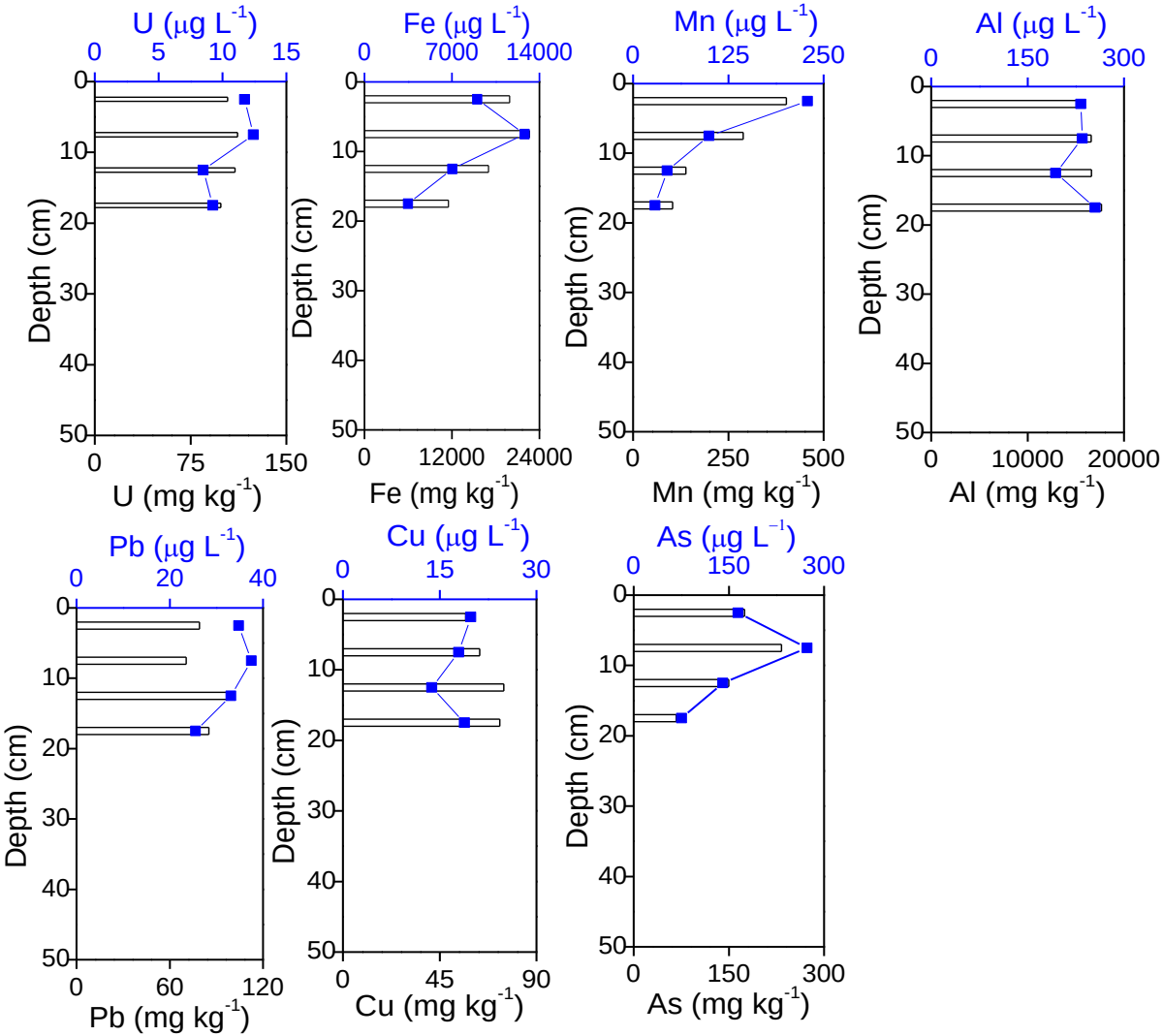

Figure 4.6: Vertical concentration profiles for U, Fe, Mn, Al, Cu, Pb and As in soil porewaters and solid phase from Core 5(the blue lines show the elemental distributions in the soil porewaters, and the bars show the elemental distributions in the soil)

The blue lines in Figure 4.4-4.6 show the elemental distributions in the soil porewaters. For Cores 3, 4 and 5, the maximum concentrations of U were 85 μg L^{-1}, 6.5 μg L^{-1} and 9.2 μg L^{-1} at depths of 16.5 cm, 10.5 cm and 7.5 cm, respectively. For Core 3, the porewater U concentrations decreased rapidly to a minimum of 7.1 μg L^{-1} at 31.5 cm; below this depth, there was a slight increase to 37 μg L^{-1} at 40.5 cm. For Core 4, the porewater U concentrations decreased to 4.3 μg L^{-1} at 19.5 cm and remained at <5 μg L^{-1} thereafter. Core 5 porewater U concentrations also decreased below 7.5 cm.

For Core 3, Fe porewater concentrations reached a value of ~290 μg L^{-1} at ~17 cm depth and then gradually decreased to a minimum of 41 μg L^{-1} at 31.5 cm. Below this, there was a sharp increase to the maximum value of 384 μg L^{-1} at 37.5 cm. For Cores 4 and 5, the positions of the porewater Fe concentration maxima were both in the 0-10 cm sections, with ~3040 μg L^{-1} and ~22600 μg L^{-1} at 7.5 cm and 7.5 cm, respectively.

The positions of Mn porewater maxima of 29 μg L^{-1}, 283 μg L^{-1}, 403 μg L^{-1} occurred in the top or second top sections of Cores 3, 4 and 5. The concentrations rapidly decreased below this point although, for Cores 3 and 4, there was an increase towards the bottom of the core.

For Cores 3 and 4, the Al porewater concentrations generally increased with increasing depth. For Core 3, the three Al porewater concentration maxima of 128 μg L^{-1}, 140 μg L^{-1} and 224 μg L^{-1} occurred at 16.5 cm, 28.5 cm and 40.5 cm, respectively. In Core 4, the Al porewater maximum of 283 μg L^{-1} was located at 31.5 cm. At Core 5, the length of the core was not great enough to observe such changes.

The Core 3 Cu porewater concentrations increased to a maximum of 68 μg L^{-1} at 16.5 cm and gradually decreased to a minimum of 5.6 μg L^{-1} at 31.5 cm before increasing to 39 μg L^{-1} at 40.5 cm. In Core 4, there was little variation over the top 0-25 cm sections but there was an increase to a maximum value of 24 μg L^{-1} at 28.5 cm. There was a small decrease to 14 μg L^{-1} at 12.5 cm for Core 5.

As for Cu, the porewater Pb concentrations did not vary greatly between 0-25 cm in Core 3. As for Al, there was an increase in porewater Pb concentrations (to ~7 μg L^{-1}) towards the bottom of the core. For Core 4, porewater Pb concentrations gradually increased and reached maximum of 12 μg L^{-1} at 28.5 cm. For Core 5, there was a small increase in

concentration at 7.5 cm and then a decrease thereafter. The porewater Pb concentrations increased with distance from the mineralisation, with values of up to 7 μg L^{-1} at Core 3, up to 24 μg L^{-1} at Core 4 and up to 101 μg L^{-1} at Core 5.

The porewater As profiles had maximum concentrations of ~210 μg L^{-1}, ~930 μg L^{-1} and ~230 μg L^{-1} in the near surface sections of Cores 3, 4 and 5, respectively. The Core 3 and 4 porewater As concentrations then decreased to ~30 cm depth, below which they increased towards the bottom of the cores.

Observations and initial interpretation

Comparison with the solid phase elemental profiles was used to identify possible factors controlling U (and other elemental) migration behaviour through the porewaters (see Appendix section 9.8, Table 9.5). For Cores 3 and 4, the porewater U concentration maxima were located ~3 cm above the respective solid phase U concentration maxima. For Core 5, there was a porewater maximum in the second section (7.5 cm) but no solid phase maximum was observed in this core. Thus processes other than a simple equilibrium between the solid and aqueous phases must be involved.

There was an obvious correlation between the porewater and solid phase Fe concentrations for all three cores. The porewater (μg L^{-1}):solid phase (% w/w) ratio for Core 3 generally ranged from 0.01 to 0.08 (except for the surface section which had a ratio value of 0.14). For Core 4, the ratio ranged between 0.05 and 0.24. For Core 5, the ratio ranged between 0.30 and 0.57. The higher values of the ratio in Cores 4 and 5 indicate a greater propensity to be in solution. An important feature in each case was that the solid and aqueous phase Fe concentration maxima were coincident. Moreover, the porewater Fe maxima occurred at the same depth as the U porewater maxima in all three cores (albeit the U maximum was coincident with the lower edge of the Fe maximum in Core 3 porewaters).

For all three cores, the porewater Mn maxima occurred either in the top or the second top section. For Core 3 and Core 5, the peak occurred in the top section and was coincident with the solid phase maximum concentration while for Cores 4, the porewater maximum occurred one section below the solid phase maxima. For Cores 4 and 5, the marked decrease in concentrations towards the bottom of each core matched well with the solid phase profiles whilst for Core 3, the increase in porewater Mn concentrations towards the

bottom of the core was disproportionate with the small increase in solid phase Mn concentrations. The relationship between the porewater and solid phase porewater Mn concentration profiles in Cores 4 and 5 is suggestive of redox cycling, where Mn is often released into the aqueous phase just below the solid phase maximum (Davison, 1993). It should be noted that, for low resolution cores, the solid and porewater maxima can appear to be co-incident and thus it shouldn't be ruled out that redox cycling of Mn is also responsible for the near surface maximum in Core 3 and Core 5 (Graham et al., 2012).

The porewater Al maxima coincided with the solid phase Al maxima in all three cores but for Core 3, there was more similarity between the porewater Al and Fe profiles than between the porewater and solid phase Al profiles. Thus, it is possible that the processes controlling release of Fe into the porewaters may also influence porewater Al.

For Core 3, the porewater Cu profile was similar in shape to the solid phase Cu profile albeit that, as for U, the porewater Cu maximum occurred slightly above the solid phase maximum. For Core 4, the porewater Cu maximum was two sections below the solid phase Cu maximum, but the shape of the porewater Cu was different from that of the solid phase Cu. Indeed, the porewater Cu showed more similarity to that of Pb. Core 5 was insufficiently long to observe the trend.

Pb concentrations in the porewater generally increased with depth for Cores 3 and 4. In each ease, the Pb maximum positions in the porewaters occurred towards the bottom of each core and below the Pb maximum in the solid phase. For Core 3, porewater Pb showed more similarity to porewater Fe and Al than to solid phase Pb. For Core 4, the shape of porewater Pb was more similar to Cu and Al than to solid phase Pb. It may be that the release of Al into the porewaters also triggers the release of Pb and Cu (from surfaces) or it could be that the increase in porewater Fe towards the bottom of the core is the key controlling factor for the observed Al, Pb and Cu behaviour at the bottom of the core.

The As porewater profiles did not correlate with the As solid phase profiles for Core 3 and Core 4; in contrast, the Core 5 depth trends for both porewater and solid phase As were almost identical. For Cores 3 and 4, although the solid phase As profiles were most similar to those for Fe, the porewater As profiles showed broad similarity to those for porewater Mn in that they both had a maximum at near surface sections. Thus, the influence of redox

processes involving Mn and Fe upon the behaviour of As in these cores is not straightforward.

4.1.7 Ultrafiltration of porewater colloids from Cores 3, 4 and 5

As described in section 2.4.9, porewaters were first isolated from each soil core section by centrifugation and then filtered through 0.2 µm hydrophilic filters. Thereafter, ultrafiltration was used to separate the porewater into large (100 kDa-0.2 µm), medium (30-100 kDa) and small (3-30 kDa) colloidal and dissolved (<3 kDa) fractions. From visual observation most of the brown colour was contained in the 100 kDa-0.2 µm fraction and hence dissolved humic substances were mainly present in the large colloid (100 kDa-0.2 µm) size fraction.

With the exception of a small number of values for individual elements (especially Al), the recoveries for each element were close to/within acceptable limits of 100±10% (mean values: U: 89±5%; Fe: 95±10%; Mn 105±13%; Al: 97±29%). It is suspected that the ultrafiltration units release small amounts of Al into the porewater samples and that this accounts for some of the higher recoveries that were excluded from the calculation of the mean. Since the contamination is not uniform (and may vary between and within batches of ultrafilters), it is difficult to correct using the standard blank subtraction method. Since Al was not the main element of interest and moreover the highest U recovery was 101%, no further action was taken.

Ultrafiltration showed that a large proportion (68-94%) of total porewater U (<0.2 µm) was containedwithin the colloid fractions (3 kDa-0.2 µm) isolated from Core 3 (20 m from the cave). This was largely (47%-76%) present in the large colloid fraction (100 kDa-0.2 µm) (Figure 4.7) withmost of the remaining colloidal U beingfound in the small fraction (3-30 kDa).There was a slight increase (from 6% at the surface to 32% at the bottom) in the importance of the dissolved fraction with increasing depth. For Core 4 and Core 5 porewaters (Figures 4.8-4.9), the general trends were similar although there was a greater proportionof dissolved U both at the very surface and towards the bottom of each of these cores. The proportion of U present in colloidal form (3 kDa-0.2 µm) was typically in the range of 60-85% at Core 4 and Core 5 (see Appendix Tables 9.13-9.15).

For all three cores, more than 80% and, in many cases, greater than 90% of porewater Fe was in the colloidal (3 kDa-0.2 μm) rather than dissolved (<3 kDa) fraction. For Core 3 and Core 4 (Figures 4.7-4.8), the percentages of Fe present in the large colloid (100 kDa-0.2 μm)fraction were very similar, from 63-82%, while for Core 5 more than 95% of Fe was in this fraction at all depths (Figure 4.9). For Core 3 porewaters, there was a general increase in the proportion of Fe inthe large colloid fraction from the near surface towards the bottom of core.The reverse trend was observed for Core 4. For Cores 4 and 5, there was slightly more Fe in the smaller colloidal and dissolved fractions with increasing depth.

For all three cores (Figures 4.7-4.9), Mn was mainly distributed between the large colloidal (100 kDa-0.2 μm) and the dissolved (<3 kDa) fractions, and the proportions of Mn in the medium colloid (30-100 kDa) and small colloid (3-30 kDa) fractionswere <2% in all cases. For Core 3, Mn was predominantly found in the large colloid fraction at the surface, but with the exception of the very bottom section of the core, there was a notable increase from 3% to 64% in the proportion of dissolved Mn with increasing depth. At Core 4, the increase in the proportion of dissolved Mn with increasing depth was more pronounced and continued to the bottom of the core.Below 20 cm depth, ~85% of Mn was in this fraction. The pattern for Core 5 was consistent with this trend but the shift from colloidal to dissolved Mn was not so strong, and there was only ~30% dissolved Mn at ~20 cm depth compared with ~50% at the same depth in Core 4.

The greatest proportion of Al was found in the large colloidal (100 kDa-0.2 μm) fraction isolated from the porewaters from all three cores. There was a clear trend, however, of increasing amounts in the dissolved fraction below 20 cm for Cores 3 and 4. For Core 3, the maximum %Al in the dissolved fraction occurred at ~35 cm, coincident with the maximum % dissolved Mn. For Core 4 (Figure 4.8), the sections below 25 cm depth had the greatest proportions of both dissolved Mn and Al. In contrast with Cores 3 and 4, almost all of the Mn in the Core 5 porewaters was in the large colloid fraction (Figure 4.9). The distribution was almost identical to that of Fe for this core.

Cu (68%-100%) was mainly found in the porewater colloids (3 kDa-0.2 μm) for Core 3, most of which (56%-94%) was within the large colloidal fraction (100 kDa-0.2 μm) (Figure 4.7). There was a small increase from 9% to 19% in the importance of dissolved Cu (<3 kDa) from the surface to 30 cm depth, but below this, the proportion of dissolved Cu

decreased to ≤5%. For Cores 4 and 5 (Figures 4.8-4.9), the general distributions of Cu showed similarity to those from Core 3, although there was increasing importance of dissolved Cu with increasing distance from the cave, e.g. 15%-28% dissolved Cu for Core 4 and 28%-32% for Core 5.

More than 86% and, in most cases, more than 90% of the Pb was found in the large colloidal fraction (100 kDa-0.2 μm) for all three cores. Generally, there was a slight increasing trend of dissolved Pb (<3 kDa) with increasing depth for all the cores (Figures 4.7-4.9).

In Cores 3 and 4 (Figures 4.7-4.8), As (62%-95%) was predominantly found in the truly dissolved phase (<3 kDa) whilst in strong contrast, most of As (73%-98%) in Core 5 porewaters was within the large colloidal fraction (100 kDa-0.2 μm) (Figure 4.9).

Observations and initial interpretation

There was no clear relationship between solid phase or porewater U concentration and distribution amongst colloidal and dissolved fractions. For Core 3, there were only very small changes towards dissolved forms with increasing depth whilst for Cores 4 and 5, the maximum large colloidal association seemed to co-incide with the maximum porewater U concentration. For Core 4, a similar pattern was observed for large colloidal As and it is postulated that this might be a consequence of release in association with large Fe colloids (cf the vast majority of porewater Fe is in the form of large colloids and the maximum porewater Fe concentration occurs at the same depth as the U maximum). For porewater As, however, the vast majority is present in dissolved forms and the similarity between the Mn and As profiles in the upper sections of each core suggests that release from the surfaces of Mn oxides may be the main transfer process from the solid to the aqueous phase.

With respect to associations of U (and Pb and Cu) within the large colloid fraction, it is clear that, in addition to humic colloids, there are significant amounts of Fe, Mn (in some cases) and Al colloids and so additional work is required to evaluate the relative importance of associations with these organic and inorganic colloids (see section 4.2).

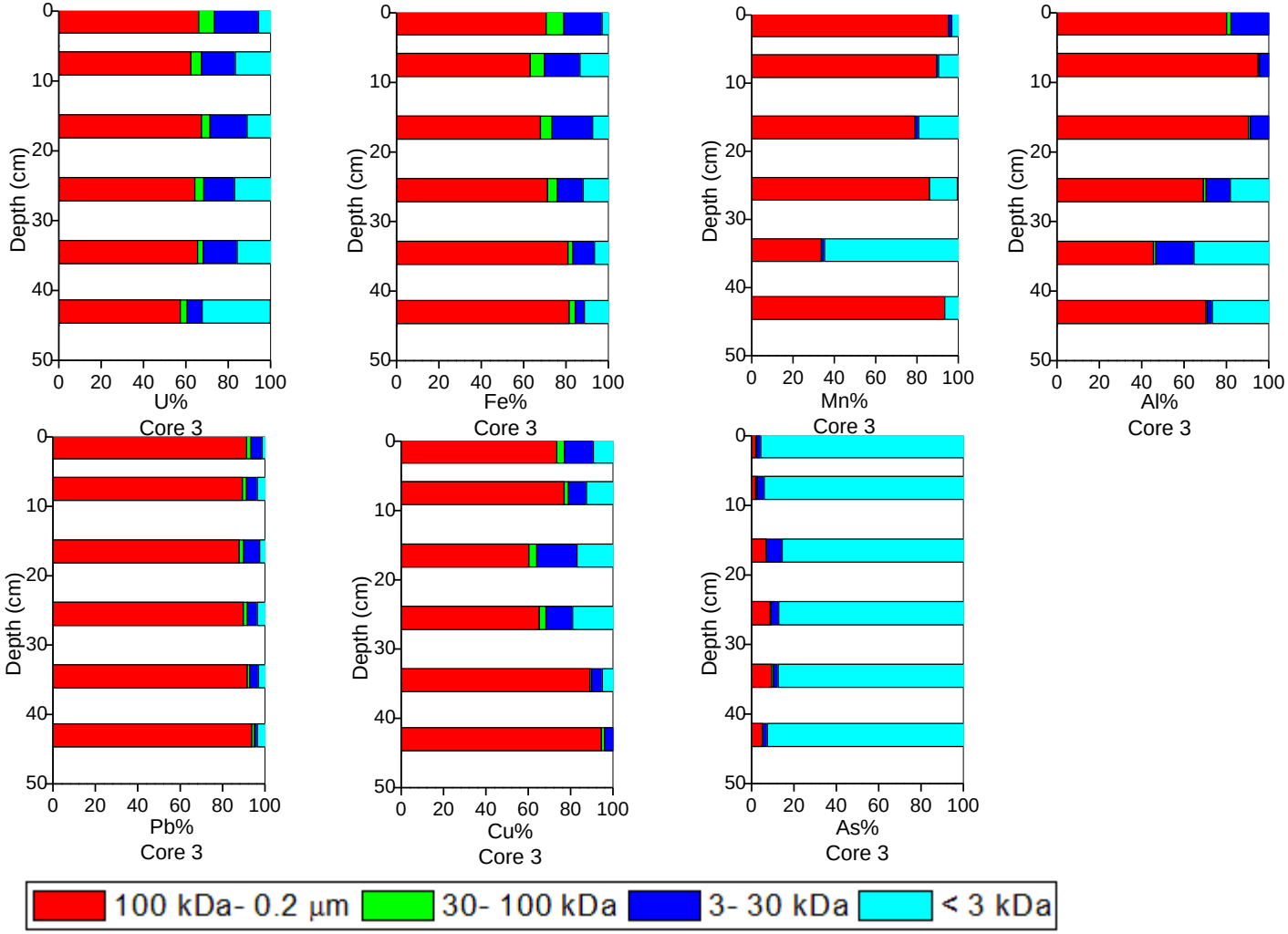

Figure 4.7: Distribution of U, Fe, Mn and Al amongst colloidal (100 kDa-0.2 µm, 30-100 kDa and 3-30 kDa) and dissolved (<3 kDa) fractions of porewaters obtained from soil Core 3

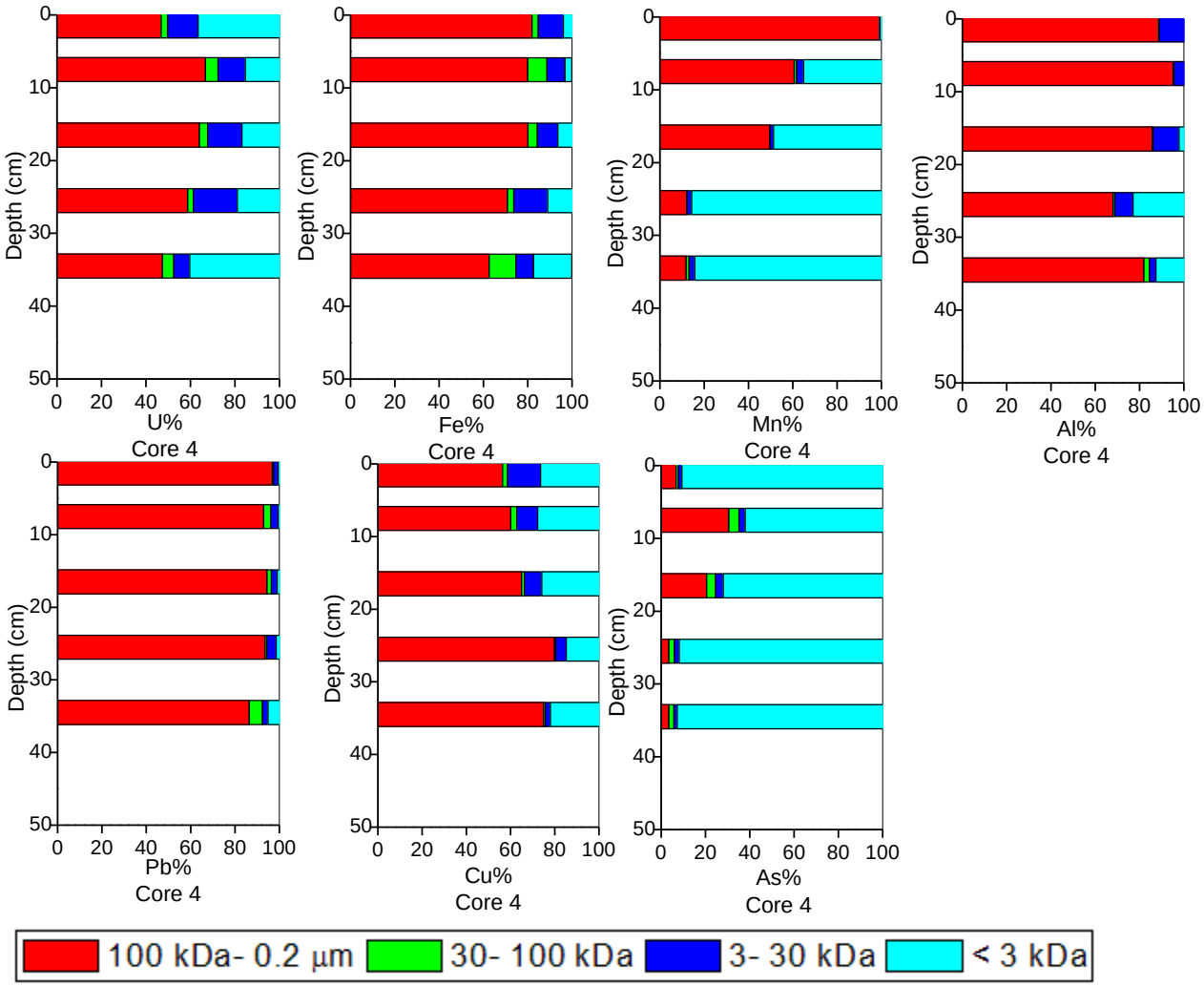

Figure 4.8: Distribution of U, Fe, Mn and Al amongst colloidal (100 kDa-0.2 µm, 30-100 kDa and 3-30 kDa) and dissolved (<3 kDa) fractions of porewaters obtained from soil Core 4

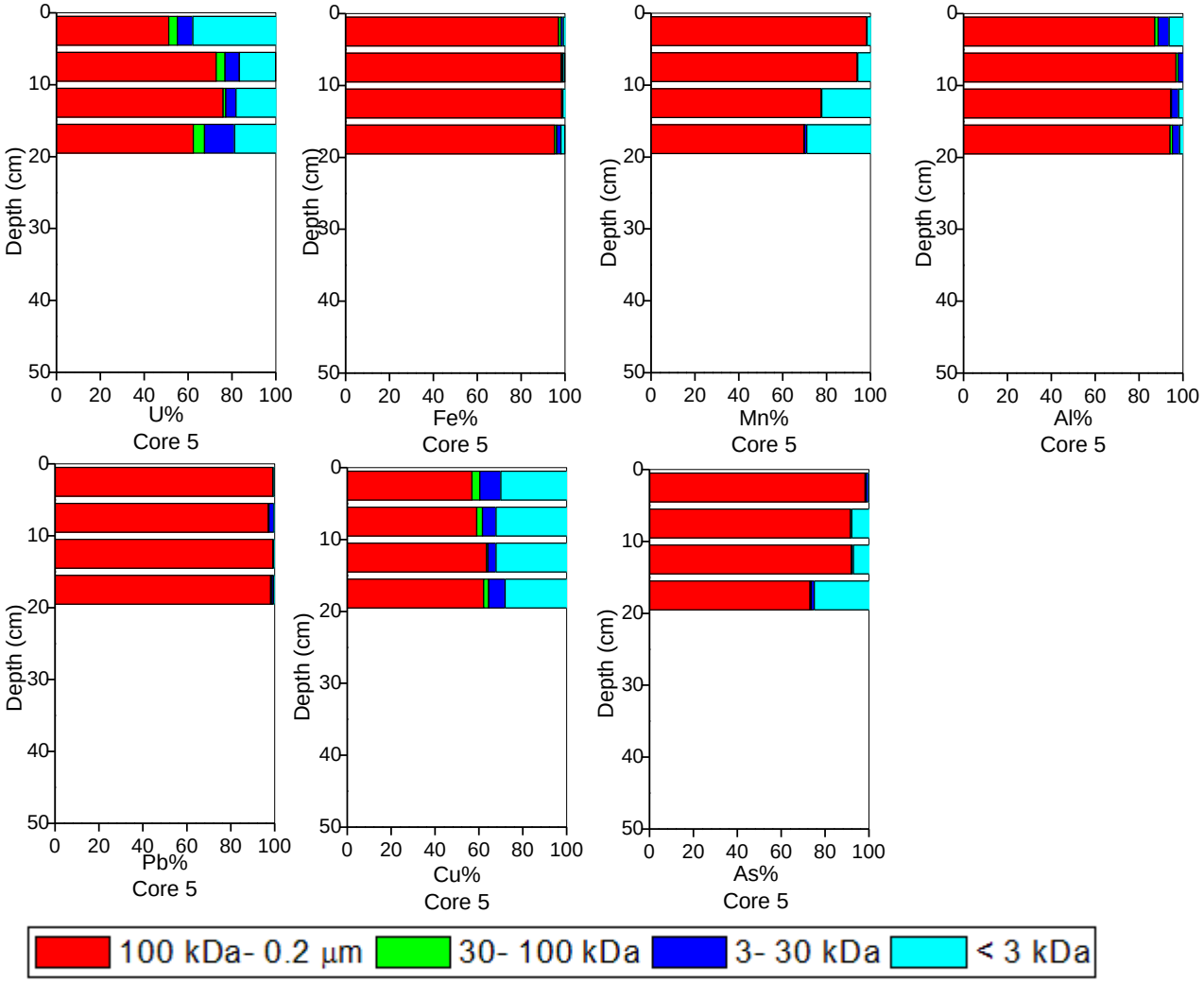

Figure 4.9: Distribution of U, Fe, Mn and Al amongst colloidal (100 kDa-0.2 µm, 30-100 kDa and 3-30 kDa) and dissolved (<3 kDa) fractions of porewaters obtained from soil Core 5

4.1.8 Sequential extraction of soil targeting for Fe phase

In section 4.1.6, it was observed that porewater U maxima did not coincide with solid phase U maxima in Cores 3 and 4. Although this was not the case for Core 5, it was sectioned into 5-cm slices which may have been too thick to reveal more detailed elemental distributions. As commented upon in section 4.1.7, there must be other factors controlling the transfer of U from the solid phase into the porewater, e.g. U may be released in association with humic colloids and/or with colloidal minerals. Amongst all the analysed elements (Fe, Mn, Al, As, Pb, Cu), Fe was found to be the only element that had a porewater maximum at the same depth as the porewater U maxima in all three cores. Since there are several kinds of Fe-containing minerals in soils which exhibit strongly contrasting behaviour, it is important to establish with which Fe phases the solid phase U is associated. In this section, sequential extraction was applied to quantify the U associations with different iron phases in the solid phase. The sequential extraction scheme was adapted from that described in Poulton and Canfield (2005) (Table 1.10 and section 2.5.11.1). The recoveries for both U and Fe were slightly elevated (U:119 ±15%; Fe:107 ±15%) but this is likely attributable to the large number of steps involved and the fact that elemental concentrations in some of the extracts were close to detection limits.

There was no U detected in F1 ($MgCl_2$) for any of the selected soil samples from Cores 3, 4 and 5 (Figure 4.10). In contrast, for all soil samples from each core, significant proportions of U was extracted in F2 (NaOAc): Core 3 - 55-73%, Core 4 – 45-63% and Core 5 – 64-67%. According to the extraction scheme, this fraction represents U that associated with the iron carbonate fraction. F3 ($NH_2OH.HCl$) represents the fraction of U that is associated with amorphous and semi-cystalline iron oxides, e.g. ferrihydrite and lepidocrocite. Only 2-7% U was extracted in F3 from each of the soil samples from Cores 3, 4 and 5. F4 (Na dithionite) extracts U associated with goethite, akaganite and hematite. Some 16-29% U at Core 3, 25-40% at Core 4 and 19-21% at Core 5 were found in this fraction. For Cores 3 and 4, only small amount of U were found in the fractions extracted after F4. Up to 11% U was extracted in F5 and up to 2% and 6% U in F6 and F7, respectively. For Core 5, slightly greater proportions were found in F7 (see Appendix section 9.11, Table 9.20).

In terms of vertical trends, there was a gradual increase (from 55 to 73%) in the amount of U extracted in F2 with increasing depth in Core 3 and a concomitant decrease in the

proportions extracted in F4 and F5. For Core 4, there was a step change (from 45-63%) between the first two samples; again, an increase in the proportion in F2 and a decrease in the percentage in F4. Below 10 cm, there was no further change. For Core 5, there was little difference in % distribution of U between the two samples.

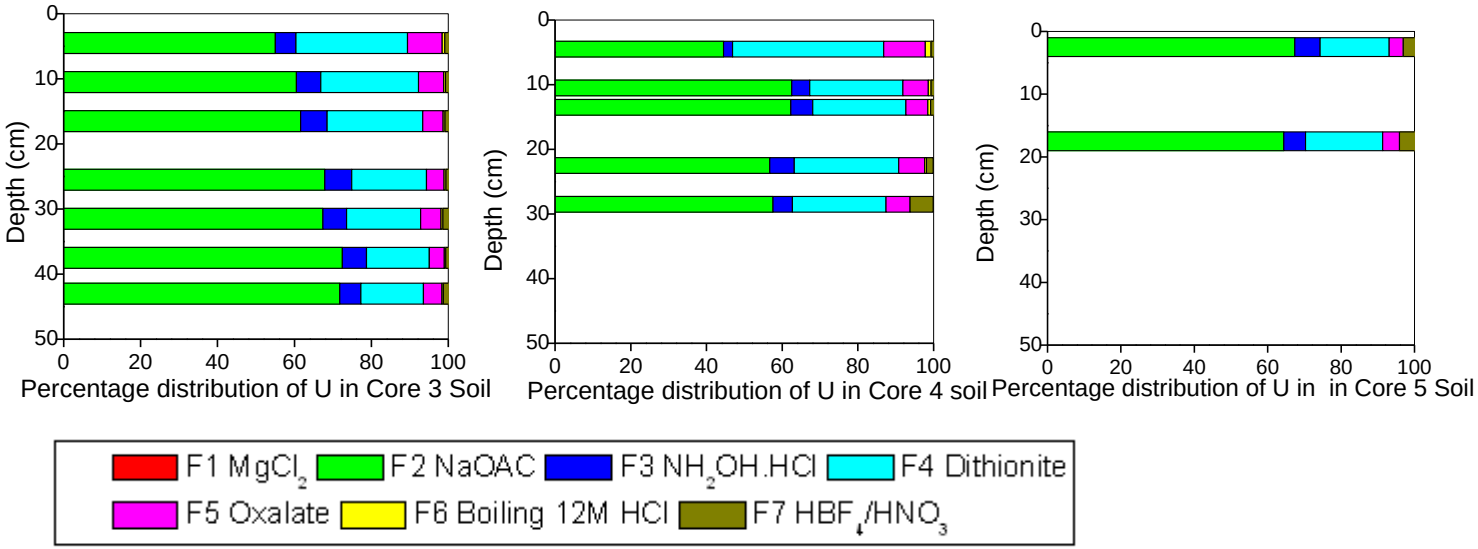

Figure 4.10 Distribution of sequentially extracted U in selected soil samples from Cores 3, 4 and 5

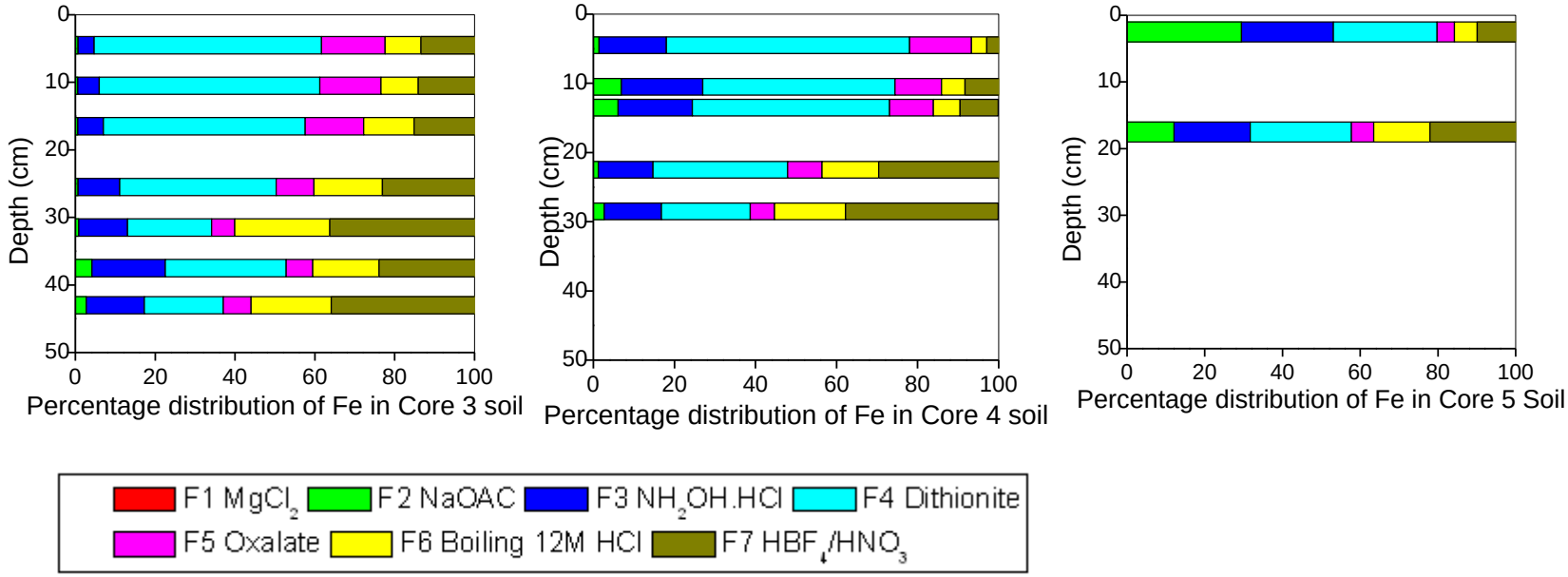

Figure 4.11: Distribution of sequentially extracted Fe in selected soil samples from Cores 3, 4 and 5

In agreement with the results for U, no detectable Fe was extracted in F1. However, the % distribution of Fe amongst the other 6 extracts differed considerably from that of U (Figure 4.11). Very little (0.6-4.2%) Fe was extracted in F2 from Core 3, only 1.2-6.9% from Core 4 and 12-29% from Core 5. Whereas only 2-7% U was extracted in F3, from each of the soil samples from Core 3 and Core 4, some 4-18% Fe for Core 3 and 14-20% for Core 4 was extracted in Fe. A similar trend was observed for Core 5. Especially in the uppermost sections, by far the greatest proportions of Fe were extracted from Cores 3 and 4 in F4: 21-57% Fe at Core 3 and 22-60% at Core 4. For Core 5, Fe was more evenly distributed across the fractions. About 10-15% Fe was extracted in F5 for the upper sections of Cores 3 and 4, but below 20 cm, significantly less than 10% of total Fe was extracted. In contrast, for F6 and F7, greater proportions of Fe were extracted in >20 cm depth sections. For Core 5, < 5% Fe was present in F5 but the trend of increasing Fe in F6 and F7 with increasing depth was again observed (see Appendix section 9.11, Table 9.21).

Observations and interpretation

The key features in the vertical distribution profiles for U and Fe in the solid phases from Cores 3, 4 and 5, were:

(i) The greatest proportion of U was extracted in F2 whilst the greatest amount of Fe was usually extracted in F4;

(ii) The proportion of U in F2 increased with increasing depth (albeit a step change in Core 4) and there was a small amount of Fe detected in F2 towards the bottom of Cores 3 and 4;

(iii) The proportion of both U and Fe in F4 decreased with increasing depth;

(iv) The proportion of Fe in F6 and F7 increased with increasing depth but did not affect the distribution of U

Since very little Fe was found in F2 extracts it is difficult to conclude with certainty that the U contained therein was associated with Fe carbonates. The high proportions of U present in F2 mean that it is a significant sink for U in these soils and it is therefore important to establish the form of U that has been extracted by the sodium acetate reagent.

The trend towards greater Fe in the later fractions with increasing depth raises the question as to whether Fe is present in the form of sulphides. This does not appear to impinge on U associations at depth within the soils but it is still important to establish whether or not sulphides may be present since this will provide evidence of the extent to which highly reducing conditions prevail.

The distribution of both U and Fe in Core 5 was significantly different from that in Cores 3 and 4, especially for Fe in F2 and F4. F2 contained much higher proportions of Fe at Core 5 whilst only a small percentage of Fe was extracted in F2 for Cores 3 and 4 samples. According to a report by Hooker (1990), the length crossing the organic-rich area from the point near the mineralisation towards the point closest to the salt marsh is ~25 m. Therefore, Core 5 (35 m from the mineralisation) is in between the peat bog and the salt marsh and so the composition of Core 5 soil is also a mixed medium which is affected by inputs of uranium-containing groundwater coming from the mineralisation and by relatively infrequent inundation with seawater. Thus the paragraphs that follow will mainly focus on Cores 3 and 4 which experience no influence from the marine system.

4.1.8.1 Additional experiment to explore the efficacy of stage 2 (Carbonate Fe) in the sequential extraction procedure

As described above, U co-extracted in F2 (Na acetate) is thought to represent that associated with the Fe carbonate fraction (Poulton and Canfield, 2005). However, as described above some 55-73% and 45-63% U were extracted in F2 along with only 0.6-4.2% Fe and 1.2-6.9% from Cores 3 and 4, respectively. Therefore, an additional experiment was added to verify whether the extracted U was associated with Fe carbonate or whether some other release mechanism was taking place. Since mineral acids will dissolve any carbonates present in soil, hydrochloric acid (c. HCl) was used to adjust the pH value of DI water. The same mass of soil and the same solution volume of pH-adjusted DI water were used so that the data in Table 4.3 can be compared directly with the results obtained during stage 2 of the sequential extraction procedure. The aim of the experiment was to change the pH from 7 (the same as that used for F1) to 4.5 (as used in F2) (see Table 4.3). The experiment started from pH 6.09 which was the value obtained when the soil was suspended in DI water. The pH was adjusted by 0.2 unit increments via addition of 0.1 M

HCl until a final value of 4.3 was reached. It should be noted that each row in Table 4.3 was a separate soil aliquot.

As shown in Table 4.3, there was no detectable U released at any of the pH values and only up to one-tenth of Fe was released when compared with the acetate extraction. The amount of Fe extracted did increase slightly from 0.02 mg L^{-1} to 0.04 mg L^{-1} as pH decreased but this was considered to be within experimental error. This experimentstrongly indicated that the U extracted by NaOAc was not associated with a carbonate fraction and so careful interpretation regarding the associations of U is required.

Table 4.3: Comparison of U and Fe concentration in pH-adjusted DI water and NaOAc extract with suspended Core 3 S4 soil (10.5 cm depth)

Adjustment of pH using 0.1 M HCl			**F2 (NaOAc at pH 4.5) in sequential extraction**	
pH	U (mg L^{-1})	Fe (mg L^{-1})	U (mg L^{-1})	Fe (mg L^{-1})
6.09	n.d.[1]	0.02	12.24	0.36
5.90	n.d.	0.02		
5.70	n.d.	0.03		
5.50	n.d.	0.03		
5.30	n.d.	0.02		
5.10	n.d.	0.03		
4.90	n.d.	0.03		
4.70	n.d.	0.03		
4.50	n.d.	0.03		
4.30[2]	n.d.	0.04		

[1]n.d.= not detected; detection limit = 0.004 mg L^{-1}

[2]Upon re-measurement after 24 hours, it was observed that the pH of the soil solution had increased by ~+0.2, so the final test was adjusted to pH 4.30 at the starting point.

4.1.8.2 Total reduced inorganic sulfur (TRIS) and acid volatile sulfide (AVS) analysis

According to the S extraction method by Fossing and Jorgensen (1989), total reduced inorganic sulfur (TRIS) includes both acid volatile sulfide (AVS: H_2S+FeS) and the remaining chromium reducible sulfur (CRS: S^0, FeS_2) (also see method section 2.4.13.3).

For Core 3, TRIS concentrations in soil increased from 90 mg kg^{-1} in the near-surface sections to 210 mg kg^{-1} near the bottom of the core. The AVS concentrations in Core 3 were close to or below detection limit for most sections, but the results may indicate that soil sections above 10.5 cm contained slightly higher amounts of AVS than those below this depth. For Core 4, there was also an increasing trend of TRIS from 150 mg kg^{-1} to 310 mg kg^{-1} towards the bottom of the core. The AVS concentrations in Core 4 samples were also higher for upper rather than the deeper sections, with more than 10 mg kg^{-1} above 20.5 cm and less than 10 mg kg^{-1} below this depth.

Since Table 4.4 showed that the AVS content was much lower in comparison with TRIS content, the S extracted by TRIS mostly represents the CRS content, which means that CRS increased with increasing depth. The Fe proportion in F7 in sequential extraction (Figure 4.11) also increased with increasing depth. This probably indicates that the Fe in F7 was at least partly in the form of pyrite.

It is also clear that Core 4 contained greater amount of TRIS and AVS than Core 3, which indicates that conditions in the soil further from the mineralization were more reducing (Table 4.4). This is consistent with the redox measurements made at the time of sample collection (section 4.1.1).

Table 4.4: Total reduced inorganic sulfur (TRIS) and acid volatile sulfide (AVS) extraction in selected subsamples of wet soil from Cores 3 and 4

Core	Depth (cm)	TRIS ($mgkg^{-1}$)	AVS ($mgkg^{-1}$)[1]
Core 3	4.5	90 ±40	n.d.[2]
	10.5	120 ±10	2.4 ±2.3
	16.5	120 ±30	n.d.
	25.5	140 ±40	n.d.
	31.5	180 ±10	0.6 ±0.8
	37.5	210 ±20	n.d.
Core 4	4.5	150 ±50	11 ±15
	10.5	150 ±60	28 ±13
	13.5	260 ±50	2.2 ±3.1
	22.5	280 ±20	9.0 ±13
	28.5	310 ±20	7.5 ±5.0

[1]The data of acid-volatile S generally have quite high standard deviation as most of them are close to detection limit by ICP-MS.

[2]n.d. = not detected; for acid-volatile S analysed by ICP-MS, the detection limit= 1 mg L^{-1}.

In section 4.1.8, sequential extraction was mainly used to explore the relationship between U and the mineral phases, specifically the iron phases in the soil. The greatest proportion of U was extracted in F2, which was supposed to indicate association with carbonate. The second largest proportion of U was released in F4, which was associated with crystalline iron oxides, e.g. goethite, akaganite and hematite. X-ray diffraction analysis is a method that can be used to quantitatively and qualitatively determine minerals in the soil. With this technique, the main types and the corresponding proportions of each mineral in the soil can be determined. It was hoped that this would provide additional information about the nature of Fe (and other) minerals present in the soils (section 4.1.9).

4.1.9 X-ray Diffraction Analysis of Soil Samples from Cores 3, 4 and 5

When selected bulk soils were initially analysed by XRD, there was a high background signal which interfered with identification of the mineral phases. This was caused by the

high organic matter content in the soil. Only up to 8 phases were recognized by XRD (data not shown) and the data were only semi-quantitative. Therefore, all the soil samples were ashed at 450 ℃ before analysis by XRD. Ashing at 450 ℃ can to some extent cause alteration or decomposition of some minerals especially some carbonate minerals, but a reasonable carbonate trend still can be found in the results (Table 4.5). Overall, ashing eliminates the organic components without affecting the majority of the crystalline components.

It should be noted that the mineral contents shown in Table 4.5 were back-calculated for the whole soil (i.e. not the ash which was analysed) and presented as a percentage of the whole soil. The detection limit for minerals in mixtures is generally ~1% w/w. As shown in Table 4.5, significant proportions of quartz were found in the samples from all three cores: Core 3 – ~7.6-25.1%, Core 4 – 9.1-50.4%, Core 5 – 29.8%, and there was a general increase with distance from the mineralisation. In terms of vertical trends, quartz content increased with depth in both Cores 3 and 4. Highest levels of calcite were found in the uppermost sections of Cores 3 and 4 (~4.7% and ~2.7% at 13.5 cm and 4.5 cm, respectively). The amount of calcite in the soil decreased with increasing distance from the mineralisation. Other carbonate minerals such as dolomite ($CaMg(CO_3)_2$) and siderite ($FeCO_3$) were present only at low concentration, with values for each of these being ≤1% in all three cores. However, as noted above, there may have been some losses due to the ashing procedure. Pyrite minerals were detected only in Core 4, which was taken from the most reducing part of the bog (see Table 4.1). The XRD detection limit for pyrite is 1% w/w so the absence of a signal for pyrite in Core 3 does not mean that it was absent from these samples. Hematite (crystalline Fe_2O_3) was found only in Cores 4 and 5 and in quite small proportions of up to ~0.14%. There was no clear trend of hematite with either vertical depth in the soil or distance from the mineralisation. Albite, anorthite, microcline and orthoclase all belong to the group of primary minerals termed feldspars. The proportion of albite increased slightly with depth, from ~1.1% to ~3.1% in Core 3 and from ~1.4% to ~5.5% in Core 4. Values for anorthite were lower than those for albite, and there was a clear trend of increasing concentration with depth for Core 3; the increase for Core 4 was more gradual. The only difference between microcline and orthoclase is the crystalline structure: microcline crystallizes in the triclinic structure while orthoclase crystallizes in the monoclinic structure. There was no clear trend in concentration for microcline or orthoclase either with vertical soil depth or distance from the mineralisation. The greatest

amounts of gypsum ($CaSO_4$) were found in Core 3, the core closest to the mineralisation. Although it needs to be taken into account that the errors were relatively large, the proportion of gypsum appeared to decrease with increasing depth in Cores 3 and 4, from ~0.4% to ~0.1% and from ~0.2% to ~0.04%, respectively. Kaolinite is a 1:1 clay mineral, and concentrations were ≤0.65% in all three cores.Illite and chlorite IIb are both 2:1 silicate clay minerals containing Fe in their structure. There were relatively high proportions of illite in all three cores: 1.9-7.8% in Core 3, 3.3-8.5% at Core 4 and 7.7% in Core 5; for Cores 3 and 4, there was a general increase with increasing soil depth. For Chlorite IIb, highest concentrations were found in Core 3, that nearest to the mineralisation. In terms of the vertical depth trend, values for chlorite IIb decreased with depth. There was no detectable anatase, a titanium dioxide, in Core 3 but further from mineralisation, anatase was present in Cores 4 and 5 at ≤~0.8%.

Observations and initial interpretation

The key features relating to the mineral composition of the ashed soils in Cores 3-5 were:

(i) Five minerals that contain Fe were detected: these included siderite, pyrite, hematite, chlorite IIb and illite. Only small amounts of siderite, pyrite and hematite were detected and the absence of other Fe oxides and hydroxides may be due to the relatively high XRD detection limits (~1% w/w). These iron phases do, however, provide large surface areas with positively charged surface sites (at pH 6-7) for sorption of negatively charged U species. The Fe present in chlorite and illite is present within the mineral structure, e.g. at octahedral sites;

(ii) Of all the minerals detected, only kaolinite, illite and chlorite IIb were clay minerals, which have large surface areas and may provide cation exchange sites for positively charged U species. Alternatively, positively charged bridging species may enable negatively charged uranium species to interact with these surfaces;

(iii) Quartz, feldspars (albite, anorthite, microcline, orthoclase) and anatase have smaller surface areas and have few exchange sites on their surfaces and are thus unlikely to constitute major sinks for aqueous phase U species;

(iv) The carbonate minerals (calcite, dolomite, siderite) were present at varying

concentrations with those for calcite being ~x10 greater than those for dolomite and siderite. From the experiments described in section 4.1.8, these minerals do not appear to be important sinks for U (section 4.1.7).

Table 4.5: Types and compositions of soil minerals in selective soil subsections of Cores 3, 4 and 5 (The detection limit is ~1% w/w, but data below this value are reserved for semi-quantitation)

Phase	Chemical formula	Core 3 (%)			Core 4 (%)			Core 5
		13.5 cm	25.5 cm	37.5 cm	4.5 cm	19.5 cm	31.5 cm	7.5 cm
Quartz	SiO_2	7.56 ±1.1	15.8 ±1.8	25.1 ±1.8	9.10 ±0.51	17.1 ±0.97	50.4 ±2.4	29.8 ±2.5
Calcite	$CaCO_3$	4.69 ±0.87	1.77 ±0.56	0.00 ±0.98	2.65 ±0.26	0.30 ±1.4	0.00 ±1.1	4.17 ±1.2
Dolomite	$CaMg(CO_3)_2$	0.20 ±0.53	0.07 ±0.40	0.18 ±0.53	0.06 ±0.30	0.00 ±2.4	0.21 ±4.8	0.08 ±4.0
Siderite	$FeCO_3$	0.22 ±0.87	0.13 ±1.0	0.06 ±1.16	0.23 ±0.79	0.28 ±0.70	0.09 ±1.0	0.02 ±2.3
Pyrite	FeS_2	-	-	-	0.02 ±1.5	0.03 ±1.2	0.07 ±2.0	-
Hematite	α-Fe_2O_3	-	-	-	0.16 ±0.61	0.04 ±1.5	0.07 ±2.6	0.04 ±2.3
Albite	$NaAlSi_3O_8$	1.16 ±0.27	2.06 ±0.47	3.07 ±0.45	1.36 ±1.5	2.07 ±2.6	5.52 ±6.2	2.71 ±0.55
Anorthite	$CaAl_2Si_2O_8$	0.24 ±1.2	0.85 ±2.2	2.31 ±3.6	0.40 ±1.2	0.73 ±1.3	1.89 ±2.6	1.05 ±2.4
Microcline max	$KAlSi_3O_8$	0.45 ±1.3	0.93 ±2.3	2.14 ±3.3	1.36 ±1.6	1.02 ±1.5	1.54 ±2.2	1.35 ±2.8
Orthoclase	$KAlSi_3O_8$	0.40 ±1.2	0.73 ±1.8	0.57 ±1.3	0.24 ±0.85	1.04 ±1.4	1.61 ±2.1	0.11 ±0.90
Gypsum	$CaSO_4$	0.47 ±1.4	0.80 ±2.3	0.10 ±4.0	0.16 ±0.47	0.22 ±0.46	0.04 ±3.2	0.39 ±1.7
Kaolinite (BISH)	$Al_2Si_2O_5(OH)_4$	0.10 ±0.53	0.19 ±0.72	0.16 ±0.67	0.13 ±0.63	0.11 ±0.52	0.18 ±6.4	0.13 ±0.60
Illite	$(Al,Mg,Fe)_2(Si,Al)_4O_{10}[(OH)_2,(H_2O)]$	1.94 ±0.49	5.32 ±1.8	7.79 ±1.4	3.28 ±0.42	6.41 ±0.79	8.50 ±1.1	7.69 ±1.5
Chlorite IIb	$(Mg,Fe)_3(Si,Al)_4O_{10}(OH)_2.(Mg,Fe)_3(OH)_6$	1.56 ±0.44	2.46 ±0.59	2.98 ±0.67	0.71 ±1.3	0.50 ±1.1	0.44 ±1.6	2.01 ±0.55
Anatase	TiO_2	-	-	-	0.38 ±0.73	0.56 ±1.0	0.82 ±1.6	0.65 ±1.7

4.1.10 Scanning electron microscopy-Energy dispersive X-ray spectroscopy (SEM-EDX)

The soil sample analysed by SEM-EDX was dried, ground intact soil (i.e. not ashed) from Core 3 S7 (19.5 cm). This sample was selected as it contained the highest amount of U amongst all the soil samples. For the SEM-EDX measurement, identification of uranium-containing particles was based on the presence of the uranium Mα X-ray line at 3.17 keV, the Mβ line at 3.34 keV, the Lα line at 13.6 keV. The SEM examination showed that uranium-enriched grain 1 was contained within particles of size ~20 μm (Figure 4.12). Grain 1 contained U and Pb with some C and O. Another U-rich particle, grain 2, found in Core 3 S7 was smaller at ~4.5 μm, and contained Si, S, C and O (Figure 4.13).

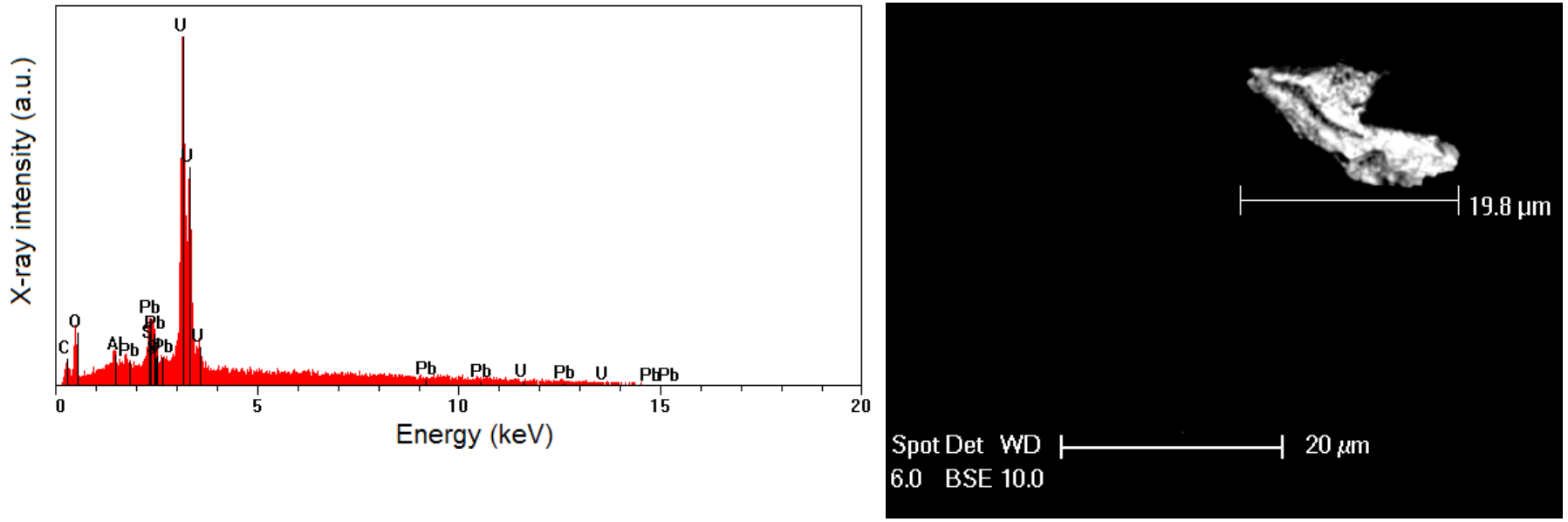

Figure 4.12: SEM-EDX spectrum and image of a precipitated U grain 1 in Core 3 S7 soil

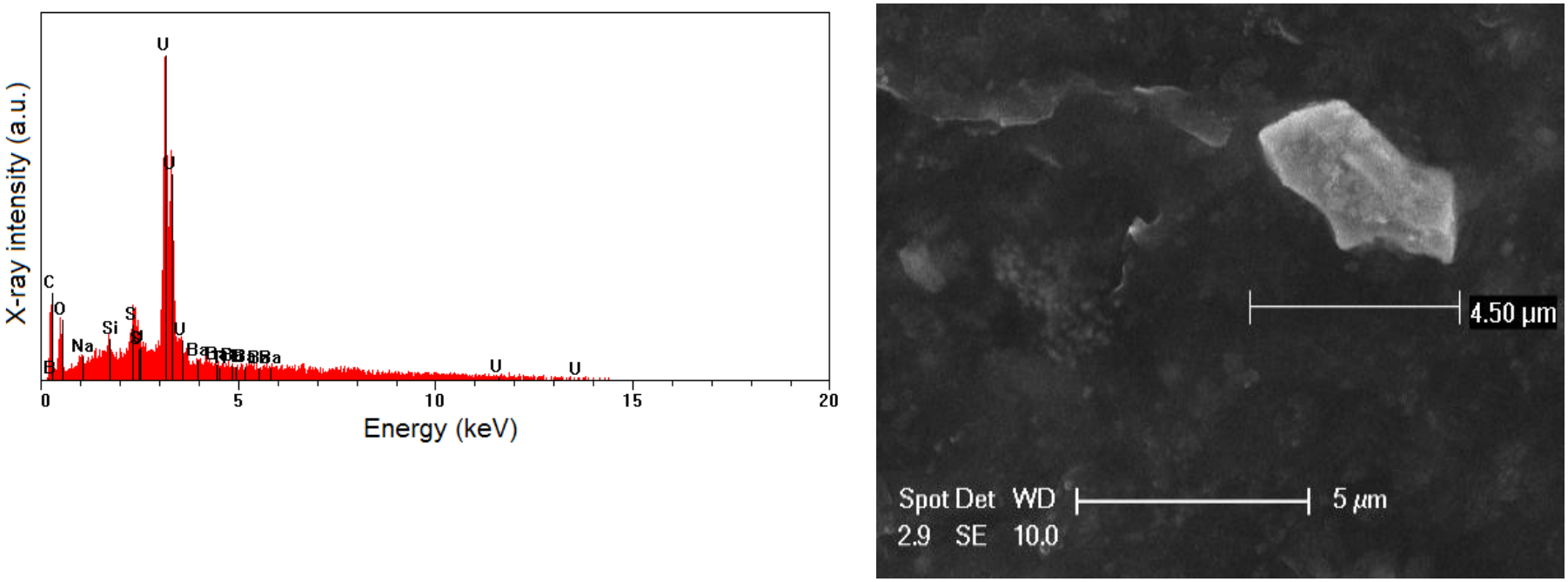

Figure 4.13: SEM-EDX spectrum and image of a precipitated U grain 2 in Core 3 S7 soil

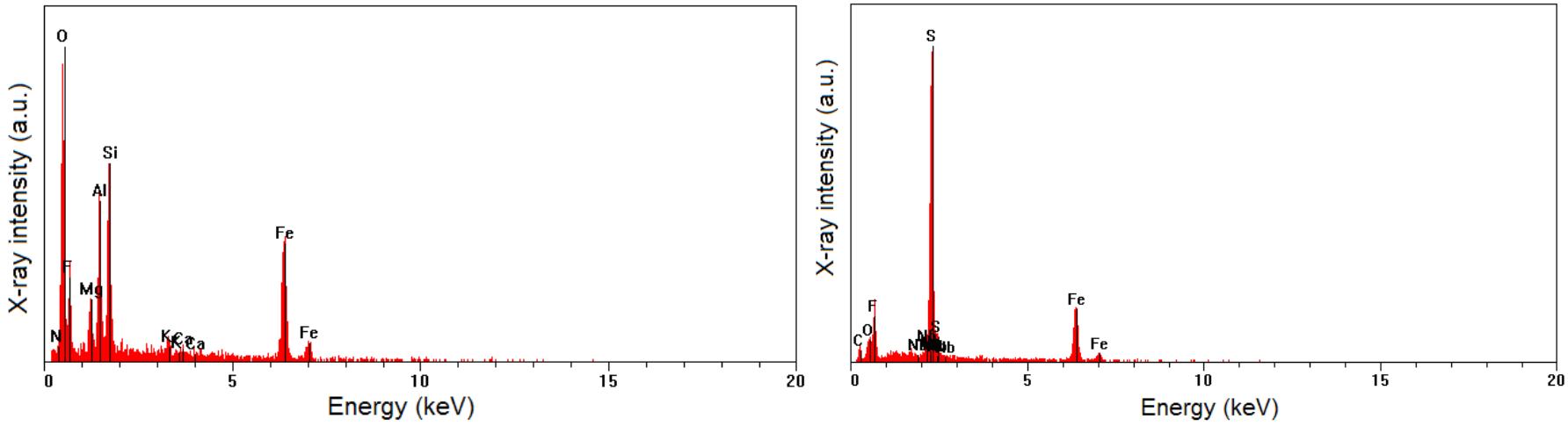

(a) **(b)**

Figure 4.14: SEM-EDX spectrums of iron minerals in Core 3 S7 soil: (a) iron containing particle along with O, F, Mg, Al and Si; (b) iron containing particle along with S, C, O and F

Two types of iron-containing particles were found in the Core 3 S7 sample: one contained Fe along with O, F, Mg, Al and Si; the other contained Fe along with S and small amounts of C, O and F (Figure 4.14). The second iron-containing particle may contain FeS_2 since this mineral was identified using XRD (see section 4.1.7). In addition, the TRIS and AVS measurements described in section 4.1.8.2 suggested that S was present either in elemental form or as FeS_2.

Overall, during 4-hour-scanning by SEM-EDX, there were only two U fragments spotted, which indicated that the U present in the Core 3 S7 soil sample was mainly in non-crystalline forms. Also the two U-rich particles did not contain Fe.

4.1.11 Sequential extraction of humic substance in conjunction with gel electrophoresis

The exhaustive humic extractions described in section 2.5.3.3 sampling trip 2, confirmed the findings of previous work (MacKenzie et al., 1991) by showing that more than 90% of U was associated with solid phase organic matter in the Needle's Eye peat bog. Moreover, the gel electrophoretic and gel filtration separations described in section 3.5.1-3.5.2 showed that the U extracted along with humic substances from these soils was almost entirely associated with the very largest size molecules. Sections 4.1.7-4.1.9 mainly tried to establish the distribution of U amongst Fe mineral phases in the soil because the shapes of vertical porewater profiles suggested that processes affecting the solubility of Fe may be controlling the U behaviour in the bog. Indeed, the solid phase sequential extraction results (section 4.1.8) identified a significant association of U with crystalline Fe oxides. In order to reconcile these contradictory findings, a set of new experiments was designed:

(I) Humic substances were isolated from two soil samples (Core 3 S6 (16.5 cm) and Core 3 S7 (19.5 cm)) and gel electrophoresis was then used to fractionate the extracts on the basis of size and charge.

(II) Humic substances were isolated from the soil AFTER (i) acetate extraction; (ii) dithionite extraction; (iii) acetate and then dithionite extraction of metals from the soil. Gel electrophoretic fractionation of the humic extract followed. The samples were labelled as Core 3 S6-1 and Core 3 S7-1.

(III) Humic substances were isolated from the soil BEFORE (i) acetate extraction; (ii) dithionite extraction; (iii) acetate and then dithionite extraction of metals from the humic extract. Gel electrophoretic fractionation of the humic extract followed. The samples were labelled as Core 3 S6-2 and Core 3 S7-2.

In the initial survey described in Chapter 3, humic substances from selected depths in Cores 1 and 2 were fractionated by gel electrophoresis (see section 3.4.1). The results showed that there were no major variations in U-humic association either with vertical soil depth or with lateral distance from the U mineralization. The humic substances in the soil seem to be uniform in composition. So in this section, Core 3 S6 and S7 were selected as pseudo-replicates.Core 3 S6 and S7 soils were selected to run the experiment because they were at the depth where U and Fe maxima occurred either in the solid phase or porewater (see Figure 4.4).

4.1.11.1 Gel electrophoretic fractionation of humic substances extracted from Core 3 soils

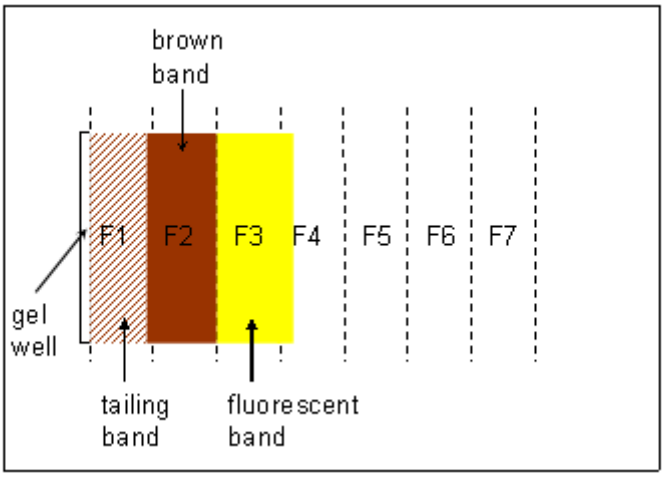

Figure 4.15: Schematic of gel electrophoresis pattern for humic substances extracted from samples Core 3 S6 and S7

For each of the humic substances from Core 3 S6 and S7, no matter which extract (I, II or III defined in section 4.1.11) was applied, the visual appearance of the gel after running for 30 minutes was very consistent. In each case a dark brown band had emerged from the gel well and migrated ~1-2 cm towards the positive electrode. There was some brown-coloured material that had only migrated 0-1 cm from the gel well and this was designated as the tailing band (F1). Viewed under UV light, a fluorescent band was observed to have migrated further from the gel well. The gel was then cut into seven 1-cm strips (F1-F7) and the positions of bands were noted. The dark brown band was mainly in F2, while the fluorescent band was mainly in F3 (some in F4), with the fluorescent being slightly ahead of the brown band (Figure 4.15).

The red bars in each of Figures 4.16-4.21 show the distribution of U, Fe, Mn and Al across each of the gels for experiment I where humic substances had been extracted directly from the soil samples. The first point to note is that the highest concentrations of each element occurred in F2, the position of the dark brown band. Lower concentrations of each element (except for Al) were found in F1, the position of the tailing band, while F3-F4 (fluorescent band) had the lowest elemental concentrations. The gel well content was also analysed and very little U, Fe, Mn or Al remained in the well. Overall, it is clear that each of these elements migrated in association with the humic substances. Importantly, almost none was detected in the fractions in front of the fluorescent band.

4.1.11.2 Selective and sequential extractions followed by extraction of humic substances: element associations with humic substances using gel electrophoresis and ICP-OES

Table 4.6 illustrates the percentage of each element remaining associated with humic substances after acetate extraction, dithionite extraction and sequential extraction. These values were obtained by summing the amount of element in each of the gel electrophoretic fractions and comparing the total value with that obtained for humic substances where no selective or sequential extraction had been carried out. Numbers exceeding 100% meant that the amount of the element associated with the humic substances had increased after reagent extraction, i.e. a portion of a mineral form of the element had been mobilised from the soil and become associated withthe humic substances after reagent extraction. Table 4.7 shows the same data but expressed as a percentage removal of each element from humic

substances after acetate extraction, dithionite extraction and sequential extraction. The summed effect of the selective reagents (acetate + dithionite) was compared with percentage of elements removed after sequential extraction. This was used to establish the selectivity of the acetate and dithionite reagents, i.e. ideally "acetate+dithionite"= "sequential".

Table 4.7 shows that 12% and 30% of the U bound to humic substances were removed from the Core 3 S6 and S7 samples, respectively, when acetate extraction of the soil was carried out before humic substance isolation form the soils (Experiment II, Table 4.7). If ~90%, i.e. almost all, of the soil U was associated with the humic substances (MacKenzie et al., 1991), then the amount of U (12-30%) released by acetate from humic substance in this experiment was much smaller than expected based on the sequential extraction results described in section 4.1.8, where ~70% of U was released from the total soil (see Figure 4.8) (see Appendix 9.13, Tables 9.28). A possible explanation is that the humic extracts were filtered through a 0.2 μm hydrophilic membrane to remove mineral matter that may have been co-extracted by 0.1 M NaOH. At the same time, this filtration would also exclude humic substances (including mineral-humic entities) that were >0.2 μm. Thus, the humic substances examined here by gel electrophoresis may not be fully representative of those in the total soil.

An unexpected feature of the results was that the amount of Fe associated with humic substances isolated after acetate extraction increased by a factor of approximately two (190% and 246% for S6 and S7, respectively) (Table 4.6). This suggests that Fe from one or more discrete mineral phases, which was not bound to OM, dissolved in the acetate solution and then re-adsorbed onto the soil, specifically onto humic substances. This partly explains why very little Fe was measured in the acetate extracts during the sequential extraction experiments described in section 4.1.8 but it should be recalled that HCl released even less Fe into solution and so it is unlikely that $FeCO_3$ is the phase that has been mobilised during experiment II.

The amount of Mn associated with the humic material isolated after acetate extraction was about seven times that associated with the humic material isolated directly from the soil (Table 4.6). This indicates that a large amount of Mn had been released from discrete mineral phases but become immediately associated with the soil humic substances.

The acetate extraction results for Al were very similar to those for Mn. The amount of Al associated with the "post-acetate extracted" humic substances increased by ~3-5 times (Table 4.5). This also indicates that a large amount of Al from discrete mineral phases was released and re-adsorbed onto the soil humic substances.

Table 4.6: Percentage of element remaining in association with humic substances isolated after acetate extraction, after dithionite extraction, and after sequential extraction

Element	Core 3 S6-1			Core 3 S7-1		
	Acetate	Dithionite	Sequential (acetate; dithionite)	Acetate	Dithionite	Sequential (acetate; dithionite)
U	88%	16%	7%	70%	13%	7%
Fe	190%	21%	21%	246%	19%	26%
Mn	671%	117%	51%	704%	136%	89%
Al	462%	145%	87%	289%	103%	78%

NB In experiment II, humic substances were isolated AFTER the selective or sequential extractions had been carried out on the soil

Table 4.7: Percentage of element removed from humic substances isolated after acetate extraction, after dithionite extraction, and after sequential extraction: comparison of the summed effect of selective reagents with the sequential extraction results

Element	Core 3 S6-1				Core 3 S7-1			
	Acetate	Dithionite	Sequential (acetate; dithionite)	Sum of acetate & dithionite	Acetate	Dithionite	Sequential (acetate; dithionite)	Sum of acetate & dithionite
U	12%	84%	***93%***	***96%***	30%	87%	***93%***	***117%***
Fe	-90%	79%	***79%***	***-11%***	-146%	81%	***74%***	***-65%***
Mn	-571%	-17%	***49%***	***-588%***	-604%	-36%	***11%***	***-640%***
Al	-362%	-45%	***13%***	***-407%***	-189%	-3%	***22%***	***-192%***

NB In experiment II, humic substances wereisolated AFTER the selective extractions had been carried out on the soil.

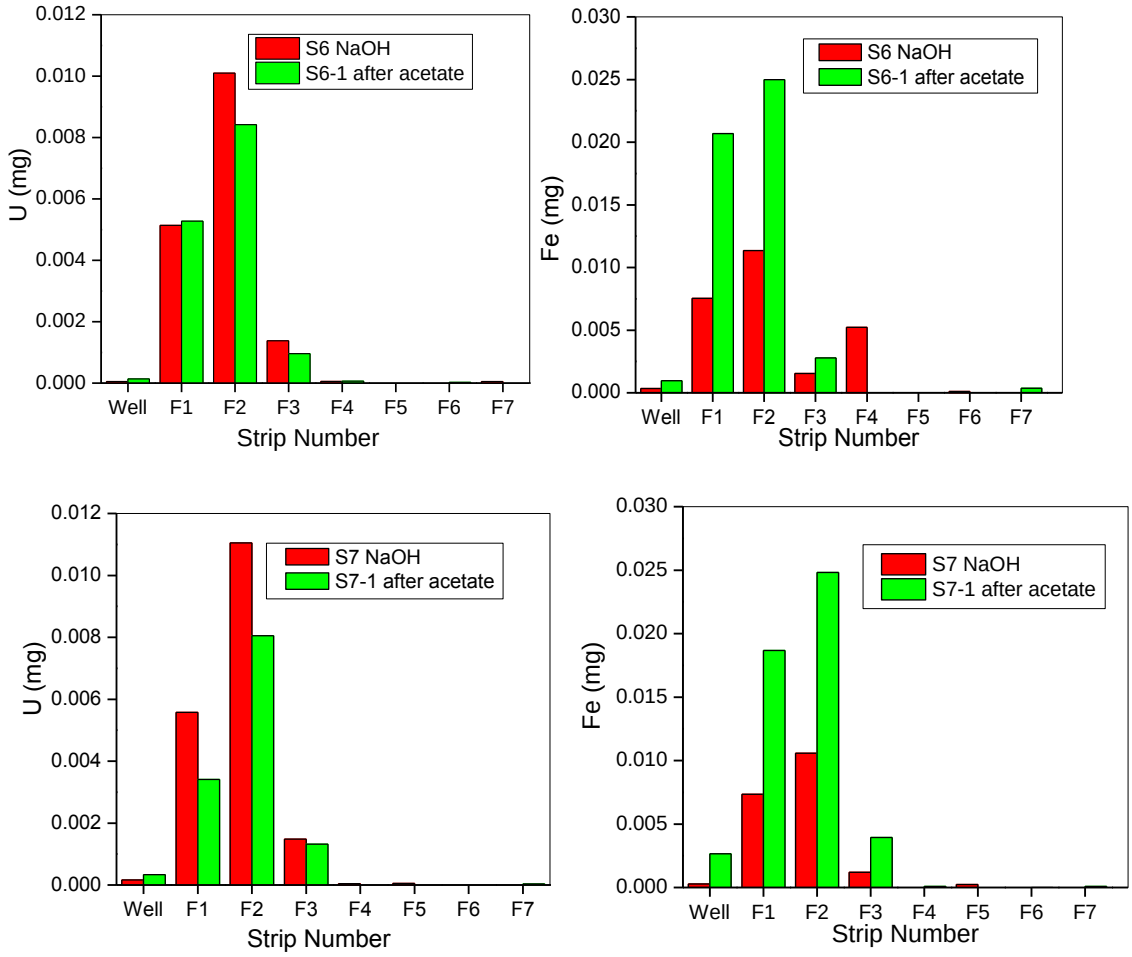

Figure 4.16(a): U and Fe associations with humic substances from Core 3 without (red bar) and with (green bar) acetate extraction (N.B. in experiment II, humic substances were isolated AFTER the selective extractions had been carried out on the soil

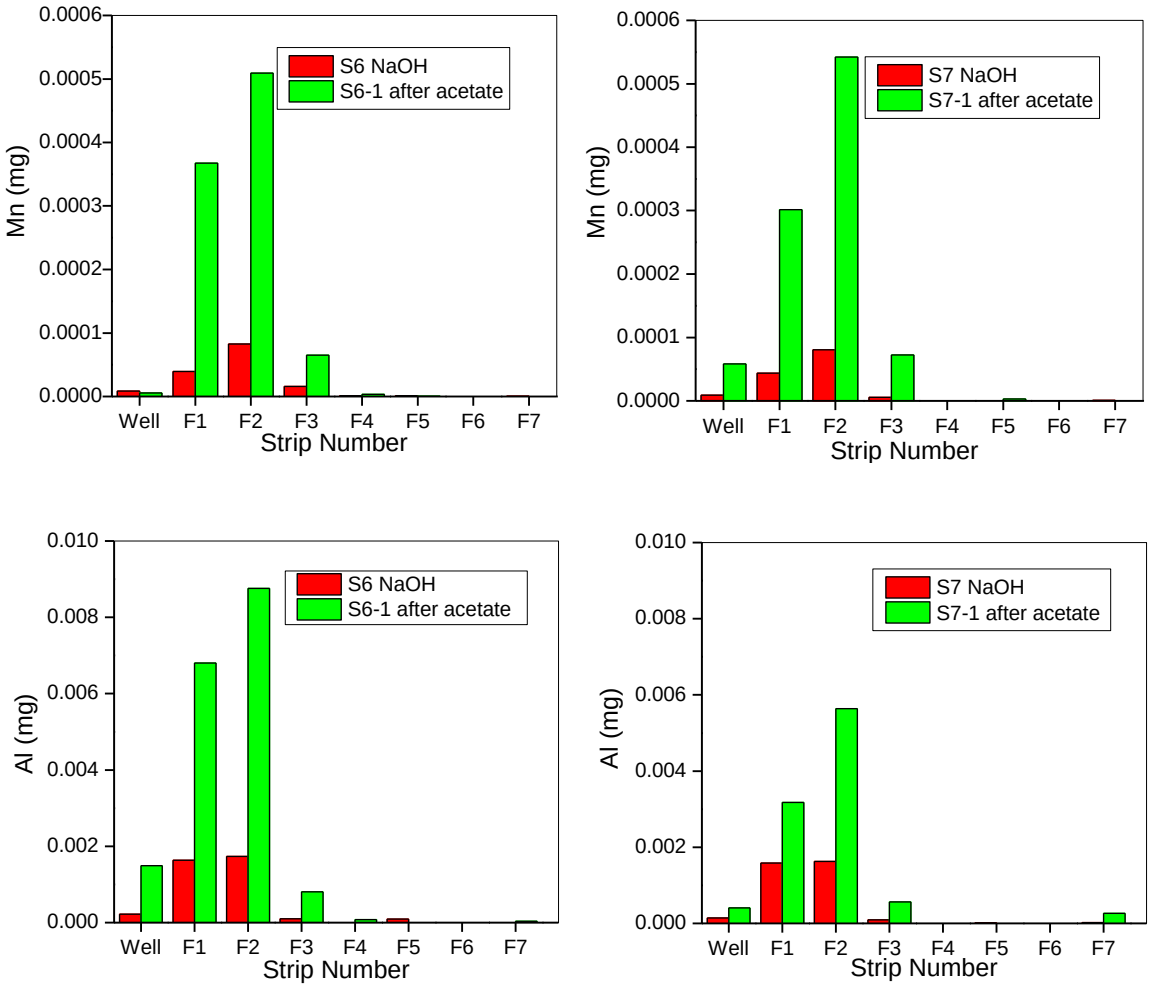

Figure 4.16(b): Mn and Al associations with humic substances from Core 3 without (red bar) and with (green bar) acetate extraction (N.B. in experiment II, humic substances were isolated AFTER the selective extractions had been carried out on the soil)

Figure 4.16-4.18 show the gel electrophoretic patterns comparing the amount of elements associated with intact humic substances (labelled as S6 NaOH and S7 NaOH) and the amount of elements associated with humic substances after acetate extraction, dithionite extraction and sequential extraction (labelled as S6-1 and S7-1).

Figure 4.16 shows that the U removed from the humic substances was predominantly from the brown band (F2) with the remainder coming from the tailing band (F1). For Fe, Mn and Al, the additional amounts of each element that have become associated with the humic substances appear to be distributed across the tailing, brown and fluorescent (F3) bands. The highest concentrations, however, were again associated with the brown band.

U, Fe, Al, Mn associations with humic substances isolated after dithionite extraction (green bars) compared with their associations with the original humic substances (red bars) are shown in Figure 4.17. In contrast with the small amounts of U removed following acetate extraction, ~85% U bound to humic substances was removed when dithionite extraction was carried out before isolating the humic material. Again this is not consistent with the previous soil sequential extraction result where only ~25% of U was removed (Figure 4.8). However, it should be remembered that dithionite is the fourth reagent used in the sequential extraction procedure and in this experiment, it is being used on its own. Thus, in addition to U associated with crystalline oxide, U in exchangeable forms and in association with weakly crystalline oxides may also have been removedby the dithionite reagent (see Table 1.11; Poulton and Canfield, 2005). In comparison with the tailing and fluorescent band material, a slightly greater proportion of the U associated with the brown band material had been removed by the dithionite reagent.

Again in contrast with the results obtained for humic substances following acetate extraction, humics isolated after dithionite extraction of the soil had significantly lower amounts of Fe than those extracted directly from the soil (Figure 4.17; Table 4.6). This suggests that, during direct extraction from the soil, amorphous/weakly crystalline and crystalline Fe oxides had been extracted in association with the original humic substances.

For the dithionite extraction, more Mn was associated with the humic extract in comparison with the original extract; however, the extent of re-adsorption was not as great as observed after the acetate extraction (Figure 4.17; Table 4.6).

The amount of Al associated with humic substances isolated after dithionite extraction was slightly enhanced compared to that associated with the original humic substances (Figure 4.17; Table 4.6).

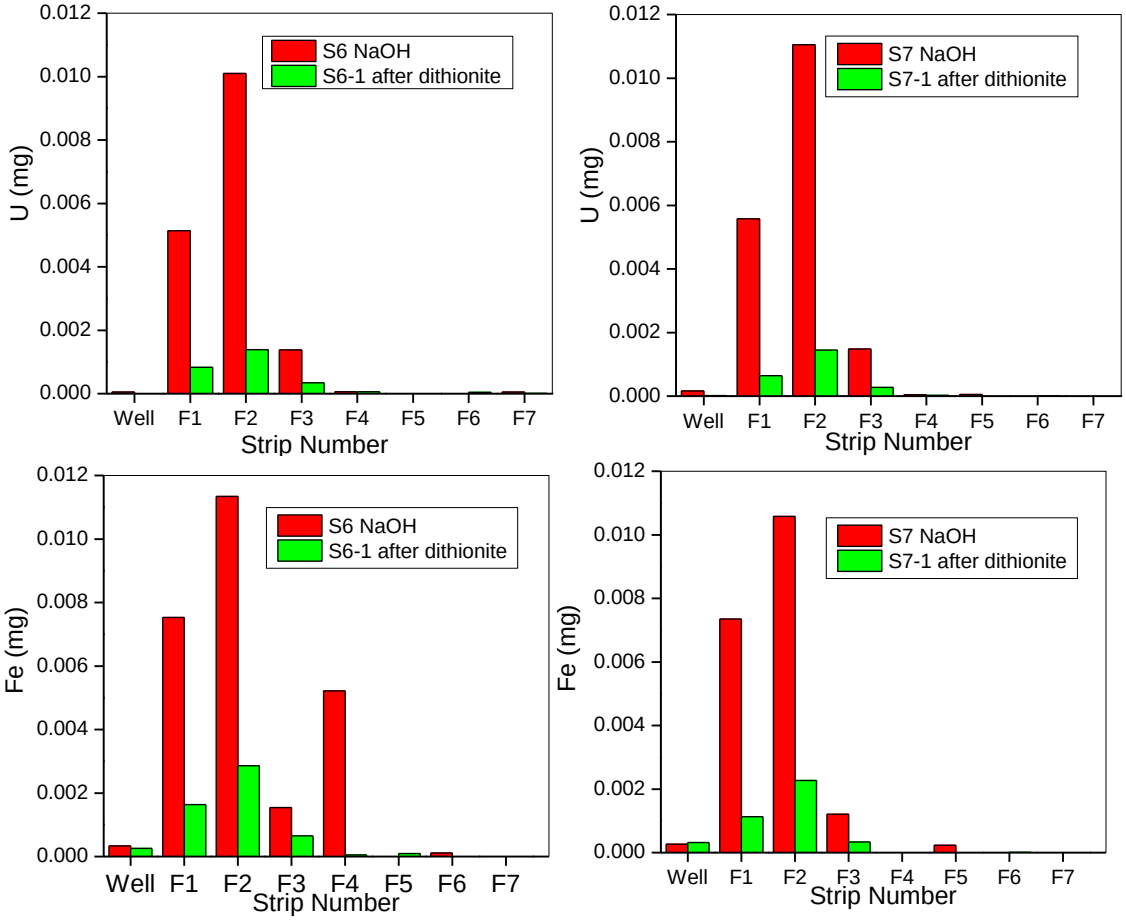

Figure 4.17(a): U and Fe associations with humic substances from Core 3 without (red bar) and with (green bar) dithionite extraction (in experiment II, humic substances were isolated AFTER the selective extractions had been carried out on the soil)

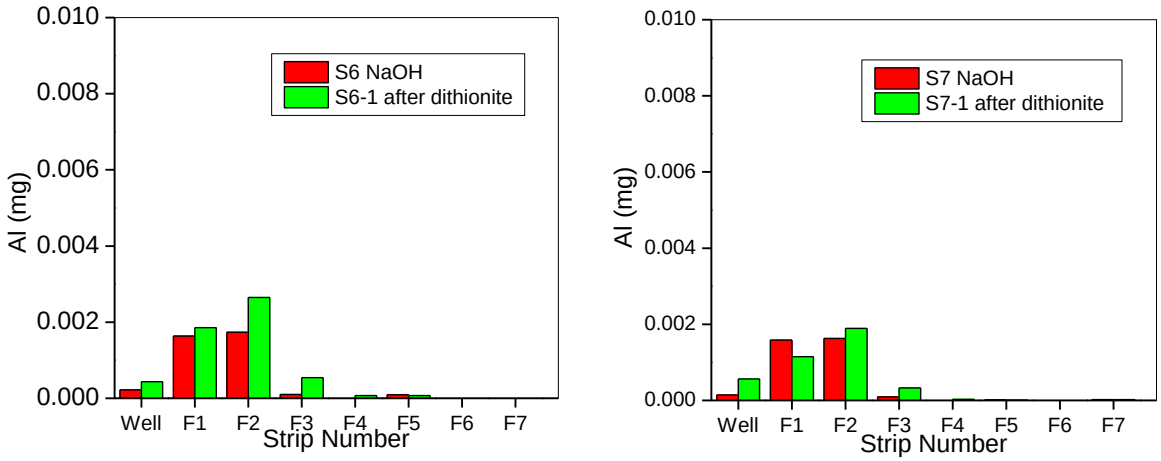

Figure 4.17(b): Mn and Al associations with humic substances from Core 3 without (red bar) and with (green bar) dithionite extraction (in experiment II, humic substances were isolated AFTER the selective extractions had been carried out on the soil)

To test the hypothesis that the dithionite reagent was removing some U that would have been isolated during the earlier sequential extraction steps, acetate followed by dithionite extraction (cf these were the two most important reagents with respect to U removal in section 4.1.8) of the soil was carried out prior to humic substance isolation (Figure 4.18). The two reagents (acetate; dithionite) were applied sequentially and for Core 3 S6, the amount of U bound to humic substances after both reagents had been applied was very close to the sum that was obtained for the two selective reagents (see Table 4.7). However, for Core 3 S7, the sum of U extracted in acetate and dithionite exceeds 100% U on the humic, which might suggest that part of the U extracted in dithionite could also be extracted by acetate. However, a contributing factor could also be the cumulative errors associated with summing the concentration measurements for each set of gel electrophoretic fractions (see Appendix 9.13, Tables 9.30).

According to Table 4.7, the amount of Fe (79% for Core 3 S6 and 74% for Core 3 S7) bound to humic substances isolated after sequential application of reagents gives the same or very similar results to those obtained after dithionite extraction (79% for Core 3 S6 and 81% for Core 3 S7), which indicates the dithionite reagent was able to remove the Fe that had re-adsorbed onto humic substances during the acetate extraction step.

When the acetate and dithionite reagents were applied sequentially, the amount of Mn remaining on the humic extract was lower than that associated with the original humic extract (Tables 4.6, 4.7; Figure 4.18). This was not expected since the amount of Mn associated with the humic extract increased considerably when the reagents had been applied selectively. Clearly dithionite was able to remove the form of Mn that had been readsorbed onto the soil humic substances after acetate extraction.

The amount of Al associated with humic substances isolated after sequential extraction of acetate and dithionite decreased by ~10-20%; this matched with the trend observed for Mn (Tables 4.6, 4.7; Figure 4.18).

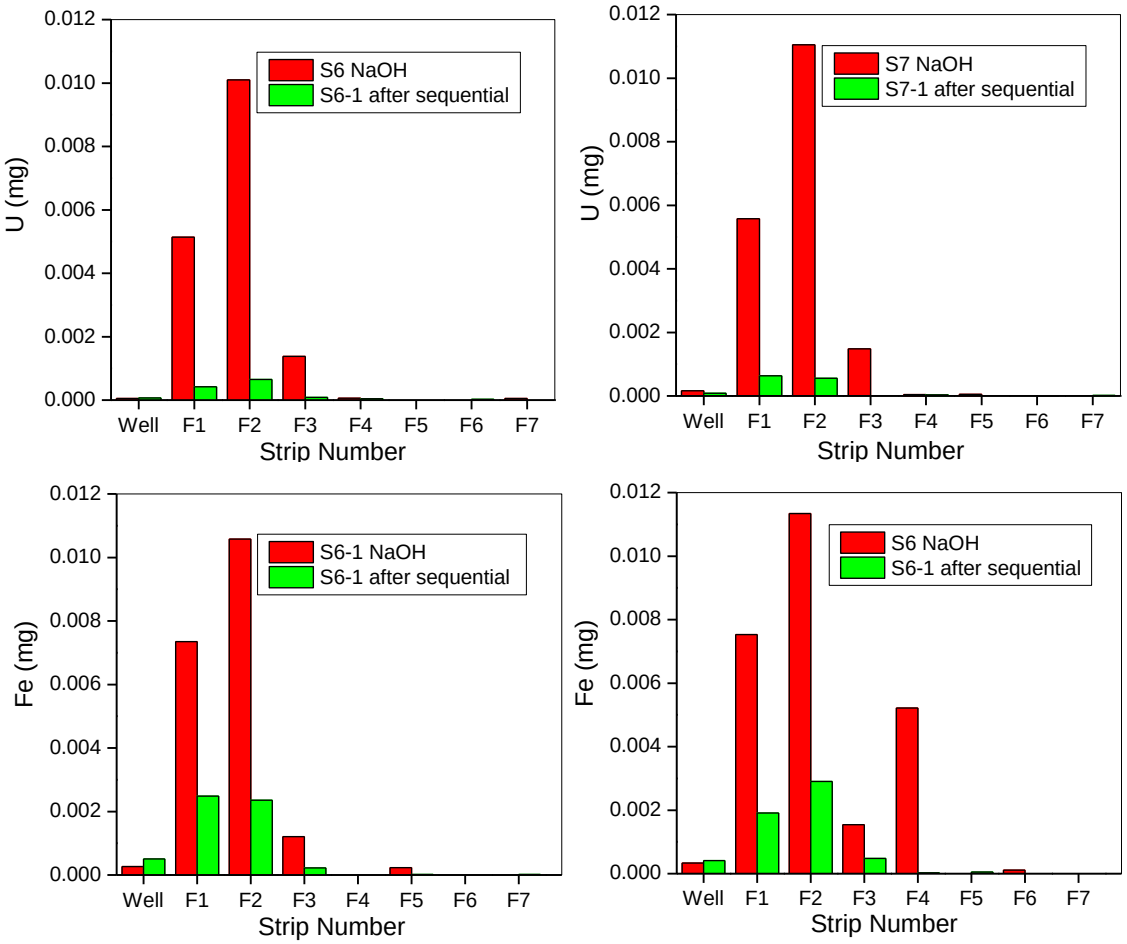

Figure 4.18(a): U and Fe associations with humic substances from Core 3 without (red bar) and with (green bar) sequential extraction (acetate; dithionite). (In experiment II, humic substances were isolated AFTER the sequential extractions had been carried out on the soil)

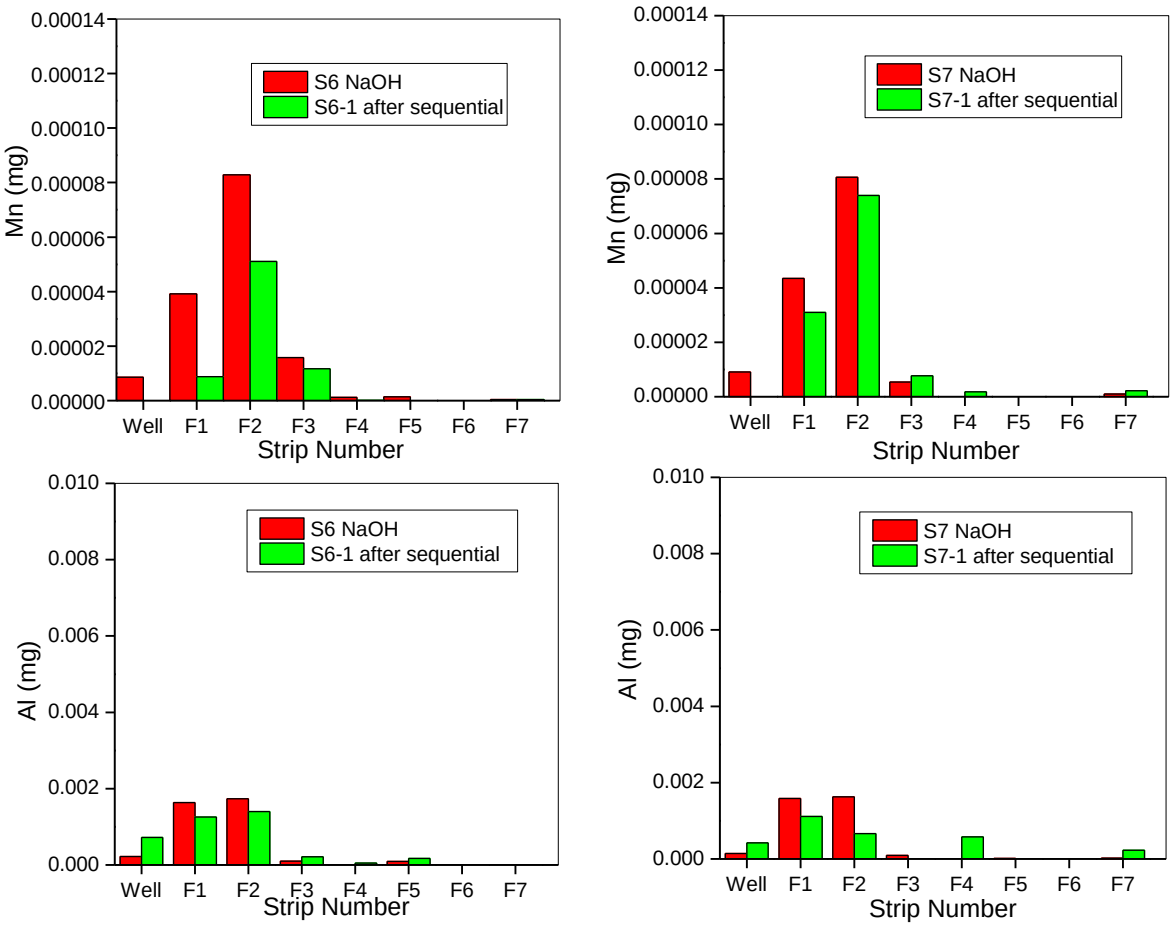

Figure 4.18(b): Mn and Al associations with humic substances from Core 3 without (red bar) and with (green bar) sequential extraction (acetate; dithionite). (In experiment II, humic substances were isolated AFTER the sequential extractions had been carried out on the soil)

Table 4.8: Percentage of element remaining in association with humic substances isolated before acetate extraction, dithionite extraction, or before sequential extraction

Element	Core 3 S6-2			Core 3 S7-2		
	Acetate	Dithionite	Sequential (acetate; dithionite)	Acetate	Dithionite	Sequential (acetate; dithionite)
U	75%	57%	40%	80%	54%	44%
Fe	101%	29%	27%	97%	36%	42%
Mn	35%	26%	17%	26%	24%	25%
Al	96%	33%	35%	94%	40%	40%

NB In experiment III, humic substances were isolated BEFORE the selective and sequential extractions were carried out on the humic extracts

Table 4.9: Percentage of element being removed from humic substances isolated before acetate extraction, dithionite extraction, or sequential extraction: comparison of summed selective extraction results with those for sequential extraction

Element	**Core 3 S6-2**				**Core 3 S7-2**			
	Acetate	**Dithionite**	**Sequential (acetate; dithionite)**	**Sum of acetate & dithionite**	**Acetate**	**Dithionite**	**Sequential (acetate; dithionite)**	**Sum of acetate & dithionite**
U	25%	43%	***60%***	***68%***	20%	46%	***66%***	***66%***
Fe	-1%	71%	***73%***	***70%***	3%	64%	***68%***	***67%***
Mn	65%	74%	***83%***	***139%***	74%	76%	***75%***	***150%***
Al	4%	67%	***65%***	***71%***	6%	60%	***60%***	***66%***

NB In experiment III, humic substances were isolated BEFORE the selective and sequential extractions were carried out on the humic extracts

4.1.11.3 Extraction of humic substances followed by selective and sequential extractions: elemental associations with humic substances using gel electrophoresis and ICP-OES

Table 4.8 illustrates the percentage of elements associated with humic substances after acetate extraction, dithionite extraction and sequential extraction had been carried out on the humic extract. Table 4.9 illustrates the percentage of elements removed from humic substances following acetate extraction, dithionite extraction and sequential extraction. The summed effectof the selective reagents (acetate + dithionite) was compared with percentage of elements removed after sequential extraction. This was again used to establish the selectivity of the acetate and dithionite reagents.

Figure 4.19-4.21 compare the amount of elements associated with the original humic substances (labelled as S6 NaOH and S7 NaOH; red bars) and the amount of elements associated with humic substanceswhich had been subjected to acetate extraction, dithionite extraction and sequential extraction (labelled as S6-2 and S7-2; green bars).

Table 4.9 and Figure 4.19 show that 20-25% of the U bound to the humic substances was removed when the humic substances were subjected to acetate extraction. This is in reasonable agreement with the results obtained (12-30%) when acetate extraction was carried out before the humic extraction.

Very little Fe was released from the humic extract during acetate extraction (Table 4.9; Figure 4.17). This is in agreement with the results from sequential extraction for the whole soil (see Figure 4.9). According to Figure 4.19, there is some re-distribution of Fe for Core 3 S6-2 after acetate extraction. A proportion of the Fe in F1 and F4 of the original humic substances had re-adsorbed to F2/F3 (see Appendix section 9.13.2, Table 9.31).

In contrast with the results for Fe, about 75% of the Mn bound to humic substances was removed when the humic substances were subjected to acetate extraction. As for Fe, however, very little (4% and 6% for S6 and S7, respectively) Al was extracted from humic substances during the acetate extraction.

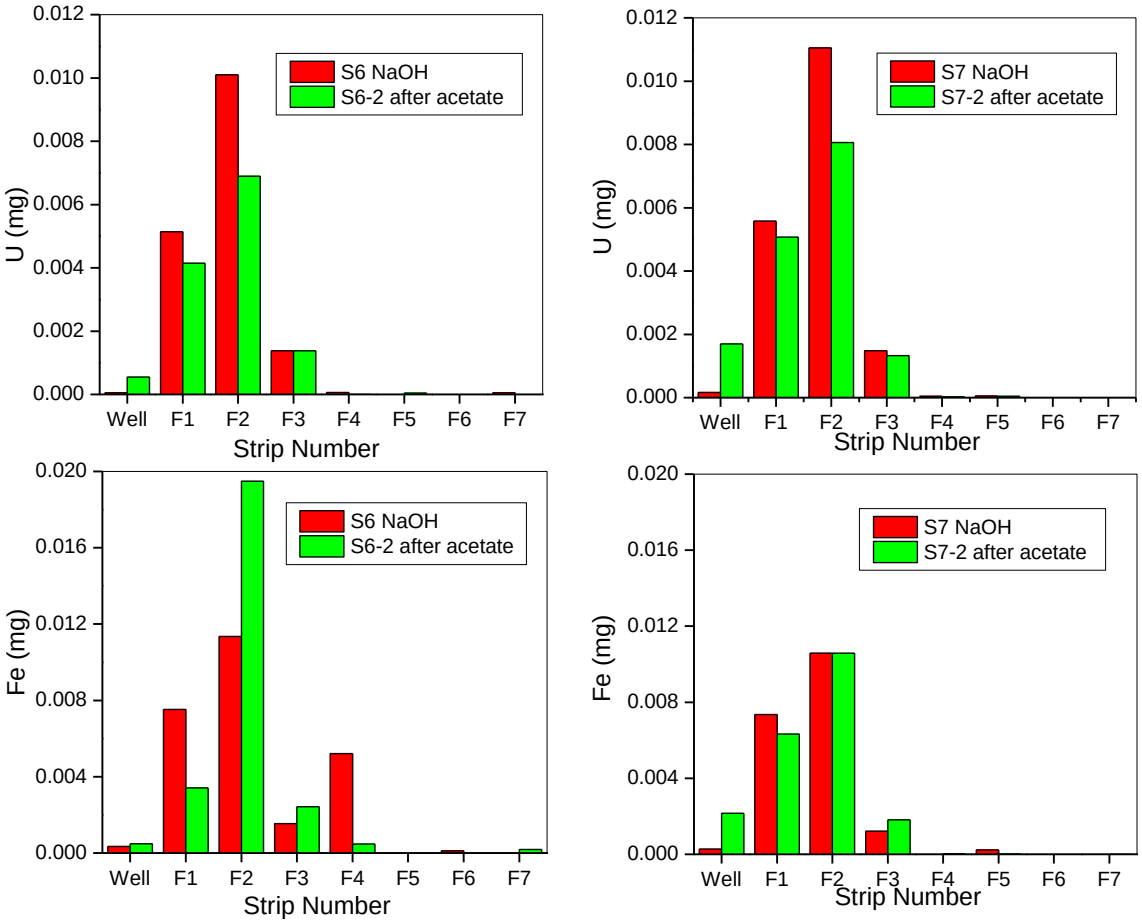

Figure 4.19(a): U and Fe associations with humic substances from Core 3 without (red bar) and with (green bar) acetate extraction (In experiment III, humic substances were isolated BEFORE the selective extractions had been carried out on the humic extract)

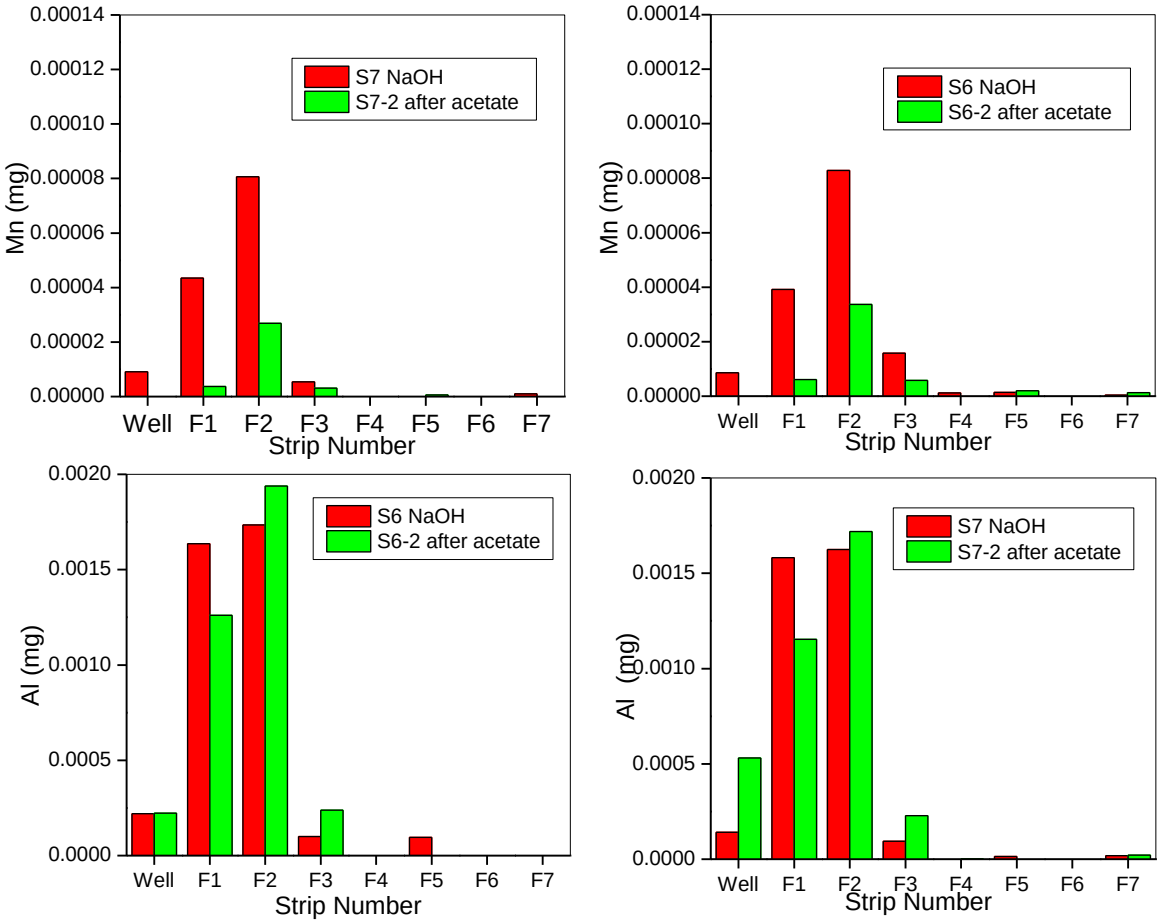

Figure 4.19(b): Mn and Al associations with humic substances from Core 3 without (red bar) and with (green bar) acetate extraction (In experiment III, humic substances were isolated BEFORE the selective extractions had been carried out on the humic extract)

Table 4.9 and Figure 4.20 show that ~45% of U was removed from the humic substances by dithionite. At the same time, ~30% of the Fe and 60-67% of the Al was released from the humic extract. About 75% of Mn was released from the humic substances after dithionite extraction, which was very close to that released after acetate extraction (see Appendix section 9.13.2, Table 9.32).

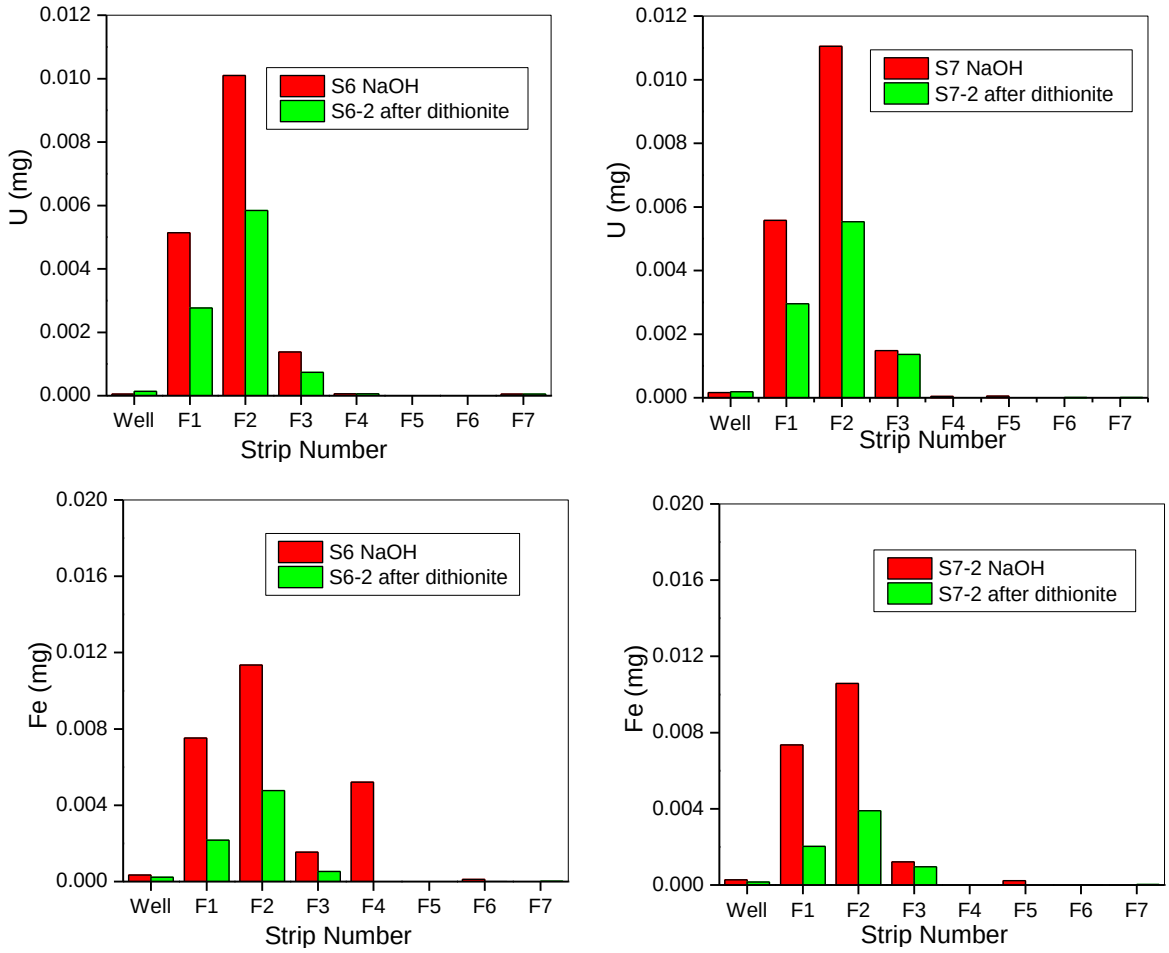

Figure 4.20(a): U and Fe associations with humic substances from Core 3 without (red bar) and with (green bar) dithionite extraction (In experiment III, humic substances were isolated BEFORE the selective extractions had been carried out on the humic extract)

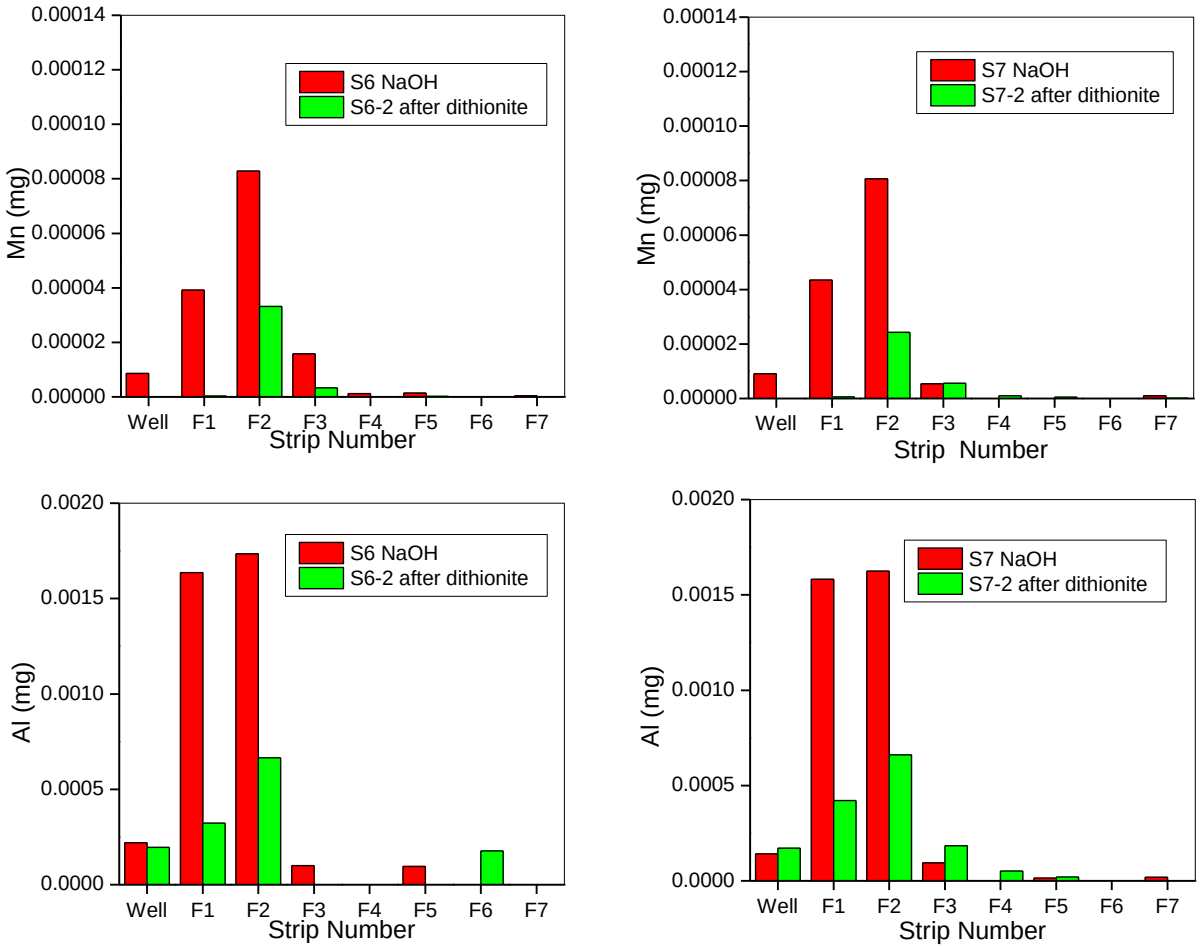

Figure 4.20(b): Mn and Al associations with humic substances from Core 3 without (red bar) and with (green bar) dithionite extraction (In experiment III, humic substances were isolated BEFORE the selective extractions had been carried out on the humic extract)

Finally, ~60-66% of the U was removed from the humic extract when both acetate and dithionite reagents were applied sequentially (Table 4.9; Figure 4.21). This was in reasonably good agreement with the sum of U selectively extracted by acetate and dithionite reagents (66-68%) (see Appendix section 9.13.2, Table 9.33).

The sequential extraction involving acetate and dithionite extracted ~70% of the Fe bound to humic substances, which was very close to the sum of Fe selectively extracted by acetate and dithionite reagents (Table 4.9; Figure 4.21).

About 83% and 75% of Mn (Core 3 S6 and S7, respectively) were removed from the humic substances after sequential extraction (Table 4.9; Figure 4.21). The sum of Mn selectively extracted by acetate and dithionite reagents was double that extracted either by acetate or dithionite, which indicated that the Mn released from humic substance in acetate could also be extracted by dithionite.

The proportions of Al (65% and 60%; Core 3 S6 and S7, respectively) sequentially extracted by acetate and dithionite were very similar to those extracted by dithionite alone (67% and 60%) (Table 4.9; Figure 4.21).

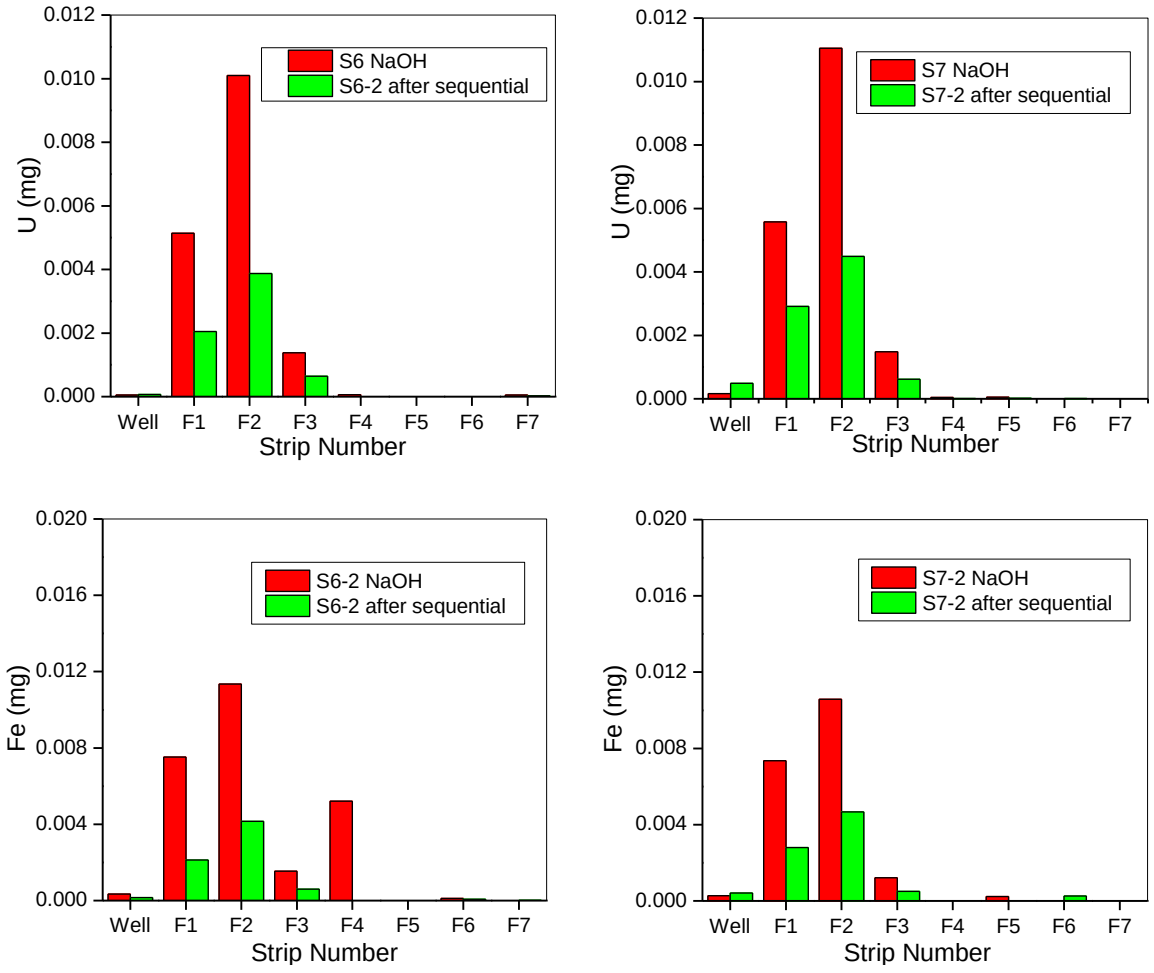

Figure 4.21(a): U and Fe associations with humic substances from Core 3 without (red bar) and with (green bar) sequential (acetate; dithionite extraction (In experiment III, humic substances were isolated BEFORE the sequential extractions had been carried out on the humic extract)

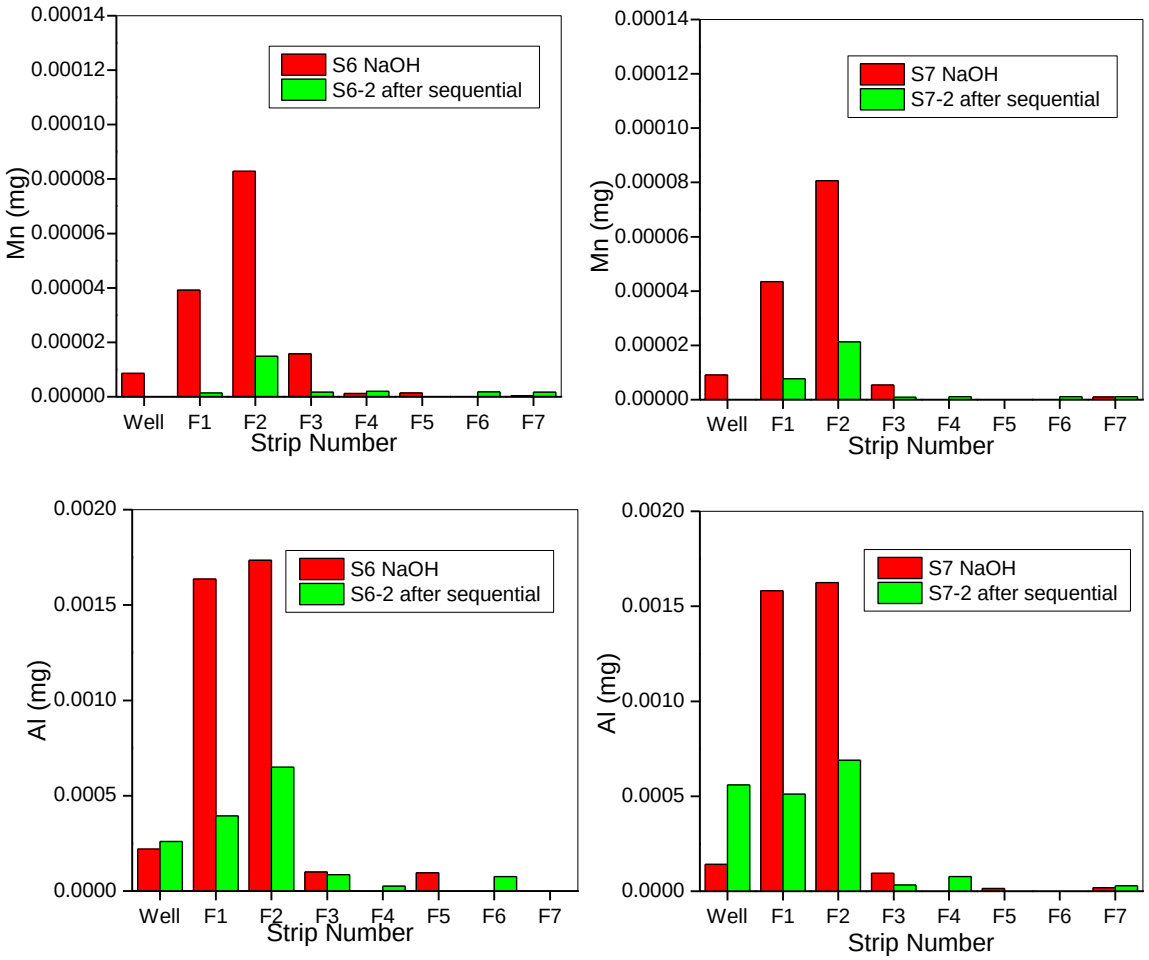

Figure 4.21(b): Mn and Al associations with humic substances from Core 3 without (red bar) and with (green bar) sequential (acetate; dithionite extraction (In experiment 3, humic substances were isolated BEFORE the sequential extractions had been carried out on the humic extract)

Observations and initial interpretation

Comparing the results presented in section 4.1.11.2 and 4.1.11.3, there are some key findings that should be noted:

(i) The proportion of U removed from humic substances did not change significantly when the acetate reagent was used directly on the soil in comparison with its use on the humic extract; in each case ~20-30% of humic-bound U was released;

(ii) When dithionite was used directly on the soil, ~85% of humic-bound U was removed; in contrast, only ~45% of humic-bound U was used when dithionite was used directly on the humic extract;

(iii) For the direct application of reagents to the humic extract, there was good agreement between the proportion of U removed by the summed selective reagents and that obtained by sequential extraction, suggesting that each reagent had removed a different form of humic-bound U;

(iv) in comparison with the values obtained when humic substance had been isolated directly from the soil samples before selectively extractions and sequential extraction, much higher concentrations of Fe (~×2), Mn (~×7), Al (~×4) were found in association with humic substance isolated from soil where acetate extraction had been carried out prior to humic extraction. This was also observed, but to a lesser extent, for Mn and Al when dithionite extraction was carried out prior to humic extraction;

(v) the reason why ~85% of humic-bound U was removed by dithionite when humic extraction was carried out after dithionite extraction on the soil while ~45% of humic-bound U was removed by dithionite when humic substances were extracted before dithionite extraction of the humic extract is not clear but it may be attributable to the loose minerals which were dissolved in dithionite and replaced the adsorption site of U.

Overall, a significant outcome of this work is that dissolution of non-target mineral phases and re-adsorption of released mineral metal components is a significant problem when Na acetate is used to determine carbonate-bound metal concentrations in soils. In this case, the released metals became associated with humic substances within the soils. It is likely that these readsorbed components were in the form of amorphous precipitates since they were largely released from the humic materials upon extraction with sodium dithionite. Importantly, it would appear that U was not significantly affected by the problems relating to mineral dissolution by the acetate reagent.

4.2 Results from sampling trip 3(26/10/2010)

In sections 4.1.6, Figures 4.4 and 4.5 showed that U concentration maxima in the porewater were not located at the same depth as those in the solid phase, but instead were located at the same depth as the Fe maxima in both porewater and solid phase. In section 4.1.7, fractionation of porewater (Figure 4.7) showed that U, Fe and humic substances were all mainly in the large colloidal fraction (100 kDa-0.2 μm). Section 4.1.11 also demonstrated that there were intimate interactions between U, Fe and humic substances within the solid phase. In section 4.2, the experimentsare mainly focused on U behaviour in soil porewaters, both with increasing soil depth and with increasing distance from the mineralisation. A transect line of sampling points NE1-NE7 (section 4.2.1) was established to investigate the lateral migration behaviour of U in porewater with increasing distance from the uranium mineralisation while Core 6 (section 4.2.2) was collected to study the vertical trends in U associations. Section 4.2.3 then presents results for carbonate content of the solid phase. This was done to provide further supporting evidence for carbonate-related results obtained by XRD characterisation of the solid phase.

4.2.1 Cave drip waters and transect line soil samples of NE1-NE7

4.2.1.1 pH values for cave drip water and porewater from NE1-NE7

As shown in Table 4.10, the pH values of cave drip waters were slightly alkaline at ca. 7.8. The pH values for the transect soil porewaters ranged from slightly acidic to alkaline (5.3-8.6). There was a sharp decrease from ~8.6 at 1 m (NE1) to 5.3 at 14 m (NE3) from the cave (Figure 4.22). Then, pH increased quickly to ~8.0 at 24.5 m (NE5) with a slight decrease to ~7.6 at 30 m (NE7) from the cave (Figure 4.24).

The pH values in soil porewaters from sampling trip 2 were in the range of ~6.0-7.2 (section 4.1.2) so the pH range for the samples collected on this trip was wider than that for samples collected during trip 2.

Table 4.10: Soil porewater pH values in surface soils NE1-NE7

Sample ID	Distance from cave (m)	pH
Drip water 6	0	7.83
Drip water 7	0	7.80
NE1	1	8.64
NE2	11	6.76
NE3	14	5.32
NE4	17	6.89
NE5	24.5	7.96
NE6	27.5	7.79
NE7	30	7.64

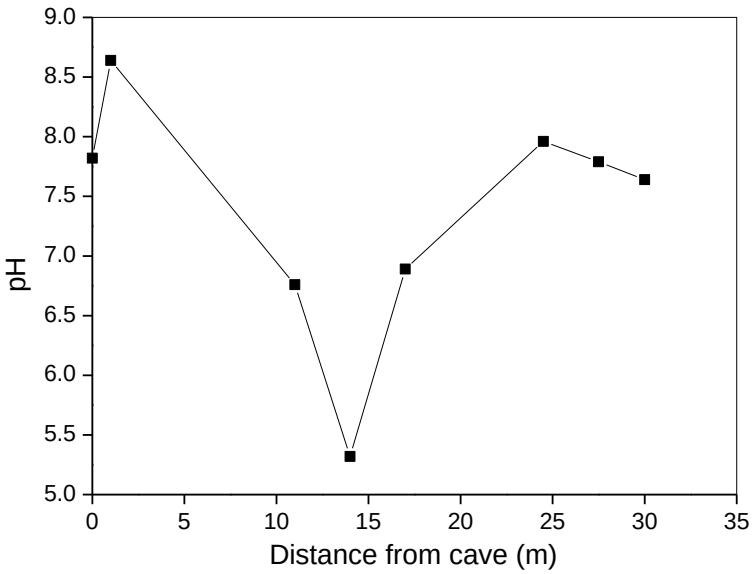

Figure 4.22: pH of cave drip waters emerging from the mineralisation and of the surface (0-5 cm) soil porewaters along a 30-m transect southwards to the edge of the boggy area

4.2.1.2 DOM (UV absorbance at 254 nm) in cave drip waters and porewaters from NE1-NE7

The UV absorbance values for the cave drip waters were low (0.023 and 0.025) in comparison with those for the transect porewaters. NE1was located at the front edge of the cave,~1 m from the drip waters (back of cave), and the soil at this location was different from that at sites NE2-NE7, which were located either in the boggy area or towards the interface with the saltmarsh. Based on the UV absorbance at 254 nm data shown in Table 4.11, the porewater from NE1 soil contained an order of magnitude greater organic carbonthan the cave drip waters. Even higher values were found for NE2-NE7, especially for NE2-NE4 porewater samples. Figure 4.24 also confirmed that NE2-NE4 had the strongest brown colour among all the porewater samples.

Table 4.11: UV absorbance at 254 nm in surface soil samples NE1-NE7 porewater (absorbance value has been dilution-corrected)

Sample ID	Distance from cave (m)	Abs at 254 nm
Drip water 6	0	0.023
Drip water 7	0	0.028
NE1	1	0.53
NE2	11	14.1
NE3	14	7.8
NE4	17	8.5
NE5	24.5	1.18
NE6	27.5	0.93
NE7	30	0.98

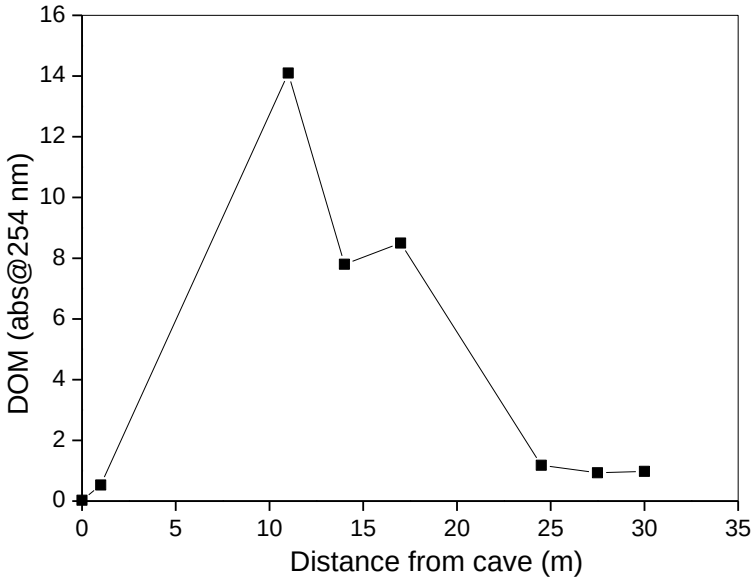

Figure 4.23: DOM in waters emerging from the mineralisation and in the surface (0-5 cm) soil porewaters along a 30-m transect southwards to the edge of the boggy area

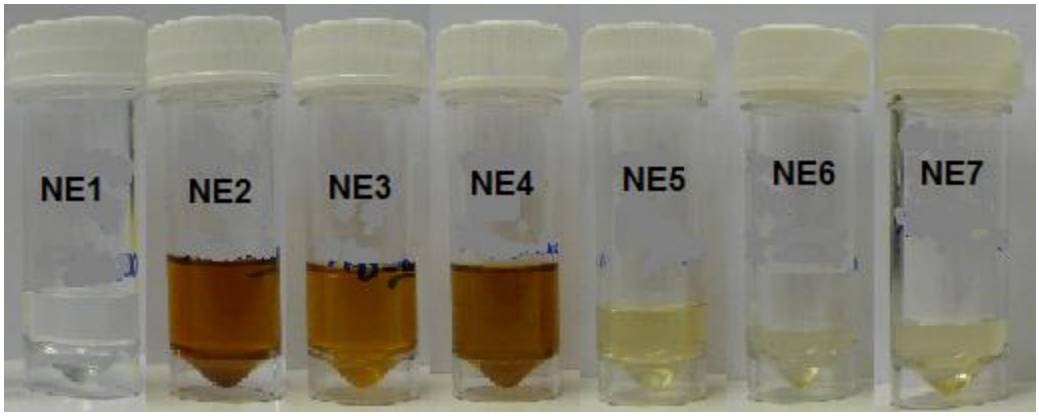

Figure 4.24: Soil porewaters from soil samples NE1-NE7 (same direction from Figure 4.23)

The UV absorbance at 254 nm for porewaters taken from Cores 3 (20 m from cave), 4 (25 m from cave) and 5 (35 m from cave) in sampling trip 2 were mainly in the range of ~0.5-2.5 (Figure 4.2). This is in reasonable agreement with the values for the NE5-NE7 (25-30 m from cave) porewaters, which were in the range of 0.93-1.18 (Table 4.11). There was also an inverse relationship between UV absorbance and pH value insomuch as the UV absorbance for drip water, NE1, NE5-7 were below 1.2, and their pH values were higher than 7.5. In contrast, the UV absorbance from NE2-4 ranged from 7.8 to 14.1, whilst their

pH values were all below 7. From the photograph shown in Figure 4.34, it was clear that the soil porewaters with higher UV absorbance (254 nm) contained the greatest amounts of dissolved humic substances. Thus, functional groups such as carboxylic group and phenolic group are likely to be major contributors to the acidity of these porewater samples (Stevenson, 1982).

4.2.1.3 Lateral variations in elemental concentrations in drip waters 6-7 and in porewaters and porewater colloids from surface soil samples NE1-NE7

The concentrations of a range of elements (U, Fe, Mn, Pb, Cu, Zn, Al, As and Ca) in Cave drip waters and soil porewaters collected during Trip 3 are shown in Table 4.12. After colloid isolation from the porewaters, colloidal element concentrations (3 kDa-0.2 μm) and truly dissolved element concentrations with the corresponding recovery rate in soil porewaters are also shown in Table 4.13. The recovery rates for U (94±11%), Fe (94±12%), Mn (96±9%), Cu (101±14%) and Ca (97±10%) were very good, i.e. mean values within 100±10%. The much higher values for Al and Zn are indicative of contamination arising from contact with the ultrafiltration tubes and thus the Al and Zn data should be viewed with extreme caution. The percentage of colloidal association and truly dissolved phase for each element in the porewaters is shown in Table 4.14.

The U concentrations in the waters emerging from the mineralization were 29 μg L^{-1} and 31 μg L^{-1}. Those values were only about one-tenth of that taken in sampling trip 2 (Table 4.2), which is attributable to heavy rainfall that had diluted the cave drip water prior to sampling. A much faster drip rate was observed at the time of sampling. In agreement with the results from trip 2 (Table 4.2), analysis of the total (<0.2 μm) soil porewater showed a general trend of decreasing U concentration with increasing distance from the mineralization (Table 4.12). U concentration in the porewater was greatest near the vicinity of the mineralization; analysis of the NE1 porewaters gave aU concentration of 547 μg L^{-1}. More than 97% passed through the 3 kDa filter and so U was primarily present in dissolved form. For NE2-4, >90% of U was found in the colloidal fraction, which are in line with high amount of DOM present in these samples (Figure 4.24). At NE5, there was a drop in the organic content of the porewaters and almost all the U was in dissolved form whilst for

NE6 and NE7, the proportion of colloidal U was 47.6% and 72.7%, respectively (Table 4.14). Overall, the results indicated there was strong relationship between colloidal U and the DOM content of the porewater.

Table 4.12: Elemental concentrations in drip waters 6 and 7 and in surface soil porewaters (NE1-7)

Sample ID	Distance from cave (m)	Element concentrations in drip waters and porewaters (<0.2 μm)								
		U (μg L^{-1})	Fe (μg L^{-1})	Mn (μg L^{-1})	Pb (μg L^{-1})	Cu (μg L^{-1})	Al (μg L^{-1})	As (μg L^{-1})	Zn (μg L^{-1})	Ca (μg L^{-1})
Dripwater 6[1]	0	29	450	n.d.	n.d.	12	50	32	34	98470
Dripwater 7[1]	0	31	330	n.d.	n.d.	12	38	20	33	98650
NE1[2]	1	547	72	4.6	6.0	23	6.6	19	25	198140
NE2[2]	11	384	42668	2595	99	259	838	279	277	123900
NE3[2]	14	197	6724	1077	19	142	376	1990	591	67290
NE4[2]	17	175	4103	1281	11	92	268	2953	482	47400
NE5[2]	24.5	33	91	19	0.1	7.6	5.5	589	24	49150
NE6[2]	27.5	2.9	614	216	0.5	5.2	9.2	72	30	26400
NE7[2]	30	2.6	842	8.4	1.1	6.9	13	89	46	30410

[1]samples were analysed by ICP-OES; n.d. = not detected (detection limits were 1 μg L^{-1} for Mn; 2 μg L^{-1} for Pb)

[2]samples were analysed by ICP-MS

Table 4.13: Colloidal (3 kDa-0.2 µm) and truly dissolved (<3 kDa) elemental concentrations in soil porewater with corresponding recovery rate for the porewater

Sample ID	Distance from cave (m)	U (µg L^{-1})		Recovery rate (%)	Fe (µg L^{-1})		Recovery rate (%)	Mn (µg L^{-1})		Recovery rate (%)	Pb (µg L^{-1})		Recovery rate (%)	Cu (µg L^{-1})		Recovery rate (%)
		C[5]	TD[5]		C	TD		C	TD		C	TD		C	TD	
NE1	1	15	-[1]	-[1]	14	-[1]	-[1]	0.7	-[1]	-[1]	0.7	-[1]	-[1]	11	-[1]	-[1]
NE2	11	351	38	101.3	31535	366	74.8[4]	1091	1705	107.7	122	1.1	124.3	266	71	129.7
NE3	14	171	36	105.1	7111	31	106.2	235	732	89.9	19	n.d.[2]	97.7	115	22	96.3
NE4	17	153	4.0	89.7	3998	62	99.0	451	903	105.7	8.7	2.3	100.8	68	16	90.5
NE5	24.5	0.3	34	104.5	94	0.5	103.8	2.0	15.0	87.3	n.d[2]	n.d[2]	n.d.[2]	5.9	1.2	93.1
NE6	27.5	1.0	1.2	78.6	543	17	91.2	23	177	92.7	0.3	n.d[2]	62.4	2.6	2.5	99.4
NE7	30	1.6	0.6	84.0	737	10	88.8	2.7	5.1	92.9	2.0	n.d[2]	188.9	4.6	2.2	98.9
Sample ID	**Distance from cave (m)**	**Al (µg L^{-1})**		**Recovery rate (%)**	**As (µg L^{-1})**		**Recovery rate (%)**	**Zn (µg L^{-1})**		**Recovery rate (%)**	**Ca (µg L^{-1})**		**Recovery rate (%)**			
		C	TD		C	TD		C	TD		C	TD				
NE1	1	6.3	-[1]	-[1]	7.1	-[1]	-[1]	5.6	-[1]	-[1]	3893	-[1]	-[1]			
NE2	11	717	107	98.3	169	16	66.0[4]	227	102	118.9	19197	33323	42.4[3 4]			
NE3	14	283	18	79.9	133	1479	81.0	232	78	52.5	13043	41480	81.0			
NE4	17	227	30	95.6	59	2555	88.6	334	328	137.4	14575	30632	95.4			
NE5	24.5	15	13	520.8[3]	12	484	84.3	29	16	185.6[3]	3248	49238	106.8			
NE6	27.5	6.9	1	85.5	44	28	100.7	27	30	191.4[3]	1245	25867	102.7			
NE7	30	12	25	284.4[3]	74	28	115.0	40	44	180.7[3]	1948	29031	101.9			

[1]Sample NE1 <3 kDa was lost, so the corresponding recovery rate cannot be calculated

[2]n.d. = not detected; detection limit for Pb = 0.08 µg L^{-1}

[3]The data with recovery rate < 50% or >200% will not be used in colloidal percentage (3 kDa-0.2 µm) and truly dissolved phase percentage (<3 kDa) calculation in Table 4.14. The reason for enhanced Al recovery rate is because the Al concentration in the porewater was much lower than the Al contaminant released from the ultrafiltrator membrane.

[4]The recovery rate of Fe, As and Ca in NE2 is low compared with the rest samples. Since the <3 kDa samples were analysed one year after the sampling trip, the elements may precipitate out in the solution. Thus those data will not be used in Figure 4.25 and the difference between total (<0.2 µm) and 3 kDa-0.2 µm fraction will be used instead.

[5]C = colloidal (3 kDa-0.2 µm); TD = truly dissolved (<3 kDa)

Table 4.14: Percentage of colloidal element (3 kD-0.2 µm) in total porewater element (< 0.2 µm)

Sample ID	Distance from cave (m)	Percentage of colloidal elements in total porewater elements (%)																	
		U		Fe		Mn		Pb		Cu		Al		As		Zn		Ca	
		C	TD	C	TD	C	TD	C	TD	C	TD	C	TD	C	TD	C	TD	C	TD
NE1	1	2.7[1]	97.3[1]	19.4[1]	80.6[1]	15.2[1]	84.8[1]	11.7[1]	88.3[1]	47.8[1]	52.2[1]	95.5[1]	4.5[1]	37.4[1]	62.6[1]	22.4[1]	77.6[1]	2.0[1]	98.0[1]
NE2	11	90.2	9.8	98.9	1.1	39.0	61.0	99.1	0.9	81.1	18.9	87.0	13	91.4	8.6	69.0	31.0	n.c.	n.c.
NE3	14	82.6	17.4	99.6	0.4	24.3	75.7	100.0	n.d.[2]	83.9	16.1	94.2	11.5	8.3	91.7	74.8	25.2	23.9	76.1
NE4	17	97.4	2.6	98.5	1.5	33.3	66.7	79.1	20.9	81.0	19.0	88.5	19.8	2.3	97.7	50.5	49.5	32.2	67.8
NE5	24.5	0.9	99.1	99.5	0.5	11.6	88.4	n.d.[2]	n.d.[2]	61.5	38.5	n.c.[3]	n.c.[3]	2.4	97.6	64.4	35.6	6.2	93.8
NE6	27.5	46.4	53.6	96.9	3.1	11.6	88.4	n.c.[3]	n.c.[3]	52.0	48.0	87.3	12.7	61.1	38.9	47.4	52.6	4.6	95.4
NE7	30	72.3	27.7	98.6	1.4	34.0	66.0	100.0	n.d.[2]	68.7	31.3	n.c.[3]	n.c.[3]	72.5	27.5	47.6	52.4	6.3	93.7

[1]Sample NE1 < 3 kDa was lost, so the percentage of 3 kDa-0.2 µm fraction and < 3 kDa fraction was calculated from porewater concentration (<0.2 µm) and 3 kDa-0.2 µm fraction concentration

[2]n.d. = not detected; detection limit=0.08 µg L^{-1}

[3]n.c. = not calculated - the recovery rates were <50% or >200% (see Table 4.13)

The Fe concentrations in the emerging cave drip waters were 450 μg L^{-1} and 330 μg L^{-1}, respectively (Table 4.12). The Fe concentration in the porewater at the front edge of the cave (NE1) was the lowest of any along the transect line. The trend in soil porewater Fe concentration for NE2-NE7 was mainly split into two parts: it decreased from ~32,000 μg L^{-1} to 4,000 μg L^{-1} between NE2 and NE4, and increased from 94 μg L^{-1} to 737 μg L^{-1} between NE5 and NE7. During the previous trip, samples were collected within the boggy área at 20 m and 25 m from the mineralisation (see Table 4.2). The conditions were more strongly reducing at the site further from the mineralisation. This would be consistent with higher concentrations of porewater Fe between NE5 and NE7. For Trip 3, however, it was observed that the UV absorbance values at 254 nm for NE2-NE4 (8.5-14.1) were much higher than those obtained for sampling trip 2 samples (0.52-2.62). Thus the higher Fe concentrations in NE2-NE4 samples were probably related to the dissolved organic matter content rather than to differences in redox potential. Fe was found mainly in the colloidal fraction in all samples except for NE1. At least 74% of total porewater Fe was retained by the 3 kDa filter for NE2 to NE7 (Table 4.14).

The Mn concentrations in the drip waters emerging from the mineralization were below the ICP-OES detection limit of 1 μg L^{-1} (Table 4.12). The trend for Mn concentration in the porewaters along the transect line was similar to the variation in UV absorbance at 254 nm in that highest values were obtained for the porewaters collected at 11 m from the cave; in both cases there was a small maximum at 17 m distance (Figure 4.25). This trend is not consistent with the earlier results (Table 4.2) which showed increasing Mn concentrations with distance from the cave. Thus it might again be considered that Mn concentration in the porewaters was being controlled by the presence of the brown colloidal organic matter. However, Mn was not so strongly associated with colloidal fraction as only 10-42% Mn was retained by the 3 kDa filter for all samples (Table 4.14).

The concentrations of Pb and Cu in the cave drip waters were below the ICP-OES detection limits of 50 μg L^{-1} and 5 μg L^{-1}, respectively, while those for Al were 50 μg L^{-1} and 38 μg L^{-1}, respectively. The variations in Pb, Cu and Al concentrations in porewaters along the transect and the proportions present in the porewater colloidal fraction were similar. The highest Pb, Cu, Al concentrations in porewaters were found to be 99 μg L^{-1}, 259 μg L^{-1}, 838 μg L^{-1}, respectively, at 11 m from the cave (Table 4.12). After that, the concentrations of Pb, Cu and Al decreased to less than 3% of the peak values at the site

furthest from the cave. At all locations, the concentrations of Pb in colloidal fractions were close to those in the total porewaters. This was also observed for Al at NE2-NE4. Cu was mainly found in colloidal fraction at NE2-4, but for the rest of the samples, the proportion of colloidal Cu decreased to below 70% (Table 4.14; Figure 4.23).

The concentrations of As in the cave drip waters were 32 μg L^{-1} and 20 μg L^{-1}, respectively (Table 4.12). The trend in porewater As concentration with distance was different from that for the other elements (U, Fe, Mn, Pb, Cu, Al); the maximum As concentration in the porewater was ~3000 μg L^{-1} at 17 m (NE4) (Figure 4.25). After being passed through a 3 kDa ultrafiltration unit, only 37.4% As was in colloidal form at NE1. NE2 had the highest proportion of colloidal As, which was in line with the highest concentration of dissolved organic matter. However, the percentage of colloidal As in porewaters of NE3-5 was extremely low (<7%), which means that As was mainly in dissolved form at these locations (Table 4.13). The proportion of colloidal As increased to more than 60-75% at NE6-7. In the main, the relationship between As and dissolved organic matter was not strong (Figure 4.25).

The Zn concentrations in drip cave waters were 33 μg L^{-1} and 34 μg L^{-1}, respectively (Table 4.12). The variation in porewater Zn concentrations with distance from the cave was different from most of the other elements (U, Fe, Mn, Pb, Cu, Al). The maximum concentration of Zn in the porewater was found to be 590 μg L^{-1} for NE3. The percentage of colloidal Zn was only 22.4% at NE1. At NE2-4, colloidal Zn made up 50-75% of the total Zn (<0.2 μm) in the porewater. With increasing distance from the cave, the proportion of colloidal Zn remained between 45% and 65% (Table 4.14).

The highest Ca concentrations of ~98,000 μg L^{-1} and ~99,000 μg L^{-1} were found in the drip waters (Table 4.12). As for U, Ca showed a general trend of decreasing concentration with increasing distance from the cave (Figure 4.23). After colloid separation, less than ~30% of the Ca was retained on the 3 kDa filter, which indicated that Ca was mainly in dissolved forms in the transect porewaters.

The coefficient of determination (r^2) was used to measure the degree of correlation between the DOM and elements (U, Fe, Mn, Pb, Cu, Al, As, Zn, Ca) or between two different elements in the porewaters NE1-NE7 (Equation 4.2). R^2 ranges between 0-1, when 0

indicates poor linear fit and 1 indicates perfect linear relationship between the two variables (Brase and Brase, 2012).

$$r = \frac{n\sum xy - \left(\sum x\right)\left(\sum y\right)}{\sqrt{n\left(\sum x^2\right) - \left(\sum x\right)^2}\sqrt{n\left(\sum y^2\right) - \left(\sum y\right)^2}}$$

Equation 4.2

where x = DOM (abs@254 nm) or total dissolved element concentration or colloidal element concentration; y = total dissolved element concentration or colloidal element concentration; n = the number of pairs of data

Table 4.15 showed the r^2 values for DOM and total dissolved (<0.2 μm) element concentrations or between pairs of total dissolved elements whilst Table 4.16 showed the r^2 between DOM and colloidal (3 kDa-0.2 μm) element concentrations or between pairs of colloidal elements. In Table 4.15, total dissolved Mn (r^2=0.978, Cu (r^2=0.937) and Al (r^2=0.940) showed strong correlation with DOM. When colloidal elements only were considered, a great improvement was noticed for U (r^2=0.977) and Ca (r^2=0.965), which also showed strong correlation with DOM (Table 4.15). For the relationships between pairs of the elements, there were generally stronger correlations for the colloidal forms compared with the total dissolved elements, e.g. r^2 of U and Fe increased from 0.166 (total) to 0.865 (colloidal).

Table 4.15: r^2 value for linear correlations between total dissolved (<0.2 µm) element and DOM concentrations

	DOM	U	Fe	Mn	Pb	Cu	Al	As	Zn	Ca
DOM	-	0.115	0.725	0.978	0.735	0.937	0.94	0.196	0.517	0.016
U	0.115	-	0.166	0.130	0.217	0.200	0.159	0.005	0.017	0.933
Fe	0.725	0.166	-	0.819	0.995	0.833	0.886	0.008	0.076	0.088
Mn	0.978	0.130	0.819	-	0.826	0.943	0.963	0.109	0.389	0.026
Pb	0.735	0.217	0.995	0.826	-	0.856	0.897	0.006	0.088	0.124
Cu	0.937	0.200	0.833	0.943	0.856	-	0.989	0.068	0.733	0.074
Al	0.940	0.159	0.886	0.963	0.897	0.989	-	0.049	0.034	0.051
As	0.196	0.005	0.008	0.109	0.006	0.068	0.049	-	0.733	0.076
Zn	0.517	0.017	0.076	0.389	0.088	0.733	0.340	0.733	-	0.010
Ca	0.016	0.933	0.088	0.026	0.124	0.074	0.051	0.076	0.010	-

Table 4.16: r^2 values for linear correlations between colloidal (3 kDa-0.2 µm) element and DOM concentrations

	DOM	U	Fe	Mn	Pb	Cu	Al	As	Zn	Ca
DOM	-	0.977	0.774	0.905	0.707	0.898	0.932	0.716	0.723	0.965
U	0.977	-	0.865	0.929	0.807	0.965	0.980	0.752	0.593	0.926
Fe	0.774	0.865	-	0.912	0.993	0.950	0.944	0.693	0.252	0.644
Mn	0.905	0.929	0.912	-	0.881	0.914	0.952	0.613	0.478	0.813
Pb	0.695	0.807	0.993	0.881	-	0.906	0.901	0.637	0.158	0.554
Cu	0.898	0.965	0.950	0.914	0.906	-	0.992	0.782	0.413	0.809
Al	0.932	0.98	0.944	0.952	0.901	0.992	-	0.761	0.467	0.842
As	0.716	0.752	0.693	0.613	0.637	0.782	0.761	-	0.387	0.602
Zn	0.723	0.593	0.252	0.478	0.158	0.413	0.467	0.387	-	0.803
Ca	0.965	0.926	0.644	0.813	0.554	0.809	0.842	0.602	0.803	-

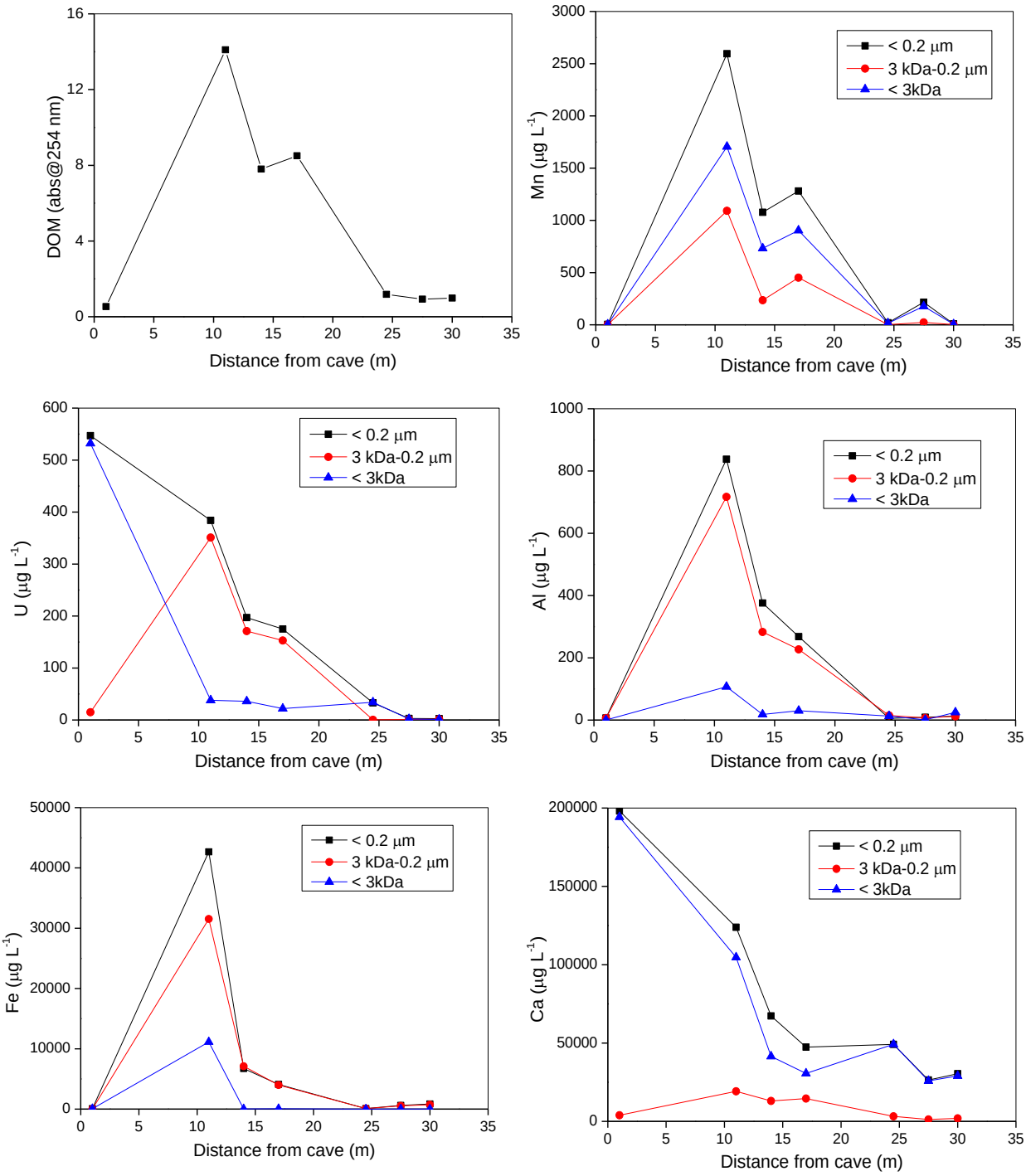

Figure 4.25(a): DOM and elemental (U, Fe, Mn, Al and Ca) concentrations in the porewater (<0.2 µm) and in corresponding porewater colloids (3 kDa-0.2 µm)

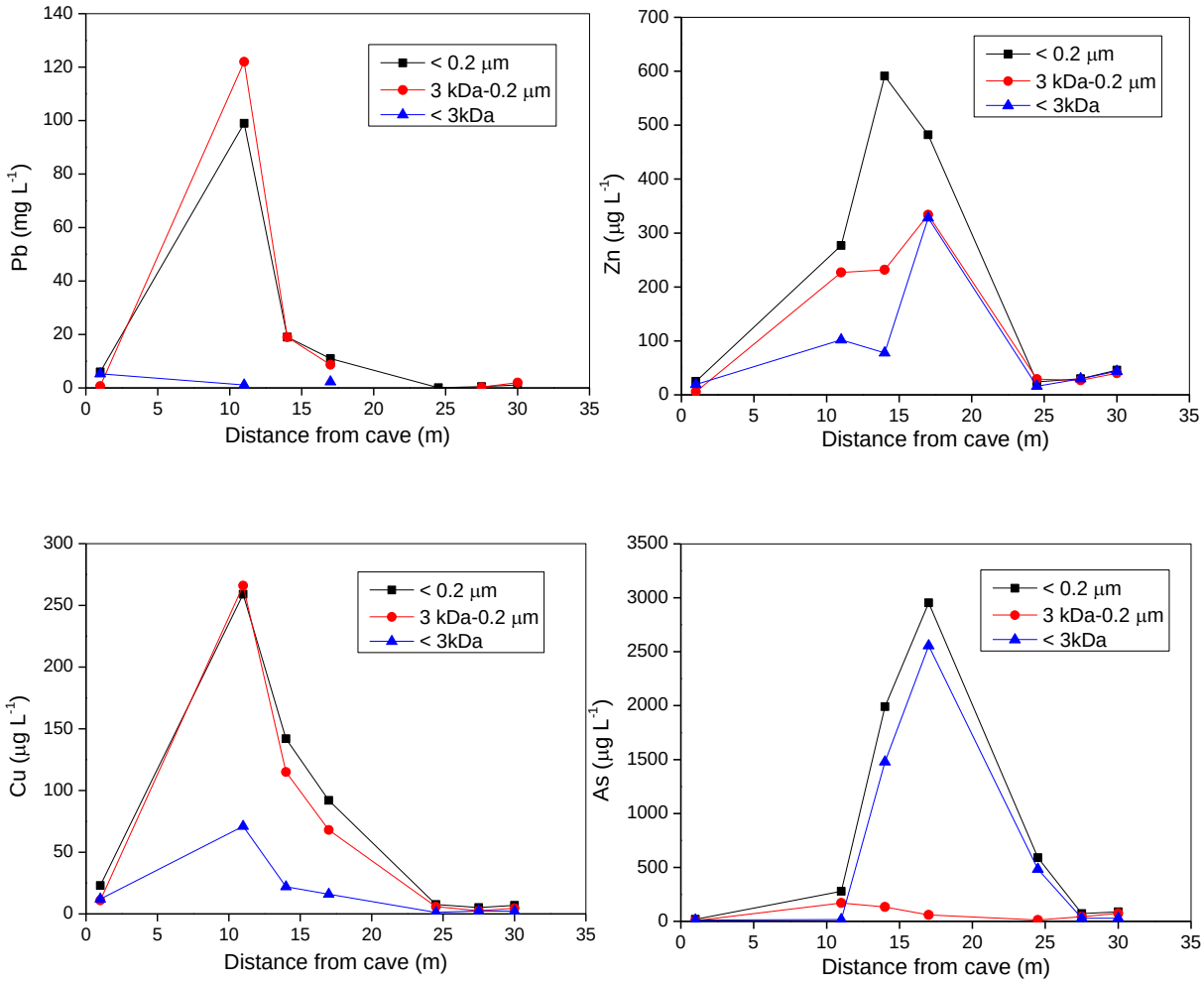

Figure 4.25(b): Elemental (Pb, Cu, Zn and As) concentrations in the porewater (<0.2 µm) and in corresponding porewater colloids (3 kDa-0.2 µm)

Observations and initial interpretation

(i) There was a clear trend of decreasing U and Ca concentrations with increasing distance from the cave. Even though the cave water samples had lower U concentrations than on previous sampling trips, there was still a tenfold decrease between the cave drip water and the soil porewaters at the furthest end of the transect (NE 6-7);

(ii) In contrast with U and Ca, the highest concentrations of all other elements (Fe, Mn, Al, Ca, Pb, Cu, Zn and As) were obtained for the porewaters with the highest DOM concentrations (NE2-NE4);

(iii) The greatest concentrations of each elements in colloidal form were again found for

porewaters with the highest DOM concentrations (NE2-NE4);

(iv) Some elements (Ca, Mn, As) were, however, present in truly dissolved form even within the NE2-NE4 samples.

Overall, it is evident that elemental speciation within the soil porewaters is strongly affected as waters emerging from the mineralisation pass through the boggy organic-rich soils along the transect. For U, this will have implications for the processes by which it is removed from the aqueous to the solid phase.

4.2.2 Characterisation of Core 6 porewaters

4.2.2.1 pH values and UV absorbance values at 254 nm for Core 6 porewaters

The maximum pH value of ~8.6 occurred in the surface section of porewatersfrom Core 6. After a sharp decrease over the first few sections, values remained in the range of ~6.7-7.1 to a depth of 30 cm, but then decreased rapidly to pH~5 between 30-40 cm before returning to pH~6 below this depth (Figure 4.26(a)) (see Appendix section 9.5, Table 9.1). The corresponding DOM profile showed an initially sharp decrease over the top 0-15 cm and then a more gradual decrease towards the bottom of the core (Figure 4.26(b)) (see Appendix section 9.6, Table 9.2).

The pH and UV absorbance profiles from Core 6 were compared with those from Core 3 (sampling trip 2) as they were both located 20 m from the cave. The pH range of Core 6 was between ~4.8-8.5, which was much wider than that of Core 3 (6.0-7.1). The trend in pH value with increasing soil depth in Core 6 was also different from that determined for Core 3. Core 3 showed a general increasing trend in the range of ~6.0-7.1 from sub-surface section to ~28 cm, and stabilized at pH 6.9 towards the bottom (see Figure 4.1). In contrast, Core 6 generally showed a decreasing trend from the surface of ~pH 8.5 to ~pH 6 at the bottom. The vertical trend in DOM concentrations for Core 6 was, however, similar to Core 3. For the latter, they gradually decreased from the surface to ~30-35 m depth, after which there was a small increase at the bottom of the core (Figure 4.2). Core 6 showed an absorbance range of ~0.1-1.5, which was generally lower than for Core 3 (~0.5-2.6).

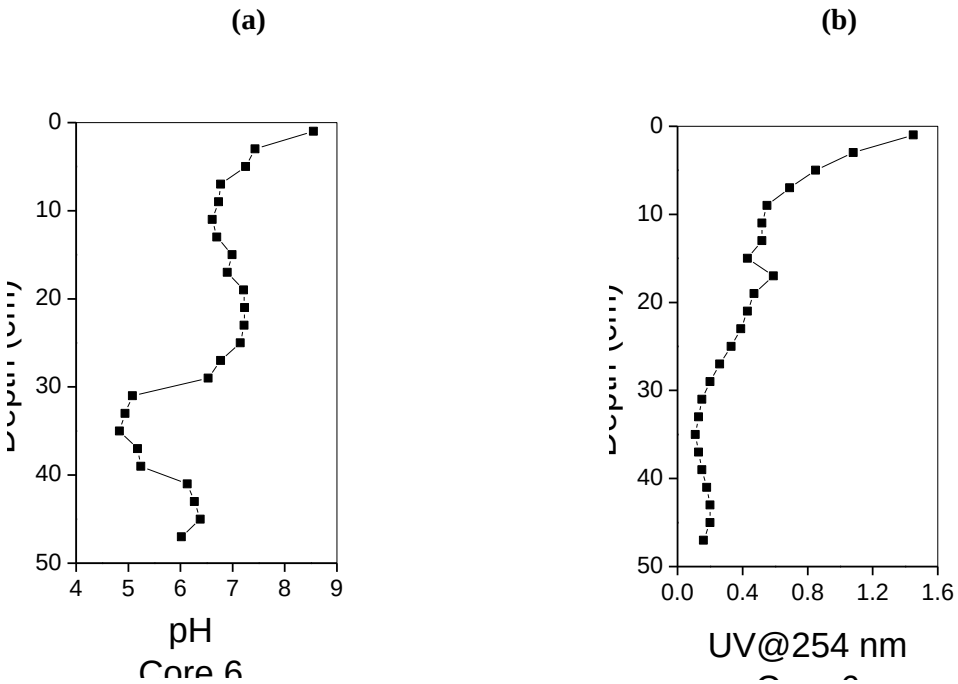

Figure 4.26: (a) pH values and (b) UV absorbance at 254 nm for Core 6 soil porewaters

4.2.2.2 Vertical concentration profiles for U and other elements in porewaters of Core 6

The vertical distribution of a range of elements (U, Fe, Mn, Al, Cu, Pb, Zn, As and Ca) in soil porewaters from Core 6 collected during sampling trip 3 is shown in Figure 4.27(see Appendix section 9.8, Table 9.8). As stated above, Core 6 and Core 3 (Figure 4.4) were both located 20 m from the cave; the element distributions of Core 3 were thus selected to compare with those of Core 6.

The U porewater profile had a maximum concentration of ~23 μg L^{-1} at 17 cm and then showed a greater than 20-fold decrease to ~1 μg L^{-1} at the bottom of the core. The porewater U from Core 6 showed a similar trend to that from Core 3 in that they both gradually increased to peak values at 15-20 cm and then decreased towards the bottom of the core afterwards.

The porewater Fe profile from Core 6 had one main maximum of 79 μg L^{-1} occurring at 17

cm, which was at the same depth as the U porewater maximum. Below this peak, there was a small increase to 28 µg L^{-1} occurring at 35 cm. The Fe porewater concentration profile from Core 3 also had two maxima occurring at 16.5 cm and 37.5 cm.

There was a broad peak towards the bottom of the Mn profile where concentrations of up to 500 µg L^{-1} were measured. On closer examination, however, there was also a peak in concentration at ~10 cm depth. Nevertheless, the position of the main Mn maximum in the porewaters from Core 6 was very different from Core 3, which had a Mn maximum in the surface section.

For the Al porewater profile, the maximum concentration of ~120 µg L^{-1} occurring at 35 cm, coinciding with the smaller Fe porewater maximum. The Al concentration profile for Core 3 was similar to Core 6 in that the main peak was located towards the bottom of the core.

The highest porewater Cu concentration of 21 µg L^{-1} occurredat 17 cm, which was at the same depth as the U and Fe concentration maxima. The Cu maximum of Core 3 occurred at a similar depth, but the peak covered a much broader depth range (10-25 cm).

The Pb porewater concentrations reached a maximum of 6 µg L^{-1} at 35 cm. The shapes of the Pb and Al porewater profiles were similar as they both had a main peak at 35 cm. The Pb porewater profile from Core 3 also had maximum values close to the bottom of the core.

For Zn, there was a small maximum of 1,350 µg L^{-1} at ~10 cm, the position of the smaller Mn maximum; below this, concentrations were almost constant to ~30 cm depth. Thereafter, there was a sharp increase from ~30 cm to a broad peak of 5,700-6,000 µg L^{-1} at 31-35 cm.

The As porewater concentration profile for Core 6 had a sub-surface maximum of ~10,400 µg L^{-1}; concentrations decreased sharply below this but there was a small increase to ~730 µg L^{-1} at 27 cm. Although a similar sub-surface As peak occurred in the Core 3 porewaters, a gradual increase in concentration continued to the bottom of the core.

The Ca porewater profile of Core 6 looked very similar to that for Mn and Zn in that they all had a small peak at 9 cm, and a major broad peak at 31-35 cm.

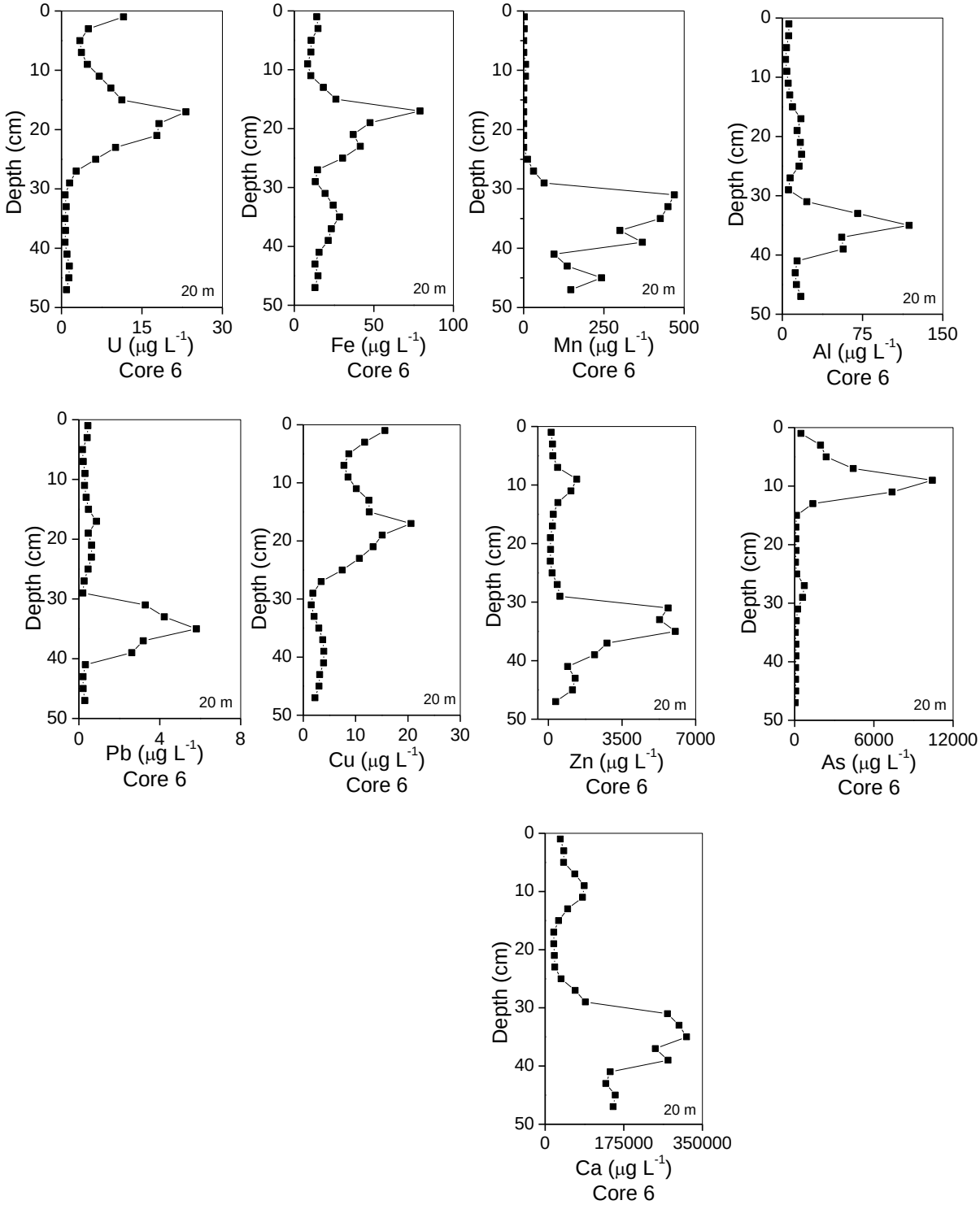

Figure 4.27: Vertical concentration profiles for U, Fe, Mn, Al, Cu, Pb, Zn, As and Ca in soil porewaters from Core 6

Observations and initial interpretation

(i) As observed for Core 3, the maximum porewater U concentration occurred in the 10-20 cm depth interval and coincided with that for Fe, strengthening the hypothesis that the behaviour of U in the Needle's Eye organic-rich soils was in some way related to that of Fe. The Cu profile was also very similar and so it is postulated that the same processes are important in controlling the mobility of all three elements;

(ii) The other elements can be grouped according to their porewater profiles, e.g. Mn, Al, Ca, Pb and Zn all have large peaks below 30 cm; Mn, As, Ca and Zn all have peaks at ~8-11 cm depth;

(iii) It is hypothesised that the peaks at depths of >30 cm are due to the reductive dissolution of Fe phases whilst those at 8-11 cm are due to the reductive dissolution of Mn phases. This would mean that the other elements are associated with these Fe and Mn phases and are released into solution as a consequence of the dissolution process.

The nature of the species in the porewater were then investigated further using ultrafiltration (section 4.2.2).

4.2.2 Ultrafiltration in conjunction with acetate extraction and ICP-MS analysis for Core 6 porewater

As described in sections 2.4.9.2 and 2.4.13.5, porewaters were first isolated from each core section by centrifugation and then filtered through 0.2 μm cellulose nitrate filters. Total porewater profiles were obtained (see Figure 4.27). Afterwards, ultafiltration was used to separate the porewaters into colloidal (3 kDa-0.2 μm) and dissolved (<3 kDa) fractions.After the dissolved fraction (<3 kDa) was transferred to the sterilin tube, 1.5 mL 1 M acetate was then added to the top section of the ultrafiltration unit and acetate extraction of the colloidal fractions for carried out on shaker over 24 hours. Ultrafiltration was then used again to separate the elements extracted by acetate and the elements remained in colloidal form. In total, there were three fractions obtained: colloidal (3 kDa-0.2 μm) fraction extracted by acetate, colloidal (3 kDa-0.2 μm) fraction remaining after acetate

extraction and truly dissolved (<3 kDa) fraction. All of these procedures were carried out both under N_2 and in air to evaluate whether or not exposure to air affected the distribution between colloidal and dissolved forms (see section 2.4.9.2).

The elemental concentrations for the acetate filtrate and the acetate retentate were summed together to give the total elemental concentrations in the colloidal (3 kDa-0.2 μm) fraction, and the acetate retentates were expressed as a percentage of this pseudo-total value in colloidal (3 kDa-0.2 μm) fractions as shown in Figures 4.30, 4.32, 4.34, 4.36.

The elemental concentrations in colloidal (3 kDa-0.2 μm) fractions are shown as red bars while those for the truly dissolved (<3 kDa) fractions are shown as blue bars in Figures 4.28, 4.30, 4.32, 4.34. The red bar values and blue bar values were summed together to give values for the total (<0.2 μm) porewater, which were compared with the measured total element concentrations in total (<0.2 μm) porewater which were displayed in Figure 4.28. The recovery rate was obtained as a percentage of calculated relative to the measured total element concentration (Appendix Tables 9.16, 9.17, 9.20, 9.21, 9.24, 9.25, 9.28, 9.29). The corresponding percentage of elemental concentrations in colloidal (3 kDa-0.2 μm) fractions and truly dissolved (<3 kDa) fraction were also shown in Figures 4.28, 4.30, 4.32, 4.34 (see Appendix Tables 9.16, 9.17 for U; 9.20, 9.21 for Fe; 9.24, 9.25 for Mn; 9.28, 9.29 for Al). Some of the data were not used to construct Figures 4.28, 4.30, 4,32 and 4.34 because the recovery rate was far beyond 100% (e.g. 2420% for Fe at 11 cm-depth sample under N_2). These data were also removed from Appendix Tables 9.16-9.31 as they were not reliable. Thus, only data for U, Fe, Mn and Al are presented.

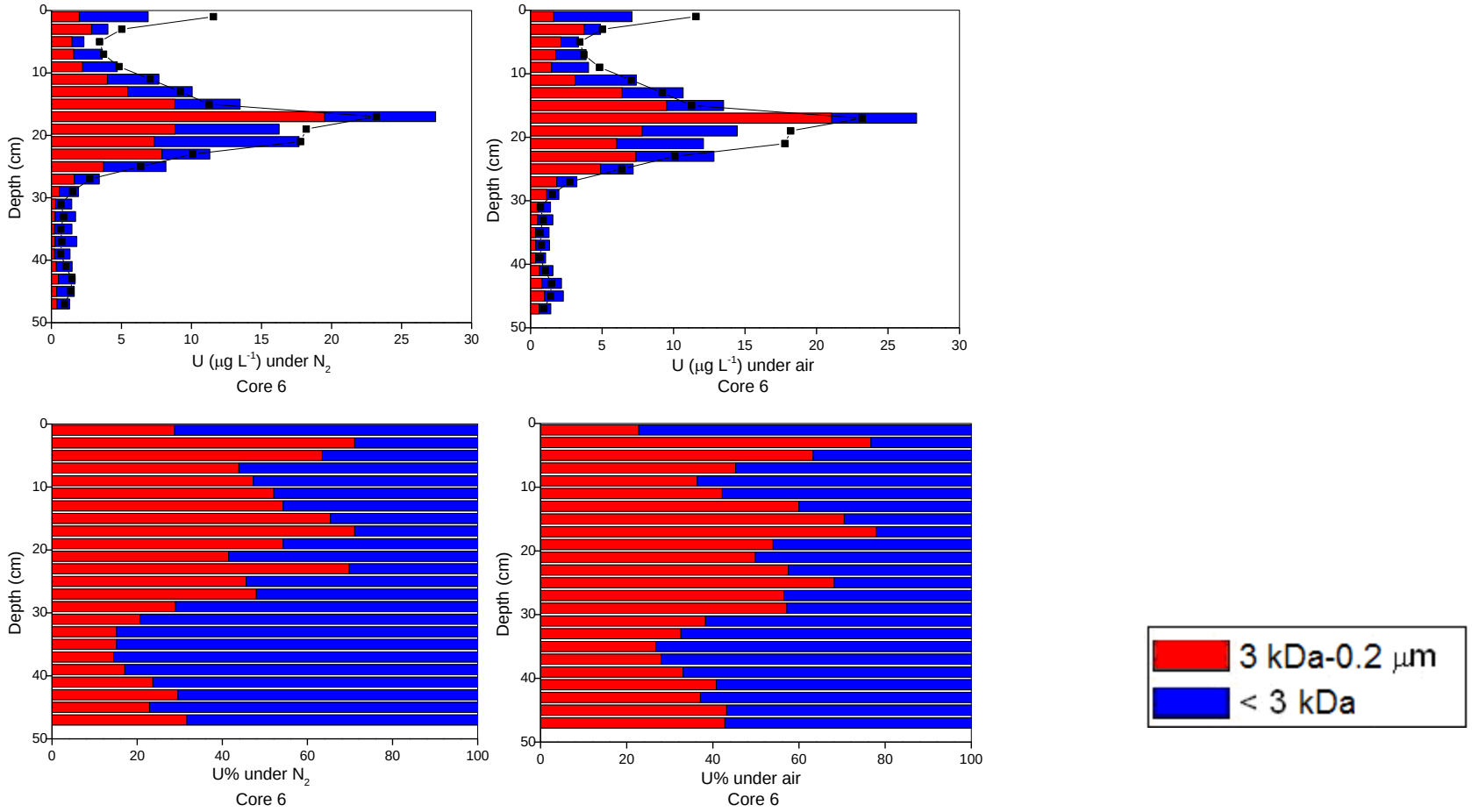

Figure 4.28: U distributions amongst colloidal (3 kDa-0.2 μm) and dissolved (<3 kDa) fractions of porewaters obtained from soil Core 6 under N_2 and in air

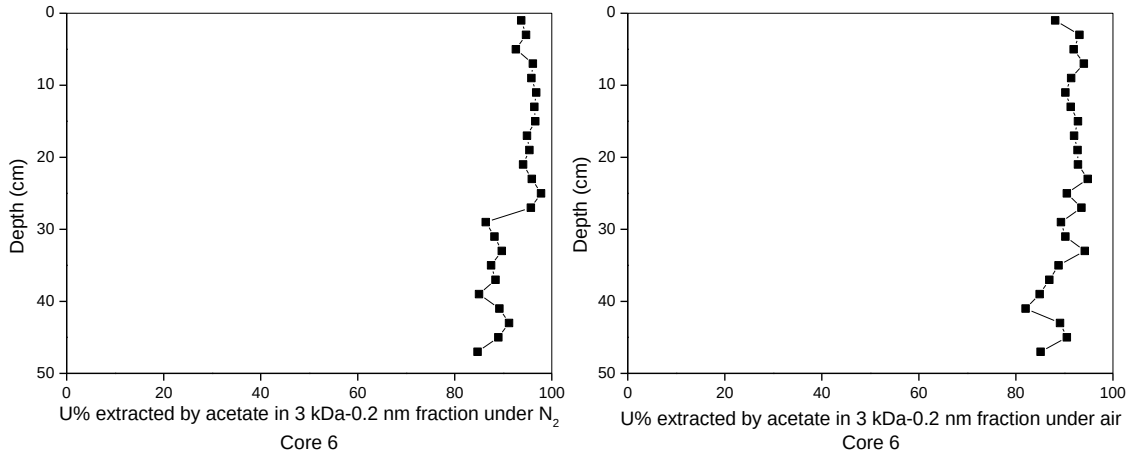

Figure 4.29: The percentage of U extracted from the colloidal (3 kDa-0.2 µm) fraction by sodium acetate

From 3-27 cm depth, ultrafiltration showed that 42-71% of U was associated with colloids (3 kDa-0.2 μm) within the porewater isolated from Core 6 soil samples under N_2 (Figure 4.28) (see Appendix section 9.10, Tables 9.16, 9.18). Below this depth there was a transformation to dissolved forms and <32% of U was in the colloidal fraction. Similarly, there was <30% colloidally associated U in the porewaters from the surface section of the core. Where the colloid isolation had been carried out aerobically, 36-78% of U was associated with colloids (3 kDa-0.2 μm) in the 3-27 cm porewaters. Below 27 cm the proportion of colloidal U generally decreased to 27-57% and so, for this depth range, there was a consistent increase of 10-20% in the proportion of U in colloidal fraction where the experiment had been carried out in air compared with under N_2.

Figure 4.28 shows the total porewater U concentration profile as a solid black line and then shows the distribution between colloidal and dissolved forms using the coloured bars. For both experiments, i.e. under N_2 and in air, the mass balance was very good for the samples which had higher U concentrations. Recoveries of significantly greater than 100% were only obtained for the very low U concentration samples towards the bottom of the core (see recovery rate in Appendix Tables 9.16, 9.17). Importantly, the general trends with depth in distribution of U between colloidal and dissolved forms obtained in air were very similar. Total and colloidal U decreased from the sub-surface section (3 cm) to ~10 cm depth, then gradually increased and reached a maximum at 17 cm; afterwards there was another major decrease from ~25 cm to 35 cm before concentrations increased towards the bottom of the core. A large proportion (82-97%) of colloidal U was extracted by acetate under both cases, and they were in the main the same (Figure 4.29, Appendix Table 9.18, 9.19). Where the experiments were carried out under N_2, there was a suggestion that the acetate extractable portion of colloidal U decreased from ~95% in the upper sections to ~80%-90% in those below 30 cm.

The depth profile pattern for Core 6 where separations were carried out in air were then compared with those for Core 3 (Figure 4.7) as they were both located at 20 m from the cave. There was a slight increase in the importance of the dissolved fraction (<3 kDa) with increasing depth in the porewaters from both Core 3 and Core 6, although Core 6 porewaters generally contained a larger proportion of U in the dissolved phase.

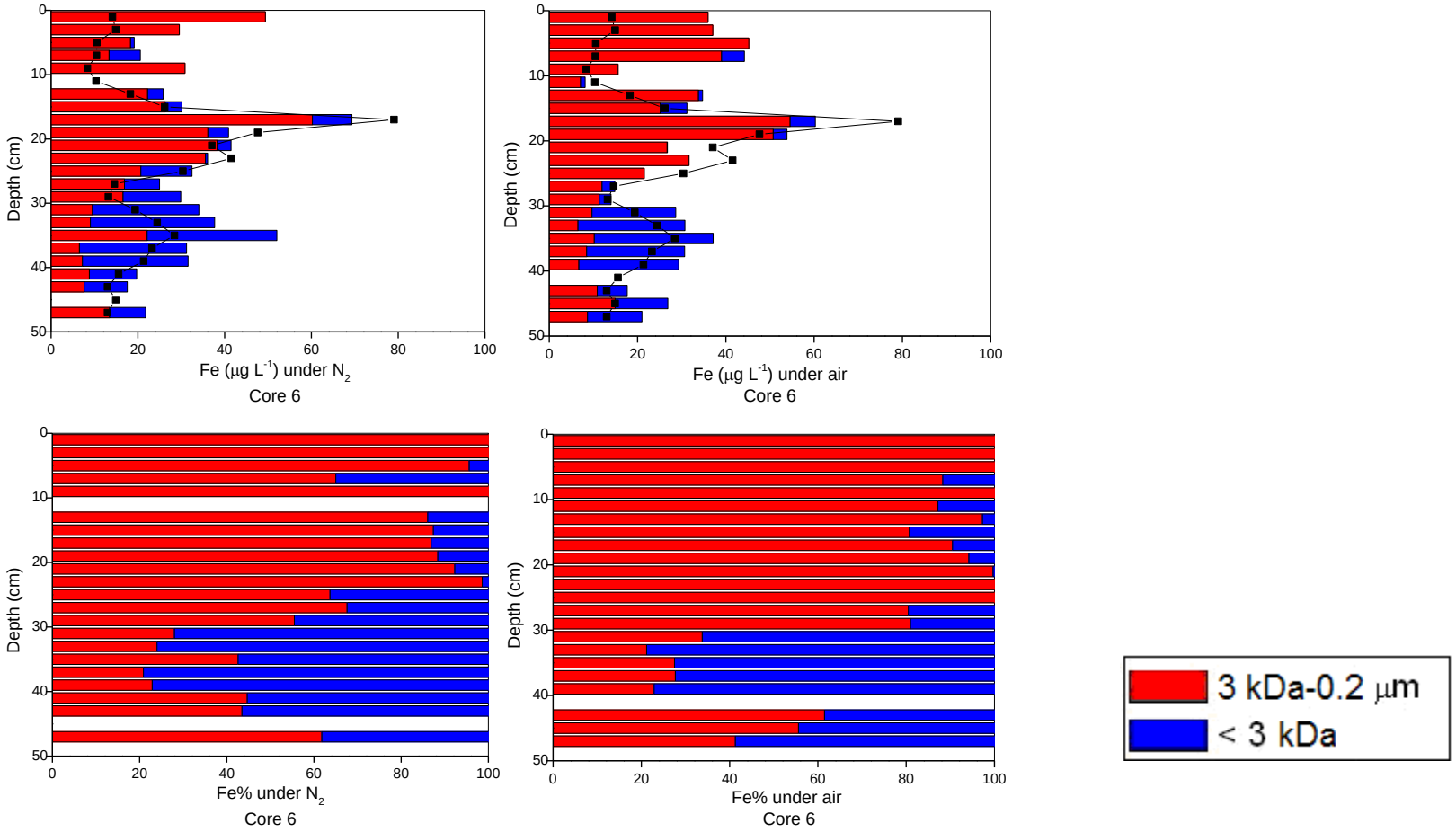

Figure 4.30: Fe distributions amongst colloidal (3 kDa-0.2 μm) and dissolved (<3 kDa) fractions of porewaters obtained from soil Core 6 under N_2 and in air

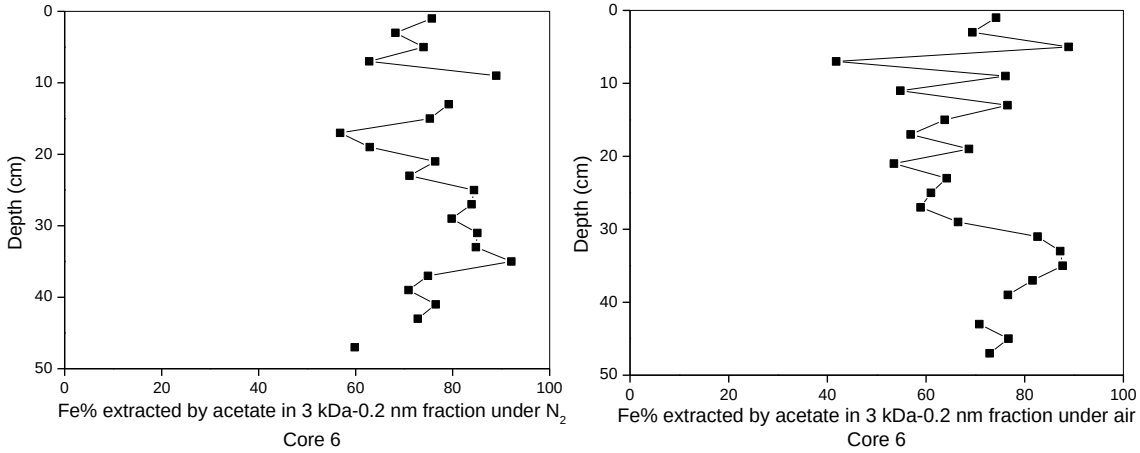

Figure 4.31: The percentage of Fe extracted from the Core 6 colloidal (3 kDa-0.2 µm) fraction by sodium acetate

As shown in Figure 4.30, the sum of Fe concentrations in three ultrafilter fractions from the bar chart does not always agree with the total porewater, Fe concentrations (solid line) i.e. before ultrafiltration. This is due to the contamination of samples following interaction of the acetate reagent with the ultrafiltration membrane. An acetate reagent blank test for elements released from the membrane was carried out before this method was applied to the Core 6 porewaters. The result showed that Fe released by acetate would not have caused such significant contamination problems if the Fe concentrations in the porewater had been as high as for Core 3 (up to ~400 μg L^{-1}). However, Fe concentrations in the Core 6 porewaters were only up to 80 μg L^{-1}, and so effects on the mass balance were clearly observed. In addition, the top five soil sections (1-9 cm depth) had much lower moisture contents as well as having relatively low Fe concentrations, and only 3.5-11 mL porewater could be used for ultrafiltration compared with 18 mL used for most of the deeper soil sections. Thus, the Fe contamination of the 1-9 cm porewaters was more obvious compared with that at increasing depths. The data for the top five sections were still retained in the graph as it can provide semi-quantitative information about the proportion of colloidal fraction in the porewater. As mentioned in section 2.5.1.2 (ultrafiltration units), a separate blank test was carried out where ~3 mL, 6.5 mL, 10 mL, 18 mL deionised water was added to the ultrafiltrator for centrifugation. The Fe concentrations in the filtrates (deionized water) were 60.3 μg L^{-1}, 12.7 μg L^{-1}, 4.2 μg L^{-1} and 5.4 μg L^{-1}. After this, 1.5 mL Na acetate was added to the same ultrafiltrator unit and the same procedure was again carried out. The Fe concentrations in the filtrates (Na acetate) were 119 μg L^{-1}, 62.1 μg L^{-1}, 85.7 μg L^{-1} and 48.0 μg L^{-1}.

In spite of the problems described above, the general concentration trends observed for the total porewater were still present after the ultrafiltration had been carried out, i.e. highest concentrations were observed at 17 cm and there was a smaller maximum at ~35 cm. There was distinct difference in Fe distribution between colloidal and dissolved forms above and below 27 cm depth where the separations had been carried out under both N_2 and in air (Figure 4.30) (also see Appendix Tables 9.20, 9.21). Above 27 cm, there was generally more than 80% of Fe associated with colloidal fraction. Below this, the proportion of colloidal Fe gradually decreased to ~20% at 39 cm. In terms of acetate extraction, there was in general a higher percentage of colloidal Fe extracted by acetate below 27 cm depth in both cases (Figure 4.31, Appendix Tables 9.22, 9.23). This change occurs at a similar depth but the direction of change is the inverse of that described for U.

As shown in Figure 4.7, greater than 85% of Fe was in colloidal fraction (3 kDa-0.2 μm) at Core 3, even for the sections below 30 cm depth. This is different from Core 6 in which less than 70% and, in many cases, only 20-45% was in the colloidal fraction below 30 cm.

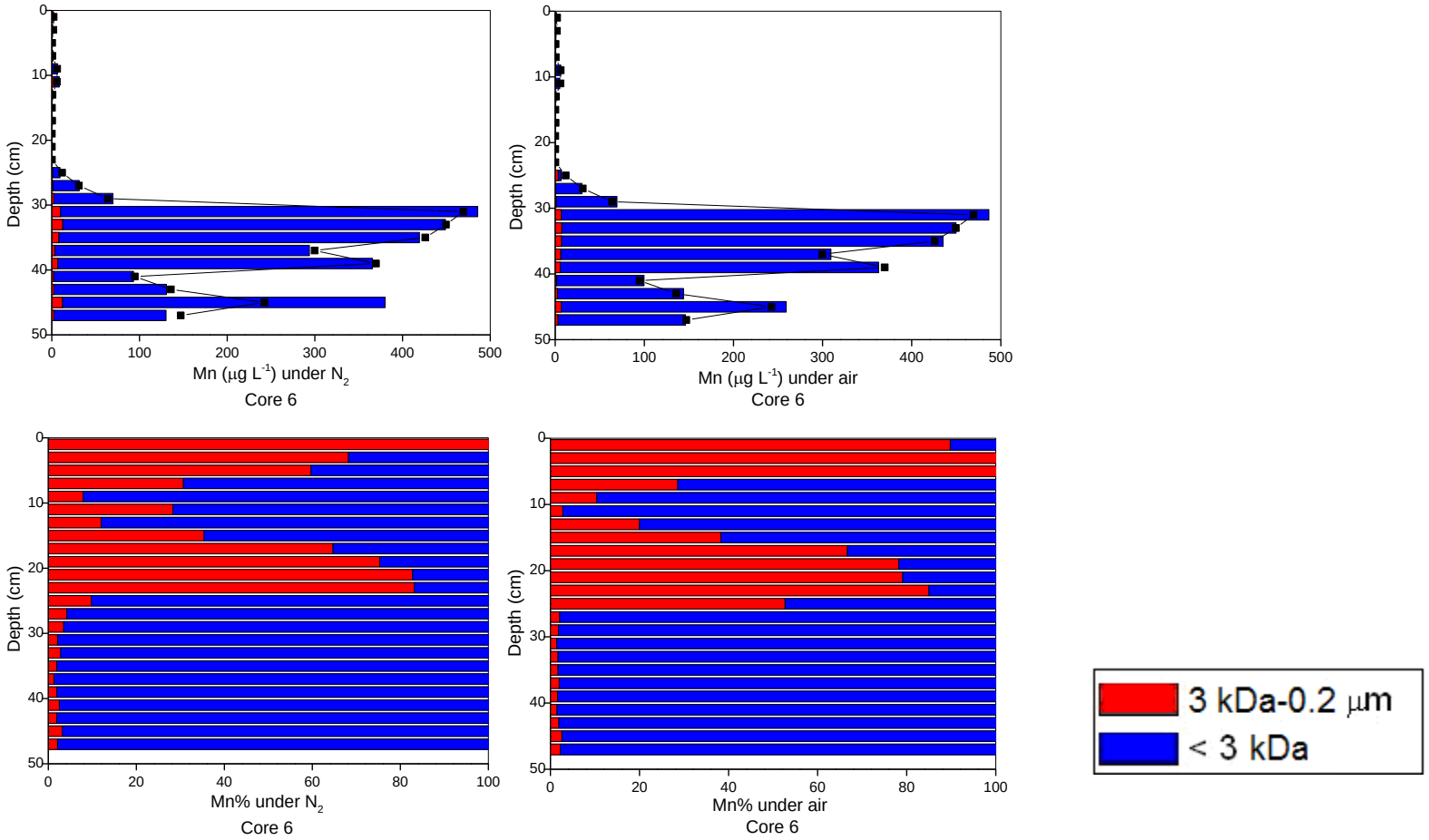

Figure 4.32: Mn distributions amongst colloidal (3 kDa-0.2 μm) and dissolved (< 3 kDa) fractions of porewaters obtained from soil Core 6 under N_2 and in air

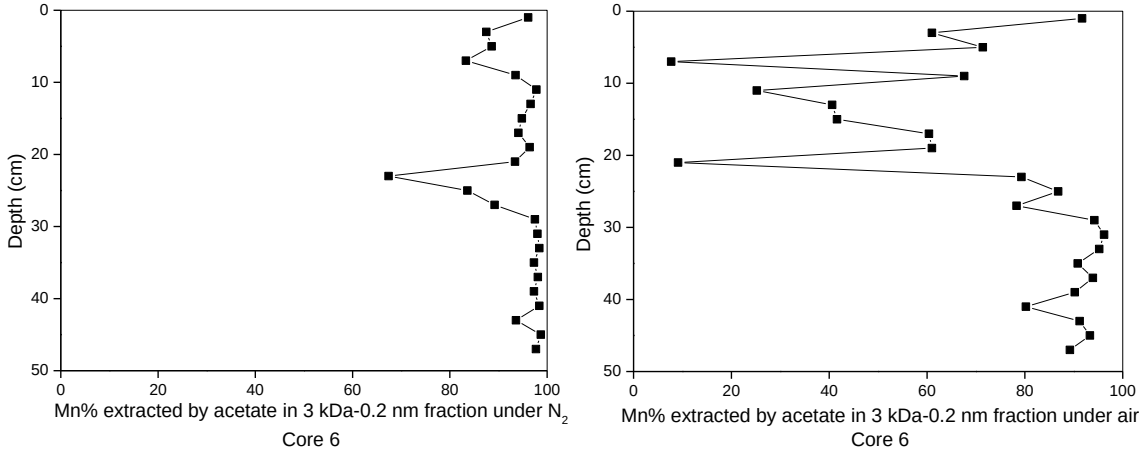

Figure 4.33: The percentage of Mn extracted from the Core 6 colloidal (3 kDa-0.2 µm) fraction by sodium acetate

Figure 4.32 shows that the highest porewater Mn concentrations were found at depths greater than 30 cm. However, it was pointed out in the preceding section that there was a small but important peak located at 10 cm depth (also see Appendix Tables 9.25, 9.26). For the 0-6 cm and 16-24 cm sections of the core, the majority of the Mn was colloidally associated. However, at ~10 cm depth and below 25 cm depth, more than 90% of Mn was in the dissolved (<3 kDa) fractions. The distribution pattern for Mn in the porewater from the 0-25 cm depth sections was interesting because there was a clear trend of decreasing amounts in colloidal fraction from the surface to ~10% at ~10 cm; below this the proportion of colloidal Mn gradually increased to 85% at 23 cm. Thus, the pattern appears to be almost symmetrical above and below10 cm depth. The distribution profiles for colloidal and dissolved fractions under N_2 and in air were very similar. However, acetate extraction carried out under the N_2 extracted a much larger amount of colloidal Mn than that extracted in air (Figure 4.33, Appendix Tables 9.26, 9.27).

In comparison with Mn distribution pattern profile from Core 3 (Figure 4.7), there were general similarities except that the bottom (43 cm) section of Core 3 contained more than 90% of the colloidal Mn whereas in Core 6 had mainly dissolved Mn.

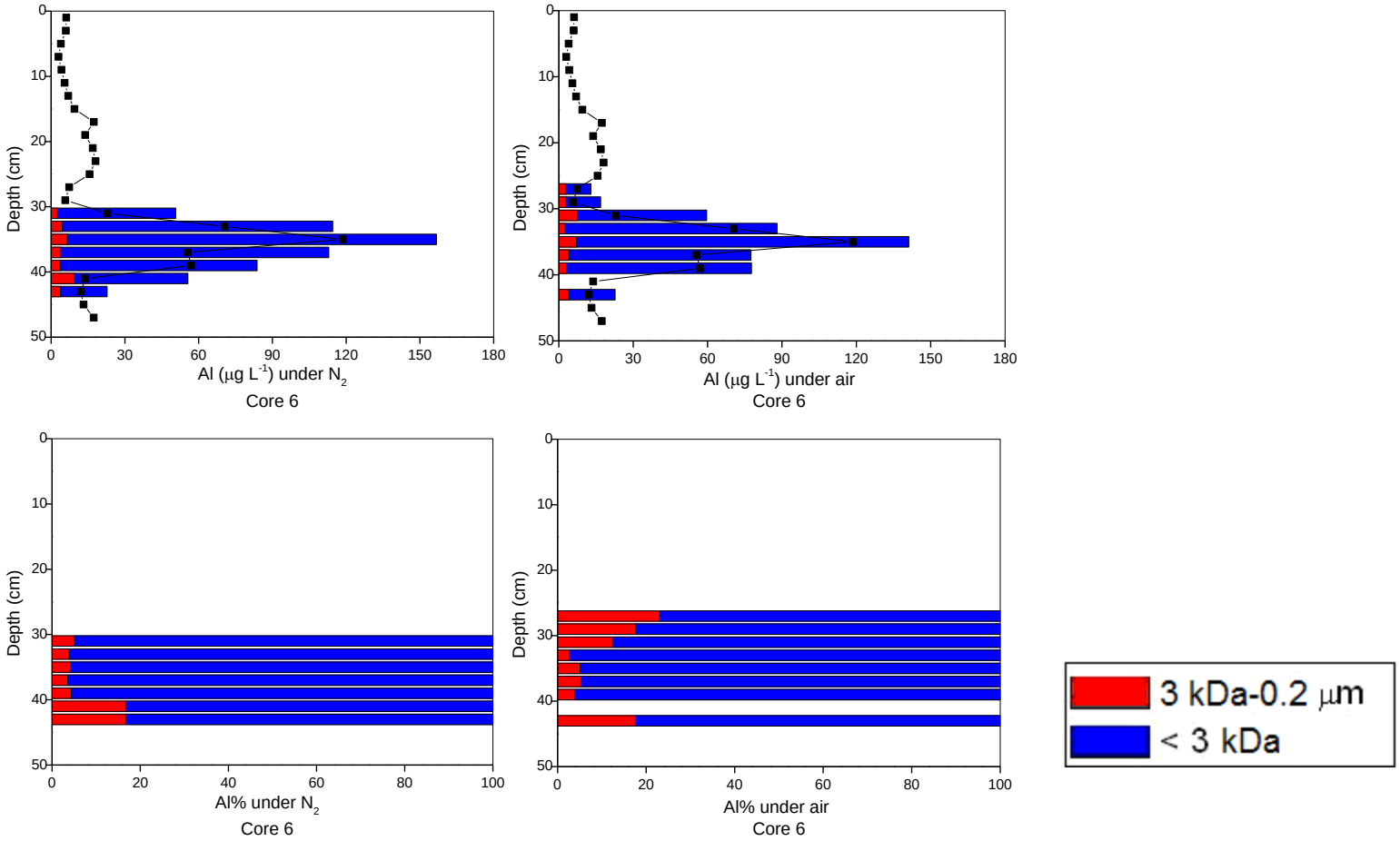

Figure 4.34: Al distributions amongst colloidal (3 kDa-0.2 µm) and dissolved (< 3 kDa) fractions of porewaters obtained from soil Core 6 under N_2 and in air

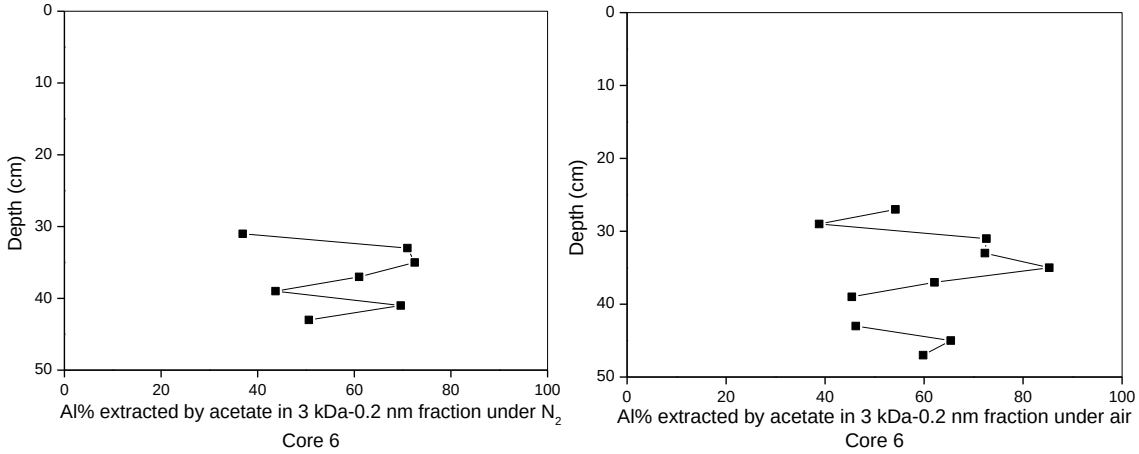

Figure 4.35: The percentage of Al extracted from the Core 6 colloidal (3 kDa-0.2 µm) fractions by sodium acetate

As shown in Figure 4.34, most of the Al data were removed because they were not reliable. This is due to the release of Al from the ultrafiltration membrane following use of the acetate reagent as well as the low Al concentrations in most porewaters from Core 6. It is possible that between-batch differences in the ultrafilter membrane account for the difference between results from the upper and lower parts of the core. Only the data for the 30-50 cm depths were retained.

Figure 4.34 shows that, as for Mn, the highest porewater Al concentrations were found towards the bottom of the core. A large proportion (mostly >80%) of this Al was present in the dissolved fraction (<3 kDa) where the separations were carried out under N_2 and in air(Figure 4.34, Appendix Table 9.28, 9.29). In both cases, greater than 70% of the colloidal Al was extractable by sodium acetate (Figure 4.35, Appendix Tables 9.30, 9.31). Importantly, Al behaved very similar as Mn that below 25 cm they were both mainly in the dissolved phase (<3 kDa).

Observations and initial interpretation

The key features of vertical distribution of colloidal (3 kDa-0.2 μm) and dissolved (<3 kDa) phases of U, Fe, Mn, Al under N_2 and in air were:

(i) The differences between the results for separations carried out under N_2 and in air were relatively small; where present, the observed differences were greater below 30 cm depth and most likely indicate that a small amount of oxidation and formation of Fe colloids occurs in air. Interaction of U with these newly formed Fe colloids would then account for the slightly greater proportions of colloidal U at such depths;

(ii) Even withstanding these small changes, the overall trends with depth are not significantly affected when the separations are carried out in air rather than under N_2;

(iii) The colloid/truly dissolved distribution patterns for U, Fe, Mn, Al showed distinct differences above 25-29 cm and below 25-29 cm. In all cases, much greater percentages of elements were found in the dissolved phase below 25-29 cm; it is

postulated that reductive dissolution of Fe phases also releases adsorbed U, Mn and Al into the porewaters;

(iv) The proportion of colloidal Mn at ~10 cm was very low, but above and below this depth, the proportion gradually increased and became the main form of Mn in the porewaters. It is proposed that reductive dissolution of Mn phases in the solid soil results in the release of truly dissolved Mn^{2+} into the soil porewaters. As both upwards and downwards diffusion take place, most of this Mn is transferred into the colloid fraction. Diffusion upwards is likely to be accompanied by re-oxidation of the Mn and the subsequent removal to the solid phase.

For the solid phase samples described in sections 3.5.1-2, U, Fe, Mn and Al were shown to be associated with extracted humic substances. Sodium acetate removed ~20-25% U, ≤3% Fe, 65-75% Mn and 4-6% Al. When the acetate reagent was applied to the porewater colloids, however, it removed ~85-95% U, ~60-80% Fe, >95% Mn (under N_2) and ~40-80% Al. Thus, all elements were present in more extractable forms in the aqueous phase compared to the solid phase.

4.2.3 Carbonate extraction from soil core 6

In section 4.2.2.1, it was shown that there was a sharp peak centered at ~17 cm and a smaller, broader peak centered at ~35 cm in the porewater Fe concentration profile for Core 6 (Figure 4.30). Section 4.2.2.2 then showed that the proportion of Fe in the dissolved fraction started to increase from ~30 cm depth. As stated above, the presence of dissolved Fe is attributed to the release of Fe from the solid phase as a consequence of reductive dissolution. However, the reason for the presence of the first Fe maximum at 17 cm is not clear. Importantly, however, there was also a maximum in porewater U (and Cu) concentration at the same depth in this core. From previous hydrogeological characterisation of the site, both surface and sub-surface flow-paths have been identified (Jamet et al., 1993). Thus it is possible that there may be lateral flow of groundwater coming from the mineralisation and transporting U through the boggy soils at this site. The waters emerging from the mineralisation are carbonate-rich but there was insufficient porewater remaining for further analyses and so the carbonate content of the solid phase was determined.

The results showed that thecarbonate content in the soil gradually decreased from 0.20 mol kg^{-1} at the surface to 0.12 mol kg^{-1} at 11 cm depth and then increased rapidly to a concentration maximum of 0.43 mol kg^{-1} at 17 cm. Below this, the trend of decreasing concentration towards the bottom of the core (Figure 4.36, Appendix Table 9.47). The maximum concentration of solid phase carbonate occurred at the same depth as that of the porewater Fe and U, consistent with the hypothesis that there was a sub-surface groundwater flow path bringing carbonate- and U-rich waters from the mineralization. It should be noted that this does not necessarily mean that either Fe or U are associated directly with carbonates.

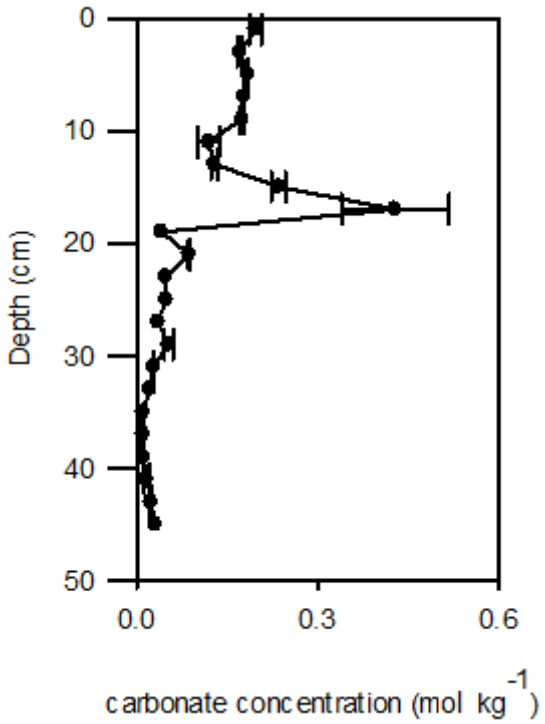

Figure 4.36: Carbonate content in solid phase from Core 6

With respect to the solid phase composition, based on a carbonate content of ~0.4 mol kg^{-1}, the maximum possible concentration of Fe in the form of $FeCO_3$ would be 2.2% w/w. More typically, the carbonate content in the top 0-20 cm sections ranged from 0.12-0.2 mol kg^{-1}, the maximum Fe concentrations would be in the range 0.7-1.1% w/w. However, the total Fe concentrations in the top 0-20 cm solid phase sections from Core 3 were typically ≤0.5% w/w and sequential extraction showed that a large proportion of this was found to be in the

form of oxides and sulfides. In addition, there was no correlation between the amount of Fe extracted from Core 3 soils by sodium acetate (supposedly carbonate bound Fe) and the amount of carbonate present in the solid phase of Core 6 (same location). Thus, the shape of the carbonate profile cannot be accounted for by the precipitation of $FeCO_3$. It is more likely that precipitation comprises $CaCO_3$. Significantly, the XRD results for Core 3 soils showed that calcite was present at up to 5% (13.5 cm depth) and that there was a marked decrease with increasing soil depth (Table 4.5).

4.3 Results from sampling trip 4 on 21/06/2011

For sampling trips 1-3(sections 3.3, 4.1, 4.2), the samples were collected during later autumn/winter (October or December). In sampling trip 4, the samples were collected during summer time (June) to compare the soil porewater parameters (pH, UV absorbance at 254 nm, element depth profiles) with the winter season (sections 4.3.1-4.3.3).

Section 4.2.2 mainly focused on the determining the distribution between colloidal and dissolved forms of the U, Fe, Mn and Al with increasing depth in Core 6 and then identified that high proportions of the colloidal forms of each of these elements were in acetate-extractable forms. However, the relationship between these elements and dissolved organic matter also required further investigation. In section 4.1.7, ultrafiltration was applied to fractionate the porewater (<0.2 μm) into large (100 kDa-0.2 μm), medium (30-100 kDa) and small (3-30 kDa) colloidal and a dissolved (<3 kDa) fractions. Visual observation confirmed the dissolved organic matter was mainly present in the large (100 kDa-0.2 μm) size fraction. In section 4.3.4, "mini-column" gel filtration, was applied to the entire colloidal fraction (3 kDa-0.2 μm) in conjunction with measurement of the UV absorbance at 254 nm and elemental concentration determination by ICP-MS to make an in-depth study of the relationship between these elements and different components of the colloidal fraction.

4.3.1 pH and UV absorbance

The pH values of the cave drip waters emerging from the mineralization were slightly alkaline (~7.6-7.7) (Table 4.17), in agreement with results from sampling trip 3 (Table 4.10). Again the organic content in these waters was very low (UV absorbance values of 0.023 and 0.025).

Table 4.17: pH and UV absorbance at 254 nm of drip waters 8 and 9 emerging from the mineralisation

Sample ID	pH	Abs at 254 nm
Drip water 8	7.56	0.023
Drip water 9	7.68	0.025

The soil porewater pH values for Core 7, ranged from 5.2-7.0 (Figure 4.37).Dissolved organic matter (DOM), as measuredby proxy (UV absorbance at 254 nm), varied with depth; the absorbance values were in the range ~0.3-1.8 (Figure 4.38).

Core 7 was compared with Core 4 as they were both located 25 m from the cave. In general, both of the pH depth profiles (Figures 4.1, 4.37) gradually decreased from the surface towards the bottom of the core, and the pH ranges were similar (see Appendix Table 9.1). The DOM depth profiles (Figures 4.2, 4.38) also showed a similar trend in that they had maximum at the surface, decreasing values with increasing depth and then a small increase towards the bottom of the cores (see Appendix Table 9.2).

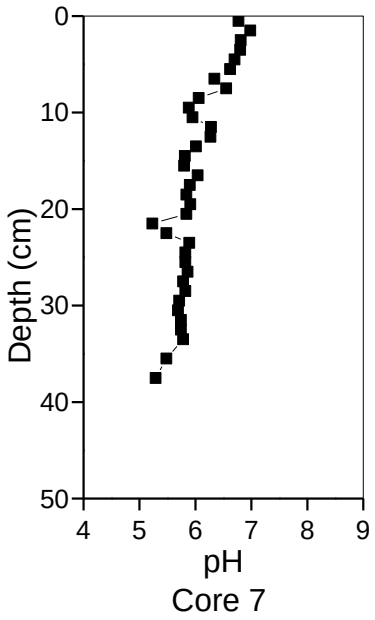

Figure 4.37: Soil porewater pH values for Core 7

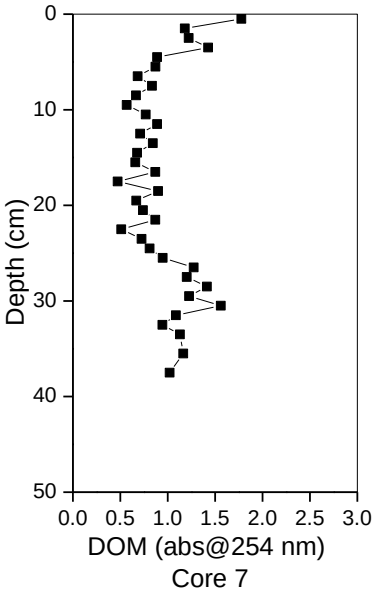

Figure 4.38: Soil porewater UV absorbance values at 254 nm for Core 7

4.3.2 Elemental concentrations in cave drip water and the soil porewater samples from Core 7

The elemental concentrations in the cave drip waters and therange of values for Core 7 porewater samples are shown in Table 4.18. U concentrations in the cave water samples were in the range 120-150 μg L^{-1}. At 25 m from the cave, U concentrations in core 7 porewaters were in the range of 10-60 μg L^{-1}. Thus by 25 m from the cave, the U concentrations are ~x2-x10 lower. For sampling trip 2, Core 4 porewaters showed a 20-fold decrease in U concentrations in comparison with those in the drip waters.

In comparison with the drip waters, higher concentrations of Fe, Mn, Pb, Cu, Al, As and Zn were found in core 7 porewaters (Table 4.18). The concentrations of Ca in the drip waters emerging from the mineralisation were ~25,300 μg L^{-1} and ~78,500 μg L^{-1}, respectively. In the porewaters from Core 7 (25 m from cave), the Ca concentrations were in the range of ~15,000-52,000 μg L^{-1}. There was no clear trend of Ca concentrations between the cave and Core 7 porewaters. In comparison with Core 4, similar results were found in that higher concentrations of Fe, Mn, Pb, Cu, Al and As were obtained in the soil core porewaters compared with the cave waters.

Table 4.18 Elemental concentration in drip waters and porewater samples of Core 7

Site	Distance from cave (m)	Water sample description	Aqueous phase concentrations								
			U ($\mu g\ L^{-1}$)	Fe ($\mu g\ L^{-1}$)	Mn ($\mu g\ L^{-1}$)	Pb ($\mu g\ L^{-1}$)	Cu ($\mu g\ L^{-1}$)	Al ($\mu g\ L^{-1}$)	As ($\mu g\ L^{-1}$)	Zn ($\mu g\ L^{-1}$)	Ca ($\mu g\ L^{-1}$)
Cave	0	Dripwater 8	123	n.d.	n.d.	n.d.	8.4	n.d.	4.4	n.d.	25300
		Dripwater 9	147	n.d.	n.d.	n.d.	7.3	n.d.	10.5	n.d.	78500
Core 7	25	Porewater	8.9-57	97-1290	17-673	0.048-20	10-60	205-2380	33-869	44-241	15700-51900

n.d. = not detected (detection limits were: Fe = 0.008 $\mu g\ L^{-1}$; Mn = 0.01 $\mu g\ L^{-1}$; Pb = 0.008 $\mu g\ L^{-1}$; Al = 1.84 $\mu g\ L^{-1}$; Zn = 1.59 $\mu g\ L^{-1}$)

4.3.3 Vertical concentration profiles for U and other elements in porewaters of Core 7

The U concentration profile decreased from30 μg L^{-1}at the surface to 10 μg L^{-1} at ~10 cm depth and then gradually increased to 57 μg L^{-1}; there was a broad maximum at 30.5-35.5cm (Figure 4.39). After reaching a maximum concentration of 1300 μg L^{-1} at 3.5 cm, Fe concentration showed a nearly 10-fold decrease towards the bottom of the core. The Mn and Ca profiles both decreased sharply from a surface maximum and then showed a similar trend of decreasing concentrations towards the bottom of the core. Al had a general trend of gradually increasing concentration with depth towards the bottom of the core. Pb concentrations gradually increased from the surface and reached a maximum value at 28.5 cm; the As profile was similar to that of Pb except for a small peak at 15.5 cm. Copper concentrations gradually increased from 12 μg L^{-1}at the surface to ~50 μg L^{-1} at 20.5 cm, but there were further increases below this depth. Zinc concentrations decreased over the 0-10 cm depth interval but then did not vary much below this depth(see Figure 4.33, Appendix Table 9.9).

Observations and initial interpretation

The porewater U depth profile for Core 7 showed a more pronounced increase towards the bottom whereas Core 4 U concentrations were relatively constant below 20 cm depth (Figure 4.5). The As depth pattern for Core 7 was also different from Core 4 in that the As maximum at Core 7 was near the bottom while that at Core 4 was ~ 5 cm depth. Since Core 7 was collected during summer time and all other cores were collected during winter, it was considered that seasonal variations in, for example, redox conditions might be a contributing factor. Although Core 7 depth profiles for other elements (Fe, Mn, Al, Cu, Pb) were quite similar to those observed for Core 4, it was clear that the maximum porewater Fe concentration occurred closer to the surface and thus more reducing conditions prevailed at the time of collection of Core 7.

Several important points emerged from these results:

(i) U and Fe porewater concentration maxima do not always co-incide;

(ii) Temporal variations in the redox intensity (as indicated by the position of the

(iii) porewater Fe maximum) influence the behaviour of U (and As)

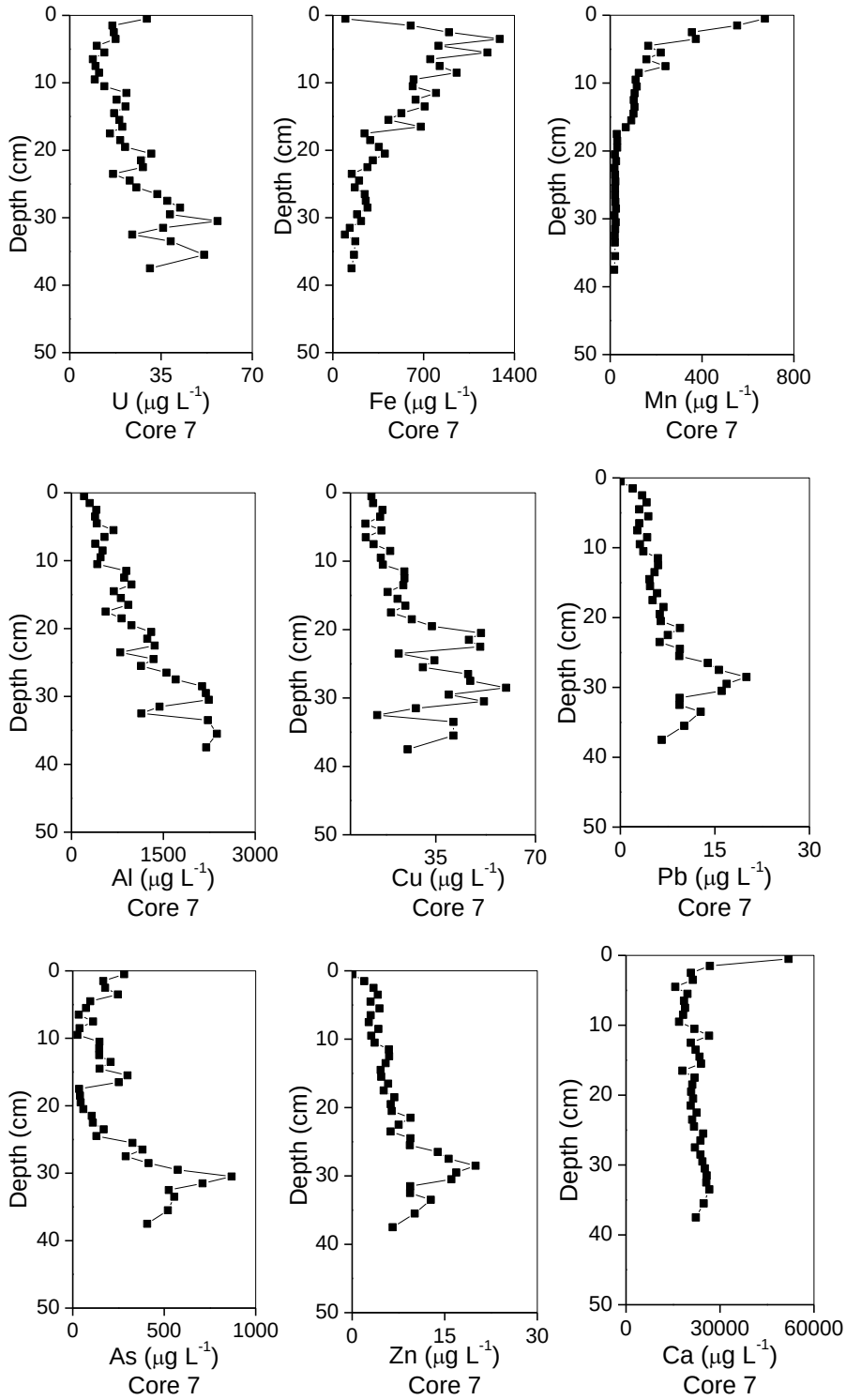

Figure 4.39: Vertical concentration profiles for U, Fe, Mn, Al, Cu, Pb, As, Zn and Ca in soil porewaters from Core 7

4.3.4 Gel filtration fractionation of porewater colloids from selected Core 7 samples

When carefully applied, gel filtration is a technique that can be used to separate the colloidal molecules according to their sizes (see section 2.4.12). It is a useful method because the sample is eluted from the column and thus the DOM content of fractions can be readily determined by UV-vis absorbance (254 nm). Here, gel filtration was used to study the interaction between elements (U, Fe, Mn, Al, Pb, Cu, Ca, Zn, As) and dissolved organic matter in colloidal fractions with increasing depth. The colloidal fractions (3 kDa-0.2 μm) were isolated from 0.2 μm-filtered porewaters using 3 kDa ultrafilter units.

G200 Sephadex gel (200 kDa MWCO) was used to prepare "mini" gel filtration columns (3 ml plastic pipette plugged with cotton wool; 3 ml of G200 gel to form gel bed; pipette bulb cut to form eluent reservoir). Dextran 2000 was again used to determine the exclusion limit (section 3.5.2). Practice runs for each sample were carried out to ensure visually that consistent elution patterns were being obtained. Figure 4.40 shows the UV absorbance values for the colloidal fractions in S4 (3.5 cm depth), S8 (7.5 cm depth), S17 (16.5 cm depth) and S35 (35.5 cm depth) porewaters, respectively. There was a broad band of dissolved organic matter with elution volume in 2-4 mL which was close to the size exclusion limit of the column. It should be recalled that the elution volume reflects the time spent on the column and that larger molecules elute before the smaller molecules. Therefore the humic colloids comprised mainly larger molecules, which is consistent with the ultrafiltration data for porewaters from Cores 3, 4 and 5 (see section 4.1.7), where most of the brown colour was present in the large colloids fractions.The maximum in UV absorbance at 254 nm in the porewaters from 3.5 cm depth occurred after 3 mL but there was quite a significant tailing off volume (absorbance dropped below 0.1 units by 6 mL). For the 7.5 cm porewaters, the maximum again occurred after 3 mL had eluted from the column but this time the drop in UV absorbance occurred more rapidly. For the 16.5 cm porewaters, the absorbance maximum occurred after 2 mL whilst at 35.5 cm, the maximum became slightly broader and more similar to the pattern observed for the 3.5 cm porewater colloids (see Appendix Table 9.50).

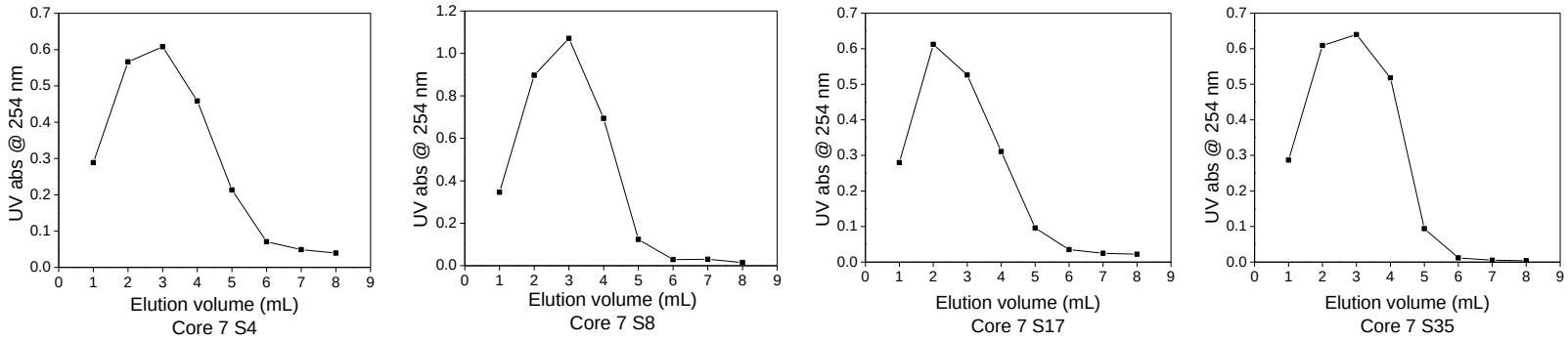

Figure 4.40: UV-visible absorbance at 254 nm for G200 gel filtration fractions for the S4, S8, S17 and S35 sections from Core 7

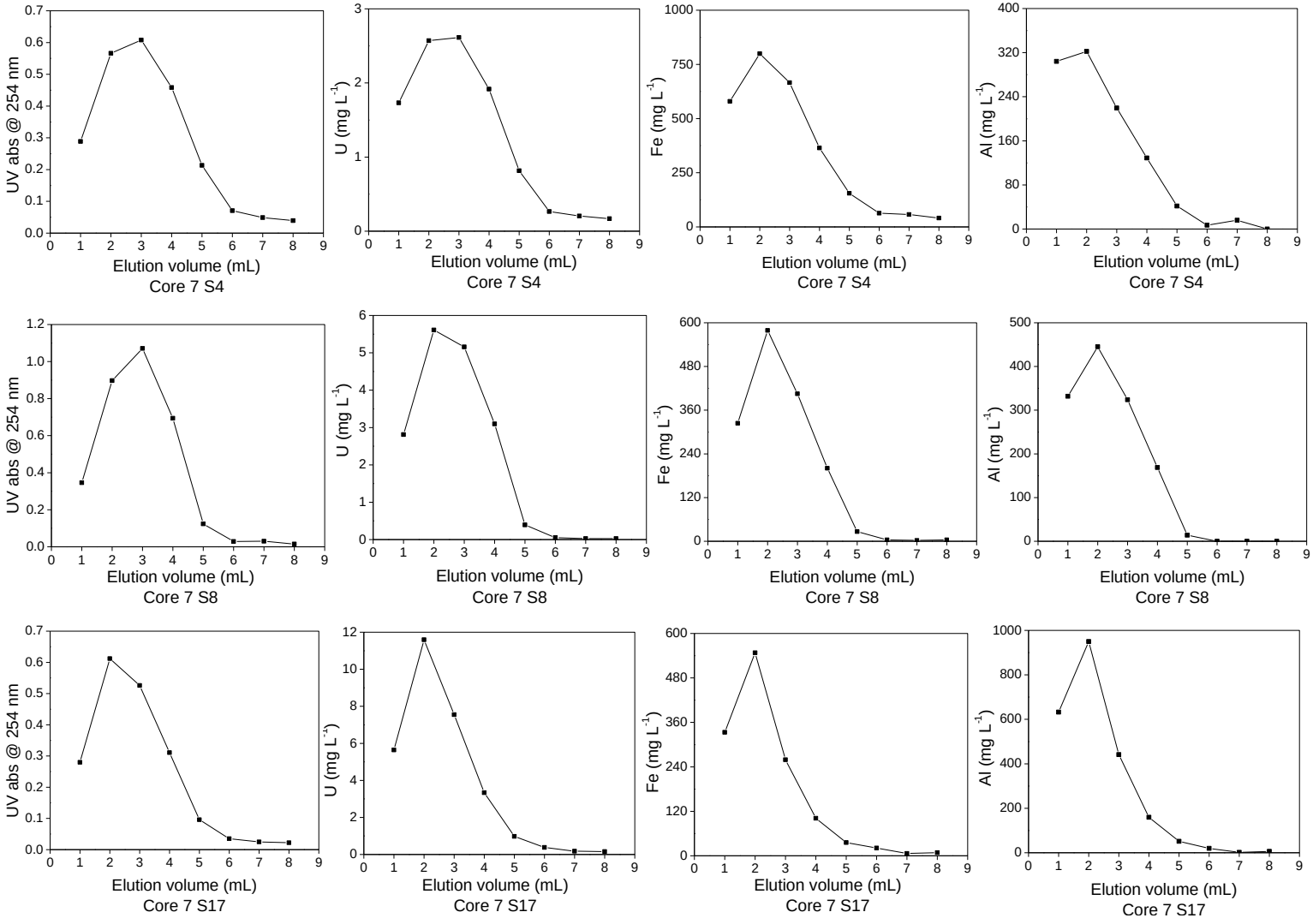
UV abs @ 254 nm
U (mg L-1)
Fe (mg L-1)
Al (mg L-1)
Elution volume (mL)
Core 7 S4
Core 7 S8
Core 7 S17

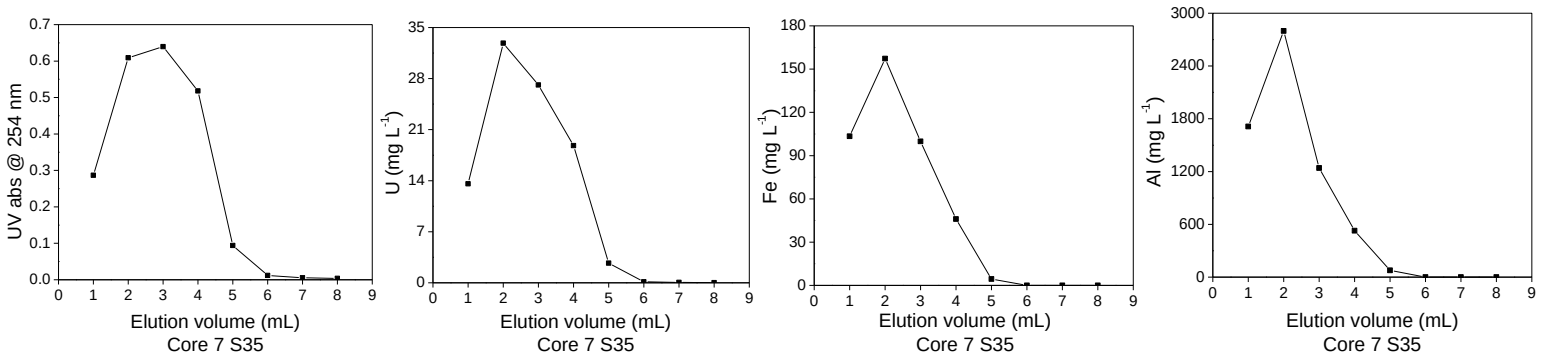

Figure 4.41: UV-visible absorbance at 254 nm and U, Fe, Al concentrations for G200 gel filtration fractions for the S4, S8, S17 and S35 sections from Core 7

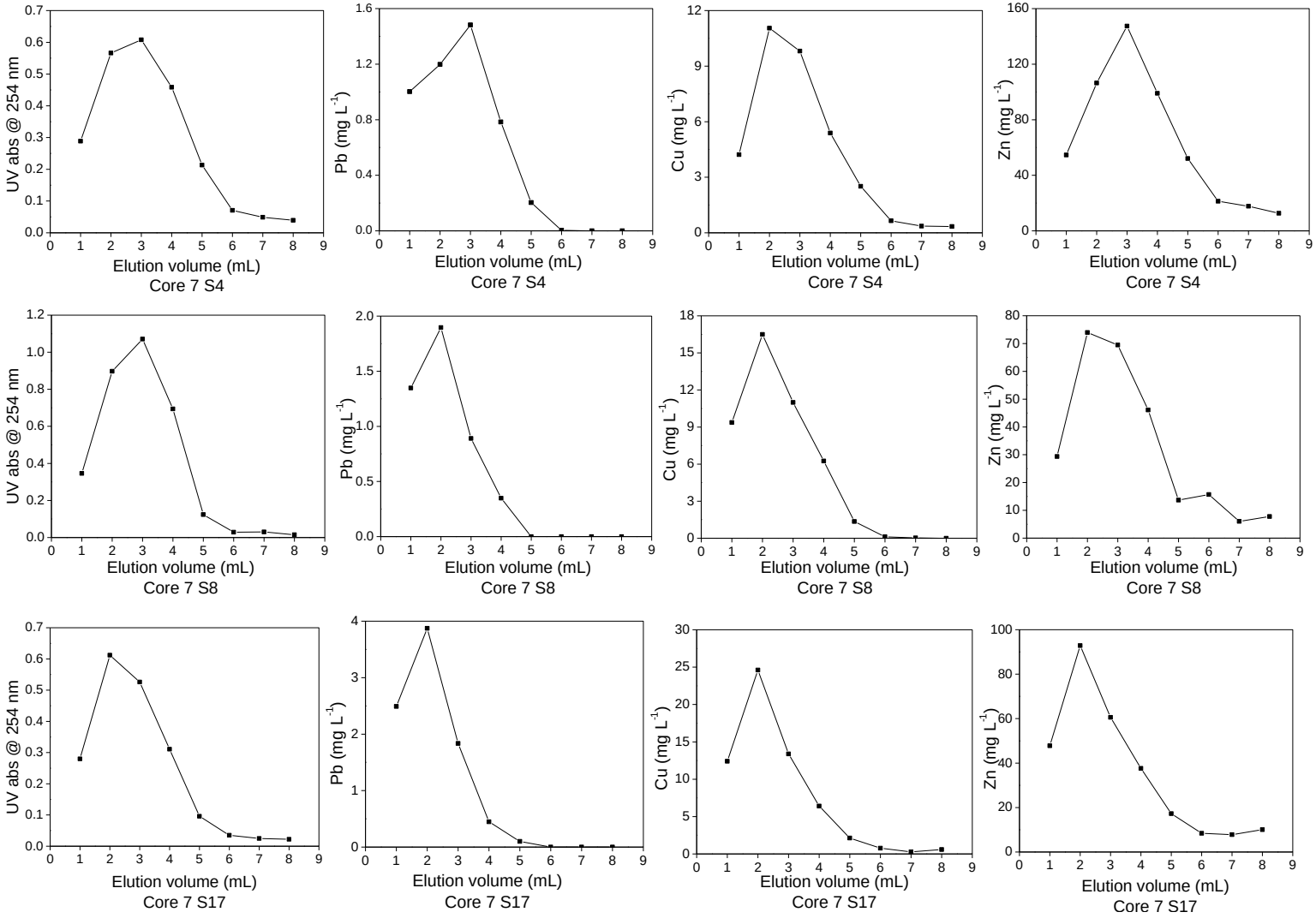
UV abs @ 254 nm
Pb (mg L-1)
Cu (mg L-1)
Zn (mg L-1)
Elution volume (mL)
Core 7 S4
Core 7 S8
Core 7 S17

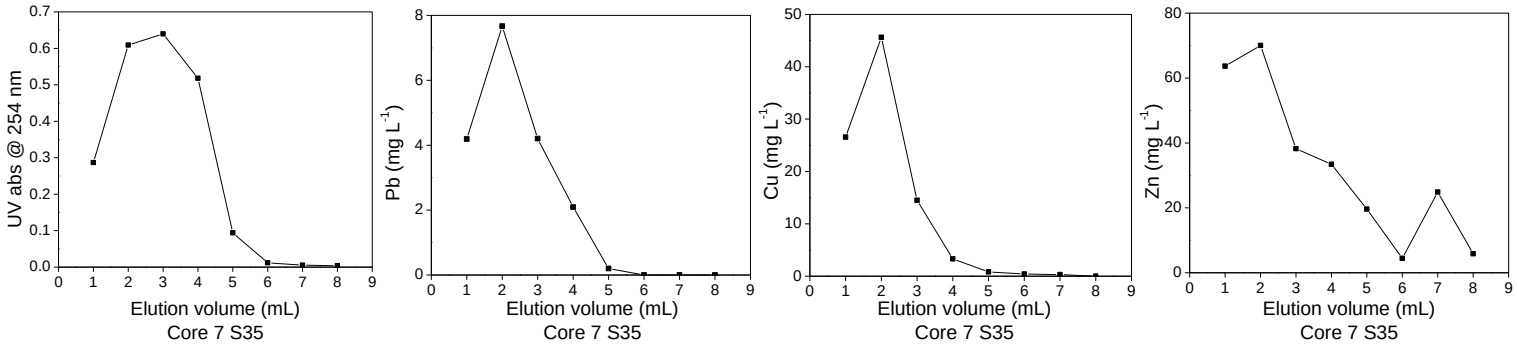

Figure 4.42: UV-visible absorbance at 254 nm and Pb, Cu, Zn concentrations for G200 gel filtration fractions for the S4, S8, S17 and S35 sections from Core 7

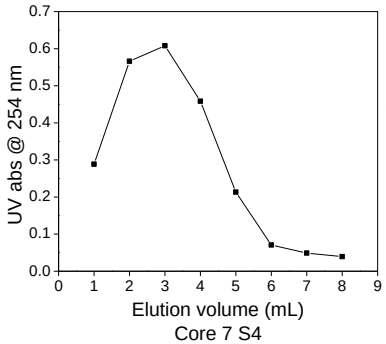
UV abs @ 254 nm
Elution volume (mL)
Core 7 S4

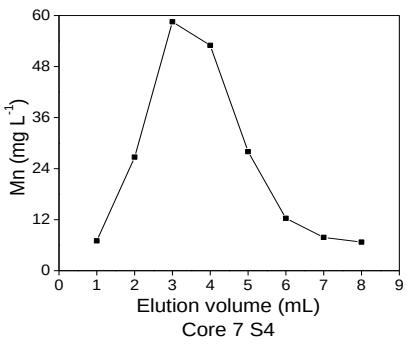
Mn (mg L-1)
Elution volume (mL)
Core 7 S4

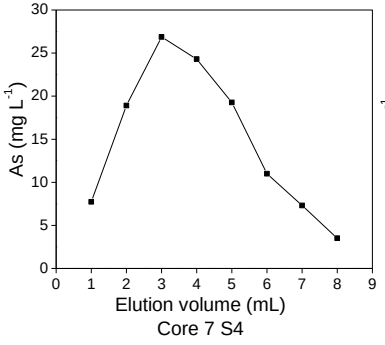
As (mg L-1)
Elution volume (mL)
Core 7 S4

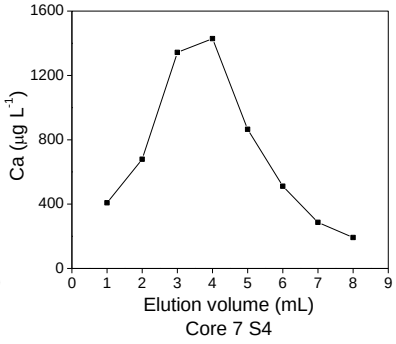
Ca (µg L-1)
Elution volume (mL)
Core 7 S4

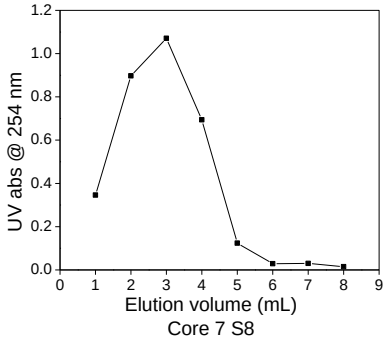
UV abs @ 254 nm
Elution volume (mL)
Core 7 S8

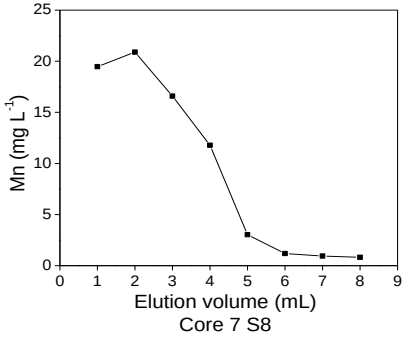
Mn (mg L-1)
Elution volume (mL)
Core 7 S8

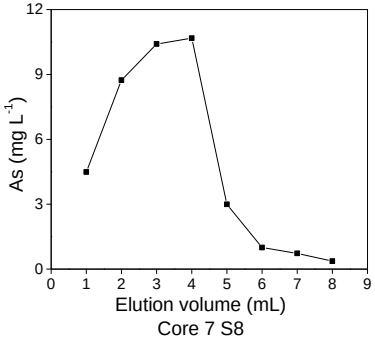
As (mg L-1)
Elution volume (mL)
Core 7 S8

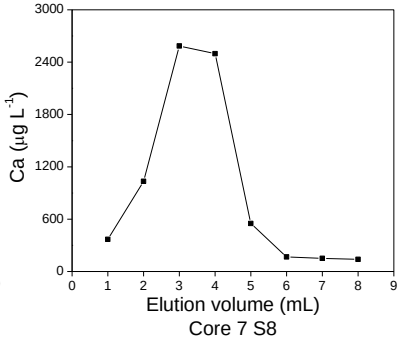
Ca (µg L-1)
Elution volume (mL)
Core 7 S8

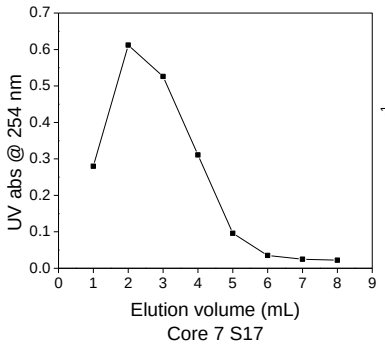
UV abs @ 254 nm
Elution volume (mL)
Core 7 S17

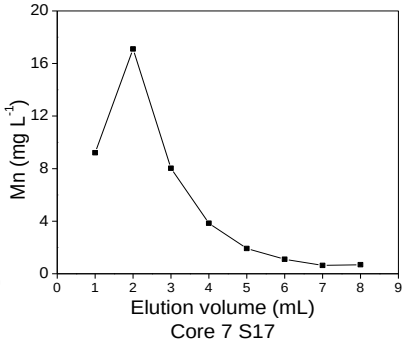
Mn (mg L-1)
Elution volume (mL)
Core 7 S17

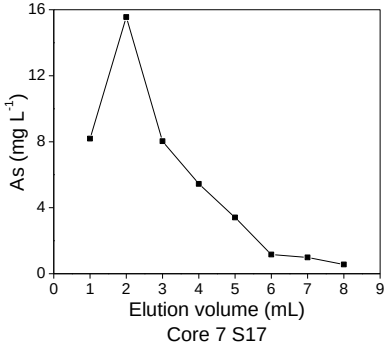
As (mg L-1)
Elution volume (mL)
Core 7 S17

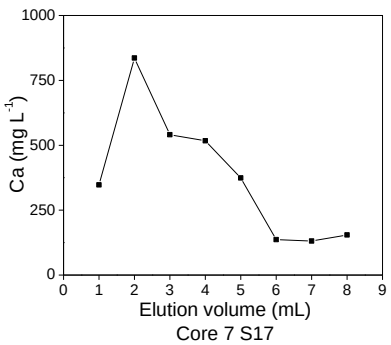
Ca (mg L-1)
Elution volume (mL)
Core 7 S17

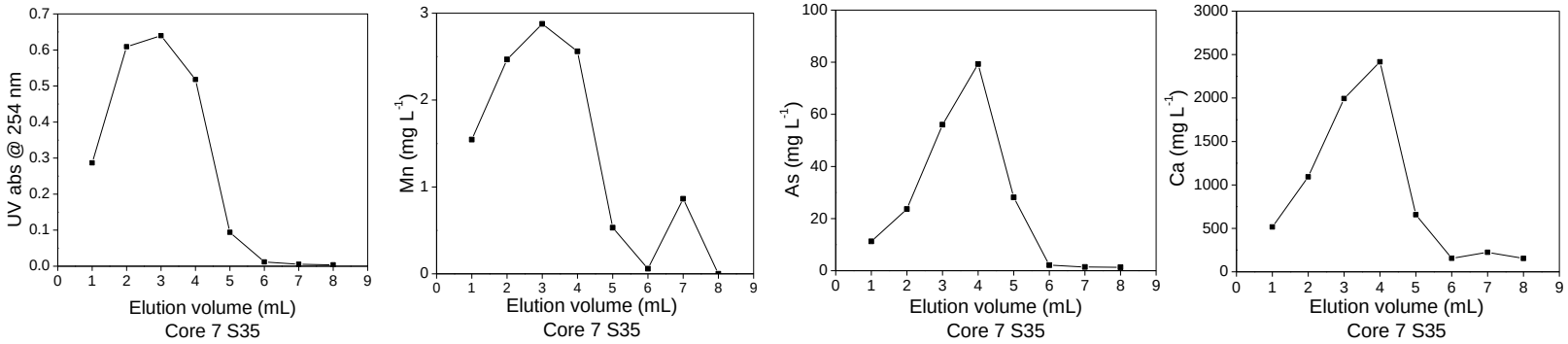

Figure 4.43: UV-visible absorbance at 254 nm and Mn, As, Ca concentrations for G200 gel filtration fractions for the S4, S8, S17 and S35 sections from Core 7

Figure 4.41 shows the UV absorbance at 254 nm and U, Fe, Al elution patterns for the colloids isolated from the Core 7 porewaters. The distribution of U was clearly influenced by that of the humic substances. The maximum U concentration was eluted after 2 mL for the colloid samples from all depths and this coincided with the position of humic substances maximum. A broader distribution of U was obtained for the nearest surface sample (S4), but with increasing depth, the U elution pattern became sharper and skewed towards the larger size fractions (see Appendix Table 9.50).

For the nearest-surface section (S4), maximum Fe and Al concentrations also eluted after 2 mL and coincided with the position of humic band (Figure 4.41). As for U, the elution patterns for Fe and Al became sharper and skewed towards the largest size fractions. In each case, however, the decrease in both Fe and Al concentrations after the maximum occurred more rapidly than for U.

Figure 4.42 shows the UV absorbance at 254 nm and Pb, Cu and Zn elution patterns for colloids isolated from the Core 7 porewaters. At each depth, the positions of the Pb and Cu maxima were coincident with the humic bands. In comparison with the other elements, the elution patterns for Pb and Cu were very similar to those for Fe; there was a broader distribution across humic size fractions in the near surface (3.5 cm depth) sample, but with increasing depth, they were skewed towards the larger fraction where a sharp peak eluted after 2 mL. The position of the Zn maximum was also coincident with that of the humic band. However, there was a less prominent peak observed in S8 and S35 after 5 mL elution, which indicates a small amount of Zn was not associated with the humic colloids. This phenomenon was also observed in the fractionation experiments described in section 3.5.1-2. For the proportion of Zn that was associated with humic band, a maximum concentration was reached after 3 mL elution at 3.5 cm depth; below this depth, a sharper peak was observed and a maximum concentration was reached after 1 mL elution at 35.5 cm depth. This again indicated a progression to association with larger humic molecules within the colloid fraction with increasing soil depth.

Figure 4.43 shows the UV absorbance at 254 nm and Mn, As, Ca distributions amongst colloidal fractions. Although Mn, As and Ca eluted in brown coloured fractions between the exclusion and permeation limits, the maximum concentrations of these elements often eluted after the maximum concentration of the humic substances, e.g. the maximum Mn

concentration eluted after 3-4 ml whilst the UV maximum appeared after 2-3 ml for the colloids from the 3.5 cm depth sample. There was no consistent trend for Mn, As and Ca with increasing depths, but, in contrast with U, Fe, Al, Cu, Pb and Zn, these elements tended to be associated with the humics in the smaller size fractions. As mentioned above, the Mn maximum occurred between 3-4 mL elution at 3.5 cm, but shifted to the larger size fractions and became more widely distributed, e.g. it eluted between 1-4 mL at 7.5 cm. Below this, the elution pattern became very sharp with a maximum at 2 mL for the 16.5 cm sample. The Mn distribution for the 35.5 cm sample was split into two parts, one eluted between 1-4 mL was associated with humic colloids and the less prominent one eluted in 7 mL which was not associated with humic colloids. Arsenic was quite widely distributed across the humic fractions in the near-surface sections but the elution pattern became increasingly sharper and skewed towards the larger size fractions by 16.5 cm. However, at 35.5 cm, As was primarily associated with smaller humic fractions. Calcium had a very similar distributions to As in that it was associated with smaller humic fraction in colloids from the 3.5 cm and 7.5 cm samples, but it skewed towards the larger size fractions at 17.5 cm before returning back to be with smaller humic fractions at 35.5 cm depth.

Observations and initial interpretation

The key features of the gel filtration results were:

(i) the analysed elements were mainly divided in two groups: U, Fe, Al, Zn, Cu, Pb were mainly associated with large humic colloids; Mn, As and Ca were mainly associated with smaller colloids;

(ii) the humic-Fe-U entities migrated together through the gel, which provided strong evidence that these components in the porewater are genuinely associated with each other;

(iii) Ca was present in high concentrations in the water samples and is likely to influence the speciation of truly dissolved U. However, it is clear that Ca associated with a different fraction of humic substances, and thus no humic-Fe-Ca-U colloids were obtained except perhaps Core 7 S17 at 16.5 cm depth, where the position of the solid phase carbonate maximum occurred (see Figure 4.36).

4.4 Results from sampling trip 5 on 11/10/2011

In sampling trip 3 (see section 4.2.2, Figure 4.30), it was found that Fe from Core 6 (20 cm from the mineralisation) was predominantly in colloidal (3 kDa-0.2 μm) form at 0-25 cm and below this, a much greater amount of Fe was in the truly dissolved (<3 kDa)fraction.Under the near-neutral conditions in the boggy soils, it was hypothesised that the colloidal Fe would be in the form of Fe^{III} while Fe in the dissolved phase would be in the form of Fe^{II}.

Core 8, which was located 25 m from mineralization, was used for investigation of Fe^{III}/Fe^{II} distribution at Needle's Eye. This was because a much higher amount of Fe could be detected at 25 m according to data from Cores 4 and 7. The porewaters from Core 8 were extracted from the soil at the sampling site. Ferrozine, a chemical that forms a magenta complex directly with Fe^{II} (see section 2.4.17), was added immediately to the porewater at the sampling site to prevent oxidation of Fe^{II} in the porewater.The Fe^{II} concentrationswere determined 3 hours later when the samples were transported to the laboratory whilst total Fe in the porewater was analysed later by ICP-OES.

The result showed that Fe in Core 8 was mainly present as Fe^{II} at all depths (Figure 4.44, Appendix Table 9.53), which indicated Core 8 had quite reducing conditions with most of the Fe in the form of Fe^{II}. The shape of the profile was very similar to that obtained for Core 7 and the Fe concentrations were also in comparable range. Thus it is likely that even where colloidal Fe is present, it is in the form of Fe^{II}. Under slightly acidic to circumneutral conditions, the colloidal forms may include $Fe(OH)_{2\,(am)}$ and HS-"Fe^{II}" species.

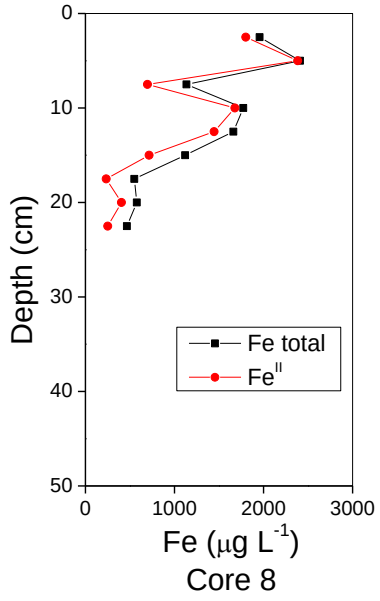

Figure 4.44: Total Fe and Fe^{II} concentration depth profile for Core 8 porewaters

4.5 Conclusions

The main findings relating to site characteristics and uranium distributions and associations from each of the four sampling trips described in this chapter were:

Trip 2

(i) The soil porewater pH values were slightly acidic to circumneutral; at 20-25 m from the cave, the soil environment was highly reducing - in contrast, the cave waters were oxic; at 20-25 m from the cave, the soils had very high organic content and the porewaters were also organic-rich; there was a major change to a more mineral-rich soil composition at depth of ~25 cm;

(ii) Aqueous phase U concentrations decreased ~20-fold from ~210-240 μg L^{-1} to ~10-15 μg L^{-1} over a distance of 35 m from the cave; U concentrations also varied with depth

and maximum values of ~85, 6.5 and 9.2 μg L^{-1} were obtained at 16.5, 10.5 and 7.5 cm depth at 20, 25, and 35 m from the cave, respectively;

(iii) Solid phase U concentrations also decreased with increasing distance from the mineralisation; again, concentrations varied with depth and maximum values of ~2400, ~190 and ~110 mg kg^{-1} were reached at ~20, 13.5 and 7.5 cm depth at 20, 25 and 35 m, respectively, from the cave;

(iv) Maximum aqueous phase concentrations at sampling locations 20 and 25 m from the mineralisation occurred at ~3 cm above those in the solid phase and were coincident with the aqueous and solid phase Fe concentration maxima;

(v) Nearly half to three-quarters of porewater U was present in the large colloid fraction. This fraction contained most of the brown humic material that was present in the porewaters. In addition, the large colloid fraction contained the vast majority of porewater Fe, Al and, in some cases, Mn. Thus it is not possible to deconvolute the roles of inorganic and organic colloids in determining U behaviour in the porewaters;

(vi) Sequential extraction targeting different Fe phases revealed that U was mainly extracted in the "carbonate-bound" and "crystalline oxide-bound" fractions; the importance of the former increased whilst the latter decreased with increasing soil depth;

(vii) Very little Fe was extracted in the "carbonate-bound" fraction and separate experiments using hydrochloric acid confirmed that dissolution of Fe carbonates was not responsible for the release of U by sodium acetate;

(viii) The decreasing amount of U in the "crystalline oxide-bound" fraction, however, was

matched by a decrease in Fe present in this form;

(ix) The gradual transformation of Fe from oxides to sulphides, suggested by the sequential extraction data and with further supporting evidence from measurements of TRIS and AVS, was not accompanied by a transformation in U associations in the solid phase.

(x) XRD characterisation identified five minerals containing Fe but quantification was unreliable due to the relatively high detection limits for XRD; however, the presence of Fe oxides means that there will be positively charged surfaces available for sorption of negatively charged uranium species and/or U-humic colloids; clays such as illite were also identified and these provide negatively charged surfaces for sorption of positively charged uranium species, for ion exchange and/or for interaction of uranium species via bridging ions; calcite was the main carbonate phase identified and its concentration decreased with distance and soil depth;

(xi) SEM-EDX revealed that there were very few crystalline particles present in the peaty soils. Only two grains containing U (in the form of uraninite) were observed; a small number of Fe-containing particles were identified – no U was detected in these particles;

(xii) Humic extraction followed by selective or sequential extraction and then gel electrophoresis showed that up to ~70% humic-bound U was removed from the humic material; about one-third of this U was removed by sodium acetate and the remainder was removed by sodium dithionite; the form of U that was removed by acetate is unclear but the latter was most likely associated with crystalline Fe oxides which were in turn associated with the humic substances;

Trip 3

(i) From a transect running southwards 30 m from the cave, U concentrations in groundwater decreased ~20-fold from ~550 to <3 μg L^{-1}; Ca concentrations showed a similar distance-related trend;

(ii) The highest concentrations of the other elements were found for soils with the highest DOM content; there was a major change in speciation as U entered the boggy soils and the distance-related trend in colloidal U correlated strongly with the DOM content of the transect porewaters;

(iii) The changes in U speciation along the transect are important when considering processe controlling its removal to the solid phase;

(iv) For a vertical soil profile taken at 20 m from the cave, the maximum U concentration was again observed at ~15-20 cm depth; Fe and Cu maxima were also observed at this depth and there was good agreement with the results for Core 3 from trip 2;

(v) Although there was still a significant proportion of U and Fe associated with colloidal material, the results for ultrafiltered porewaters revealed a trend of decreasing colloidal association of U, Fe, Mn and Al with increasing soil depth;

(vi) Carrying out the porewater isolation and ultrafiltration under N_2 only had a significant effect on U distribution below ~30 cm depth, where the "in-air" results gave an ~10% greater association with porewater colloids; this was attributed to partial oxidation of Fe and the formation of Fe colloids with which the U became associated;

(vii) Sodium acetate extraction of the porewater colloids released >85% of the colloidal U; in general, all of the elements (U, Fe, Mn, and Al) were more readily extracted by this reagent from the porewater colloids than from solid phase humic substances;

(viii) Finally, solid phase carbonate concentration generally decreased with increasing soil depth, in agreement with the XRD results for calcite. A sharp peak at ~17 cm coincided with the porewater Fe and U concentration maxima.

Trip 4

(i) Analysis of porewaters obtained from a core collected at a distance of 25 m from the cave during summer showed that the maximum concentrations of U and Fe do not always coincide and this was attributed to variations in the prevailing redox conditions;

(ii) Following isolation of the porewater colloids, gel chromatography was used for colloid fractionation because the colloids could be recovered for UV as well as ICP-MS analysis. With the exception of Zn and Mn, all of the elements analysed by ICP-MS eluted along with the brown-coloured colloids;

(iii) Two groups of elements were identified; U, Fe, Al, Zn, Cu and Pb were mainly associated with large humic colloids whilst Mn, As and Ca were mainly associated with smaller colloids;

(iv) Importantly, it was demonstrated that U, Fe and humic substances were genuinely associated with each other within the soil porewaters.

Trip 5

(i) The shape of the Fe porewater profile for Core 8 was very similar to those obtained for Core 7 and it was shown that almost all of the Fe was present as Fe^{II}, confirming that strongly reducing conditions prevailed even in the near-surface sections of the peaty soils at this location.

5 Synthesis and Discussion

The original hypothesis of this project was that U derived from the natural mineralisation at Needle's Eye was immobilised by direct interaction with OM in the boggy soils at the base of the cliff (Figure 2.3). This was based on previous work, e.g. by MacKenzie et al. (1991), which showed that 80-90% U was retained by OM within the boggy Needle's Eye soils. Other work by Read et al. (1993) concluded that U was strongly held by direct interaction with OM in Broubster peaty soils, NE Scotland. Regenspurg et al. (2010) also showed that U was almost entirely bound to OM in organic-rich soils in Dischma, Switzerland. While the results presented in sections 3.5.1 and 3.5.2 again showed that U was associated primarily with very large humic molecules, it quickly became clear in this study that the mechanisms by which U is immobilised were more complicated and that, in particular, the inter-relation between U-Fe-OM in organic-rich soils was not well-understood. Therefore the main part of this PhD project was re-focused to investigate these relationships as presented in Chapter 4. The purpose of this chapter is to combine the results from all of the sampling trips (Chapters 3 and 4) to address the following questions:

(i) Is the change in the aqueous speciation of U when the waters emerging from the cliff comes into contact with the boggy soils attributable to the presence of organic/inorganic colloids or to the change in redox status?
(ii) How is U retained within the boggy soils and how does this relate to its aqueous phase speciation?
(iii) Do transformations in U associations occur within the soil and, if so, do these influence its mobility?
(iv) What forms of U are transported out of the boggy soils towards the saltmarsh?

and then to set the findings in the context of the wider literature.

In section 5.1, the ancillary data for pH, DOM, SOM, SoilAl will first be used to characterise the geochemical and hydrological conditions prevailing at the Needle's Eye site. Then, in section 5.2, the near-surface water data for the lateral transect will be used in conjunction with the vertical soil porewater profiles to establish the effect of changing conditions on U mobility. Section 5.3.1-3 will consider the solid phase soil profiles and the possible mechanisms by which U is being removed from groundwater at the Needle's Eye Site. Section 5.3.4 will consider the evidence from sequential extraction experiments relating to the role of Fe minerals in U removal processes. Section 5.3.5-6 will address the issue of Fe binding to organic matter and attempt to distinguish between U interactions directly with organic matter and those which involve interactions with OM-bound Fe. Finally section 5.4 will focus on the U remaining in the soil porewaters and establish the nature of interactions between U and the porewater colloids that are being transported out of the boggy soils.

5.1 Geochemical and hydrological conditions at the Needle's Eye site

5.1.1 Vertical porewater pH and DOM profiles for Cores 3-7

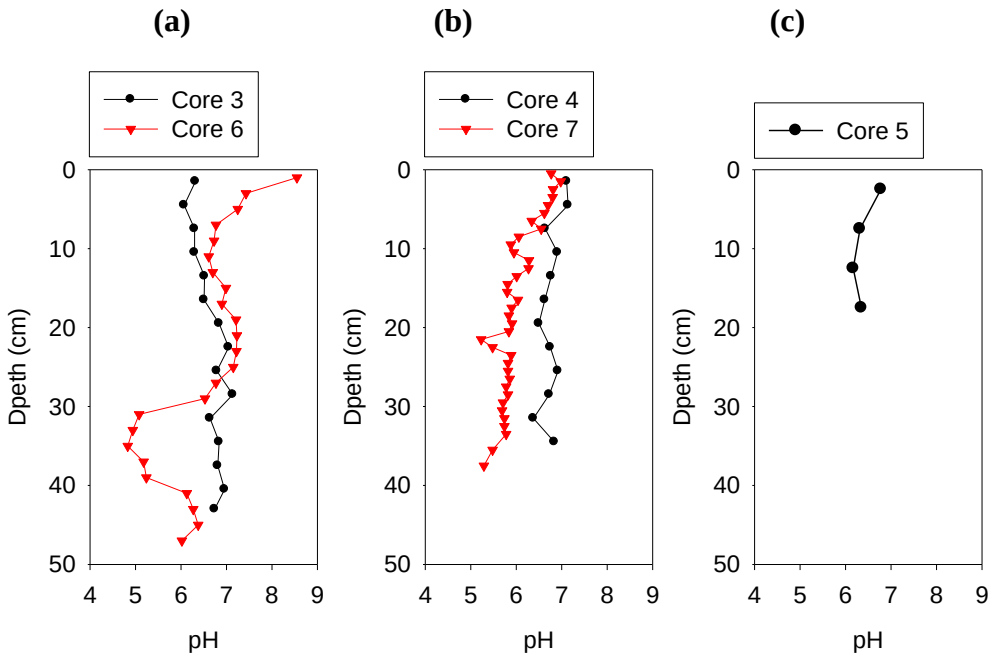

Figure 5.1: Soil porewater pH values in Cores 3-7: (a) cores 3 and 6, (b) cores 4 and 7 and (c) core 5 are located 20 m, 25 m and 35 m, respectively, from the uranium mineralisation

Soil porewater from Cores 3-7 were mainly found to be slightly acidic to near-neutral, and the ranges of soil porewater pH values in these cores were 6.1-7.1, 6.4-7.1, 6.2-6.8, 4.8-8.6, 5.2-7.0, respectively. These pH values were typical of those measured in groundwaters from the boggy area during a previous study at Needle's Eye (Jamet et al., 1993). Although, Jamet et al. (1993) collected groundwater from 1.00-1.80 m depth, the values were still in the range 5.9-7.1. Jamet et al. (1993) observed some variation in pH across the boggy area: the part closest to the cliff had constant values of ~6.5 over the depth interval 1.00-1.80 m but with increasing distance in the seawards direction, there was a decrease in pH from

6.8-7.1 at 1.2-1.4 m to 5.9-6.2 at 1.8 m depth. The reasons for these variations were not specifically discussed in Jamet et al. (1993) but it has been documented that there is a second peaty layer at depth and this may account for the lower pH values.

In this study, there was a common trend of decreasing pH with increasing depth: surface values of ~6.8-8.6 decreased to ~5.3-6.8 towards the bottom of Cores 4-7. Although the pH of UK rainwater has increased over recent years (Curtis and Simpson, 2012), it is unlikely that values of ≥6.8 would be observed. Thus, the high values at the surface likely reflect the influence of surface flows of carbonate-rich waters derived from the cliff (Hooker, 1989). Piezometric measurements indicated positive water pressures near the base of the cliff and extending across the boggy area. The high flow at the base of the sediments had the highest hydraulic pressure. The rest water level is close to slightly (0-5 cm) above ground level (Hooker, 1989).

Cores 3 and 6: 20 m from the cave

The Core 3 profile was the exception to the above, with values of ~6.1 at the surface and then values of ~6.6 below 20 cm depth. Moreover, although Core 3 and Core 6 were both located at ~20 m from the mineralization, the general shapes of the vertical profiles were very different. There was a trend of increasing pH over the 0-20 cm depth interval for Core 3 but a general trend of decreasing pH for Core 6 (Figure 5.1(a)). Although collected in different years (2008 and 2010, respectively), both were collected in October and so the reason for the variations was not seasonally related. A potential explanation may involve the soil porewater DOM. The DOM (absorbance at 254 nm used as proxy) profiles for these two cores were, at a first glance, very similar in that the highest values were found for the surface section, there was a sharp decrease of the 0-5 cm depth sections and then a gradual decline in absorbance towards the bottom of the profiles. However, there was approximately twice as much DOM present in the Core 3 porewaters compared with those for Core 6 (Figure 5.2(a)). The lower pH values for the near-surface sections may therefore

be attributable to the much higher DOM concentrations.

Both Cores 3 and 6 also have slightly higher pH values of ~7.2 at ~20 cm. Although not conclusive, these higher pH values at ~20 cm depth may be indicative of lateral flow of groundwater from the mineralisation. The emerging waters from the cliff were ~7.6-7.8, again in good agreement with those published by Hooker (1989) and Jamet et al. (1993). Interaction with groundwaters along the flow path, especially those containing DOM could account for the lowering of the pH from 7.6-7.8 to ~7.2. It is well-documented that such flow paths exist at the Needle's Eye Site (Hooker, 1989; Jamet et al., 1993) and their existence has been attributed to the permeability variations within laminated silts which underlie the boggy area and which impose a horizontal vector upon the groundwater flow (Hooker, 1989). The vertical depth at which such flows operate may vary depending on the actual sampling location and perhaps may also be affected by seasonal factors. Further evidence for the positioning of a lateral flow of cliff-derived groundwater will be considered in the sections that follow.

Cores 4 and 7: 25 m from the cave

In contrast with the profile described for Core 3, Cores 4 and 7, both located at ~25 m from the cliff, showed similar trends of generally decreasing pH towards the bottom of the core (Figure 5.1(b)). These cores were collected in October 2008 and June 2011, respectively, and so again there was no obvious seasonal effect on the profile shapes.

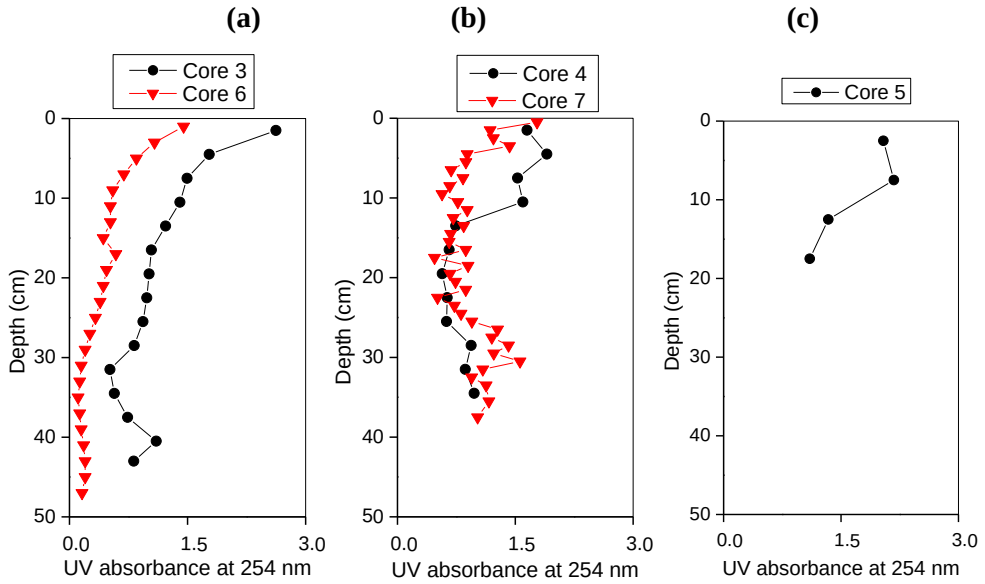

Figure 5.2: Comparison of the DOM (UV absorbance at 254 nm used as proxy profiles for (a) Cores 3 and 6; (b) Cores 4 and 7; (c) Core 5

The DOM profiles for Cores 4 and 7 were in reasonably good agreement with each other and also with those for Cores 3 and 6, with higher values in the near-surface sections and then a general decrease with increasing depth (Figure 5.2(b)). Although the high surface pH values are most likely indicative of cliff-derived surface flows, the high DOM concentrations at the surface are not; the absorbance values for the waters emerging from the cliff are extremely low and the waters were indeed crystal clear. In explanation, the boggy area is extremely organic-rich and the trend of decreasing DOM with increasing depth is fairly typical for organic soils, e.g. Xi et al. (2007), reflecting the rapid initial breakdown of fresh organic matter to form less soluble, more stable forms of OM. Figure 5.3 shows the relationship between DOM and solid phase OM for Cores 3-5.

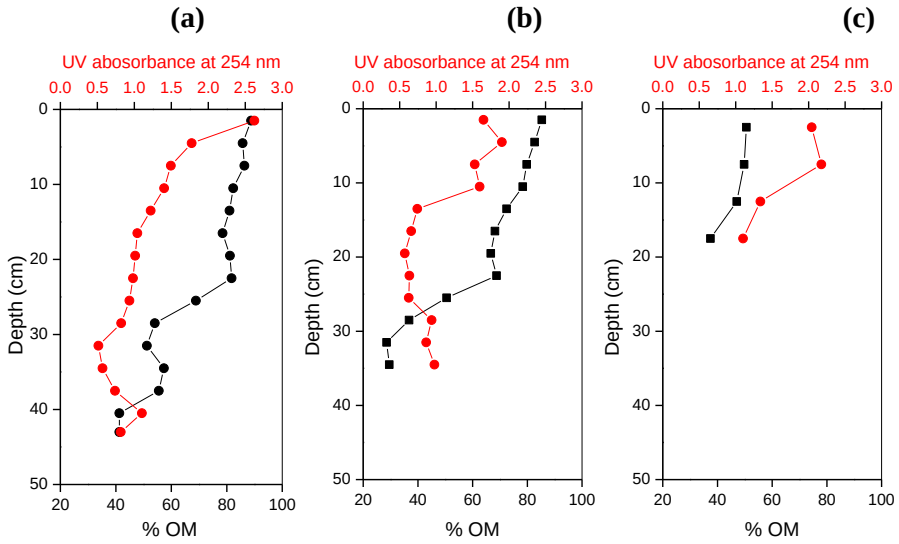

Figure 5.3 (a)-(c): Comparison of DOM and SOM profiles for Cores 3-5

The solid phase OM profiles for all three cores show slight decreases with increasing depth down to ~25 cm (~20 cm for Core 5) whilst the DOM profiles showed a more rapid decline over the top 0-10 cm (Figure 5.3 (a)-(c)). This relationship is, however, quite commonly observed in organic-rich soils and, as noted above, simply reflects the rapid decrease in the amount of soluble organic matter which is accompanied by a much slower loss of stable soil OM. Below 20-25 cm in Cores 3-4, however, there is a major change in the OM content, indicative of a transition to a more mineral-rich solid substrate.

5.1.2 Solid phase OM, Al and carbonate profiles for Cores 3-6

The elemental composition of the solid phase soil was further examined and it was determined that there was a marked increase in the concentration of Al at the same depth as the decline in solid phase OM in Cores 3-4 (Figure 5.4(a)-(b)).

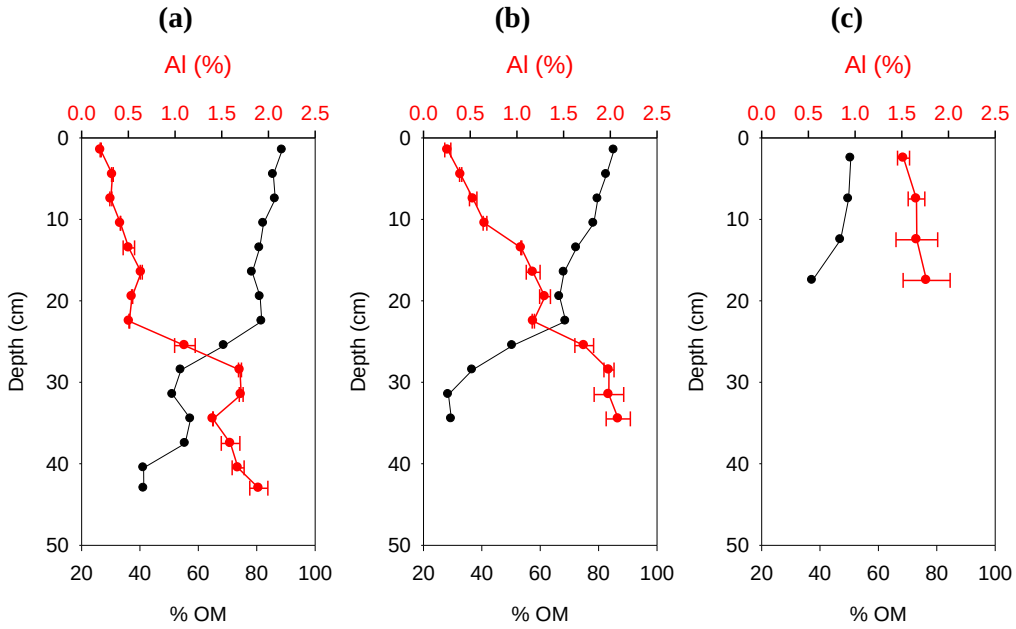

Figure 5.4 (a)-(c): Core 3, 4 and 5 %OM (w/w) and %Al (w/w)

For Core 5, the OM content in the top 0-20 cm section was lower than that for Cores 3-4 and this was accompanied by a generally higher Al content (Figure 5.4(c)); at 35 m from the mineralisation, this core is considered to be from beyond the southern limit of the boggy area. Nevertheless, the OM content is still significantly greater than in the saltmarsh sediments (2-3% OM w/w) which form part of the Southwick Merse (Allan, 1993; Graham, 1995). Aluminium content has been used widely in studies of ombrotrophic peats as a measure of crustal-derived mineral inputs from the atmosphere (e.g. Shotyk et al., 2002) and it is proposed that it can also be used in this context as a proxy for mineral content of the organic-rich Needle's Eye soils, specifically to indicate transitions to mineral-rich materials which are known to occur at the Needle's Eye site (Hooker, 1989). The total concentration of Al may only be ~2% (w/w) but this would equate to a soil content of, for example, 17.8% (w/w) K-feldspar ($KAlSi_3O_8$), a common primary mineral identified by XRD in these soil samples (Section 4.1.9; Table 4.5). The XRD results showed that the total feldspar content (Na, K and Ca) was approximately 10% w/w towards the bottom of core 3 and there was a trend of increasing concentration with increasing soil depth. Other

likely contributions to the increased mineral content will be from Si present as quartz (SiO_2), which is a ubiquitous feature of almost all mineral soils. Although Si was not directly measured in this study, the XRD results showed that greater amounts of quartz were present in samples from the bottom of the core, e.g. ~25% and 50% w/w for Cores 3 and 4, respectively (Table 4.5). Consequently, the decrease from ~80% to ~40% in OM content can be readily explained.

The position of the transition from organic-rich to mineral-rich soil may be highly significant since the higher density, underlying mineral-rich soil may be influential in directing the lateral sub-surface flow of carbonate-rich waters emerging from the mineralisation. To this end, carbonate determination was carried out on the solid phase soils from Core 6 (Figure 4.35). The general trend was of higher concentrations at the surface of the soil and then a gradual decrease with increasing soil depth. This likely reflects the long-term surface flow of carbonate-rich waters from the mineralisation through the boggy area. This trend is also in agreement with the XRD data for Core 3 (collected at the same location), which showed a decrease in calcite concentration with increasing soil depth (Table 4.5).

Although not a strong relationship, the general trend of decreasing carbonate concentration was in reasonable agreement (r^2=0.49) with the overall decrease in pH with increasing depth (Figure 5.5) for this core and so there is a plausible explanation for the general pH trends observed in the boggy area.

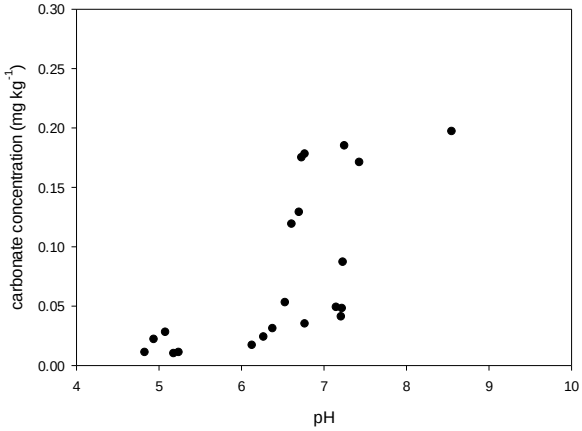

Figure 5.5: Relationship between solid phase carbonate concentration and soil porewater pH (omitting the two peak points in carbonate concentration)

The sharp peak in carbonate content was not reflected in a change in porewater pH nor in a change in DOM. It is postulated that water flowpath from the mineralisation is affected by the underlying mineral-rich substrate and that oversaturation with respect to calcium carbonate occurs just above this transition. Thus the sharp peak in Figure 4.36 is indicative of a significant oversaturation and removal of calcite ($K_{SP} = 3.36x10^{-9}$) to the solid phase.

5.1.3 pH and DOM in emerging waters and surface (0-5 cm) soil porewaters along a lateral transect southwards from the mineralisation

In order to advance the interpretation relating to prevailing conditions at the Needle's Eye site, it is now useful to consider the pH and DOM for the surface (0-5 cm) soil porewaters obtained for a transect running from the base of the cliff southward to the edge of the boggy area.

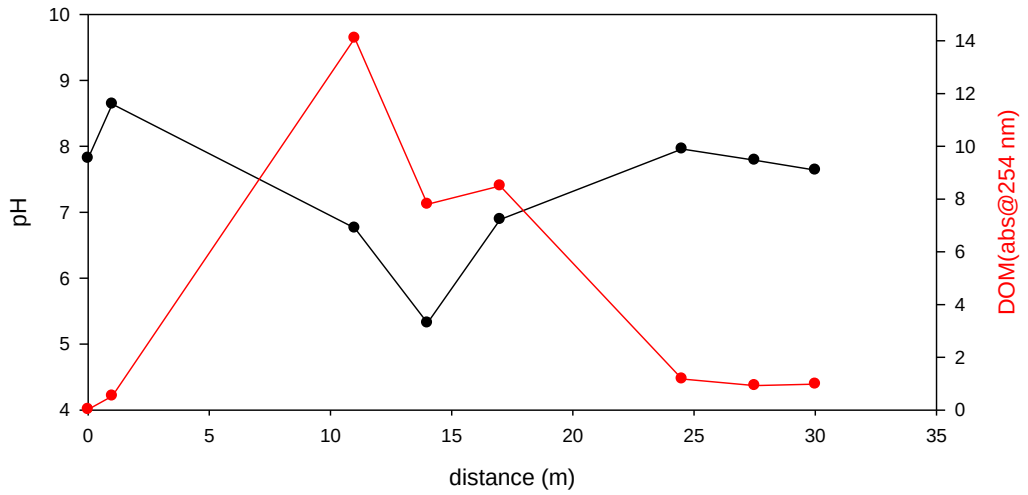

Figure 5.6: pH and DOM for water emerging from the cliff and in soil porewaters obtained from 0-5 cm soils along a 30-m transect southwards to the edge of the boggy area

Following collection of the waters emerging from the cliff, the first surface soil sample was taken at a distance of 1 m, which corresponds to the outer edge of the cave at the base of the cliff. It was not possible to get any soil samples between 1 m and 10 m from the cliff due to the stony nature of the ground. The sample taken at 11 m represents the start of the boggy area and it is clear that, upon entering the bog, the pH for the surface soil porewaters dropped quite rapidly from values of ~8.6 to ~5.3 and the DOM content of the waters had increased markedly (Figure 5.6). With increasing distance towards the saltmarsh end of the bog, the pH of the surface soil porewaters increased to values of >7 and the DOM content dramatically decreased (Figure 5.6). Although the relationship between pH and DOM is not particularly strong (r^2=0.49) the locations with the highest DOM concentrations do have the lowest pH values and it is clear that the pH of the surface waters flowing from the cliff is most strongly modified by the presence of DOM at the northern end of the boggy area.

Overall, the surface soil porewater pH data are consistent with the flow of carbonate-rich waters from the cliff which are impacted by DOM deriving from the boggy soils at

distances of ~11-25 m along the surface flow path.

5.2 Mobility of U in surface and groundwater flows emerging from the mineralization and traversing the boggy soils at the base of the cliff

5.2.1 Lateral transect from the cliff base traversing the boggy soils

Past work showed that the ancient cliff at Needle's Eye contains leachable pitchblende within polymetallic-carbonate breccias veins. These act as a source of soluble uranium to the sedimentary deposits stretching from the base of the cliff in a seaward direction. The mobile species were shown to be U^{VI} carbonate complexes which are stable at Eh=+400 mV, pH 7.8 and $pCO_2=10^{-3.2}$ (Hooker, 1989). It is considered that these highly soluble U^{VI} complexes are transported via surface flow from the cliff and artesian flow from underlying rocks (Hooker, 1989) through the boggy area towards the coastal sediments. In this past work, the measured U concentrations in the drip waters from the cliff were up to 594 μg L^{-1} (Hooker, 1989).

Throughout the study period (October 2007-October 2011), the concentrations of U in the cave drip waters varied from ~30-250 μg L^{-1}. Several samples were collected on each occasion and the variability on any one sampling date was significantly smaller than that between sampling dates (Figure 5.7).

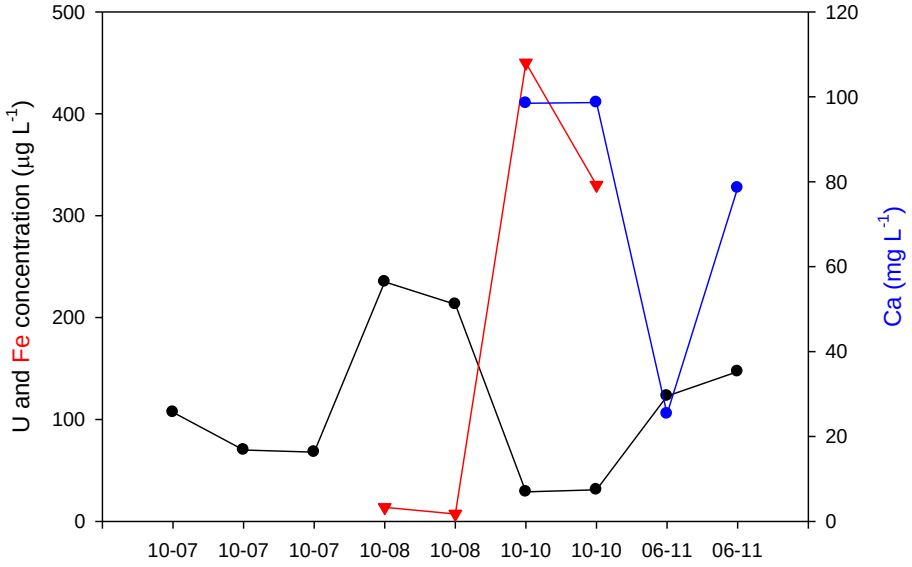

Figure 5.7: U, Fe and Ca concentrations in drip waters obtained from the cliff at Needle's Eye over the sampling period October 2007-June 2011

Although no flow rate measurements were made during this study, past work showed that there was an inverse relationship between flow rate and uranium concentration in the cave drip water (MacKenzie et al., 1991). Uranium concentrations ranged from ~20-150 µg L^{-1}, in close agreement with the ones obtained in this study. Since Smith (2004) states that the U concentration in natural waters is typically <1 µg L^{-1}, U concentrations in the cave waters are clearly elevated. Indeed all of the waters collected in this study and during previous work (Hooker, 1989; MacKenzie et al., 1991) contained U at concentrations close to or above the WHO safe level for drinking water of 30 µg L^{-1} (WHO, 2012).

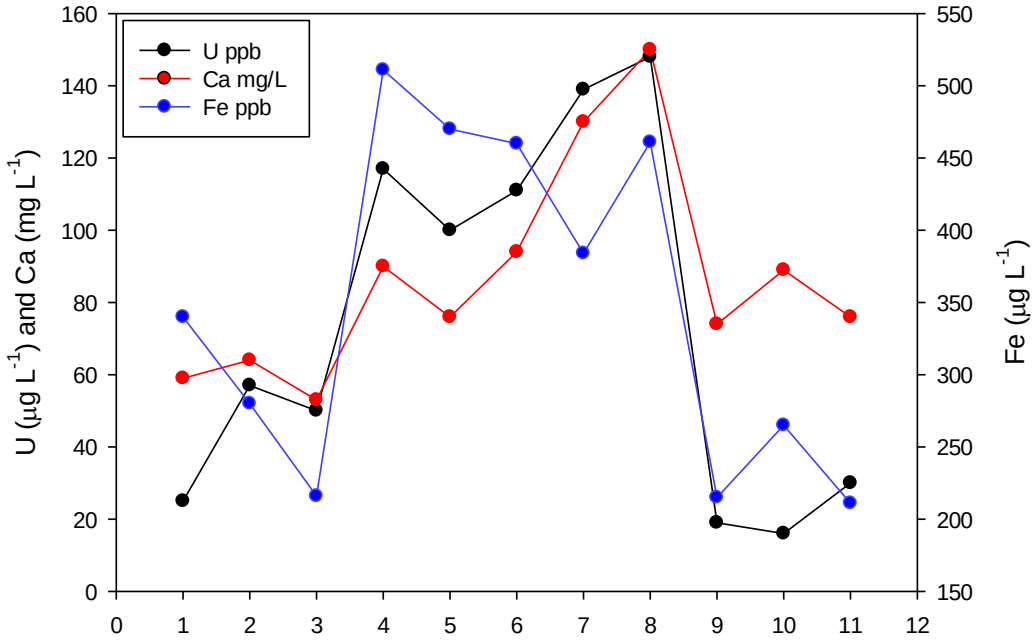

Figure 5.8: Monthly data for a 1-year sampling period 03/90-03/91 (adapted from MacKenzie et al., 1991)

From the limited data available from this study in conjunction with the previously published seasonal study (MacKenzie et al., 1991), there is no clear relationship between U and Fe concentrations or between Ca and U concentrations (Figures 5.7-5.8). As expected on the basis of previous work (Hooker, 1989; MacKenzie et al., 1989), however, the cliff waters were oxidizing (Eh=~300 mV) and as such U^{VI} would be the prevailing OS. In carbonate-rich waters, at pH 7.6-7.8, the main species is likely to be $UO_2(UO_3)_3^{4-}$ with smaller amounts of $UO_2(CO_3)_2^{2-}$. In waters with significant Ca^{2+} concentrations, $Ca_2UO_2(CO_3)_3^{0}$ and $CaUO_2(CO_3)_3^{2-}$ are thought to be the dominant species (Kelly et al., 2007). In this study, Ca concentrations of ~80-100 mg L^{-1} equate to 2000-2500 µM Ca^{2+}. According to Figure 1.22, the main species in solution are likely to be $CaUO_2(CO_3)_3^{2-}$ (~60%), $Ca_2UO_2(CO_3)_3^{0}$ (~25%), $UO_2(CO_3)_3^{4-}$ (~15%) (Guillaumont and Mompean, 2003).

Other workers have also observed the formation of ternary Ca-U^{VI}-CO_3 ternary complexes

(e.g. Bernhard et al., 2001) and have suggested that they may diminish enzymatic and chemical reduction rates (Brooks et al., 2003; Stewart et al., 2007; Neiss et al., 2007). Such complexation may thus inhibit the reduction of U^{VI} as the cliff waters enter the boggy soils at Needle's Eye.

Jamet et al. (1993) considered that leached U from the pitchblende veins in the cliff was transported in the groundwater for distances of up to 50 m from the base of the cliff (also Hooker, 1990; Hooker et al, 1986; Jamet, 1989a). Their transect extended into the Merse sediments but in this study we only looked at 30 m because this was the extent of the peaty area, marked also by the presence of marine debris beyond this point.

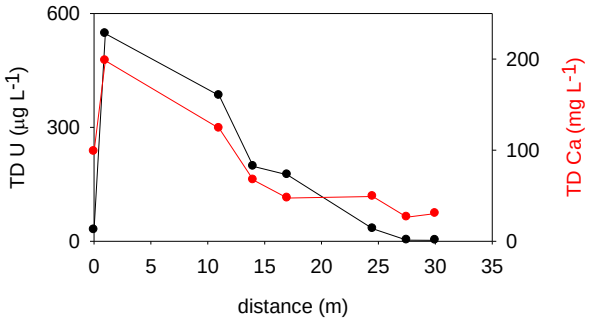

Figure 5.9: TD (<0.2 µm) U and Ca concentrations in soil porewaters along the southwards transect from the cliff base through the boggy soils

Figure 5.9 shows the relationship between total dissolved (TD) U and Ca concentrations in the porewater samples along the southwards transect from the cliff through the boggy soils towards the Southwick Merse sediments. The trends in TD U and Ca concentration with increasing distance from the mineralisation were relatively similar (r^2=0.933; Table 4.15); the highest porewater concentrations for both elements were obtained at the edge of the cave, followed by a gentle decline over 11 m and then a sharper decline between 11 and 14 m from the cliff base. The TD U concentrations continued to decrease towards the edge of the boggy area, whilst TD Ca concentrations remained relatively constant. A halving distance for U concentration of 10 m determined by MacKenzie et al. (1989) does hold for

the first 20 m from the cave but a decrease in TD U concentration of more than 100-fold was observed from ~11 m to ~30 m from the cliff base (Table 4.12). The major drop in TD U concentration by 24 m corresponded to the sharp drop in DOM (Table 4.11).

Clearly, upon entering the boggy area, both Ca and U are being removed from solution. This could be related to changes in: (i) pH (from 7.8-~5.5-6.5 in this study); (ii) extent of over-saturation with respect to certain minerals; (iii) redox potential (from 300 mV to ~48 mV by 25 m from the cave in this study); (iv) DOM (from ~0.025 to ~14 absorbance units in this study). Past work at Needle's Eye modeled U solubility on the basis of uraninite (UO_2) and liebigite ($Ca_2(UO_2)(CO_3)_3.10H_20$) saturation indices (Basham et al., 1989). It was possible to reproduce the U concentrations in groundwater based on the precipitation of liebigite, a U^{VI} phase (see section 1.4.1; Table 1.8), but SEM studies did not find it in the solid phase and the idea that U^{VI} would not be reduced was considered to be incompatible with prevailing redox conditions. Instead, Basham et al. (1989) invoked reduction and precipitation of UO_2 as the important removal process. In support, some uraninite-like phases were identified in the solid phase (Basham et al., 1989). However, Hooker (1989) commented that this model may not be satisfactory since it contradicted fission track results which pointed to organic matter as being directly responsible for the fixation of U. Thus, although it is clear that U is being removed from the water flowing along the transect, the mechanisms by which this is happening need to be re-examined.

The following paragraphs will consider the extent to which changes in pH/redox/DOM conditions along the flow path affect the behaviour of U and other elements that are present in the soil porewaters, leading to conclusions about the main mechanisms by which U is being removed from the transect waters.

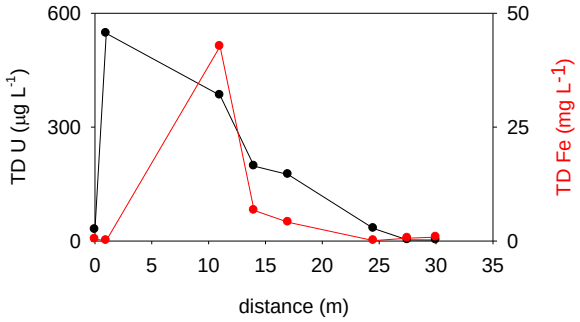

Figure 5.10: TD U and Fe concentrations in the surface (0-5 cm) soil porewaters along the southwards transect from the cliff base through the boggy soils

A strong contrast between TD U and Fe is evident in Figure 5.10; whilst TD U concentrations were highest at the cave edge, the maximum TD Fe concentrations were observed in the porewaters from the 11 m sample. The TD Fe concentrations decreased sharply from 11 to 14 m and then more gradually until the 24.5 m sample; a very slight increase was observed for the two samples furthest from the cliff base. The change from 11m to 14 m suggests a markedly different behavior for U and Fe which may be related to redox conditions and/or to the presence of dissolved humic substances in the boggy soil porewaters.

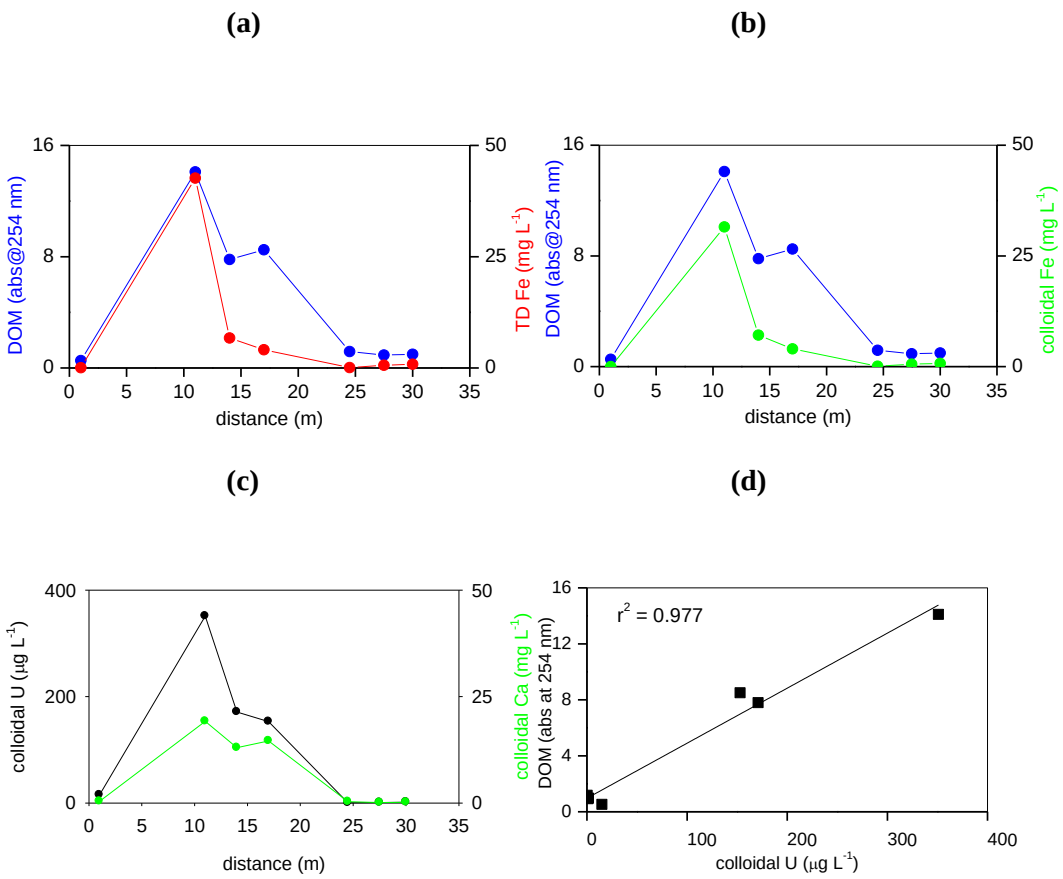

Figure 5.11: (a) DOM and TD Fe concentrations; (b) DOM and colloidal Fe concentrations; (c) colloidal U and colloidal Ca concentrations in surface (0-5 cm) soil porewaters along the transect from the cliff base southwards through the boggy area; (d) relationship between colloidal U and DOM concentrations

Figure 5.11(a) shows the good match between DOM and TD Fe concentrations in the first part of the transect but, at 14 m, the TD Fe concentration dropped markedly whilst there was a shoulder in the DOM profile (r^2 = 0.725; Table 4.15). Figure 5.11 (b) shows the same DOM data but this time includes colloidal Fe (3 kDa-0.2 µm). Almost all the Fe present in the soil porewaters is in the form of colloidal Fe and so there is no significant improvement in the relationship between Fe and DOM in the second part of the transect (r^2 = 0.774; Table 4.16).

Figure 5.11(c) shows the transect concentrations of colloidal U and colloidal Ca. In contrast with colloidal Fe, there was a good match between colloidal U and colloidal DOM (r^2 = 0.977; Table 4.16). This is indicative of a major change in speciation of U upon contact with the organic-rich groundwater of the boggy area. Although there was a trend of decreasing U concentration with distance from the cliff base, the U remaining in solution was primarily colloidal U whilst that in the cliff waters was truly dissolved U. As would be expected for Ca, only a small proportion was colloidally associated (Figures 5.11(c) and 5.9(a)) but the trend for colloidal Ca does match the DOM pattern (r^2 =0.965; Table 4.16).

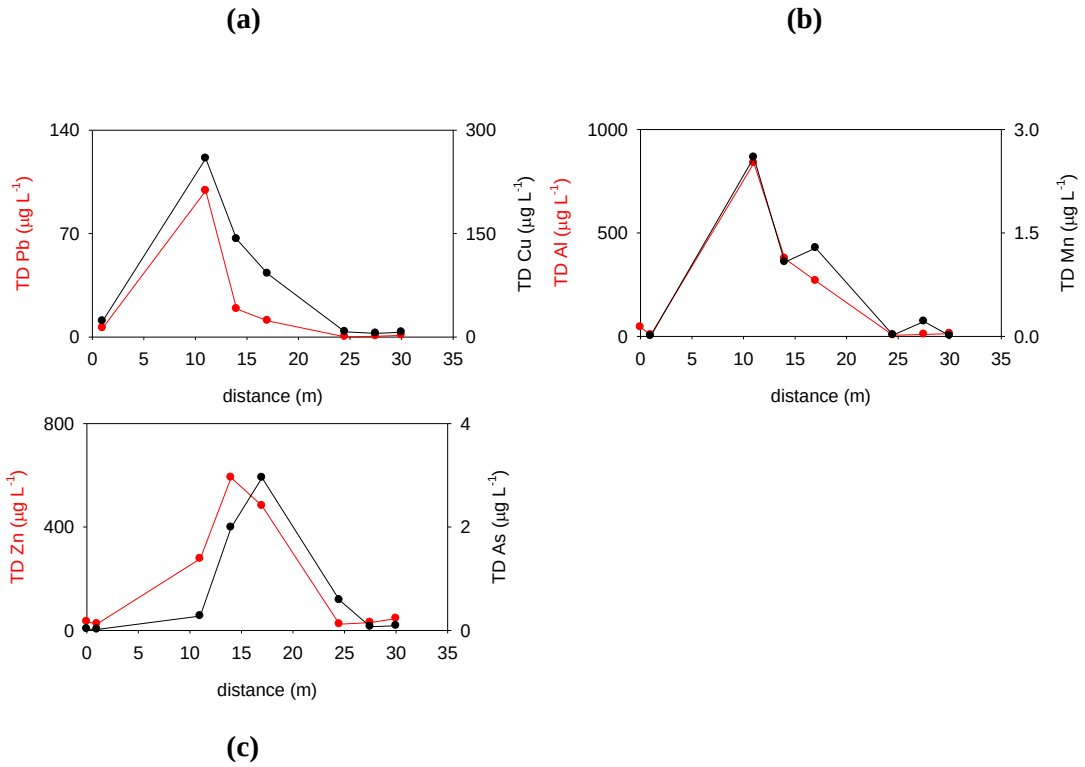

Figure 5.12: TD (<0.2 µm) (a) Pb and Cu; (b) Al and Mn; (c) Zn and As concentrations in surface (0-5 cm) soil porewaters along the transect from the cliff base southwards through the boggy soils

Figure 5.12(a) shows the TD Pb and Cu concentrations in solution. The pattern for TD Pb matched closely with that for Fe (r^2=0.995; Table 4.15) whilst that for TD Cu showed a little more similarity to the DOM profile (although no shoulder at 17 m). Figure 5.12(b)

shows the TD Al and TD Mn concentrations in solution. The pattern for TD Al was very similar to that for TD Cu while the pattern for TD Mn matched most closely the DOM profile. The latter might not be expected since Mn does not associate strongly with DOM; it does, however, form outer sphere complexes with humic substances (Gavin et al., 2001). Although there was a strong correlation between colloidal Mn and DOM (r^2=0.905) (Figure 5.13(b)), this represented only a small portion (10-40%) of total Mn (Figure 5.12(b)) and so the results were in keeping with the expected behaviour of Mn in aquatic environments.

The trends shown in Figure 5.12(c) were very different from those observed for all other elements since the peaks for TD Zn and TD As occur at 14 m and 17 m from the cliff base, respectively. Since there was no obvious relationship with the patterns for the other elements, nor with DOM itself, these results could indicate that redox conditions may be a contributing factor. This will be explored further in the sections that follow.

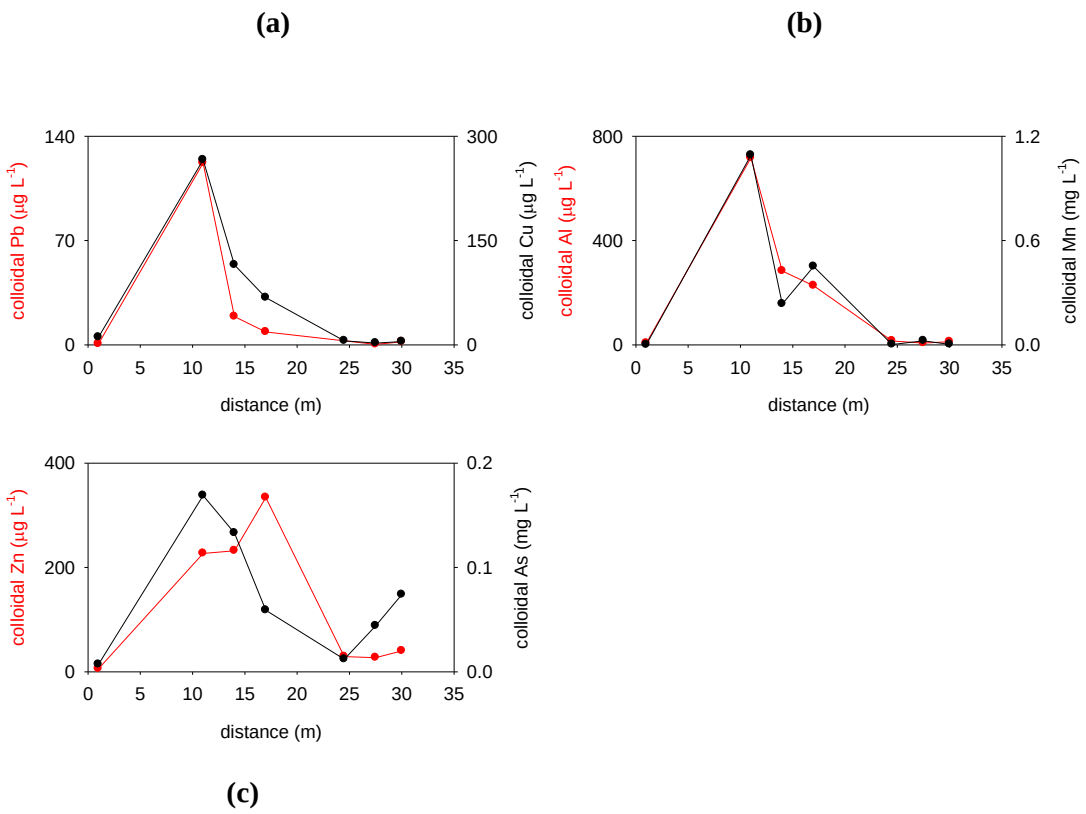

Figure 5.13: Colloidal concentrations of (a) Pb and Cu; (b) Al and Mn; (c) Zn and As in surface (0-5 cm) soil porewaters along the transect from the cliff base southwards through the boggy area

The patterns for colloidal Pb and colloidal Cu were very similar to those for the TD concentrations of these elements (Figure 5.13(a) and Figure 5.12(a)), i.e. most (70-100%) of the Pb and Cu is in colloidal form. For Pb, this is to be expected since thetrue solubility of Pb (based on the free aquated ion) is very low. For example, especially in carbonate-rich environments, at pH~6.5-8, the solubilities of cerrusite ($Pb(CO_3)$) and hydrocerussite ($Pb_3(CO_3)_2(OH)_2$), which are likely solubility controlling solid phases, are extremely low (Figure 5.14) (Scheetz and Rimstidt, 2009).

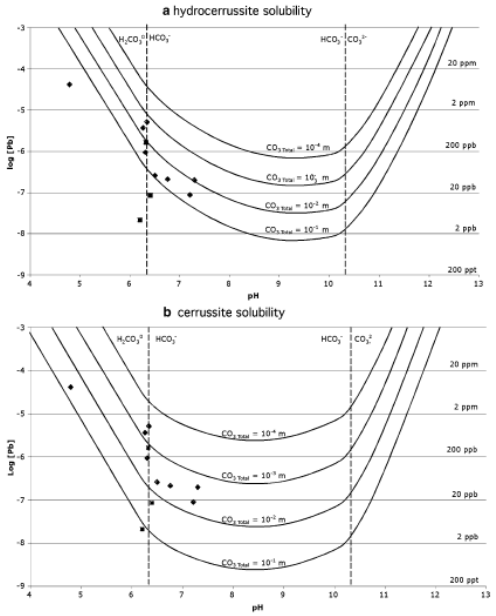

Figure 5.14: The pH dependence of the solubility of (a) hydrocerrusite and (b) cerussite under varying concentrations of dissolved $CO_{2(aq)}$ (Scheetz and Rimstidt, 2009)

The pattern for colloidal Pb was again very similar to that for colloidal Fe (r^2 = 0.994) and it may be that Pb is associated with Fe colloids in the soil porewater (Figures 5.13(a) and 5.11(b)). Alternatively, it is possible that the Pb is associated with OM-bound Fe within the colloidal fraction but the fact that the sharp decrease in both Fe colloidal and Pb colloidal concentrations at 15 m from the cliff base suggests that there is a single process affecting both elements and this appears to be unrelated to DOM content (Figure 5.11(a)).

A vast number of studies have observed strong interactions between Cu and OM and so it is not surprising that the pattern for colloidal Cu is quite strongly related to the DOM pattern (r^2 = 0.898; Table 4.16). Approximately 75-100% Al was in colloidal form and the pattern for colloidal Al is similar to that for both Cu (r^2 = 0.992) (Figures 5.13(a) and (b)) and DOM (r^2 = 0.932), again suggesting an association with DOM.

Although the TD porewater Zn pattern (Figure 5.12(c)) seemed different from the other elements, the pattern for colloidal Zn (Figure 5.13(c)) was more similar to that of DOM (although r^2 = 0.723 was indicative of a weaker correlation than for the other elements). Colloidal As (Figure 5.13(c)) constituted only a small portion of total As, especially from 14 m to 24.5 m from the cliff base (2-7% in colloidal form). Again, as for colloidal Zn, there was a weaker correlation between colloidal As concentrations and DOM (r^2 = 0.716).

Finally, it is important to consider the changes in truly dissolved concentrations of each element along the transect as this may be important with respect to further delineating zones of change across the bog.

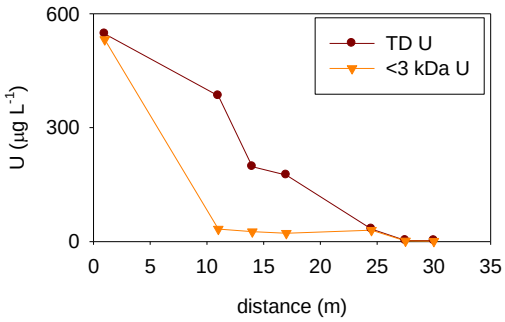

Figure 5.15: Total dissolved (TD; <0.2 µm) and truly dissolved (<3 kDa) U in the surface (0-5 cm) soil porewaters along a transect from the cliff base southwards across the boggy area

Figure 5.15 shows that truly dissolved U concentrations dropped immediately from ~550 µg L^{-1} at 1 m from the cliff base to ~20-30 µg L^{-1} upon entering the boggy area. They remained at this level until 25 m from the cliff base before dropping to ~1-1.5 µg L^{-1}. Clearly the decrease in truly dissolved U occurs much more rapidly than for TD U, suggesting that colloidal organic matter is instrumental in maintaining the amounts of U remaining in the aqueous phase as groundwater passes through the bog. This is important with respect to establishing transport processes through the geosphere and eventual fate of U and so discussion of the likely interactions between U and OM will form part of the later

sections of this chapter (see sections 5.3.5-6).

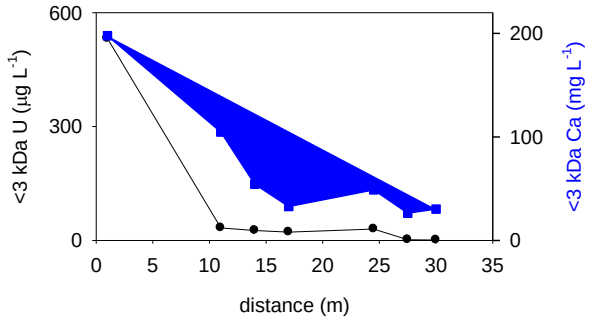

Figure 5.16(a): Comparison of truly dissolved U and Ca in the surface (0-5 cm) soil porewaters along a transect from the cliff base southwards across the boggy area

As for U, truly dissolved Ca also decreases upon entering the bog (Figure 5.16(a)). Although its concentration did not decrease as markedly as for U, near constant values were reached after ~17 m from the cliff base. The more dramatic drop upon entering the boggy soils could be an indication that transition to reducing conditions particularly affects truly dissolved U (since Ca does not display redox-related behaviour). For example, Hooker (1989) suggested that, on contact with the highly reducing organic-rich soils, U^{VI} was reduced to U^{IV} and precipitated as uraninite with a rate constant of 1 d^{-1}. He observed that a steady state was reached after 1 month (Hooker, 1989). However, as previously discussed, precipitation as UO_2 contradicted the fission track results which pointed to organic matter as being directly responsible for the fixation of U. The change in speciation from dissolved to organic colloidal U observed in this study supports the latter interpretation.

Jamet et al. (1993) also considered that the uranium was reduced as a consequence of the impact of humic matter on the redox potential of the bog. As in this study, they found that the Eh values for the bog were typically about 100-200 mV lower than the water emerging

from the cliff. They considered that uraninite and liebigite were two likely candidates for solid phase uranium but noted that the latter was a U^{VI} phase. It is relatively rare but has been found as a coating in the hydrocarbon fractures in the main pitchblende-bearing vein of the cliff (Basham et al., 1989). It has never been recorded in a reducing sedimentary environment and the authors considered that it was difficult to explain the role of redox potential if uranium retention in the boggy soils was governed by U^{VI} precipitation. Their field analyses failed to reveal pH contrasts large enough for this hexavalent mineral to precipitate. Usually, liebigite precipitates under weakly to strongly basic conditions (Finch and Murakami, 1999) whilst the conditions in the peaty soils are acidic-to-near-neutral. In this study, only two crystalline grains containing U (in the form of uraninite) were identified using SEM-EDX (section 4.1.10; Figures 4.12-4.13). Clearly, reduction and precipitation of U in mineral forms is not the major process occurring at the Needle's Eye site.

In contrast with U, Figure 4.25(a) showed that the majority of Ca was present in the truly dissolved form and thus the decrease in Ca concentration with distance from the mineralisation may either be due to dilution with increasing distance or be indicative of removal via precipitation. Jamet et al. (1993) calculated the saturation indices of selected minerals in contact with groundwater along a N-S transect and at varying depths in order to deduce flow paths. They considered that oversaturation or equilibrium with calcite suggested that there must be a vertically ascending component of the flow from the limestone substratum. As discussed above, this study showed that calcite concentrations were greatest in the near-surface soils and decreased with increasing soil depth and with distance from the mineralisation. Thus the removal of calcite is consistent with the observed trend in the porewater transect data.

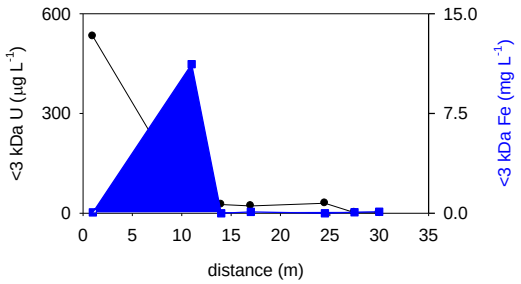

Figure 5.16(b): Comparison of truly dissolved U and Fe in the surface (0-5 cm) soil porewaters along a transect from the cliff base southwards across the boggy area

Figure 5.16(b) illustrates the strong contrast between the pattern for truly dissolved Fe and that for truly dissolved U. Whereas truly dissolved U decreases markedly upon entering the bog, the reverse was observed for truly dissolved Fe. The truly dissolved Fe concentration at 11 m was ~10 mg L^{-1} which is many orders of magnitude higher than could be sustained by simple equilibrium between hydrous iron oxides and a pure aqueous phase (see Figure 1.13). Complexation, e.g. by carbonate (at pH~6.8, $FeHCO_3^{2+}$) or perhaps by truly dissolved organic ligands, may explain this observation. The very much lower concentrations of truly dissolved Fe from 14 m to 30 m from the bog was an interesting feature. Indeed the decrease in truly dissolved Fe concentrations was even more marked than for colloidal Fe (Figure 5.11(b)). The pH increased from ~5.5 to >7 which will affect the speciation of Fe. An increase in colloidal forms of Fe, e.g. $Fe(OH)_2$, $Fe(OH)_3$, possibly $Fe(OH)_2$-humic, $Fe(OH)_3$-humic, would be expected. Colloid formation is often considered to be the first step in removal to the solid phase and so it is postulated that this accounts for the sharp decrease in both truly dissolved and TD Fe concentrations.

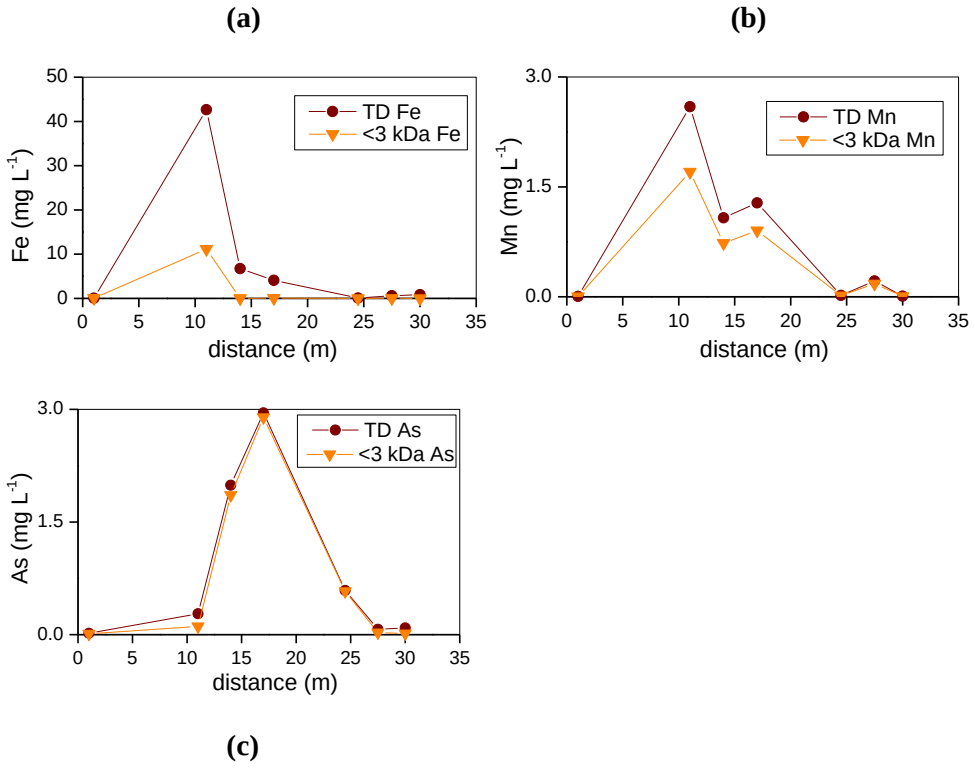

Figure 5.17: Comparison of TD and truly dissolved (a) Fe; (b) Mn; (c) As in the surface (0-5 cm) soil porewaters along a transect from the cliff base southwards across the boggy area

Figure 5.17 shows the relationships between TD and truly dissolved concentrations of the redox-active (Fe and Mn) and redox-affected (As) elements in the soil porewaters. Differences between the behaviour of Mn and Fe are evident at distances of greater than 11 m from the cliff base (Figures 5.17(b) and (a)). Here there is a second component in the Mn pattern that is absent from that of Fe which could suggest a decoupling of the Mn and Fe behaviour. Comparison of the pattern for truly dissolved As (Figure 5.17(c)) with that for truly dissolved Fe also reveals an interesting relationship. As the Fe concentrations in solution decrease, the As concentrations increase. This is not likely to be a direct causal relationship and will be investigated further via the vertical profiles (i.e. it is not removal of Fe from the aqueous phase that is causing As to go into solution).

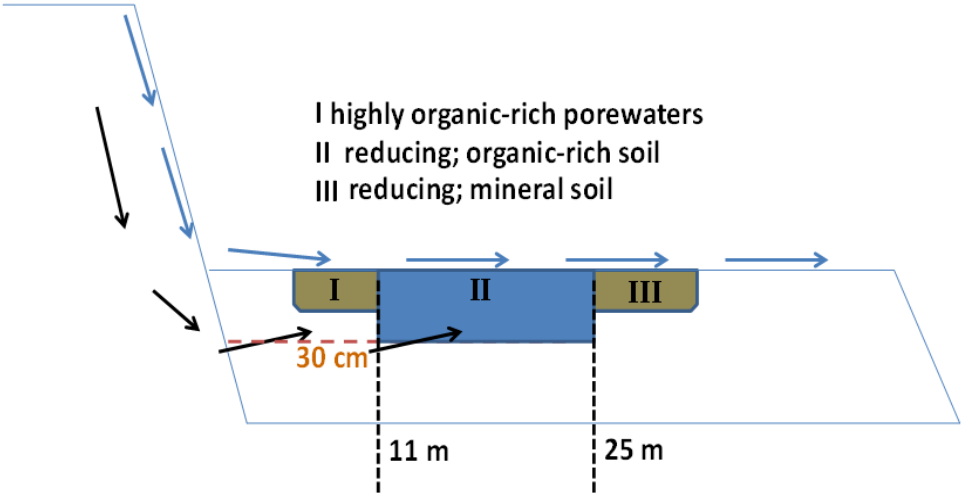

Figure 5.18: Model of the hydrological and the redox conditions for the boggy soils at Needle's Eye

The model shown in Figure 5.18 combines the hydrological information about flow paths with the geochemical information obtained in this study (pH, DOM, SOM, Al, carbonate concentration data, elemental data for the lateral transect through 0-5 cm surface soils).

Upon entering the highly organic-rich boggy soils (zone I), some TD U is immediately removed to the solid phase but most becomes associated with the organic colloids. During transport through zone II of the bog, it is the colloidal U that is then being removed from solution as shown by the decrease in TD U from 11 m to 14-17 m from the cliff base (truly dissolved U is constant at ~20-30 μg L^{-1} across this section of the transect). At 25 m from the cave, colloidal U concentration drops to ~1% of TD U and this corresponds to the point where DOM concentrations also drop significantly; beyond this point, both truly dissolved and colloidal U were ~1-1.5 μg L^{-1}. This marks the transition from the boggy area towards the Merse sediments.

The validity of the model will be explored further during the discussion of the vertical soil porewater profiles.

5.2.2 Vertical soil porewater profiles – redox conditions

The vertical porewater concentration profiles for redox-active elements, Fe and Mn, and redox-affected element, as will be considered together (Figures 5.19-5.22).

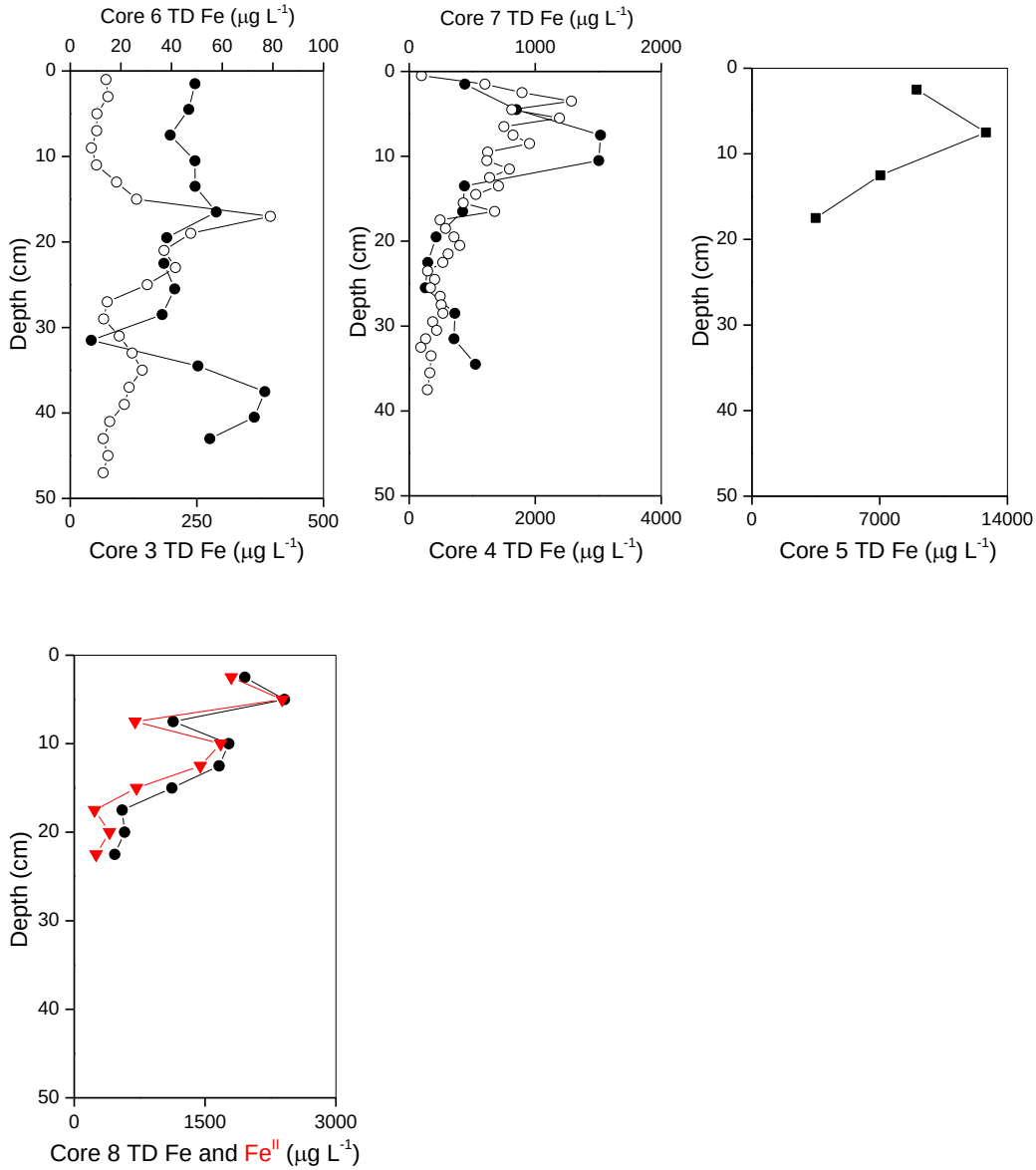

Figure 5.19: Porewater Fe concentrations in cores 3-8 from the boggy area at Needle's Eye

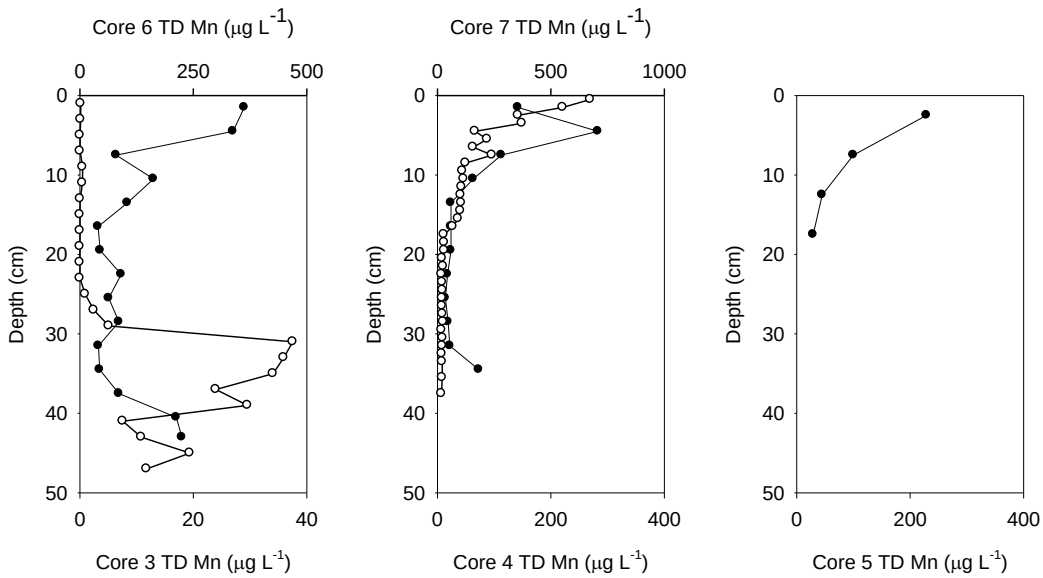

Figure 5.20: Porewater Mn concentrations in cores 3-7 from the boggy area at Needle's Eye

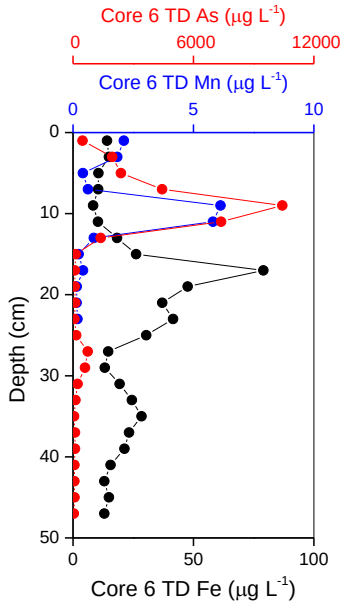

Figure 5.21: Comparison of near-surface TD Mn peak with those for TD Fe and TD As in Core 6

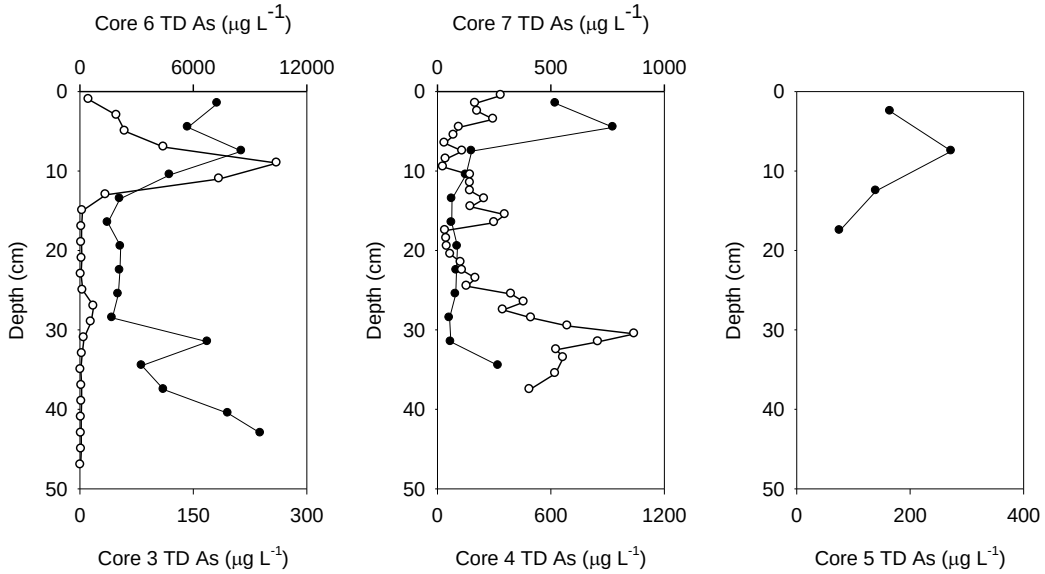

Figure 5.22: Porewater As concentrations in cores 3-7 from the boggy area at Needle's Eye

In the main, the concentrations of porewater Mn, Fe and As from cores 3-4 (20 m and 25 m from the cave, respectively) were consistent with those for the lateral transect at distances of 17-27.5 m from the base of the cliff (cf. NE4-NE6 in Table 4.12).

5.2.2.1 Fe

For cores 3 and 4, the nearest-surface maximum Fe concentrations occurred at 10-20 cm and ~10 cm, respectively (Figure 5.19). For core 4 in particular, the Fe peak occurred below the porewater Mn maximum and was coincident with a broad solid phase Fe concentration maximum. Taken together, these factors strongly suggest redox-controlled behaviour, i.e. a transition from solid phase Fe^{III} to aqueous phase Fe^{II}. For core 3, the presence of such a transition is not so clear and there may be other factors contributing to the slight enhancement of porewater Fe concentrations in the 10-20 cm depth sections. Again for core 3, the maximum concentrations in both the porewater and solid phase Fe profiles occurred towards the bottom of the core (Figure 4.4); in this instance, redox-related

processes may well be involved since a transition to sulfidic conditions was supported by the sequential extraction data for these cores (section 4.1.8 and Table 4.4).

In explanation of the latter, equilibrium between pyrite and Fe^{II} in the aqueous phase can give rise to increased porewater Fe concentrations such as those observed at depths of >30 cm in Core 3. Equation 5.1 shows one such relationship (Rickard and Luther III, 2007) but clearly the precise chemical equations involved cannot be elucidated from this work.

$$FeS_{2(s)} + H^+ \leftrightharpoons Fe^{2+} + HS^- + S^0$$
$$H^+ + HS^- \leftrightharpoons H_2S$$

$$FeS_{2(s)} + 2H^+ \leftrightharpoons Fe^{2+} + H_2S + S^0 \qquad K=10^{-7.2} \qquad \text{Equation 5.1}$$

Cores 3 and 6: 20 m from the cave

Core 6 was collected at the same time as the lateral transect and at the same location as core 3. The concentrations in the near-surface (0-5 cm) sections were very low, in agreement with the transect data. In comparison with Core 3, the Core 6 porewater Fe profile has a much more pronounced subsurface maximum in the 10-20 cm sections of the core and this could be indicative of the transition from Fe^{III}/Fe^{II} as described in the previous section or it might reflect the effects of lateral flow of water from the mineralisation. More than 90% of Fe was colloidally associated at these depths, consistent with the core 3 profile.

The peak at depths >30 cm was not as pronounced as for Core 3, but ultrafiltration showed that most of this Fe was in dissolved form, consistent with the mechanism of release from sulfides proposed above.

Cores 4 and 7: 25 m from the cave

Core 7 was collected at the same location as core 4 but during the summer rather than late autumn. Although the porewater Fe profiles had a similar shape, the position of the sub-surface maximum was closer to the soil surface for Core 7 (Figure 5.19). This indicated that conditions had become even more reducing. This was supported by the data for core 8 which showed that, when the Fe maximum was very close to the surface, the Fe in solution was present as Fe^{II} (Figure 5.19).

5.2.2.2 Mn

The Mn profiles for cores 3, 4, 5 and 7 all had peaks in the 0-5 cm section; thereafter, concentrations decreased dramatically (Figure 5.20). The high near-surface concentrations are consistent with those observed in zone II of the bog, as per the model shown in Figure 5.18. For core 7, the Mn peak was in the very surface section, just above that of Fe. This is consistent with the explanation proposed for porewater Fe in Core 7, i.e. the presence of both Mn and Fe peaks in the top 0-5 cm sections is consistent with strongly reducing conditions.

For core 6, there was a very large peak at depth which distorted the overall profile. On closer examination of the near-surface sections, however, there was a peak in porewater Mn concentration at ~10 cm depth, which occurred above that of Fe (Figures 5.19-5.20).

5.2.2.3 As

For cores 3, 4 and 6, there was a strong relationship between the position of the As peak and that of Mn (Figures 5.21 and 5.22) and it is proposed that As is being released as a consequence of the reductive dissolution of Mn oxides, not in relation to the formation and removal of Fe colloids (*cf* section 5.2.1). For core 5 (Figure 5.22), the behaviour of As is

more typical of that found in many sediments, i.e. it was controlled by the reductive dissolution of Fe oxides (e.g. Erbs et al., 2010). For Core 7, however, there is a large increase in porewater As towards the bottom of the core and yet neither Fe or Mn concentrations were found to increase. Instead, Al was found to increase at depths of >30 cm. Table 5.1 shows the characteristics of the bottom sections of cores 3, 4, 6 and 7.

Table 5.1 Characteristics of the bottom sections of Cores 3, 4, 6 and 7

Core	Elements with a porewater maximum below 30 cm depth	pH change	DOM maximum below 30 cm	Elements with solid phase maximum below 30 cm
3	Al Mn Fe As U Cu Pb	No	Small increase	Al Fe As
4	Al Fe Cu Pb	No	Small increase	Al (Fe)
6	Al Mn (Fe) As U Pb Zn	Yes (suddenly to pH 6)	-	n.a.
7	Al As U Cu Pb	Yes (gradually to pH 6)	Small increase	n.a.

n.a. = not applicable

Thus it would appear that the change to mineral-rich conditions below 30 cm is accompanied by higher porewater concentrations of many elements, including those which may have been present on the mineral surfaces prior to dissolution. Dissolution of Al and/or Fe phases is invoked to account for the observed profiles. However, there is no single controlling factor, e.g. pH, redox, DOM, that can be invoked to explain all of the profiles.

Overall, the results are largely consistent with those for the transect and the proposed model for the Needle's Eye site. Cores 3, 4, 6, 7 and 8 lie within zone II of the bog where As release is mainly coupled to reductive dissolution of Mn oxides in the top 0-5 cm sections of bog and where mineral dissolution processes occur at depths below ~30 cm. Some variation in the position of Fe redox boundaries was evident: at 25 m from the cliff, the Fe^{II}/Fe^{III} redox boundary had moved closer to the bog surface on some sampling dates.

5.2.3 Vertical soil porewater profiles – U mobility in Needle's Eye soils

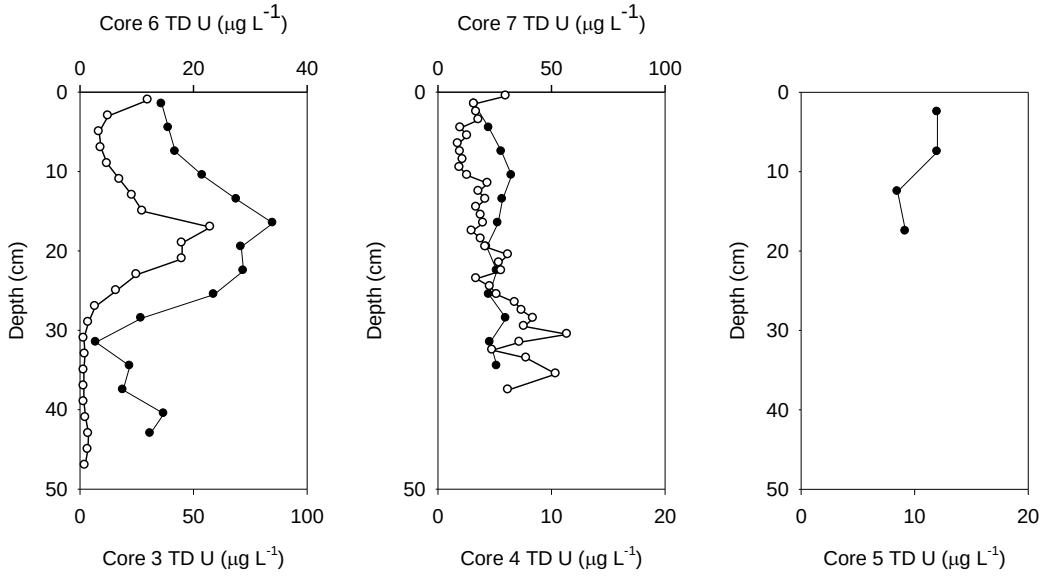

Figure 5.23: Porewater U concentrations in cores 3-8 from the boggy area at Needle's Eye

The near-surface U concentrations for the soil porewaters from cores 3, 4, 6 and 7 were broadly in agreement with those for the 0-5 cm transect porewaters at 20-25 m from the mineralisation (Figure 5.23 and Table 4.12). Admittedly the concentrations in the 0-5 cm sections of core 4 were lower than those found for NE5 (24.5 m) but the general trend of decreasing concentration between 20 and 25 m was as expected from the lateral transect.

Cores 3 and 6: 20 m from the cave

The difference between the ranges of U concentrations for core 3 and core 6 fitted with the change in DOM concentrations, i.e. a x2 drop in DOM was accompanied by a x2 drop in porewater U concentration (Figure 4.4 and Figure 4.27), providing further evidence for the role of DOM in stabilizing U in the soil porewaters. However, the porewater maximum for Core 3 occurred ~3 cm above the solid phase U concentration maximum and, for both Cores 3 and 6, the porewater maxima coincided with maxima in the porewater Fe profiles (Figures 4.4 and 4.27). Although there was evidence for lateral water flow, the potential importance of redox-related processes involving Fe on the behaviour of U within these highly organic-rich soils couldn't be overlooked. For the upper sections (0-30 cm) of Core 3, the ultrafiltration data showed that most of the colour and the Fe and U were present in the large colloid (100 kDa-0.2 μm) fraction (Figure 4.7). Thus, Fe, U and humic substances may be intimately associated and this became the focus of further experimental work to elucidate the processes controlling U mobility.

The decrease in porewater and solid phase U concentration especially below 30 cm coincided with the major change from organic-rich to mineral-rich soil (Figure 5.4(a)). For Core 6, the small amount of U in the porewaters at such depths was predominantly in the dissolved form; this may indicate release following dissolution of solid phase minerals. The solid phase sequential extraction results showed that although there was a transformation from crystalline Fe oxides to FeS_2 at depth, this did not result in a concomitant transfer of U to the sulfides (Figure 4.10). Consequently pyrite dissolution is unlikely to have caused the release of dissolved forms of U (or other elements, i.e. Al, Mn). Future work will require to more fully investigate the behaviour of U in relation to the mineral phases towards the bottom of these cores.

Cores 4 and 7: 25 m from the cave

For core 4, the porewater U maximum was again ~3 cm above the solid phase maximum and also coincided with the Fe porewater maximum (Figures 4.5 and 4.40). Ultrafiltration results for Core 4 showed that U was present in both large colloidal and dissolved forms while Fe was mainly in large colloidal form (Figure 4.7). The porewater U profile from Core 7, which was collected during summer (June 2011), was distinctly different from that obtained for Core 4. There was a small near-surface peak co-incident with the position of the Mn peak and a larger maximum towards the bottom of the core. Since there was no

significant difference between the DOM profiles for the two cores, the higher U concentrations, especially towards the bottom of the core, must in some way be related to the more intensely reducing and more acidic conditions prevailing at the time of sample collection.

5.2.3.1 Comparison of colloidal associations of elements in vertical soil porewaters and 0-5 cm transect soil porewaters

Cores 3 and 4 vs transect porewaters

As discussed in the preceding section, the greatest proportion of U along with most of the brown colour (humic substances) was typically in the large colloid fraction (60-90%) with the remainder split between the small colloids and the dissolved fraction. The extent of colloidal association was similar to that reported by Graham et al. (2011) but much higher than in some other studies, e.g. Crancon *et al.* (2010) estimated that a maximum of 10% of the total dissolved U^{VI} species may be bound to humic colloids. Although small, this fraction was still found to be responsible for the rapid and far-reaching transport of U into nearby aquatic systems.

For Cores 3 and 4, the split between colloidal and dissolved U for the 0-5 cm sections was in good agreement with the results for the transect (17-25 m from the cliff base) since the proportion of dissolved U is increasing from ~10% (Core 3) to ~40% (Core 4) of the total. Thus, as concluded from the transect results alone, the decrease in total porewater U concentrations going from Core 3 to Core 4 can be attributed to the removal of colloidal U from the porewaters. Interestingly, there was also a decrease in the proportion of colloidal U with increasing soil depth which was attributable to a loss of large colloidal forms and then a loss of small colloidal forms of U towards the bottom of the core. This trend with increasing depth was also in very good agreement with Graham et al. (2011) who showed that small colloidal forms of U were present in near-surface soils but decreased with increasing soil depth (the difference in this study was that the small colloidal forms are not Fe-free). The colloid distribution pattern for Core 5 (35 m from cave) continued the trend observed for Core 4 and also that observed from the lateral transect in that the smaller amounts of U remaining in the 0-5 cm soil porewaters were spilt ~55:45 between colloidal and dissolved forms (Figure 4.9). Below this depth, there was an increase in the proportion of U in colloidal forms but the core was not long enough to observe any transition to

dissolved forms below 30-40 cm.

Most of the Fe present in the 0-5 cm porewaters was associated with colloids, in very good agreement with the transect data. For Cores 3 and 4, Fe was predominantly found within the large colloid fraction with most of the remainder in the small colloid fraction; for Core 5, Fe was almost exclusively in the large colloid fraction. The core 5 results were similar to the findings of Graham et al. (2011) for soils with a similar organic content. For core 3, the proportion of large colloidal Fe increased with increasing depth whilst that of small colloidal Fe decreased (Figure 4.7). In contrast, for core 4, large colloidal Fe decreased and there was an increase in dissolved Fe concentrations towards the bottom of the core, as was observed for U (Figure 4.8).

In comparison with the transect porewaters, there was a greater proportion of colloidal Mn in the soil core porewaters but the trends from colloidal to dissolved Mn with increasing depth in the vertical porewater profiles are readily explained. The transition to dissolved forms is a consequence of the reduction of MnO_2 to Mn^{2+} as was observed by Graham et al. (2011) in soils from SW Scotland. Truly dissolved Mn is released into the porewaters. Upwards diffusion is accompanied by re-oxidation and removal to the solid phase. The formation of colloidal forms of Mn (*cf* almost all Mn was in this form in the top sections of Cores 3 and 4), is the first step towards removal of Mn^{IV} from the porewaters to the solid phase. If the cores had been more finely sectioned, e.g. in sub-cm sections then the position of release of reduced Mn would have been more readily distinguished from the point of removal of oxidized Mn. Although fine-sectioning (e.g. at 2-mm intervals) can be achieved for lake sediments (e.g. Gavin et al., 2001; Graham et al., 2012), it is not possible to do this for peaty soils.

For Al, the trends were very similar to those for Fe; again colloidal forms are dominant at all depths and the dominant association was with the large colloidal fraction. The trend of increasing proportion of Al in the dissolved fraction with increasing depth below 20 cm was similar to that for Mn, albeit not so marked. Below 35 cm depth, however, there was an increase in large colloidal Al for both core 3 and 4 and for core 3, and this was accompanied by an major increase in colloidal Mn. This speciation change occurred in the mineral-rich section of these cores at the position of the porewater maxima for these elements.

Core 3 vs core 6 porewaters: 20 m from the cave

For Core 6, only total colloidal (3 kDa-0.2 μm) and dissolved (<3 kDa) forms of U, Fe, Mn and Al were separated as the purpose was to isolate the total colloid fraction for other experiments which are discussed later. It is also important to recognize that Core 6 was sectioned into 1-cm depth sections and so the profiles for this core are much more detailed than those for Core 3. Nevertheless, it is useful to consider the distribution between dissolved and colloidal forms isolated both under nitrogen and in air. The 'in air' results for Core 6 are directly comparable with those obtained for Core 3. In the top 0-30 cm sections, up to 80% U was present in colloidal form, in reasonable agreement with the Core 3 data. For >30 cm depth, this dropped to ~30-40% which was lower than obtained for Core 3. The direction of change was, however, consistent between the two cores.

For the "under N_2" experiments, up to ~70% U was in colloidal form over the top 0-30 cm. Below 30 cm, the amount in dissolved form increased to ~70-80%. Thus, the effect of exposure to air was a small increase in the percentage of U in colloidal form (~10%) in the upper sections. The same effect was observed to a greater extent (~20%) at depth. Based on the "under N_2" results, however, the extent of colloidal association of U at the Needle's Eye site was still significantly greater than reported by Crancon et al. (2010) for laboratory experiments involving sandy soils.

For Fe, the mass balance (colloidal+dissolved vs total) was not as good as on previous occasions for the reasons described in section 4.2.2. However, the vertical trends in colloidal+dissolved Fe did follow those of total dissolved Fe (Figure 4.30). In the surface sections, all of the Fe was in colloidal form whilst below 27 cm, the majority was in dissolved form. There was very little difference between the colloid-dissolved distribution when separations had been carried out under N_2 compared with under air (Figure 4.30), suggesting that the previous sample processing protocols (under air) had not caused significant artifact generation (e.g. formation of Fe colloids due to prolonged exposure to air). Thus the differences in Fe speciation between Cores 3 and 6 in the deeper part of the profile are real and the form of Fe being released at depth in Core 6 is dissolved rather than colloidal Fe. In the 30-40 cm depth interval, there was a significant decrease in pH from ~7 to ~6 which coincides with the porewater maximum and the transition to dissolved forms. This also appeared to be highly significant in terms of the release of Mn and Al into the porewaters since both these elements have extremely large dissolved phase peaks at below 30 cm. Thus a process involving mineral dissolution is resulting in the release of truly

dissolved U as well as Fe, Mn, Al into the porewaters.

As already mentioned in section 5.2.2.2, there was an additional feature in the core 6 Mn profile that was being dwarfed by the results for the bottom of the core. Figure 4.32 shows the % distribution between colloidal and truly dissolved forms of Mn and it is clear that it is truly dissolved Mn that is present at the position of the small porewater maximum (~10 cm depth); above and below this point Mn is in colloidal form. This is consistent with reductive dissolution of Mn and concomitant release of truly dissolved Mn into the porewater (Davison, 1993). The higher sampling resolution of this core has enabled these features to be observed. This release of truly dissolved Mn, however, also affects the speciation of U and Fe, e.g. a change of ~20% U and ~20% Fe towards the truly dissolved form at this depth, and so dissolution of Mn oxides releases some dissolved U and Fe into the porewaters. Similar processes leading to the release of U from soils were also identified in Graham et al. (2011).

In summary, U is present in dissolved forms in the cave waters emerging from the mineralisation. Formation of ternary U^{VI}-Ca-CO_3 complexes inhibits reduction to U^{IV} and instead, as the U-bearing waters enter the boggy soils, the results of this study strongly suggest that a high proportion of this U becomes associated with humic colloids. The remainder is removed to the solid phase. As the waters continue to flow through the boggy soils, colloidal U is removed to the solid phase in preference to dissolved forms (concentrations remain constant). When the waters reach the transition between the boggy soils and the saltmarsh, concentrations of both colloidal and dissolved forms were markedly reduced (<3 μg L^{-1}) and the ratio of colloidal:dissolved was ~55:45. These stages are represented in Figure 5.24.

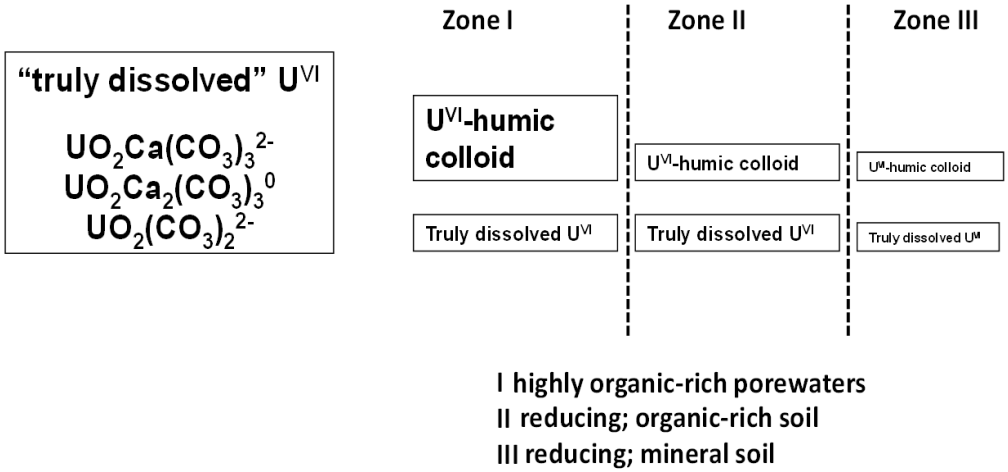

Figure 5.24: Changes in speciation of U as it passes from the mineralisation through the 0-30 cm boggy soils and reaches the transition to the saltmarsh at the Needle's Eye site

Although reductive dissolution of Mn has a small effect on the speciation of U (transition to dissolved forms), it has a very limited effect on the overall concentration of U present in the porewaters. On several sampling occasions, however, the positions of U and Fe maxima within the 10-20 cm sections of the porewaters coincided and, since both elements remained colloidally associated, the sections that follow will mainly focus on establishing how U interacts with both Fe phases and organic components of the solid phase as well as with the colloidal components identified above.

5.3 Retention of U in solid phase soils within the boggy area at the base of the cliff at Needle's Eye

5.3.1 Mechanisms of U immobilization in peat reported in the literature

Researchers from the U.S. Geological Survey have reported elevated U concentrations in woody peat and organic-rich sediments at the Flodelle Creek wetland, Washington, Rocky Mountains, Sierra Nevada (Owen and Otten, 1995). The high concentrations were due to nearby inputs of naturally U-enriched groundwaters. Although some peats had U concentrations in the range 1,000-3,000 mg kg^{-1}, the majority of peat samples contained less than 150 mg kg^{-1} and significant variations over short distances within the same wetland were observed (Owen and Otten, 1995). Maximum U concentrations of nearly 1%

w/w have been reported by Schöner et al. (2006) for peat horizons in wetlands of the Wismut region (Germany). These had been contaminated by seepage from adjacent tailings of former U mills.

Several mechanisms by which U can be retained by peat bogs have been proposed. These include: sorption onto organic material, sorption onto mineral phases, and co-precipitation of U along with secondary minerals. With respect to the role of organic matter, Schöner et al. (2006) remarked that mechanisms responsible for the removal and fixation of dissolved uranium from water are still not sufficiently understood. Many, however, consider that sorption to organic matter is the major mechanism for immobilizing dissolved U from the water phase. Owen and Otten (1995) found that the complexation of the uranyl cation (UO_2^{2+}) by carboxyl groups, and the formation of insoluble uranyl humates, contributed significantly to the retention of U in peat but other researchers consider that metals in general are initially only loosely adsorbed to peat and may subsequently be reduced to more stable forms (Nakashima et al., 1984). The interactions of cations with humic materials is, however, of very limited importance for this study since, at the Needle's Eye site, the main solution phase species will be negatively charged.

Another school of thought is that U becomes associated with humic acids in solution and then sorption of humic acids to mineral surfaces occurs. Sorption generally increases when the pH is lowered and the ionic strength of the solution rises and Feng et al. (2005) considered that this would be unlikely to be an issue in a peat bog as the pH decrease would have to be substantial. Feng et al.(2005) showed in batch experiments that peat humic acid is sorbed to different clay minerals (kaolinite and montmorillonite) via cation bridging, ligand exchange and van der Waals forces. The presence of multivalent cations, such as Ca^{2+} and $Al^{3+,}$ can largely enhance organic acid adsorption to clay through cation bridges.

Crancon et al. (2010) stated that the sorption of humic substances onto mineral surfaces created hydrophobic mixtures that stabilize organic matter in soils. The stability of these aggregates was, in turn, dependent on soil moisture as well as the flow velocity and chemistry of the porewater. Uranium species may also adsorb directly to freshly precipitated iron hydroxides or iron oxides as well as to clay minerals. Negatively charged U species will sorb onto positively charged iron (hydr)oxides whilst positively charged U species will sorb onto negatively charged clay minerals. Crancon et al. (2010) found that

complete sorption of U onto clay and other surfaces typically occurred within a period of a few days. Krepelova et al. (2006) found that U^{VI} adsorption to clay (kaolinite) under acidic conditions increased if humic acids were present due to the formation of additional binding sites for U coming from the adsorption of humic acids to kaolinite. For this study, the sorption of negatively charged U species onto positively charged Fe surfaces are most relevant to the situation at Needle's Eye.

5.3.2 Removal processes at Needle's Eye: evidence from solid phase profiles in conjunctions with the transect porewater data

The solid phase U vertical concentration profiles for Cores 3 and 4 both have sub-surface maxima at ~10-20 cm depth. The highest concentrations of ~2,400 mg kg^{-1} found for core 3 (20 m from the cave) were similar to the highest concentrations reported by Owen and Otten (1995) for peaty soils in the US. Below the transition to mineral-rich soil composition, the U concentrations decrease markedly. This is consistent with the major flow of U-rich groundwater occurring above the mineral-rich layer. The pattern for Cu is very similar, again consistent with the results obtained for the soil porewaters. The vertical profiles for Mn are very much as would be expected for a highly reducing environment, with relatively low concentrations overall (<700 mg kg^{-1}) and with highest concentrations in the top section of the cores followed by a decline with increasing soil depth. The Fe profiles for the two cores differ in the same way as the porewater profiles, i.e. Core 3 had higher concentrations towards the bottom of the core whilst core 4 had highest concentrations at ~10 cm. The shoulder in the solid phase profile for Core 3 does, however, occur at the same position as the main peak in core 4. Overall, the solid phase profiles for Core 3 and 4 can be split into 3 groups: those having a surface maximum (Mn), those having a broad maximum at ~10-20 cm (U, Cu, Fe), and those having a maximum towards the bottom of the core (Fe, Al, As, Pb). The focus of this section will be on the middle group.

In section 5.1 it was proposed that the lower permeability of the mineral-rich layer underlying the organic-rich material means that sub-surface water flow is directed through the organic-rich layer (0-30 cm). By 11 m from the cave, most of the transported U is associated with very large organic colloids and it is these that are being removed from the aqueous phase with increasing distance. Thus, continuous movement of waters from the mineralization through the sub-surface results in accumulation of U at ~10-20 cm depth.

The similarity of the Core 3 Cu and U profiles suggests that the same processes are affecting both elements at this location. This is in agreement with the behaviour observed in the transect porewater data; both were predominantly in colloidal form at 11 m from the cave (Table 5.2). Several other elements (Fe, Pb, Al and As) were also predominantly present in colloidal form at this point on the transect but all four showed weaker correlations with organic matter (Table 5.2).

The U and Cu enhancements in the 15-25 cm sections of Core 4 were again coincident. Moreover, the maximum concentrations in the solid and aqueous phase were a factor of 10 and 20 lower, respectively, compared with Core 3. The transect data suggested continued removal of organic colloidal U from the porewater to the solid phase and this is reflected in the continued accumulation of U and Cu within the organic soils even at 25 m from the cave.

Table 5.2 Colloidal elemental association at 11 m from the cave and correlation between colloidal elemental concentrations and DOM along the 30 m transect from the mineralization.

Element	% colloid association at 11 m from cave	Overall r^2 (colloidal element vs DOM)
U	90.2	0.977
Cu	81.1	0.898
Fe	98.9	0.774
Pb	99.1	0.707
Al	87.0	0.716
Mn	39.0	0.905
As	91.4	0.716
Ca	15.5	0.965
Zn	69.0	0.723

5.3.3 Association of U with humic substances: evidence from solid phase humic extraction/fractionation and from colloid fractionation

In agreement with previous work (MacKenzie et al, 1991), more than 90% U was extracted along with the solid phase humic substances and both gel electrophoretic and gel

chromatographic fractionation showed that most was associated with the largest humic substances (sections 3.5.1-2). The results for gel chromatographic fractionation of Core 7 porewater colloids also showed U association with large humic colloids (section 4.3.4), in good agreement with the solid phase data. The mechanism proposed in the previous section relating to the removal of U along with large humic colloids is therefore consistent with both the aqueous and the solid phase data. However, Fe was also associated with these fractions and it cannot be ruled out that U was directly associated with iron oxides which were intimately associated with humic substances in both the porewater and the solid phase. The affinity of Fe (hydr)oxides for trace metals combined with their high surface area and prevalence in natural systems makes them ideal sorbents for uranium. This is especially important because the main truly dissolved U species in the waters are either negatively charged or neutral and thus an interaction with positively charged Fe surfaces would be highly favourable. In addition, uranium has been found in coprecipitates (e.g. U/Fe) in various geochemical settings (e.g. Sato et al., 1997; Pett-Ridge et al., 2007) and so it was important to consider the importance of U-Fe interactions as a retention mechanism in the Needle's Eye soils.

5.3.4 U association with Fe phases: evidence from solid phase sequential extraction

Sequential extraction targeting Fe phases showed that 60-80% U was extracted in the "Fe-carbonate-bound" fraction with most of the remaining 20-40% being associated with crystalline Fe oxides in the solid phases from cores 3 and 4 (section 4.1.8). There was a gradual transformation in the nature of the Fe phases from crystalline oxides in the near-surface sections to sulfides at depth. This was reflected in a decrease in U associated with the crystalline oxides; however, there was no transition to association with sulfides (Figures 4.10-4.11). Instead, there was an increase in U in the "Fe-carbonate-bound" fraction. Very little Fe was co-extracted and further work demonstrated that carbonate dissolution was not responsible for the release of U by the acetate reagent (section 4.1.8.1).

Further consideration of the literature relating to the use of sodium acetate revealed the following points. In relation to its effectiveness as an extractant, Pickering (1986) noted that metal complexes with acetate were generally more stable than chloro-complexes. It was also suggested that the use of this reagent favoured exchange processes and that acetate-complex formation reduced re-adsorption or precipitation of the extracted metals.

Where the pH of the reagent has been adjusted to 2, the carbonate fraction could also be attacked and it is this characteristic that has been exploited in many sequential extraction schemes. However, sodium acetate may also access U specifically sorbed to surface clays, organic matter and Fe/Mn oxy-hydroxides and thus the results obtained in this study may be explained: it is proposed that a large proportion of U is held at surface sites on the organic matter/Fe oxides, and that acetate is helping to release the U by (i) competing for surface sites on the organic matter/Fe oxides and (ii) forming soluble U complexes.

It is well-known that U^{VI} forms strong soluble complexes with acetate (Rao et al., 2005). Significantly, U^{IV}-acetate complexes have low solubility (Jelenic et al., 1964). In addition, the uranyl phosphate chernikovite $[UO_2HPO_4(H_2O)_4]$ and metaautunite $[Ca(UO_2)_2(PO_4)_2(H_2O)_x]$ have also been found to be resistant to dissolution in acetic acid (Sowder et al., 2001) with half-times of weeks to years in a 1 mM system, so this is another form of solid phase uranium that can be ruled out.

The proportion of U in the acetate-extracted fraction from Cores 3 and 4 increased with increasing soil depth (Figure 4.3). Although sections 3.5.1-2 demonstrated that U was associated with large humic molecules at all depth within these soils, Fe was again associated with the same fractions and so it still cannot be ruled out that U is held by Fe surfaces which are intimately associated with humic substances.

5.3.5 Association of U with humic-bound Fe: evidence from sequential extraction combined with humic extraction and gel electrophoresis

In a novel set of experiments, the results for sequential extraction followed by humic extraction and then gel electrophoretic fractionation demonstrated that non-humic associated Fe/Mn/Al mineral dissolution and readsorption to the humic substances occurred during sodium acetate extraction (section 4.1.11). This did not affect the results for U since U^{VI} is strongly complexed by acetate as described above (Rao et al., 2005). Acetate extracted ~12-30% U whilst dithionite removed 85% U (including the acetate-extractable fraction) and almost all of the readsorbed Fe/Mn/Al.

An improved experimental approach was then developed whereby the humic substances were first extracted and then the acetate and dithionite reagents were applied directly to the

humic substances. Here 20-25% of U was removed from the humic substances by acetate. Importantly, almost no Fe was removed and so the acetate was removing U that was sorbed either directly to the humics or to humic-bound Fe minerals (not carbonates). Almost half of the "humic-bound" U was removed along with crystalline iron oxides (almost 70% Fe removed in this fraction). The crystalline Fe-ox-bound Fe is most likely to be in the form of co-precipitates since surface-bound forms would have been removed by the acetate. Finally, only ~30% U was strongly complexed directly by the humic substances and was unable to be released by either of these reagents. On the basis of these results, it is proposed that there are three main associations of U within the solid phase:

U^{VI}---(humic/Fe)	exchangeable/weak surface complex
U^{VI}-$FeOx_{cryst}$-humic	co-precipitate
U^{VI}-humic	strong complexation

5.3.6 Associations of U within the soil porewaters: evidence from gel filtration chromatography and sequential extraction combined with colloid isolation

Importantly, as already discussed in the preceding sections, gel chromatographic fractionation of the porewater colloids demonstrated that the U and Fe (and Cu) were again associated with the largest humic colloids whilst other elements such as Mn, As and Ca were associated with smaller humic colloids and Zn could be easily removed from the humic colloids.

In order to compare the solid phase associations of U with those in the aqueous phase, the acetate reagent was applied to the colloid fraction isolated the porewaters from a soil profile (section 4.2.2). This demonstrated that 85-95% colloidal-associated U was removed by the acetate reagent and thus dithionite was not applied (Figure 4.29). Importantly, there was no difference between the results from experiments carried out in air or under N_2 and so it is highly unlikely that U^{IV} was being released, oxidized and then U^{VI} complexed by the acetate reagent, a process which had been identified by Jelenic et al. (1964). Clearly, the results from this study support only one main association between U^{VI} and the porewater colloids:

U^{VI}---(humic/Fe)	exchangeable/weak surface complex

Interestingly, 60-80% Fe was also removed from the colloids and so there was very little, if any, in the form of crystalline oxides. Thus Fe within the colloid fraction of the porewaters was also held either at exchangeable sites or in the form of weak surface complexes. The same applies to Mn and Al associations with the humic-rich colloids.

Once removed to the solid phase, there is a loss of the exchangeable/weak complexes of Fe, Mn and Al from the humic material. Redox transformation of Fe within the solid phase leads to the intimate association of crystalline FeOx with the humic material and a gradual transformation in the associations of U. In the upper sections (0-30 cm), crystalline FeOx account for ~40% of U binding within the soils but at greater depth there is a return to exchangeable forms, i.e. whereby U is associated with humic substances. Figure 5.25 summarises the transformations of U associations within the porewaters and solid phase soils at the Needle's Eye site.

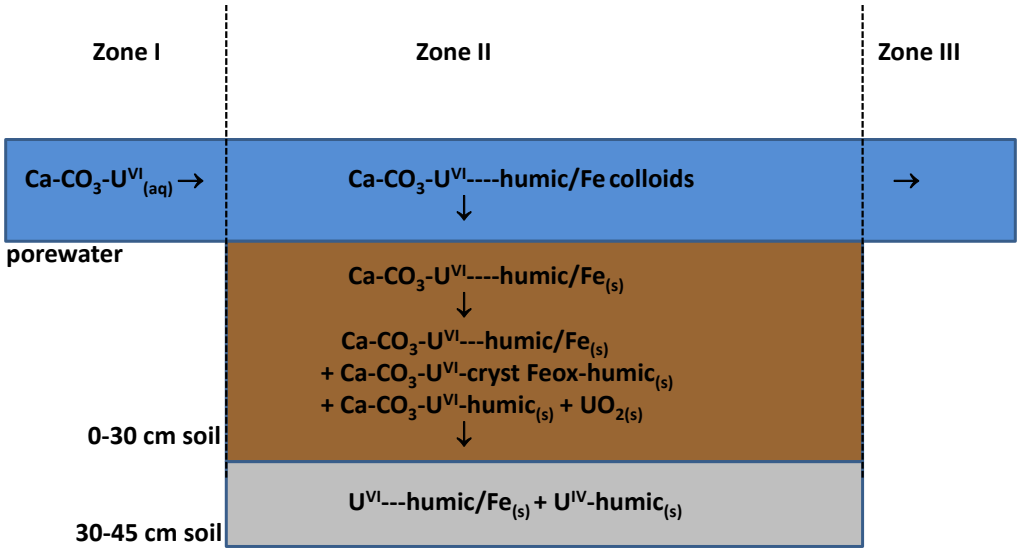

Figure 5.25 Conceptual model of transformations in U associations within the organic-rich soils and associated porewaters at the Needle's Eye site

Although the formation of calcium carbonato complexes has been shown to inhibit the reduction of U^{VI} (e.g. Stewart et al., 2007) and there is strong evidence from the results of this study that U^{VI} becomes associated with humic/Fe colloids, a key question remains: how do negatively charged U^{VI} species such as $UO_2(CO_3)_2^{2-}$ and $CaUO_2(CO_3)_3^{2-}$ interact with negatively charged humic colloids? Very recently, Steudtner et al. (2011a) used Time Resolved Laser Induced Fluorescence Spectroscopy (TRLIFS) to demonstrate the

formation of ternary U^{VI} humate complexes in solutions containing dissolved CO_2.The stability constant for$UO_2(CO_3)$HAwas found to be 24.47±0.70, indicating that a strong complex had been formed (Steudtner et al., 2011a). In this study, it is proposed that this type of interaction accounts for the ~30% U^{VI} that is directly bound to the humic substances and is not removed by either the acetate or dithionite reagents.

Wazne et al. (2003) studied the effects of carbonate complexation on hexavalent uranium adsorption by Fe oxyhydroxides. They concluded that the effects on sorption and on mobility of U(VI) were dramatic. U^{VI} was present as cationic species in the absence of carbonate and as anionic species in the presence of carbonate at neutral pH. FTIR spectra showed that, in the presence of carbonate, adsorbed U^{VI} was retained as uranyl carbonate complexes on the surface of iron oxyhydroxides. Bargar et al. (2000) showed that sorption of such complexes caused the reversal in the zeta potential of the Fe surfaces in the pH range 6.5-8.0 and the magnitude of the reversal increased with increasing total U^{VI} concentration. Reversal was attributed to formation of anionic ternary uranyl surface complexes ($UO_2(CO_3)^0$ at pH<7.6 – no effect on charge; $UO_2(CO_3)_2^{2-}$ at pH>7.6 – reversal of charge). Wazne et al. (2003) also modeled the speciation of U^{VI} in the presence and absence of carbonate. In carbonate-free systems, $(UO_2)_3(OH)_5^+$ was the main species present in solution at pH 6-8 whilst in the presence of carbonate, the double negatively charged carbonate was the main species with the neutral carbonate species as the other species in solution. The model output indicated that the bicarbonate species interacted via bidentate co-ordination. Thus, the weak interaction occurring between U^{VI} and the humic/Fe colloids within the porewaters at Needle's Eye may involve similar co-ordination via the bicarbonate ligand.

Wazne et al. (2003) also investigated the effect of increasing carbonate concentration and found that, at higher concentrations, the multicarbonate complexes become dominant and started to form at lower pH values. This favoured U^{VI} remaining in solution by the formation of stable complexes but the carbonate ion also competed with U^{VI} for surface sites, again favouring U^{VI} remaining in solution. This may explain why, for example, ~10% U^{VI} remains in the truly dissolved fraction of the Zone I soil porewaters.

Once removed from the porewaters, the results for Zone II soils indicated a transformation to U associations with crystalline Fe oxides (Figure 5.26) and there was also evidence to support fluctuations in the position of the Fe^{III}/Fe^{II} redox boundary at some locations (e.g.

25 m from the cave). Uranium has been found in coprecipitates (U/Cu/Fe) in various geochemical settings, including organic-rich soils (e.g. Sato et al., 1997; Pett-Ridge et al., 2007). It remains unresolved, however, as to how U is incorporated into these solids and what factors control their solubility. U sorption to oxide surfaces followed by incorporation into the oxide structure as well as U and Fe coprecipitation have been postulated as potential explanations (Murakami et al., 1997; Gu et al., 2003; Payne et al., 1996). An important point is that U^{VI} incorporation into mineral phases has the potential to occur readily under geochemical conditions that do not promote U^{VI} reduction, e.g. in the presence of $Ca\text{-}UO_2\text{-}CO_3$ complexes.

In a recent study, Stewart et al. (2009) investigated the stability of uranium incorporated into Fe (hydr)oxides under fluctuating redox conditions. Uranium in U^{VI}-ferrihydrite-Fe^{II} systems was separated into 4 pools – dissolved U^{VI}, U^{VI} adsorbed onto surfaces of Fe hydroxides (estimated by $KHCO_3$ desorption treatment), U incorporated into the Fe mineral structure and solid phase $U^{IV}O_2$.

In systems without Fe^{II}, U^{VI} resided in the aqueous phase or was adsorbed onto mineral surfaces during anoxic-to-oxic experiments. In systems where Fe^{II} was present, there was no U^{VI} in solution. Instead, U^{VI} was either adsorbed onto mineral surfaces or incorporated into Fe mineral structures. Where Fe^{II} concentrations were high (10 mM = ~5.6 mg L^{-1}), some U was present as $UO_{2(s)}$. Such concentrations were considered to be likely under stimulated (artificially added labile OM) reducing conditions. In this study, the maximum Fe concentration within the Zone II soil porewaters was ~3.2 mg L^{-1} and typically values were <1 mg L^{-1}. At lower Fe^{II} concentrations, however, Stewart et al. (2009), found that the U^{VI} incorporated into $Fe^{II/III}$ mineral structures was less affected by fluctuations in redox conditions. Transformation of Fe oxides through dissolution-precipitation coupled with the formation of ternary $Ca\text{-}UO_2\text{-}CO_3$ complexes was considered to be the key to U^{VI} incorporation into stable iron oxide solids. In this study, the role of humic-bound crystalline Fe oxides in retaining U^{VI} in the solid phase is evident over the 0-30 cm depth sections. Only below 30 cm, where conditions become sufficiently reducing for Fe sulphide formation, is this sink for U lost.

Overall, the majority of literature studies suggest that negatively charged U^{VI} species can interact with both humic substances and humic-associated Fe in both the porewater and the solid phase at the Needle's Eye site. Initially, this is a weak interaction but over time, some

of this U^{VI} becomes incorporated into crystalline Fe phases within the solid phase and some becomes directly and strongly bound to the humic substances. Small-scale U^{VI} reduction to U^{IV} and precipitation as crystalline $UO_{2(s)}$ was also evident from the detection of a small number of such particles within the peat (Figure 4.12).

5.4 Characteristics of U species remaining in the soil porewaters beyond the limits of the boggy soils

The results of this study suggest that ~55% of the small amounts of U exiting the boggy area was in colloidal form. From the core 5 data, most of this was associated with large humic colloids and further removal to the solid phase with increasing distance would be predicted. The highest amounts of truly dissolved U were found in the surface 0-5 cm sections of the soil porewaters and, given that the pH of these waters was ~8, negatively charged carbonate species would again be expected. These may interact with solid phase substrates in the same way as described for the boggy soil although it should be borne in mind that the greater mineral contents of the saltmarsh soils may influence the relative importance of different binding modes identified for the boggy soils.

6 Conclusions

The following questions were posed at the beginning of chapter 5:

(i) Is the change in the aqueous speciation of U when the waters emerging from the cliff comes into contact with the boggy soils attributable to the presence of organic/inorganic colloids or to the change in redox status?

(ii) How is U retained within the boggy soils and how does this relate to its aqueous phase speciation?

(iii) Do transformations in U associations occur within the soil and, if so, do these influence its mobility?

(iv) What forms of U are transported out of the boggy soils towards the saltmarsh?

In conclusion:

Question (i):

Uranium in the cave waters emerging from the mineralization was present at concentrations of up to 240 μg L^{-1}, primarily in dissolved forms, e.g. $CaUO_2(CO_3)_3^{2-}$, $Ca_2UO_2(CO_3)_3^{0}$ and $UO_2(CO_3)^{2-}$. Although Ca-U-CO_3 ternary complexes are thought to inhibit U^{VI} reduction, porewater U concentrations decreased by a factor of up to ~100 by a distance of ~30 m from the cave. Upon entering the boggy soils in Zone I, most of the U remaining in solution was weakly associated with humic-Fe colloids.

Question (ii)

Within Zone II soils, evidence from the gel chromatographically fractionated porewater colloids showed preferential association of U with the largest humic-Fe colloids and fractionation of solid phase humic substances again showed preferential association with the largest humic-Fe molecules. It was proposed that the main mechanism of U removal from the porewaters to the Zone II soils was by sorption of large U-Fe-humic colloids to the solid phase.

Question (iii)

Within the Zone II soils, redox-related processes involving transformation of Fe phases led to the incorporation of U^{VI} into humic-bound crystalline Fe oxides which were stable to depths of >30 cm. Redox-related processes were also implicated in the formation of small amounts of crystalline $U^{IV}O_2$. In the 0-30 cm sections, strong Ca-UO_2-CO_3-humic complexes were also formed. At depths of >30 cm, weaker interactions between U^{VI} and humic-Fe entities again prevailed as the crystalline Fe oxides were transformed to Fe sulfides. There was evidence from some cores that truly dissolved U was released into the porewaters and this appeared to be related to dissolution of mineral phases within the mineral-rich sections of the soils (30-45 cm) but the controlling mechanisms were not fully elucidated.

Question (iv)

The concentrations of U in porewaters in Zone III were <15 μg L^{-1} and, on some occasions <3 μg L^{-1}. In the 0-5 cm sections of the soils, ~55% was in colloidal form whilst, at depths of 5-20 cm, the proportion in colloidal form was >80%. Since the majority was present in large colloidal form, it is likely that most of this will be attenuated within the solid phase before reaching the Southwick Water.

Wider implications

This study has demonstrated that U^{VI} can prevail even under highly reducing conditions within organic-rich soils and this has implications for its long-term fate since U^{VI} is generally considered to be much more mobile than U^{IV}. However, U^{VI} was efficiently removed from the aqueous phase following interaction with humic-Fe colloids and such processes appear to be effective in the long-term storage of U within the organic-rich soils. Clearly, changes in U association occur following deposition and the incorporation into stable crystalline Fe oxides (bound to humic substances) may be a major factor influencing the long-term storage in the solid phase.

Should the predicted effects of climate change, resulting in warmer and drier conditions, lead to drying out of organic-rich soils, degradation of the organic matter could lead to the release of humic-Fe-U colloids into soil porewaters. At the Needle's Eye site, these colloids were found to be very large in size but alteration of the organic matter might yield lower molecular weight, more mobile species and thus large quantities of U could be transported

over considerable distances. This would also apply to other U-contaminated organic-rich soils such as those found in Switzerland and the US.

7 Further Work

Since this project involved detailed characterisation of U associations with different fractions within the soil, determination of U oxidation state was considered to be beyond the scope of current XAS techniques. However, recent literature suggests that the concentrations of U associated with humic substances within the Needle's Eye soils might be now above detectable limits and so future work should focus on applying XAS in conjunction with the methods developed to distinguish the three different associations (direct/indirect) of U with solid phase humic substances.

The novel experiments developed in this study to distinguish between U bound to humic-bound Fe phases and that bound directly to humic substances can be applied to study other current environmental issues. For example, the associations of As in groundwaters from West Bengal (and other such regions where As is considered to be a major threat to human health) could be readily investigated using the ultrafiltration/sequential extraction method.

Colloid characterisation could also be enhanced by the determination of zeta potential as a measure of surface charge as well as by the use of SEM-EDX to identify mineral components and the presence of organic coatings.

The processes resulting in the release of truly dissolved U, Mn, Fe and Al at depths of >30 cm require more thorough evaluation. This would require further characterisation of the solid phase and relationships with porewater chemistry. In order to minimise future disturbance of the boggy area, this may be best achieved via installation of porewater sampling devices. Isolation and fractionation of such porewaters should be carried out under N_2 since this study has demonstrated that changes in the distribution of U between colloidal and truly dissolved forms do occur in air.

Finally, previous work has suggested that U accumulates around root channels in the boggy soils and that the presence of U-As-Cu and Bi bearing minerals indicated that fungi were important in attenuating mobile U (Basham et al., 1989; Hooker et al., 1989). A comparison of the behaviour of U and Th (including analysis of their radioactive decay products) could be useful in elucidating such attenuation processes.

8 References

Abdelouas, A. (2006). Uranium mill tailings: geochemistry, mineralogy, and environmental impact. *Elements*, *2*(6), 335-341.

Abiven, S., Menasseri, S., & Chenu, C. (2009).The effects of organic inputs over time on soil aggregate stability–A literature analysis.*Soil Biology and Biochemistry*, *41*(1), 1-12.

Agilent Technologies, (2005), Agilent 7500 ICP- MS Hardware Manual.

Ahearne, J. F. (1997). Radioactive waste: the size of the problem. *Physics Today*, *50*, 24.

Ahonen, L., Ervanne, H., Ruskeeniemi, T., Jaakkola, T., & Blomqvist, R. (1992). Uranium Mineral–Groundwater Equilibration at the Palmottu Natural Analogue Study Site, Finland.In *MRS Proceedings* (Vol. 294).Cambridge University Press.

Aiken, G. R., McKnight, D. M., Thorn, K. A., & Thurman, E. M. (1992). Isolation of hydrophilic organic acids from water using nonionic macroporous resins. *Organic Geochemistry*, *18*(4), 567-573.

Alianiello, F. (2003).Isoelectric focusing in soil science.*Journal of separation science*, *26*(5), 387-391.

Allan, R. L. (1993). *Distribution, geochemistry and geochronology of Sellafield waste in contaminated Solway Firth floodplain deposits* (Doctoral dissertation, University of Glasgow).

Alwan, A. K., & Williams, P. A. (1980).The aqueous chemistry of uranium minerals.Part 2.Minerals of the liebigite group.*Mineralogical Magazine*, *43*(329), 665-667.

Amezketa, E. (1999). Soil aggregate stability: A review. *Journal of sustainable agriculture*, *14*(2-3), 83-151.

Artinger, R., Rabung, T., Kim, J. I., Sachs, S., Schmeide, K., Heise, K. H., ...& Nitsche, H. (2002). Humic colloid-borne migration of uranium in sand columns.*Journal of contaminant hydrology*, *58*(1), 1-12.

Arunachalam, J., Emons, H., Krasnodebska, B., & Mohl, C. (1996). Sequential extraction studies on homogenized forest soil samples. *Science of the total environment*, *181*(2), 147-159.

Ashman, M., & Puri, G. (2008).*Essential soil science: a clear and concise introduction to soil science*. Wiley-Blackwell.

Bacon, J. R., & Davidson, C. M. (2008). Is there a future for sequential chemical extraction?.*Analyst*, *133*(1), 25-46.

Bargar, J. R., Reitmeyer, R., Lenhart, J. J., & Davis, J. A. (2000). Characterization of U (VI)-carbonato ternary complexes on hematite: EXAFS and electrophoretic mobility measurements. *Geochimica et Cosmochimica Acta*, *64*(16), 2737-2749.

Bargar, J. R., Kubicki, J. D., Reitmeyer, R., & Davis, J. A. (2005). ATR-FTIR spectroscopic characterization of coexisting carbonate surface complexes on hematite. *Geochimica et cosmochimica acta*, *69*(6), 1527-1542.

Basham, I. R., Milodowski, A. E., & Hyslop, E. K. (1989).*The Location of Uranium in Source Rocks and Sites of Secondary Deposition in the Needle's Eye Natural Analogue Site, Dumfries and Galloway*. Great Britain, Her Majesty's Inspectorate of Pollution.

Bazilevskaya, E., Archibald, D. D., Aryanpour, M., Kubicki, J. D., & Martínez, C. E. (2011). Aluminum coprecipitates with Fe (hydr) oxides: Does isomorphous substitution of Al^{3+} for Fe^{3+} in goethite occur?.*Geochimica et Cosmochimica Acta*, *75*(16), 4667-4683.

Beck, H. L., & Miller, K. M. (1980).Some radiological aspects of coal combustion.*Nuclear Science, IEEE Transactions on*, *27*(1), 689-694.

Becker, S. (2008). *Inorganic mass spectrometry: principles and applications*. Wiley-Interscience.

Bednar, A. J., Medina, V. F., Ulmer-Scholle, D. S., Frey, B. A., Johnson, B. L., Brostoff, W. N., & Larson, S. L. (2007). Effects of organic matter on the distribution of uranium in soil and plant matrices. *Chemosphere*, *70*(2), 237-247.

Bernhard, G., Geipel, G., Reich, T., Brendler, V., Amayri, S., & Nitsche, H. (2001). Uranyl (VI) carbonate complex formation: Validation of the $Ca_2UO_2(CO_3)_3$ (aq.) species. *Radiochimica Acta*, *89*(8), 511.

Berrow, M. L., & Mitchell, R. L. (1980). Location of trace elements in soil profiles: total and extractable contents of individual horizons. *Transactions of the Royal Society of Edinburgh: Earth Sciences*, *71*(2), 103-121.

Biederbeck, V. O., & Paul, E. A. (1973).Fractionation of soil humate with phenolic solvents and purification of the nitrogen-rich portion with polyvinylpyrrolidone.*Soil Science*, *115*(5), 357-366.

Bleise, A., Danesi, P. R., & Burkart, W. (2003). Properties, use and health effects of depleted uranium (DU): a general overview. *Journal of Environmental Radioactivity*, *64*(2), 93-112.

Blomqvist, R., Ruskeeniemi, T., Kaija, J., Ahonen, L., Paananen, M., Smellie, J., ...& Frape, S. (2000). The Palmottu natural analogue project(Phase II, Transport of radionuclides in a natural flow system at Palmottu). *EUR(Luxembourg)*.

Boss, C. B., & Fredeen, K. J. (2004). *Concepts, instrumentation and techniques in inductively coupled plasma optical emission spectrometry* (Vol. 997). Norwalk: Perkin Elmer.

Bosshard, E., Zimmerli, B., & Schlatter, C. (1992). Uranium in the diet: risk assessment of its nephro-and raditoxicity. *Chemosphere*, *24*(3), 309-322.

Brady, N. C., & Weil, R. R. (2007). *The nature and properties of soils* (No.Ed. 14). Prentice-Hall Inc..

Braithwaite, A., Livens, F. R., Richardson, S., Howe, M. T., & Goulding, K. W. T. (1997). Kinetically controlled release of uranium from soils.*European journal of soil science*, *48*(4), 661-673.

Brase, C. H., & Brase, C. P. (2012).*Understanding basic statistics*.Brooks/Cole.

Bricker, O. P. (1964). *Stability Relations in the System Mn-O2-H2O at 25° C and One Atmosphere Total Pressure* (Doctoral dissertation).

British Standards Institution, (1996). British Standard, Water quality, determination of alkalinity, determination of total and composite alkalinity, BS EN ISO 9963-1:1996, BS

6068-2.51:1996.

Bronick, C. J., & Lal, R. (2005). Soil structure and management: a review. *Geoderma*, *124*(1), 3-22.

Brooks, S. C., Fredrickson, J. K., Carroll, S. L., Kennedy, D. W., Zachara, J. M., Plymale, A. E., ... & Fendorf, S. (2003). Inhibition of bacterial U (VI) reduction by calcium.*Environmental science & technology*, *37*(9), 1850-1858.

Bruland, K. W., Rue, E. L., Donat, J. R., Skrabal, S. A., & Moffett, J. W. (2000). Intercomparison of voltammetric techniques to determine the chemical speciation of dissolved copper in a coastal seawater sample. *Analytica Chimica Acta*, *405*(1), 99-113.

Bruno, J., Casas, I., Cera, E., & Duro, L. (1997). Development and application of a model for the long-term alteration of UO_2 spent nuclear fuel Test of equilibrium and kinetic mass transfer models in the Cigar Lake ore deposit. *Journal of contaminant hydrology*, *26*(1), 19-26.

Bruno, J., Duro, L., & Grivé, M. (2002). The applicability and limitations of thermodynamic geochemical models to simulate trace element behaviour in natural waters. Lessons learned from natural analogue studies. *Chemical Geology*, *190*(1), 371-393.

Burba, P., Aster, B., Nifant'eva, T., Shkinev, V., & Spivakov, B. Y. (1998). Membrane filtration studies of aquatic humic substances and their metal species: a concise overview: Part 1. Analytical fractionation by means of sequential-stage ultrafiltration.*Talanta*, *45*(5), 977-988.

Canfield, D. E. (1988).*Sulfate reduction and the diagenesis of iron in anoxic marine sediments*. Yale University.

Catalano, J. G., Heald, S. M., Zachara, J. M., & Brown, G. E. (2004). Spectroscopic and diffraction study of uranium speciation in contaminated vadose zone sediments from the Hanford Site, Washington State. *Environmental science & technology*, *38*(10), 2822-2828.

Calmano, W., & Förstner, U. (1983).Chemical extraction of heavy metals in polluted river sediments in central Europe.*Science of the total Environment*, *28*(1), 77-88.

Cavani, L., Trubetskaya, O., Grigatti, M., Trubetskoj, O., & Ciavatta, C. (2008).Electrofocusing the compost organic matter obtained by coupling SEC–PAGE.*Bioresource technology*, *99*(10), 4360-4367.

Chao, T. T., & Zhou, L. (1983). Extraction techniques for selective dissolution of amorphous iron oxides from soils and sediments.*Soil Science Society of America Journal*, *47*(2), 225-232.

Chamberlain, A. C. (1981). *Emission of fission products and other activities during the accident to Windscale Pile No. 1 in October 1957*. UKAEA Atomic Energy Research Establishment, Harwell, Environmental & Medical Sciences Division.

Chapman, N. A., McKinley, I. G., Shea, M. E., & Smellie, J. A. T. (1993). The Poços de Caldas project: Natural Analogues of Processes in a Radioactive Waste Repository. *Journal of Geochemical Exploration*, *45*(1-3).

Charles, M. W., & Harrison, J. D. (2007). Hot particle dosimetry and radiobiology—past and present. *Journal of Radiological Protection*, *27*(3A), A97.

Chen, J., Gu, B., Royer, R. A., & Burgos, W. D. (2003). The roles of natural organic matter in chemical and microbial reduction of ferric iron.*Science of the total environment*, *307*(1), 167-178.

Cheng, T., Barnett, M. O., Roden, E. E., & Zhuang, J. (2006). Effects of solid-to-solution ratio on uranium (VI) adsorption and its implications.*Environmental science & technology*, *40*(10), 3243-3247.

Choppin, G. R., & Allard, B. E. R. T. (1985). Complexes of actinides with naturally occurring organic compounds.*Handbook on the Physics and Chemistry of the Actinides*, *3*, 407.

Choppin, G. R. (1992). The role of natural organics in radionuclide migration in natural aquifer systems.*Radiochimica Acta*, *58*, 113-113.

Christl, I., Knicker, H., Kögel‐Knabner, I., & Kretzschmar, R. (2000). Chemical heterogeneity of humic substances: characterization of size fractions obtained by hollow‐fibre ultrafiltration. *European Journal of Soil Science*, *51*(4), 617-625.

Chorover, J., Zhang, J., Amistadi, M. K., & Buffle, J. (1997). Comparison of hematite coagulation by charge screening and phosphate adsorption: Differences in aggregate structure. *Clays and clay minerals*, *45*(5), 690-708.

Chuan, M. C., Shu, G. Y., & Liu, J. C. (1996). Solubility of heavy metals in a contaminated soil: effects of redox potential and pH. *Water, Air, and Soil Pollution*, *90*(3-4), 543-556.

Clarke, R. H. (1974). An analysis of the 1957 Windscale accident using the WEERIE code.*Annals of Nuclear Science and Engineering*, *1*(2), 73-82.

Claveranne-Lamolère, C., Lespes, G., Dubascoux, S., Aupiais, J., Pointurier, F., & Potin-Gautier, M. (2009). Colloidal transport of uranium in soil: Size fractionation and characterization by field-flow fractionation–multi-detection. *Journal of Chromatography A*, *1216*(52), 9113-9119.

Claveranne-Lamolère, C., Aupiais, J., Lespes, G., Frayret, J., Pili, E., Pointurier, F., & Potin-Gautier, M. (2011). Investigation of uranium–colloid interactions in soil by dual field-flow fractionation/capillary electrophoresis hyphenated with inductively coupled plasma-mass spectrometry. *Talanta*, *85*(5), 2504-2510.

Cook, G. T., Baxter, M. S., Duncan, H. J., & Malcolmson, R. (1984). Geochemical associations of plutonium and γ-emitting radionuclides in Caithness soils and marine particulates.*Journal of Environmental Radioactivity*, *1*(2), 119-131.

Courchesne, F., & Turmel, M. C. (2007).Extractable Al, Fe, Mn, and Si.*Soil sampling and methods of analysis. 2nd ed. CRC Press, Boca Raton, FL*, 307-315.

Craft, E. S., Abu-Qare, A. W., Flaherty, M. M., Garofolo, M. C., Rincavage, H. L., & Abou-Donia, M. B. (2004). Depleted and natural uranium: chemistry and toxicological effects. *Journal of Toxicology and Environmental Health, Part B*, *7*(4), 297-317.

Crancon, P., Pili, E., & Charlet, L. (2010). Uranium facilitated transport by water-dispersible colloids in field and soil columns. *Science of the Total Environment*, *408*(9), 2118-2128.

Cramer, J. J., & Smellie, J. A. (1994).Final report of the AECL/SKB Cigar Lake analog study.*AECL research/Atomic energy of Canada ltd*.

Cresser, M., Killham, K., & Edwards, A. (1993).*Soil chemistry and its applications* (Vol. 5). Cambridge University Press.

Curtis, C. J., & Simpson, G. L. (2012). Trends in bulk deposition of acidity in the UK, 1988–2007, assessed using additive models. *Ecological Indicators*.

Davison, W. (1993). Iron and manganese in lakes.*Earth-Science Reviews*, *34*(2), 119-163.

De Nobili, M., Bragato, G., Alcaniz, J. M., Puigbo, A., & Comellas, L. (1990).Characterization of electrophoretic fractions of humic substances with different electrofocusing behavior.*Soil Science*, *150*(5), 763-770.

Deffeyes, K. S., & MacGregor, I. D. (1980). World uranium resources. *Scientific American*, *242*(1), 66-76.

Dobbs, R. A., Wise, R. H., & Dean, R. B. (1972). The use of ultra-violet absorbance for monitoring the total organic carbon content of water and wastewater.*Water Research*, *6*(10), 1173-1180.

Dodge, C. J., Francis, A. J., Gillow, J. B., Halada, G. P., Eng, C., & Clayton, C. R. (2002). Association of uranium with iron oxides typically formed on corroding steel surfaces. *Environmental science & technology*, *36*(16), 3504-3511.

Dong, W., Xie, G., Miller, T. R., Franklin, M. P., Oxenberg, T. P., Bouwer, E. J., ...& Halden, R. U. (2006). Sorption and bioreduction of hexavalent uranium at a military facility by the Chesapeake Bay.*Environmental Pollution*, *142*(1), 132-142.

Dong, W., & Brooks, S. C. (2006). Determination of the formation constants of ternary complexes of uranyl and carbonate with alkaline earth metals (Mg2+, Ca2+, Sr2+, and Ba2+) using anion exchange method. *Environmental science & technology*, *40*(15), 4689-4695.

Dreissig, I., Weiss, S., Hennig, C., Bernhard, G., & Zänker, H. (2011). Formation of uranium (IV)-silica colloids at near-neutral pH.*Geochimica et Cosmochimica Acta*, *75*(2), 352-367.

Duff, M. C., Coughlin, J. U., & Hunter, D. B. (2002). Uranium co-precipitation with iron oxide minerals.*Geochimica et Cosmochimica Acta*, *66*(20), 3533-3547.

Duxbury, J. M. (1989). Studies of the molecular size and charge of humic substances by electrophoresis.*MB Hayes, P. MacCarthy, RL Malcolm and RS Swift,"Humic Substances II, In Search of Structure*, *1*, 257-409.

Echevarria, G., Sheppard, M. I., & Morel, J. (2001). Effect of pH on the sorption of uranium in soils.*Journal of Environmental Radioactivity*, *53*(2), 257-264.

Egeberg, P. K., & Alberts, J. J. (2002). Determination of hydrophobicity of NOM by RP-HPLC, and the effect of pH and ionic strength. *Water research*, *36*(20), 4997-5004.

Emeis, K. C., Struck, U., Leipe, T., Pollehne, F., Kunzendorf, H., & Christiansen, C. (2000). Changes in the C, N, P burial rates in some Baltic Sea sediments over the last 150 years—relevance to P regeneration rates and the phosphorus cycle. *Marine Geology*, *167*(1), 43-59.

ENRESA (1996).TRAnSin, versión ii.Fortran code for solving the coupled flow and transport inverse problem in saturated conditions. El Berrocal Project.Characterization and validation of natural radionuclide migration processes under real conditions on the fissured granitic environment.

Erbs, J. J., Berquó, T. S., Reinsch, B. C., Lowry, G. V., Banerjee, S. K., & Penn, R. L. (2010). Reductive dissolution of arsenic-bearing ferrihydrite.*Geochimica et Cosmochimica Acta*, *74*(12), 3382-3395.

Essington, M. E. (2003). *Soil and water chemistry: An integrative approach*. CRC press.

ESFA (2009). Uranium in foodstuffs, in particular mineral water.Scientific Opinion of the Panel on Contaminants in the Food Chain.*The European Food Safety Authority.*

Farmer, J. G., Thomas, R. P., Graham, M. C., Geelhoed, J. S., Lumsdon, D. G., & Paterson, E. (2002). Chromium speciation and fractionation in ground and surface waters in the vicinity of chromite ore processing residue disposal sites.*Journal of Environmental Monitoring*, *4*(2), 235-243.

Farrah, H., & Pickering, W. F. (1993).Factors influencing the potential mobility and bioavailability of metals in dried lake sediments.*Chemical Speciation and Bioavailability*, *5*(3), 81-96.

Feng, X., Simpson, A. J., & Simpson, M. J. (2005).Chemical and mineralogical controls on humic acid sorption to clay mineral surfaces.*Organic Geochemistry*, *36*(11), 1553-1566.

Ferreira, J. A., Nascimento, O. R., & Martin-Neto, L. (2001).Hydrophobic interactions between spin-label 5-SASL and humic acid as revealed by ESR spectroscopy.*Environmental science & technology*, *35*(4), 761-765.

Filgueiras, A. V., Lavilla, I., & Bendicho, C. (2002).Chemical sequential extraction for metal partitioning in environmental solid samples.*Journal of Environmental Monitoring*, *4*(6), 823-857.

Finch, R., & Murakami, T. (1999). Systematics and paragenesis of uranium minerals. *Reviews in Mineralogy and Geochemistry*, *38*(1), 91-179.

Forstner, U. (1983). Bonding Forms of Heavy Metals in Sediments and Sludges: Sorption/Mobilization, Chemical Extraction and Bioavailability (Bindungsformen von Schwermetallen in Sedimenten und Schlammen: Sorption/Mobilisierung, chemische Extraktion und Bioverfugbarkeit). *Fresenius Zeitschrift fur Analytische Chemie*, *316*(6).

Fossing, H., & Jørgensen, B. B. (1989). Measurement of bacterial sulfate reduction in sediments: evaluation of a single-step chromium reduction method. *Biogeochemistry*, *8*(3), 205-222.

Francis, A. J., Gillow, J. B., Dodge, C. J., Harris, R., Beveridge, T. J., & Papenguth, H. W. (2004). Uranium association with halophilic and non-halophilic bacteria and archaea.*Radiochimica Acta/International journal for chemical aspects of nuclear science and technology*, *92*(8/2004), 481-488.

Gaffney, J. W., White, K. N., & Boult, S. (2008). Oxidation state and size of Fe controlled by organic matter in natural waters.*Environmental science & technology*, *42*(10), 3575-3581.

Garfin, D., & Ahuja, S. (Eds.). (2005). Overview.*Handbook of isoelectric focusing and proteomics* (Vol. 7). Academic Press.

Garland, J. A., & Wakeford, R. (2007).Atmospheric emissions from the Windscale accident of October 1957. *Atmospheric Environment*, *41*(18), 3904-3920.

Gavin, K. G., Farmer, J. G., Graham, M. C., Kirika, A., & Britton, A. (2001).Manganese-humic interactions in the catchment, water and sediment of Loch Bradan, SW Scotland.*Understanding and managing Organic Matter in Soils, Sediments and Waters.IHSS*.

Geckeis, H., Rabung, T., Manh, T. N., Kim, J. I., & Beck, H. P. (2002). Humic colloid-borne natural polyvalent metal ions: dissociation experiment. *Environmental science & technology*, *36*(13), 2946-2952.

Gleyzes, C., Tellier, S., & Astruc, M. (2002). Fractionation studies of trace elements in contaminated soils and sediments: a review of sequential extraction procedures. *TrAC Trends in Analytical Chemistry*, *21*(6), 451-467.

González A, Z. I., Krachler, M., Cheburkin, A. K., & Shotyk, W. (2006). Spatial distribution of natural enrichments of arsenic, selenium, and uranium in a minerotrophic peatland, Gola di Lago, Canton Ticino, Switzerland. *Environmental science & technology*, *40*(21), 6568-6574.

Graham, M. C. (1995). *An investigation of actinide interactions with humic substances* (PhD thesis, University of Glasgow).

Graham, M. C., Vinogradoff, S. I., Abbott, A., & Farmer, J. G. (2000). Application of gel electrophoretic techniques to the investigation of actinide-humic interactions in soils.*Radiochimica Acta*, *88*(9-11), 77-7785.

Graham, M. C., Gavin, K. G., Farmer, J. G., Kirika, A., & Britton, A. (2002).Processes controlling the retention and release of manganese in the organic-rich catchment of Loch Bradan, SW Scotland. *Applied geochemistry*, *17*(8), 1061-1067.

Graham, M. C., Vinogradoff, S. I., Chipchase, A. J., Dunn, S. M., Bacon, J. R., & Farmer, J. G. (2006). Using size fractionation and Pb isotopes to study Pb transport in the waters of an organic-rich upland catchment. *Environmental science & technology*, *40*(4), 1250-1256.

Graham, M. C., Oliver, I. W., MacKenzie, A. B., Ellam, R. M., & Farmer, J. G. (2008). An integrated colloid fractionation approach applied to the characterisation of porewater uranium–humic interactions at a depleted uranium contaminated site. *Science of the Total Environment*, *404*(1), 207-217.

Graham, M. C., Oliver, I. W., MacKenzie, A. B., Ellam, R. M., & Farmer, J. G. (2011). Mechanisms controlling lateral and vertical porewater migration of depleted uranium (DU) at two UK weapons testing sites. *Science of the Total Environment*, *409*(10), 1854-1866.

Graham, M. C., Gavin, K. G., Kirika, A., & Farmer, J. G. (2012). Processes controlling manganese distributions and associations in organic-rich freshwater aquatic systems: The example of Loch Bradan, Scotland. *Science of the Total Environment*, *424*(1), 239-250.

Gray, J., Jones, S. R., & Smith, A. D. (1995).Discharges to the environment from the Sellafield site, 1951-1992. *Journal of Radiological Protection*, *15*(2), 99.

Greenwood, N. N., Earnshaw, A., & Earnshaw, A. (1997).*Chemistry of the Elements* (Vol. 1341). Oxford: Butterworth-Heinemann.

Groenenberg, J. E., Dijkstra, J. J., Bonten, L. T., de Vries, W., & Comans, R. N. (2012). Evaluation of the performance and limitations of empirical partition-relations and process based multisurface models to predict trace element solubility in soils. *Environmental Pollution*, *166*, 98-107.

Gu, B., Brooks, S. C., Roh, Y., & Jardine, P. M. (2003). Geochemical reactions and dynamics during titration of a contaminated groundwater with high uranium, aluminum, and calcium.*Geochimica et cosmochimica acta*, *67*(15), 2749-2761.

Gu, B., & Chen, J. (2003). Enhanced microbial reduction of Cr (VI) and U (VI) by different natural organic matter fractions.*Geochimica et cosmochimica acta*, *67*(19), 3575-3582.

Gu, B., Wu, W. M., Ginder-Vogel, M. A., Yan, H., Fields, M. W., Zhou, J., ...& Jardine, P. M. (2005). Bioreduction of uranium in a contaminated soil column.*Environmental science & technology*, *39*(13), 4841-4847.

Guest, C. A., Schulze, D. G., Thompson, I. A., & Huber, D. M. (2002).Correlating manganese X-ray absorption near-edge structure spectra with extractable soil manganese.*Soil Science Society of America Journal*, *66*(4), 1172-1181.

Guillaumont, R., & Mompean, F. J. (2003). Update on the chemical thermodynamics of uranium, neptunium, plutonium, americium and technetium.

Günther, A., Geipel, G., & Bernhard, G. (2007). Complex formation of uranium (VI) with the amino acids l-glycine and l-cysteine: A fluorescence emission and UV–Vis absorption study. *Polyhedron*, *26*(1), 59-65.

Guo, L., & Santschi, P. H. (1996).A critical evaluation of the cross-flow ultrafiltration technique for sampling colloidal organic carbon in seawater.*Marine Chemistry*, *55*(1), 113-127.

Guo, L., Warnken, K. W., & Santschi, P. H. (2007). Retention behavior of dissolved uranium during ultrafiltration: Implications for colloidal U in surface waters. *Marine Chemistry*, *107*(2), 156-166.

Haas, J. R., & Northup, A. (1999). Effects of aqueous complexation on reductive precipitation of uranium by Shewanella putrefaciens. *Geochemical Transactions*, *5*(3), 41.

Hainfeld, J. F., Dilmanian, F. A., Slatkin, D. N., & Smilowitz, H. M. (2008). Radiotherapy enhancement with gold nanoparticles. *Journal of Pharmacy and Pharmacology*, *60*(8), 977-985.

Halliday, A. N., Stephens, W. E., & Harmon, R. S. (1980). Rb-Sr and O isotopic relationships in 3 zoned Caledonian granitic plutons, Southern Uplands, Scotland: evidence for varied sources and hybridization of magmas. *Journal of the Geological Society*, *137*(3), 329-348.

Hamilton, E. I. (1981). α-Particle radioactivity of hot particles from the Esk estuary.

Hayes, M. H. B., MacCarthy, P., Malcolm, R. L., & Swift, R. S. (1989). The search for structure: setting the scene. *Humic substances II: in search of structure. Chichester: J. Wiley*, 3-33.

Hiemstra, T., Riemsdijk, W. H. V., Rossberg, A., & Ulrich, K. U. (2009). A surface structural model for ferrihydrite II: Adsorption of uranyl and carbonate. *Geochimica et Cosmochimica Acta*, *73*(15), 4437-4451.

Hooker, P. J., MacKenzie, A. B., Scott, R. D., Ivanovich, M., Ball, T. K., Basham, I. R., ... & Roberts, P. D. (1986). Natural analogue of radionuclide migration: reconnaissance study of sites. *NERC Report FLPU*, *86*(6), 26.

Hooker, P. J. (1989). Modelling of the Needle's Eye natural analogue site. *BGS Technical Report* WE/90/5

Hooker, P. J. (1991). The geology, hydrogeology and geochemistry of the Needle's Eye natural analogue site. *BGS Technical Report* WE/90/5

Hostetler, P. B., & Garrels, R. M. (1962). Transportation and precipitation of uranium and vanadium at low temperatures, with special reference to sandstone-type uranium deposits.*Economic Geology*, *57*(2), 137-167.

Hu, Q. H., Weng, J. Q., & Wang, J. S. (2010). Sources of anthropogenic radionuclides in the environment: a review. *Journal of environmental radioactivity*, *101*(6), 426-437.

Hursh, J. B., & Spoor, N. L. (1973). Data on man.*Handbook of experimental pharmacology*, *36*, 197-240.

IAEA, (2008). The Semipalatinsk Test Site, Kazakhstan.

Ikeda-Ohno, A., Hennig, C., Tsushima, S., Scheinost, A. C., Bernhard, G., & Yaita, T. (2009).Speciation and structural study of U (IV) and-(VI) in perchloric and nitric acid solutions. *Inorganic chemistry*, *48*(15), 7201-7210.

Jackson, B. P., Ranville, J. F., Bertsch, P. M., & Sowder, A. G. (2005). Characterization of colloidal and humic-bound Ni and U in the “dissolved” fraction of contaminated sediment extracts. *Environmental science & technology*, *39*(8), 2478-2485.

Jacobsen, O. H., Moldrup, P., Larsen, C., Konnerup, L., & Petersen, L. W. (1997). Particle transport in macropores of undisturbed soil columns. *Journal of Hydrology*, *196*(1-4), 185-203.

James, R. O., & Parks, G. A. (1982). Characterization of aqueous colloids by their electrical double-layer and intrinsic surface chemical properties.In *Surface and colloid science* (pp. 119-216).Springer US.

Jamet, P., Doublet, R., Soubeyran R. (1989a). Hydrogeochemistry of the Needle’s Eye site-first interpretation. *BGS Technical Report* WE/89/55

Jamet, P., Lachassagne, P., Doublet, R., Ledoux, E. (1989b). Modelling of the Needle's Eye natural analogue. *BGS Technical Report* WE/89/64

Jamet, P., Hooker, P. J., Schmitt, J. M., Ledoux, E., & Des Orres, P. E. (1993). Hydrogeochemical modelling of an active system of uranium fixation by organic soils and sediments (Needle's Eye, Scotland). *Mineralium Deposita*, *28*(1), 66-76.

Janoš, P. (2003). Separation methods in the chemistry of humic substances. *Journal of Chromatography A*, *983*(1), 1-18.

Jelenic, I., Grdenic, D., & Bezjak, A. (1964). The crystal structure of uranium (IV) acetate. *Acta Crystallographica*, *17*(6), 758-759.

Jiménez, M. S., Gomez, M. T., Rodriguez, L., Velarte, R., & Castillo, J. R. (2010). Characterization of metal–humic acid complexes by polyacrylamide gel electrophoresis–laser ablation-inductively coupled plasma mass spectrometry. *Analytica chimica acta*, *676*(1), 9-14.

JNCC, (2001).UK Special Protection Areas and Wetlands of International Importance (Ramsar Sites).Status tracking report as at 31 March 2001.

Kampf, N., Scheinost, A. C., & Schulze, D. G. (2000).Oxide minerals.*Handbook of soil science. CRC Press, Boca Raton, FL*, 125-168.

Karim, S., Okuyama, Y., & Aoyama, M. (2013). Separation and characterization of the constituents of compost and soil humic acids by two-dimensional electrophoresis.*Soil Science and Plant Nutrition*, *59*(2), 130-141.

Kazi, T. G., Jamali, M. K., Kazi, G. H., Arain, M. B., Afridi, H. I., & Siddiqui, A. (2005). Evaluating the mobility of toxic metals in untreated industrial wastewater sludge using a BCR sequential extraction procedure and a leaching test. *Analytical and bioanalytical chemistry*, *383*(2), 297-304.

Keating, G. E., McCartney, M., & Davidson, C. M. (1996). Investigation of the technological enhancement of natural decay series radionuclides by the manufacture of phosphates on the Cumbrian coast.*Journal of environmental radioactivity*, *32*(1), 53-66.

Kelly, S. D., Kemner, K. M., & Brooks, S. C. (2007). X-ray absorption spectroscopy identifies calcium-uranyl-carbonate complexes at environmental concentrations. *Geochimica et cosmochimica acta*, *71*(4), 821-834.

Kelly, S. D. (2010). Uranium Chemistry in Soils and Sediments. *Developments in Soil Science*, *34*, 411-466.

Killops, S. D., & Killops, V. J. (2009). *An introduction to organic geochemistry*.Wiley-Blackwell.

Knicker, H., Almendros, G., González-Vila, F. J., Lüdemann, H. D., & Martin, F. (1995).^{13}C and ^{15}N NMR analysis of some fungal melanins in comparison with soil organic matter.*Organic Geochemistry*, *23*(11), 1023-1028.

Kopáček, P., Kaniansky, D., & Hejzlar, J. (1991).Characterization of humic substances by capillary isotachophoresis.*Journal of Chromatography A*, *545*(2), 461-470.

Krachler, M., Mohl, C., Emons, H., & Shotyk, W. (2002). Analytical procedures for the determination of selected trace elements in peat and plant samples by inductively coupled plasma mass spectrometry. *Spectrochimica Acta Part B: Atomic Spectroscopy*, *57*(8), 1277-1289.

Krawczyk-Bärsch, E., Arnold, T., Reuther, H., Brandt, F., Bosbach, D., & Bernhard, G. (2004).Formation of secondary Fe-oxyhydroxide phases during the dissolution of chlorite–effects on uranium sorption.*Applied Geochemistry*, *19*(9), 1403-1412.

Kremleva, A., Krüger, S., & Rösch, N. (2009). Role of aliphatic and phenolic hydroxyl groups in uranyl complexation by humic substances. *Inorganica Chimica Acta*, *362*(8), 2542-2550.

Krepelova, A., Sachs, S., & Bernhard, G. (2006). Uranium (VI) sorption onto kaolinite in the presence and absence of humic acid.*Radiochimica Acta*, *94*(12), 825-833.

Krepelová, A., Brendler, V., Sachs, S., Baumann, N., & Bernhard, G. (2007). U (VI)-kaolinite surface complexation in absence and presence of humic acid studied by TRLFS. *Environmental science & technology*, *41*(17), 6142-6147.

Kř'ibek, B., & Podlaha, J. (1980).The stability constant of the UO UO_2^{2+}-humic acid complex.*Organic Geochemistry*, *2*(2), 93-97.

Krivácsy, Z., Kiss, G., Varga, B., Galambos, I., Sárvári, Z., Gelencser, A., ...& Persson, L. (2000). Study of humic-like substances in fog and interstitial aerosol by size-exclusion chromatography and capillary electrophoresis.*Atmospheric Environment*, *34*(25), 4273-4281.

Krivankova, L., Gebauer, P., &Bocek, P.(1996).Isotachophoresis.*High Resolution separation and Analysis of Biological Macromolecules,* PartA.

Kurttio, P., Auvinen, A., Salonen, L., Saha, H., Pekkanen, J., Mäkeläinen, I., ... & Komulainen, H. (2002). Renal effects of uranium in drinking water. *Environmental health perspectives*, *110*(4), 337.

Kurttio, P., Harmoinen, A., Saha, H., Salonen, L., Karpas, Z., Komulainen, H., & Auvinen, A. (2006).Kidney toxicity of ingested uranium from drinking water.*American journal of kidney diseases*, *47*(6), 972-982.

Langmuir, D. (1978). Uranium solution-mineral equilibria at low temperatures with applications to sedimentary ore deposits. *Geochimica et Cosmochimica Acta*, *42*(6), 547-569.

Langmuir, D., Hall, P., & Drever, J. I. (1997). *Environmental Geochemistry* (pp. 88-153). Englewood Cliffs: Prentice-Hall.

Leenheer, J. A., Rostad, C. E., Barber, L. B., Schroeder, R. A., Anders, R., & Davisson, M. L. (2001). Nature and chlorine reactivity of organic constituents from reclaimed water in groundwater, Los Angeles County, California. *Environmental science & technology*, *35*(19), 3869-3876.

Lenhart, J. J., & Honeyman, B. D. (1999). Uranium (VI) sorption to hematite in the presence of humic acid. *Geochimica et Cosmochimica Acta*, *63*(19), 2891-2901.

Lenhart, J. J., Cabaniss, S. E., MacCarthy, P., & Honeyman, B. D. (2000).Uranium (VI) complexation with citric, humic and fulvic acids.*Radiochimica Acta*, *88*(6/2000), 345.

Leo, G. W. (1960). Autunite from Mt. Spokane, Washington.*Am. Mineralogist*, *45*.

León Vintró, L., Mitchell, P. I., Omarova, A., Burkitbayev, M., Jiménez Nápoles, H., & Priest, N. D. (2009).Americium, plutonium and uranium contamination and speciation in well waters, streams and atomic lakes in the Sarzhal Region of the Semipalatinsk nuclear test site, Kazakhstan.*Journal of environmental radioactivity*, *100*(4), 308-314.

Li, W. C., Victor, D. M., & Chakrabarti, C. L. (1980).Effect of pH and uranium concentration on interaction of uranium (VI) and uranium (IV) with organic ligands in aqueous solutions.*Analytical Chemistry*, *52*(3), 520-523.

Lottermoser, B. G., & Ashley, P. M. (2005). Tailings dam seepage at the rehabilitated Mary Kathleen uranium mine, Australia. *Journal of Geochemical Exploration*, *85*(3), 119-137.

Louvat, D., Michaud, V., & von Maravic, H. (1998, June). Oklo Working Group. In *Proceedings of the first joint EC-CEA Workshop on the Oklo Natural Analogue Phase II Project Held in Helsinki* (Vol. 16).

Lovley, D. R. (1991). Dissimilatory Fe (III) and Mn (IV) reduction. *microbiological reviews*, *55*(2), 259.

Lovley, D. R., Coates, J. D., Blunt-Harris, E. L., Phillips, E. J., & Woodward, J. C. (1996). Humic substances as electron acceptors for microbial respiration. *Nature*, *382*(6590), 445-448.

Lyklema, J. (1987). Structure of solid/liquid interface and the electric double layer. *Solid/liquid Dispersions*, *34*, 63-90.

Luessenhop, A. J., Gallimore, J. C., Sweet, W. H., Struxness, E. G., & Robinson, J. (1958).The toxicity in man of hexavalent uranium following intravenous administration. *The American journal of roentgenology, radium therapy, and nuclear medicine*, *79*(1), 83.

Lyvén, B., Hassellöv, M., Turner, D. R., Haraldsson, C., & Andersson, K. (2003). Competition between iron-and carbon-based colloidal carriers for trace metals in a freshwater assessed using flow field-flow fractionation coupled to ICPMS. *Geochimica et Cosmochimica Acta*, *67*(20), 3791-3802.

McDonald, P., Cook, G. T., & Baxter, M. S. (1991). Natural and artificial radioactivity in coastal regions of UK. In *Radionuclides in the study of marine processes* (pp. 329-339). Springer Netherlands.

MacKenzie, A. B., Scott, R. D., Linsalata, P., Miekeley, N., Osmond, J. K., & Curtis, D. B. (1990). Natural radionuclide and stable element studies of rock samples from the Osamu Utsumi uranium mine and Morro do Ferro analogue sites, Poços de Caldas, Brazil. *Poços de Caldas Technical Report Series*, (7), 90-25.

MacKenzie, A. B., Whitton, A. N., Shimmield, T. M., Jemielita, R. A. (1991). Natural decay series radionuclide studies at the Needle's Eye Natural Analogue Site, II, 1989-1991. *BGS Technical Report* WE/91/37

MacKenzie, A. B., Scott, R. D., Linsalata, P., & Miekeley, N. (1992). Natural decay series studies of the redox front system in the Pocos de Caldas uranium mineralization. *Journal of Geochemical Exploration*, *45*(1), 289-322.

MacKenzie, A. B., Scott, R. D., Allan, R. L., Ben Shaban, Y. A., Cook, G. T., & Pulford, I. D. (1994). Sediment radionuclide profiles: implications for mechanisms of Sellafield waste dispersal in the Irish Sea. *Journal of environmental radioactivity*, *23*(1), 39-69.

MacKenzie, A. B., Logan, E. M., Cook, G. T., & Pulford, I. D. (1998). A historical record of atmospheric depositional fluxes of contaminants in west-central Scotland derived from an ombrotrophic peat core. *Science of the total environment*, *222*(3), 157-166.

Mann, A. W. (1974). Chemical ore genesis models for the precipitation of carbonite in calcrete. *Rept. FP7, CRISO Minerals Research Labs. Div. of Minerology.*

Mann, A. W., & Deutscher, R. L. (1978).Genesis principles for the precipitation of carnotite in calcrete drainages in Western Australia. *Economic Geology*, *73*(8), 1724-1737.

McBride, M. B. (1979). Chemisorption and precipitation of Mn2+ at $CaCO_3$ surfaces. *Soil Science Society of America Journal*, *43*(4), 693-698.

McCartney, M., Kershaw, P. J., & Allington, D. J. (1990).The behaviour of ^{210}Pb and ^{226}Ra in the eastern Irish Sea. *Journal of Environmental Radioactivity*, *12*(3), 243-265.

McCartney, M., Kershaw, P. J., Allington, D. J., Young, A. K., & Turner, D. (1992).Industrial sources of naturally occurring radionuclides in the eastern Irish Sea. *Radiation Protection Dosimetry*, *45*(1-4), 711-714.

McDonald, C. F. (1991). Nuclear/coal synergy early in the 21_{st} century with advanced bi-modal mhr. *IECEC Proc*, *5*, 20-24.

McGrath, S. P., & Cegarra, J. (1992).Chemical extractability of heavy metals during and after long‐term applications of sewage sludge to soil. *Journal of Soil Science*, *43*(2), 313-321.

McLaren, R. G., Lawson, D. M., & SWIFT, S. (1986). The forms of cobalt in some Scottish soils as determined by extraction and isotopic exchange. *Journal of soil science*, *37*(2), 223-234.

Mehra, O. P., & Jackson, M. L. (1960). Iron oxide removal from soils and clays by a dithionite-citrate system buffered with sodium bicarbonate. In *Proc. 7th nat. Conf. Clays.*(Vol. 5, pp. 317-327).

Meinrath, G., & Kimura, T. (1993). Carbonate complexation of the uranyl (VI) ion. *Journal of Alloys and Compounds*, *202*(1), 89-93.

Memon, J. R., Hallam, K. R., Bhanger, M. I., El-Turki, A., & Allen, G. C. (2009).Evaluation of sorption of uranium onto metakaolin using X-ray photoelectron and Raman spectroscopies. *Analytica chimica acta*, *631*(1), 69-73.

Mester, Z., & Sturgeon, R. (Eds.).(2003). *Sample preparation for trace element analysis* (pp. 207-210). Amsterdam: Elsevier.

Mibus, J., Sachs, S., Pfingsten, W., Nebelung, C., & Bernhard, G. (2007). Migration of uranium (IV)/(VI) in the presence of humic acids in quartz sand: A laboratory column study. *Journal of contaminant hydrology*, *89*(3), 199-217.

Michel, F. M., Barrón, V., Torrent, J., Morales, M. P., Serna, C. J., Boily, J. F., ...& Brown, G. E. (2010). Ordered ferrimagnetic form of ferrihydrite reveals links among structure, composition, and magnetism. *Proceedings of the National Academy of Sciences*, *107*(7), 2787-2792.

Mikkelsen, S. R., & Cortón, E. (2004). *Bioanalytical chemistry*.Wiley-interscience.

Miller, W. M., Chapman, N., McKinley, I., Alexander, R., & Smellie, J. A. T. (2011). *Natural analogue studies in the geological disposal of radioactive wastes* (Vol. 57). Elsevier Science.

Miller, J. M., & Taylor, K. (1966).Uranium mineralization near Dalbeattie, Kirkcudbrightshire.*Bulletin of the Geological Survey of Great Britain*, *25*, 1-18.

Mitsch, W. J., & Gosselink, J. G. (2007).Wetlands. Hoboken.

Morris, D. E., Allen, P. G., Berg, J. M., Chisholm-Brause, C. J., Conradson, S. D., Donohoe, R. J., ... & Tait, C. D. (1996). Speciation of uranium in Fernald soils by molecular spectroscopic methods: Characterization of untreated soils. *Environmental science & technology*, *30*(7), 2322-2331.

Moyes, L. N., Parkman, R. H., Charnock, J. M., Vaughan, D. J., Livens, F. R., Hughes, C. R., & Braithwaite, A. (2000). Uranium uptake from aqueous solution by interaction with goethite, lepidocrocite, muscovite, and mackinawite: An X-ray absorption spectroscopy study. *Environmental science & technology*, *34*(6), 1062-1068.

Mudd, G. M. (2000). Remediation of uranium mill tailings wastes in Australia: a critical review. *Contaminated Site Remediation: From Source Zones to Ecosystems. CSRC, Melbourne*, *106*, 777-282.

Munier-Lamy, C., Adrian, P., Berthelin, J., & Rouiller, J. (1986). Comparison of binding abilities of fulvic and humic acids extracted from recent marine sediments with UO_2^{2+}. *Organic geochemistry*, *9*(6), 285-292.

Murakami, T., Ohnuki, T., Isobe, H., & Sato, T. (1997).Mobility of uranium during weathering. *American Mineralogist*, *82*(9), 888-899.

Nadkarni, R. A. (1984). Applications of microwave oven sample dissolution in analysis. *Analytical Chemistry*, *56*(12), 2233-2237.

Nagyová, I., & Kaniansky, D. (2001).Discrete spacers for photometric characterization of humic acids separated by capillary isotachophoresis. *Journal of Chromatography A*, *916*(1), 191-200.

Nakashima, S., Disnar, J. R., Perruchot, A., & Trichet, J. (1984).Experimental study of mechanisms of fixation and reduction of uranium by sedimentary organic matter under diagenetic or hydrothermal conditions. *Geochimica et Cosmochimica Acta*, *48*(11), 2321-2329.

Neiss, J., Stewart, B. D., Nico, P. S., & Fendorf, S. (2007). Speciation-dependent microbial reduction of uranium within iron-coated sands. *Environmental science & technology*, *41*(21), 7343-7348.

Nguyen Trung, C., Begun, G. M., & Palmer, D. A. (1992).Aqueous uranium complexes. 2. Raman spectroscopic study of the complex formation of the dioxouranium (VI) ion with a variety of inorganic and organic ligands. *Inorganic Chemistry*, *31*(25), 5280-5287.

Nico, P. S., Stewart, B. D., & Fendorf, S. (2009). Incorporation of oxidized uranium into Fe (hydr) oxides during Fe (II) catalyzed remineralization. *Environmental science & technology*, *43*(19), 7391-7396.

Nriagu, J., Nam, D. H., Ayanwola, T. A., Dinh, H., Erdenechimeg, E., Ochir, C., & Bolormaa, T. A. (2012).High levels of uranium in groundwater of Ulaanbaatar, Mongolia.*Science of the Total Environment*, *414*, 722-726.

NWQMS (National Water Quality Management Strategy) (2000).Australian and New Zealand guidelines for fresh and marine water quality, Vols. 1, 2. Australia and New Zealand Environment and Conservation Council and Agriculture and Resource Management Council of Australia and New Zealand, Canberra

Ochiai, E. I. (1977). *Bioinorganic chemistry: an introduction*. Boston: Allyn and Bacon.

Ochiai, E. I. (1987). *General principles of biochemistry of the elements* (Vol. 38). New York: Plenum Press.

Ohnuki, T., Kozai, N., Sakamoto, F., Ozaki, T., Nankawa, T., Suzuki, Y., & Francis, A. J. (2010). Association of actinides with microorganisms and clay: Implications for radionuclide migration from waste-repository sites. *Geomicrobiology Journal*, *27*(3), 225-230.

Oliver, I. W., Graham, M. C., MacKenzie, A. B., Ellam, R. M., & Farmer, J. G. (2007). Assessing depleted uranium (DU) contamination of soil, plants and earthworms at UK weapons testing sites. *Journal of Environmental Monitoring*, *9*(7), 740-748.

Oliver, I. W., Graham, M. C., MacKenzie, A. B., Ellam, R. M., & Farmer, J. G. (2008a). Depleted uranium mobility across a weapons testing site: isotopic investigation of porewater, earthworms, and soils. *Environmental Science & Technology*, *42*(24), 9158-9164.

Oliver, I. W., Graham, M. C., MacKenzie, A. B., Ellam, R. M., & Farmer, J. G. (2008b). Distribution and partitioning of depleted uranium (DU) in soils at weapons test ranges–Investigations combining the BCR extraction scheme and isotopic analysis. *Chemosphere*, *72*(6), 932-939.

Opel, K., Weiß, S., Hübener, S., Zänker, H., & Bernhard, G. (2007). Study of the solubility of amorphous and crystalline uranium dioxide by combined spectroscopic methods. *Radiochimica Acta*, *95*(3), 143-149.

Owen, D. E., & Otton, J. K. (1995). Mountain wetlands: Efficient uranium filters—Potential impacts. *Ecological Engineering*, *5*(1), 77-93.

Pandey, A. K., Pandey, S. D., & Misra, V. (2000).Stability constants of metal–humic acid complexes and its role in environmental detoxification.*Ecotoxicology and Environmental Safety*, *47*(2), 195-200.

Papastefanou, C. (2010). Escaping radioactivity from coal-fired power plants (CPPs) due to coal burning and the associated hazards: a review.*Journal of Environmental Radioactivity*, *101*(3), 191-200.

Payne, T. E., Davis, J. A., & Waite, T. D. (1996). Uranium adsorption on ferrihydrite: Effects of phosphate and humic acid. *Radiochimica Acta*, *74*, 239-243.

Payne, T. E., Lumpkin, G. R., & Waite, T. D. (1998).Uranium "Adsorption on Model Minerals.*Adsorption of Metals by Geomedia: Variables, Mechanisms, and Model Applications*, 75.

Pearce, G. (2007). Introduction to membranes: Filtration for water and wastewater treatment. *Filtration & Separation*, *44*(2), 24-27.

Penners, N. H. G., Koopal, L. K., & Lyklema, J. (1986). Interfacial electrochemistry of haematite (α-Fe_2O_3): homodisperse and heterodisperse sols. *Colloids and Surfaces*, *21*, 457-468.

Pérez-Sanz, A., Lucena, J. J., & Graham, M. C. (2006). Characterization of Fe–humic complexes in an Fe-enriched biosolid by-product of water treatment. *Chemosphere*, *65*(11), 2045-2053.

Pett-Ridge, J. C., Monastra, V. M., Derry, L. A., & Chadwick, O. A. (2007).Importance of atmospheric inputs and Fe-oxides in controlling soil uranium budgets and behavior along a Hawaiian chronosequence. *Chemical Geology*, *244*(3), 691-707.

Pfeifer, H. R., Vust, M., Meisser, N., Doppenberg, R., Torti, R. C., Domergue, F. L., ...& Hunziker, J. (1994). Uranium-enrichment in soils and plants in the vicinity of a pitchblende vein at La Creusaz/Les Marecottes (W of Martigny, Valais, Switzerland). *Eclogae Geologicae Helvetiae*, *87*(2), 491-501.

Pharmacia LKB (1991). Principles and methods.*Pharmacia technical booklet. Pharmacia LKB Biotechnology, S-75182 Uppsala, Sweden*.

Piccolo, A. (1988). Characteristics of soil humic extracts obtained by some organic and inorganic solvents and purified by HCl-HF treatment. *Soil Science*, *146*(6), 418-426.

Piccolo, A., Conte, P., Cozzolino, A., & Spaccini, R. (2001).Molecular sizes and association forces of humic substances in solution.*Humic Substances and Chemical Contaminants*, (humicsubstancesa), 89-118.

Pickering, W. F. (1986). Metal ion speciation—soils and sediments (a review). *Ore Geology Reviews*, *1*(1), 83-146.

Pitty, A. F. (1979).*Geography and soil properties*. London: Methuen.

Pokrovsky, O. S., & Schott, J. (2002). Iron colloids/organic matter associated transport of major and trace elements in small boreal rivers and their estuaries (NW Russia). *Chemical Geology*, *190*(1), 141-179.

Pokrovsky, O. S., Dupré, B., & Schott, J. (2005). Fe–Al–organic colloids control of trace elements in peat soil solutions: results of ultrafiltration and dialysis. *Aquatic Geochemistry*, *11*(3), 241-278.

Pokrovsky, O. S., Viers, J., Shirokova, L. S., Shevchenko, V. P., Filipov, A. S., & Dupré, B. (2010). Dissolved, suspended, and colloidal fluxes of organic carbon, major and trace elements in the Severnaya Dvina River and its tributary. *Chemical Geology*, *273*(1), 136-149.

Pompe, S., Schmeide, K., Bubner, M., Geipel, G., Heise, K. H., Bernhard, G., & Nitsche, H. (2000). Investigation of humic acid complexation behavior with uranyl ions using modified synthetic and natural humic acids. *Radiochimica Acta*, *88*(9-11/2000), 553.

Poulton, S. W., & Canfield, D. E. (2005). Development of a sequential extraction procedure for iron: implications for iron partitioning in continentally derived particulates. *Chemical Geology*, *214*(3), 209-221.

Priest, N. D. (2001).Toxicity of depleted uranium. *The Lancet*, *357*(9252), 244-246.

Raff, O., & Wilken, R. D. (1999).Removal of dissolved uranium by nanofiltration.*Desalination*, *122*(2), 147-150.

Raiswell, R., Canfield, D. E., & Berner, R. A. (1994).A comparison of iron extraction methods for the determination of degree of pyritisation and the recognition of iron-limited pyrite formation. *Chemical Geology*, *111*(1), 101-110.

Ralph, J. P., & Catcheside, D. E. A. (1996).Size-exclusion chromatography of solubilised low-rank coal. *Journal of Chromatography A*, *724*(1), 97-105.

Ranville, J. F., Hendry, M. J., Reszat, T. N., Xie, Q., & Honeyman, B. D. (2007). Quantifying uranium complexation by groundwater dissolved organic carbon using asymmetrical flow field-flow fractionation. *Journal of Contaminant Hydrology*, *91*(3), 233-246.

Rao, L., Choppin, G. R., & Clark, S. B. (1994).A study of metal-humate interactions using cation exchange. *Radiochimica Acta*, *66*, 141-141.

Rao, L., Zanonato, P., & Di Bernardo, P. L. I. N. I. O. (2005). Interaction of actinides with carboxylates in solution: complexation of U (VI), Th (IV), and Nd (III) with acetate at variable temperatures. *Journal of Nuclear and Radiochemistry*, *6*(1), 31-37.

Rapin, F., & Förstner, U. (1983). Sequential leaching techniques for particulate metal speciation: the selectivity of various extractants. In *Proceedings of the 4th International Conference on Heavy Metals in the Environment* (Vol. 2, pp. 1074-1077).

Rauret, G., Lopez-Sanchez, J. F., Sahuquillo, A., Rubio, R., Davidson, C., Ure, A., & Quevauviller, P. (1999).Improvement of the BCR three step sequential extraction procedure prior to the certification of new sediment and soil reference materials. *Journal of Environmental Monitoring*, *1*(1), 57-61.

Read, D., Bennett, D. G., Hooker, P. J., Ivanovich, M., Longworth, G., Milodowski, A. E., & Noy, D. J. (1993). The migration of uranium into peat-rich soils at Broubster, Caithness, Scotland, UK. *Journal of contaminant hydrology*, *13*(1), 291-308.

Regenspurg, S., Margot-Roquier, C., Harfouche, M., Froidevaux, P., Steinmann, P., Junier, P., & Bernier-Latmani, R. (2010). Speciation of naturally-accumulated uranium in an organic-rich soil of an alpine region (Switzerland). *Geochimica et Cosmochimica Acta*, *74*(7), 2082-2098.

Reich, T., Moll, H., Arnold, T., Denecke, M. A., Hennig, C., Geipel, G., ...& Shuh, D. K. (1998). An EXAFS study of uranium (VI) sorption onto silica gel and ferrihydrite. *Journal of electron spectroscopy and related phenomena*, *96*(1), 237-243.

Renshaw, J. C., Handley-Sidhu, S., & Brookshaw, D. R. (2011). Pathways of radioactive substances in the environment. *Nuclear Power and the Environment*, 152-176.

Richard, C., Guyot, G., Rivaton, A., Trubetskaya, O., Trubetskoj, O., Cavani, L., & Ciavatta, C. (2007). Spectroscopic approach for elucidation of structural peculiarities of Andisol soil humic acid fractionated by SEC-PAGE setup.*Geoderma*, *142*(1), 210-216.

Rickard, D., & Luther, G. I. (2007). Chemistry of iron sulfides.*Chemical Reviews-Columbus*, *107*(2), 514-562.

Robie, R. A., Hemingway, B. S., & Fisher, J. R. (1978). *Thermodynamic properties of minerals and related substances at 298.15 K and 1 bar (10/sup 5/pascals) pressure and at higher temperatures* (No.USGS-BULL-1452).Geological Survey, Washington, DC (USA).

Rossiter, H., Graham, M. C., & Schäfer, A. I. (2010). Impact of speciation on behaviour of uranium in a solar powered membrane system for treatment of brackish groundwater.*Separation and Purification Technology*, *71*(1), 89-96.

Russell, J. E. (2008). Soil conditions and plant growth. *Daya Books.*

Ryan, J. N., Illangasekare, T. H., Litaor, M. I., & Shannon, R. (1998). Particle and plutonium mobilization in macroporous soils during rainfall simulations. *Environmental science & technology*, *32*(4), 476-482.

Sachs, S., Geipel, G., Mibus, J., & Bernhard, G. (2006). Impact of humic acid on the uranium migration in the environment.In *Uranium in the Environment* (pp. 107-116).Springer Berlin Heidelberg.

Sachs, S., Brendler, V., & Geipel, G. (2007). Uranium (VI) complexation by humic acid under neutral pH conditions studied by laser-induced fluorescence spectroscopy.*Radiochimica Acta*, *95*(2), 103-110.

Sandino, A., & Bruno, J. (1992). The solubility of $(UO_2)_3(PO_4)_2.4H_2O(s)$and the formation of U (VI) phosphate complexes: Their influence in uranium speciation in natural waters.*Geochimica et Cosmochimica Acta*, *56*(12), 4135-4145.

Sato, T., Murakami, T., Yanase, N., Isobe, H., Payne, T. E., & Airey, P. L. (1997). Iron nodules scavenging uranium from groundwater. *Environmental science & technology*, *31*(10), 2854-2858.

Schaetzl, R. J., & Anderson, S. (2005). Soils. *Cambridge University Press.*

Scheetz, C. D., & Rimstidt, J. D. (2009). Dissolution, transport, and fate of lead on a shooting range in the Jefferson National Forest near Blacksburg, VA, USA.*Environmental geology*, *58*(3), 655-665.

Schmidt, M. W. I., Knicker, H., Hatcher, P. G., & Kogel-Knabner, I. (1997). Improvement of ^{13}C and ^{15}N CPMAS NMR spectra of bulk soils, particle size fractions and organic material by treatment with 10% hydrofluoric acid. *European Journal of Soil Science*, *48*(2), 319-328.

Schmidt, M. W., Torn, M. S., Abiven, S., Dittmar, T., Guggenberger, G., Janssens, I. A., ...& Trumbore, S. E. (2011). Persistence of soil organic matter as an ecosystem property.*Nature*, *478*(7367), 49-56.

Schnitzer, M., & Schuppli, P. (1989). The extraction of organic matter from selected soils and particle size fractions with 0.5 M NaOH and 0.1 M Na4P2O7 solutions. *Canadian Journal of Soil Science*, *69*(2), 253-262.

Schöner, A., Sauter, M., & Büchel, G. (2006). Uranium in natural wetlands: a hydrogeochemical approach to reveal immobilization processes. In *Uranium in the Environment* (pp. 389-397).Springer Berlin Heidelberg.

Schöner, A., Noubactep, C., Büchel, G., & Sauter, M. (2009). Geochemistry of natural wetlands in former uranium milling sites (eastern Germany) and implications for uranium retention.*Chemie der Erde-Geochemistry*, *69*, 91-107.

Schwertmann, U., Fitzpatrick, R. W., Taylor, R. M., & Lewis, D. G. (1979). The influence of aluminum on iron oxides. Part II. Preparation and properties of Alsubstituted hematites.*Clays Clay Miner*, *27(2)*, 105-112.

Schwertmann, U. (1988). Goethite and hematite formation in the presence of clay minerals and gibbsite at 25 C. *Soil Science Society of America Journal*, *52*(1), 288-291.

Schwertmann, U., & Cornell, R. M. (2000).*Iron oxides in the laboratory*.Wiley-Vch.

Schwertmann, U., Wagner, F., & Knicker, H. (2005). Ferrihydrite–Humic Associations.*Soil Science Society of America Journal*, *69*(4), 1009-1015.

Scott, T. B., Riba Tort, O., & Allen, G. C. (2007). Aqueous uptake of uranium onto pyrite surfaces; reactivity of fresh versus weathered material.*Geochimica et Cosmochimica Acta*, *71*(21), 5044-5053.

Shafer, M. M., Overdier, J. T., Hurley, J. P., Armstrong, D., & Webb, D. (1997). The influence of dissolved organic carbon, suspended particulates, and hydrology on the concentration, partitioning and variability of trace metals in two contrasting Wisconsin watersheds (USA).*Chemical Geology*, *136*(1), 71-97.

Schäfer, A. I., Fane, A. G., & Waite, T. D. (1998). Nanofiltration of natural organic matter: removal, fouling and the influence of multivalent ions. *Desalination*, *118*(1), 109-122.

Shelobolina, E. S., Konishi, H., Xu, H., & Roden, E. E. (2009). U (VI) sequestration in hydroxyapatite produced by microbial glycerol 3-phosphate metabolism.*Applied and environmental microbiology*, *75*(18), 5773-5778.

Sheppard, S. C., Evenden, W. G., & Pollock, R. J. (1989). Uptake of natural radionuclides by field and garden crops.*Canadian Journal of Soil Science*, *69*(4), 751-767.

Sherman, D. M., Peacock, C. L., & Hubbard, C. G. (2008). Surface complexation of U (VI) on goethite (α-FeOOH).*Geochimica et Cosmochimica Acta*, *72*(2), 298-310.

Shotyk, W. (1996). Natural and anthropogenic enrichments of As, Cu, Pb, Sb, and Zn in ombrotrophic versus minerotrophic peat bog profiles, Jura Mountains, Switzerland.*Water, Air, and Soil Pollution*, *90*(3-4), 375-405.

Shotyk, W., Weiss, D., Heisterkamp, M., Cheburkin, A. K., Appleby, P. G., & Adams, F. C. (2002). New peat bog record of atmospheric lead pollution in Switzerland: Pb

concentrations, enrichment factors, isotopic composition, and organolead species. *Environmental science & technology*, *36*(18), 3893-3900.

Shultis, J. K., & Faw, R. E. (2007). Fundamentals of Nuclear Science and Engineering *Second Edition*. *CRC Press*.

Shuman, L. M. (1982). Separating soil iron-and manganese-oxide fractions for microelement analysis.*Soil Science Society of America Journal*, *46*(5), 1099-1102.

Silva, R. J., & Nitsche, H. (1996). Actinide environmental chemistry.*100 Years after the Discovery of Radiochemistry*, *70*(71), 377-396.

Simonart, P., Batistic, L., & Mayaudon, J. (1967). Isolation of protein from humic acid extracted from soil. *Plant and Soil*, *27*(2), 153-161.

Simpson, A. J. (2002). Determining the molecular weight, aggregation, structures and interactions of natural organic matter using diffusion ordered spectroscopy. *Magnetic Resonance in Chemistry*, *40*(13), S72-S82.

Simpson, A. J., Kingery, W. L., & Hatcher, P. G. (2003). The identification of plant derived structures in humic materials using three-dimensional NMR spectroscopy. *Environmental science & technology*, *37*(2), 337-342.

Skipperud, L., Strømman, G., Yunusov, M., Stegnar, P., Uralbekov, B., Tilloboev, H., ...& Salbu, B. (2012). Environmental impact assessment of radionuclide and metal contamination at the former U sites Taboshar and Digmai, Tajikistan. *Journal of Environmental Radioactivity*.

Smedley, P. L., Smith, B., Abesser, C., & Lapworth, D. (2006). Uranium occurrence and behaviour in British groundwater.*BGS Technical Report CR/06/050 N.*

Smellie, J. A., & Karlsson, F. (1999). The use of natural analogues to assess radionuclide transport. *Engineering Geology*, *52*(3), 193-220.

Smellie, J. (2009). Analogue evidence from uranium orebodies. *Nuclear Decomissioning Authority Report.*

Smith, B.. (2004). Uranium in groundwater. Impacts on health, geochemical exploration and radwaste disposal, *British Geology Survey*, Earthwise issue 21.

Sowder, A. G., Clark, S. B., & Fjeld, R. A. (2001). The impact of mineralogy in the U (VI)—Ca—PO4 system on the environmental availability of uranium.*Journal of Radioanalytical and Nuclear Chemistry*, *248*(3), 517-524.

Sparks, D. L. (2003). Environmental soil chemistry. *Academic press*.

Steelink, C. (2002). Peer Reviewed: investigating humic acids in soils. *Analytical chemistry*, *74*(11), 326-A.

Steudtner, R., Müller, K., Schmeide, K., Sachs, S., & Bernhard, G. (2011a). Binary and ternary uranium (vi) humate complexes studied by attenuated total reflection Fourier-transform infrared spectroscopy. *Dalton Transactions*, *40*(44), 11920-11925.

Steudtner, R., Sachs, S., Schmeide, K., Brendler, V., & Bernhard, G. (2011b). Ternary uranium (VI) carbonato humate complex studied by cryo-TRLFS.*Radiochimica Acta*, *99*(11), 687-692.

Stevenson, F. J. (1982). Humus Chemistry, J. *Wiley&Sons, NY*.

Stewart, B. D., Neiss, J., & Fendorf, S. (2007). Quantifying constraints imposed by calcium and iron on bacterial reduction of uranium (VI). *Journal of environmental quality*, *36*(2), 363-372.

Stewart, B. D., Nico, P. S., & Fendorf, S. (2009). Stability of uranium incorporated into Fe (hydr) oxides under fluctuating redox conditions. *Environmental science & technology*, *43*(13), 4922-4927.

Stewart, B. D., Mayes, M. A., & Fendorf, S. (2010). Impact of uranyl− calcium− carbonato complexes on uranium (VI) adsorption to synthetic and natural sediments.*Environmental science & technology*, *44*(3), 928-934.

Stone, M., & Droppo, I. G. (1996). Distribution of lead, copper and zinc in size-fractionated river bed sediment in two agricultural catchments of southern Ontario, Canada.*Environmental Pollution*, *93*(3), 353-362.

Stumm, W., & Morgan, J. J. (1995). Aquatic chemistry: chemical equilibria and rates in natural waters. *John Wiley& Sons, NY.*

Summers, L., Hsu, P. C., von Holtz, E., Hipple, D., Wang, F., Adamson, M. (1997). Removal of uranium from spent salt from the molten salt oxidation process,UCRL-ID-126857.

Susanto, H., & Ulbricht, M. (2006). Performance of surface modified polyethersulfone membranes for ultrafiltration of aquatic humic substances. *Performance of surface modified polyethersulfone membranes for ultrafiltration of aquatic humic substances*, *199*(1-3), 384-386.

Suter, D., Siffert, C., Sulzberger, B., & Stumm, W. (1988). Catalytic dissoluion of iron (III)(hydr) oxides by oxalic acid in the presence of Fe (II). *Naturwissenschaften*, *75*(11), 571-573.

Sutton, R., & Sposito, G. (2005). Molecular structure in soil humic substances: the new view. *Environmental Science & Technology*, *39*(23), 9009-9015.

Swift, R. S., & Posner, A. M. (1971). Gel chromatography of humic acid. *Journal of Soil Science*, *22*(2), 237-249.

Sylwester, E. R., Hudson, E. A., & Allen, P. G. (2000). The structure of uranium (VI) sorption complexes on silica, alumina, and montmorillonite.*Geochimica et Cosmochimica Acta*, *64*(14), 2431-2438.

Taylor, H. E. (2001). *Inductively coupled plasma-mass spectrometry: practices and techniques*.Academic Press.

Tessier, A., Campbell, P. G., & Bisson, M. (1979). Sequential extraction procedure for the speciation of particulate trace metals. *Analytical chemistry*, *51*(7), 844-851.

Thomas, R. P., Ure, A. M., Davidson, C. M., Littlejohn, D., Rauret, G., Rubio, R., & López-Sánchez, J. F. (1994). Three-stage sequential extraction procedure for the determination of metals in river sediments.*Analytica Chimica Acta*, *286*(3), 423-429.

Tinsley, J., & Salam, A. (1961). Extraction of soil organic matter with aqueous solvents.*Soils and Fertilizers*, *24*(2), 81-84.

Temminghoff, E. J., Van der Zee, S. E., & de Haan, F. A. (1997). Copper mobility in a copper-contaminated sandy soil as affected by pH and solid and dissolved organic matter. *Environmental Science & Technology*, *31*(4), 1109-1115.

Trubetskoj, O. A., Kudryavceva, L. Y., & Shirshova, L. T. (1991). Characterization of soil humic matter by polyacrylamide gel electrophoresis in the presence of denaturating agents.*Soil Biology and Biochemistry*, *23*(12), 1179-1181.

Trubetskoj, O. A., Trubetskaya, O. E., Afanas' eva, G. V., Reznikova, O. I., & Sáiz-Jiménez, C. (1997). Polyacrylamide gel electrophoresis of soil humic acid fractionated by size-exclusion chromatography and ultrafiltration.*Journal of Chromatography A*, *767*(1), 285-292.

Ulrich, K. U., Rossberg, A., Foerstendorf, H., Zänker, H., & Scheinost, A. C. (2006). Molecular characterization of uranium (VI) sorption complexes on iron (III)-rich acid mine water colloids. *Geochimica et cosmochimica acta*, *70*(22), 5469-5487.

Ure, A. M., Quevauviller, P., Muntau, H., & Griepink, B. (1993). Speciation of heavy metals in soils and sediments.An account of the improvement and harmonization of extraction techniques undertaken under the auspices of the BCR of the Commission of the European Communities.*International journal of environmental analytical chemistry*, *51*(1-4), 135-151.

Ure, A., & Davidson, C. (Eds.). (2008). *Chemical speciation in the environment*. Wiley-Blackwell.

Van der Heide, P. (2011). *X-ray Photoelectron Spectroscopy: An Introduction to Principles and Practices*. Wiley.

Van der Lee, J., Ledoux, E., & De Marsily, G. (1992). Modeling of colloidal uranium transport in a fractured medium.*Journal of Hydrology*, *139*(1), 135-158.

Van Horn, J. D., & Huang, H. (2006).Uranium (VI) bio-coordination chemistry from biochemical, solution and protein structural data.*Coordination chemistry reviews*, *250*(7), 765-775.

Vandecasteele, C., & Block, C. B. (1997). *Modern methods for trace element determination*. Wiley.

Vandenhove, H., Van Hees, M., Wouters, K., & Wannijn, J. (2007). Can we predict uranium bioavailability based on soil parameters? Part 1: Effect of soil parameters on soil solution uranium concentration. *Environmental Pollution*, *145*(2), 587-595.

Vanhaecke, F., Balcaen, L., & Malinovsky, D. (2009). Use of single-collector and multi-collector ICP-mass spectrometry for isotopic analysis.*Journal of Analytical Atomic Spectrometry*, *24*(7), 863-886.

Vasyukova, E. V., Pokrovsky, O. S., Viers, J., Oliva, P., Dupré, B., Martin, F., & Candaudap, F. (2010). Trace elements in organic-and iron-rich surficial fluids of the boreal zone: Assessing colloidal forms via dialysis and ultrafiltration. *Geochimica et Cosmochimica Acta*, *74*(2), 449-468.

Venugopal, B., & Luckey, T. D. (1978). Chemical toxicity of metals and metalloids.*Metal Toxicity in Mammals. 2nd ed. New York: Plenum*, 229-31.

Vepraskas, M. J., & Faulkner, S. P. (2001). Redox chemistry of hydric soils.*Wetland soils: Genesis, hydrology, landscapes, and classification*, 85-106.

Vilks, P., Cramer, J. J., Bachinski, D. B., Doern, D. C., & Miller, H. G. (1993). Studies of colloids and suspended particles, Cigar Lake uranium deposit, Saskatchewan, Canada. *Applied Geochemistry*, *8*(6), 605-616.

Vinogradoff S. I., Abbott A., Graham M.C., Farmer J.G. (1998). The influence of microbial alteration of humic macromolecules on humic-actinide binding: implications for actinide mobility in soils, *Proc. Sixth Intern. FZK/TNO Conf. Contaminated Soil*, 2, 931-32.

Viollier, E., Inglett, P. W., Hunter, K., Roychoudhury, A. N., & Van Cappellen, P. (2000). The ferrozine method revisited: Fe (II)/Fe (III) determination in natural waters. *Applied Geochemistry*, *15*(6), 785-790.

Vorenhout, M., van der Geest, H. G., van Marum, D., Wattel, K., & Eijsackers, H. J. (2004). Automated and continuous redox potential measurements in soil. *Journal of environmental quality*, *33*(4), 1562-1567.

Waite, T. D., Davis, J. A., Payne, T. E., Waychunas, G. A., & Xu, N. (1994). Uranium (VI) adsorption to ferrihydrite: Application of a surface complexation model. *Geochimica et Cosmochimica Acta*, *58*(24), 5465-5478.

Walter, M., Arnold, T., Reich, T., & Bernhard, G. (2003). Sorption of uranium (VI) onto ferric oxides in sulfate-rich acid waters.*Environmental science & technology*, *37*(13), 2898-2904.

Wan, J., Kim, Y., Tokunaga, T. K., Wang, Z., Dixit, S., Steefel, C. I., ...& Tamura, N. (2009). Spatially resolved U (VI) partitioning and speciation: Implications for plume scale behavior of contaminant U in the Hanford vadose zone. *Environmental science & technology*, *43*(7), 2247-2253.

Wang, Z., Zachara, J. M., Yantasee, W., Gassman, P. L., Liu, C., & Joly, A. G. (2004). Cryogenic laser induced fluorescence characterization of U (VI) in Hanford vadose zone pore waters. *Environmental science & technology*, *38*(21), 5591-5597.

Warwick, P., Allinson, S., Beckett, K., Eilbeck, A., Fairhurst, A., Russel-Flint, K., & Verrall, K. (2002). Sampling and analyses of colloids at the Drigg low level radioactive waste disposal site. *Journal of Environmental Monitoring*, *4*(2), 229-234.

Wazne, M., Korfiatis, G. P., & Meng, X. (2003). Carbonate effects on hexavalent uranium adsorption by iron oxyhydroxide. *Environmental science & technology*, *37*(16), 3619-3624.

Wise, S. S., Thompson, W. D., Aboueissa, A. M., Mason, M. D., & Wise, J. P. (2007). Particulate depleted uranium is cytotoxic and clastogenic to human lung cells. *Chemical research in toxicology*, *20*(5), 815-820.

World Health Organization.(2012). Guideline for drinking water quality. Geneva. *World Health Organization*.

Worobey, B. L., & Webster, G. B. (1981). Indigenous 13C-NMR structural features of soil humic substances.*Nature, 292*, 526-529.

Xi, M., Lu, X. G., Li, Y., & Kong, F. L. (2007). Distribution characteristics of dissolved organic carbon in annular wetland soil-water solutions through soil profiles in the Sanjiang Plain, Northeast China.*Journal of Environmental Sciences*, *19*(9), 1074-1078.

Yafa, C., Farmer, J. G., Graham, M. C., Bacon, J. R., Barbante, C., Cairns, W. R. L., ... & Kylander, M. (2004). Development of an ombrotrophic peat bog (low ash) reference material for the determination of elemental concentrations. *Journal of Environmental Monitoring*, *6*(5), 493-501.

Yafa, C., & Farmer, J. G. (2006). A comparative study of acid-extractable and total digestion methods for the determination of inorganic elements in peat material by inductively coupled plasma-optical emission spectrometry. *Analytica chimica acta*, *557*(1), 296-303.

Yang, R., & van den Berg, C. M. (2009). Metal complexation by humic substances in seawater.*Environmental science & technology*, *43*(19), 7192-7197.

Yang, Y., Saiers, J. E., Xu, N., Minasian, S. G., Tyliszczak, T., Kozimor, S. A., ...& Barnett, M. O. (2012). Impact of Natural Organic Matter on Uranium Transport through Saturated Geologic Materials: From Molecular to Column Scale. *Environmental science & technology*, *46*(11), 5931-5938.

Zänker, H., Ulrich, K. U., Opel, K., & Brendler, V. (2007). The role of colloids in uranium transport: a comparison of nuclear waste repositories and abandoned uranium mines. In *IMWA Symposium*.

Zavarin, M. (1999). *Sorptive properties of synthetic and soil carbonates for selenium, nickel, and manganese* (Doctoral dissertation, University of California, Berkeley).

Zeh, P., Czerwinski, K. R., & Kim, J. I. (1997). Speciation of uranium in Gorleben groundwaters.*Radiochimica acta*, *76*(1-2), 37-44.

Zhou, Q., Cabaniss, S. E., & Maurice, P. A. (2000). Considerations in the use of high-pressure size exclusion chromatography (HPSEC) for determining molecular weights of aquatic humic substances.*Water Research*, *34*(14), 3505-3514.

9 Appendix

9.1 Preparation of nitric acid solutions

9.1.1 Preparation of 5 M nitric aicd

A volume of 960 mL concentrated HNO_3 (69%, Analar, VWR) was added in 2040 mL deionised water in a beaker.

9.1.2 Preparation of 2 % v/v nitric acid

A 40 mL aliquot of concentrated HNO_3 (69%, Aristar, VWR) was made up to volume in a 2 L flask with deionised water. The molarity of 2% v/v nitric acid solution is 0.311 M.

9.2 Preparation of 0.045 M Tris-borate buffer solution (pH 8.5) for gel electrophoresis

Masses of 54.0 g Tris and 27.5 g Orthoboric acid were dissolved in deionised water and the solution made up to volume in a 1 L volumetric flask. This solution was transferred to a 10 L plastic aspirator and diluted by addition of 9 L deionised water.

9.3 Preparation of 0.05 M Tris-HCl (pH 8.5) loading buffer solution for gel electrophoresis

A mass of 1.2 g Tris was dissolved in deionised water and made up to 100 mL in a flask. 0.31 mL concentrated HCl was added to deionised water and made up to 100 mL in a flask. The prepared Tris and HCl solutions were mixed together in a reagent bottle.

9.4 Preparation of reagents used for sequential extraction and Fe^{II} measurement

9.4.1 Preparation of 1 M $MgCl_2$ solution (pH 7)

A mass of 95.22 g $MgCl_2$ was dissolved into approximate 990 mL deionised water, then

was titrated to pH7 with HCl and solution was made up to 1L with deionised water.

9.4.2 Preparation of 1 M CH3COONa solution (pH 4.5)

A mass of 136 g $CH_3COONa.3H_2O$ was dissolved into approximate 750 mL deionised water, then was titrated to pH 4.5 with acetic acid. The solution was made up to 1 L with deionised water.

9.4.3 Preparation of 1 M hydroxylamine-HCl solution

A mass of 67.5 g NH_2OH-HCl was dissolved in approximate 500 mL deionised water and transferred into a 1 L flask, and 250 mL acetic acid was then added to the flask. The solution was made up to 1 L with deionised water.

9.4.4 Preparation of 50 g L^{-1} sodium dithionite solution (pH 4.8)

Masses of 50 g sodium $Na_2S_2O_4$ and 58.82 g sodium citrate were dissolved in approximate 500 mL deionised water and transferred into a 1 L flask. 20.02 mL acetic acid was then added to the flask. The solution was made up to 1 L with deionised water.

9.4.5 Preparation of 0.2 M ammonium oxalate solution (pH 3.2)

Masses of 28.42 g ammonium oxalate and 15.31 g oxalic acid were dissolved in deionised water and solution was made up to 1L with deionised water.

9.4.6 Preparation of ferrozine for Fe^{II} measurement

A solution of 0.1 M ammonium acetate was prepared by adding 0.7708 g ammonium acetate in deionised water and the solution was made up to 100 mL with deionised water. 0.0492 g ferrozine was dissolved in 0.1 M ammonium acetate solution and the solution was made up to 10 mL with 0.1 M ammonium acetate solution.

9.5 Soil porewater pH data for Cores 3, 4, 5, 6 and 7

Table 9.1 Soil porewater pH data in Cores 3, 4, 5, 6 and 7

Core 3		Core 4		Core 5		Core 6				Core 7			
Depth (cm)	**pH**	**Depth (cm)**	**pH**	**Depth (cm)**	**pH**	**Depth (cm)**	**pH**	**Depth (cm)**	**pH**	**Depth (cm)**	**pH**	**Depth (cm)**	**pH**
1.5	6.32	1.5	7.11	2.5	6.78	1	8.55	37	5.18	0.5	6.77	18.5	5.84
4.5	6.07	4.5	7.14	7.5	6.32	3	7.43	39	5.24	1.5	6.98	19.5	5.91
7.5	6.30	7.5	6.64	12.5	6.17	5	7.25	41	6.13	2.5	6.81	20.5	5.84
10.5	6.30	10.5	6.91	17.5	6.35	7	6.77	43	6.27	3.5	6.80	21.5	5.23
13.5	6.52	13.5	6.77			9	6.73	45	6.38	4.5	6.70	22.5	5.48
16.5	6.51	16.5	6.63			11	6.61	47	6.02	5.5	6.62	23.5	5.89
19.5	6.84	19.5	6.5			13	6.7			6.5	6.34	24.5	5.82
22.5	7.05	22.5	6.75			15	6.99			7.5	6.55	25.5	5.82
25.5	6.79	25.5	6.92			17	6.9			8.5	6.06	26.5	5.86
28.5	7.14	28.5	6.73			19	7.21			9.5	5.88	27.5	5.78
31.5	6.64	31.5	6.38			21	7.23			10.5	5.95	28.5	5.82
34.5	6.84	34.5	6.84			23	7.22			11.5	6.28	29.5	5.71
37.5	6.81					25	7.15			12.5	6.27	30.5	5.69
40.5	6.96					27	6.77			13.5	6.01	31.5	5.74
43	6.74					29	6.53			14.5	5.81	32.5	5.74
						31	5.08			15.5	5.80	33.5	5.78
						33	4.94			16.5	6.04	35.5	5.48
						35	4.83			17.5	5.90	37.5	5.29

9.6 Soil porewater UV absorbance data for Cores 3, 4, 5, 6 and 7

Table 9.2 Soil porewater UV absorbance data for Core 3, 4, 5, 6 and 7

Core 3		Core 4		Core 5		Core 6				Core 7			
Depth (cm)	UV abs @254 nm	Depth (cm)	UV abs @254 nm	Depth (cm)	UV abs @254 nm	Depth (cm)	UV abs @254 nm	Depth (cm)	UV abs @254 nm	Depth (cm)	UV abs @254 nm	Depth (cm)	UV abs @254 nm
1.5	2.623	1.5	1.650	2.5	2.042	1	1.45	37	0.13	0.5	1.777	18.5	0.899
4.5	1.776	4.5	1.902	7.5	2.175	3	1.08	39	0.15	19.5	1.180	19.5	0.669
7.5	1.494	7.5	1.529	12.5	1.338	5	0.85	41	0.18	20.5	1.222	20.5	0.740
10.5	1.403	10.5	1.597	17.5	1.101	7	0.69	43	0.20	21.5	1.426	21.5	0.870
13.5	1.222	13.5	0.743			9	0.55	45	0.20	22.5	0.889	22.5	0.510
16.5	1.041	16.5	0.658			11	0.52	47	0.16	23.5	0.871	23.5	0.724
19.5	1.012	19.5	0.571			13	0.52			24.5	0.683	24.5	0.810
22.5	0.982	22.5	0.634			15	0.43			25.5	0.835	25.5	0.947
25.5	0.934	25.5	0.625			17	0.59			26.5	0.666	26.5	1.275
28.5	0.822	28.5	0.939			19	0.47			27.5	0.568	27.5	1.201
31.5	0.515	31.5	0.864			21	0.43			28.5	0.768	28.5	1.414
34.5	0.571	34.5	0.977			23	0.39			29.5	0.889	29.5	1.225
37.5	0.739					25	0.33			30.5	0.709	30.5	1.560
40.5	1.103					27	0.26			31.5	0.843	31.5	1.086
43	0.817					29	0.20			14.5	0.678	32.5	0.944
						31	0.15			15.5	0.659	33.5	1.129
						33	0.13			16.5	0.870	35.5	1.164
						35	0.11			17.5	0.472	37.5	1.020

9.7 Loss of ignition (L.O.I.) data for Cores 3, 4 and 5

Table 9.3 Loss of ignition data at Cores 3, 4 and 5

Core 3		Core 4		Core 5	
Depth (cm)	**LOI (%)**	**Depth (cm)**	**LOI (%)**	**Depth (cm)**	**LOI (%)**
1.5	88.77	1.5	85.28	2.5	50.56
4.5	85.72	4.5	82.68	7.5	49.77
7.5	86.35	7.5	79.77	12.5	47.07
10.5	82.33	10.5	78.34	17.5	37.42
13.5	81.01	13.5	72.44		
16.5	78.48	16.5	68.17		
19.5	81.16	19.5	66.63		
22.5	81.74	22.5	68.76		
25.5	68.86	25.5	50.49		
28.5	54.06	28.5	36.78		
31.5	51.2	31.5	28.55		
34.5	57.34	34.5	29.55		
37.5	55.5				
40.5	41.28				
43	41.29				

9.8 Element concentrations in soil porewater for Cores 1, 2, 3, 4, 5, 6, 7 and in solid phase for Cores 3, 4 and 5

Table 9.4 Vertical concentration data for U, Fe, Mn, Pb, Cu in soil porewaters from Cores 1 and 2

Core 1						**Core 2**					
Depth (cm)	**U (µg L^{-1})**	**Fe (mg L^{-1})**	**Mn (mg L^{-1})**	**Pb (mg L^{-1})**	**Cu (mg L^{-1})**	**Depth (cm)**	**U (µg L^{-1})**	**Fe (mg L^{-1})**	**Mn (mg L^{-1})**	**Pb (mg L^{-1})**	**Cu (mg L^{-1})**
2.5	40	0.387	0.012	0.027	0.077	2.5	4.8	0.715	0.024	0.026	0.026
7.5	59	0.382	0.009	0.023	0.079	7.5	7.6	1.50	0.031	0.028	0.024
13	55	0.457	0.006	0.031	0.078	12.5	6.7	1.27	0.019	0.027	0.024
19	24	0.439	0.005	0.021	0.049	17.5	5.8	1.34	0.018	0.026	0.022
25	34	0.307	0.004	0.030	0.040	22.5	4.4	0.336	0.006	0.028	0.018
31	18	0.212	0.005	0.025	0.033	27.5	5.1	0.284	0.006	0.027	0.020
37	8.4	0.099	0.018	0.022	0.023	32.5	5.1	0.279	0.005	0.031	0.030
42.5	5.6	0.155	0.009	0.028	0.027	38.5	1.9	0.439	0.008	0.026	0.026

Table 9.5 Vertical concentration data for U, Fe, Mn, Al, Cu, Pb in soil porewaters and solid phase from Core 3

Depth (cm)	U (mg kg^{-1})	U (µg L^{-1})	Fe (mg kg^{-1})	Fe (µg L^{-1})	Fe porewater/ solid phase ratio	Mn (mg kg^{-1})	Mn (µg L^{-1})	Al (mg kg^{-1})	Al (µg L^{-1})	Cu (mg kg^{-1})	Cu (µg L^{-1})	Pb (mg kg^{-1})	Pb (µg L^{-1})	As (mg kg^{-1})	As (µg L^{-1})
1.5	386 ±3	36	1780 ±36	246	0.14	371 ±2	29	2046 ±50	84	124 ±1	31	n.d.	2.9	15 ±0.9	182
4.5	676 ±18	39	2770 ±34	234	0.08	270 ±4	27	3305 ±87	76	197 ±9	31	17 ±7	2.9	24 ±2	143
7.5	754 ±12	42	2620 ±229	197	0.08	227 ±2	6.4	3131 ±112	78	211 ±3	34	27 ±3	2.5	28 ±2	214
10.5	1161 ±18	54	3460 ±4	246	0.07	182 ±3	13	4162 ±15	109	364 ±62	53	30 ±17	3.2	29 ±5	119
13.5	1710 ±67	69	3660 ±290	246	0.07	143 ±8	8.4	5060 ±608	105	404 ±5	64	61 ±11	2.8	26 ±5	53
16.5	1880 ±39	85	5400 ±380	288	0.05	130 ±11	3.2	6389 ±109	128	501 ±17	68	65 ±11	3.3	48 ±3	37
19.5	2440 ±16	71	4960 ±23	191	0.04	215 ±2	3.6	5408 ±58	85	571 ±5	55	70 ±13	2.5	61 ±0.4	54
22.5	2470 ±29	72	4880 ±238	185	0.04	196 ±9	7.3	5110 ±35	74	563 ±9	57	67 ±12	2.3	65 ±5	53
25.5	1190 ±42	59	4710 ±64	206	0.04	135 ±4	5.1	11100 ±1100	109	368 ±13	53	115 ±16	4.0	44 ±1	51
28.5	441 ±9	27	5270 ±310	182	0.03	81 ±3	6.9	17000 ±160	140	203 ±13	33	114 ±4	4.6	46 ±2	43
31.5	229 ±3	7.1	6010 ±240	41	0.01	57 ±4	3.3	17100 ±210	18	171 ±3	5.6	103 ±5	0.9	91 ±4	169
34.5	416 ±5	22	6870 ±200	252	0.04	60 ±1	3.5	14100 ±32	81	201 ±4	22	92 ±17	4.1	145 ±5	82
37.5	390 ±21	19	8140 ±760	384	0.05	66 ±8	6.9	16000 ±998	119	178 ±12	23	91 ±11	5.4	186 ±14	111
40.5	351 ±26	37	7120 ±220	364	0.05	107 ±2	17	16800 ±650	224	141 ±7	39	57 ±16	6.6	89 ±1	196
43	358 ±3	31	6860 ±59	276	0.04	96 ±2	18	19000 ±970	191	126 ±9	33	47 ±6	5.2	86 ±1	239

n.d. for Pb = 0.2 mg kg^{-1}

Table 9.6 Vertical concentration data for U, Fe, Mn, Al, Cu, Pb in soil porewaters and solid phase from Core 4

Depth (cm)	U (mg kg^{-1})	U (µg L^{-1})	Fe (mg kg^{-1})	Fe (µg L^{-1})	Fe porewater/ solid phase ratio	Mn (mg kg^{-1})	Mn (µg L^{-1})	Al (mg kg^{-1})	Al (µg L^{-1})	Cu (mg kg^{-1})	Cu (µg L^{-1})	Pb (mg kg^{-1})	Pb (µg L^{-1})	As (mg kg^{-1})	As (µg L^{-1})
1.5	48 ±5	3.2	5790 ±37	883	0.15	598 ±63	142	2600 ±330	51	43 ±5	15	20 ±3	3.3	135 ±13	625
4.5	68 ±5	4.5	9620 ±160	1700	0.18	499 ±6	283	3990 ±120	36	54 ±2	11	8 ±8	3.4	122 ±4	930
7.5	95 ±7	5.6	12600 ±410	3036	0.24	244 ±13	113	5330 ±400	42	76 ±5	15	55 ±10	4.4	185 ±11	182
10.5	119 ±7	6.5	15300 ±380	3009	0.20	180 ±4	63	6590 ±200	47	93 ±4	15	47 ±7	5.1	258 ±3	151
13.5	189 ±6	5.7	10400 ±100	878	0.08	117 ±2	24	10500 ±61	55	139 ±1	13	82 ±8	5.3	164 ±7	77
16.5	158 ±7	5.3	9420 ±10	849	0.09	106 ±1	24	11700 ±710	67	126 ±0.5	14	90 ±0.2	5.5	155 ±5	76
19.5	127 ±6	4.3	6370 ±650	427	0.07	77 ±4	24	13000 ±580	63	110 ±3	11	130 ±14	5.6	137 ±10	106
22.5	133 ±10	5.2	5150 ±6	295	0.06	71 ±0.4	18	11800 ±120	77	142 ±1	15	105 ±1	6.4	193 ±6	101
25.5	68 ±3	4.5	5670 ±57	256	0.05	65 ±2	14	17200 ±1000	107	89 ±6	13	140 ±9	5.3	117 ±8	97
28.5	43 ±1	6.0	6400 ±260	724	0.12	64 ±1	19	19900 ±540	258	67 ±0.5	24	80 ±17	12	95 ±6	64
31.5	23 ±2	4.6	7140 ±43	713	0.10	67 ±4	22	19900 ±1600	283	46 ±2	15	27 ±8	6.7	65 ±1	71
34.5	29 ±2	5.2	6110 ±250	1052	0.16	76 ±1	73	20900 ±1300	181	52 ±0.3	7.7	95 ±19	5.8	77 ±4	323

Table 9.7 Vertical concentration data for U, Fe, Mn, Al, Cu, Pb in soil porewaters and solid phase from Core 5

Depth (cm)	U (mg kg^{-1})	U (µg L^{-1})	Fe (mg kg^{-1})	Fe (µg L^{-1})	Fe porewater/ solid phase ratio	Mn (mg kg^{-1})	Mn (µg L^{-1})	Al (mg kg^{-1})	Al (µg L^{-1})	Cu (mg kg^{-1})	Cu (µg L^{-1})	Pb (mg kg^{-1})	Pb (µg L^{-1})	As (mg kg^{-1})	As (µg L^{-1})
2.5	104 ±11	12	19900 ±780	9022	0.45	403 ±8	229	15200 ±640	233	57 ±4	20	79 ±15	35	175 ±13	165
7.5	112 ±6	12	22600 ±11	12820	0.57	289 ±2	100	16600 ±890	235	64 ±0.1	18	71 ±1	38	233 ±2	273
12.5	110 ±3	8.5	17000 ±380	7036	0.41	139 ±3	45	16600 ±2200	194	75 ±2	14	101 ±10	33	150 ±0.4	140
17.5	99 ±2	9.2	11500 ±670	3487	0.30	104 ±10	29	17700 ±2500	255	73 ±5	19	85 ±7	26	67 ±4	76

Table 9.8 Vertical concentration data for U, Fe, Mn, Al, Cu, Pb, Zn, As and Ca in soil porewaters from Core 6

Depth (cm)	U (µg L^{-1})	Fe (µg L^{-1})	Mn (µg L^{-1})	Al (µg L^{-1})	Cu (µg L^{-1})	Pb (µg L^{-1})	Zn (µg L^{-1})	As (µg L^{-1})	Ca (µg L^{-1})
1	12	14	2.1	6.1	16	0.4	131	475	34100
3	5.0	15	1.8	6.0	12	0.4	198	1956	41400
5	3.4	11	0.4	4.0	8.7	0.2	209	2388	41000
7	3.7	10	0.6	3.0	7.8	0.2	441	4438	66300
9	4.8	8.4	6.1	4.2	8.6	0.3	1350	10400	86900
11	7.0	10	5.8	5.5	10	0.3	1070	7380	83300
13	9.2	18	0.9	6.9	13	0.4	455	1378	50300
15	11	26	0.2	9.5	13	0.5	233	138	30100
17	23	79	0.4	17	21	0.9	194	96	19200
19	18	48	0.2	14	15	0.5	95	87	19100
21	18	37	0.2	17	13	0.6	103	113	20800
23	10	42	0.2	18	11	0.6	94	68	21400
25	6.4	30	11.8	16	7.5	0.5	176	156	35600
27	2.7	15	31.0	7.4	3.4	0.3	419	733	67000
29	1.5	13	63.9	5.8	1.8	0.2	548	599	89800
31	0.7	19	470	23	1.5	3.3	5690	227	272000
33	0.9	24	450	70	2.1	4.2	5290	123	298000
35	0.7	28	426	119	3.0	5.8	6030	53	315000
37	0.7	23	300	56	3.7	3.2	2790	98	245000
39	0.7	21	370	57	3.9	2.6	2200	99	274000
41	1.0	16	94.8	14	3.9	0.3	919	72	145000
43	1.5	13	136	12	3.1	0.2	1280	71	135000
45	1.4	15	243	13	3.0	0.2	1150	78	156000
47	0.9	13	147	17	2.2	0.3	349	43	151000

Table 9.9 Vertical concentration data for U, Fe, Mn, Al, Cu, Pb, Zn, As and Ca in soil porewaters from Core 7

Depth (cm)	U (μg L^{-1})	Fe (μg L^{-1})	Mn (μg L^{-1})	Al (μg L^{-1})	Cu (μg L^{-1})	Pb (μg L^{-1})	Zn (μg L^{-1})	As (μg L^{-1})	Ca (μg L^{-1})
0.5	30	97	674	205	12	n.d.	241	281	51900
1.5	16	601	553	297	13	2.0	184	167	26800
2.5	17	896	356	406	16	3.5	159	177	20700
3.5	18	1287	373	385	15	4.2	140	247	21400
4.5	10	814	166	412	10	3.0	112	96	15700
5.5	13	1192	220	686	16	4.4	196	73	19600
6.5	8.9	752	158	540	10	3.0	144	33	18500
7.5	9.9	824	241	388	13	2.7	94	111	18800
8.5	11	955	125	509	19	4.2	113	38	18200
9.5	9.6	623	111	476	16	3.1	77	26	16900
10.5	13	616	116	422	16	3.7	69	146	21800
11.5	22	796	107	894	24	6.0	105	145	26500
12.5	18	639	103	860	24	6.0	86	145	20700
13.5	21	709	106	979	24	5.4	66	207	22200
14.5	17	529	102	692	18	4.6	57	147	23500
15.5	19	429	92	807	22	4.7	58	299	23900
16.5	20	678	68	929	24	5.8	44	252	18000
17.5	15	245	29	557	19	5.1	107	35	21900
18.5	19	288	31	818	27	6.8	114	40	21200
19.5	21	355	31	979	34	6.2	98	43	20800
20.5	31	402	21	1300	51	6.4	91	58	21400
21.5	27	309	26	1240	47	9.5	96	104	20600
22.5	28	267	19	1360	51	7.5	99	110	22600
23.5	17	146	22	796	22	6.2	73	169	21100
24.5	23	202	23	1340	35	9.4	100	130	21700
25.5	26	169	21	1140	30	9.3	78	326	24700
26.5	34	247	21	1550	46	14	100	382	23800
27.5	37	254	23	1700	47	16	99	290	22000
28.5	42	268	26	2130	60	20	148	414	23800
29.5	38	187	19	2190	40	17	142	574	24400
30.5	57	218	24	2240	52	16	104	869	25200
31.5	36	131	22	1440	28	9.4	91	709	25800
32.5	24	93	20	1140	14	9.4	144	525	25600
33.5	39	174	21	2230	41	13	126	555	27000
35.5	52	164	21	2380	41	10	84	520	24800
37.5	31	144	18	2200	25	6.6	83	407	22300

n.d. for Pb = 0.05 μg L^{-1}

9.9 Ultrafiltration data for soil porewater from Cores 1, 2, 3, 4 and 5

Table 9.10 Total vertical concentration data for U, Fe, Mn, Cu, Pb in soil porewater and corresponding colloidal associations from selected depths for Core 1

Element	Depth (cm)	Concentration (µg L^{-1})	100 kDa-0.2 µm (µg L^{-1})	30-100 kDa (µg L^{-1})	3-30 kDa (µg L^{-1})
U	2.5	40	42	3.0	4.7
	7.5	59			
	13	55			
	19	24	19	0.9	13
	25	34			
	31	18			
	37	8.4			
	42.5	5.6	5.1	n.d.	1.3
Element	**Depth (cm)**	**Concentration (mg L^{-1})**	**100 kDa-0.2 µm (mg L^{-1})**	**30-100 kDa (mg L^{-1})**	**3-30 kDa (mg L^{-1})**
Fe	2.5	0.39	0.26	0.03	0.05
	7.5	0.38			
	13	0.46			
	19	0.44	0.27	0.02	0.10
	25	0.31			
	31	0.21			
	37	0.10			
	42.5	0.16	0.10	0.01	0.04
Mn	2.5	0.012	0.008	0.001	0.001
	7.5	0.009			
	13	0.006			
	19	0.005	0.002	0.001	0.001
	25	0.004			
	31	0.005			
	37	0.018			
	42.5	0.009	0.001	0.001	0.001
Cu	2.5	0.08	0.03	0.007	0.02
	7.5	0.08			
	13	0.08			
	19	0.05	0.01	0.003	0.02
	25	0.04			
	31	0.03			
	37	0.02			
	42.5	0.03	0.01	0.002	0.004
Pb	2.5	0.03	0.009	0.005	0.007
	7.5	0.02			
	13	0.03			
	19	0.02	0.008	0.005	0.006
	25	0.03			
	31	0.03			
	37	0.02			
	42.5	0.03	0.006	0.006	0.004

n.d. for U = 0.001 µg L^{-1}

Table 9.11 Total vertical concentration data for U, Fe, Mn, Cu, Pb in soil porewater and corresponding colloidal association data from selected depths for Core 2

Element	Depth (cm)	Concentration (µg L^{-1})	100 kDa-0.2 µm (µg L^{-1})	30-100 kDa (µg L^{-1})	3-30 kDa (µg L^{-1})
U	2.5	4.8	1.9	n.d.	1.8
	7.5	7.6			
	12.5	6.7			
	17.5	5.8	1.9	n.d.	2.3
	22.5	4.4			
	27.5	5.1			
	32.5	5.1			
	38.5	1.9	1.3	n.d.	0.4
Element	**Depth (cm)**	**Concentration (mg L^{-1})**	**100 kDa-0.2 µm (mg L^{-1})**	**30-100 kDa (mg L^{-1})**	**3-30 kDa (mg L^{-1})**
Fe	2.5	0.72	0.46	0.007	0.050
	7.5	1.50			
	12.5	1.27			
	17.5	1.34	0.61	0.010	0.070
	22.5	0.34			
	27.5	0.28			
	32.5	0.28			
	38.5	0.44	0.26	0.009	0.050
Mn	2.5	0.024	0.015	0.0005	0.0007
	7.5	0.031			
	12.5	0.019			
	17.5	0.018	0.0076	0.0005	0.0007
	22.5	0.006			
	27.5	0.006			
	32.5	0.005			
	38.5	0.008	0.0019	0.0007	0.001
Cu	2.5	0.03	0.004	0.002	0.007
	7.5	0.02			
	12.5	0.02			
	17.5	0.02	0.004	0.002	0.006
	22.5	0.02			
	27.5	0.02			
	32.5	0.03			
	38.5	0.03	0.010	0.002	0.004
Pb	2.5	0.03	0.007	0.004	0.007
	7.5	0.03			
	12.5	0.03			
	17.5	0.03	0.009	0.006	0.006
	22.5	0.03			
	27.5	0.03			
	32.5	0.03			
	38.5	0.03	0.007	0.006	0.005

n.d. for U = 0.001 µg L^{-1}

Table 9.12 Data of U, Fe, Mn, Pb, Cu distributions in soil porewater and bog water amongst colloidal (100 kDa-0.2 µm, 30-100 kDa and 3-30 kDa) fractions and recovery rate in the form of percentage for Cores 1 and 2

Element	Core 1					Core 2				
	Depth (cm)	100 kDa-0.2 µm (%)	30-100 kDa (%)	3-30 kDa (%)	Recovery rate (%)	Depth (cm)	100 kDa-0.2 µm (%)	30-100 kDa (%)	3-30 kDa (%)	Recovery rate (%)
U	2.5	103.9	7.5	11.8	123.3	2.5	39.6	n.d.	38.2	77.1
	19	78.1	3.6	54.7	136.4	17.5	32.8	n.d.	39.7	72.4
	42.5	91.1	n.d.	23.2	114.3	38.5	68.4	n.d.	21.1	89.5
	Bog water	0.6	0.2	12.4	13.3	Bog water	1.4	n.d.	11.2	12.6
Fe	2.5	103.9	7.5	11.8	123.3	2.5	64.2	1.0	13.7	78.9
	19	78.1	3.6	54.7	136.4	17.5	45.8	0.8	4.9	51.5
	42.5	91.4	0.2	23.9	115.5	38.5	58.5	2.0	10.6	71.1
	Bog water	0.6	0.2	12.4	13.3	Bog water	28.1	6.1	41.5	75.6
Mn	2.5	67.1	6.5	8.5	82.0	2.5	62.7	2.1	3.0	67.8
	19	49.4	15.8	15.2	80.4	17.5	42.2	3.0	3.9	49.1
	42.5	14.6	8.9	11.9	35.5	38.5	23.2	8.5	8.5	40.2
	Bog water	11.6	13.3	18.6	43.5	Bog water	31.3	15.0	15.0	61.3
Pb	2.5	34.5	19.1	25.4	79.0	2.5	25.6	15.2	27.8	68.6
	19	37.6	23.8	27.8	89.2	17.5	33.5	24.6	22.8	80.9
	42.5	22.5	22.0	15.4	59.9	38.5	25.9	22.4	18.6	66.9
	Bog water	23.1	28.2	36.5	87.8	Bog water	16.9	22.5	31.1	70.5
Cu	2.5	44.1	8.7	21.5	74.3	2.5	14.2	7.6	28.8	50.6
	19	24.2	5.9	35.8	65.8	17.5	19.8	8.5	29.1	57.4
	42.5	45.8	6.9	15.9	68.6	38.5	40.1	6.5	15.8	62.5
	Bog water	7.0	41.7	44.3	93.0	Bog water	19.2	14.3	45.6	79.1

n.d. for U = 0.001 µg L^{-1}

Table 9.13 Data of U, Fe, Mn and Al distributions amongst colloidal (100 kDa-0.2 µm, 30-100 kDa and 3-30 kDa) and dissolved (<3 kDa) fractions of soil porewaters and recovery rate in the form of percentage from Core 3

Element	Depth (cm)	100 kDa-0.2 µm (%)	30-100 kDa (%)	3-30 kDa (%)	<3 kDa (%)	Recovery rate (%)
U	1.5	66.1	7.5	20.8	5.6	82.5
	7.5	62.4	5.0	16.0	16.6	92.0
	16.5	67.4	4.0	17.5	11.1	91.7
	25.5	64.2	4.3	14.5	17.0	89.1
	34.5	65.5	2.6	16.1	15.8	86.2
	43	57.4	3.3	7.0	32.2	81.7
Fe	1.5	70.6	8.4	18.1	2.9	88.5
	7.5	63.2	6.6	16.8	13.4	98.9
	16.5	67.9	5.6	19.1	7.4	92.4
	25.5	71.3	4.7	12.2	11.8	95.8
	34.5	81.0	2.3	10.2	6.5	113
	43	81.5	2.8	4.4	11.4	108
Mn	1.5	95.1	0.3	1.5	3.1	113
	7.5	89.4	n.d.[1]	1.1	9.5	135
	16.5	79.1	n.d.[1]	1.8	19.1	120
	25.5	86.1	n.d.[1]	n.d.	13.4	112
	34.5	33.7	n.d.[1]	1.6	64.7	132
	43	93.5	n.d.[1]	n.d.	6.5	79.2
Al	1.5	80.1	2.1	17.8	n.d.[2]	107
	7.5	95.0	0.5	4.5	n.d.[2]	308
	16.5	90.4	1.0	8.6	n.d.[2]	85.4
	25.5	69.2	1.2	11.5	18.1	144
	34.5	45.6	1.1	18.0	35.3	76.0
	43	70.4	0.6	2.4	26.6	142

n.d.[1] for Mn = 0.057 µg L^{-1}

n.d.[2] Ultrafiltration released small amount of Al, thus the Al data showed negative value after being corrected using standard blank subtraction method.

Table 9.14 Data of U, Fe, Mn and Al distributions amongst colloidal (100 kDa-0.2 µm, 30-100 kDa and 3-30 kDa) and dissolved (<3 kDa) fractions of soil porewaters and recovery rate in the form of percentage from Core 4

Element	Depth (cm)	100 kDa-0.2 µm (%)	30-100 kDa (%)	3-30 kDa (%)	<3 kDa (%)	Recovery rate (%)
U	1.5	46.9	2.9	13.7	36.5	101
	7.5	66.7	5.7	12.3	15.3	94.5
	16.5	64.0	3.7	15.5	16.8	89.7
	25.5	58.8	2.5	19.8	18.9	88.3
	34.5	47.4	5.1	7.2	40.4	84.8
Fe	1.5	82.0	2.8	11.3	4.0	83.5
	7.5	80.0	8.7	8.2	3.0	90.6
	16.5	80.1	4.2	9.3	6.4	111
	25.5	70.9	2.8	15.3	11.0	81.7
	34.5	62.6	12.1	7.9	17.3	88.4
Mn	1.5	99.3	n.d.[1]	0.1	0.6	115
	7.5	60.7	1.0	3.2	35.1	89.7
	16.5	49.5	0.1	1.6	48.7	107
	25.5	12.1	0.2	2.1	85.6	121
	34.5	11.8	1.4	2.6	84.2	94.3
Al	1.5	88.6	0.3	11.1	n.d.[2]	187
	7.5	95.1	0.5	4.4	n.d.[2]	272
	16.5	85.7	0.3	11.8	2.2	85.0
	25.5	68.1	0.7	8.2	23.0	135
	34.5	81.9	2.6	2.9	12.6	67.3

n.d.[1] for Mn = 0.057 µg L^{-1}

n.d.[2] Ultrafiltration released small amount of Al, thus the Al data showed negative value after being corrected using standard blank subtraction method.

Table 9.15 Data of U, Fe, Mn and Al distributions amongst colloidal (100 kDa-0.2 µm, 30-100 kDa and 3-30 kDa) and dissolved (<3 kDa) fractions of soil porewaters and recovery rate in the form of percentage from Core 5

Element	Depth (cm)	100 kDa-0.2 µm (%)	30-100 kDa (%)	3-30 kDa (%)	<3 kDa (%)	Recovery rate (%)
U	2.5	51.2	3.9	7.1	37.9	88.2
	7.5	72.8	4.1	6.5	16.5	89.3
	12.5	76.0	1.2	4.7	18.1	89.2
	17.5	62.4	5.1	13.7	18.9	87.2
Fe	2.5	97.1	1.0	1.1	0.8	88.4
	7.5	98.3	0.4	0.4	0.8	98.9
	12.5	98.5	0.2	0.3	1.0	104
	17.5	95.2	1.0	1.9	1.8	93.2
Mn	2.5	98.3	0.03	0.1	1.5	88.8
	7.5	94.1	0.04	0.2	5.7	108
	12.5	77.6	n.d.	0.2	22.1	108
	17.5	69.7	0.2	1.0	29.0	109
Al	2.5	87.2	1.5	5.0	6.3	62.9
	7.5	96.9	0.9	2.2	0.0	80.6
	12.5	94.3	0.5	3.2	2.0	72.7
	17.5	94.1	1.1	3.2	1.6	106

n.d. for Mn = 0.057 µg L^{-1}

9.10 Ultrafiltration in conjunction with acetate extraction data for soil porewater from Core 6

Table 9.16 U distributions amongst colloidal (3 kDa-0.2 µm) and dissolved (<3 kDa) fractions of porewaters and its recovery rate obtained from soil Core 6 under N_2

Depth (cm)	N_2						
	colloidal (3 kDa-0.2 µm) (µg L^{-1})	% colloidal	truly dissolved (< 3 kDa) (µg L^{-1})	% truly dissolved	Calculated total (< 0.2 µm) porewater (µg L^{-1})	measured total (< 0.2 µm) porewater (µg L^{-1})	Recovery rate (%)
1	0.99	28.8	4.92	71.2	6.91	12	59.8
3	2.86	71.1	1.17	28.9	4.03	5.0	80.2
5	1.47	63.5	0.85	36.5	2.32	3.4	67.5
7	1.59	43.9	2.04	56.1	3.63	3.7	97.5
9	2.22	47.3	2.48	52.7	4.70	4.8	97.6
11	4.00	52.1	3.68	47.9	7.68	7.0	109
13	5.46	54.3	4.59	45.7	10.0	9.2	109
15	8.82	65.4	4.66	34.6	13.5	11	120
17	19.5	71.1	7.93	28.9	27.4	23	118
19	8.83	54.3	7.43	45.7	16.3	18	89.4
21	7.35	41.5	10.3	58.5	17.7	18	99.4
23	7.90	69.8	3.41	30.2	11.3	10	112
25	3.72	45.6	4.45	54.4	8.17	6.4	128
27	1.64	48.0	1.78	52.0	3.42	2.7	125
29	0.56	29.0	1.38	71.0	1.94	1.5	128
31	0.30	20.7	1.15	79.3	1.45	0.7	212
33	0.26	15.2	1.47	84.8	1.73	0.9	197
35	0.22	15.2	1.24	84.8	1.46	0.7	221
37	0.26	14.5	1.55	85.5	1.81	0.7	244
39	0.23	17.1	1.11	82.9	1.34	0.7	204
41	0.35	23.7	1.13	76.3	1.48	1.0	145
43	0.50	29.6	1.19	70.4	1.69	1.5	116
45	0.37	22.9	1.26	77.1	1.63	1.4	119
47	0.41	31.7	0.89	68.3	1.30	0.9	140

Table 9.17 U distributions amongst colloidal (3 kDa-0.2 μm) and dissolved (<3 kDa) fractions of porewaters and its recovery rate obtained from soil Core 6 in air

Depth (cm)	Air						
	$U_{pseudo-total}$ in colloidal (3 kDa-0.2 μm) fraction (μg L^{-1})	U% of colloidal (3 kDa-0.2 μm) fraction	U in truly dissolved (< 3 kDa) fraction (μg L^{-1})	U% of truly dissolved (< 3 kDa) fraction	$U_{pseudo-total}$ in total (< 0.2 μm) porewater (μg L^{-1})	U_{total} in total (<0.2 μm) porewater (μg L^{-1})	Recovery rate (%)
1	1.62	22.8	5.47	77.2	6.91	12	59.8
3	3.75	76.7	1.14	23.3	4.03	5.0	80.2
5	2.12	63.3	1.23	36.7	2.32	3.4	67.5
7	1.77	45.3	2.12	54.7	3.63	3.7	97.5
9	1.48	36.4	2.58	63.6	4.70	4.8	97.6
11	3.12	42.2	4.27	57.8	7.68	7.0	109
13	6.41	60.0	4.27	40.0	10.1	9.2	109
15	9.52	70.5	3.98	29.5	13.5	11	120
17	21.1	78.0	5.95	22.0	27.4	23	118
19	7.80	54.0	6.65	46.0	16.3	18	89.4
21	6.04	49.9	6.06	50.1	17.7	18	99.4
23	7.37	57.5	5.45	42.5	11.3	10	112
25	4.90	68.2	2.28	31.8	8.17	6.4	128
27	1.83	56.5	1.41	43.5	3.42	2.7	125
29	1.13	57.2	0.85	42.8	1.94	1.5	128
31	0.53	38.3	0.86	61.7	1.45	0.7	212
33	0.51	32.6	1.05	67.4	1.73	0.9	197
35	0.35	26.8	0.95	73.2	1.46	0.7	221
37	0.37	28.0	0.96	72.0	1.81	0.7	244
39	0.35	33.1	0.71	66.9	1.34	0.7	204
41	0.64	40.8	0.92	59.2	1.48	1.0	145
43	0.80	37.1	1.36	62.9	1.69	1.5	116
45	0.99	43.2	1.30	56.8	1.63	1.4	119
47	0.60	42.8	0.81	57.2	1.30	0.9	140

Table 9.18 U distributions amongst acetate extracted colloidal (3 kDa-0.2 μm) fraction and residue after acetate extraction, and the percentage of U extracted from colloidal (3 kDa-0.2 μm) fraction by acetate from soil Core 6 under N_2

Depth (cm)	N_2			
	U in colloidal (3 kDa-0.2) μm fraction extracted by acetate (μg L^{-1})	U in colloidal (3 kDa-0.2 μm) fraction after acetate extraction (μg L^{-1})	$U_{pseudo-total}$ in colloidal (3 kDa-0.2 μm) fraction (μg L^{-1})	U% extracted by acetate of $U_{pseudo-total}$ in colloidal (3 kDa-0.2 μm)fraction
1	1.86	0.13	1.99	93.7
3	2.71	0.15	2.86	94.7
5	1.36	0.11	1.47	92.6
7	1.53	0.06	1.59	96.1
9	2.13	0.09	2.22	95.8
11	3.87	0.13	4.00	96.8
13	5.26	0.20	5.46	96.4
15	8.52	0.30	8.82	96.6
17	18.5	1.00	19.5	94.9
19	8.42	0.41	8.83	95.4
21	6.91	0.44	7.35	94.1
23	7.57	0.33	7.90	95.9
25	3.64	0.08	3.72	97.8
27	1.57	0.07	1.64	95.7
29	0.49	0.08	0.56	86.5
31	0.27	0.04	0.30	88.2
33	0.24	0.03	0.26	89.7
35	0.20	0.03	0.22	87.5
37	0.23	0.03	0.26	88.4
39	0.19	0.03	0.23	85.0
41	0.31	0.04	0.35	89.2
43	0.46	0.04	0.50	91.2
45	0.33	0.04	0.37	88.9
47	0.35	0.06	0.41	84.6

Table 9.19 U distributions amongst acetate extracted colloidal (3 kDa-0.2 µm) fraction and residue after acetate extraction, and the percentage of U extracted from colloidal (3 kDa-0.2 µm) fraction by acetate from soil Core 6 in air

Depth (cm)	Air			
	U in colloidal (3 kDa-0.2) µm fraction extracted by acetate (µg L^{-1})	U in colloidal (3 kDa-0.2 µm) fraction after acetate extraction (µg L^{-1})	$U_{pseudo-total}$ in colloidal (3 kDa-0.2 µm) fraction (µg L^{-1})	U% extracted by acetate of $U_{pseudo-total}$ in colloidal (3 kDa-0.2 µm)fraction
1	1.43	0.19	1.62	88.1
3	3.49	0.26	3.75	93.1
5	1.95	0.17	2.12	91.9
7	1.66	0.11	1.77	94.0
9	1.35	0.13	1.48	91.5
11	2.81	0.31	3.12	90.2
13	5.85	0.56	6.41	91.2
15	8.83	0.69	9.52	92.8
17	19.4	1.67	21.1	92.1
19	7.23	0.57	7.80	92.7
21	5.60	0.44	6.04	92.8
23	6.99	0.38	7.37	94.8
25	4.43	0.47	4.90	90.5
27	1.71	0.12	1.83	93.5
29	1.01	0.12	1.13	89.3
31	0.48	0.05	0.53	90.2
33	0.48	0.03	0.51	94.2
35	0.31	0.04	0.35	88.8
37	0.32	0.05	0.37	86.9
39	0.30	0.05	0.35	84.9
41	0.52	0.12	0.64	81.9
43	0.71	0.09	0.80	89.1
45	0.90	0.09	0.99	90.6
47	0.51	0.09	0.60	85.1

Table 9.20 Fe distributions amongst colloidal (3 kDa-0.2 μm) and dissolved (<3 kDa) fractions of porewaters and its recovery rate obtained from soil Core 6 under N_2

Depth (cm)	N_2						
	$Fe_{pseudo-total}$ in colloidal (3 kDa-0.2 μm) fraction (μg L^{-1})	Fe% of colloidal (3 kDa-0.2 μm) fraction	Fe in truly dissolved (< 3 kDa) fraction (μg L^{-1})	Fe% of truly dissolved (< 3 kDa) fraction	$Fe_{pseudo-total}$ in total (< 0.2 μm) porewater (μg L^{-1})	Fe_{total} in total (<0.2 μm) porewater (μg L^{-1})	Recovery rate (%)
1	49.4	100	n.d.	n.d.	49.4	14	353
3	29.6	100	n.d.	n.d.	29.6	15	197
5	18.4	95.6	0.84	4.40	19.2	11	175
7	13.4	65.0	7.21	35.0	20.6	10	206
9	30.9	100	n.d.	n.d.	30.9	8.4	368
11	-	-	-	-	-	-	-
13	22.2	86.1	3.60	13.9	25.8	18	143
15	26.3	87.4	3.80	12.6	30.1	26	116
17	60.2	86.9	9.10	13.1	69.3	79	87.7
19	36.1	88.4	4.75	11.6	40.9	48	85.2
21	38.2	92.3	3.21	7.70	41.4	37	112
23	35.6	98.6	0.50	1.40	36.1	42	86.0
25	20.7	63.7	11.8	36.3	32.5	30	108
27	16.9	67.6	8.09	32.4	25.0	15	167
29	16.6	55.5	13.3	44.5	29.9	13	230
31	9.52	28.0	24.5	72.0	34.0	19	179
33	9.06	24.0	28.6	76.0	37.7	24	157
35	22.2	42.6	29.9	57.4	52.1	28	186
37	6.52	20.9	24.7	79.1	31.2	23	136
39	7.22	22.9	24.4	77.1	31.6	21	151
41	8.82	44.7	10.9	55.3	19.7	16	123
43	7.64	43.5	9.93	56.5	17.6	13	135
45	-	-	-	-	-	-	-
47	13.5	61.8	8.32	38.2	21.8	13	168

n.d. for Fe = 0.08 μg L^{-1}

Table 9.21 Fe distributions amongst colloidal (3 kDa-0.2 µm) and dissolved (<3 kDa) fractions of porewaters and its recovery rate obtained from soil Core 6 in air

Depth (cm)	Air						
	$Fe_{pseudo-total}$ in colloidal (3 kDa-0.2 µm) fraction (µg L^{-1})	Fe% of colloidal (3 kDa-0.2 µm) fraction	Fe in truly dissolved (< 3 kDa) fraction (µg L^{-1})	Fe% of truly dissolved (< 3 kDa) fraction	$Fe_{pseudo-total}$ in total (< 0.2 µm) porewater (µg L^{-1})	Fe_{total} in total (<0.2 µm) porewater (µg L^{-1})	Recovery rate (%)
1	36.0	100	n.d.	n.d.	36.0	14	257
3	37.0	100	n.d.	n.d.	37.0	15	247
5	45.	100	n.d.	n.d.	45.2	11	411
7	39.0	88.3	5.17	11.7	44.2	10	442
9	15.6	100	n.d.	n.d.	15.6	8.4	186
11	7.08	87.2	1.04	12.8	8.12	10	81.2
13	33.9	97.3	0.93	2.70	34.8	18	194
15	25.1	80.7	6.03	19.3	31.1	26	120
17	54.5	90.5	5.70	9.50	60.2	79	76.2
19	50.8	94.2	3.11	5.80	53.9	48	112
21	26.7	99.7	0.08	0.30	26.8	37	72.4
23	31.6	100	n.d.	n.d.	31.6	42	75.2
25	21.5	100	n.d.	n.d.	21.5	30	71.7
27	12.0	80.5	2.89	19.5	14.9	15	99.3
29	11.3	81.0	2.66	19.0	14.0	13	107
31	9.69	33.8	19.0	66.2	28.7	19	151
33	6.52	21.2	24.2	78.8	30.7	24	128
35	10.2	27.5	26.9	72.5	37.1	28	133
37	8.48	27.7	22.2	72.3	30.7	23	133
39	6.71	22.9	22.6	77.1	29.3	21	140
41	-	-	-	-	-	-	-
43	10.9	61.5	6.80	38.5	17.7	13	136
45	15.0	55.6	11.9	44.4	26.9	15	179
47	8.67	41.3	12.3	58.7	21.0	13	161

n.d. for Fe = 0.08 µg L^{-1}

Table 9.22 Fe distributions amongst acetate extracted colloidal (3 kDa-0.2 µm) fraction and residue after acetate extraction, and the percentage of Fe extracted from colloidal (3 kDa-0.2 µm) fraction by acetate from soil Core 6 under N_2

Depth (cm)	N_2			
	Fe in colloidal (3 kDa-0.2) µm fraction extracted by acetate (µg L^{-1})	Fe in colloidal (3 kDa-0.2 µm) fraction after acetate extraction (µg L^{-1})	$Fe_{pseudo-total}$ in colloidal (3 kDa-0.2 µm) fraction (µg L^{-1})	Fe% extracted by acetate of $Fe_{pseudo-total}$ in colloidal (3 kDa-0.2 µm)fraction
1	37.4	12.0	49.4	75.7
3	20.2	9.39	29.6	68.3
5	13.6	4.77	18.4	74.0
7	8.40	4.97	13.4	62.8
9	27.5	3.38	30.9	89.1
11	-	-	-	-
13	17.6	4.64	22.2	79.1
15	19.8	6.51	26.3	75.3
17	34.2	26.0	60.2	56.8
19	22.7	13.4	36.1	62.9
21	29.2	9.03	38.2	76.4
23	25.3	10.3	35.6	71.1
25	17.5	3.22	20.7	84.5
27	14.2	2.72	16.9	83.9
29	13.2	3.36	16.6	79.7
31	8.10	1.42	9.52	85.1
33	7.68	1.38	9.06	84.8
35	20.4	1.75	22.2	92.1
37	4.88	1.64	6.52	74.8
39	5.12	2.10	7.22	70.9
41	6.75	2.07	8.82	76.5
43	5.56	2.08	7.64	72.8
45	-	-	-	-
47	8.06	5.42	13.5	59.8

Table 9.23 Fe distributions amongst acetate extracted colloidal (3 kDa-0.2 µm) fraction and residue after acetate extraction, and the percentage of Fe extracted from colloidal (3 kDa-0.2 µm) fraction by acetate from soil Core 6 in air

Depth (cm)	Air			
	Fe in 3 kDa-0.2 µm fraction extracted by acetate (µg L^{-1})	Fe in 3 kDa-0.2 µm fraction after acetate extraction (µg L^{-1})	$Fe_{pseudo-total}$ in 3 kDa-0.2 µm fraction (µg L^{-1})	Fe % extracted by acetate of $U_{pseudo-total}$ fraction
1	26.7	9.29	36.0	74.2
3	25.7	11.3	37.0	69.5
5	40.2	5.00	45.2	88.9
7	16.3	22.7	39.0	41.8
9	11.9	3.73	15.6	76.1
11	3.88	3.20	7.08	54.8
13	25.9	7.95	33.9	76.5
15	16.0	9.10	25.1	63.7
17	31.0	23.5	54.5	56.9
19	34.9	15.9	50.8	68.7
21	14.3	12.4	26.7	53.6
23	20.3	11.3	31.6	64.2
25	13.1	8.40	21.5	60.9
27	7.05	4.91	12.0	58.9
29	7.54	3.79	11.3	66.5
31	8.01	1.68	9.69	82.7
33	5.68	0.84	6.52	87.2
35	8.96	1.25	10.2	87.8
37	6.92	1.56	8.48	81.6
39	5.14	1.57	6.71	76.6
41	-	-	-	-
43	7.70	3.18	10.9	70.8
45	11.5	3.48	15.0	76.8
47	6.32	2.35	8.67	72.9

Table 9.24 Mn distributions amongst colloidal (3 kDa-0.2 µm) and dissolved (<3 kDa) fractions of porewaters and its recovery rate obtained from soil Core 6 under N_2

Depth (cm)	N_2						
	$Mn_{pseudo-total}$ in colloidal (3 kDa-0.2 µm) fraction (µg L^{-1})	Mn% of colloidal (3 kDa-0.2 µm) fraction	Mn in truly dissolved (< 3 kDa) fraction (µg L^{-1})	Mn% of truly dissolved (< 3 kDa) fraction	$Mn_{pseudo-total}$ in total (< 0.2 µm) porewater (µg L^{-1})	Mn_{total} in total (<0.2 µm) porewater (µg L^{-1})	Recovery rate (%)
1	2.09	100	n.d.	n.d.	2.09	2.1	99.5
3	0.56	68.2	0.26	31.8	0.83	1.8	45.8
5	0.31	59.7	0.21	40.3	0.51	0.4	128
7	0.45	30.7	1.02	69.3	1.47	0.6	245
9	0.52	7.90	6.12	92.1	6.64	6.1	109
11	2.43	28.3	6.16	71.7	8.59	5.8	148
13	0.12	12.0	0.90	88.0	1.03	0.9	114
15	0.14	35.4	0.26	64.6	0.41	0.2	204
17	0.42	64.7	0.23	35.3	0.65	0.4	163
19	0.24	75.3	0.08	24.7	0.32	0.2	158
21	0.32	82.8	0.07	17.2	0.39	0.2	193
23	0.36	83.2	0.07	16.8	0.44	0.2	218
25	0.93	9.80	8.52	90.2	9.45	11.8	80.1
27	1.30	4.20	30.0	95.8	31.3	31.0	101
29	2.45	3.50	67.3	96.5	69.8	63.9	109
31	9.98	2.10	476	97.9	486	469	104
33	12.5	2.80	436	97.2	449	450	99.9
35	8.10	1.90	411	98.1	419	426	98.4
37	3.70	1.30	290	98.7	294	300	98.1
39	6.87	1.90	359	98.1	366	370	99.0
41	2.30	2.50	90.9	97.5	93.2	94.8	98.3
43	2.44	1.90	128	98.1	130	136	95.7
45	12.3	3.20	368	96.8	380	243	157
47	2.75	2.10	128	97.9	131	147	89.1

n.d. for Mn = 0.009 µg L^{-1}

Table 9.25 Mn distributions amongst colloidal (3 kDa-0.2 μm) and dissolved (<3 kDa) fractions of porewaters and its recovery rate obtained from soil Core 6 in air

Depth (cm)	Air						
	$Mn_{pseudo-total}$ in colloidal (3 kDa-0.2 μm) fraction (μg L^{-1})	Mn% of colloidal (3 kDa-0.2 μm) fraction	Mn in truly dissolved (< 3 kDa) fraction (μg L^{-1})	Mn% of truly dissolved (< 3 kDa) fraction	$Mn_{pseudo-total}$ in total (< 0.2 μm) porewater (μg L^{-1})	Mn_{total} in total (<0.2 μm) porewater (μg L^{-1})	Recovery rate (%)
1	1.19	89.8	0.14	10.2	1.33	2.1	63.3
3	0.91	100	n.d.	n.d.	0.91	1.8	50.7
5	0.72	100	n.d.	n.d.	0.72	0.4	179
7	0.23	28.6	0.56	71.4	0.79	0.6	131
9	0.67	10.4	5.75	89.6	6.42	6.1	105
11	0.14	2.80	5.02	97.2	5.16	5.8	89.0
13	0.21	20.0	0.83	80.0	1.03	0.9	114
15	0.20	38.3	0.32	61.7	0.52	0.2	262
17	0.39	66.7	0.19	33.3	0.58	0.4	145
19	0.40	78.2	0.11	21.8	0.51	0.2	253
21	0.39	79.1	0.10	20.9	0.49	0.2	247
23	0.54	85.0	0.09	15.0	0.63	0.2	315
25	3.49	52.7	3.13	47.3	6.62	11.8	56.1
27	0.64	2.10	29.4	97.9	30.0	31.0	96.8
29	1.22	1.80	68.1	98.2	69.3	63.9	109
31	6.84	1.40	480	98.6	487	469	104
33	7.49	1.70	442	98.3	449	450	99.9
35	7.24	1.70	428	98.3	435	426	102
37	6.29	2.00	303	98.0	309	300	103
39	5.65	1.60	357	98.4	363	370	98.2
41	1.52	1.50	98.2	98.5	99.7	94.8	105
43	2.67	1.90	141	98.1	144	136	106
45	6.84	2.60	252	97.4	259	243	107

n.d. for Mn = 0.009 μg L^{-1}

Table 9.26 Mn distributions amongst acetate extracted colloidal (3 kDa-0.2 μm) fraction and residue after acetate extraction, and the percentage of Mn extracted from colloidal (3 kDa-0.2 μm) fraction by acetate from soil Core 6 under N_2

Depth (cm)	N_2			
	Mn in 3 kDa-0.2 μm fraction extracted by acetate (μg L^{-1})	Mn in 3 kDa-0.2 μm fraction after acetate extraction (μg L^{-1})	$Mn_{pseudo\text{-}total}$ in 3 kDa-0.2 μm fraction (μg L^{-1})	Mn % extracted by acetate of $U_{pseudo\text{-}total}$ fraction
1	2.01	0.08	2.09	96.1
3	0.49	0.07	0.56	87.5
5	0.27	0.03	0.31	88.6
7	0.38	0.08	0.45	83.2
9	0.49	0.03	0.52	93.5
11	2.38	0.05	2.43	97.8
13	0.12	0.004	0.12	96.6
15	0.14	0.01	0.14	94.8
17	0.40	0.02	0.42	94.1
19	0.23	0.01	0.24	96.4
21	0.30	0.02	0.32	93.4
23	0.24	0.12	0.36	67.4
25	0.78	0.15	0.93	83.5
27	1.16	0.14	1.30	89.2
29	2.39	0.06	2.45	97.5
31	9.78	0.20	9.98	98.0
33	12.3	0.20	12.5	98.4
35	7.88	0.22	8.10	97.3
37	3.63	0.07	3.70	98.1
39	6.69	0.18	6.87	97.3
41	2.26	0.04	2.30	98.4
43	2.28	0.16	2.44	93.6
45	12.1	0.16	12.3	98.7
47	2.69	0.06	2.75	97.7

Table 9.27 Mn distributions amongst acetate extracted colloidal (3 kDa-0.2 µm) fraction and residue after acetate extraction, and the percentage of Mn extracted from colloidal (3 kDa-0.2 µm) fraction by acetate from soil Core 6 in air

Depth (cm)	Air			
	Mn in 3 kDa-0.2 µm fraction extracted by acetate (µg L^{-1})	Mn in 3 kDa-0.2 µm fraction after acetate extraction (µg L^{-1})	$Mn_{pseudo\text{-}total}$ in 3 kDa-0.2 µm fraction (µg L^{-1})	Mn % extracted by acetate of $U_{pseudo\text{-}total}$ fraction
1	1.09	0.10	1.19	91.7
3	0.56	0.36	0.91	61.0
5	0.51	0.21	0.72	71.4
7	0.02	0.21	0.23	7.6
9	0.45	0.22	0.67	67.6
11	0.04	0.11	0.14	25.1
13	0.08	0.12	0.21	40.6
15	0.08	0.12	0.20	41.7
17	0.23	0.15	0.39	60.5
19	0.24	0.15	0.40	61.0
21	0.04	0.36	0.39	9.1
23	0.43	0.11	0.54	79.3
25	3.03	0.46	3.49	86.9
27	0.50	0.14	0.64	78.3
29	1.15	0.07	1.22	94.2
31	6.58	0.26	6.84	96.2
33	7.13	0.36	7.49	95.2
35	6.57	0.67	7.24	90.8
37	5.90	0.39	6.29	93.9
39	5.10	0.55	5.65	90.2
41	1.22	0.30	1.52	80.2
43	2.43	0.24	2.67	91.1
45	6.38	0.46	6.84	93.3
47	2.88	0.35	3.23	89.2

Table 9.28 Al distributions amongst colloidal (3 kDa-0.2 μm) and dissolved (<3 kDa) fractions of porewaters and its recovery rate obtained from soil Core 6 under N_2

Depth (cm)	N_2						
	$Al_{pseudo-total}$ in colloidal (3 kDa-0.2 μm) fraction (μg L^{-1})	Al% of colloidal (3 kDa-0.2 μm) fraction	Al in truly dissolved (< 3 kDa) fraction (μg L^{-1})	Al% of truly dissolved (< 3 kDa) fraction	$Al_{pseudo-total}$ in total (< 0.2 μm) porewater (μg L^{-1})	Al_{total} in total (<0.2 μm) porewater (μg L^{-1})	Recovery rate (%)
1	-	-	-	-	-	-	-
3	-	-	-	-	-	-	-
5	-	-	-	-	-	-	-
7	-	-	-	-	-	-	-
9	-	-	-	-	-	-	-
11	-	-	-	-	-	-	-
13	-	-	-	-	-	-	-
15	-	-	-	-	-	-	-
17	-	-	-	-	-	-	-
19	-	-	-	-	-	-	-
21	-	-	-	-	-	-	-
23	-	-	-	-	-	-	-
25	-	-	-	-	-	-	-
27	-	-	-	-	-	-	-
29	-	-	-	-	-	-	-
31	2.60	5.10	48.0	94.9	50.6	23	220
33	4.49	3.90	110	96.1	114	70	163
35	6.58	4.20	150	95.8	157	119	132
37	4.03	3.60	109	96.4	113	56	202
39	3.68	4.40	80.1	95.6	83.8	57	147
41	9.42	16.9	46.2	83.1	55.6	14	397
43	3.86	16.9	18.9	83.1	22.8	12	190
45	21.8	45.0	26.6	55.0	48.4	13	372
47	17.3	27.1	46.6	72.9	63.9	17	376

Table 9.29 Al distributions amongst colloidal (3 kDa-0.2 μm) and dissolved (<3 kDa) fractions of porewaters and its recovery rate obtained from soil Core 6 in air

Depth (cm)	Air						
	$Al_{pseudo-total}$ in colloidal (3 kDa-0.2 μm) fraction (μg L^{-1})	Al% of colloidal (3 kDa-0.2 μm) fraction	Al in truly dissolved (< 3 kDa) fraction (μg L^{-1})	Al% of truly dissolved (< 3 kDa) fraction	$Al_{pseudo-total}$ in total (< 0.2 μm) porewater (μg L^{-1})	Al_{total} in total (<0.2 μm) porewater (μg L^{-1})	Recovery rate (%)
1	-	-	-	-	-	-	-
3	-	-	-	-	-	-	-
5	-	-	-	-	-	-	-
7	-	-	-	-	-	-	-
9	-	-	-	-	-	-	-
11	-	-	-	-	-	-	-
13	-	-	-	-	-	-	-
15	-	-	-	-	-	-	-
17	-	-	-	-	-	-	-
19	-	-	-	-	-	-	-
21	-	-	-	-	-	-	-
23	-	-	-	-	-	-	-
25	-	-	-	-	-	-	-
27	-	-	-	-	-	-	-
29	-	-	-	-	-	-	-
31	7.51	12.6	52.1	87.4	59.6	23.0	259
33	2.43	2.80	85.6	97.2	88.0	70.0	126
35	7.25	5.10	134	94.9	141	119	119
37	4.14	5.30	73.4	94.7	77.5	56.0	138
39	3.13	4.00	74.6	96.0	77.7	57.0	136
41	-	-	-	-	-	-	-
43	3.99	17.6	18.7	82.4	22.7	12.0	189
45	-	-	-	-	-	-	-
47	-	-	-	-	-	-	-

Table 9.30 Al distributions amongst acetate extracted colloidal (3 kDa-0.2 μm) fraction and residue after acetate extraction, and the percentage of Al extracted from colloidal (3 kDa-0.2 μm) fraction by acetate from soil Core 6 under N_2

Depth (cm)	N_2			
	Al in 3 kDa-0.2 μm fraction extracted by acetate (μg L^{-1})	Al in 3 kDa-0.2 μm fraction after acetate extraction (μg L^{-1})	$Al_{pseudo-total}$ in 3 kDa-0.2 μm fraction (μg L^{-1})	Al % extracted by acetate of $U_{pseudo-total}$ fraction
1	-	-	-	-
3	-	-	-	-
5	-	-	-	-
7	-	-	-	-
9	-	-	-	-
11	-	-	-	-
13	-	-	-	-
15	-	-	-	-
17	-	-	-	-
19	-	-	-	-
21	-	-	-	-
23	-	-	-	-
25	-	-	-	-
27	-	-	-	-
29	-	-	-	-
31	0.96	1.64	2.60	36.9
33	3.19	1.30	4.49	71.0
35	4.77	1.81	6.58	72.5
37	2.46	1.57	4.03	61.0
39	1.61	2.07	3.68	43.8
41	6.56	2.86	9.42	69.6
43	1.95	1.91	3.86	50.5
45	-	-	-	-
47	-	-	-	-

Table 9.31 Al distributions amongst acetate extracted colloidal (3 kDa-0.2 μm) fraction and residue after acetate extraction, and the percentage of Al extracted from colloidal (3 kDa-0.2 μm) fraction by acetate from soil Core 6 in air

Depth (cm)	Air			
	Al in 3 kDa-0.2 μm fraction extracted by acetate (μg L^{-1})	Al in 3 kDa-0.2 μm fraction after acetate extraction (μg L^{-1})	$Al_{pseudo-total}$ in 3 kDa-0.2 μm fraction (μg L^{-1})	Al % extracted by acetate of $U_{pseudo-total}$ fraction
1	-	-	-	-
3	-	-	-	-
5	-	-	-	-
7	-	-	-	-
9	-	-	-	-
11	-	-	-	-
13	-	-	-	-
15	-	-	-	-
17	-	-	-	-
19	-	-	-	-
21	-	-	-	-
23	-	-	-	-
25	-	-	-	-
27	1.62	1.37	2.99	54.2
29	1.16	1.83	2.99	38.8
31	5.45	2.06	7.51	72.6
33	1.76	0.67	2.43	72.3
35	6.18	1.07	7.25	85.2
37	2.57	1.57	4.14	62.1
39	1.42	1.71	3.13	45.4
41	-	-	-	-
43	1.84	2.15	3.99	46.1
45	4.13	2.18	6.31	65.5
47	3.45	2.31	5.76	59.9

9.11 Sequential extraction data for selective soils from Cores 3, 4 and 5

Table 9.32 Distribution of sequentially extracted U (n=2or 3) for selected soil samples in the form of percentage and concentration from Cores 3, 4 and 5

Sample ID	Depth (cm)	Distribution of U in each fraction (%)							Recovery rate (%)	Distribution of U in each fraction (mg L^{-1})						
		F1	F2	F3	F4	F5	F6	F7		F1	F2	F3	F4	F5	F6	F7
Core 3	4.5	n.d.	55.1	5.3	29.0	9.0	0.7	0.9	127.9	n.d.	6.00±1.04	0.58±0.07	3.16±0.25	0.98±0.17	0.08±0.00	0.10±0.02
	10.5	n.d.	60.5	6.3	25.4	6.5	0.5	0.7	121.8	n.d.	12.24±0.04	1.28±0.10	5.14±0.18	1.32±0.11	0.09±0.01	0.15±0.02
	16.5	n.d.	61.6	6.8	24.9	5.3	0.5	0.9	125.1	n.d.	22.65±0.27	2.51±0.05	9.14±0.33	1.95±0.25	0.18±0.00	0.31±0.13
	25.5	n.d.	67.9	7.0	19.4	4.6	0.5	0.6	142.7	n.d.	18.10±0.38	1.87±0.09	5.18±0.23	1.23±0.02	0.13±0.05	0.16±0.01
	31.5	n.d.	67.4	6.1	19.3	5.3	0.4	1.4	104.4	n.d.	5.00±0.07	0.46±0.03	1.43±0.05	0.39±0.01	0.03±0.01	0.11±0.00
	37.5	n.d.	72.5	6.3	16.3	3.9	0.3	0.7	119.5	n.d.	6.91±0.28	0.60±0.02	1.56±0.06	0.38±0.04	0.03±0.01	0.07±0.01
	43	n.d.	71.8	5.5	16.3	4.8	0.3	1.3	111.8	n.d.	6.92±0.32	0.53±0.02	1.57±0.13	0.47±0.04	0.03±0.00	0.13±0.03
Core 4	4.5	n.d.	44.5	2.4	39.9	11	1.5	0.7	126.5	n.d.	0.57±0.02	0.03±0.00	0.51±0.01	0.14±0.00	0.02±0.00	n.d.
	10.5	n.d.	62.5	4.8	24.6	6.7	0.7	0.7	176.6	n.d.	1.89±0.05	0.14±0.00	0.74±0.00	0.20±0.02	0.02±0.00	0.02±0.00
	13.5	n.d.	62.3	5.8	24.6	5.8	0.7	0.8	130.2	n.d.	2.52±0.04	0.23±0.03	0.99±0.05	0.24±0.01	0.03±0.00	0.03±0.01
	22.5	n.d.	56.7	6.5	27.6	6.8	0.5	1.8	84.3	n.d.	1.50±0.25	0.17±0.03	0.73±0.08	0.18±0.02	0.01±0.01	0.05±0.01
	28.5	n.d.	57.6	5.1	24.7	6.4	n.d.	6.1	149.4	n.d.	1.15±0.15	0.10±0.02	0.49±0.07	0.13±0.02	n.d.	0.12±0.02
Core 5	2.5	n.d.	67.4	6.9	18.8	3.9	n.d.	3.1	156.6	n.d.	2.40±0.08	0.25±0.00	0.67±0.05	0.14±0.01	n.d.	0.11±0.03
	17.5	n.d.	64.4	5.9	21.0	4.6	n.d.	4.1	137.9	n.d.	2.48±0.02	0.23±0.02	0.81±0.04	0.18±0.02	n.d.	0.16±0.01

n.d. = 0.004 mg L^{-1}

Table 9.33 Distribution of sequentially extracted Fe (n=2) in selected soil samples in the form of percentage and concentration from Cores 3, 4 and 5

Sample ID	Depth (cm)	Distribution of Fe in each fraction (%)							Recovery rate (%)	Distribution of Fe in each fraction (mg L^{-1})						
		F1	F2	F3	F4	F5	F6	F7		F1	F2	F3	F4	F5	F6	F7
Core 3	4.5	n.d.	0.7	4.0	57.0	15.9	9.0	13.4	116.8	n.d.	0.29 ±0.02	1.65 ±0.54	23.57 ±1.38	6.57 ±1.20	3.73 ±0.43	5.55 ±1.25
	10.5	n.d.	0.6	5.4	55.2	15.3	9.3	14.1	123.3	n.d.	0.36 ±0.13	3.26 ±0.33	33.25 ±0.10	9.24 ±0.77	5.61 ±0.13	8.50 ±0.22
	16.5	n.d.	0.6	6.4	50.5	14.6	12.7	15.2	107.1	n.d.	0.51 ±0.02	5.47 ±0.28	42.88 ±4.61	12.41 ±0.08	10.74 ±1.54	12.86 ±2.18
	25.5	n.d.	0.6	10.5	39.2	9.5	17.1	23.1	122.1	n.d.	0.56 ±0.06	9.20 ±0.03	34.42 ±0.03	8.30 ±0.22	15.05 ±6.07	20.27 ±2.19
	31.5	n.d.	0.8	12.2	21.1	5.8	23.8	36.3	102.3	n.d.	1.18 ±0.08	16.95 ±0.29	29.15 ±1.47	7.99 ±0.02	32.96 ±5.66	50.17 ±4.59
	37.5	n.d.	4.2	18.4	30.3	6.6	16.6	23.9	93.3	n.d.	6.35 ±0.93	27.98 ±1.58	46.18 ±2.85	10.13 ±1.55	25.34 ±1.39	36.46 ±2.81
	43	n.d.	2.7	14.6	19.8	6.9	20.1	35.9	103.7	n.d.	4.59 ±1.24	24.34 ±0.30	33.08 ±0.51	11.61 ±2.11	33.60 ±2.35	60.00 ±7.30
Core 4	4.5	n.d.	1.4	16.6	60	15.3	3.8	2.9	118.2	n.d.	2.47 ±0.43	29.24 ±5.88	105.95 ±6.83	27.03 ±2.72	6.78 ±0.19	5.09 ±0.78
	10.5	n.d.	6.9	20.1	47.4	11.5	5.8	8.4	89.5	n.d.	12.97 ±0.91	37.80 ±3.78	89.36 ±2.32	21.59 ±0.88	10.84 ±1.02	15.88 ±1.19
	13.5	n.d.	6.1	18.3	48.7	10.8	6.6	9.4	121.6	n.d.	12.13 ±1.95	36.31 ±0.53	96.65 ±4.37	21.47 ±2.66	13.08 ±0.63	18.68 ±2.67
	22.5	n.d.	1.2	13.5	33.2	8.5	14	29.6	99.7	n.d.	1.31 ±0.07	15.18 ±0.15	37.25 ±4.07	9.52 ±0.64	15.75 ±0.58	33.16 ±1.85
	28.5	n.d.	2.7	14.1	21.9	6	17.5	37.7	78.3	n.d.	4.36 ±1.09	22.36 ±1.41	34.87 ±4.00	9.59 ±0.39	27.84 ±8.77	59.98 ±12.51
Core 5	2.5	n.d.	29.5	23.6	26.6	4.5	5.8	9.9	127.9	n.d.	165.75 ±14.97	132.98 ±1.86	149.86 ±7.66	25.31 ±1.48	32.76 ±2.25	55.81 ±2.22
	17.5	n.d.	12.1	19.6	26.0	5.7	14.5	22.0	96.4	n.d.	35.99 ±9.79	58.51 ±8.17	77.56 ±6.59	17.04 ±0.35	43.15 ±2.14	65.69 ±7.12

n.d. = 0.001 mg L^{-1}

9.12 Gel electrophoresis data

9.12.1 Data of validation of the gel electrophoretic fractionation procedure

Table 9.34: Gel strip mass and corresponding element content in the gel without and with application of gel electrophoresis

Strip number	Gel weight (g)	Without application gel electrophoresis						Under application of gel electrophoresis						
		U (mg)	Fe (mg)	Zn (mg)	Mn (mg)	Cu (mg)	Pb (mg)	Gel weight (g)	U (mg)	Fe (mg)	Zn (mg)	Mn (mg)	Cu (mg)	Pb (mg)
F1	4.708	9.91E-04	9.81E-04	8.07E-03	n.d.	n.d.	n.d.	4.717	1.30E-03	4.72E-04	7.33E-03	n.d.	n.d.	n.d.
F2	4.314	8.97E-04	3.65E-04	6.84E-03	n.d.	n.d.	n.d.	3.787	1.04E-03	4.49E-04	6.43E-03	n.d.	n.d.	n.d.
F3	4.107	1.00E-03	3.04E-04	7.18E-03	n.d.	n.d.	n.d.	3.991	1.00E-03	8.22E-04	5.17E-03	n.d.	n.d.	n.d.
F7	4.312	9.57E-04	3.64E-04	5.20E-03	n.d.	n.d.	n.d.	4.181	1.12E-03	4.24E-04	4.58E-03	n.d.	n.d.	n.d.
F8	4.298	1.06E-03	3.85E-04	4.54E-03	n.d.	n.d.	n.d.	3.954	9.59E-04	3.35E-04	3.26E-03	n.d.	n.d.	n.d.
F12	3.962	1.15E-03	3.15E-04	6.07E-03	n.d.	n.d.	n.d.	4.204	9.11E-04	7.67E-04	7.18E-03	n.d.	n.d.	n.d.
F13	4.502	9.77E-04	3.59E-04	7.78E-03	n.d.	n.d.	n.d.	4.023	1.10E-03	4.35E-04	8.41E-03	n.d.	n.d.	n.d.
F14	4.666	9.76E-04	5.49E-04	1.63E-02	n.d.	n.d.	n.d.	4.595	1.17E-03	4.19E-04	2.02E-02	n.d.	n.d.	n.d.

n.d. for Mn = 0.0002 mg L^{-1}

n.d. for Cu = 0.003 mg L^{-1}

n.d. for Pb = 0.002 mg L^{-1}

9.12.2 Data of gel electrophoresis for soil humic substances from Cores 1 and 2

Table 9.35: Mass of elements (U, Fe, Mn, Pb and Cu) in gel electrophoretic fractions from Core 1 0-5 cm and Core 2 0-5 cm

Strip number	Core 1 0-5 cm					Core 2 0-5 cm				
	U (mg)	Fe (mg)	Mn (mg)	Pb (mg)	Cu (mg)	U (mg)	Fe (mg)	Mn (mg)	Pb (mg)	Cu (mg)
F1	2.55E-03	1.31E-02	3.79E-04	3.59E-04	2.99E-03	2.62E-04	1.42E-02	5.61E-05	1.00E-04	5.10E-04
F2	2.14E-03	1.72E-02	3.04E-04	3.12E-04	2.33E-03	1.11E-03	4.37E-02	4.00E-05	2.05E-04	1.37E-03
F3	3.87E-04	1.12E-03	n.d.	3.93E-05	3.45E-04	1.30E-04	3.90E-03	n.d.	3.02E-05	1.11E-04
F4	n.d.	3.05E-03	n.d.	6.04E-05	3.13E-04	n.d.	1.94E-04	n.d.	n.d.	n.d.
F5	5.79E-05	n.d.	n.d.	n.d.	n.d.	n.d.	2.70E-04	n.d.	n.d.	n.d.
F6	1.22E-05	n.d.	n.d.	n.d.	n.d.	n.d.	9.17E-05	n.d.	n.d.	n.d.
F7	n.d.	4.12E-05	n.d.	4.26E-05	n.d.	2.05E-05	3.63E-05	n.d.	7.25E-06	n.d.
F8	1.18E-05	8.33E-05	n.d.	n.d.	n.d.	n.d.	n.d.	n.d.	n.d.	n.d.

n.d. for U = 0.004 mg L^{-1}

n.d. for Fe = 0.001 mg L^{-1}

n.d. for Mn = 0.0002 mg L^{-1}

n.d. for Cu = 0.003 mg L^{-1}

n.d. for Pb = 0.002 mg L^{-1}

Table 9.36: Mass of U in gel electrophoretic fractions at different depths of Core 1 and Core 2

Strip number	**U (mg) in Core 1**							
	0-5 cm	**5-10 cm**	**10-16 cm**	**16-22 cm**	**22-28 cm**	**28-34 cm**	**34-40 cm**	**40-45 cm**
F1	2.55E-03	1.12E-03	1.10E-03	4.28E-03	3.87E-04	3.40E-04	3.13E-04	6.73E-05
F2	2.14E-03	7.24E-04	3.68E-03	3.88E-03	2.99E-03	2.01E-03	1.18E-03	1.18E-03
F3	3.87E-04	3.44E-04	3.85E-04	3.21E-04	8.17E-04	4.30E-04	1.92E-04	3.44E-04
F4	n.d.	5.12E-05	n.d.	4.21E-05	4.52E-05	n.d.	1.43E-05	n.d.
F5	5.79E-05	3.50E-05	n.d.	n.d.	3.35E-05	4.78E-05	3.23E-05	n.d.
F6	1.22E-05	n.d.	n.d.	n.d.	1.98E-07	n.d.	n.d.	n.d.
F7	n.d.	2.01E-05	n.d.	1.43E-05	n.d.	1.35E-05	5.64E-05	n.d.
F8	1.18E-05	1.48E-06	1.64E-05	8.16E-06	1.19E-05	n.d.	n.d.	4.72E-05
Strip number	**U (mg) in Core 2**							
	0-5 cm	**5-10 cm**	**10-15 cm**	**15-20 cm**	**20-25 cm**	**25-30 cm**	**30-35 cm**	**35-42 cm**
F1	2.62E-04	8.19E-04	1.15E-03	1.22E-03	1.52E-03	1.10E-04	1.27E-03	5.17E-04
F2	1.11E-03	2.10E-03	1.05E-03	1.52E-03	2.21E-03	8.16E-04	1.55E-03	7.07E-04
F3	1.30E-04	2.03E-04	3.19E-04	2.26E-04	2.60E-04	7.74E-05	2.53E-04	3.94E-05
F4	n.d.	4.53E-06	n.d.	1.02E-05	5.10E-06	8.70E-08	5.48E-05	n.d.
F5	n.d.	n.d.	n.d.	3.63E-05	1.63E-05	8.26E-05	n.d.	n.d.
F6	n.d.	6.21E-06	n.d.	n.d.	n.d.	n.d.	2.05E-06	1.74E-05
F7	2.05E-05	2.49E-05	n.d.	n.d.	1.18E-06	3.43E-05	3.92E-05	n.d.
F8	n.d.	n.d.	5.67E-05	6.15E-05	3.21E-06	2.77E-06	n.d.	n.d.

n.d. for U = 0.004 mg L^{-1}

Table 9.37: Mass of Fe in gel electrophoretic fractions at different depths of Core 1 and Core 2

Strip number	**Fe (mg) in Core 1**							
	0-5 cm	**5-10 cm**	**10-16 cm**	**16-22 cm**	**22-28 cm**	**28-34 cm**	**34-40 cm**	**40-45 cm**
F1	1.31E-02	2.45E-02	3.03E-03	2.92E-02	3.28E-03	3.70E-03	1.89E-02	2.28E-03
F2	1.72E-02	8.71E-03	1.27E-02	2.21E-02	1.85E-02	2.20E-02	2.40E-02	2.08E-02
F3	1.12E-03	1.82E-04	9.03E-04	1.07E-03	3.00E-03	4.11E-03	2.15E-03	4.39E-03
F4	3.05E-03	n.d.	n.d.	5.14E-05	n.d.	5.66E-05	n.d.	n.d.
F5	n.d.	n.d.	n.d.	4.21E-06	6.90E-05	3.66E-04	1.71E-04	1.68E-04
F6	n.d.	n.d.	n.d.	3.45E-04	2.48E-06	9.88E-06	1.49E-04	3.58E-05
F7	4.12E-05	n.d.	n.d.	n.d.	5.19E-05	n.d.	n.d.	n.d.
F8	8.33E-05	1.09E-04	3.85E-04	n.d.	n.d.	n.d.	n.d.	3.37E-06
Strip number	**Fe (mg) in Core 2**							
	0-5 cm	**5-10 cm**	**10-15 cm**	**15-20 cm**	**20-25 cm**	**25-30 cm**	**30-35 cm**	**35-42 cm**
F1	1.42E-02	4.94E-02	7.97E-02	6.30E-02	1.63E-02	1.09E-02	2.25E-02	2.91E-02
F2	4.37E-02	7.50E-02	3.71E-02	2.73E-02	1.89E-02	2.58E-02	2.61E-02	3.07E-02
F3	3.90E-03	6.97E-03	2.71E-03	2.36E-03	1.12E-03	1.31E-03	3.52E-03	1.94E-03
F4	1.94E-04	2.76E-05	4.96E-04	n.d.	n.d.	2.28E-03	3.69E-05	1.80E-04
F5	2.70E-04	n.d.	1.12E-04	9.03E-06	n.d.	2.14E-04	n.d.	n.d.
F6	9.17E-05	1.47E-04	3.09E-05	4.92E-05	n.d.	2.36E-05	n.d.	1.65E-04
F7	3.63E-05	n.d.	1.08E-04	n.d.	9.19E-05	n.d.	2.03E-05	n.d.
F8	n.d.	n.d.	n.d.	n.d.	n.d.	n.d.	7.32E-05	n.d.

n.d. for Fe = 0.001 mg L^{-1}

Table 9.38: Mass of Mn in gel electrophoretic fractions at different depths of Core 1 and Core 2

Strip number	**Mn (mg) in Core 1**							
	0-5 cm	**5-10 cm**	**10-16 cm**	**16-22 cm**	**22-28 cm**	**28-34 cm**	**34-40 cm**	**40-45 cm**
F1	3.79E-04	1.51E-04	n.d.	1.23E-04	n.d.	n.d.	n.d.	n.d.
F2	3.04E-04	n.d.	5.43E-05	n.d.	n.d.	n.d.	n.d.	n.d.
F3	n.d.	n.d.	n.d.	n.d.	n.d.	n.d.	n.d.	n.d.
F4	n.d.	n.d.	n.d.	n.d.	n.d.	n.d.	n.d.	n.d.
F5	n.d.	n.d.	n.d.	n.d.	n.d.	n.d.	n.d.	n.d.
F6	n.d.	n.d.	n.d.	n.d.	n.d.	n.d.	n.d.	n.d.
F7	n.d.	n.d.	n.d.	n.d.	n.d.	n.d.	n.d.	n.d.
F8	n.d.	n.d.	n.d.	n.d.	n.d.	n.d.	n.d.	n.d.
Strip number	**Mn (mg) in Core 2**							
	0-5 cm	**5-10 cm**	**10-15 cm**	**15-20 cm**	**20-25 cm**	**25-30 cm**	**30-35 cm**	**35-42 cm**
F1	5.61E-05	2.17E-04	3.93E-04	1.81E-04	n.d.	6.67E-05	n.d.	9.41E-05
F2	4.00E-05	3.90E-04	4.75E-06	5.56E-05	n.d.	n.d.	n.d.	1.32E-04
F3	n.d.	n.d.	n.d.	n.d.	n.d.	n.d.	n.d.	n.d.
F4	n.d.	n.d.	n.d.	n.d.	n.d.	n.d.	n.d.	n.d.
F5	n.d.	n.d.	n.d.	n.d.	n.d.	n.d.	n.d.	n.d.
F6	n.d.	n.d.	n.d.	n.d.	n.d.	n.d.	n.d.	n.d.
F7	n.d.	n.d.	n.d.	n.d.	n.d.	n.d.	n.d.	n.d.
F8	n.d.	n.d.	n.d.	n.d.	n.d.	n.d.	n.d.	n.d.

n.d. for Mn = 0.0002 mg L^{-1}

Table 9.39: Mass of Pb in gel electrophoretic fractions at different depths of Core 1 and Core 2

Strip number	**Pb (mg) in Core 1**							
	0-5 cm	**5-10 cm**	**10-16 cm**	**16-22 cm**	**22-28 cm**	**28-34 cm**	**34-40 cm**	**40-45 cm**
F1	3.59E-04	6.76E-04	1.68E-04	7.53E-04	8.98E-04	1.26E-04	1.92E-04	6.62E-05
F2	3.12E-04	2.80E-04	4.98E-04	5.14E-04	5.99E-04	6.03E-04	4.26E-04	4.77E-04
F3	3.93E-05	1.52E-05	5.14E-05	6.54E-05	1.11E-04	1.14E-04	4.65E-05	1.09E-04
F4	6.04E-05	7.60E-06	2.25E-05	4.02E-05	1.00E-05	9.46E-06	4.98E-06	1.43E-05
F5	n.d.	9.22E-06	2.48E-05	3.20E-05	n.d.	n.d.	n.d.	n.d.
F6	n.d.	n.d.	5.40E-06	n.d.	n.d.	n.d.	n.d.	n.d.
F7	4.26E-05	2.14E-05	n.d.	6.99E-06	n.d.	n.d.	n.d.	n.d.
F8	n.d.	n.d.	n.d.	n.d.	n.d.	n.d.	n.d.	n.d.
Strip number	**Pb (mg) in Core 2**							
	0-5 cm	**5-10 cm**	**10-15 cm**	**15-20 cm**	**20-25 cm**	**25-30 cm**	**30-35 cm**	**35-42 cm**
F1	1.00E-04	2.58E-04	6.91E-04	3.52E-04	4.37E-04	2.41E-04	5.22E-04	2.74E-04
F2	2.05E-04	2.11E-04	1.95E-04	1.98E-04	4.88E-04	4.12E-04	5.32E-04	2.76E-04
F3	3.02E-05	6.05E-06	1.99E-05	4.03E-05	4.54E-05	1.92E-05	8.09E-05	3.72E-06
F4	n.d.	8.02E-06	n.d.	1.01E-05	7.12E-06	1.02E-05	4.99E-08	n.d.
F5	n.d.	1.34E-06	n.d.	1.51E-05	7.37E-06	1.03E-05	n.d.	6.14E-06
F6	n.d.	3.18E-07	2.60E-05	n.d.	n.d.	n.d.	n.d.	5.86E-06
F7	7.25E-06	n.d.	n.d.	4.93E-06	9.30E-06	8.38E-06	1.86E-06	n.d.
F8	n.d.	6.77E-06	n.d.	n.d.	5.54E-06	2.31E-06	5.20E-06	5.46E-06

n.d. for Pb = 0.002 mg L^{-1}

Table 9.40: Mass of Cu in gel electrophoretic fractions at different depths of Core 1 and Core 2

Strip number	**Cu (mg) in Core 1**							
	0-5 cm	**5-10 cm**	**10-16 cm**	**16-22 cm**	**22-28 cm**	**28-34 cm**	**34-40 cm**	**40-45 cm**
F1	2.99E-03	0.00337	9.55E-04	0.00644	0.00294	5.37E-04	5.11E-04	1.93E-04
F2	2.33E-03	0.00112	0.00263	0.00553	0.00329	0.00227	0.00115	0.00133
F3	3.45E-04	3.14E-05	2.01E-04	3.79E-04	6.64E-04	4.33E-04	1.03E-04	2.57E-04
F4	3.13E-04	n.d.	n.d.	n.d.	5.02E-06	n.d.	n.d.	n.d.
F5	n.d.	n.d.	n.d.	n.d.	n.d.	n.d.	n.d.	n.d.
F6	n.d.	n.d.	n.d.	n.d.	n.d.	n.d.	n.d.	n.d.
F7	n.d.	n.d.	n.d.	n.d.	n.d.	n.d.	n.d.	n.d.
F8	n.d.	n.d.	2.54E-05	n.d.	n.d.	n.d.	n.d.	n.d.
Strip number	**Cu (mg) in Core 2**							
	0-5 cm	**5-10 cm**	**10-15 cm**	**15-20 cm**	**20-25 cm**	**25-30 cm**	**30-35 cm**	**35-42 cm**
F1	5.10E-04	0.00105	0.00175	0.00132	0.00105	7.29E-04	9.67E-04	8.73E-04
F2	1.37E-03	0.00203	0.00128	0.00135	9.42E-04	9.69E-04	7.74E-04	6.57E-04
F3	1.11E-04	2.01E-04	1.12E-04	1.34E-04	n.d.	5.47E-05	4.61E-05	9.73E-06
F4	n.d.	n.d.	n.d.	n.d.	n.d.	1.11E-04	n.d.	n.d.
F5	n.d.	n.d.	n.d.	n.d.	n.d.	n.d.	n.d.	n.d.
F6	n.d.	n.d.	n.d.	n.d.	n.d.	n.d.	n.d.	n.d.
F7	n.d.	n.d.	n.d.	n.d.	n.d.	n.d.	n.d.	n.d.
F8	n.d.	n.d.	n.d.	n.d.	n.d.	n.d.	n.d.	n.d.

n.d. for Cu = 0.003 mg L^{-1}

9.13 Data of selective and sequential extractions followed by gel electrophoresis for soil humic substances from Core 3

9.13.1 Humic substances were extracted from the soil AFTER (i) acetate extraction; (ii) dithionite extraction; (iii) acetate and then dithionite extraction of metals from the soil followed by gel electrophoresis

Table 9.41: Data for U, Fe, Mn and Al association with humic substances from Core 3 before and after acetate extraction

Element ID	Strip number	Core 3 S6-1		Core 3 S7-1	
		NaOH (mg)	After acetate extraction (mg)	NaOH (mg)	After acetate extraction (mg)
U	Well	5.18E-05	1.37E-04	1.60E-04	3.34E-04
	F1	5.14E-03	5.28E-03	5.58E-03	3.41E-03
	F2	1.01E-02	8.42E-03	1.11E-02	8.06E-03
	F3	1.38E-03	9.60E-04	1.49E-03	1.32E-03
	F4	5.63E-05	6.36E-05	4.39E-05	n.d.
	F5	n.d.	n.d.	4.90E-05	n.d.
	F6	n.d.	2.64E-05	n.d.	n.d.
	F7	4.98E-05	n.d.	n.d.	3.72E-05
Fe	Well	3.37E-04	9.58E-04	2.69E-04	2.65E-03
	F1	7.53E-03	2.07E-02	7.34E-03	1.87E-02
	F2	1.13E-02	2.50E-02	1.06E-02	2.48E-02
	F3	1.54E-03	2.77E-03	1.21E-03	3.94E-03
	F4	5.21E-03	n.d.	n.d.	7.73E-05
	F5	n.d.	n.d.	2.29E-04	n.d.
	F6	1.12E-04	n.d.	n.d.	3.30E-06
	F7	n.d.	3.71E-04	n.d.	8.10E-05
Mn	Well	8.63E-06	5.43E-06	9.12E-06	5.81E-05
	F1	3.92E-05	3.67E-04	4.35E-05	3.01E-04
	F2	8.29E-05	5.09E-04	8.07E-05	5.42E-04
	F3	1.58E-05	6.50E-05	5.40E-06	7.24E-05
	F4	1.23E-06	3.63E-06	n.d.	n.d.
	F5	1.41E-06	4.00E-07	n.d.	2.84E-06
	F6	n.d.	n.d.	n.d.	n.d.
	F7	4.01E-07	n.d.	9.60E-07	n.d.
Al	Well	2.20E-04	1.49E-03	1.41E-04	4.07E-04
	F1	1.64E-03	6.80E-03	1.58E-03	3.18E-03
	F2	1.73E-03	8.76E-03	1.62E-03	5.64E-03
	F3	1.00E-04	8.09E-04	9.43E-05	5.61E-04
	F4	n.d.	7.64E-05	n.d.	n.d.
	F5	9.55E-05	n.d.	1.47E-05	n.d.
	F6	n.d.	n.d.	n.d.	n.d.
	F7	n.d.	3.71E-05	1.85E-05	2.64E-04

n.d. for U = 0.004 mg L^{-1}

n.d. for Fe = 0.001 mg L^{-1}

n.d. for Mn = 0.0002 mg L^{-1}

n.d. for Al = 0.001 mg L^{-1}

Table 9.42 Data of U, Fe, Mn, Al association with humic substances from Core 3 before and after dithionite extraction

Element ID	Strip number	Core 3 S6-1		Core 3 S7-1	
		NaOH (mg)	After dithionite (mg)	NaOH (mg)	After dithionite (mg)
U	Well	5.18E-05	n.d.	1.60E-04	1.55E-05
	F1	5.14E-03	8.34E-04	5.58E-03	6.45E-04
	F2	1.01E-02	1.38E-03	1.11E-02	1.45E-03
	F3	1.38E-03	3.41E-04	1.49E-03	2.73E-04
	F4	5.63E-05	6.09E-05	4.39E-05	2.51E-05
	F5	n.d.	n.d.	4.90E-05	n.d.
	F6	n.d.	4.10E-05	n.d.	1.15E-05
	F7	4.98E-05	7.87E-06	n.d.	n.d.
Fe	Well	3.37E-04	2.60E-04	2.69E-04	3.14E-04
	F1	7.53E-03	1.64E-03	7.34E-03	1.13E-03
	F2	1.13E-02	2.86E-03	1.06E-02	2.27E-03
	F3	1.54E-03	6.54E-04	1.21E-03	3.33E-04
	F4	5.21E-03	5.09E-05	n.d.	n.d.
	F5	n.d.	9.47E-05	2.29E-04	n.d.
	F6	1.12E-04	n.d.	n.d.	9.05E-06
	F7	n.d.	n.d.	n.d.	n.d.
Mn	Well	8.63E-06	n.d.	9.12E-06	n.d.
	F1	3.92E-05	2.04E-05	4.35E-05	1.31E-05
	F2	8.29E-05	1.12E-04	8.07E-05	1.35E-04
	F3	1.58E-05	2.69E-05	5.40E-06	2.51E-05
	F4	1.23E-06	4.90E-06	n.d.	2.98E-06
	F5	1.41E-06	n.d.	n.d.	n.d.
	F6	n.d.	1.22E-06	n.d.	n.d.
	F7	4.01E-07	n.d.	9.60E-07	1.85E-06
Al	Well	2.20E-04	4.35E-04	1.41E-04	5.62E-04
	F1	1.64E-03	1.85E-03	1.58E-03	1.15E-03
	F2	1.73E-03	2.64E-03	1.62E-03	1.89E-03
	F3	1.00E-04	5.42E-04	9.43E-05	3.32E-04
	F4	n.d.	7.48E-05	n.d.	2.73E-05
	F5	9.55E-05	6.81E-05	1.47E-05	8.63E-06
	F6	n.d.	n.d.	n.d.	n.d.
	F7	n.d.	n.d.	1.85E-05	2.36E-05

n.d. for U = 0.004 mg L^{-1}

n.d. for Fe = 0.001 mg L^{-1}

n.d. for Mn = 0.0002 mg L^{-1}

n.d. for Al = 0.001 mg L^{-1}

Table 9.43: Data for U, Fe, Mn, Al association with humic substances from Core 3 before and after sequential extraction (acetate; dithionite)

Element ID	Strip number	Core 3 S6-1		Core 3 S7-1	
		NaOH (mg)	After sequential (mg)	NaOH (mg)	After sequential (mg)
U	Well	5.18E-05	6.54E-05	1.60E-04	8.43E-05
	F1	5.14E-03	4.16E-04	5.58E-03	6.33E-04
	F2	1.01E-02	6.52E-04	1.11E-02	5.56E-04
	F3	1.38E-03	8.82E-05	1.49E-03	n.d.
	F4	5.63E-05	4.54E-05	4.39E-05	3.12E-05
	F5	n.d.	n.d.	4.90E-05	n.d.
	F6	n.d.	2.87E-05	n.d.	2.33E-06
	F7	4.98E-05	n.d.	n.d.	1.73E-05
Fe	Well	3.37E-04	4.11E-04	2.69E-04	5.01E-04
	F1	7.53E-03	1.91E-03	7.34E-03	2.48E-03
	F2	1.13E-02	2.90E-03	1.06E-02	2.36E-03
	F3	1.54E-03	4.80E-04	1.21E-03	2.24E-04
	F4	5.21E-03	2.76E-05	n.d.	n.d.
	F5	n.d.	4.98E-05	2.29E-04	1.36E-05
	F6	1.12E-04	n.d.	n.d.	n.d.
	F7	n.d.	n.d.	n.d.	1.41E-05
Mn	Well	8.63E-06	n.d.	9.12E-06	n.d.
	F1	3.92E-05	8.79E-06	4.35E-05	3.10E-05
	F2	8.29E-05	5.11E-05	8.07E-05	7.40E-05
	F3	1.58E-05	1.17E-05	5.40E-06	7.65E-06
	F4	1.23E-06	9.65E-08	n.d.	1.75E-06
	F5	1.41E-06	n.d.	n.d.	n.d.
	F6	n.d.	n.d.	n.d.	n.d.
	F7	4.01E-07	3.92E-07	9.60E-07	2.21E-06
Al	Well	2.20E-04	7.19E-04	1.41E-04	4.22E-04
	F1	1.64E-03	1.25E-03	1.58E-03	1.11E-03
	F2	1.73E-03	1.40E-03	1.62E-03	6.65E-04
	F3	1.00E-04	2.14E-04	9.43E-05	n.d.
	F4	n.d.	5.22E-05	n.d.	5.79E-04
	F5	9.55E-05	1.74E-04	1.47E-05	n.d.
	F6	n.d.	n.d.	n.d.	n.d.
	F7	n.d.	n.d.	1.85E-05	2.27E-04

n.d. for U = 0.004 mg L^{-1}

n.d. for Fe = 0.001 mg L^{-1}

n.d. for Mn = 0.0002 mg L^{-1}

n.d. for Al = 0.001 mg L^{-1}

9.13.2 Humic substances were extracted from the soil BEFORE (i) acetate extraction; (ii) dithionite extraction; (iii) acetate and then dithionite extraction of metals from the HS followed by gel electrophoresis

Table 9.44: Data of U, Fe, Mn, Al association with humic substances from Core 3 before and after dithionite extraction

Element ID	Strip number	Core 3 S6-2		Core 3 S7-2	
		NaOH (mg)	After acetate (mg)	NaOH (mg)	After acetate (mg)
U	Well	5.18E-05	5.49E-04	1.60E-04	1.69E-03
	F1	5.14E-03	4.15E-03	5.58E-03	5.07E-03
	F2	1.01E-02	6.90E-03	1.11E-02	8.06E-03
	F3	1.38E-03	1.38E-03	1.49E-03	1.33E-03
	F4	5.63E-05	1.74E-06	4.39E-05	2.34E-05
	F5	n.d.	4.68E-05	4.90E-05	4.18E-05
	F6	n.d.	n.d.	n.d.	n.d.
	F7	4.98E-05	n.d.	n.d.	n.d.
Fe	Well	3.37E-04	4.79E-04	2.69E-04	2.16E-03
	F1	7.53E-03	3.41E-03	7.34E-03	6.33E-03
	F2	1.13E-02	1.95E-02	1.06E-02	1.06E-02
	F3	1.54E-03	2.42E-03	1.21E-03	1.81E-03
	F4	5.21E-03	4.76E-04	n.d.	3.35E-05
	F5	n.d.	n.d.	2.29E-04	1.22E-05
	F6	1.12E-04	n.d.	n.d.	n.d.
	F7	n.d.	1.91E-04	n.d.	2.95E-06
Mn	Well	8.63E-06	n.d.	9.12E-06	n.d.
	F1	3.92E-05	6.08E-06	4.35E-05	3.72E-06
	F2	8.29E-05	3.37E-05	8.07E-05	2.69E-05
	F3	1.58E-05	5.75E-06	5.40E-06	3.05E-06
	F4	1.23E-06	n.d.	n.d.	n.d.
	F5	1.41E-06	1.99E-06	n.d.	6.06E-07
	F6	n.d.	n.d.	n.d.	n.d.
	F7	4.01E-07	1.33E-06	9.60E-07	n.d.
Al	Well	2.20E-04	2.22E-04	1.41E-04	5.31E-04
	F1	1.64E-03	1.26E-03	1.58E-03	1.15E-03
	F2	1.73E-03	1.94E-03	1.62E-03	1.72E-03
	F3	1.00E-04	2.38E-04	9.43E-05	2.28E-04
	F4	n.d.	n.d.	n.d.	1.79E-06
	F5	9.55E-05	n.d.	1.47E-05	n.d.
	F6	n.d.	n.d.	n.d.	n.d.
	F7	n.d.	n.d.	1.85E-05	2.20E-05

n.d. for U = 0.004 mg L^{-1}

n.d. for Fe = 0.001 mg L^{-1}

n.d. for Mn = 0.0002 mg L^{-1}

n.d. for Al = 0.001 mg L^{-1}

Table 9.45: Data of U, Fe, Mn, Al association with humic substances from Core 3 before and after dithionite extraction

Element ID	Strip number	Core 3 S6-2		Core 3 S7-2	
		NaOH (mg)	After dithionite (mg)	NaOH (mg)	After dithionite (mg)
U	Well	5.18E-05	1.36E-04	1.60E-04	1.92E-04
	F1	5.14E-03	2.76E-03	5.58E-03	2.95E-03
	F2	1.01E-02	5.84E-03	1.11E-02	5.53E-03
	F3	1.38E-03	7.39E-04	1.49E-03	1.36E-03
	F4	5.63E-05	5.81E-05	4.39E-05	n.d.
	F5	n.d.	n.d.	4.90E-05	n.d.
	F6	n.d.	n.d.	n.d.	6.24E-06
	F7	4.98E-05	5.50E-05	n.d.	8.24E-06
Fe	Well	3.37E-04	2.27E-04	2.69E-04	1.58E-04
	F1	7.53E-03	2.18E-03	7.34E-03	2.03E-03
	F2	1.13E-02	4.77E-03	1.06E-02	3.90E-03
	F3	1.54E-03	5.27E-04	1.21E-03	9.53E-04
	F4	5.21E-03	n.d.	n.d.	n.d.
	F5	n.d.	n.d.	2.29E-04	n.d.
	F6	1.12E-04	2.81E-07	n.d.	2.74E-07
	F7	n.d.	1.03E-05	n.d.	2.49E-05
Mn	Well	8.63E-06	n.d.	9.12E-06	n.d.
	F1	3.92E-05	3.16E-07	4.35E-05	6.43E-07
	F2	8.29E-05	3.31E-05	8.07E-05	2.43E-05
	F3	1.58E-05	3.27E-06	5.40E-06	5.59E-06
	F4	1.23E-06	n.d.	n.d.	1.00E-06
	F5	1.41E-06	2.14E-07	n.d.	4.80E-07
	F6	n.d.	n.d.	n.d.	n.d.
	F7	4.01E-07	n.d.	9.60E-07	1.10E-07
Al	Well	2.20E-04	1.95E-04	1.41E-04	1.71E-04
	F1	1.64E-03	3.22E-04	1.58E-03	4.21E-04
	F2	1.73E-03	6.65E-04	1.62E-03	6.60E-04
	F3	1.00E-04	n.d.	9.43E-05	1.84E-04
	F4	n.d.	n.d.	n.d.	5.21E-05
	F5	9.55E-05	n.d.	1.47E-05	1.95E-05
	F6	n.d.	1.77E-04	n.d.	n.d.
	F7	n.d.	n.d.	1.85E-05	n.d.

n.d. for U = 0.004 mg L^{-1}

n.d. for Fe = 0.001 mg L^{-1}

n.d. for Mn = 0.0002 mg L^{-1}

n.d. for Al = 0.001 mg L^{-1}

Table 9.46: Data of U, Fe, Mn, Al association with humic substances from Core 3 before and after after sequential extraction (acetate; dithionite)

Element ID	Strip number	Core 3 S6-2		Core 3 S7-2	
		NaOH (mg)	After sequential (mg)	NaOH (mg)	After sequential (mg)
U	Well	5.18E-05	6.50E-05	1.60E-04	4.87E-04
	F1	5.14E-03	2.05E-03	5.58E-03	2.91E-03
	F2	1.01E-02	3.87E-03	1.11E-02	4.48E-03
	F3	1.38E-03	6.43E-04	1.49E-03	6.16E-04
	F4	5.63E-05	n.d.	4.39E-05	9.10E-06
	F5	n.d.	n.d.	4.90E-05	2.10E-05
	F6	n.d.	n.d.	n.d.	9.15E-06
	F7	4.98E-05	2.81E-05	n.d.	n.d.
Fe	Well	3.37E-04	1.52E-04	2.69E-04	4.14E-04
	F1	7.53E-03	2.13E-03	7.34E-03	2.80E-03
	F2	1.13E-02	4.15E-03	1.06E-02	4.66E-03
	F3	1.54E-03	6.00E-04	1.21E-03	5.02E-04
	F4	5.21E-03	n.d.	n.d.	n.d.
	F5	n.d.	n.d.	2.29E-04	n.d.
	F6	1.12E-04	7.48E-05	n.d.	2.53E-04
	F7	n.d.	9.38E-06	n.d.	n.d.
Mn	Well	8.63E-06	n.d.	9.12E-06	n.d.
	F1	3.92E-05	1.38E-06	4.35E-05	7.74E-06
	F2	8.29E-05	1.49E-05	8.07E-05	2.13E-05
	F3	1.58E-05	1.72E-06	5.40E-06	9.15E-07
	F4	1.23E-06	1.97E-06	n.d.	1.10E-06
	F5	1.41E-06	n.d.	n.d.	n.d.
	F6	n.d.	1.75E-06	n.d.	1.10E-06
	F7	4.01E-07	1.74E-06	9.60E-07	1.08E-06
Al	Well	2.20E-04	2.60E-04	1.41E-04	5.59E-04
	F1	1.64E-03	3.95E-04	1.58E-03	5.11E-04
	F2	1.73E-03	6.50E-04	1.62E-03	6.89E-04
	F3	1.00E-04	8.50E-05	9.43E-05	3.24E-05
	F4	n.d.	2.64E-05	n.d.	7.68E-05
	F5	9.55E-05	n.d.	1.47E-05	n.d.
	F6	n.d.	7.52E-05	n.d.	n.d.
	F7	n.d.	n.d.	1.85E-05	2.86E-05

n.d. for U = 0.004 mg L^{-1}

n.d. for Fe = 0.001 mg L^{-1}

n.d. for Mn = 0.0002 mg L^{-1}

n.d. for Al = 0.001 mg L^{-1}

9.14 Data of vertical carbonate concentration for from Core 6

Table 9.47 Data for carbonate concentration from Core 6 soil (n=1 or 2)

Depth (cm)	carbonate (mol kg^{-1} soil)
1	0.197 ±0.010
3	0.171 ±0.004
5	0.185 ±0.001
7	0.178 ±0.001
9	0.175 ±0.002
11	0.119 ±0.018
13	0.129 ±0.006
15	0.235 ±0.012
17	0.429 ±0.089
19	0.041
21	0.087 ±0.001
23	0.048
25	0.049
27	0.035
29	0.053 ±0.007
31	0.028 ±0.001
33	0.022 ±0.000
35	0.011 ±0.000
37	0.010 ±0.002
39	0.011 ±0.001
41	0.017 ±0.004
43	0.024 ±0.002
45	0.031

9.15 Data for gel filtration fractionation

9.15.1 Data of distribution of elements from humic substances of Core 2 under gel filtration

Table 9.48 Data of distribution of elements (U, Fe, Mn, Pb, Cu, Zn) in gel filtration fractionation of Needle's Eye humic substances from Core 2

Strip number	Fe (mg L^{-1})	U (mg L^{-1})	Mn (mg L^{-1})	Pb (mg L^{-1})	Cu (mg L^{-1})	Zn (mg L^{-1})
F1	3.62	0.004	0.023	0.010	0.068	0.144
F2	16.61	0.035	0.113	0.052	0.399	0.542
F3	7.533	0.031	0.02	0.014	0.346	0.216
F4	2.298	0.018	n.d.	n.d.	0.265	0.056
F5	1.508	0.008	n.d.	n.d.	0.236	0.043
F6	1.053	0.007	n.d.	n.d.	0.207	0.039
F7	0.724	0.004	n.d.	n.d.	0.173	0.034
F8	0.491	n.d.	n.d.	n.d.	0.136	0.029
F9	0.331	n.d.	n.d.	n.d.	0.099	0.028
F10	0.227	n.d.	n.d.	n.d.	0.070	0.025
F11	0.151	n.d.	n.d.	n.d.	0.041	0.023
F12	0.106	n.d.	n.d.	n.d.	0.020	0.021
F13	0.081	n.d.	n.d.	n.d.	0.004	0.021
F14	0.061	n.d.	n.d.	n.d.	n.d.	0.021
F15	0.048	n.d.	n.d.	n.d.	n.d.	0.022
F16	0.036	n.d.	n.d.	n.d.	n.d.	0.024
F17	0.027	n.d.	n.d.	n.d.	n.d.	0.026
F18	0.022	n.d.	n.d.	n.d.	n.d.	0.030
F19	0.017	n.d.	n.d.	n.d.	n.d.	0.037
F20	0.014	n.d.	n.d.	n.d.	n.d.	0.067

n.d. for U = 0.004 mg L^{-1}

n.d. for Mn = 0.0002 mg L^{-1}

n.d. for Pb = 0.002 mg L^{-1}

n.d. for Cu = 0.003 mg L^{-1}

Table 9.49: Data of distribution of elements from humic substances of Core 1 under gel filtration

Strip number	U (mg L^{-1}) in Core 1			Fe (mg L^{-1}) in Core 1			Mn (mg L^{-1}) in Core 1			Pb (mg L^{-1}) in Core 1			Cu (mg L^{-1}) in Core 1			Zn (mg L^{-1}) in Core 1		
	28-34 cm	34-40 cm	40-45 cm	28-34 cm	34-40 cm	40-45 cm	28-34 cm	34-40 cm	40-45 cm	28-34 cm	34-40 cm	40-45 cm	28-34 cm	34-40 cm	40-45 cm	28-34 cm	34-40 cm	40-45 cm
F1	0.006	0.008	0.010	1.088	1.250	2.646	n.d.	n.d.	n.d.	n.d.	n.d.	n.d.	0.174	0.06	0.151	0.076	0.050	0.143
F2	0.044	0.058	0.051	4.034	7.217	7.300	n.d.	0.025	n.d.	n.d.	0.025	n.d.	0.707	0.43	0.527	0.255	0.299	0.357
F3	0.046	0.074	0.055	3.662	7.716	5.527	n.d.	0.015	n.d.	n.d.	0.015	n.d.	0.743	0.516	0.536	0.201	0.265	0.236
F4	0.027	0.060	0.026	1.779	4.341	2.014	n.d.	n.d.	n.d.	n.d.	n.d.	n.d.	0.518	0.409	0.347	0.079	0.135	0.059
F5	0.015	0.033	0.018	0.856	1.768	1.235	n.d.	n.d.	n.d.	n.d.	n.d.	n.d.	0.362	0.261	0.293	0.034	0.039	0.028
F6	0.011	0.021	0.014	0.633	1.296	0.844	n.d.	n.d.	n.d.	n.d.	n.d.	n.d.	0.314	0.223	0.248	0.029	0.03	0.017
F7	0.006	0.017	0.009	0.428	0.92	0.598	n.d.	n.d.	n.d.	n.d.	n.d.	n.d.	0.258	0.182	0.202	0.023	0.023	0.012
F8	n.d.	0.012	0.005	0.277	0.605	0.416	n.d.	n.d.	n.d.	n.d.	n.d.	n.d.	0.206	0.152	0.166	0.018	0.015	0.009
F9	n.d.	0.008	n.d.	0.182	0.408	0.283	n.d.	n.d.	n.d.	n.d.	n.d.	n.d.	0.161	0.130	0.133	0.014	0.01	0.006
F10	n.d.	0.006	n.d.	0.114	0.276	0.192	n.d.	n.d.	n.d.	n.d.	n.d.	n.d.	0.115	0.112	0.106	0.01	0.005	n.d.
F11	n.d.	0.005	n.d.	0.073	0.191	0.135	n.d.	n.d.	n.d.	n.d.	n.d.	n.d.	0.079	0.093	0.082	0.006	n.d.	n.d.
F12	n.d.	n.d.	n.d.	0.049	n.d.	0.099	n.d.	n.d.	n.d.	n.d.	n.d.	n.d.	0.047	n.d.	0.057	0.005	n.d.	n.d.
F13	n.d.	0.006	n.d.	0.033	0.110	0.072	n.d.	n.d.	n.d.	n.d.	n.d.	n.d.	0.023	0.041	0.032	n.d.	n.d.	n.d.
F14	n.d.	n.d.	n.d.	0.023	0.087	0.053	n.d.	n.d.	n.d.	n.d.	n.d.	n.d.	0.009	0.020	0.015	n.d.	n.d.	n.d.
F15	n.d.	0.004	n.d.	0.015	0.067	0.041	n.d.	n.d.	n.d.	n.d.	n.d.	n.d.	n.d.	0.006	0.006	n.d.	n.d.	n.d.
F16	n.d.	n.d.	n.d.	0.01	0.055	0.033	n.d.	n.d.	n.d.	n.d.	n.d.	n.d.	n.d.	n.d.	n.d.	n.d.	0.007	0.005
F17	n.d.	0.003	n.d.	0.007	0.048	0.027	n.d.	n.d.	n.d.	n.d.	n.d.	n.d.	n.d.	n.d.	n.d.	0.005	0.008	0.005
F18	n.d.	n.d.	n.d.	0.004	0.042	0.021	n.d.	n.d.	n.d.	n.d.	n.d.	n.d.	n.d.	n.d.	n.d.	0.006	0.008	0.006
F19	n.d.	n.d.	n.d.	0.002	0.038	0.018	n.d.	n.d.	n.d.	n.d.	n.d.	n.d.	n.d.	n.d.	n.d.	0.008	0.010	0.007
F20	n.d.	0.005	n.d.	0.001	0.034	0.016	n.d.	n.d.	n.d.	n.d.	n.d.	n.d.	n.d.	n.d.	n.d.	0.011	0.012	0.011
F21		0.004	n.d.		0.032	0.014		n.d.	n.d.		n.d.	n.d.		n.d.	n.d.		0.016	0.014
F22		0.004	n.d.		0.027	0.011		n.d.	n.d.		n.d.	n.d.		n.d.	n.d.		0.023	0.022
F23		0.005	n.d.		0.024	0.010		n.d.	n.d.		n.d.	n.d.		n.d.	n.d.		0.033	0.034
F24		0.004	n.d.		0.022	0.009		n.d.	n.d.		n.d.	n.d.		n.d.	n.d.		0.056	0.051
F25		0.004	n.d.		0.020	0.008		n.d.	n.d.		n.d.	n.d.		n.d.	n.d.		0.095	0.083

n.d. for U = 0.004 mg L^{-1}, n.d. for Fe = 0.001 mg L^{-1}, n.d. for Mn = 0.0002 mg L^{-1}, n.d. for Pb = 0.002 mg L^{-1}, n.d. for Cu = 0.003 mg L^{-1}, n.d. for Zn = 0.005 mg L^{-1}

9.15.2 Distribution of elements from soil porewater colloids (3 kDa-0.2 µm) from Core 7 under gel filtration

Table 9.50: Gel filtration for Core 7 G200

Sample ID	Elution volume (mL)	UV abs at 254 nm	U (µg L^{-1})	Fe (µg L^{-1})	Al (µg L^{-1})	Pb (µg L^{-1})	Cu (µg L^{-1})	Zn (µg L^{-1})	Mn (µg L^{-1})	As (µg L^{-1})	Ca (µg L^{-1})
Core 7 S4	1	0.289	1.7	588	286	1.3	4.2	55	7.0	7.7	414
	2	0.566	2.6	811	303	1.9	11	106	27	19	690
	3	0.608	2.6	676	207	0.9	10	147	59	27	1360
	4	0.458	1.9	364	129	0.3	5.4	99	53	24	1450
	5	0.213	0.8	155	42	1.3	2.5	52	28	19	864
	6	0.071	0.3	64	7.1	n.d.	0.6	21	12	11	511
	7	0.049	0.2	57	16	n.d.	0.4	18	7.8	7.3	286
	8	0.039	0.2	41	n.d.	n.d.	0.3	13	6.7	3.5	193
Core 7 S8	1	0.346	2.8	324	332	2.5	9.4	29	19	4.5	369
	2	0.897	5.6	579	445	3.9	16	74	21	8.7	1030
	3	1.071	5.2	405	324	1.8	11	69	17	10	2590
	4	0.694	3.1	201	169	0.4	6.3	46	12	11	2500
	5	0.124	0.4	27	14	0.1	1.4	14	3.0	3.0	550
	6	0.029	0.05	4.0	n.d.	n.d.	0.1	16	1.2	1.0	167
	7	0.030	0.03	2.2	n.d.	n.d.	n.d.	6.1	0.9	0.7	155
	8	0.015	0.03	3.9	n.d.	n.d.	n.d.	7.8	0.8	0.4	140
Core 7 S17	1	0.280	5.6	333	632	13.6	12	48	9.2	4.5	348
	2	0.612	11.6	548	950	32.8	25	93	17	8.7	836
	3	0.526	7.5	259	441	27.1	13	61	8.0	10	541
	4	0.311	3.3	101	156	18.8	6	38	3.8	11	517
	5	0.096	1.0	34	51	2.7	2.1	17	1.9	3.0	336
	6	0.035	0.4	21	20	0.1	0.8	8.4	1.1	1.0	136
	7	0.025	0.2	6.2	n.d.	0.1	0.3	7.8	0.6	0.7	131
	8	0.022	0.2	8.5	5.9	n.d.	0.6	10	0.7	0.4	155
Core 7 S35	1	0.287	13.6	103	1710	4.2	27	64	1.5	11	515
	2	0.609	32.8	157	2800	7.7	46	70	2.5	24	1090
	3	0.640	27.1	102	1330	4.2	14	38	2.9	56	2000
	4	0.518	18.8	46	527	2.1	3.3	33	2.6	79	2420
	5	0.094	2.7	4.4	77	0.2	0.8	20	0.5	28	657
	6	0.012	0.1	n.d.	n.d.	n.d.	0.4	4.4	0.1	2.2	156
	7	0.005	0.06	n.d.	n.d.	n.d.	0.3	25	0.9	1.4	224
	8	0.004	0.01	n.d.	n.d.	n.d.	n.d.	5.9	n.d.	1.3	154

n.d. for Fe = 0.008 µg L^{-1}, n.d. for Al = 1.84 µg L^{-1}, n.d. for Pb = 0.008 µg L^{-1}, n.d. for Cu = 0.05 µg L^{-1}, n.d. for Mn = 0.01 µg L^{-1}

9.16 Data of total Fe and Fe^{II} concentrations in soil porewater from Core 8

Table 9.51 Calibration curve (absorbance vs. Fe^{II} concentration)

Fe^{II} (µg L^{-1})	Abs@562 nm
75.4	0.065
161	0.106
393	0.208
821	0.391
1620	0.736
4096	1.702

Table 9.52 Data of total Fe and Fe^{II} concentrations

Depth (cm)	Fe_{tot} (µg L^{-1})	Fe^{II} (µg L^{-1})
2.5	1960	1800
5	2410	2380
7.5	1140	697
10	1770	1680
12.5	1660	1450
15	1120	715
17.5	549	233
20	577	404
22.5	465	250